A MATHEMATICAL MODEL OF INTERSTITIAL TRANSPORT AND MICROVASCULAR EXCHANGE

By

David G. Taylor

B. A. Sc. (Engineering Science) University of Toronto

A THESIS SUBMITTED IN PARTIAL FULFILMENT OF

THE REQUIREMENTS FOR THE DEGREE OF

DOCTOR OF PHILOSOPHY

in

THE FACULTY OF GRADUATE STUDIES

CHEMICAL ENGINEERING

We accept this thesis as conforming

to the required standard

In presenting this thesis in partial fulfilment of the requirements for an advanced degree at the University of British Columbia, I agree that the Library shall make it freely available for reference and study. I further agree that permission for extensive copying of this thesis for scholarly purposes may be granted by the head of my department or by his or her representatives. It is understood that copying or publication of this thesis for financial gain shall not be allowed without my written permission.

Chemical Engineering

The University of British Columbia

2075 Wesbrook Place

Vancouver, Canada

V6T 1W5

Date:

_____20/04/90_____

Abstract

A generalized mathematical model is developed to describe the transport of fluid and plasma proteins or other macromolecules within the interstitium. To account for the effects of plasma protein exclusion and interstitial swelling, the interstitium is treated as a multiphase deformable porous medium. Fluid flow is assumed proportional to the gradient in fluid chemical potential and therefore depends not only on the local hydrostatic pressure but also on the local plasma protein concentrations through appropriate colloid osmotic pressure relationships. Plasma protein transport is assumed to occur by restricted convection, molecular diffusion, and convective dispersion.

A simplified version of the model is used to investigate microvascular exchange of fluid and a single 'aggregate' plasma protein species in mesenteric tissue. The interstitium is approximated by a rigid, rectangular, porous slab displaying two fluid pathways, only one of which is available to plasma proteins.

The model is first used to explore the effects the interstitial plasma protein diffusivity, the tissue hydraulic conductivity, the restricted convection of plasma proteins, and the mesothelial transport characteristics have on the steady-state distribution and transport of plasma proteins and flow of fluid in the tissue. The simulations predict significant convective plasma protein transport and complex fluid flow patterns within the interstitium. These flow patterns can produce local regions of high fluid and plasma protein exchange along the mesothelium which might be erroneously identified as 'leaky sites'. Further, the model predicts significant interstitial osmotic gradients in some instances, suggesting that the Darcy expression invoked in a number of previous models appearing in the literature, in which fluid flow is assumed to be driven by hydrostatic pressure gradients alone, may be inadequate.

Subsequent transient simulations of hypoproteinemia within the model tissue indicate that

the interstitial plasma protein content decreases following this upset. The simulations therefore support (qualitatively, at least) clinical observations of hypoproteinemia. Simulations of venous congestion, however, demonstrate that changes in the interstitial plasma protein content following this upset depends, in part, on the relative sieving properties of the filtering and draining vessels. For example, when the reflection coefficients of these two sets of boundaries are similar, the interstitial plasma protein content increases with time due to an increased plasma protein exchange rate across the filtering boundaries and sieving of interstitial plasma proteins at the draining boundaries. (This effect is supported by the clinical observation that interstitial plasma protein content in liver increases during venous congestion.) As the reflection coefficient of the draining boundaries decreases relative to that of the filtering boundaries, there is a net loss of plasma proteins from the interstitium, resulting in a decrease in the total interstitial plasma protein content over time (i.e., the familiar 'plasma protein washout'). Further, the model predicts increased fluid transfer from the interstitium to the peritoneum during venous congestion, supporting the clinical observation of ascites.

Finally, the model is used to study the effects of interstitial plasma protein convection and diffusion, plasma protein exclusion, and the capillary transport properties on the transit times of two macromolecular tracers representative of albumin and γ-globulin within a hypothetical, one-dimensional tissue. As was expected, the transit times of each of the tracers through the model tissue varied inversely with the degree of convective transport. Increasing the interstitial diffusivity of the albumin tracer also led to a moderate decrease in the transit time for that tracer. The capillary wall transport properties, meanwhile, had only a marginal effect on the transit time for the range of capillary permeabilities and reflection coefficients considered. However, these properties (and, in particular, the reflection coefficient) had a more pronounced effect on the ultimate steady-state concentration of the tracer in the outlet stream.

It was the interstitial distribution volume of a given tracer that had the greatest impact on the time required for the outlet tracer concentration to reach 50 % of its steady-state value. This was attributed to the increased filling times associated with larger interstitial distribution

volumes. These findings suggest that the 'gel chromatographic effect' observed in some tissues could possibly be explained on the basis of varying distribution volumes.

Table of Contents

List of Tables

List of Figures

Acknowledgements

I would like to express my sincere gratitude to the following individuals:

- my advisors, Drs. J.L. Bert and B.D. Bowen, for their direction, enthusiasm, and understanding;

- the other members of my committee, Drs. K.L. Pinder, R. Pearce, D. Brooks, J. Piret, D. Thompson, and L. Smith, for their helpful suggestions throughout this work;

- Dr. R. Reed of the University of Bergen, Norway, whose clinical expertise is much appreciated;

- Dr. M. Olsen, for his advice on some of the numerical procedures used in this dissertation; and

- Dr. Clive Brereton, Dr. Frank Laytner, and Mr. Clive Chapple, for their friendship and support.

I will praise thee;

for I am fearfully and wonderfully made:

marvellous are thy works,

and that my soul knoweth right well.

My substance was not hid from thee,

when I was made in secret,

and curiously wrought in the lowest parts of the earth.

Thine eyes did see my substance,

yet being unperfect;

and in thy book all my members were written,

which in continuance were fashioned,

when as yet there were none of them.

Ps. 139: 14-16.

This thesis is dedicated to my parents, Ron and Vi, my wife, Charmayne, and my children,

Joseph and Kara, whom I love.

Chapter 1

Introduction

The systemic blood circulation consists of a complex network of vessels that form a closed loop, passing through the various body tissues before completing the circuit. Blood, driven by the pumping action of the heart, travels through a set of small, permeable blood vessels where it exchanges fluid and solutes, including the plasma proteins, with the surrounding tissue. Fluid and solutes are drained from the tissue spaces by an additional circulatory system, called the lymphatics. This exchange is essential both for providing nutrients to the tissue cells and for removing metabolic wastes from the cells' environment. Further, the exchange of fluid and plasma proteins between the blood, the tissue space and the lymph plays an essential part in balancing fluid within the body.

The various physiological elements involved in the exchange of materials within tissues constitute the *microvascular exchange system*. A disturbance to the system, be it from an extrinsic source (such as a burn or hemorrhage) or an intrinsic one (such as venous congestion or hypoproteinemia), compromises the health and well-being of the individual. For example, following a burn, large quantities of fluid may shift from the blood stream to the tissues. The resultant loss of blood volume can be life threatening. A fundamental understanding of the forces and mechanisms governing exchange is therefore of interest to physiologists and clinicians alike.

During exchange, fluid and plasma proteins encounter three principle resistances: the capillary wall and basement membrane, the tissue space (i.e., the interstitium), and the lymphatic wall. These are the major barriers encountered during the transfer of materials from the blood stream to the lymphatic circulation.

1

To describe the mechanisms governing mass exchange within the microvascular exchange system and, ultimately, to predict its response to physiological upsets, the transport characteristics of each of the resistances must be known. Due to the complexity of the system, and as a complement to experimental studies, mathematical models have been developed to describe microvascular exchange. Much of the effort has been directed to modelling the transport properties of the capillary wall (see, for example, [30, 31, 58, 71, 75, 81]). However, over the years researchers have identified the interstitium as another important component of the microvascular exchange system. General models of this system must therefore include mathematical descriptions of the interstitium and its physicochemical properties.

Two basic modelling approaches have been adopted. In the first of these, the microvascular exchange system is reduced to a set of subsystems, or compartments. Material is exchanged between compartments according to the driving forces present (such as differences in fluid chemical potential or solute concentration between compartments) and the transport properties of the intervening boundary. Each compartment is assumed to be homogeneous; i.e., spatial heterogeneities in the material properties of that part of the system represented by the compartment are not accounted for. Furthermore, the compartment is assumed to be well–mixed, so that incoming material is instantaneously dispersed throughout its entire volume. Therefore, the solute concentrations, fluid pressures, and fluid volume associated with a given compartment represent average quantities.

Because of the well–mixed assumption invoked in compartmental models, the driving forces for mass exchange between compartments will, in general, differ from the local driving forces found in the real system. This limits the model's ability to simulate the real system, particularly under transient conditions. In addition, compartmental models tell us nothing about mass transport within an individual compartment and its effect on the overall behavior of the system. However, the assumption of a well–mixed, homogeneous compartment simplifies the modelling problem immensely, because it reduces the number of parameters needed to characterize the system (since the transport properties of the compartment itself are neglected), and because

it simplifies the mathematical description of the system. Hence, complex phenomena, such as tissue swelling, can be included fairly easily in these models. For these reasons compartmental models are frequently used to simulate whole organ and body fluid and plasma protein exchange under both normal and pathological states [108, 18, 14, 3, 70].

Recent advances in microfluorometry, electron microscopy and digital image analysis now permit much more detailed experimental studies of interstitial fluid and protein transport than were previously possible [61, 40, 115], including measurements of interstitial plasma protein gradients. Mathematical models of interstitial transport are therefore required to interpret this expanding body of experimental data. The requisite model must include mathematical descriptions of the physicochemical properties of the interstitium, such as plasma protein exclusion and interstitial swelling characteristics, which impact on fluid and protein transport. It must also be able to predict possible variations in the distribution of fluid pressure and protein within the interstitial space [40, 61, 110]. Compartmental models are incapable of this. Such detailed descriptions are only possible with a distributed (i.e., spatially varying) model of interstitial transport.

Unlike compartmental models, the distributed models of the microvascular exchange system do not assume that the various body compartments are well–mixed so that, in principle at least, these models more closely describe the real system. Distributed models can therefore be used to investigate the influence of mass transport within a given compartment (such as the blood or the interstitial space) on microvascular exchange. In addition, since the distributed models eliminate the artificial dispersion caused by the well–mixed assumption, they better describe transient processes.

The advantages associated with the distributed models are not without their costs. First, these models require far more detailed information about the structure, transport properties and spatial distribution of the various compartments. This leads naturally to a larger number of system parameters which need to be quantified, such as the interstitial hydraulic conductivity, plasma protein effective diffusivity, and capillary vessel diameter. More often than not,

many of these quantities must be estimated due to a lack of experimental data. In such instances it is necessary to conduct numerical experiments to determine the sensitivity of the model's predictions to the values assumed for the estimated parameters. Given the degree of uncertainty associated with these estimates, the results from distributed models are more often qualitative than quantitative. Despite these limitations, distributed models provide a powerful tool for investigating the mechanisms governing interstitial transport and their influence on microvascular exchange.

A number of distributed models have already been proposed to describe fluid and/or protein transport within the interstitium. These models vary both in detail and in complexity. Blake and Gross [22] and Fleischman et al. [36] investigated fluid exchange within idealized tissues consisting of ordered arrays of capillaries. In both cases the interstitial space was treated as an isotropic, homogeneous, rigid porous medium. In addition, interstitial fluid flow was described by a form of Darcy's Law in which the authors assumed that the local fluid flux is proportional to the local gradient in hydrostatic pressure. Hence both models neglect the influence of osmotic pressure gradients on local fluid movement. Furthermore, neither model considers protein transport within the interstitium.

Several investigators have addressed protein transport through the interstitial space. For example, Baxter et al. [7] assumed that protein transport occurs strictly by diffusion. Convective contributions were not accounted for. Fry [43] considered both convection and diffusion in his model of interstitial transport of multiple protein species. However, Fry's model requires prior knowledge of the fluid velocities throughout the interstitial space. Furthermore, it makes no attempt to describe the effect of interstitial swelling on protein transport.

Salathé and Venkataraman [87] presented equations to describe both fluid and protein transport within the interstitium. Again, fluid flow was assumed proportional to the gradient in hydrostatic pressure. The equation of protein transport included both convective and diffusive terms. However, their model does not distinguish between those regions of the interstitium which are accessible to protein and those from which protein is excluded. Hence, their model

neglects the intrinsic heterogeneities within the interstitium resulting from plasma protein exclusion. Furthermore, the model is limited to steady-state conditions. It is therefore incapable of predicting the time-dependent response of the interstitial fluid and protein distributions to a variety of systemic perturbations.

Each of the models cited above provides insights into various aspects of interstitial transport. However, in each case the mathematical model is limited in scope. The objective of the present work, therefore, is to develop a more general mathematical model which describes the combined effects of interstitial swelling and plasma protein exclusion on the transient re-distribution of fluid and any number of macromolecular species within the interstitium. Local fluid flow is related to the gradient in total fluid chemical potential rather than hydrostatic pressure alone. Thus fluid movement is linked to gradients in solute concentration through associated colloid osmotic pressure gradients. Protein transport occurs by convective, dispersive and diffusive mechanisms, thereby providing further linkage between fluid and solute behavior. As a consequence, the equations governing fluid and protein movement within the deforming interstitium must always be solved as a coupled set rather than as the independent equations often assumed in previous analyses.

This dissertation is divided into seven remaining chapters. Chapter 2 provides an overview of the physiology of the microvascular exchange system. In Chapter 3, the general model of interstitial transport is developed. Chapter 4 applies a simplified version of the general model to investigate the mechanisms governing the steady-state exchange of fluid and macromolecules within mesenteric tissue. In Chapter 5, the analysis is extended to transient conditions and considers the response of the model system to two specific systemic perturbations. Chapter 6 adds a further dimension to the problem by investigating the simultaneous transport of multiple plasma protein species through the interstitium. Finally, Chapters 7 and 8 summarize the findings and ramifications of the dissertation and recommend several additional studies.

Chapter 2

Physiological Overview of the Microvascular Exchange System

Fluid and various solute species contained within blood are transported to the body tissues and organs via a complex network of vessels forming the *systemic blood circulation*. Upon entering a specific organ, blood passes through a system of small, permeable blood vessels that constitute the *microcirculation* (see Figure (2.1)). It is here that nutrients and metabolic wastes exchange between the blood and the tissues cells. In addition, fluid and various macromolecules (in particular, the *plasma proteins*) are transported across the walls of the exchange vessels to enter the surrounding tissue space called the *interstitium*.

The *blood capillaries* are the principal vessels responsible for exchange between the blood and the interstitium. However, the blood vessels supplying the capillaries, namely the *arterioles*, and those which drain the capillary bed, i.e., the *venules*, are also known to participate in the exchange process [82]. The exchange vessels are of minute dimensions; capillary diameters, for example, average 6 μm in humans [46].

In addition to the blood vasculature, the body contains another circulatory network, called the *lymphatic system,* that drains fluid and solutes from the interstitial space. The lymphatic vessels return material to the systemic circulation, emptying into the venous portion of the latter network in the vicinity of the heart [46].

The exchange vessels of the blood vasculature (namely, the arterioles, the capillaries and the venules), the interstitium, and the tissue drainage system (such as the terminal lymphatic vessels) constitute the *microvascular exchange system*. Based on this anatomical definition, the microvascular exchange system can be viewed as a series of resistances that fluid and solutes encounter in their journey from blood to lymph. These resistances may be loosely defined
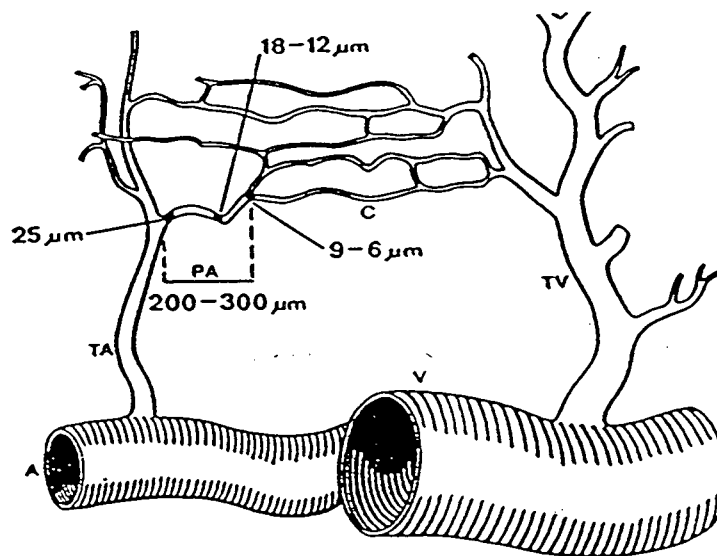
Figure 2.1: The network of permeable vessels constituting the microcirculation. Blood enters via the arteriolar vessel (A). A portion of this is drawn into the terminal arteriole (TA), passes through the network of capillaries (C), is taken up by the terminal venule (TV), and returned to the venule (V). During this time fluid and solutes, including plasma proteins, leak from the blood to the surrounding tissue spaces [109].

as the capillary wall and basement membrane, the interstitium, and the wall of the terminal lymphatic vessel. A discussion of each of these three components follows.

2.1 The Capillary Wall and Basement Membrane

2.1.1 General Description

The capillary wall is composed of a single layer of flattened *endothelial cells* that rest on a specialized region of the interstitial matrix call the *basement membrane* or *basal lamina* [90, 13]. The latter structure consists largely of specialized forms of collagen that are not to be found elsewhere within the interstitial matrix [13] (see Section 2.2.1 for a further discussion of collagen). The basal lamina carries a net negative charge. It is believed to both provide mechanical support to the endothelial cells and to act as an additional transport barrier [112]. Together, the capillary wall and basal lamina act as a semi-permeable membrane that separates the blood and the interstitial compartments. Fluid and solutes selectively pass from the blood to the interstitium, driven by the local differences in the hydrostatic pressures, colloid osmotic pressures, and solute concentrations between the two compartments.

The endothelial cell consists of the aqueous *cytoplasm* of the cell interior surrounded by a *plasma membrane*, the latter being comprised largely of lipids and protein. Within the cytoplasm are small spherical bodies 60 to 80 nm in diameter, called *plasmalemmal vesicles* [90]. These appear open on the luminal (blood) and interstitial surfaces of the cell and as free bodies within the cytoplasm [112]. The vesicles are thought to play a role in the transfer of macromolecules across the endothelial barrier. Several mechanisms have been suggested, including the shuttling of material from the luminal surface to the interstitial side by individual vesicles. It is also postulated that several vesicles may fuse to form temporary water channels across the width of the cell (see Figure (2.2)). Evidence suggests that vesicular uptake of macromolecules is selective [112]. For example, vesicles found in the microvessels of adipose tissue will take up native ferritin, but not native albumin, although the latter is smaller.

The outer surface of the endothelial cells are covered with delicate, negatively charged fibers,
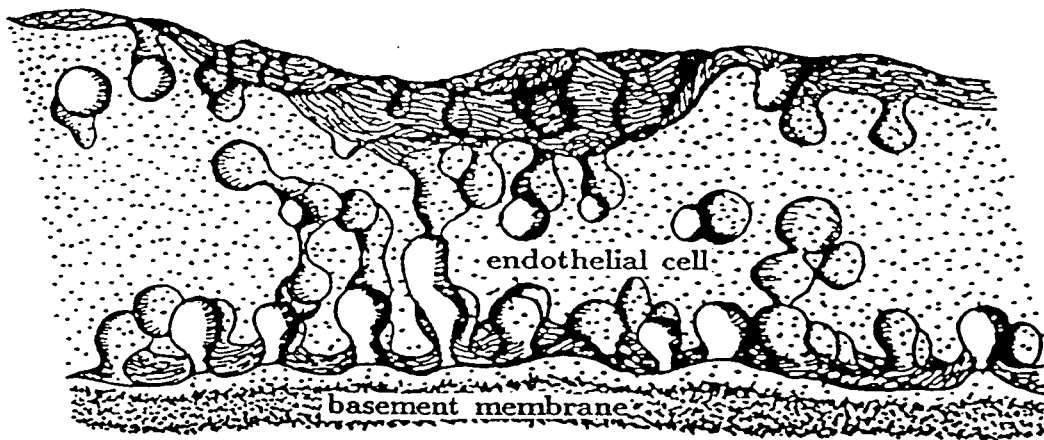
Figure 2.2: **This figure depicts vesicular transport pathways within a cross-section of an endothelial cell resting on the basement membrane below. Proposed vesicular transport mechanisms include the formation of temporary fluid channels due to fusion of several vesicles bridging the endothelial cell (modified after [103]).**

thought to be glycosaminoglycans, that form a coat 10 to 20 nm thick [90]. This felt-like cover also lines the inner surface of the vesicles. It is thought to serve as an additional diffusion barrier, repelling like-charged particles such as the red blood cells.

Adjacent endothelial cells meet at *intercellular clefts* that are typically 10 to 20 nm wide [44]. In all tissues except the brain, the intercellular clefts and plasmalemmal vesicles provide the major transport pathways for water and macromolecules [83]. However, certain portions of the clefts may be sealed due to contacting of apposing cells. In the case of the capillaries of the brain, the contacting cells fuse, eliminating the cleft altogether. Such seals prohibit the transport of larger molecules through intercellular junctions, confining exchange along this pathway to water, salts, and other small molecules [32].

Individual capillary vessels fall into one of three classifications, depending on the structural characteristics of their endothelia: namely *continuous, fenestrated,* or *discontinuous* capillaries. Continuous vessels are common to the microvascular beds of the lung, the nervous system,

skeletal muscle, and skin, among others [90]. As the name implies, the endothelia of these vessels form a continuous layer 0.2 to 0.3 μm thick, interrupted only by the intercellular clefts. The basement membrane is likewise continuous.

Fenestrated vessels are characterized by the presence of disk shaped regions, typically 60 to 80 nm in diameter, located on the vessel wall. These regions, called *fenestrae,* are due to an attenuation of the endothelial cell to a thickness of 6 to 8 nm [90]. The attenuated cellular matter forms a diaphragm, the structure of which differs from the rest of the cell membrane in that it is thought to be composed largely of hydrophilic elements [112]. In some cases, such as the glomerular capillaries of the kidney, the fenestrae lack diaphragms altogether. The basement membrane of fenestrated vessels is continuous. The enhanced permeability of these vessels to plasma proteins suggests that the fenestrae provide a major pathway for the transport of macromolecules across the capillary wall [84]. Fenestrated vessels are found within the microvasculature of the pancreas, the endocrine glands, and the gastrointestinal tract.

Discontinuous vessels, also called *sinusoids,* are identified by large gaps in the endothelial layer and basement membrane. Fenestrae hundreds of nm in diameter may also be present [90]. While their structure would suggest that discontinuous vessels are highly permeable to various plasma proteins, lymph composition from tissues containing these vessels indicates that sieving of certain plasma protein species occurs even here [93].

2.1.2   Transport Pathways Across the Capillary Barrier

Several transport pathways have been identified for passage of fluid and various solute species across the capillary wall. These are summarized below [84]:

1. through the cell itself which includes two layers of cell membrane and the intervening cytoplasm;

2. within the endothelial cell membrane by lateral diffusion through intercellular junctions or lipid phase vesicular channels;

3. through interendothelial junctions in the aqueous extracellular phase (these pathways consist both of highly restrictive channels that are virtually impermeable to plasma proteins and less restrictive channels that permit exchange of these macromolecules);

4. via endothelial cell fenestrae; and

5. by vesicular transport, which includes shuttling of material within individual vesicles (i.e., *transcytosis*) and the fusion of several vesicles to form temporary fluid filled channels across the cell.

These pathways are illustrated in Figure (2.3).
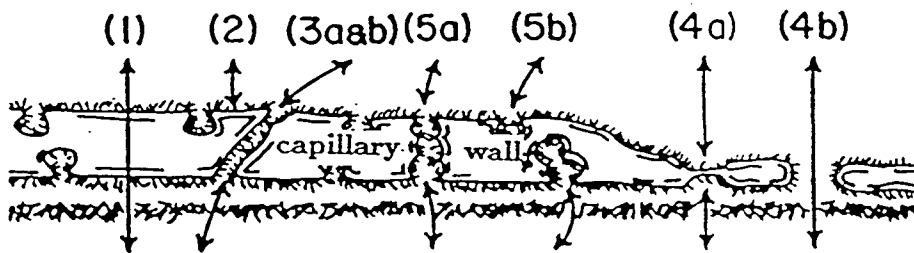
Figure 2.3: **This figure illustrates a cross-sectional slice of the capillary wall. Transport pathways across the capillary wall include direct routes across the cell (1), through the cell membrane (2), via intercellular pathways (3), across fenestrae (4), and via vesicular mechanisms (5a, 5b) (modified after [31]).**

Transport directly through the cell matter is limited to the diffusion of water and small lipid soluble molecules. Convective transport of fluid along this path is negligible [84]. In all likelihood virtually all respiratory gases are exchanged directly through the cell. In addition, substantial amounts of fatty acids and other lipids cross the capillary wall. However, these

substances cannot penetrate the cell cytoplasm and are therefore limited to transport through the cell membrane and lipid vesicles.

Finally, the lipid insoluble materials, including small ions and the plasma proteins, are limited to the paracellular pathways (i.e., across open fenestrae, in fluid filled vesicles and across aqueous vesicular channels, and via interendothelial junctions). The permeability of these substances decreases with increasing molecular size, suggesting that these pathways display sieving characteristics [84]. Charge may also play a role in determining solute permeability. For example, the capillaries of the brain are more permeable to transferrin than to albumin, although transferrin is a larger molecule [83]. Transferrin, however, carries a smaller net negative charge.

2.1.3 Quantifying Transport Across the Capillary Wall

We have seen that the capillary wall offers several different routes for the transport of material. While attempts have been made to delineate between these different pathways (see, for example, [83]), transcapillary exchange is typically quantified using expressions analogous to those for porous membranes. These describe mass exchange rates in terms of both the principal driving forces present and lumped parameters that characterize transcapillary resistance.

Fluid is driven across the capillary wall by differences in the effective fluid chemical potential from one side of the barrier to the other. This driving force can be resolved into two principal components: a hydrostatic pressure difference and an osmotic pressure difference. The latter reflects the reduction in fluid chemical potential due to the presence of solute species within the fluid. The osmotic pressure of a particular solute species is typically a nonlinear function of the solute concentration. Each solute species present in the plasma and interstitial fluid can potentially influence fluid exchange across the capillary wall.

In fact, the degree to which a particular solute species alters transcapillary fluid exchange depends on the ease with which the given solute crosses the capillary wall. Only those solutes to which the capillary wall is impermeable exert their entire osmotic pressure. The effective

osmotic pressure of those solutes that can penetrate the capillary barrier varies inversely with the solute's permeability.

The fraction of the total osmotic pressure of a solute species i that acts on the capillary membrane is represented by the reflection coefficient for that solute species, σ_i. A σ of 0 indicates that the solute's permeability across the capillary wall is equal to that of water [80]. If the membrane is completely impermeable to a given solute, σ equals 1. Most small lipid-insoluble solutes, such as NaCl, have reflection coefficients below 0.1, while σ for most plasma proteins approaches 0.9 - 1.0 [80]. Further, since the capillary wall is very permeable to these small solutes and ions, any differences in their osmotic pressures across the membrane are quickly dissipated [71]. It is the plasma proteins, then, that contribute most to the overall osmotic driving force for fluid exchange across the capillary wall.

If we treat the array of plasma proteins as an aggregate species exerting an overall osmotic pressure of Π and having an effective reflection coefficient of σ, then the fluid flux across the capillary wall, j_v, is given by the Starling equation [81]:

$$j_v = L_p \left[P^P - \left[P^{int} \right]_b - \sigma \left(\Pi^P - \left[\Pi^{int} \right]_b \right) \right], \qquad (2.1)$$

where L_p is the hydraulic conductance of the capillary membrane, and P^P and $[P^{int}]_b$ are the hydrostatic pressure in the plasma and in the interstitial space adjacent the boundary, respectively. Π^P and $[\Pi^{int}]_b$ denote the plasma protein osmotic pressures in the plasma and in the interstitial space adjacent the capillary wall, respectively.

We will now turn to the exchange of plasma proteins across the capillary wall. Again, for convenience, we will limit the discussion to a single (possibly 'aggregate') species. More detailed discussions can be found in any one of many reviews on the subject [80, 82, 84, 31, 71, 93, 75, 58]. Assuming that plasma protein convection and diffusion occur along the same paracellular pathways, the exchange of these substances is described by the nonlinear flux equation (see, for example, [71]):

$$j_s = j_v(1 - \sigma) \frac{\left[C^P - \left[C^{int} \right]_b \cdot e^{-Pe} \right]}{\left[1 - e^{-Pe} \right]}, \qquad (2.2)$$

where j_s is the local flux of plasma proteins from blood to tissue, C^P and $[C^{int}]_b$ are the plasma protein concentrations in the plasma and the interstitial plasma protein distribution volume adjacent the boundary respectively, and where Pe is a modified Peclet number, defined as

$$Pe = \frac{(1 - \sigma)j_v}{D}.$$ (2.3)

D refers here to the permeability of the capillary wall to the plasma proteins. The modified Peclet number indicates the relative contributions of convection and diffusion to the total exchange of plasma proteins. As Pe approaches ∞, the exchange is dominated by convection. A Pe of 0, on the other hand, indicates purely diffusive exchange. Equations (2.2) and (2.3) have been used to describe transcapillary macromolecular exchange in a range of tissues (see, for example, [80]).

2.2 The Interstitium

2.2.1 Structure and Composition

The interstitium has been likened to a three-dimensional meshwork of fibrous elements embedded in a gel-like substance, referred to as *ground substance,* created by soluble polymers in an aqueous solution [26, 53] (see Figure (2.4)). The interstitium is therefore a composite of elements, each element contributing to the overall behavior of this medium. The principal components determining the gross characteristics of the interstitium include the following: collagen, elastin, the glycosaminoglycan and proteoglycan elements, and the interstitial plasma proteins. Each of these will now be discussed briefly.

Collagen Collagen is the primary structural protein of the body [57]. It is formed from a precursor molecule, *procollagen,* that consists of three extended polypeptide chains wound to form a triple helix [4]. The helical configuration is stabilized by interchain hydrogen and covalent bonds [57]. The procollagen molecules combine to form the collagen monomer, a rod-like molecule 300 μm long and having a diameter of approximately 1.5 nm [26]. The

Collagenous fiber   Proteoglycan

Hyaluronate   Plasma protein
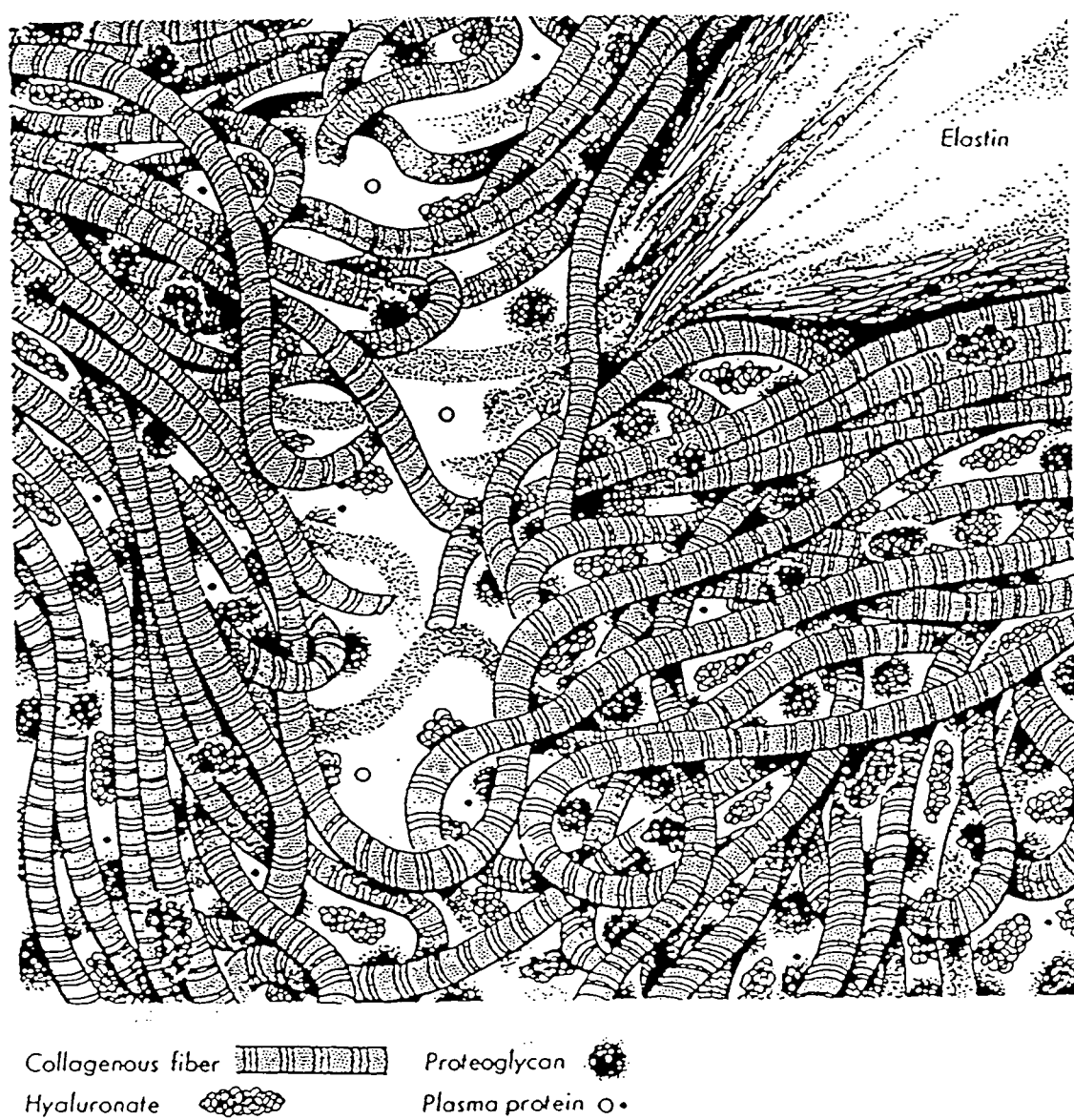
Figure 2.4: An artist's concept of the interstitium shows the fibrous collagen mesh-work [13].

monomers spontaneously form aggregates through covalent bonding and crosslinks [57], yielding the collagen fibrils. The fibrils further combine to give collagen fibers (Figure (2.5)).
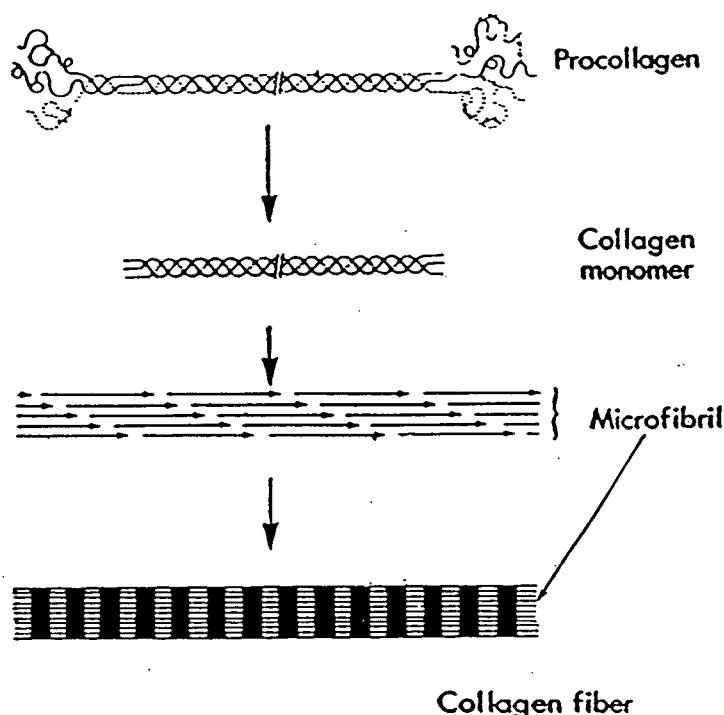
Figure 2.5: **The hierarchy of collagen elements is shown above. Procollagen combines to give the collagen monomers that aggregate to give collagen fibrils which, in turn, combine to yield the collagen fiber (modified after [26]).**

Numerous distinct collagen types have been identified within the interstitia of various tissues [5, 13]. The extent to which a particular collagen type is found within the interstitium varies from tissue to tissue. Each of the collagen types, however, forms molecules of similar structure and dimensions.

Collagen is *polyampholytic;* that is, it is capable of bearing both positive and negative charges. The former are due to amino groups present in collagen, while the latter are attributed to carboxyl groups [57]. However, at physiological pH most of these are neutralized, so that collagen bears only a slight positive charge.

Functionally, collagen fibers provide tensile strength to the tissue, resisting changes in tissue

volume when stressed along the longitudinal axis of the fiber [4]. This is due to the covalent cross-linkages that form between collagen molecules [26]. By forming a meshwork, the fibers tend to immobilize the polymers responsible for the interstitial gel (i.e., the glycosaminoglycans and proteoglycans) [26]. Finally, collagen is partly responsible for the excluding properties of the interstitium [13], to be discussed later.

Elastic Fibers   While collagen fibers impart tensile strength to a tissue, elastic fibers provide it with elasticity [13]. Elastic fibers occur in small quantities (relative to collagen content) in most interstitia, with the possible exception of certain specialized tissues such as the greater arteries [53] that display a high degree of elasticity.

Elastic fibers consist of two principal components: an amorphous mass of elastin surrounded by microfibrils of protein [13]. Elastin is one of the most apolar proteins known [57], providing it with a hydrophobic nature [13].

At physiological pH, elastic fibers contain approximately 0.56 ml of water per ml of elastin [13]. Most of this water is likely accessible to small molecules and ions, such as sucrose, urea, sodium, and chloride. Larger molecules, such as the plasma proteins, however, are thought to be excluded from this fluid space.

Glycosaminoglycans and Proteoglycans   Glycosaminoglycans are linear polymer chains of disaccharide units common to all tissues [4]. Essentially all of the charge groups associated with these polymers are ionized at physiological pH [57]. Glycosaminoglycans therefore attract counterions, thereby creating a Donnan distribution of mobile ions that exert an osmotic pressure [4].

One of the most prevalent of the glycosaminoglycans is hyaluronate. In its hydrated state, hyaluronate forms an unbranched, random coil that occupies a solvent domain some 1000 times greater than the polymer volume [4]. Further, the mutual repulsion of negative charges present along the hyaluronate chains tends to expand the coil [13]. Therefore, even at concentrations

as low as 0.1 percent by weight, hyaluronate molecules become entangled [4]. It is the entanglement of hyaluronate and other glycosaminoglycans and proteoglycans that gives the ground substance its gel-like properties. Gersh and Catchpole [47] also identified 'water-rich, colloid poor' regions within the interstitial matrix, leading some to postulate the existence of free fluid channels within the interstitium (see, for example [104]). However, the original study made no mention of such continuous structures; rather, the authors simply identified heterogeneities in glycosaminoglycan distribution within the matrix [4]. Other early ultrastructural studies have identified transient, submicroscopic fluid vacuoles within the interstitium, but later studies have not confirmed their existence [4]. In fact, the preparative procedures used in many of these studies are known to extract ground substance [53], suggesting that the 'free fluid phase' may well be an artifact of these early experiments. However, as Aukland and Nicolaysen [4] point out, this does not preclude the possibility of heterogeneities within the interstitial gel, due to local rarefactions in polysaccharide content, that might provide preferential channels for fluid and solute transport.

Except for hyaluronate, glycosaminoglycans exist *in vivo* not as free polymers, but covalently bound to a protein core [13]. Such structures are termed *proteoglycans*. These can further bind to hyaluronate molecules to form *proteoglycan aggregates*, having molecular weights in excess of 2×10^8 Daltons. At physiological pH, proteoglycans display a high charge density [13]. These structures are also known to bind to collagen [26].

The glycosaminoglycan and proteoglycan elements contribute to the interstitium's resistance to bulk fluid movement [13]. Their water retaining properties also enhance the stability of collagen-glycosaminoglycan solutions, resisting volume changes under compression [26]. This has been demonstrated experimentally using prepared solutions of collagen and hyaluronate, for example. *In vitro* mixtures of thermally precipitated collagen and hyaluronate produce structures that resist compression during centrifugation [13].

The Interstitial Plasma Proteins Plasma proteins represent a broad group of macromolecules. Various types of these are transported across the endothelial membrane into the

interstitium. They range in size, displaying Stokes' radii anywhere from 1 to 11 nm [13]. At physiological pH, most plasma proteins carry a net negative charge [13].

Interstitial plasma proteins exert an osmotic pressure that is a nonlinear function of plasma protein concentration. However, the major part of the osmotic pressure is due to a single species – albumin [13].

Albumin is the most plentiful of the plasma proteins, constituting approximately 60 % of the serum protein content in humans [46]. It has a molecular weight of 6.6×10^4 Daltons and a Stokes' radius of 3.5 nm [13]. With an isoelectric point at a pH of 4.7, albumin bears a net negative charge at physiological pH. Experimental studies of extravascular albumin indicate that significant quantities of this protein lie outside of the blood stream, largely in the interstitia of muscle and skin [13]. This suggests that the interstitium may act as a reservoir for osmotically active macromolecules [13].

2.2.2 Volume Exclusion within the Interstitium

As mentioned earlier, the various components of the interstitium, particularly the glycosamino-glycans, occupy a volume in solution that far exceeds the volume of the polymers themselves. Even at low concentrations, the solvent domains associated with these polymers overlap to create a meshwork of molecular dimensions [53]. A given interstitial solute species will distribute throughout only those spaces in the meshwork that have dimensions larger than the solute itself. The remaining regions of the meshwork are inaccessible to the solute. As a consequence, the space available to certain interstitial solutes (i.e., the solute's *distribution volume*) is considerably less than the total interstitial fluid volume. This phenomenon has been termed *volume exclusion*.

The glycosaminoglycans have traditionally been identified as the principal components responsible for the exclusion of plasma proteins from regions of the interstitium [4]. The fraction of total fluid volume inaccessible to plasma proteins in hyaluronate solutions, for example, can be significant, even at low concentrations. A 0.5 % by weight solution of hyaluronate excludes

albumin from 25 % of the solution space. As the hyaluronate concentration is raised to 1.5 % by weight, the excluded volume increases to 75 % of the solution volume [13]. However, because of its abundance relative to the glycosaminoglycans in certain tissues such as dermis, collagen may well be the major source of plasma protein exclusion in some instances [13].

Exclusion bears upon the processes within the interstitial space. It is the effective concentration of a given solute species (i.e., the concentration based on the solute's distribution volume rather than the total fluid volume) that determines its chemical activity, which in turn affects chemical equilibria, osmotic properties, solubilities, and driving forces for diffusion within the system [27].

By treating the interstitial solute species as spheres contained in a random meshwork of rods, Ogston and co-workers [72] developed the following equation to calculate volume exclusion:

$$ \mathrm{fe} = 1 - e^{-[(r_s+r_f)/r_f]^2 V_f C_f}, \tag{2.4} $$

where fe is the excluded volume fraction, r_s and r_f are the solute radius and radius of the rods making up the meshwork, respectively, V_f is the partial specific volume of the rod material, and C_f is the mass concentration of rods in the system. This analysis would suggest that exclusion increases with increased concentration of excluding species (i.e., the rods) and increased solute radius, but decreases with increasing rod diameter. Similar expressions have been developed for single rod-sphere and sphere-sphere systems (see [13] for details).

The above analysis of exclusion considers only geometric factors. However, since the glycosaminoglycans are negatively charged, electrostatic effects may also play a role in determining the exclusion properties of specific tissue-solute systems. This may be true, in particular, for tissues such as cartilage that display a high interstitial charge density [53]. In fact, the exclusion of low molecular weight anionic tracers has been demonstrated, but the effect is unpredictable [4].

2.2.3 Characterizing Interstitial Swelling

The glycosaminoglycans and the collagen fibers are the principal components within the interstitium that determine the mechanical properties of connective tissues [4, 53, 117, 89]. It is generally thought that the glycosaminoglycan element provides the tissue with its swelling tendency by virtue of its osmotic activity. As a polymer solution, the glycosaminoglycans (and their aggregates) exert an osmotic pressure that tends to imbibe fluid. The charged groups associated with the polymers create a mutual repulsive force that may further tend to expand the network [4]. The stiff collagen meshwork, on the other hand, imparts rigidity to the tissue, acting to limit volume changes within the interstitium.

The relative influences of the glycosaminoglycans and of the collagen on tissue hydration are well demonstrated experimentally. Degradation of the collagen by chemical treatment causes umbilical cord to swell [53]. Destruction of hyaluronate in swollen tissue, on the other hand, leads to a reduction in tissue hydration [53]. Theoretical interpretations of the swelling process, however, are clouded in controversy (see, for example, [53, 89, 107]). Much of the confusion seems to lie in the delineation of the various forces acting on the system into the mechanical components responsible for deformation (i.e., the mechanical stresses within the system) and the forces responsible for fluid exchange within the system (namely differences in fluid chemical potential between vascular and tissue compartments).

Typically, the swelling properties of a tissue are characterized by an experimentally determined relationship between the equilibrium tissue hydration and the interstitial fluid pressure, i.e., the *tissue compliance relationship*. The interstitial fluid pressure within a tissue is measured at various states of hydration using microneedles, wicks, or implanted capsules. The major problem in such experiments lies with interpreting the reading provided by the pressure measuring device (see, for example, [107]). Again, there seems to be a great deal of confusion regarding whether such devices measure an equivalent interstitial fluid chemical potential, which would include both hydrostatic and colloid osmotic pressures, or whether they isolate the hydrostatic component. A fundamental understanding of the operation of these pressure
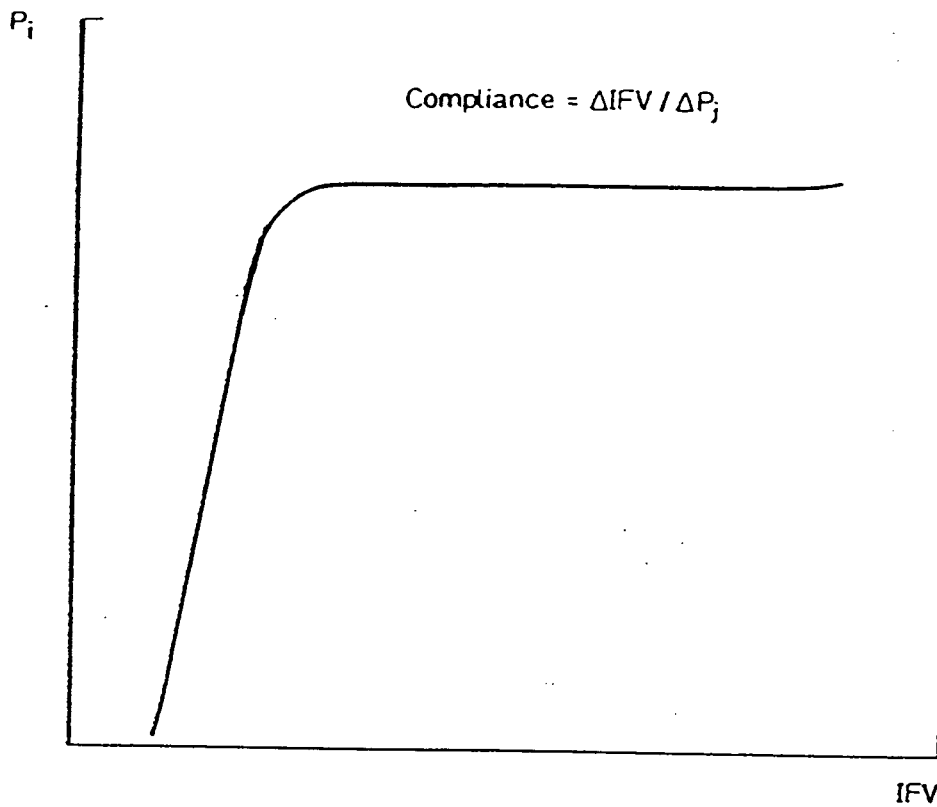
Figure 2.6: **This figure shows the general trend in the change in interstitial fluid volume (IFV), given along the x-axis, following a change in interstitial fluid pressure, shown on the y-axis (modified after [5]) .**

measuring devices within tissues is therefore needed before tissue hydration data can be reliably interpreted.

The general shape of the pressure–volume curves typical of tissues is given in Figure (2.6). Generally, the change in tissue hydration per unit change in interstitial fluid pressure is low at the lower tissue hydrations, increasing as the tissue becomes swollen. The high resistance to tissue hydration in the initial part of the curve suggests a mechanism to ward off edema formation. Specifically, a small change in interstitial hydration is accompanied by a substantial increase in the interstitial fluid pressure. According to the Starling equation (see Eq. (2.1)), this increase in interstitial fluid pressure reduces the driving force for fluid transport from the blood to the tissue space, thereby reducing the threat of severe tissue swelling [13].

2.3   The Lymphatic System

2.3.1   General Description

In contrast to the abundance of data on the exchange vessels of the blood vasculature, there appears to be a dearth of information regarding the operation of the lymphatic network. Several reviews [4, 117, 77, 49] are available in the literature, however, and the reader is referred to these for more detailed discussions of this system. Only a brief description will be provided here that focuses on the withdrawal of interstitial fluid and plasma proteins by the permeable vessels of the lymphatic network.

Lymphatic vessels occur in most tissues; exceptions include the brain, the retina, and bone marrow [5]. Unlike the arterio-venous blood system, the lymphatic network typically begins with bulbous *terminal lymphatic vessels* located in close proximity to the blood capillaries. These bulbous structures are typically 20 to 80 μm in diameter, although they can reach diameters of 720 μm in some tissues (e.g., the bat wing) [49]. The terminal lymphatic vessels are unevenly distributed within the microcirculation, being more prominent at the venous side of the microvascular bed where the blood vessels are most permeable [77]. Further, they occur less frequently than the blood capillaries [5]. Figure (2.7) illustrates the structure and orientation of these vessels within the microcirculation.

Fluid and solutes that have been withdrawn from the tissue space are carried along the lymphatic network via collecting vessels. These empty their contents into the *left* and *right* *subclavial veins* [46], thereby returning fluid and solutes to the blood circulation. In the average human, an estimated 25 % to 50 % of the total circulating plasma proteins are returned to the blood circulation along this route on a daily basis, while 2 to 4 liters of fluid enter the lymphatics from the interstitial space each day [46].

Figure 2.7: The lymphatic vessels within the bat wing are illustrated above in solid black. The system begins with the bulbous terminal lymphatic vessels, located close to the blood capillaries. These drain into collecting vessels that eventually return fluid and solutes to the blood vasculature (modified after [49]).

2.3.2 The Terminal Lymphatic Vessels

The terminal lymphatic vessels are responsible for draining fluid and solutes from the interstitial space. The wall of the terminal lymphatic vessel is similar to that of the blood capillary in that it consists of a single layer of flat endothelial cells [77]. However, it differs from the capillary wall in several respects [49]. First, the interendothelial junctions appear more loose, the cells overlapping each other at times. The basement membrane is poorly developed or absent altogether. Furthermore, while the endothelial cells of the terminal lymphatic vessels contain vesicles, fenestrae have not been observed. The terminal lymphatics display irregular geometries with bulbous sacs and constricted regions along the vessel length. The vessels are easily collapsed, making pressure measurements within terminal lymphatics difficult [77].

The wall of the terminal lymphatic vessel is anchored to the surrounding interstitial matrix by fine strands of reticular fibers and collagen [49] (see Figure (2.8)). It is thought that the anchoring filaments aid in the withdrawal of fluid from the interstitial space. As fluid accumulates within the tissue spaces, the tissue expands, placing the anchoring filaments under tension. This tensile stress keeps the lymphatic vessel from collapsing under the increased tissue fluid pressure associated with the accumulation of fluid there. The terminal lymphatic is then able to withdraw fluid and solutes from the interstitium [49, 77].

Interstitial fluid is thought to cross the terminal lymphatic wall via diffusion through the endothelial cell, by vesicular pathways, and through the intercellular junctions [49]. The relative importance of these pathways in lymphatic filling is, as yet, unknown. A number of theories for the filling of the terminal lymphatic vessels have been proposed, including vesicular, osmotic pressure driven, and hydraulic (i.e., hydrostatic pressure) driven mechanisms. To date, there is little to no experimental evidence to support the first two hypotheses [5]. However, it has been demonstrated experimentally that lymph flow increases with increased interstitial fluid pressure in a number of tissues, including dog hindpaw, the small intestine, the liver, the myocardium, and rat kidney [5]. Hence, it is frequently assumed that the rate of lymph formation in the terminal vessel is a direct function of the local tissue fluid pressure (see, for example, [108, 14]).
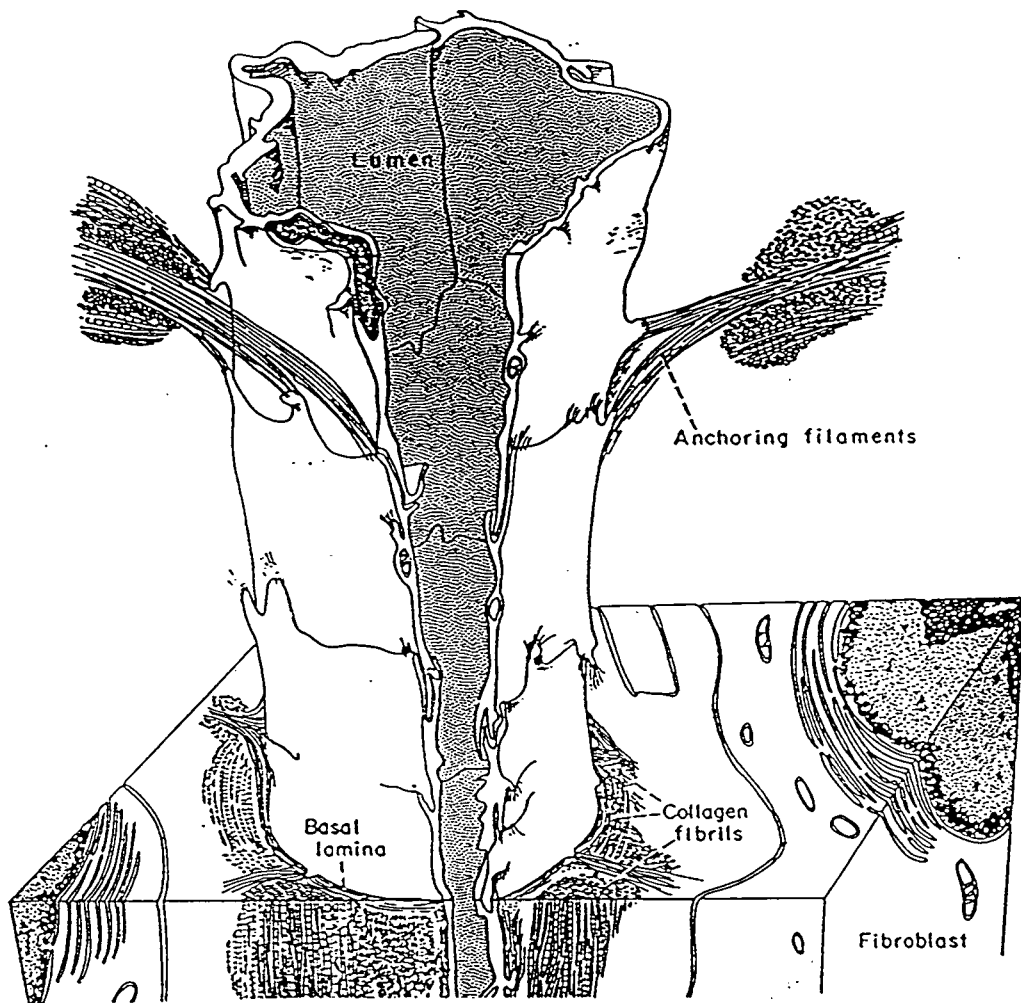
Figure 2.8: The structure of the terminal lymphatic vessel is shown, illustrating the anchoring filaments that serve to keep the vessel patent under increased tissue fluid pressure [49].

In the absence of injury, tissue swelling, or muscular activity, the intercellular junctions are typically closed. However, given any of these circumstances, the junctions open to permit large particles to pass through [49]. Experiments with labelled particles suggest that both intercellular junctions and vesicular mechanisms serve as routes for macromolecules, although the relative importance of these two pathways is debated [49]. However, it is typically assumed that the composition of lymph in the terminal lymphatic vessel is the same as the interstitial fluid in the adjacent tissue space [117].

The walls of most collecting lymphatic vessels contain smooth muscle [5]. The collecting vessels propel fluid and solutes along the network in response to both extrinsic forces (such as limb movements, respiratory pressure variations, and massage) and spontaneous, coordinated contractions of the muscle within the vessel walls [49]. The intrinsic contractile behavior of the lymphatic vessels appears driven by the increased stress (hoop pressure) within the vessel walls that accompanies the uptake of fluid from the surrounding interstitial space. The amplitude of the contraction is proportional to the degree of wall stretch [77].

Lymph flow within the collecting vessels remains uni-directional by virtue of one-way valves found within the vessels [77]. These valves occur in abundance along the lymphatic network; the average spacing between valves ranges from 2.3 mm to 4.0 mm in the upper arm in humans, for example [49]. The valves of the larger vessels can withstand back-pressures as high as 60 mmHg [77], far above typical pressure drops reported within the lymphatic network (see [49]).

Chapter 3

Formulation of the General Model of Interstitial Transport

3.1   A Continuum Representation of the Interstitium

At the microscopic level, the transport of fluid and plasma proteins through the interstitium represents an extremely complex process. Fluid and plasma proteins interact as they traverse the interstitial space along tortuous pathways. Furthermore, plasma proteins may encounter barriers resulting from electrostatic forces and/or the architectural configuration of various structural components, such as hyaluronate, proteoglycans, collagen, and elastin, all of which exclude proteins from regions of the interstitium. These structural components deform under a complex set of forces as the tissue hydration changes.

A detailed description of interstitial transport is impractical. Instead, we adopt the concept of a continuum to represent the interstitium (see [106, 8, 28] for details). Here each principle phase, such as fluid or structural elements, is represented by a hypothetical continuum which is distributed throughout the interstitium. The properties of these continua, as well as the processes occurring within them, represent spatial averages of the properties and processes found at the microscopic level. The characteristic dimension of the elementary volume over which this averaging procedure takes place is large relative to the microscopic dimensions (represented, for example, by the diameter of a collagen fiber bundle), yet small relative to the characteristic dimension of the system as a whole (such as the total distance traversed by fluid and plasma proteins in their journey from the blood to the lymphatic circulations). The resulting averaged properties are assigned to the point about which the elementary volume is centered. The volume is then centered about an adjacent point, and the averaging process is performed again. The procedure is repeated throughout the domain, transforming the complex, heterogeneous

28

system into a hypothetical continuum to which the laws of differential calculus apply. The averaging process introduces parameters associated with the continuum, such as the interstitial fluid conductivity, the effective protein diffusivities, and the excluded volume fractions. These represent the averaged effects of the complex structure and molecular interactions at the level of the microscale. The parameters are then used to describe interstitial transport when approximating the real system by the continuum.

The principle of spatial averaging is applied here to analyze the transient flow and distribution of fluid and any number of macromolecular species through the interstitium, which is treated as an isotropic, deformable porous medium. Since crystalloid solutions are exchanged rapidly, compared to the plasma proteins [71], any disturbances to the system with respect to small ion distribution is likely dissipated quickly. Therefore, interstitial gradients in small ion concentrations and the influence of tissue cells on fluid exchange will be neglected here. Hence the analysis cannot describe hypertonic fluid resuscitation, for example. Since the total plasma protein concentration in plasma is small (6 gm/dl in humans [46]), the interstitial fluid and plasma proteins form a dilute, incompressible solution. The solid components of the interstitium are also considered incompressible. Hence interstitial deformation results from the spatial reorientation (e.g. bending) of the solid elements relative to each other. Exclusion is accounted for by assigning different distribution volume fractions to the various plasma protein species. These distribution volume fractions are functions of the solid phase volume fraction, and therefore vary with interstitial hydration. Fluid and protein transport parameters may vary between individual distribution volume fractions and with interstitial hydration.

In the remainder of this section we present mathematical descriptions of each of the following aspects of the interstitial continuum:

1. plasma protein exclusion and its effect on local protein partitioning, colloid osmotic pressures, and fluid chemical potential;

2. the relationship between fluid transport and fluid chemical potential; and

3. protein transport mechanisms within the interstitium.

These relationships are then used in the following section to develop the mass balance equations which govern the time-dependent distributions of solids, fluid and protein species in a deforming interstitium.

3.1.1 Plasma Protein Partitioning within the Interstitium: Exclusion

Plasma protein exclusion in tissues can be substantial; for example, albumin is excluded from 60 percent of the total interstitial volume in canine smooth muscle [13]. Because of exclusion, the effective concentration of an interstitial plasma protein species (i.e., its mass per unit volume of available space) is higher than its concentration based on the total fluid volume. The effective concentration plays an important role in interstitial fluid and protein transport because it determines the protein osmotic pressures, convective protein fluxes, and the diffusional driving force within the interstitium [27]. A complete description of interstitial transport must therefore include a treatment of exclusion and its effect on local plasma protein distribution and fluid chemical potential. We will now discuss how the principle of volume averaging can be employed to describe exclusion of multiple solute species.

Figure (3.1) is a schematic diagram of a typical elementary volume centered about some point within the interstitium, over which the averaging process has been performed. The volume element contains m protein species and m+3 distinct volume fractions:

1. a total mobile fluid volume fraction (n^0);

2. m volume fractions corresponding to the distribution volume fractions for each of the m protein species (n^k, $k = 1, 2, ...m$);

3. a solid phase volume fraction (n^s) comprised of structural elements such as collagen, glycosaminoglycans, proteoglycans, and elastin, which form the solid skeleton of the porous structure; and

4. an immobile water volume fraction consisting of water trapped and/or bound to the solid phase (n^{im}).

The immobile fluid phase will, in general, depend on the amount and composition of the solid phase. For a given tissue, then, n^{im} will be a function of n^s:

$$n^{im} = F^s(n^s), \tag{3.1}$$

where F^s is an empirical function relating the two volume fractions. If, for example, we assume that the immobile fluid is largely made up of the intrafibrillar water of collagen and that the collagen is uniformly distributed throughout the solid phase, then n^{im} is directly proportional to the solid phase volume fraction:

$$n^{im} = \beta^* \cdot n^s, \tag{3.2}$$

where β^* is an experimentally determined constant of proportionality. The remaining distribution volume fractions are indexed such that

$$n^0 > n^1 > n^2 > ... > n^{m-1} > n^m. \tag{3.3}$$

We also define a set of incremental volume fractions, δn^k, where

$$\delta n^k = n^k - n^{k+1}, \quad k = 0, 1, 2, ..., m - 1. \tag{3.4}$$

That is, the incremental volume fraction δn^k represents the difference between the distribution volume fractions of species k and species k+1. Note that, by this definition, δn^m equals n^m. As we will see shortly, these incremental volume fractions are needed to describe the plasma protein and fluid pressure distributions within the volume element.

The total excluded volume for a given protein species depends on the amount of interstitial solid components present in the elementary volume [53]. Therefore the fraction of total mobile and immobile fluid from which plasma protein species k is excluded, n^{ek}, is a function of n^s:

$$n^{ek} = F^k(n^s), \quad k = 1, 2, ..., m, \tag{3.5}$$
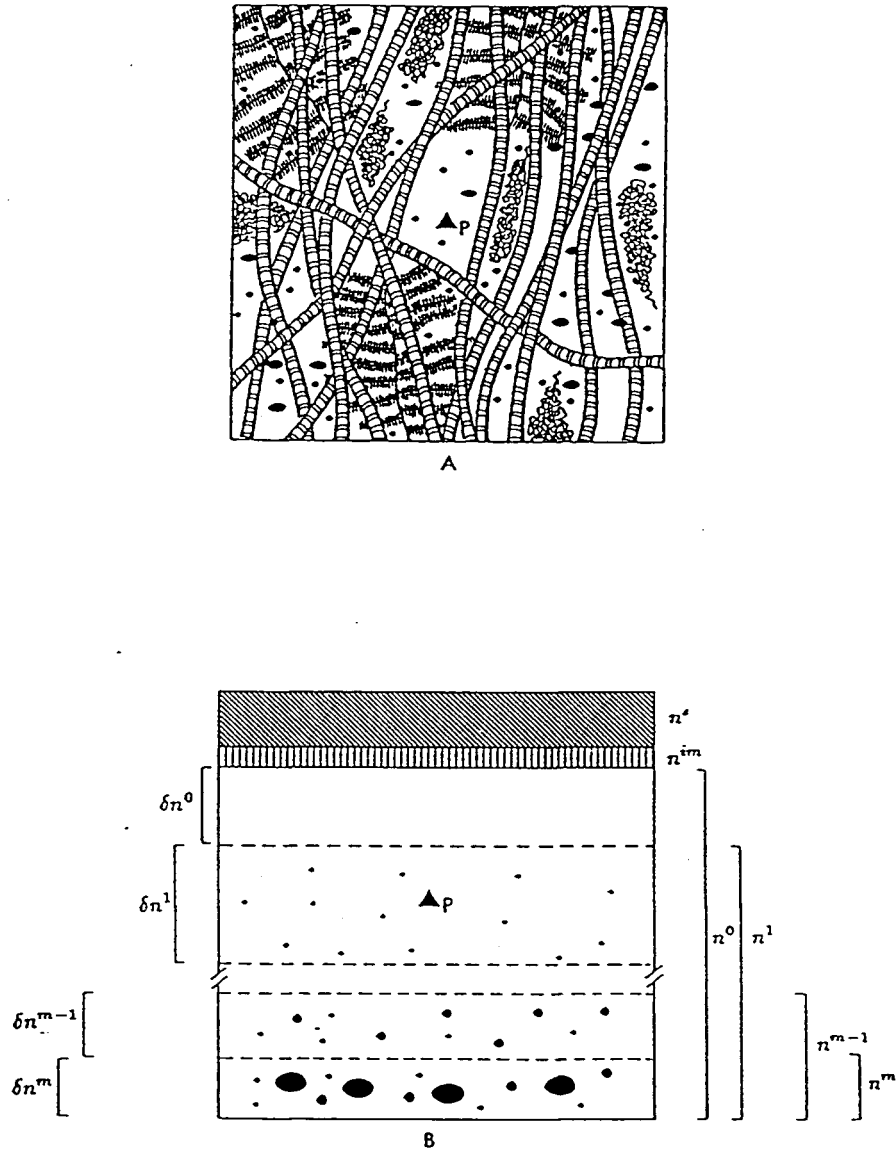
Figure 3.1: Elementary volume of interstitium before (A) and after (B) volume averaging. The various incremental volume fractions, δn^i, distribution volume fractions, n^i, solid phase volume fraction, n^s, and immobile fluid phase volume fraction, n^{im}, are associated with the point, P, in the continuum about which the elementery volume is centered. The heterogeneous interstitium is thereby transformed into a multiphase continuum.

where F^k is an empirical function for the kth protein species. By definition, the sum of the distribution volume fraction and the excluded volume fraction for species k must equal the total fluid volume fraction (i.e., $1 - n^s$). That is,

$$n^k = 1 - n^s - n^{ek}. \tag{3.6}$$

It therefore follows from Eqs. (3.5) and (3.6) that

$$n^k = 1 - n^s - F^k(n^s), \tag{3.7}$$

while from Eqs. (3.4) and (3.7) we have

$$\delta n^k = F^{k+1}(n^s) - F^k(n^s), \quad k = 1, ..., m - 1. \tag{3.8}$$

Hence all pertinent fluid volume fractions ($n^k, \delta n^k, n^{ek}$, and n^{im}) may be expressed in terms of n^s for a given tissue using Eqs. (3.1), (3.5), (3.7), and (3.8).

To describe fluid and protein transport through the interstitium, we must make some assumptions regarding the distribution of proteins and the variation of fluid chemical potential throughout the incremental volume fractions within the elementary volume. Consider first the distribution of plasma proteins within the volume element. The incremental volume fraction δn^0 contains no protein (see Figure (3.1)). Each subsequent incremental volume fraction contains an additional protein species. Let $C^{k,l}$ represent the concentration of protein species k in δn^l. Assuming that, for each volume element, the protein has a uniform concentration C^k within its distribution volume n^k, then

$$C^{k,l} = C^k, \quad l \geq k, \tag{3.9}$$

and

$$C^{k,l} = 0, \quad l < k. \tag{3.10}$$

Hence only one value, C^k, is needed to describe the local concentration of protein species k throughout all of the incremental volume fractions in the elemental volume which are accessible to that species.

Assuming an isothermal system free of external forces, the chemical potential of the fluid in δn^l, μ_w^l, is [62]

$$\mu_w^l = \mu_w^{ref} + \bar{V}_w^l P^l + RT \cdot \ln\left(\gamma_w X_w^l\right),\tag{3.11}$$

where μ_w^{ref} is the reference chemical potential, equal to the chemical potential of the pure fluid at standard conditions, $\bar{V}_w^l$ and P^l are the fluid's partial molar volume and hydrostatic pressure in δn^l, respectively, R is the universal gas constant, T is the absolute temperature, γ_w is the activity coefficient for the fluid, and X_w^l is the mole fraction of fluid in δn^l. For dilute solutions, variations in $\bar{V}_w^l$ are negligible. Using the Gibbs-Duhem relation, the chemical potential can be expressed alternatively in terms of hydrostatic and colloid osmotic pressures [117] as

$$\mu_w^l = \mu_w^{ref} + \bar{V}_w\left(P^l - \sum_{k=1}^{l} \Pi^k\right),\quad l = 1, 2, ..., m,\tag{3.12}$$

where $\bar{V}_w^l$ has been replaced by $\bar{V}_w$, the molar volume of pure fluid, due to the assumption of a dilute solution.

The colloid osmotic pressure exerted by plasma protein species k in δn^l, $\Pi^{k,l}$, is a function of the protein concentration in δn^l, i.e.,

$$\Pi^{k,l} = G^k(C^{k,l}),\tag{3.13}$$

where G^k is the colloid osmotic pressure relationship for plasma protein species k. By virtue of Eqs. (3.9), (3.10) and (3.13),

$$\Pi^{k,l} = \Pi^k,\quad l \geq k,\tag{3.14}$$

and

$$\Pi^{k,l} = 0,\quad l < k.\tag{3.15}$$

In δn^0 we have

$$\mu_w^0 = \mu_w^{ref} + \bar{V}_w\left(P^0 - \Pi^0\right)\tag{3.16}$$

where P^0 is the hydrostatic pressure in δn^0, and Π^0 is the sum of any additional osmotic terms associated with δn^0, such as Donnan and polysaccharide osmotic pressure contributions.

If the relative amounts of these osmotically active components are known, then Π^0 can be determined through an appropriate osmotic relationship. Assuming that the fluid throughout the elementary volume is in thermodynamic equilibrium, it follows that

$$P^0 - \Pi^0 = P^1 - \Pi^1 = P^2 - \Pi^1 - \Pi^2 = ... = P^m - \sum_{k=1}^{m} \Pi^k. \qquad (3.17)$$

Hence the fluid hydrostatic pressure in any of the incremental volume fractions may be expressed in terms of a single hydrostatic pressure (P^m) and the various osmotic pressures (Π^k, $k = 0, 1, 2, ...m$).

The concepts and definitions presented here are best illustrated with a simple example. Consider an elementary volume of interstitium containing a single plasma protein species k, as shown in Figure (3.2A). By definition, the sum of the solid phase volume fraction, n^s, the excluded volume fraction, n^{ek}, and the plasma protein's distribution volume fraction, n^k, equals 1. Since we are considering only a single plasma protein species, it follows from Eq. (3.4) that δn^k equals n^k. Also, since we have assumed local thermodynamic equilibrium within the elementary volume, the sum of the hydrostatic and colloid osmotic pressures in the distribution volume, $P^k - \Pi^k$, equals the sum of pressures in the excluded volume, $P^0 - \Pi^0$.

Figure (3.2B) shows the same elementary volume following an increase in hydration accompanying, for example, an increase in local fluid hydrostatic pressure. If we assume that the local concentration in protein species k remains the same, then the local fluid chemical potential in n^k, $P^k - \Pi^k$, will increase. Since the fluid within the volume is in local thermodynamic equilibrium, $P^0 - \Pi^0$ will also increase by the same amount. Since the hydration has increased, the local solid phase volume fraction is reduced. This results in a reduction in the excluded volume fraction as well, since the latter depends only on the amount of solid phase present in the volume. Consequently, the volume available to the plasma proteins increases, so that n^k increases. We will now discuss how such a change in tissue hydration may be described in more rigorous terms.
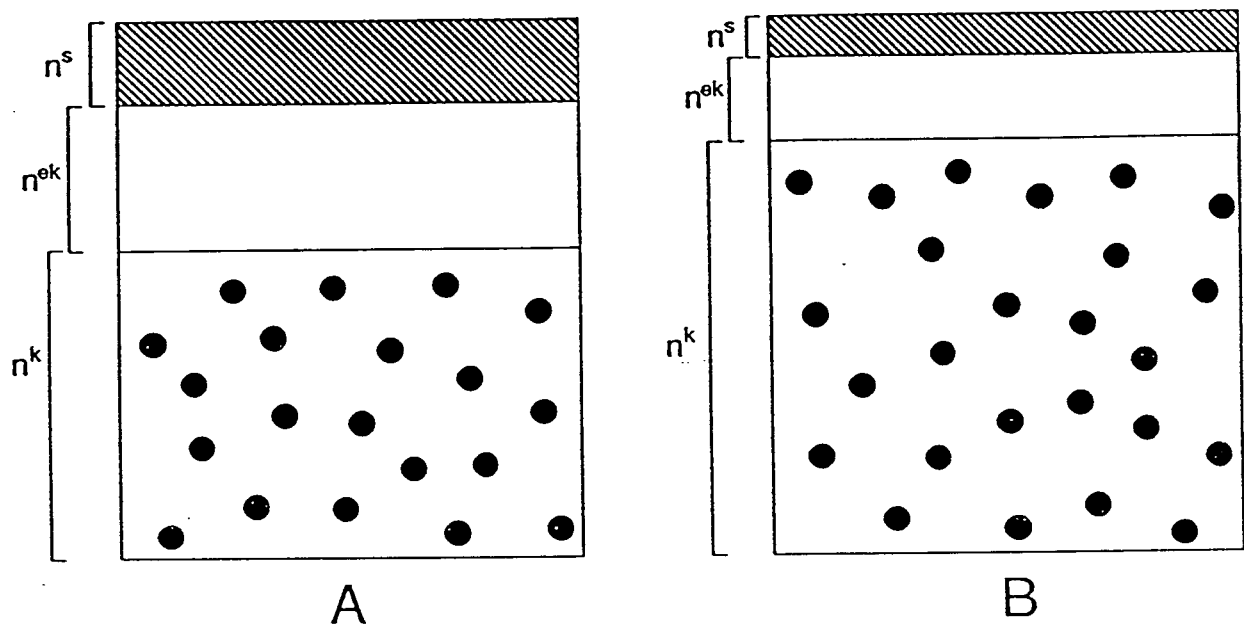
Figure 3.2: An elementary volume of interstitium containing a single plasma protein species k before (A) and after (B) an increase in local hydration. Following hydration, the local solids phase volume fraction, n^s, decreases, resulting in a decrease in the excluded phase volume fraction, n^{ek}, as well. By definition, the fraction of total fluid available to the plasma proteins, n^k, increases.

3.1.2 Tissue Strain, Volumetric Dilation, and Tissue Compliance

Changes in interstitial hydration result from a net flow of fluid into or out of the interstitium. Swelling is therefore linked to the forces governing fluid exchange, including interstitial hydrostatic and colloid osmotic pressures. As interstitial solid components deform there is an accompanying change in the solid stress. The system maintains mechanical equilibrium by a concomitant change in the hydrostatic pressure of the interstitial fluid [53, 89, 117]. This change in hydrostatic pressure, together with the change in interstitial hydration and possible net exchange of plasma proteins, alters the driving forces for fluid exchange. Interstitial swelling therefore involves a complex set of coupled processes that depend on the mechanical characteristics and transport properties of the microvasacular exchange system.

A rigorous examination of swelling in a porous medium requires a complete description of the stress distribution throughout the medium, together with constitutive relationships between solid stress and deformation. This type of analysis has been used to describe fluid movement in deformable porous rocks [19, 28]. To apply the principles underlying this theory to biological systems in turn requires detailed information regarding the mechanical properties of the interstitium and its boundaries. Such information is not available for most tissues. Therefore a simpler – albeit less rigorous – approach is adopted which follows the method used by Terzaghi [98] to analyze land subsidence following the removal of large volumes of groundwater [28]. The method assumes that the local deformation at any point in the interstitium is a function of the local fluid hydrostatic pressure (see [89]). The problem of swelling then reduces to determining the distribution of fluid pressure within the interstitium. This is accomplished by solving the set of transport equations which are developed in Section 3.2. Fatt and Goldstick [35] and Friedman [41] have used similar approaches to study swelling in corneal stroma. In these cases, however, swelling is linked to a 'swelling pressure', rather than the hydrostatic fluid pressure. In addition, their analyses are limited to a single dimension. The present analysis applies to the case of isotropic, three–dimensional swelling in which the influence of shear stresses is neglected. As such it represents only a first approximation to the complete description of
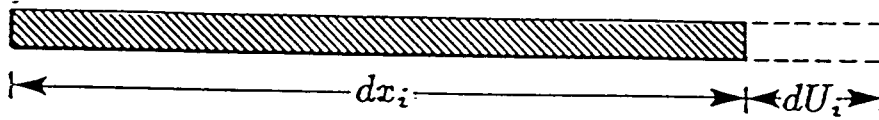
Figure 3.3: **Linear deformation of a differential segment, dx_i, by an amount dU_i.**

The following discussion is limited to the case of small deformations described by classical elastic theory. Therefore the equations do not apply, for example, to the development of severe edema. We begin with a brief description of deformation theory. Let dU_i represent the deformation in the x_i direction of a small element of initial length dx_i (see Figure (3.3)). By definition, the local solid strain in the x_1 direction, ϵ_1, is equal to the change in length of the element divided by its initial length, i.e.,

$$\epsilon_1 = \frac{\partial U_1}{\partial x_1}.$$ (3.18)

Similar equations apply for the strains in the x_2 and x_3 directions. The local volumetric dilation, ϵ_v, of an infinitesimal volume element, dV^0, undergoing deformation is defined as

$$\epsilon_v = \frac{dV^1 - dV^0}{dV^0},$$ (3.19)

where dV^1 is the volume of the deformed element (see Figure (3.4)). For small strains, ϵ_v is equal to the sum of the individual linear strains [102]:

$$\epsilon_v = \sum_{i=1}^{3} \epsilon_i.$$ (3.20)

That is,

$$\epsilon_v = \frac{\partial U_i}{\partial x_i},$$ (3.21)

where the right hand side of Eq. (3.21) is written in tensor notation (see [99]).
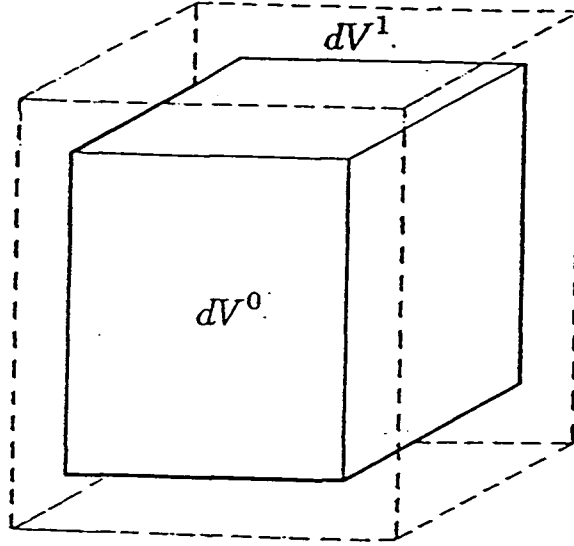
Figure 3.4: **Volumetric dilation of a differential volume element from an unstrained volume, dV^0, to a strained volume, dV^1.**

To relate the volumetric dilation, ϵ_v, to the local fluid hydrostatic pressure we begin with Terzaghi's concept of effective stress, which forms the basis for describing deformation in porous media [19, 59, 101, 67]. The total stress is set equal to the sum of the local fluid pressure and an effective stress responsible for the deformation of the solid skeleton as follows [102]:

$$\sigma_{ij} = \sigma_{ij}^{eff} - P\delta_{ij},$$ (3.22)

where σ_{ij} and σ_{ij}^{eff} are the components of the total stress tensor and the effective stress tensor, respectively, P denotes the local hydrostatic fluid pressure, and δ_{ij} is the Kronecker delta function (see [99]). The negative sign in front of the pressure term results from defining the

pressure as positive in compression, while the remaining stresses are defined as positive in tension. Furthermore, Eq. (3.22) assumes that the pressure in the fluid creates a normal stress of equal magnitude in the solid skeleton, and that both the fluid and the solid skeleton are incompressible. The effective stress then represents the additional stress within the solid phase that causes the solid components to reorient themselves relative to each other, resulting in the deformation of the medium.

If, for the small range of volume changes considered, we neglect any changes in the overall stress in the system which might occur, for example, due to changes in the applied stresses at the interstitial boundaries, then

$$\Delta\sigma_{ij}^{eff} = \Delta P \delta_{ij}. \tag{3.23}$$

Equation (3.23) implies that the local volumetric dilation is a function only of the local hydrostatic pressure within the system.

This function is provided by the interstitial compliance, Ω, [4] defined here as

$$\Omega(P) = \frac{\Delta V}{\Delta P}, \tag{3.24}$$

where ΔV is the change in the interstitial fluid volume, relative to a reference volume, in response to a change in fluid hydrostatic pressure, relative to the corresponding reference pressure. The compliance can be expressed in terms of the volumetric dilation, ϵ_v, by dividing Eq. (3.24) by the reference volume. Then, in the limit of infinitesimal volumes, the specific compliance, $\hat{\Omega}$, is

$$\hat{\Omega}(P) = \frac{d\epsilon_v}{dP}. \tag{3.25}$$

In the multiphase system proposed here the question arises as to which of the m+1 hydrostatic pressures (corresponding to the m+1 incremental fluid volume fractions) are to be used in the compliance relationship. Following Lewis and Schrefler [67], the average local hydrostatic pressure,

$$P_{av} = \frac{1}{n^0} \cdot \sum_{k=0}^{m} \delta n^k \cdot P^k, \tag{3.26}$$

will be used. The exact form of Eq. (3.26) will depend on the experimental method used to measure interstitial fluid pressures when determining the compliance of a given tissue. For example, the average pressure given above assumes that the measuring device (such as a micropipette) cannot distinguish between the hydrostatic pressures in the various fluid phases, and hence yields a composite value.

Together, Eqs. (3.21), (3.25) and (3.26) define the relationship between the local hydrostatic pressures in each of the incremental volume fractions, the local linear strains, and the local volumetric dilation. These equations will be used when developing expressions for the distribution of fluid pressure and various plasma protein species within the deformable interstitial space.

To determine the geometry of the deformed medium, it is necessary to calculate the linear displacements, U_i, $i = 1, 2, 3$, throughout the interstitial space as functions of the local average hydrostatic pressure. The spatial components of the deformed medium are then evaluated from these displacements, i.e.,

$$x_i' = x_i + U_i(x_i),$$

(3.27)

where x_i' is the x_i location after deformation of a point that was originally positioned at x_i. Hence $U_i(x_i)$ represents the total displacement of a point from its original (unstressed) position, x_i. The displacements are found by introducing the solid displacement potential, Φ, where [59]

$$\frac{\partial \Phi}{\partial x_i} = U_i.$$

(3.28)

Φ is therefore related to ϵ_v by (see Eq. (3.18))

$$\frac{\partial^2 \Phi}{\partial x_i^2} = \epsilon_v.$$

(3.29)

Upon determining the local average fluid pressure from the transport equations and Eq. (3.26), the volumetric dilation, ϵ_v, the displacement potential, Φ, and the individual local solid phase displacements, U_i, are calculated from Eqs. (3.25), (3.29), and (3.28) respectively. The deformed geometry of the interstitial space is then calculated using Eq. (3.27). Together, these equations describe the local interstitial deformation associated with variations in local fluid hydration.

3.1.3 A Constitutive Relationship between Fluid Flow and Fluid Chemical Potential

At low Reynolds numbers, the creeping flow of a homogeneous Newtonian fluid through an isotropic porous medium is described by Darcy's Law:

$$j_{w_i}^0 = -K^0 \cdot \frac{\partial P}{\partial x_i}, \tag{3.30}$$

where $j_{w_i}^0$ is the total local volumetric fluid flux in the x_i direction, K^0 is the hydraulic conductivity of the porous medium-fluid system, and P is the fluid hydrostatic pressure. The hydraulic conductivity is a function of the structure of the porous medium and the absolute viscosity, μ, of the fluid. However, the specific hydraulic conductivity, K', equal to K/μ, is a material property of the porous medium and therefore does not depend on the type of fluid flowing within the system [31, 66, 60].

In deforming porous media, $j_{w_i}^0$ represents the fluid flux relative to the moving solids [20]. It is related to the absolute fluid flux, $q_{w_i}^0$ (where $q_{w_i}^0$ is the fluid flux relative to stationary coordinates), and the local solid phase velocity, v_{s_i} (taken with respect to the same set of stationary coordinates), by

$$q_{w_i}^0 = j_{w_i}^0 + n^0 \cdot v_{s_i}, \tag{3.31}$$

where, as before, n^0 is the mobile fluid volume fraction.

In the case of solutions, the presence of solutes influences the flux of solvent. This interaction is described by the phenomenological relationships of irreversible thermodynamics. These relationships, which have been used to quantify mass exchange across the vascular wall, relate the fluid flux to the colloid osmotic pressure and hydrostatic pressure driving forces present in the system. The exact way in which the colloid osmotic and hydrostatic pressures within the interstitial space affect the local interstitial fluid flux remains unresolved. However, as a starting point, it is assumed here that the local fluid flux through an incremental volume fraction is proportional to the local gradient in fluid chemical potential there, i.e.,

$$j_{w_i} \propto \frac{\partial \mu_w}{\partial x_i}. \tag{3.32}$$

While Eq. (3.32) is a postulate only, it should provide a satisfactory first approximation for quantifying the effect of colloid osmotic pressure gradients on the solvent flux. This dependence of fluid flux through a porous medium on the gradient in fluid chemical potential was first proposed by Biot [21], and has been suggested by several researchers to describe interstitial fluid transport [57, 26, 69]. However, Eq. (3.32) does not consider the influence of solute mobility in determining the effective colloid osmotic pressure driving fluid within the interstitium. It will therefore most likely over-estimate the effect of colloid osmotic pressure gradients on fluid flow. Further research is needed to determine the influence of osmotic pressures on interstitial fluid flow and, hence, the appropriate form of Eq. (3.32).

Since we have assumed local thermodynamic equilibrium with respect to the fluid chemical potential in each of the incremental volume fractions, the total local fluid flux for our system is

$$j_{w_i}^0 = -K^0 \cdot \frac{\partial}{\partial x_i} \left(P^m - \sum_{k=1}^{m} \Pi^k \right).$$
(3.33)

Equation (3.33), because it incorporates colloid osmotic effects in the fluid flow relationship, represents a more general version of Eq. (3.30). The assumption of local thermodynamic equilibrium in fluid chemical potential implies that the local driving force for fluid flow in each of the incremental volume fractions within an elementary volume of interstitium is the same. That is

$$\frac{\partial \mu_w^0}{\partial x_i} = \frac{\partial \mu_w^1}{\partial x_i} = \cdots = \frac{\partial \mu_w^m}{\partial x_i}.$$
(3.34)

The local fluid flux associated with the distribution volume fraction n^k, expressed in terms of hydrostatic and colloid osmotic pressure gradients, is then

$$j_{w_i}^k = -K^k \frac{\partial}{\partial x_i} \left(P^m - \sum_{k=1}^{m} \Pi^k \right),$$
(3.35)

where $j_{w_i}^k$ is the local fluid flux and K^k is the hydraulic conductivity associated with the distribution volume fraction of protein species k. It follows from Eqs. (3.34) and (3.35) that the fraction of the total volumetric fluid flux that is associated with the distribution volume fraction n^k is

$$j_{w_i}^k = \frac{K^k}{K^0} \cdot j_{w_i}^0.$$
(3.36)

In general, K^0, and hence K^k, will vary with interstitial hydration (see, for example, [53]). For a discussion of interstitial hydraulic conductivity and its dependence on hydration and on solid phase composition, the reader is referred to the recent review by Levick [66]. The local fluid flux through any of the protein distribution volume fractions can then be calculated using Eqs. (3.33) and (3.36).

3.1.4 Protein Transport Mechanisms within the Interstitium

The transport of a solute through a porous medium occurs via convective and diffusive mechanisms. The relative contributions of these two processes to the overall solute flux will depend on the fluid velocities within the medium and the system's transport properties with respect to that particular solute. When modelling the interstitial transport of plasma proteins it is often assumed that molecular diffusion dominates [38, 65, 7]. However, given the comparatively high hydraulic conductivity of certain tissues, such as tumours [61], cases may exist in which convective transport plays an important role. In addition, convective transport in porous media can result in mechanical dispersion which, while bearing a resemblance to diffusion, is dependent on the solute convective velocities [8]. A general description of interstitial protein transport must consider the possible contributions of each of these mechanisms to the overall protein flux.

Molecular diffusion is the result of random thermal motions of the solute. When coupled with convective transport, the diffusive flux represents the solute flux relative to the convective component. In a porous medium the apparent diffusive flux of the solute is somewhat hindered, due to both the increased pathlength of the tortuous channels that the solute must follow and the reduced cross-sectional area available to the solute due to the presence of the solid matrix [88].

In dilute solutions, interactions between solute molecules are negligible [91]. The local diffusive flux of protein species k through the interstitium is then described by Fick's Law:

$$j_{d_i}^k = n^k \cdot D_{\text{eff}}^k \cdot \frac{\partial C^k}{\partial x_i},$$

(3.37)

where $j_{d_i}^k$ is the diffusive flux of protein species k in the x_i direction. The effective molecular

diffusion coefficient, D_{eff}^k, is typically less than the protein's free diffusion coefficient, reflecting the hindering effects of the matrix components. Therefore, as interstitial hydration increases, D_{eff}^k approaches the free diffusion coefficient [53, 4, 27]. Comparison of the diffusion of plasma proteins and various dextrans within tissues suggests that charge and molecular size also play a major role in determining the effective diffusivity of individual macromolecular species [61].

The local convective velocity of an interstitial plasma protein may be somewhat less than the local fluid velocity, due to the hydrodynamic interaction between the protein molecule and the solid matrix [92, 87, 61]. This phenomenon has been analyzed, from a theoretical standpoint, for the case of neutrally buoyant spheres travelling through narrow cylindrical channels (e.g. [23, 31]). The extent to which a particle is hindered (given by the ratio of the local particle velocity to the local fluid velocity, v^*) depends both on the position of the particle relative to the wall and the ratio of the particle radius to the channel radius, λ [23].

Brenner and Gaydos [23] estimate the mean velocity of particles in the channel for cases where λ is less than or equal to 0.2. Their analysis reveals two opposing effects. On the one hand, the velocity ratio v^* decreases with increasing particle radius, due to hydrodynamic interaction. However, the larger particles are also restricted, due to steric exclusion, to the more central portions of the flow field where the local fluid velocities are higher. For this range of λ, Brenner and Gaydos predict mean particle velocities that are greater than the mean fluid velocity within the channel, even though the local particle velocities are always less than the local fluid velocities.

Because of the complex geometry of the interstitium, the extent to which this type of interaction influences interstitial protein transport is unknown. Based on the foregoing discussion however, we assume that the mean convective velocity of protein species k in the x_i direction, $\bar{v}_{c_i}^k$, is related to the mean interstitial fluid velocity within the protein's distribution volume, $\bar{v}_{w_i}^k$, by

$$\bar{v}_{c_i}^k = \zeta^k \cdot \bar{v}_{w_i}^k, \tag{3.38}$$

where the fluid and protein velocities are defined relative to the solid phase velocity. The

convective hindrance of the protein, ξ^k, is less than or equal to 1. Since ξ^k is a function of λ, it will vary with interstitial hydration. The mean interstitial fluid velocity in the x_i direction is related to the fluid flux through the distribution volume, $j_{w_i}^k$, by

$$\bar{v}_{w_i}^k = \frac{j_{w_i}^k}{n^k}. \tag{3.39}$$

The total convective flux of protein species k in the x_i direction, $j_{c_i}^k$, relative to the moving solid phase is

$$j_{c_i}^k = n^k \cdot \xi^k \cdot \bar{v}_{w_i}^k \cdot C^k, \tag{3.40}$$

which states that the convective solute flux is equal to the net fluid flux through the protein's distribution volume fraction $(n^k \cdot \bar{v}_{w_i}^k)$ times the protein's convective hindrance (ξ^k) and the local protein concentration (C^k). This expression can be rewritten in terms of the total fluid flux, $j_{w_i}^0$, relative to the solid phase by noting that

$$n^k \cdot \bar{v}_{w_i}^k = \frac{K^k}{K^0} \cdot j_{w_i}^0. \tag{3.41}$$

Equation (3.40) then becomes

$$j_{c_i}^k = \left[\xi^k \frac{K^k}{K^0} \right] j_{w_i}^0 \cdot C^k, \tag{3.42}$$

where the bracketed term may be identified as the retardation factor, R_f^k, [92, 61] associated with protein species k.

In light of the preceding discussion, it does not necessarily follow that the mean convective velocity of the protein m exceeds the mean velocity of some larger protein n. According to Eqs. (3.38) and (3.41), the ratio of these two velocities depends on the quantity $(\xi^m K^m n^n)/(\xi^n K^n n^m)$. This suggests a new, alternative mechanism for the 'gel chromatographic effect' where the mean transit time through the interstitium for larger protein molecules is less than that for smaller proteins [104]. This mechanism is quite different from the one proposed by Watson and Grodins [104], who divided the interstitial space into a 'gel phase', in which proteins move by restricted diffusion, and a 'free fluid phase', in which proteins are transported by convection and free diffusion. In their model the smaller proteins, which access a greater percentage of

the gel phase, are retarded compared to the bigger proteins, which are largely restricted to the free fluid channels. Equations (3.38) and (3.41) together suggest that protein exclusion in a continuum may be sufficient to account for the gel chromatographic effect without introducing open channels in the description of the interstitium.

The contribution of mechanical dispersion to the total interstitial plasma protein flux has neither been addressed experimentally nor theoretically. The mechanical dispersive flux arises from variations in the true microscopic convective velocity of the protein from the mean convective velocity given by Eq. (3.38). This includes the phenomenon of Taylor dispersion [96, 97] which results from local velocity profiles within a given channel, and the fact that the protein, because of its finite size, cannot access the entire channel cross-section [23]. Mechanical dispersion in porous media also results from deviations in the microscopic flow paths of the solute particles from the direction of bulk convective flow [8]. Like diffusion, mechanical dispersion tends to spread an advancing solute front. It is therefore generally assumed that the mechanical dispersive flux obeys Fick's Law (see Anderson for details [1]):

$$j^k_{md_i} = -n^k \vartheta^k_{ij} \frac{\partial C^k}{\partial x_j}, \qquad (3.43)$$

where $j^k_{md_i}$ is the flux of protein species k in the x_i direction resulting from mechanical dispersion, and ϑ^k_{ij} is the protein's coefficient of mechanical dispersion, a second rank tensor. In general, the dispersive flux is some fraction of the total convective flux. It is therefore significant only when the magnitude of the convective protein flux is large compared to the diffusive flux.

Mechanical dispersion is a function of both the local convective protein velocity and the structure of the porous medium. The latter effect is characterized by a set of parameters, the longitudinal and transverse dispersivities (α_l and α_t). For an isotropic medium, ϑ^k_{ij} is related to the components of the mean protein convective velocity and the dispersivities by [8]

$$\vartheta^k_{ij} = \alpha^k_t \left| \bar{v}^k_c \right| \delta_{ij} + \left(\alpha^k_l - \alpha^k_t \right) \frac{\bar{v}^k_{c_i} \cdot \bar{v}^k_{c_j}}{\left| \bar{v}^k_c \right|}, \qquad (3.44)$$

where $\left| \bar{v}^k_c \right|$ is the magnitude of the mean convective velocity of the protein, i.e.,

$$\left| \bar{v}^k_c \right| = \left[\left(\bar{v}^k_1 \right)^2 + \left(\bar{v}^k_2 \right)^2 + \left(\bar{v}^k_3 \right)^2 \right]^{\frac{1}{2}}. \qquad (3.45)$$

While the dispersivities depend on the medium's pore geometry, no analytical expressions exist to link these parameters to other appropriate material properties, such as the solid phase volume fraction and the medium's hydraulic conductivity. Hence, in practical applications, the dispersivities are adjusted to give the best possible agreement between experimental observations and model predictions [1]. Since the dispersivities reflect, for example, the tortuosity of the pathways available to the various plasma protein species, they will vary with tissue hydration. Furthermore, since the pathways for different protein species will vary as a result of exclusion, the dispersivities may also be expected to vary amongst protein species.

The sum of the diffusive flux (Eq. (3.37)), the convective flux (Eq. (3.42)), and the mechanical dispersive flux (Eq. (3.43)) gives the total protein flux at any point within the interstitium, relative to the moving solid phase. Equations (3.37), (3.42), and (3.43) will be used in Section 3.2.3 to develop expressions for the transient distributions of the various macromolecular species within the interstitial space.

3.2 Mass Balance Equations for Solid, Fluid, and Solute Species

In the previous section we developed mathematical expressions for the flow of solid, fluid and protein species within a deformable interstitium. We will now develop the equations that describe the transient distribution of these phases within the interstitium. The equations describing fluid transport through a porous medium subject to small deformations have been applied in a number of fields, including groundwater hydrology and soil mechanics [19, 8, 101]. The equations are based on differential mass balances for the solid and fluid phases, combined with an appropriate description of deformation. A similar approach is adopted here. Likewise, the equations describing the distribution of various plasma protein species within the interstitial space are based on differential mass balances on each of the protein species contained within the interstitium. Because of the linkages existing between the fluid flux and the protein osmotic pressures, between the convective protein flux and the fluid flux, and between the various transport properties and the tissue hydration, the material balances result in a set of coupled

partial differential equations which must be solved simultaneously. We will now consider each of the material balances individually.

3.2.1 Material Balance on the Solid and Immobile Fluid Phases

The solid and immobile fluid phases have much the same impact on mass flow within the interstitium in that they both reduce the volume available to mobile fluid and plasma proteins. Furthermore, given that the immobile fluid phase volume fraction is a function of the solid phase volume fraction, it is convenient to consider the two as a single composite phase $(n^s + F^s(n^s))$ when carrying out mass balances on the various components within the interstitium.

Assuming that the density of the solid phase is constant, a material balance on the solid and immobile fluid phases within a differential volume of interstitium gives

$$-\frac{\partial(n^s + F^s)}{\partial t} = \frac{\partial([n^s + F^s] \cdot v_{s_i})}{\partial x_i}, \qquad (3.46)$$

where $[n^s + F^s] \cdot v_{s_i}$ is the net flux of the composite phase, per unit volume, at a point within the interstitium. Equation (3.46) states that the net rate of change in the composite phase volume per unit volume of interstitium at some point is equal to the net flux of the phase at that point. The solid phase velocity, v_{s_i}, relative to a fixed coordinate system, is related to the solid displacement in the x_i direction, U_i, by [101]

$$v_{s_i} = \frac{\partial U_i}{\partial t}. \qquad (3.47)$$

Since the volumetric dilation, ϵ_v, is equal to $\partial U_i/\partial x_i$, then

$$\frac{\partial v_{s_i}}{\partial x_i} = \frac{\partial \epsilon_v}{\partial t}. \qquad (3.48)$$

The local solid phase velocity can therefore be related to the local average hydrostatic pressure through the compliance relationship (Eq. (3.25)). Together, Eqs. (3.46) and (3.48) describe the distribution of solid material and immobile fluid in response to variations in the local average hydrostatic pressure.

3.2.2 Material Balance on the Fluid Phase

Consider the flow of fluid-protein solution within the interstitium. For dilute solutions, variations in density can be neglected. Furthermore the volumetric flux of solution is approximately equal to the total solvent flux, $q_{w_i}^0$. A material balance on the total fluid-protein mixture within a differential volume of interstitium then gives

$$-\frac{\partial n^0}{\partial t} = \frac{\partial q_{w_i}^0}{\partial x_i}. \qquad (3.49)$$

The total mobile fluid volume fraction, n^0, can be rewritten in terms of the solid phase volume fraction, i.e.,

$$n^0 = 1 - n^s - F^s(n^s). \qquad (3.50)$$

Furthermore, the total solvent flux relative to fixed coordinates, $q_{w_i}^0$, may be expressed in terms of solvent flux relative to the solid phase, $j_{w_i}^0$, the solid phase velocity, v_{s_i}, and n^s using Eqs. (3.31) and (3.50), i.e.,

$$q_{w_i}^0 = j_{w_i}^0 + (1 - n^s - F^s(n^s)) \cdot v_{s_i}. \qquad (3.51)$$

The second term of Eq. (3.51) represents the flux of mobile water at the solid phase velocity. Equation (3.49) can now be expressed in terms of $j_{w_i}^0$, n^s, F^s, and v_{s_i} using Eq. (3.51) to give

$$-\left[\frac{\partial(n^s + F^s)}{\partial t} + \frac{\partial([n^s + F^s] \cdot v_{s_i})}{\partial x_i}\right] + \frac{\partial v_{s_i}}{\partial x_i} + \frac{\partial j_{w_i}^0}{\partial x_i} = 0. \qquad (3.52)$$

Since the solid phase and immobile fluid phases are conserved, the sum in square brackets is zero (see Eq. (3.46)). Also, the second term in Eq. (3.52) is equal to $\partial \epsilon_v / \partial t$, so that Eq. (3.52) becomes

$$\frac{\partial \epsilon_v}{\partial t} = -\frac{\partial j_{w_i}^0}{\partial x_i} \qquad (3.53)$$

which states that the rate of volumetric dilation at a given point in the interstitium is equal to the net rate of fluid inflow to that point.

Finally, using the expressions for $j_{w_i}^0$ and ϵ_v developed earlier (see Eqs. (3.35), (3.24) and (3.25)), Eq. (3.53) can be rewritten in terms of the local average hydrostatic pressure and the

local fluid chemical potential to give

$$\hat{\Omega}\frac{\partial P_{av}}{\partial t} = \frac{\partial}{\partial x_i}\left(K^0\frac{\partial}{\partial x_i}\left(P^m - \sum_{k=1}^m \Pi^k\right)\right). \tag{3.54}$$

3.2.3 Material Balance on Protein Species k

The net rate of increase in the mass of protein species k contained in a differential element within the interstitium is equal to the net diffusive, dispersive and convective flows of protein into the element. In a fixed coordinate reference frame

$$\frac{\partial(n^k C^k)}{\partial t} = \frac{\partial}{\partial x_i}\left(n^k\left[\vartheta_{ij}^k + D_{eff}^k\delta_{ij}\right]\frac{\partial C^k}{\partial x_j}\right) - \frac{\partial}{\partial x_i}\left(\left[n^k v_{s_i} + R_f^k j_{w_i}^0\right]C^k\right) \tag{3.55}$$

where $-n^k(\vartheta_{ij}^k + D_{eff}^k\delta_{ij})\partial C^k/\partial x_j$ is the total dispersive and diffusive flux, $n^k v_{s_i} C^k$ is the convective protein flux at the solid phase velocity, and $R_f^k j_{w_i}^0 C^k$ is the additional convective protein flux due to the motion of the fluid relative to the solid phase. R_f^k is the retardation factor for protein species k, defined in Section 3.2.2.

Equation (3.55) is combined with the equation for volumetric dilation (Eq. (3.48)) to give

$$\frac{\partial(n^k C^k)}{\partial t} + n^k C^k\frac{\partial\epsilon_v}{\partial t} + v_{s_i}\frac{\partial(n^k C^k)}{\partial x_i} + \frac{\partial(R_f^k j_{w_i}^0 C^k)}{\partial x_i}$$
$$-\frac{\partial}{\partial x_i}\left(n^k\left[\vartheta_{ij}^k + D_{eff}^k\delta_{ij}\right]\frac{\partial C^k}{\partial x_j}\right) = 0 \tag{3.56}$$

Equation (3.56) may be interpreted as follows. The first term represents the net rate of change in protein content, per unit volume of interstitium, within the element. The second term represents the change in protein content associated with deformation within the interstitium. The third term represents the net convective flow of protein, at the solid phase velocity, out of the element, while the fourth term is the remaining convective flow associated with the solute motion relative to the solid phase. The final term represents the net dispersive and diffusive flows leaving the element.

3.2.4 Summary of Governing Equations

Table (3.1) summarizes the equations describing fluid, solids, and protein transport in a deforming interstitium. Alongside are listed the primary dependent variables obtained as the solution

of each equation. The equations and dependent variables are grouped into one of three categories: those describing interstitial deformation, those describing interstitial fluid transport and distribution, and those pertaining to solute transport and distribution within the interstitium.

The first category includes equations for the conservation of solid phase and local solid phase velocity (Eqs. (3.46) and (3.47)), relationships linking the geometry of the deformed interstitium to the local volumetric dilation (Eqs. (3.27) and (3.28)), and constitutive relationships expressing volumetric dilation as a function of the local average hydrostatic pressure (Eqs. (3.25) and (3.26)). The second category consists of an equation for the conservation of fluid mass within the system (Eq. (3.54)), expressions relating local fluid fluxes to gradients in local fluid hydrostatic and colloid osmotic pressures (Eq. (3.35)), and colloid osmotic relationships (Eq. (3.13). The final category is comprised of the conservation equations for the various protein species (Eq. (3.56)), expressions linking each of the distribution volume fractions to the solid phase volume fraction (Eq. (3.7)), and relationships used to define the various protein and fluid fluxes and velocities (Eqs. (3.36), (3.37), (3.38), (3.39) and (3.43)).

Together these equations form a coupled system that must be solved simultaneously. For example, the total local volumetric fluid flux, $j_{w_i}^0$, is a function of the local colloid osmotic pressures, Π^k, $k = 1, 2, ...m$, and hence the local concentrations of the various plasma protein species, C^k, $k = 1, 2, ...m$. In the next three chapters, we demonstrate how the method of Finite Elements can be used to solve sets of coupled equations, based on those shown in Table (3.1), for a number of simplified circumstances.

UNKNOWN	GOVERNING EQUATION	LOCATION IN TEXT
	I. INTERSTITIAL DEFORMATION	
n^s		
$v_{s_i},\ i = 1,2,3$	$-\dfrac{\partial(n^s + F^s)}{\partial t} = \dfrac{\partial([n^s + F^s]\cdot v_{s_i})}{\partial x_i}.$	$Eq.\ (3.46),\ Sec.\ 3.2.1$
$U_i,\ i = 1,2,3$	$v_{s_i} = \dfrac{\partial U_i}{\partial t}.$	$Eq.\ (3.47),\ Sec.\ 3.2.1$
Φ	$\dfrac{\partial \Phi}{\partial x_i} = U_i.$	$Eq.\ (3.28),\ Sec.\ 3.1.2$
ϵ_v	$\dfrac{\partial^2 \Phi}{\partial x_i^2} = \epsilon_v.$	$Eq.\ (3.29),\ Sec.\ 3.1.2$
P_{av}	$\hat{\Pi}(P_{av}) = \dfrac{d\epsilon_v}{dP}.$	$Eq.\ (3.25),\ Sec.\ 3.1.2$
$P^k,\ k = 1,2,3,...,m-1$	$P_{av} = \dfrac{1}{n^0}\cdot\sum_{k=0}^{m}\delta n^k \cdot P^k.$	$Eq.\ (3.26),\ Sec.\ 3.1.2$
	$P^0 - \Pi^0 = P^1 - \Pi^1 = P^2 - \Pi^1 - \Pi^2 = ... = P^m - \sum_{k=1}^{m}\Pi^k$	$Eq.\ (3.17),\ Sec.\ 3.1.1$
	II. FLUID TRANSPORT	
P^m	$\hat{\Pi}\dfrac{\partial P_{av}}{\partial t} = \dfrac{\partial}{\partial x_i}\left(K^0 \dfrac{\partial}{\partial x_i}\left(P^m - \sum_{k=1}^{m}\Pi^k\right)\right).$	$Eq.\ (3.54),\ Sec.\ 3.2.2$
$\Pi^k\ k = 1,2,...,m$	$\Pi^k = G^k(C^k).$	$Eq.\ (3.13),\ Sec\ 3.1.1$
$j^0_{w_i},\ i = 1,2,3$	$j^0_{w_i} = -K^0 \cdot \dfrac{\partial}{\partial x_i}\left(P^m - \sum_{k=1}^{m}\Pi^k\right).$	$Eq.\ (3.33),\ Sec.\ 3.1.3$
	III. PLASMA PROTEIN TRANSPORT	
$n^k,\ k = 1,2,...,m$	$n^k = 1 - n^s - F^k(n^s).$	$Eq.\ (3.6),\ Sec.\ 3.1.1$
$C^k,\ k = 1,2,...,m$	$\dfrac{\partial(n^k C^k)}{\partial t} = \dfrac{\partial}{\partial x_i}\left(n^k\left[\vartheta^k_{ij} + D^k_{eff}\delta_{ij}\right]\dfrac{\partial C^k}{\partial x_j}\right) - \dfrac{\partial}{\partial x_i}\left(\left[n^k v_{s_i} + R^k_j j^0_{w_i}\right]C^k\right)$	$Eq.\ (3.56),\ Sec.\ 3.2.3$
$\vartheta^k_{ij},\ i=1,2,3;\ j=1,2,3$	$\vartheta^k_{ij} = \alpha^k_t |\bar{v}^k_c|\delta_{ij} + (\alpha^k_l - \alpha^k_t)\dfrac{\vartheta^k_{c_i}\cdot\vartheta^k_{c_j}}{|\bar{v}^k_c|}.$	$Eq.\ (3.44),\ Sec.\ 3.1.4$
$\bar{v}^k_{w_i},\ i = 1,2,3$	$\bar{v}^k_{w_i} = \dfrac{j^k_{w_i}}{n^k}.$	$Eq.\ (3.39),\ Sec.\ 3.1.4$
$\bar{v}^k_{c_i},\ i = 1,2,3$	$\bar{v}^k_{c_i} = \xi^k \cdot \bar{v}^k_{w_i}.$	$Eq.\ (3.38),\ Sec.\ 3.1.4$
$j^k_{w_i},\ i = 1,2,3$	$j^k_{w_i} = \dfrac{K^k}{K^0}\cdot j^0_{w_i}.$	$Eq.\ (3.36),\ Sec.\ 3.1.3$

Table 3.1: Summary of the model equations.

3.3 Concluding Remarks

In the preceding two sections, mathematical relationships were developed to describe the transient flow and distribution of fluid and plasma proteins within the interstitium, resulting in a system of coupled, nonlinear partial differential equations which must be solved simultaneously (see Table (3.1)). Despite the complexity of the model, it is limited in several respects. First, the description of interstitial deformation applies to small strains only (on the order of ten percent). The model is therefore unsuitable for analysing extreme cases of edema formation. However, the model could be expanded to consider large deformations by introducing a more general and, as a result, a more complex finite deformation theory (e.g., [21]). Furthermore, the model uses a compliance relationship to characterize deformation, which assumes that any change in volume is a function of the hydrostatic pressure within the system. This neglects the influence of shear stresses on deformation. However, we are interested primarily in the effect of volume changes on the various transport properties and material characteristics of the interstitial space (such as the hydraulic conductivity, effective diffusivities, and various distribution volume fractions), rather than a description of the deformed geometry of the interstitium. We therefore consider this approach a reasonable first approximation to the complete theory developed by Biot [19]. A more detailed analysis of deformation would require additional information about the material properties of the various interstitial components, such as their stress-strain characteristics.

Fluid flow within the interstitium is assumed to be proportional to the gradient in fluid chemical potential alone, thus neglecting any coupling between fluid flow and solute chemical potential, for example. The theory presented here could easily be modified to include these additional effects, given better information about the nature of fluid transport in the interstitium. Previous models of interstitial fluid transport have considered the effect of hydrostatic pressure gradients only [22, 36, 87]. Therefore, because it includes the influence of colloid osmotic as well as hydrostatic pressure gradients, the interstitial fluid flux representation given here is considered to be more general than that offered by any previous interstitial transport

models. However, further research in the area of fluid flow within osmotically active, partially restricting matrices (such as the interstitium) is needed.

Despite its limitations, the model describes the combined effects of a number of interstitial properties (such as exclusion and swelling characteristics) and transport mechanisms (such as protein convection, diffusion, and dispersion) on interstitial fluid and plasma protein transport. It therefore provides a far more comprehensive description of interstitial transport than has been offered by any of the previous models. The model can be used to study numerous aspects of interstitial transport over a wide range of physiological conditions. When combined with mathematical descriptions of fluid and protein exchange across the capillary wall and, where appropriate, the lymphatic wall, the model provides a tool to investigate the sensitivity of the microvascular exchange system to any number of parameters characterizing its transport behaviour. The next three chapters give examples of the model's utility in this respect by investigating fluid and plasma protein exchange, both in mesentery and a hypothetical tissue, under steady-state and transient conditions and for a number of systemic upsets.

Chapter 4

Steady-State Exchange in Mesenteric Tissue

In the previous chapter we presented a general mathematical model describing the transport and distribution of fluid and macromolecules within the interstitium, which is treated as a multiphase, deforming porous medium. In this chapter, a simplified version of the model, in which the interstitium is approximated as a rigid porous medium containing a single plasma protein species, is combined with mathematical descriptions of transport across the interstitial boundaries to study steady-state fluid and protein exchange within the mesentery. The mesentery was selected both for its simple geometry and because a number of its transport parameters have been measured. Furthermore, the mesentery remains a popular tissue for experimental studies of microvascular exchange [30] and interstitial transport [115, 40].

The mesentery consists of a thin sheet of loose connective tissue, the upper and lower surfaces of which are bounded by a serous membrane (the mesothelium) made of a single layer of epithelial cells [50]. In some respects, then, fluid and plasma protein exchange across the mesothelium may resemble that of the capillary wall. While it is generally accepted that fluid and plasma proteins are able to cross this boundary and enter the surrounding peritoneal fluid [50, 37], the mesothelium's exchange properties remain poorly defined. Therefore, one objective of this study is to explore the potential influence of the mesothelium on the steady-state exchange of fluid and a single plasma protein species within the mesentery. Three scenarios are considered:

1. the mesothelium is impermeable to fluid and proteins;

2. the mesothelium's transport properties are identical to those of the capillary wall; and

3. the resistance of the mesothelium to fluid and plasma protein exchange is substantially

lower than that of the capillary wall.

These three cases were selected so as to encompass a wide range of mass transport characteristics.

We also investigate the sensitivity of microvascular exchange in the mesentery to a select number of interstitial parameters, namely the tissue hydraulic conductivity, the protein effective diffusion coefficient and the protein convective hindrance. The possible influence of dispersion on interstitial transport is not considered in this study. (In fact, the effects of mechanical dispersion on mass exchange within this model tissue are tentatively in Appendix C.) The model equations are recast in dimensionless form. This reduces the number of interstitial parameters that must be varied from the three listed above to two equivalent dimensionless groups. A brief description of the model follows.

4.1 Defining the System

Figure (4.1) is a schematic diagram of a cross-sectional portion of mesenteric tissue of uniform thickness. For simplicity we will assume that the conditions in the tissue are independent of the z-direction, thereby limiting the flow field to the two remaining dimensions. The interstitium is bounded left and right by arteriolar and venular capillaries respectively. It is assumed that the tissue thickness, H, is small relative to the distance, L, separating the vessels, so that the system can be approximated by the two-dimensional rectangular domain shown in Figure (4.2). In addition, the hydrostatic pressure and plasma protein concentration in each of the vessels are assumed uniform along the vascular walls. The upper and lower boundaries of Figure (4.1) represent the mesothelial layers. For simplicity, and for lack of additional information, it is assumed that the peritoneal fluid is well-mixed, semi-infinite in extent, and subject to a uniform hydrostatic pressure along the length of the mesothelium.

The following notation will apply in the remainder of the paper. A superscript '0' denotes a quantity associated with the total mobile fluid phase (defined below), while a superscript '1' identifies a parameter associated with the accessible volume phase (also defined below).
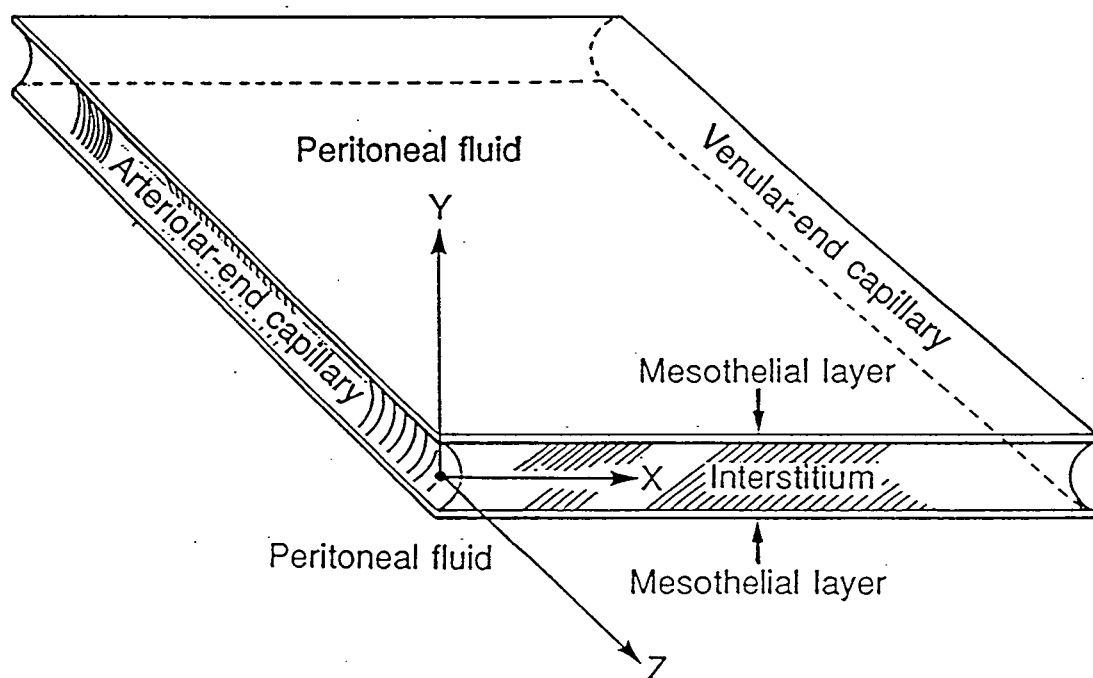
Figure 4.1: **Schematic diagram of a cross-sectional slice of mesentery. The shaded area represents the region of interest.**
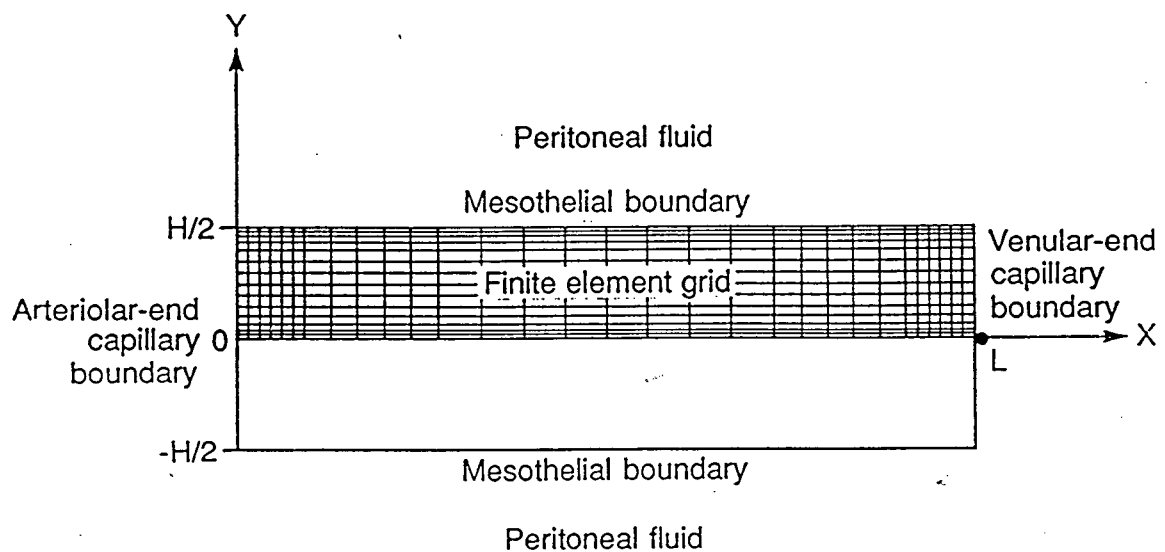
Figure 4.2: Schematic diagram of the tissue segment studied. The system is assumed symmetric about the x-axis; hence only the upper half of the tissue is modelled. The finite element grid is superimposed on this portion of tissue. The aspect ratio (H/L) is 0.1. For simplicity, the curvature associated with the vessels' walls is neglected.

Parameters associated with the arteriolar capillary, the venular capillary, and the mesothelium are identified by superscripts 'art', 'ven', and 'mes', respectively. Finally, a superscript 'b' will be used to identify parameters associated with a general permeable boundary or with the well–mixed fluid on the luminal side of the boundary.

The mathematical description of interstitial transport developed in the previous chapter is applied here, along with these additional simplifying assumptions.

1. Since detailed information on the swelling properties of mesentery is unavailable, it is assumed that the tissue behaves as a rigid porous medium. Furthermore, for lack of additional information, the material properties of the tissue are considered to be spatially invariant.

2. In this study we are not concerned with the relative transport rates of individual plasma protein species within the interstitium. Therefore, the array of interstitial plasma protein species is treated as a single aggregate displaying averaged properties. In fact, several steady-state simulations were performed to investigate the effects of treating the plasma and interstitial fluid as aqueous solutions containing two different osmotically active plasma proteins representative of albumin and globulin. The results of that study, not presented here, identified albumin as the dominant osmotically active plasma protein, when these species are present in physiological concentrations. These findings substantiate the notion that albumin is the major contributor to the colloid osmotic driving forces within tissues.

3. In light of assumption 2, the interstitium contains two distinct mobile fluid phases, only one of which is accessible to proteins (see Figure (4.3)). The accessible volume fraction is denoted by n^1, while the total mobile fluid volume fraction is represented by n^0. In addition to the two mobile fluid phases, the interstitium contains a 'solid' phase, n^s, composed of elements such as hyaluronate, elastin, collagen and proteoglycans, and an immobile fluid phase, n^{im}. It is recognized that, under some conditions, hyaloronate

may be mobile [5]. However, provided that the relative amount of mobile hyaloronate is small, and assuming that interstitial hyaloronate lost to the circulation is replaced, so that the physicochemical properties of the tissue does not change, it is reasonable to neglect movement of this component. Further, the intrafibrillar water of the collagen is included in the immobile phase, due to the comparatively low hydraulic conductivity of the intrafibrillar spaces [66].

4. The total interstitial hydraulic conductivity, K^0, is divided between the accessible fluid phase and the excluded mobile fluid phase according to their proportionate share of the total mobile fluid volume. Hence,

$$K^1 = \frac{n^1}{n^0} \cdot K^0. \tag{4.1}$$

Equation (4.1) therefore neglects any variations in flow resistance between the accessible fluid phase pathways and the pathways of the excluded fluid phase. Given further information about the relative resistances of these two pathways, an alternative expression relating K^1 to K^0 can be substituted for Eq. (4.1).

5. Interstitial protein transport occurs via molecular diffusion and restricted convection only; i.e., mechanical dispersion is not considered. This represents a significant limitation only in convectively dominant problems.

6. Body forces, such as gravity, are neglected.

7. The system is at steady-state.

Since the tissue is assumed rigid, a material balance on the fluid within a differential volume of interstitial space gives (see Eq. (3.53) in Chapter 3)

$$\frac{\partial j^0_{w_x}}{\partial x} + \frac{\partial j^0_{w_y}}{\partial y} = 0, \tag{4.2}$$

where $j^0_{w_i}$ is the local total fluid flux in the x_i direction. This fluid flux is related to the gradient in hydrostatic pressure in the accessible fluid phase, P^1, and the gradient in plasma protein
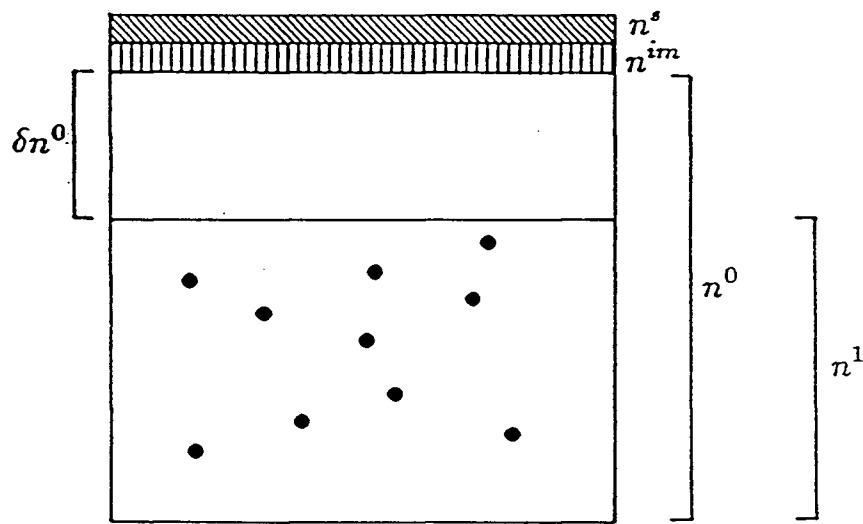
Figure 4.3: **A schematic diagram of an elementary volume of interstitium illustrating the different volume fractions associated with any one point in the continuum representation of the interstitial space.**

osmotic pressure, Π^1, according to Eq. (3.33) in Chapter 3. That is,

$$j_{w_i}^0 = -K^0 \frac{\partial(P^1 - \Pi^1)}{\partial x_i}. \tag{4.3}$$

The local protein osmotic pressure depends on the local plasma protein concentration in the accessible volume, C^1, according to a polynomial relationship:

$$\Pi^1 = A_1 \cdot C^1 + A_2 \cdot \left(C^1\right)^2 + A_3 \cdot \left(C^1\right)^3. \tag{4.4}$$

Substituting Eq. (4.3) in Eq. (4.2) gives

$$\frac{\partial^2(P^1 - \Pi^1)}{\partial x^2} + \frac{\partial^2(P^1 - \Pi^1)}{\partial y^2} = 0. \tag{4.5}$$

The local flux of plasma proteins within the interstitial space consists of a convective component, j_{c_i}, and a diffusive component, j_{d_i}. The first of these is given by Eq. (3.42) in Chapter 3:

$$j_{c_i} = \xi \cdot \frac{K^1}{K^0} \cdot j_{w_i}^0 \cdot C^1, \tag{4.6}$$

where ξ is the convective hindrance. The diffusive flux is defined by Eq. (3.37) in that same chapter:

$$j_{d_i} = -n^1 D_{\text{eff}} \frac{\partial C^1}{\partial x_i}. \tag{4.7}$$

A material balance on the plasma proteins within a differential volume of interstitium then gives (see Eq. (3.56) in Chapter 3)

$$n^1 \cdot D_{\text{eff}} \left[\frac{\partial^2 C^1}{\partial x^2} + \frac{\partial^2 C^1}{\partial y^2} \right] - \xi \cdot \frac{K^1}{K^0} \left[j_{w_x}^0 \frac{\partial C^1}{\partial x} + j_{w_y}^0 \frac{\partial C^1}{\partial y} \right] = 0. \tag{4.8}$$

The first term in Eq. (4.8) represents the net diffusive flux of plasma proteins at a point within the interstitium, per unit volume of interstitial space. The second term is the net convective protein flux, per unit volume of interstitium, at that point. Since the system is at steady-state, the net accumulation of plasma proteins at the point (the right-hand side of Eq. (4.8)) is zero.

Boundary conditions are needed to complete the description of fluid and protein exchange. Their forms depend on the physical nature of the boundaries themselves. We will consider three

boundary types in our system: a symmetry boundary (i.e., from (0,0) to (0,L) in Figure (4.2)),
an impermeable boundary (i.e., from (0,H/2) to (L,H/2), corresponding to the case where
the mesothelium is treated as an impermeable barrier), and the permeable boundaries (i.e.,
from (0,0) to (0,H/2) and from (L,0) to (L,H/2), corresponding to the arteriolar and venular
capillary walls, respectively, and from (0,H/2) to (L,H/2), for those cases where the mesothelium
is permeable).

In the case of a symmetry boundary, the gradients in plasma protein concentration and fluid
chemical potential normal to the boundary are zero. That is,

$$\left[\frac{\partial(P^1 - \Pi^1)}{\partial x} \right]_b \cdot l_x + \left[\frac{\partial(P^1 - \Pi^1)}{\partial y} \right]_b \cdot l_y = 0, \tag{4.9}$$

and

$$\left[\frac{\partial C^1}{\partial x} \right]_b \cdot l_x + \left[\frac{\partial C^1}{\partial y} \right]_b \cdot l_y = 0, \tag{4.10}$$

where l_x and l_y are the x and y components of the unit outward normal to the boundary (see
Figure (4.4)), and where $[\cdot]_b$ implies an interstitial quantity evaluated at a point along the
boundary.

At an impermeable boundary the fluid flux and plasma protein flux normal to the boundary
are zero. That is,

$$\left[j_{w_x}^0 \right]_b \cdot l_x + \left[j_{w_y}^0 \right]_b \cdot l_y = 0, \tag{4.11}$$

and

$$([j_{d_x}]_b + [j_{c_x}]_b) \cdot l_x + ([j_{d_y}]_b + [j_{c_y}]_b) \cdot l_y = 0. \tag{4.12}$$

Upon substituting Eqs. (4.3), (4.6), and (4.7) into these last two expressions, Eqs. (4.11) and
(4.12) reduce to Eqs. (4.9) and (4.10), respectively, cited for the symmetry boundary.
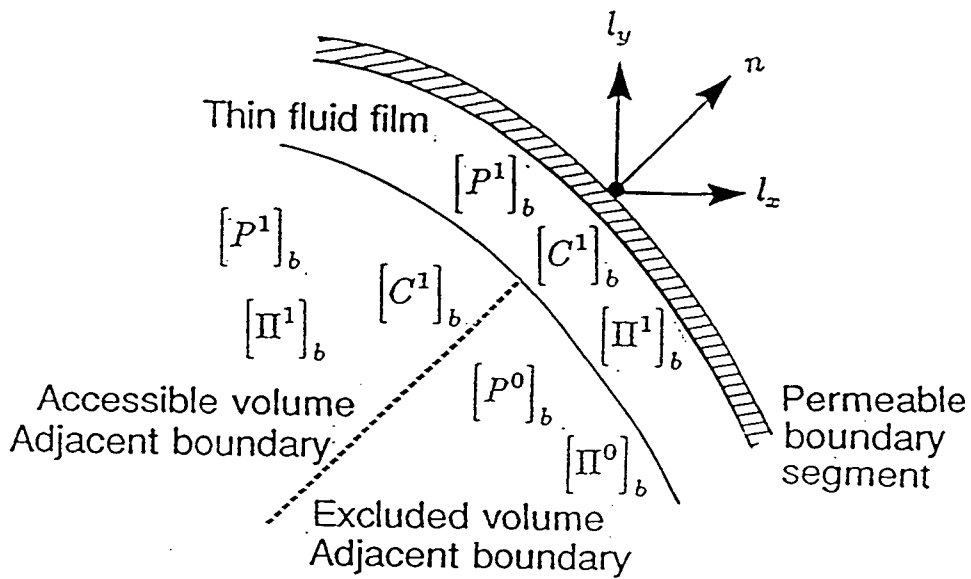
Figure 4.4: An elementary volume representing a point in the interstitial continuum adjacent a permeable boundary. The fluid film of infinitesimal thickness is in local equilibrium with the fluid in the accessible space at that point in the continuum. The vectors l_x and l_y represent the x and y components of the unit outward normal, n.

Fluid flow across a permeable boundary is described by Starling's Law. This is equated to the total fluid flux to the boundary from within the interstitium to give

$$-K^1 \left(\left[\frac{\partial(P^1 - \Pi^1)}{\partial x} \right]_b \cdot l_x + \left[\frac{\partial(P^1 - \Pi^1)}{\partial y} \right]_b \cdot l_y \right) =$$
$$L_p^b \left(\left[P^1 \right]_b - P^b - \sigma^b \left(\left[\Pi^1 \right]_b - \Pi^b \right) \right),$$ (4.13)

where L_p^b and σ^b are the hydraulic conductivity and reflection coefficient, respectively, of the boundary, while P^b and Π^b represent the hydrostatic and colloid osmotic pressures on the luminal side of the boundary.

Plasma protein exchange across a permeable boundary obeys the nonlinear flux equation [76, 71]. Equating the plasma protein flux across the boundary with the sum of the diffusive and convective protein fluxes through the available space to the boundary then gives

$$\left(\left[j_{w_x}^0 \right]_b \cdot l_x + \left[j_{w_y}^0 \right]_b \cdot l_y \right) \cdot \left(1 - \sigma^b \right) \cdot \left(\frac{[C^1]_b - C^b e^{(-Pe)}}{1 - e^{(-Pe)}} \right) =$$
$$-n^1 \cdot D_{eff} \left(\left[\frac{\partial C^1}{\partial x} \right]_b \cdot l_x + \left[\frac{\partial C^1}{\partial y} \right]_b \cdot l_y \right) \div$$
$$+ \xi \cdot \frac{K^1}{K^0} \left(\left[j_{w_x}^0 \right]_b \cdot l_x + \left[j_{w_y}^0 \right]_b \cdot l_y \right) \cdot \left[C^1 \right]_b,$$ (4.14)

where C^b is the plasma protein concentration on the luminal side of the boundary, and where Pe, the local Peclet number for the boundary, is defined by

$$Pe = \frac{\left([j_{w_x}^0]_b \cdot l_x + \left[j_{w_y}^0 \right]_b \cdot l_y \right) \cdot \left(1 - \sigma^b \right)}{D^b}.$$ (4.15)

D^b represents the boundary's permeability to plasma proteins.

The boundary conditions defined by Eqs. (4.13) and (4.14) assume that a thin fluid film exists between the boundary and the interstitial space (see Figure (4.4)) . This fluid is in local equilibrium with the interstitial fluid within the perivascular region of the accessible space, and is therefore at a hydrostatic pressure $[P^1]_b$ and protein concentration $[C^1]_b$. By this assumption we circumvent the need to distinguish between the transport properties of the boundary segment exposed to the accessible space from those of the boundary segment exposed to the excluded

space. It therefore represents a mathematical convenience rather than a physiological condition. However, since it is impossible to distinguish between these two segments when measuring the transport parameters for a given permeable boundary, Eqs. (4.13) and (4.14) are considered reasonable approximations to the conditions prevailing *in vivo* .

In the case of m different plasma protein species, it is assumed that the fluid film is in equilibrium with the material contained in the distribution volume m. Hence, the thin film concentration of each plasma protein species is equal to the concentration within that protein's distribution volume, C^k. The mathematical formulation is therefore consistent with the fact that it is the distribution volume concentration of a plasma protein species, and not the concentration based on the total fluid volume, that determines, for example, the interstitial osmotic pressure influencing fluid exchange across the capillary wall [26].

To minimize the number of independent parameters that must be evaluated in the numerical simulations, the equations governing fluid and protein transport are recast in dimensionless form. This is accomplished by introducing the following nondimensional parameters: $\tilde{P} = P/P^{art}$, $\tilde{C} = C/C^{art}$, $\tilde{\Pi} = \Pi/P^{art}$, $\tilde{x} = x/L$, $\tilde{y} = y/L$, $\tilde{H} = H/L$, $\alpha = (K^0 \cdot P^{art})/D_{eff}$, $\beta = K^1/K^0$, $\tilde{j}^0_{w_i} = j^0_{w_i}L/D_{eff}$, $\tilde{j}_{d_i} = j_{d_i}L/(D_{eff}C^{art})$, $\tilde{j}_{c_i} = j_{c_i}L/(D_{eff}C^{art})$, $\tilde{A}_1 = A_1 \cdot C^{art}/P^{art}$, $\tilde{A}_2 = A_2 \cdot (C^{art})^2/P^{art}$, $\tilde{A}_3 = A_3 \cdot (C^{art})^3/P^{art}$, $\tilde{L}^b_p = (L^b_p \cdot L)/K^0$, and $\tilde{D}^b = (D^b \cdot L)/D_{eff}$.

The governing equations and auxiliary relationships then take the following form.

1. Fluid transport within the interstitium:

$$\frac{\partial^2\left(\tilde{P}^1 - \tilde{\Pi}^1\right)}{\partial\tilde{x}^2} + \frac{\partial^2\left(\tilde{P}^1 - \tilde{\Pi}^1\right)}{\partial\tilde{y}^2} = 0, \qquad (4.16)$$

$$\tilde{\Pi}^1 = \tilde{A}_1 \cdot \tilde{C}^1 + \tilde{A}_2 \cdot \left(\tilde{C}^1\right)^2 + \tilde{A}_3 \cdot \left(\tilde{C}^1\right)^3, \qquad (4.17)$$

$$\tilde{j}^0_{w_i} = -\alpha\frac{\partial\left(\tilde{P}^1 - \tilde{\Pi}^1\right)}{\partial\tilde{x}_i}. \qquad (4.18)$$

2. Plasma protein transport within the interstitium:

$$n^1 \cdot \left[\frac{\partial^2\tilde{C}^1}{\partial\tilde{x}^2} + \frac{\partial^2\tilde{C}^1}{\partial\tilde{y}^2}\right] - \xi \cdot \beta \cdot \left[\tilde{j}^0_{w_x} \cdot \frac{\partial\tilde{C}^1}{\partial\tilde{x}} + \tilde{j}^0_{w_y} \cdot \frac{\partial\tilde{C}^1}{\partial\tilde{y}}\right] = 0, \qquad (4.19)$$

$$\tilde{j}_{c_i} = \xi \cdot \beta \cdot \tilde{j}^0_{w_i} \cdot \tilde{C}^1, \tag{4.20}$$

$$\tilde{j}_{d_i} = -n^1 \cdot \frac{\partial C^1}{\partial \tilde{x}_i}. \tag{4.21}$$

The boundary conditions are rewritten in dimensionless form as follows.

1. Conditions at a symmetry boundary or impermeable boundary:

$$\left[\frac{\partial\left(\tilde{P}^1 - \tilde{\Pi}^1\right)}{\partial \tilde{x}}\right]_b \cdot l_x + \left[\frac{\partial\left(\tilde{P}^1 - \tilde{\Pi}^1\right)}{\partial \tilde{y}}\right]_b \cdot l_y = 0, \tag{4.22}$$

$$\left[\frac{\partial \tilde{C}^1}{\partial \tilde{x}}\right]_b \cdot l_x + \left[\frac{\partial \tilde{C}^1}{\partial \tilde{y}}\right]_b \cdot l_y = 0. \tag{4.23}$$

2. Fluid flow across a permeable boundary:

$$-\left[\frac{\partial\left(\tilde{P}^1 - \Pi^1\right)}{\partial \tilde{x}}\right]_b \cdot l_x \div \left[\frac{\partial\left(\tilde{P}^1 - \Pi^1\right)}{\partial \tilde{y}}\right]_b \cdot l_y =$$
$$\tilde{L}^b_p \left(\left[\tilde{P}^1\right]_b - \tilde{P}^b - \sigma^b \cdot \left(\left[\tilde{\Pi}^1\right]_b - \tilde{\Pi}^b\right)\right). \tag{4.24}$$

3. Protein transport across a permeable boundary:

$$\left(1 - \sigma^b\right) \cdot \left(\left[\tilde{j}^0_{w_x}\right]_b \cdot l_x + \left[\tilde{j}^0_{w_y}\right]_b \cdot l_y\right) \cdot \left(\frac{\left[\tilde{C}^1\right]_b - \tilde{C}^b e^{(-\tilde{P}e^b)}}{1 - e^{(-\tilde{P}e^b)}}\right) =$$
$$\left(\left[\tilde{j}^0_{w_x} \cdot \beta \cdot \xi \cdot \tilde{C}^1\right]_b - n^1 \cdot \left[\frac{\partial \tilde{C}^1}{\partial \tilde{x}}\right]_b\right) \cdot l_x -$$
$$+ \left(\left[\tilde{j}^0_{w_y} \cdot \beta \cdot \xi \cdot \tilde{C}^1\right]_b - n^1 \cdot \left[\frac{\partial \tilde{C}^1}{\partial \tilde{y}}\right]_b\right) \cdot l_y, \tag{4.25}$$

$$\tilde{P}e^b = \left(1 - \sigma^b\right) \cdot \frac{\left(\left[\tilde{j}^0_{w_x}\right]_b \cdot l_x + \left[\tilde{j}^0_{w_y}\right]_b \cdot l_y\right)}{\tilde{D}^b}. \tag{4.26}$$

Equations (4.16) to (4.26) fully describe the system.

4.2 Case Studies

Values for the various system parameters are reported in Table (4.1), while Table (4.2) lists values for the corresponding dimensionless parameters used in the numerical simulations. The

values presented in Table (4.1) were drawn from the literature, where available. However, several of the variables had to be estimated, including the permeabilities of the vascular walls, D^{art} and D^{ven}, the plasma protein reflection coefficients, σ^{art} and σ^{ven}, the immobile fluid volume fraction, n^{im}, and the accessible volume fraction, n^1. In addition, values for the tissue dimensions, H and L, the mesothelial transport parameters, and the peritoneal fluid properties were assumed.

The permeabilities D^{art} and D^{ven} were assigned values of 2.4×10^{-8} cm/s and 3.6×10^{-6} cm/s, respectively, which lie within the range of capillary permeabilities to albumin reported for a variety of tissues (see [83]). Furthermore, these values were selected so that the ratio D^{art}/D^{ven} equaled the ratio L_p^{art}/L_p^{ven} reported for mesentery [39]. The protein reflection coefficients for the arteriolar and venular capillaries were both allotted a value of 0.85, which falls within the normal range reported for continuous capillaries (see [83]).

It was assumed that the principal component of the immobile fluid volume was the intrafibrillar water of the collagen. The immobile volume fraction was then calculated assuming that the specific volume of intrafibrillar water equalled 1.14 cm^3/gm of collagen [66], and that the volume fraction of collagen in mesentery equalled that found in subcutaneous tissue. This yielded a value of 0.128 for n^{im}. The accessible fluid volume fraction was assigned a value of 0.68, which lies within the range reported for albumin in skin (see [18]). Since , by definition, the sum of n^s, n^{im} and n^0 equals 1.0 (see Figure (4.3)), a value of 0.089 for n^s [66] implies that n^0 equals 0.783.

H was assumed to equal 3×10^{-3} cm, which is the same order of magnitude as the microvessels. L was assigned a value of 3×10^{-2} cm. The peritoneal fluid was assumed to be at atmospheric pressure, with a plasma protein content of 0.015 gm/cm^3. The transport parameters L_p^{mes}, D^{mes}, and σ^{mes} were varied to simulate three different boundary conditions along the mesothelium. In boundary condition 1, L_p^{mes} and D^{mes} were set to zero, thus describing an impermeable boundary. In boundary condition 2, L_p^{mes}, D^{mes}, and σ^{mes} were set equal to the corresponding parameters for the arteriolar capillary. Finally, in boundary condition 3, L_p^{mes}

and D^{mes} were assigned values 100 times greater than L_p^{art} and D^{art}, respectively, while σ^{mes} was assigned a value of zero, thereby reducing substantially the resistance of the mesothelium, compared to the resistances of the other two permeable boundaries.

According to Eqs. (4.18), and (4.20), the dimensionless parameters ζ and α are key to characterizing the interstitial transport of fluid and plasma proteins. The first of these, the convective hindrance, is a measure of the local convective velocity of the solute relative to the local fluid velocity (see Chapter 3). The parameter α, on the other hand, is a measure of the resistance of the interstitium to plasma protein diffusion, relative to its resistance to fluid flow. Together, these two parameters determine the relative role of convection and diffusion in transporting plasma proteins through the interstitium.

A series of numerical simulations were performed to investigate the coupled effects of ζ and α on microvascular exchange within the model tissue for each of the three mesothelial boundary conditions outlined above. For each boundary condition, ζ was assigned values of 1.0, 0.5, and 0.0, while α was given values of 9.117, 0.9117, and 0.09117, resulting in a $3 \times 3 \times 3$ factorial study. The results of the study are presented in Section 4.4.

4.3 Numerical Procedure

A form of the Finite Element Method using isoparametric elements [59] was used to solve the system of coupled partial differential equations presented in Section 4.1. The interstitial space was first divided into a set of rectangular subdomains of variable dimensions (see Figure (4.2)). To enhance the accuracy of the solution, the element size was reduced in the vicinity of the interstitial boundaries, where fluid pressure and solute concentration gradients were typically greatest. Associated with each element were eight nodes representing discrete locations within the domain. The dependent variables, $\bar{P}^1$ and $\bar{C}^1$, were approximated in each element by a set of biquadratic interpolating functions, which in turn depended on the nodal values of $\bar{P}^1$ and $\bar{C}^1$. By following the Galerkin procedure [59], the partial differential equations were reduced to a set of coupled algebraic expressions for these nodal values (see Appendix B for details). The

Parameter	Value	Tissue	Source
A_1	2.8×10^5 dyne $-$ cm/gm	plasma	[64]
A_2	2.1×10^6 dyne $-$ cm^2/gm^2	plasma	[64]
A_3	1.2×10^7 dyne $-$ cm^3/gm^3	plasma	[64]
C^{art}	0.06 gm/cm^3	human serum	[46]
C^{mes}	0.015 gm/cm^3	$-$	Assumed
C^{ven}	0.06 gm/cm^3	human serum	[46]
D^{art}	2.4×10^{-8} cm/s	$-$	See text
D^{mes}	$0 - 2.4 \times 10^{-6}$ cm/s	$-$	See text
D^{ven}	3.6×10^{-8} cm/s	$-$	See text
H	3.0×10^{-3} cm	$-$	Assumed
K^0	3.1×10^{-12} cm^4/(dyne $-$ s)	mesentery	[111] in [66]
L	3.0×10^{-2} cm	$-$	Assumed
L_p^{art}	1.35×10^{-9} cm^3/(dyne $-$ s)	mesentery	[39]
L_p^{mes}	$0 - 1.35 \times 10^{-9}$ cm^3/(dyne $-$ s)	$-$	See text
L_p^{ven}	2.02×10^{-9} cm^3/(dyne $-$ s)	mesentery	[39]
$n^1 \cdot D_{eff}$	6.8×10^{-8} cm^2/s	mesentery	[38]
n^{im}	0.128	subcutaneous	See text
n^s	0.089	subcutaneous	[66]
n^1	0.68	rabbit skin	[86] in [13]
P^{art}	2.942×10^4 dyne/cm^2	mesentery	[63]
P^{mes}	0.0 dyne/cm^2	$-$	Assumed
P^{ven}	1.667×10^4 dyne/cm^2	mesentery	[63]
Π^{art}	2.707×10^4 dyne/cm^2	$-$	Eq. (4.4) in text
Π^{mes}	0.472×10^4 dyne/cm^2	$-$	Eq. (4.4) in text
Π^{ven}	2.707×10^4 dyne/cm^2	$-$	Eq. (4.4) in text
σ^{art}	0.85	$-$	See text
σ^{mes}	$0 - 0.85$	$-$	See text
σ^{ven}	0.85	$-$	See text
ξ	$0.0 - 1.0$	$-$	See text

Table 4.1: **Values of model parameters assumed in the simulations.**

Parameter	Value
$\tilde{A}_1$	0.571
$\tilde{A}_2$	0.261
$\tilde{A}_3$	0.881
$\tilde{C}^{art}$	1.0
$\tilde{C}^{mes}$	0.25
$\tilde{C}^{ven}$	1.0
$\tilde{D}^{art}$	0.0072
$\tilde{D}^{mes}$	0. - 0.72
$\tilde{D}^{ven}$	0.0180
$\tilde{H}$	0.1
$\tilde{L}_p^{art}$	13.06
$\tilde{L}_p^{mes}$	0. - 1306.
$\tilde{L}_p^{ven}$	19.55
n^{im}	0.128
n^s	0.089
n^1	0.68
$\tilde{P}^{art}$	1.00
$\tilde{P}^{mes}$	0.00
$\tilde{P}^{ven}$	0.57
α	0.09117 - 9.117
β	0.87
$\tilde{\Pi}^{art}$	0.92
$\tilde{\Pi}^{mes}$	0.16
$\tilde{\Pi}^{ven}$	0.92
σ^{art}	0.85
σ^{mes}	0.00 - 0.85
σ^{ven}	0.85
ξ	0.0 - 1.0

Table 4.2: **Values of dimensionless parameters assumed in the simulations.**

system of algebraic equations was then solved using a banded matrix technique [100].

Because of their coupled nature, the fluid and protein material balance equations were solved iteratively. An initial guess of $\tilde{C}^1$ was used to calculate the local gradients in plasma protein osmotic pressure, by differentiating Eq. (4.17). The hydrostatic pressure distribution was then calculated using Eq. (4.16) and its corresponding boundary conditions. Using this solution of $\tilde{P}^1$ and Eq. (4.18), the local fluid fluxes throughout the interstitial space were determined. An updated estimate of $\tilde{C}^1$ was then obtained by solving Eq. (4.19), subject to the assigned concentration boundary conditions.

The iteration procedure was terminated when one of the following two criteria was met.

1. The change in the value of the dependent variables at each node during successive iterations satisfied the conditions

$$\left| \frac{\tilde{P}^1_{i,j} - \tilde{P}^1_{i-1,j}}{\tilde{P}^1_{i,max}} \right| < 10^{-5}, \tag{4.27}$$

and

$$\left| \frac{\tilde{C}^1_{i,j} - \tilde{C}^1_{i-1,j}}{\tilde{C}^1_{i,max}} \right| < 10^{-5}, \tag{4.28}$$

where $\psi_{i,j}$ denotes value of some variable ψ at node j, calculated in the ith iteration, and where $\psi_{i,max}$ represents the maximum nodal value of ψ from that iteration.

2. The total number of iterations exceeded 200.

In the latter case convergence was not achieved to within the specified tolerance, and the solutions were rejected. Under-relaxation techniques [24] were used where needed to achieve convergence. As an additional check of the numerical solution's accuracy, overall material balances were performed around the boundaries of the system. In all cases, the total inflow of fluid and plasma proteins equalled the total outflow, to within .005 percent. Finally, numerical tests were performed to determine the sensitivity of the solution to grid size. Increasing the grid density from 501 to 971 elements produced less than one percent change in the calculated fluid and protein exchanges across each of the permeable boundaries. Thus, all of the results presented in the next section were produced with a grid having 501 elements.

4.4 Results and Discussion

The large number of simulations performed makes it impractical to discuss each one in detail. Instead the following discussion focuses on selected examples of how the model can be used to investigate microvascular exchange in this system. The discussion is divided into four parts. In the first part we demonstrate with a specific example how the model can be used to predict fluid and plasma protein flow patterns and plasma protein transport mechanisms within the interstitium. The second part discusses the influence of ζ, α, and the mesothelial transport properties on the net fluid exchange across each of the permeable boundaries while the third part considers the influence of these parameters on net plasma protein exchange across the boundaries. In the final section we discuss the effects of ζ, α, and the mesothelial transport parameters on plasma protein distribution and transport within the interstitial space.

4.4.1 A Specific Case of Interstitial Transport

The analysis of fluid and plasma protein transport within the interstitium is complex, due to the coupled nature of the transport equations and the nonlinear effects arising from the osmotic activity of the interstitial plasma proteins. In the following discussion we will seek a mechanistic interpretation of the model predictions for the specific case where ζ equals 0.5, α equals 9.117, and the mesothelial transport properties are described by boundary condition 2. However, this interpretation is only possible with the detailed description of interstitial fluid and plasma protein flow patterns and plasma protein distribution afforded by the model itself; the results are not intuitively obvious.

The solution of Eqs. (4.16) and (4.19), with the appropriate auxiliary equations and boundary conditions, yields the steady-state distributions of both the dimensionless hydrostatic pressure, $\tilde{P}^1$, and the dimensionless plasma protein concentration, $\tilde{C}^1$, throughout the interstitial space. Combining this information with the expressions for the local interstitial fluid flux (Eq. (4.18)), the local convective protein flux (Eq. (4.20)) and the local diffusive protein flux (Eq. (4.21)) gives a complete description of fluid and plasma protein transport within the modelled

interstitium.

Figure (4.5) presents plots of the distribution in the interstitium of the dimensionless hydrostatic pressure and the dimensionless total plasma protein concentration, $\tilde{C}^t$, where

$$\tilde{C}^t = \frac{n^1}{(1 - n^s)} \cdot \tilde{C}^1, \tag{4.29}$$

i.e., the plasma protein concentration based on the total fluid volume. $\tilde{C}^t$ represents the concentration that would be calculated, for example, from measurements of fluid and plasma protein content within the interstitium using ultraviolet absorbance techniques. Figure (4.5) also contains a plot of the distribution of $\tilde{P}^1 - \tilde{\Pi}^1$, which is a measure of the local fluid chemical potential (see Eq. (3.12) in Chapter 3). In each plot the x/L axis corresponds to the symmetry boundary in Figure (4.2), while the y/L axis lies on the arteriolar capillary wall.

The concentration plot reveals a local ridge of high plasma protein content near the arteriolar capillary, and a trough near the venular capillary corresponding to a local region of low plasma protein concentration. As we will see, the profile is a direct consequence of the transport of fluid and plasma proteins from the arteriolar end of the interstitium into the peritoneal fluid and the entry of fluid and proteins from the peritoneum to the interstitium at the venular end of the system, together with the sieving properties of the mesothelium. $\tilde{P}^{mes} - \sigma^{mes} \cdot \tilde{\Pi}^{mes}$, is a measure of the driving force for fluid exchange at the mesothelium. Its value lies between $\tilde{P}^{art} - \sigma^{art} \cdot \tilde{\Pi}^{art}$ and $\tilde{P}^{ven} - \sigma^{ven} \cdot \tilde{\Pi}^{ven}$. Therefore, fluid entering the interstitium from the arteriolar capillary is drawn to the mesothelium due to the lower chemical potential of the peritoneal fluid, carrying with it plasma proteins. The plasma proteins are sieved at the mesothelium where their concentration builds up. At the venular end of the system, fluid is drawn into the interstitium from the peritoneum and then removed from the interstitium by the venular capillary. Again proteins are sieved at the mesothelium so that the fluid–plasma protein solution entering the interstitium is diluted somewhat, causing the local washout of proteins seen in the surface plot. Interstitial plasma proteins carried by the fluid to the venular capillary once again build up due to the sieving properties of this boundary. Hence, the peritoneum acts here as both an infinite source and an infinite sink for fluid and plasma proteins. A substantial portion of the fluid and

(i)

(ii)

(iii)
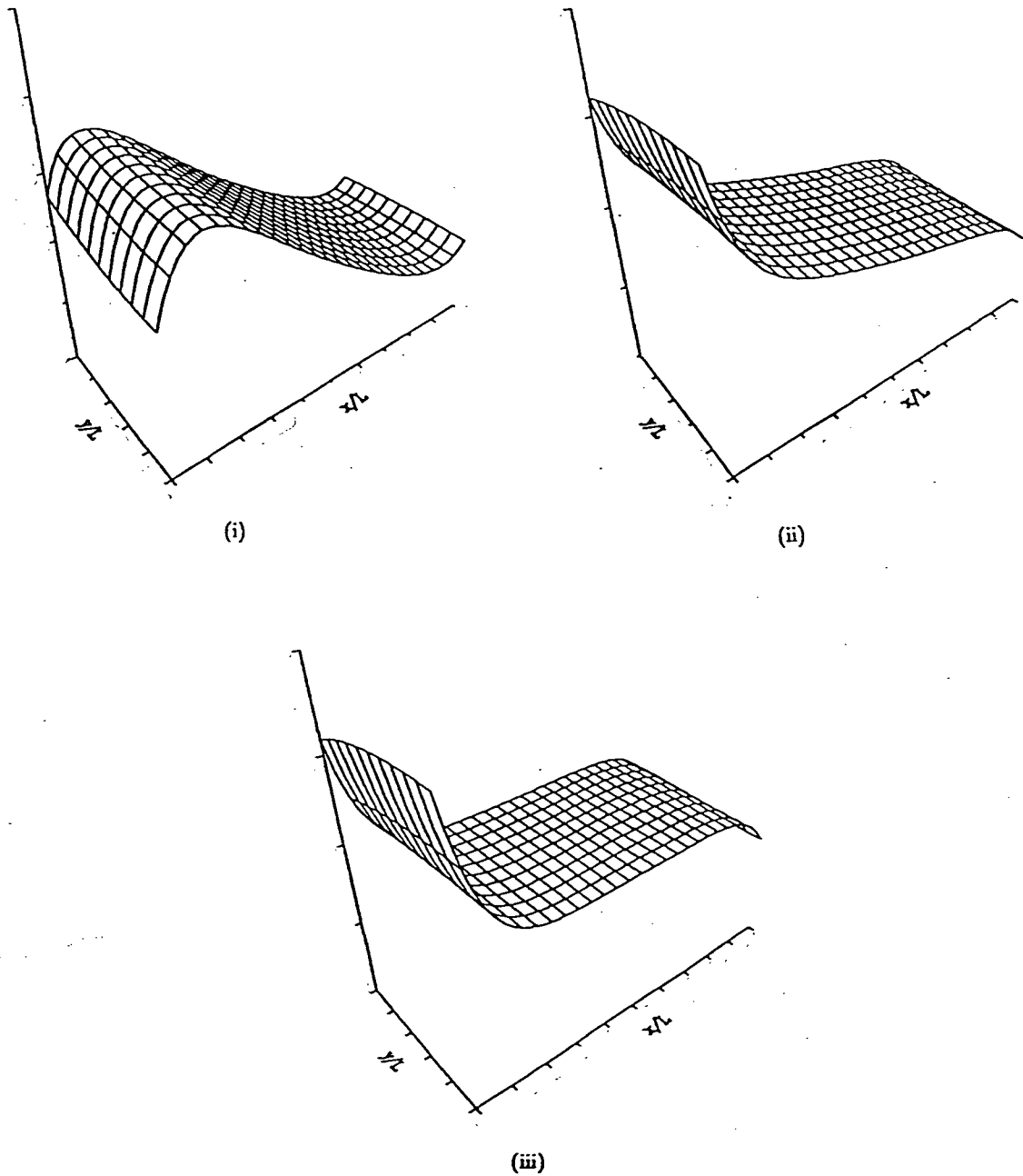
Figure 4.5: **Surface plots of the distribution of (i) dimensionless total concentration, (ii) dimensionless hydrostatic pressure, and (iii) dimensionless fluid chemical potential (expressed as an equivalent pressure, $P^1 - \Pi^1$) in the interstitium, for the case where $\xi = 0.5$, $\alpha = 9.117$, and the mesothelial transport properties are defined by boundary condition 2. The x/L axis represents the symmetry boundary, while the y/L axis lies on the arteriolar-end capillary boundary. Note that the tissue's aspect ratio, $\tilde{H}$, is exaggerated in these figures to provide greater detail.**

plasma proteins entering the interstitium from the arteriolar capillary are transported into the peritoneum at the arteriolar end of the system. Some fraction of this re-enters the interstitium in the vicinity of the venular capillary, bypassing the central region of the interstitium altogether.

The local gradient $\tilde{P}^1 - \tilde{\Pi}^1$ gives the driving force for fluid flow within the interstitium. Comparing the surface plots of $\tilde{P}^1$ and $\tilde{P}^1 - \tilde{\Pi}^1$ (Figures (4.5) (ii) and (iii), respectively), it is clear that the colloid osmotic pressure contributes significantly to the overall driving force for interstitial fluid transport. The local ridge of high plasma protein concentration in the vicinity of the arteriolar capillary creates a local minimum in fluid chemical potential there, while the region of low plasma protein content produces a local maximum in fluid chemical potential in the vicinity of the venular capillary. Therefore, while the gradients in fluid hydrostatic pressure would suggest a flow of fluid from the arteriolar end of the system to the venular end, the gradients in fluid chemical potential produce a complex recirculating flow pattern. This is illustrated in Figure (4.6) (i). However, since the fluid chemical potential varies only marginally in the central regions of the interstitium, the fluid flow associated with the recirculation is comparatively small. It is also apparent from these surface plots that, for this case at least, the gradients in the y-direction are small compared to those in the x-direction, indicating that the mesentery acts here as a one-dimensional tissue. In fact, this is investigated for all of the cases considered here in detail in Appendix A and taken advantage of in subsequent chapters.

The convective plasma protein flux pattern follows that of the fluid. However, the diffusive flux pattern must be calculated from the plasma protein concentration distribution using Eq. (4.21). The latter pattern, illustrated in Figure (4.6) (ii), reveals that the diffusive protein flux also recirculates. However, the diffusive flux often occurs in a direction opposite to the local convective plasma protein flux, particularly in the vicinity of the capillary boundaries. The sum of these two flow patterns gives the net protein flow pattern within the interstitium shown in Figure (4.6) (iii). The combined convective and diffusive patterns produce a net flow of plasma proteins from the arteriolar end of the system to the venular end. Note that the plasma protein transport characteristics could have been presented in terms of local Peclet numbers, given by
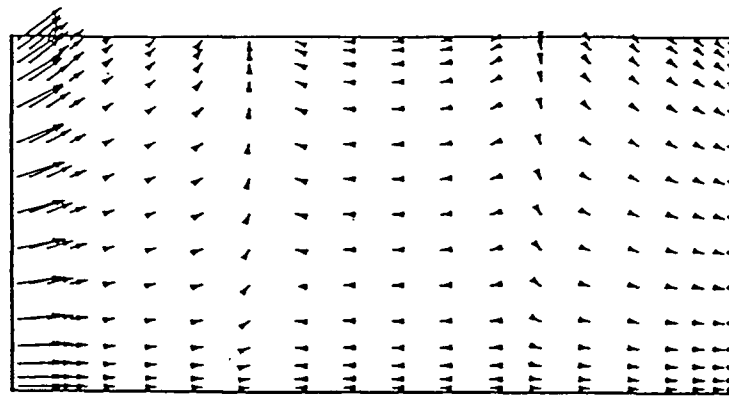
(i)
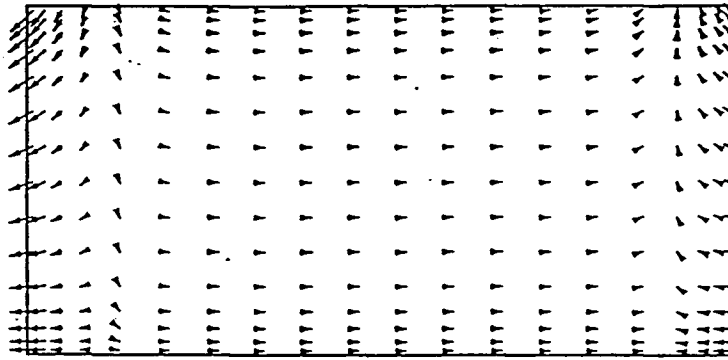
(ii)
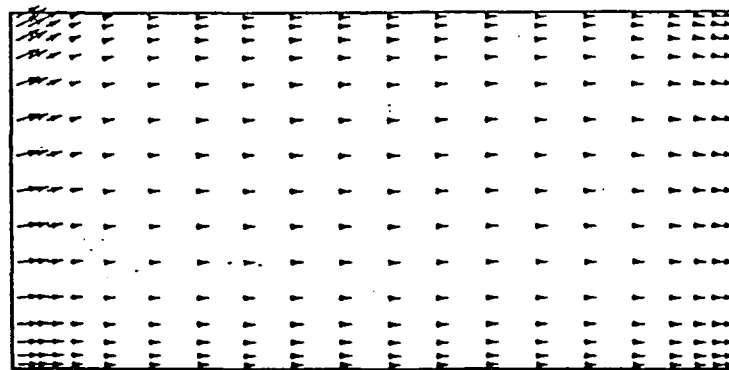
(iii)

Figure 4.6: **Flux patterns for the case where $\xi = 0.5$, $\alpha = 9.117$, and the mesothelial transport properties are defined by boundary condition 2.** Plot (i) shows the fluid flux pattern, or equivalently, the convective plasma protein flux pattern within the interstitial space. Plot (ii) is the diffusive flux, and plot (iii) illustrates the total (convective plus diffusive) plasma protein flux. The arrows show the local directions of the fluxes at the positions corresponding to their origins and their lengths are proportional to the magnitudes of the local flux vectors. Note that the tissue aspect ratio, $\bar{H}$, is exaggerated in these figures to provide greater detail.

the ratio of the magnitude of the local convective flux to the magnitude of the local diffusive flux. However, the Peclet number fails to account for direction. Therefore, in Figure (4.6), we have chosen to present the predicted flux patterns.

The opposing effects of the convective and diffusive plasma protein fluxes on the net protein transport are further illustrated in plots (iii) and (iv) of Figure (4.7). These panels of Figure (4.7) show, respectively, the local interstitial convective and diffusive plasma protein fluxes normal to the mesothelial boundary as a function of position, $\bar{x}$, along the mesothelium. At the arteriolar end of the boundary the convective flux transports plasma proteins to the mesothelium from within the interstitium, while the diffusive flux draws protein from the mesothelial boundary into the adjoining interstitial space. These trends are reversed near the venular end of the mesothelium. The lack of convective and diffusive protein transport to the mesothelium in the central portions of the boundary implies that these fluxes run parallel to the boundary in this region. The sum of the local convective and diffusive plasma protein fluxes normal to the mesothelium gives the net protein flux crossing the boundary, as a function of position $\bar{x}$ (see Figure (4.7) (ii)). For this particular case the magnitude of the normal interstitial convective plasma protein flux to the mesothelium is greater than that of the normal interstitial diffusive flux of plasma proteins from that boundary, resulting in a net transport of plasma proteins into the peritoneum. Associated with this steady-state condition, and as a result of the resistance of the mesothelial barrier to plasma protein transport, there is local high concentration of interstitial plasma proteins near the arteriolar end of the system, and a local dilution of plasma proteins near the venular end.

From the above example it is clear that transport within the system can be complex. In some cases this yields surprising behavior that could be subject to misinterpretation. Consider, for example, the fluid and plasma protein exchange across the mesothelial boundary when its transport properties are defined by boundary condition 2, with $\xi = 1.0$, and $\alpha = 9.117$. Panels (i) and (ii) of Figure (4.8) show these fluxes as a function of $\bar{x}$. Despite uniform mesothelial transport properties, there is a localized region of high fluid and plasma protein exchange,
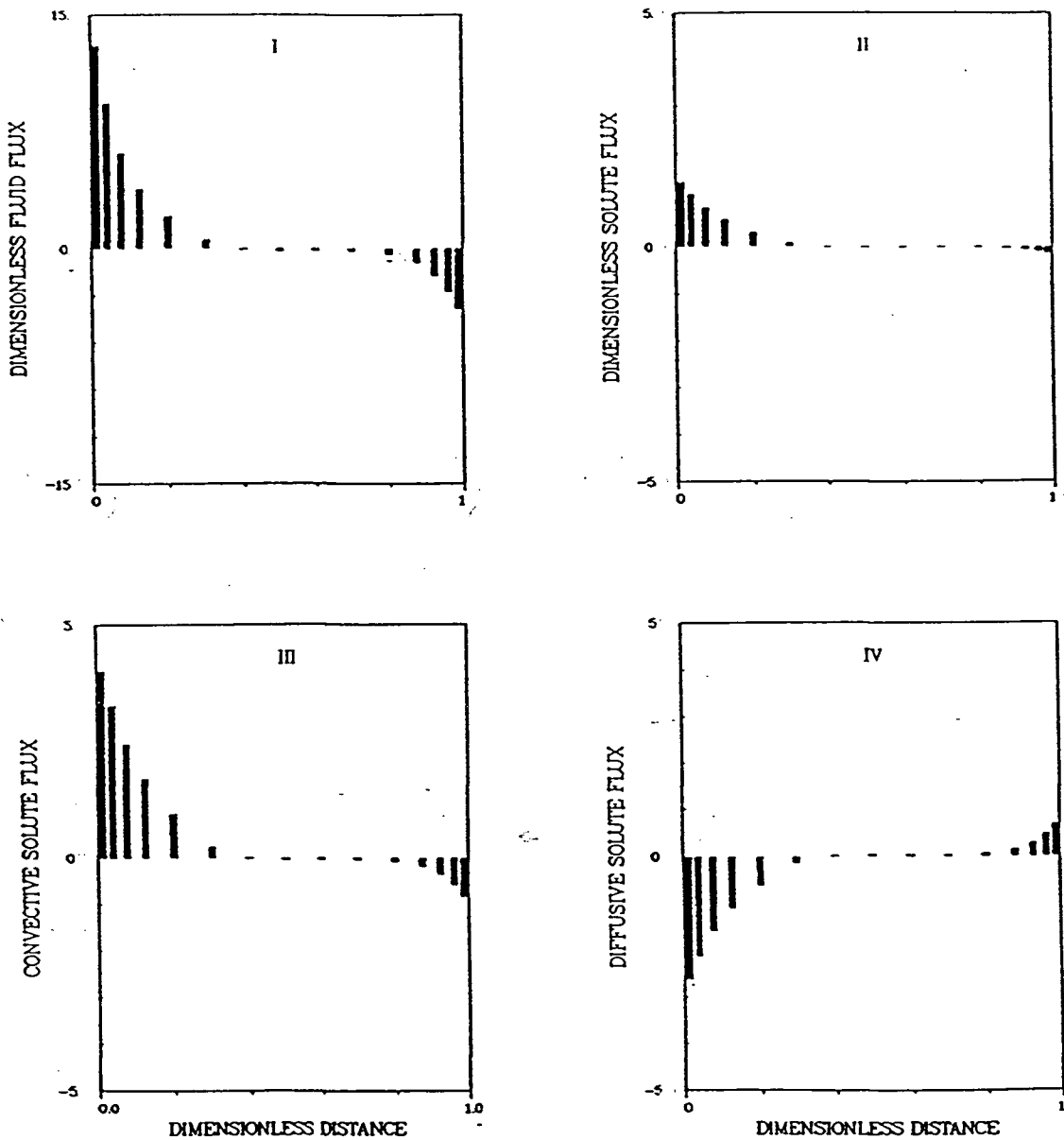
Figure 4.7: Panels (i) and (ii) represent local dimensionless fluid fluxes and plasma protein fluxes crossing the mesothelium, as a function of position along the boundary, when $\xi = 0.5$, $\alpha = 9.117$, and the mesothelial transport properties are given by boundary condition 2. Panels (iii) and (iv) show the local dimensionless convective protein flux and the local dimensionless diffusive protein flux reaching the mesothelium from within the adjacent regions of the interstitium. The sum of (iii) and (iv) yields the net protein flux crossing the mesothelium (panel (ii)). A negative value represents a flux directed into the interstitial space, while a positive quantity denotes a flux directed into the peritoneal fluid.

located at approximately $\bar{x} = 0.2$, that could be erroneously interpreted as a 'leaky site' in the mesothelial layer.

4.4.2 Fluid Exchange across the Boundaries of the Interstitium

Table (4.3) lists the average fluid fluxes crossing each of the permeable boundaries for the various cases studied. Note that, with $\xi = 1$, $\alpha = 9.117$, and the mesothelial transport properties defined by boundary condition 3, the simulation failed to converge to the required tolerances. Hence, no numerical results are reported for this case. (In fact, in this case the solution suffered from oscillations from one iteration to the next, suggesting that alternate choices for the relaxation parameters could possibly alleviate the problem.)

ξ	α	Boundary Condition 1			Boundary Condition 2			Boundary Condition 3		
		Art	Ven	Mes	Art	Ven	Mes	Art	Ven	Mes
1.0	0.09117	-0.04	0.04	—	-0.22	0.06	0.01	-0.31	0.09	0.01
1.0	0.9117	-0.40	0.40	—	-2.30	0.63	0.08	-2.87	0.65	0.11
1.0	9.117	-4.49	4.49	—	-25.16	6.84	0.92	No Convergence		
0.5	0.09117	-0.04	0.04	—	-0.22	0.06	0.01	-0.31	0.09	0.01
0.5	0.9117	-0.37	0.37	—	-2.26	0.61	0.08	-2.87	0.66	0.11
0.5	9.117	-4.30	4.30	—	-24.90	6.46	0.92	-26.14	2.47	1.18
0.0	0.09117	-0.03	0.03	—	-0.22	0.06	0.01	-0.31	0.09	0.01
0.0	0.9117	-0.34	0.34	—	-2.21	0.60	0.08	-2.86	0.66	0.11
0.0	9.117	-2.42	2.42	—	-20.20	5.70	0.72	-25.58	2.92	1.13

Table 4.3: **Average dimensionless fluid fluxes across permeable boundaries. A negative value indicates a flux entering the interstitium, while a positive value denotes a flux leaving the interstitial space.**

As seen in Table (4.3), an increase in α led consistently to an increase in the net fluid exchange across each of the permeable boundaries. For example, increasing α from 0.9117 to 9.117, with ξ equal to 0.5 and the mesothelial transport properties given by boundary condition 2, increases the fluid exchange across each of the permeable boundaries by an order of magnitude.

It should be noted that α, which is defined as $K^0 P^{art}/D_{eff}$, was increased by increasing the
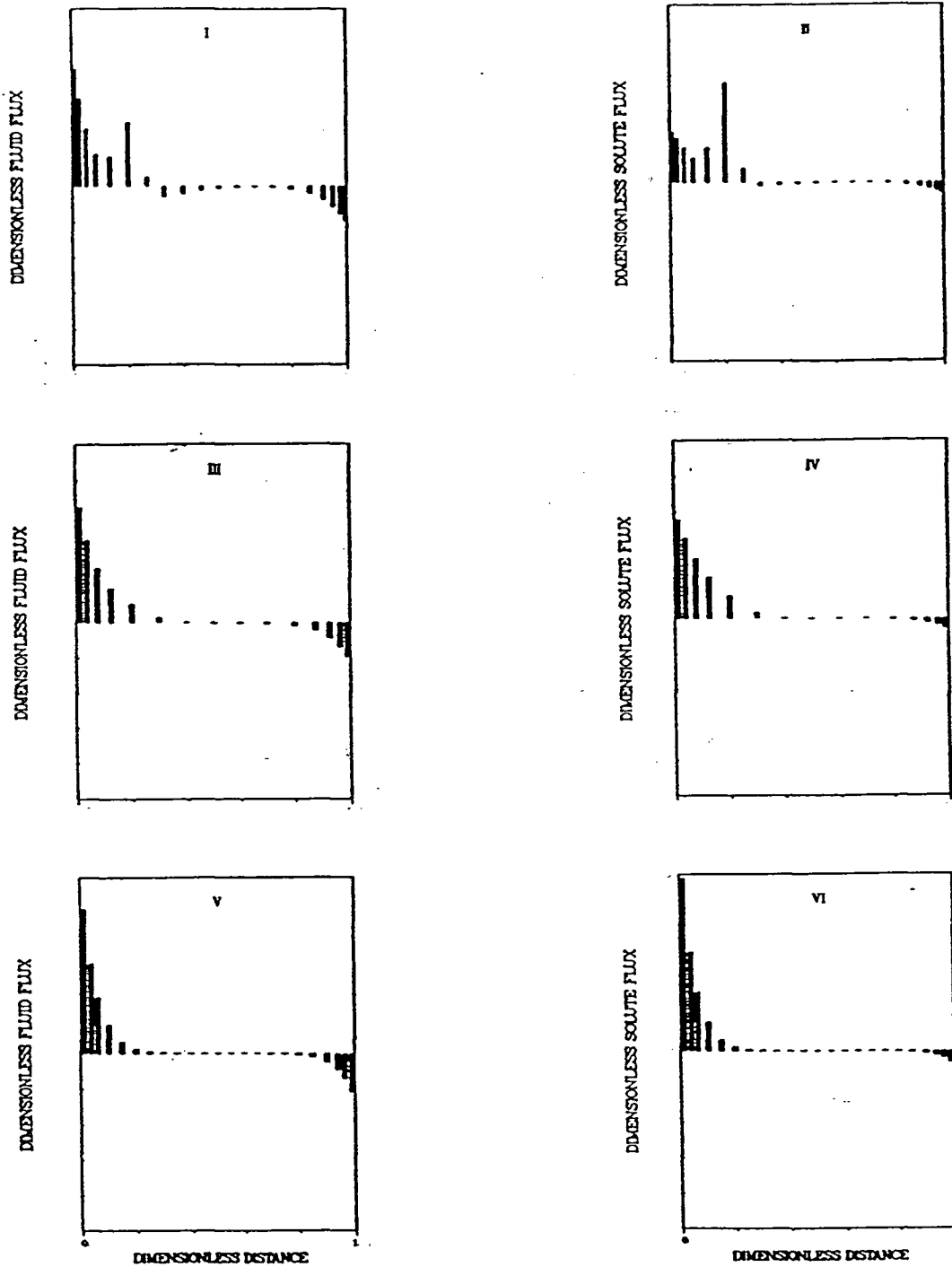
Figure 4.8: Comparison of the local dimensionless fluid fluxes and plasma protein fluxes as a function of position along the mesothelium for various values of ζ, assuming $\alpha = 9.117$, and the mesothelial transport properties are defined by boundary condition 2. In panels (i) and (ii) $\zeta=1.0$, in panels (iii) and (iv) $\zeta=0.5$, and in panels (v) and (vi) $\zeta=0.0$.

value of K^0. Furthermore, $\tilde{L}_p^b$ is defined as $L_p^b L/K^0$. To maintain $\tilde{L}_p^b$ constant, L_p^b was increased by a proportionate amount. The increase in fluid exchange accompanying an increase in α is therefore attributed to the enhanced fluid transport properties of both the interstitium and the permeable boundaries.

As previously mentioned, the fluid exchange rate within the system depends on the values of $\tilde{P}^b$ and $\tilde{\Pi}^b$, which are the driving forces, as well as the transport properties of each of the permeable boundaries. While ξ affects the plasma protein transport mechanisms within the interstitium it does not influence the transport properties of the permeable boundaries, nor does it alter the fluid chemical potential in the blood or the peritoneal fluid. In these cases, where the principal resistances to fluid flow are at the boundaries, a change in ξ generally had only a marginal effect on the net fluid exchange to or from the interstitium. However, ξ did influence substantially the distribution of fluid flux crossing the mesothelium, since it affected the distribution of interstitial plasma proteins and therefore the distribution of interstitial fluid chemical potential. This is illustrated in panels (i), (iii), and (v) of Figure (4.8), which show the distribution of fluid fluxes crossing the mesothelium when ξ equals 1.0, 0.5, and 0.0, respectively, for the case where α equals 9.117 and the mesothelial transport properties are defined by boundary condition 2.

Enhancing the transport characteristics of the mesothelium typically led to a moderate increase in fluid exchange across the arteriolar capillary, due to the increased capacity for the system to exchange fluid with the peritoneum. Consider, for example, the case where $\xi = 0.5$, and $\alpha = 0.9117$. Altering the mesothelial transport properties from those given by boundary condition 2 to those of boundary condition 3 increased the fluid flux across the arteriolar capillary from 2.26 to 2.87.

4.4.3 Plasma Protein Exchange across the Interstitial Boundaries

Table (4.4) reports the average plasma protein fluxes across the permeable boundaries for each of the 26 successful simulations. The enhanced fluid exchange associated with an increase

in α produced a concomitant increase in the convective plasma protein exchange across the permeable boundaries, thereby increasing the total exchange of plasma proteins within the system.

ξ	α	Boundary Condition 1			Boundary Condition 2			Boundary Condition 3		
		Art	Ven	Mes	Art	Ven	Mes	Art	Ven	Mes
1.0	0.09117	-0.005	0.005	—	-0.034	0.000	0.002	-0.046	0.001	0.002
1.0	0.9117	-0.060	0.060	—	-0.345	0.069	0.014	-0.430	0.029	0.020
1.0	9.117	-0.673	0.673	—	-3.774	0.396	0.169	No Convergence		
0.5	0.09117	-0.005	0.005	—	-0.034	-0.000	0.002	-0.046	-0.001	0.002
0.5	0.9117	-0.056	0.056	—	-0.339	0.064	0.014	-0.430	0.029	0.020
0.5	9.117	-0.645	0.645	—	-3.736	0.512	0.161	-3.920	0.130	0.189
0.0	0.09117	-0.005	0.005	—	-0.034	-0.000	0.002	-0.046	0.001	0.002
0.0	0.9117	-0.051	0.051	—	-0.332	0.060	0.014	-0.430	0.028	0.020
0.0	9.117	-0.364	0.364	—	-3.030	0.433	0.130	-3.840	0.144	0.184

Table 4.4: **Average dimensionless plasma protein fluxes across permeable boundaries. A negative value indicates a flux entering the interstitium, while a positive value denotes a flux leaving the interstitial space.**

Material balances dictate that the net amount of plasma proteins entering the venular capillary and the peritoneum must equal the net amount of plasma proteins entering the interstitium from the arteriolar capillary. In general the exchange of plasma protein across the arteriolar capillary was predominantly convective. Since ξ had negligible effect on the net fluid influx across the arteriolar boundary, it had little impact on the net amount of plasma proteins entering the system. However, since ξ had a strong influence on the distribution of fluid flux crossing the mesothelium, it also influenced the distribution of plasma protein fluxes crossing that boundary (see panels (ii), (iv), and (vi) of Figure (4.8)).

The influence of the mesothelium on net plasma protein exchange paralleled its influence on net fluid exchange across each of the permeable boundaries. For example, a change from boundary condition 2 to boundary condition 3, with $\xi = 0.5$ and $\alpha = 0.9117$, increased plasma protein exchange across the arteriolar capillary from 0.339 to 0.430. Again, this behavior is attributed to the increased capability of the interstitium to exchange material with the

peritoneum.

4.4.4 Interstitial Plasma Protein Convection, Diffusion, and Distribution

According to Eq. (4.20), interstitial plasma protein convection is directly proportional to the interstitial fluid flux available to transport proteins, as well as the local concentration of plasma proteins within the interstitium. Plasma protein diffusion, on the other hand, is proportional to the local gradient in plasma protein concentration (see Eq. (4.21)). Therefore, the influence of ξ, α, and the mesothelial transport properties on protein convection and diffusion within the interstitium will depend upon the effect of these parameters on each of the interstitial fluid flux, the local interstitial plasma protein concentration, and the interstitial plasma protein gradients.

Consider first the influence of the parameters on convective plasma protein transport. Since an increase in α typically enhanced fluid flow through certain regions of the interstitium (particularly in the vicinity of the arteriolar capillary), such a change promoted protein convection there. Likewise, reducing the resistance of the mesothelium to fluid and protein exchange increased fluid transport through these regions of the interstitial space. However, such a change also tended to decrease the average value of $\bar{C}^t$ within the entire interstitium (see Table (4.5)); i.e., as the resistance and plasma protein sieving properties of the mesothelium were decreased, the interstitial fluid composition approached that of the peritoneal fluid. For example, a change from boundary condition 2 to boundary condition 3, holding ξ and α constant at 0.5 and 0.9117 respectively, reduced the average value of $\tilde{C}^t$ within the interstitium from 0.54 to 0.18. (It is worth noting that those mean dimensionless interstitial concentrations in the range of 0.31 to 0.37 predicted by a number of the simulations agree closely with the typical value of 0.33 reported by Drake and Gabel [45].) The overall influence of the mesothelium on plasma protein convection therefore depended on the relative magnitudes of the two opposing effects of increased fluid flow and reduced interstitial plasma protein concentration. Finally, while ξ had only a limited influence on the magnitude of net exchange of fluid between the interstitium and the vascular system, it determined the degree of convective hindrance for plasma protein

transport (see Eq. (4.20)). It therefore played a key role in determining the degree of plasma protein convection within the interstitium.

ξ	α	Boundary Condition 1	Boundary Condition 2	Boundary Condition 3
1.0	0.09117	0.74	0.31	0.19
1.0	0.9117	0.61	0.55	0.18
1.0	9.117	0.24	0.37	No Convergence
0.5	0.09117	0.74	0.31	0.19
0.5	0.9117	0.69	0.54	0.18
0.5	9.117	0.42	0.54	0.19
0.0	0.09117	0.75	0.31	0.19
0.0	0.9117	0.77	0.53	0.18
0.0	9.117	0.95	0.52	0.20

Table 4.5: **Mean values for the total plasma protein concentration, $\tilde{C}^t$, for each of the simulations.**

The plot of $\tilde{C}^t$ (Figure (4.5) (i)) reveals comparatively small gradients in the $\bar{y}$ direction. This suggests that averaging the concentration in this dimension will still provide a reasonable picture of the plasma protein distribution within the interstitium. Furthermore, a $\bar{y}$-averaged profile approximates more closely the plasma protein distributions obtained experimentally using, for example, ultraviolet light absorbance techniques [40, 115]. We will therefore refer to these averaged profiles in our discussion of diffusion within the interstitial space.

The $\bar{y}$-averaged plasma protein concentration profile of each of the 26 cases is given in Figure (4.9). A single plot is reported for each of the nine possible combinations of ξ and mesothelial boundary conditions. Each plot contains up to three curves corresponding to the three values of α considered. Comparing plot (ii) to plot (iii), for example, it is evident that enhancing the transport properties of the mesothelium reduced the plasma protein concentration gradients within the central regions of the interstitium, suggesting reduced diffusion there. In Figure (4.9) (ii), with α equal to 9.117, the high convective flux of plasma proteins encountered a barrier at the mesothelium, creating a local buildup of proteins that promoted diffusion

towards the central portions of the interstitial space. As the mesothelium became more permeable to fluid and proteins, the plasma protein buildup was eliminated, and the diffusive flux was reduced, producing the corresponding profile in plot (iii).

A decrease in α promoted plasma protein diffusion relative to convection within the interstitium, since α is a measure of the resistance of the interstitium to diffusion relative to its resistance to fluid flow. Furthermore, a reduction in α resulted in less protein exchange across the permeable boundaries, as discussed earlier. The enhanced protein diffusivity, relative to fluid conductivity, and the reduced quantity of plasma proteins entering the interstitium caused a flattening of the interstitial plasma protein concentration profiles in all of the plots.

With ξ equal to zero, interstitial plasma protein transport was limited to diffusion alone (see Eq. (4.21)), so that the protein concentration profiles were often altered substantially from those in which protein convection occurred. For example, the local buildup of plasma proteins due to the high convective plasma protein flux to the mesothelium discussed earlier (see plots (ii) and (iv)) is absent in plot (viii) where plasma protein transport is by diffusion only.

It is not generally possible, however, to identify the dominant transport mechanism on the basis of the averaged concentration profile alone. Compare, for example, the curves in plot (vi), corresponding to a value of 0.5 for ξ to the curves in plot (ix) in which ξ equals 0.0. The curves closely resemble one another. However, in the former case, the ratio of the average interstitial plasma protein convective flux in the $\bar{x}$ direction to the diffusive flux in that direction ranges from 1.52 to 2.34 in the vicinity of the arteriolar capillary, indicating significant plasma protein convection in this region for all values of α considered (see Table (4.6)). In plot (ix), however, interstitial plasma protein transport is by diffusion alone.

Based on the above discussion, it is clear that no single parameter can be identified that fully characterizes fluid or plasma protein transport within the interstitium. It is the combined influence of the various transport parameters that determine the relative importance of interstitial plasma protein convection to diffusion. This is illustrated in Table (4.6). No clear
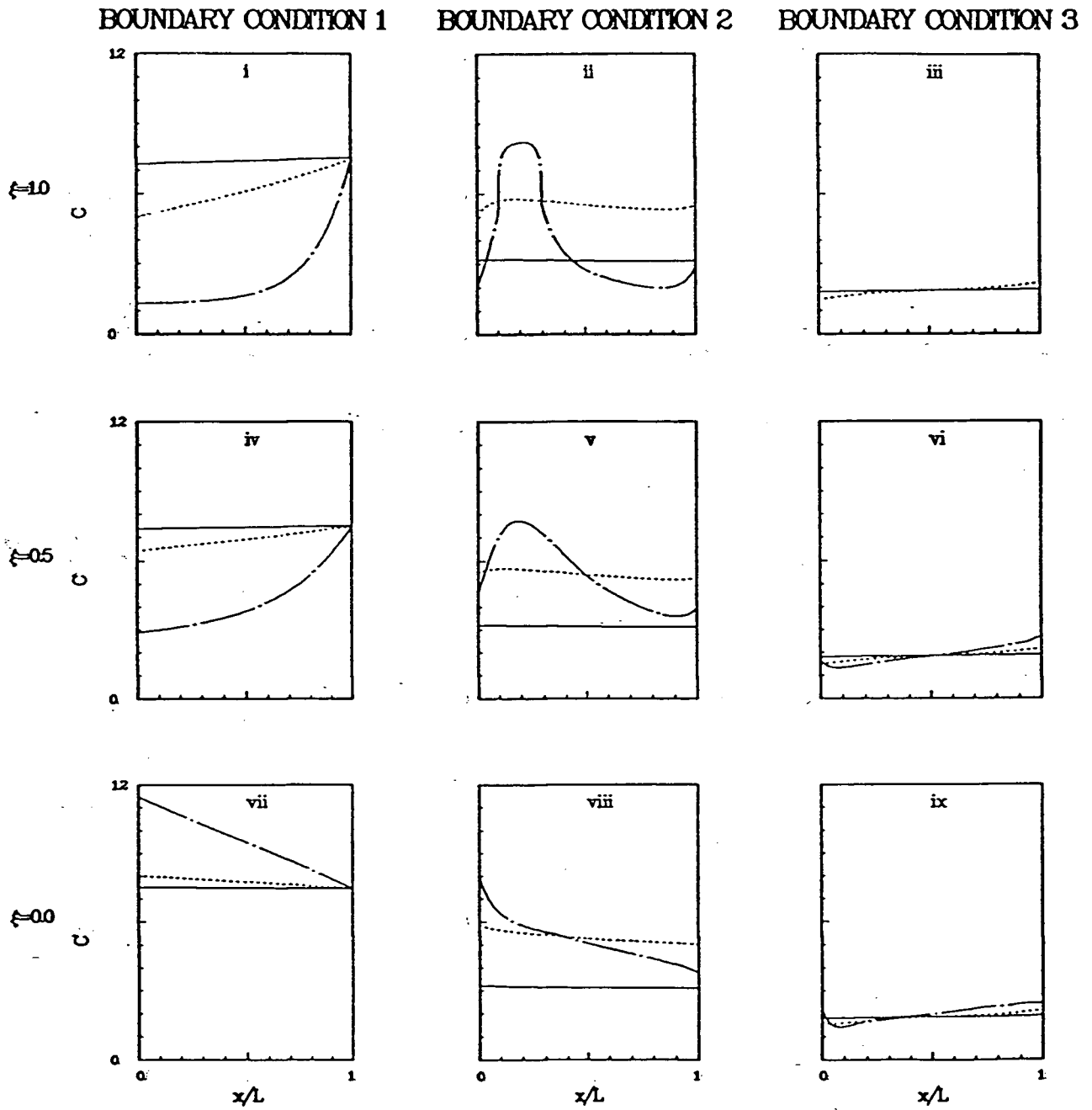
Figure 4.9: The thickness-averaged dimensionless total concentration, C^t/C^{art}, as a function of position, x/L. The nine plots correspond to the nine different combinations of boundary conditions (columns) and values of ξ (rows) studied. Each plot contains up to three curves corresponding to the three values of α considered (i.e., the solid line corresponds to α equal to 0.09117, the dotted line corresponds to α equal 0.9117, and the chain-dot line corresponds to α equal to 9.117).

ξ	α	Boundary Condition 1			Boundary Condition 2			Boundary Condition 3		
		Art	Ven	Mes	Art	Ven	Mes	Art	Ven	Mes
1.0	0.09117	-1.22	-1.21	—	-1.69	-0.99	-2.26	-3.54	-0.97	23.22
1.0	0.9117	-1.35	-1.21	—	-1.34	-1.21	-1.34	-7.89	-1.21	5.73
1.0	9.117	-64.51	-1.21	—	-2.71	-1.21	-1.23	No Convergence		
0.5	0.09117	-1.55	-1.53	—	-5.28	-0.98	9.16	2.34	-0.93	0.92
0.5	0.9117	-1.67	-1.53	—	-1.89	-1.53	-1.98	1.52	-1.53	0.75
0.5	9.117	-9.22	-1.53	—	-2.30	-1.53	-1.62	1.80	-1.53	0.71

Table 4.6: **Ratio of average plasma protein convection to average plasma protein diffusion normal to each of the permeable boundaries, evaluated in the interstitial space adjacent the respective boundaries. A negative values indicates that convection and diffusion are in opposite directions.**

trend appears relating the ratio of convective to diffusive protein transport to α, the mesothelial transport properties, and non-zero values of ξ. However, the data reported in Table (4.6) emphasize the importance of convection in the model's prediction of interstitial plasma protein transport for all cases in which ξ is non-zero.

Finally it is noted that, under certain circumstances, the local concentration of interstitial plasma proteins in the accessible space, $\tilde{C}^1$, exceeded that in the blood. Consider, for example, the case where $\alpha=9.117$, $\xi=1.0$, and the mesothelial transport properties are given by boundary condition 2. The buildup of plasma proteins at the mesothelium discussed earlier caused $\tilde{C}^t$ to reach a value of 0.8 at $\tilde{x}=0.2$, which corresponds to a value of 1.07 for $\tilde{C}^1$. A more dramatic concentrating effect was observed for the case where the mesothelium was assumed impermeable, α equalled 9.117, and ξ equaled 0 (corresponding to diffusion only within the interstitium). In this case the large convective flux of plasma proteins crossing the arteriolar capillary caused a buildup of protein in the interstitial space, until the plasma protein gradient was sufficient to transport proteins by diffusion at the same rate as they entered the interstitium at the arteriolar capillary.

4.4.5   Comparison of Model Predictions to Experimental Data

To date, there is little experimental data in the literature describing the distribution of native interstitial plasma proteins within a specific tissue. Recently, however, Friedman and Witte [40] measured the interstitial plasma protein concentration profile in rat mesentery. We will therefore refer to this data set in the following discussion. Furthermore, B.J. Barber of the University of Wisconsin has improved on the technique used by Friedman and Witte and is currently using it to determine plasma protein content and distribution within mesentery. It is therefore expected that even better data will be available in the near future.

Friedman and Witte employed ultraviolet light absorbance techniques and fluorescent tracers to determine local interstitial plasma protein content and interstitial fluid content, respectively, as a function of position in the ileal mesentery of the rat. A segment of the tissue bounded by arteriolar and venular microvessels was selected for study, where the distance separating the two vessels was approximately 295 μm.

The experimental determination of the local interstitial plasma protein content was based on the fact that aromatic amino acids have maximum light absorption at a wavelength of 280 nm and negligible absorption at 320 nm. Therefore, by performing two measurements of light absorbance using these wavelengths, the authors were able, in principle, to distinguish between the absorbance due to the interstitial plasma proteins the absorbance associated with other non-specific material. Local fluid volume was determined by measuring the light intensity from the fluorescent tracers (in this case, sodium and FITC-dextran) that distribute rapidly throughout the entire interstitial fluid volume. From the measurements of local plasma protein content and fluid content, and employing some simplifying assumptions regarding the geometry of the tissue (e.g., that the thickness of the mesenteric tissue segment is constant), the authors estimated the variation in the local concentration of interstitial plasma proteins (i.e., $\tilde{C}^t$) with position. The results of the experimental study are presented in Figure (4.10). Due to the considerable scatter in the data, the authors calculated two profiles based on the upper and lower limits in the scatter, as well as an average profile lying between these two limits. The top graph of

Figure (4.10) shows upper and lower bounds of the concentration profile associated with local fluctuations in the measurements, while the bottom graph plots the mean value of these two curves.

The boundary parameters and interstitial transport parameters of the model were adjusted to obtain a reasonable fit between the model predictions of $\bar{C}^t$ and the mean concentration profile shown in Figure (4.10). This was done for two different scenarios: one in which it was assumed that interstitial plasma protein transport occurs by diffusion alone (i.e., ξ equal to 0), and one in which both convection and diffusion take place (i.e., a non-zero value for ξ). In both cases, the parameter values were determined by trial-and-error using only a few iterations. A rigorous least-squares fit was not attempted. Hence, it is conceivabe that other choices of parameters might lead to even better agreement between model predictions and experimental data.

With ξ equal to zero, a reasonable match between the model predictions and experimental data was obtained by adjusting the following parameters as stated, keeping the other variables at their baseline values: $L_p^{art} = 1.5 \times 10^{-8} cm^3/(dyne\text{-}s)$, $L_p^{ven} = 3.0 \times 10^{-8} cm^3/(dyne\text{-}s)$, $L_p^{mes} = 1.0 \times 10^{-9} cm^3/(dyne\text{-}s)$, $\sigma^{art} = 0.85$, $\sigma^{ven} = 0.80$, $\sigma^{mes} = 0.70$, $P^{ven} = 2.207 \times 10^4 dyne/cm^2$, $C^{mes} = 3.0\ gm/dl$, $K^0 = 3.0 \times 10^{-11} cm^4/(dyne\text{-}s)$, and $D_{eff} = 2.0 \times 10^{-7} cm^2/s$. L_p^{art} and L_p^{ven} are therefore somewhat higher than reported for mesentery, but not outside the general range of values reported in the literature [71]. A similar profile could also be obtained assuming ξ equalled 0.35 and the assigning these same parameters the following values: $L_p^{art} = 1.4 \times 10^{-8} cm^3/(dyne\text{-}s)$, $L_p^{ven} = 1.6 \times 10^{-8} cm^3/(dyne\text{-}s)$, $L_p^{mes} = 5.0 \times 10^{-9} cm^3/(dyne\text{-}s)$, $\sigma^{art} = 0.75$, $\sigma^{ven} = 0.70$, $\sigma^{mes} = 0.51$, $P^{ven} = 2.207 \times 10^4 dyne/cm^2$, $C^{mes} = 3.6\ gm/dl$, $K^0 = 3.0 \times 10^{-11} cm^4/(dyne\text{-}s)$, and $D_{eff} = 1.0 \times 10^{-7} cm^2/s$. Again, while L_p^{art} and L_p^{ven} are elevated, they remain within the range reported in the literature. The arteriolar and venular capillary reflection coefficients, meanwhile, are somewhat lower than reported in the literature for mesentery. But again, the values lie within the range reported for single capillaries in frog mesentery, for example [71]. The resulting profiles for these two cases are compared to the experimental data
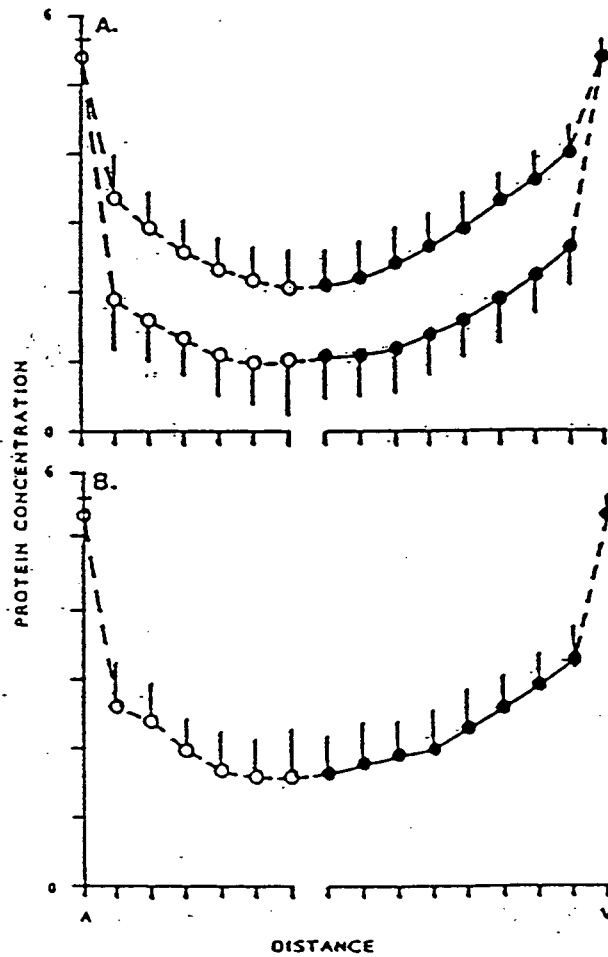
Figure 4.10: The upper graph shows the maxima and minima associated with the experimental determination of interstitial plasma protein concentration distribution in rat mesentery by Friedman and Witte [40]. The lower graph plots the average between these two.

in Figure (4.11).
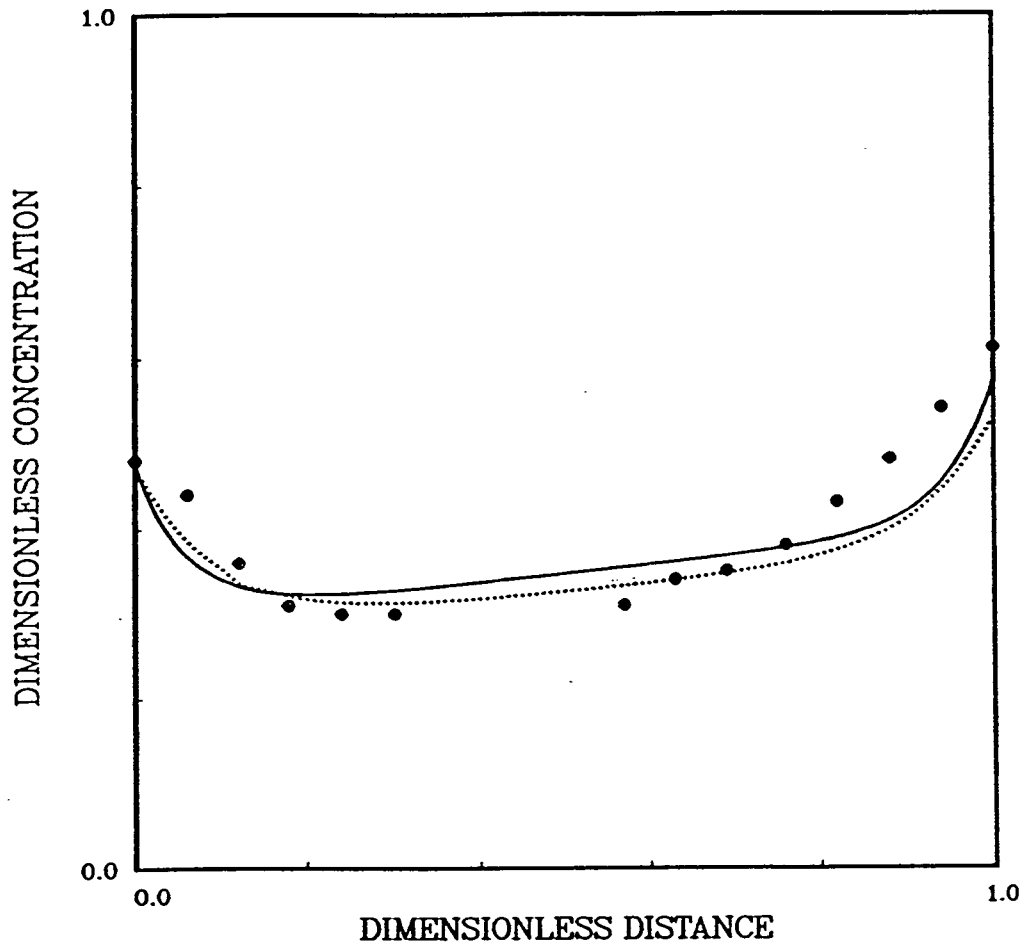
Figure 4.11: **The model predictions of $\tilde{C}^t$ assuming ξ is zero (solid line) and assuming ξ is 0.35 (dotted line) are compared here to the mean concentration profile determined by Friedman and Witte.**

In both cases, fluid and plasma proteins enter the interstitial space from the two vascular compartments and leave the interstitium via the mesothelium. Clearly, when ξ is zero, all plasma protein transport is by diffusion alone. However, when ξ is 0.35, there is substantial convective transport of plasma proteins within the interstitium. For example, the ratio of convection to diffusion at the arteriolar, venular and mesothelial boundaries is 3.36, 2.56, and

1.63 respectively. It is also interesting to note that neither of these scenarios agrees with Friedman's and Witte's interpretation of the data. These authors assumed that fluid and plasma proteins entered the interstitium across the arteriolar wall, some of the proteins then crossing the mesothelium to cause the local gradient in concentration near that vessel. However, in contrast to the model predictions, they further assumed that proteins were transported by convection to the venular vessel where they were reabsorbed into the blood.

It is clear from Figure (4.11) that reasonable agreement between experimental data of Friedman and Witte and model predictions is possible assuming drastically different interstitial plasma protein transport mechanisms. In both cases, however, the hydraulic conductivities of the vascular boundaries had to be increased by an order of magnitude, while decreasing the reflection coefficients for these vessels somewhat, to match the experimental data. More importantly (and contrary to opinions expressed by some [115, 74]), it is evident from this example that, without reasonable estimates of the transport properties of arteriolar, venular and mesothelial boundaries, one cannot draw definitive conclusions regarding interstitial plasma protein transport mechanisms from concentration profiles in mesentery.

4.5 Concluding Remarks

In the preceding sections we applied a simplified version of the general model of interstitial transport developed in Chapter 3 to study the influence of a number of transport parameters on microvascular exchange in mesentery. The analysis was limited in several respects. First, the simplified model failed to account for possible deformation resulting from pressure gradients within the interstitium. The extent to which this limits the analysis depends on the deformation characteristics of the mesentery, which remain poorly defined. Second, the study focussed on steady-state exchange only. Since the model considered only a single 'average' plasma protein species, it neglected the possible influence of several distinct plasma protein species on the overall exchange of fluid and proteins in the system. Thirdly, values for a number of the model parameters were unknown and had to be estimated from the best available data.

Finally, the largest fluid and plasma protein fluxes occurred in the vicinity of the arteriolar and venular capillaries, which were approximated by rectangular boundaries. The vessels' curvature may have to be considered to provide a more accurate description of fluid and plasma protein exchange in these regions.

The findings of the study are therefore hypothetical. However, several points are noted which warrant further attention. These are summarized below.

1. A recent experimental study of the movement of labelled albumin in rat mesentery suggests that convection plays a significant role in interstitial plasma protein transport [115, 74]. Our numerical investigation further suggests this even at reduced values of convective hindrance, ξ. Hence, diffusion models [38, 7] may represent an oversimplification of interstitial plasma protein transport in this tissue. However, the model also shows that steady-state interstitial plasma protein concentration profiles alone yield insufficient information to determine the principal mechanisms of plasma protein transport within the interstitium. In some cases where plasma protein transport was predominantly convective, the profiles are virtually indistinguishable from those in which plasma protein transport is purely diffusive. These profiles are strongly influenced by the transport properties of the mesothelium, for example. Further information about the mesothelium's exchange characteristics, as well as other system parameters, is needed to interpret interstitial plasma protein distribution data (see, for example, [40]).

2. Because it is influenced by osmotic as well as hydrostatic pressure gradients, the hydrodynamics within the interstitium can be quite complex, culminating, for some circumstances, in the recirculation of fluid within the interstitium. The hydrodynamics, in combination with the sieving properties of the bounding walls, can also result in irregularities in the distribution of fluid and plasma protein fluxes crossing a permeable boundary, such as the mesothelium, even when the boundary's transport properties are uniform. This could lead to the erroneous identification of 'leaky sites' within the system.

3. The colloid osmotic pressure gradients exert a strong influence on the flux patterns within the interstitium, suggesting that the Darcy expression evoked in a number of previous models [22, 36, 87], which considers hydrostatic gradients only, is inadequate for describing interstitial fluid transport.

The model presented here can be adapted readily to simulate microvascular exchange in a variety of tissues. The changes might include, for example, the addition of a lymphatic vessel as an interstitial boundary, the inclusion of multiple plasma protein species in the analysis, and extension to transient conditions. In fact these changes are incorporated into the model formulation in subsequent chapters. In this way the model provides a powerful tool to investigate microvascular exchange under transient conditions and for other tissue systems, providing insights into the behavior of the system that may not be identified readily in laboratory studies.

Chapter 5

Transient Exchange in Mesentery Following a Systemic Upset

In the previous chapter we studied the steady–state exchange of fluid and plasma proteins within a segment of mesentery as a function of interstitial transport mechanisms (i.e., restricted convection and molecular diffusion) and the transport properties of the mesothelial layer. In this chapter we will extend the analysis to consider the transient behavior of the system following a systemic perturbation. Specifically, we will look at exchange within the mesenteric slab in response to two different upsets: a sustained reduction in plasma protein concentration in the blood (i.e., *hypoproteinemia*), and a sustained elevation in systemic blood pressure (i.e., *venous congestion*). As before, the system response to these perturbations will be investigated as a function of mesothelial transport properties and interstitial transport mechanisms. Since the tissue segment is assumed to be rigid, however, edema formation will not be addressed here.

The remaining portion of this chapter is divided as follows. In Section 5.1 we present the transient version of the system equations. Section 5.2 specifies the cases making up the study, while Section 5.3 outlines the numerical procedures employed in the simulations. A discussion of the results is found in Section 5.4. Finally, Section 5.5 summarizes the findings of the investigation.

5.1 The Governing Equations

In Chapter 4 the mesentery was treated as a two-dimensional, rectangular slab. The results of that study suggested that, in many cases at least, the two–dimensional tissue could be adequately approximated by an equivalent one–dimensional system. This suspicion was further substantiated by a series of numerical experiments in which the simulations performed

in Chapter 4 were repeated assuming a one–dimensional mesentery. The development of the one–dimensional equations and the results of that analysis are presented in Appendix A. Based on those findings, all subsequent simulations have assumed the one–dimensional geometry.

Consider first the material balance equation for the interstitial fluid. Since the tissue is assumed to be rigid and the fluid is incompressible, the local interstitial fluid flux adjusts instantaneously to any changes that occur in the interstitial colloid osmotic pressure distribution. Hence, the interstitial fluid mass balance equation is the same as for the steady-state case. That is, the sum of the net local efflux of interstitial fluid, per unit volume of interstitium, and the net loss of interstitial fluid to the peritoneum, per unit volume of interstitium, must equal zero. Hence, for the one–dimensional mesentery we have

$$\frac{dj_w^0}{dx} + \frac{2}{H} \cdot j_w^{mes} = 0, \tag{5.1}$$

where j_w^0 is the local interstitial fluid flux at some point x in the system, H is the tissue thickness, and j_w^{mes} is the local fluid flux crossing either of the two mesothelial boundaries at that same point. (By virtue of the symmetry of the system, the fluid fluxes across the upper and lower mesothelial boundaries are identical.)

The local interstitial fluid flux is given by the extended Darcy expression:

$$j_w^0 = -K^0 \frac{d\left(P^1 - \Pi^1\right)}{dx}, \tag{5.2}$$

where, as before, the colloid osmotic pressure, Π^1, is related to the local interstitial plasma protein concentration, C^1, via a third-order polynomial. The fluid exchange rate between the interstitium and the peritoneum, meanwhile, is described by Starling's Law:

$$j_w^{mes} = L_p^{mes} \left[P^1 - P^{mes} - \sigma^{mes} \left(\Pi^1 - \Pi^{mes}\right)\right]. \tag{5.3}$$

Substituting Eqs. (5.2) and (5.3) into Eq. (5.1) gives the final form of the fluid mass balance equation:

$$\frac{d^2(P^1 - \Pi^1)}{dx^2} - \frac{2L_p^{mes}}{HK^0} \left[P^1 - P^{mes} - \sigma^{mes} \left(\Pi^1 - \Pi^{mes}\right)\right] = 0. \tag{5.4}$$

A material balance on the plasma proteins within a differential volume of interstitium under transient conditions gives the following:

$$\xi\,\beta\left[j_w^0 \cdot \frac{dC^1}{dx} - \frac{2}{H}C^1 j_w^{mes}\right] - n^1\frac{d^2C^1}{dx^2} + j_s^{mes} = -n^1\frac{\partial C^1}{\partial t}, \qquad (5.5)$$

where j_s^{mes} is given by the nonlinear flux equation, i.e.,

$$j_s^{mes} = (1 - \sigma^{mes}) \cdot j_w^{mes} \cdot \frac{[C^1 - C^{mes}\exp(-Pe^{mes})]}{[1 - \exp(-Pe^{mes})]}, \qquad (5.6)$$

Pe being the modified Peclet number given by Eq. (4.15) of Chapter 4. Substituting Eq. (5.6) into Eq. (5.5) then gives

$$\xi\,\beta\left[j_w^0 \cdot \frac{dC^1}{dx} - \frac{2}{H}C^1 j_w^{mes}\right] - n^1\frac{d^2C^1}{dx^2} +$$

$$+ \frac{2}{H}\cdot(1 - \sigma^{mes})j_w^{mes}\frac{[C^1 - C^{mes}\exp(-Pe^{mes})]}{[1 - \exp(-Pe^{mes})]} = -n^1\frac{\partial C^1}{\partial t}. \qquad (5.7)$$

The first set of terms of Eq. (5.7) found within the square brackets represents the net convective efflux of plasma proteins from a point within the interstitium, per unit volume of interstitial space, while the second term is the net diffusive efflux of proteins, per unit volume of interstitium (mechanical dispersion effects are neglected here). The third term represents the net loss of plasma proteins to the peritoneal fluid (j_s^{mes}), per unit volume of interstitium. The sum of these three terms equals the local net rate of decrease in interstitial plasma proteins per unit volume of interstitium, given by the right-hand-side of the equation.

Equations (5.4) and (5.7) must be combined with the pertinent set of boundary and initial conditions. The boundary conditions at the arteriolar and venular capillaries remain unchanged from the steady-state analysis, and so are given by Eqs. (4.13), (4.14), and (4.15) of Chapter 4. The initial conditions, meanwhile, can be calculated by solving the steady-state versions of the transport equations using appropriate boundary conditions.

The interstitial fluid and plasma protein mass balance equations are cast in dimensionless form using the same set of dimensionless groups as before, along with the dimensionless time, $\bar{t}$, equal to $t\,D_{eff}/L^2$. The fluid mass balance equation then becomes

$$\frac{d^2(\tilde{P}^1 - \tilde{\Pi}^1)}{d\tilde{x}^2} - \frac{2}{\tilde{H}}\tilde{L}_p^{mes}\left[\tilde{P}^1 - \tilde{P}^{mes} - \sigma^{mes}\left(\tilde{\Pi}^1 - \tilde{\Pi}^{mes}\right)\right] = 0. \qquad (5.8)$$

The plasma protein mass balance equation, meanwhile, is given by

$$\xi \cdot \beta \cdot \left[\tilde{j}_w^0 \cdot \frac{d\tilde{C}^1}{d\tilde{x}} - \frac{2}{\tilde{H}} \cdot \tilde{j}_w^{mes} \cdot \tilde{C}^1 \right] - n^1 \cdot \frac{d^2\tilde{C}^1}{d\tilde{x}^2} +$$

$$+ \frac{2}{\tilde{H}} \cdot (1 - \sigma^{mes}) \cdot \tilde{j}_w^{mes} \cdot \frac{\left[\tilde{C}^1 - \tilde{C}^{mes} \exp(-\tilde{P}e^{mes}) \right]}{\left[1 - \exp(-\tilde{P}e^{mes}) \right]} = 0, \qquad (5.9)$$

where $\tilde{P}e^{mes}$ is given by Eq. (4.26), and where $\tilde{j}_w^{mes}$ is

$$\tilde{j}_w^{mes} = \alpha \cdot \tilde{L}_p^{mes} \left[\tilde{P}^1 - \tilde{P}^{mes} - \sigma^{mes} \left(\tilde{\Pi}^1 - \tilde{\Pi}^{mes} \right) \right]. \qquad (5.10)$$

This completes the mathematical formulation of the transient mass balance equations.

5.2 Case Studies

As was mentioned at the beginning of this chapter, two systemic perturbations were simulated, namely the case of sustained hypoproteinemia and that of sustained venous congestion. These two upsets are discussed below.

Hypoproteinemia Hypoproteinemia is characterized by a drop in the plasma protein concentration within the blood. In the simulations presented here, it was assumed that C^{art} and C^{ven} fell instantaneously to 50 % of their original value (that is, from 6 gm/dl to 3 gm/dl). C^{mes}, on the other hand, was kept at its original value of 1.5 gm/dl. While an instantaneous drop in plasma protein content is not representative of a typical pathological state, it does provide a reasonable starting point for simulating the effects of a injection of saline into the vascular system, for example, provided that the time course for the injection is much shorter than the response time of the system.

Venous Congestion The arteriolar and venular capillary pressures can be related to the venous and arterial blood pressures (P^{VEN} and P^{ART}, respectively) through the following resistance relationships [108]:

$$P^{art} = P^{VEN} + k_1 \left(P^{ART} - P^{VEN} \right), \qquad (5.11)$$

$$P^{ven} = P^{VEN} + k_2 \left(P^{ART} - P^{VEN} \right), \tag{5.12}$$

where k_1 and k_2 are the fractions of the systemic resistances associated with the branch of the blood vasculature from the arteriolar end of the network to the heart and from the venular end of the network to the heart, respectively. Given that, in the simulations, P^{art} equals 2.942×10^4 dyne/cm^2 (22 mmHg) while P^{ven} equals 1.667×10^4 dyne/cm^2 (12.5 mmHg), and assuming that P^{ART} and P^{VEN} are 1.337×10^5 dyne/cm^2 (100 mmHg) and 1.605×10^4 dyne/cm^2 (12 mmHg), respectively, [108], then k_1 becomes 0.1136 while k_2 assumes a value of 0.0057.

During venous congestion, P^{VEN} is elevated. This results in an increase in both P^{art} and P^{ven} according to Eqs. (5.11) and (5.12). In the venous congestion case studies it is assumed that P^{VEN} increases to 3.342×10^4 dyne/cm^2 (25 mmHg), raising P^{art} and P^{ven} to 4.4825×10^4 dyne/cm^2 (33.52 mmHg) and 3.400×10^4 dyne/cm^2 (25.43 mmHg), respectively. Hence the arteriolar capillary pressure increases by 52 % of its original value, while the venular capillary pressure increases by 103 % of its baseline value. Again, it is assumed that these shifts in hydrostatic pressures occur instantaneously, so that the simulations provide only a first approximation to the onset of venous congestion.

Computer Simulations The three different mesothelial boundary conditions described in Chapter 4 were simulated to determine the influence of this boundary on the transient response of the system to each of the two systemic perturbations cited above. In addition, the plasma protein convective hindrance was varied to consider two extreme cases of interstitial plasma protein transport: pure diffusion (ξ equal to 0), and full convection (ξ equal to 1). All other system parameters were maintained at their baseline values during the simulations. Hence α, for example, remained 0.9117. These alterations in ξ and the mesothelial transport properties resulted in a 2 × 3 factorial study for each of the perturbations considered.

Finally, it is noted that the initial conditions of each of the simulations were calculated from the steady–state model, assuming pre-perturbation conditions, while the final steady-state conditions were determined using the same model and assuming the perturbed conditions

prevailed.

5.3 Numerical Procedures

As before, the finite element method was used to reduce the fluid mass balance equation to a set of coupled, algebraic expressions that could be solved iteratively using matrix techniques. The interstitial plasma protein mass balance equation, however, contains both spatial and temporal terms. In this case the finite element method was applied to the spatial terms of the equation, while a Crank-Nicolsen finite difference scheme was used to approximate the temporal term. A detailed discussion of this combined technique, as it applies to the plasma protein mass balance equation, can be found in Appendix B.

The interstitial plasma protein concentration distribution and the interstitial hydrostatic pressure field were determined using the following iterative procedure. A fully explicit finite difference formulation was used to obtain a first estimate of the plasma protein concentration distribution at some time $\Delta \bar{t}$ after initiation of the system upset, using the specified initial conditions. This initial estimate of $\bar{C}^1$ was used to update the hydrostatic pressure distribution, $\bar{P}^1$, using the finite element formulation. Having an estimate of both $\bar{C}^1$ and $\bar{P}^1$ at the new time, the Crank-Nicolsen finite difference scheme could then be used during subsequent iterations at this same time step to obtain new estimates of $\bar{C}^1$ at $\Delta \bar{t}$. Upon each iteration, the appropriate finite element matrices and vectors were revised to reflect the updated estimates of the plasma protein concentration distribution and hydrostatic pressure field. The iterative procedure was repeated until the convergence requirements outlined in Section 4.3 of Chapter 4 were met. This overall process was repeated at each new time step to determine the plasma protein concentration distribution and hydrostatic pressure field as functions of space and time. Typically, the system required less than 10 iterations to achieve convergence at any one time-step.

The simulation specifications were as follows. The domain was divided into 25 quadratic elements (i.e., each element contained 3 nodes) to give a total of 51 nodes within the one-dimensional tissue space. This choice of step size was based on the favourable results of the

one-dimensional simulations performed in Appendix A. Lagrange basis functions were used to approximate the spatial variations of $\tilde{C}^1$ and $\tilde{P}^1$. The initial time-step size was chosen so that the Courant number did not exceed a specified value (see Section B.4 in Appendix B for details). For a number of cases, the value of the initial Courant number was varied over a range of values from 0.0001 to 0.01 to assure a consistent estimate of the dependent variables. The validity of the transient simulations was further confirmed by allowing selected simulations to reach steady–state. These estimates of the new system steady–state conditions were then compared to the steady–state conditions calculated by the one–dimensional steady–state simulator. In all cases, the two predictions showed excellent agreement.

5.4 Results and Discussion

We will now consider, individually, the results of the transient simulations of hypoproteinemia and venous congestion. In each case we will address the effects of the mesothelial transport properties and the interstitial transport mechanisms on the transient exchange of fluid and plasma proteins within the system, as well as their effect on the distribution of interstitial plasma proteins over time.

5.4.1 Transient Exchange in Sustained Hypoproteinemia

The transient exchange rates of fluid and plasma proteins and the changes in interstitial plasma protein distribution within the mesenteric tissue segment following a drop in the vascular plasma protein content are all affected by the transport properties of the mesothelial layer and the mechanisms governing interstitial plasma protein transport. However, before discussing how these factors influence the behavior of the system during hypoproteinemia, it seems appropriate to consider briefly the effect that this perturbation has on the overall driving forces for fluid and plasma protein exchange within the system.

The Effect of Hypoproteinemia on Luminal Driving Forces

The overall driving forces for the exchange of fluid and plasma proteins within the model tissue consist of the differences in the effective fluid chemical potential and plasma protein concentration, respectively, between each of three luminal fluids in the system (i.e., the arteriolar capillary fluid, the venular capillary fluid, and the peritoneal fluid). Clearly, a drop in plasma protein content in the blood reduces the overall driving force for diffusive exchange of plasma proteins in the system. Likewise, this reduction in vascular protein content would tend to reduce the net convective exchange of plasma proteins, since less protein would accompany the fluid transported across the vascular boundaries. However, the convective transport of plasma proteins, and hence the total exchange of proteins, also depends on the total volume of fluid exchanged between the various luminal compartments. Hence, we must also consider how the lower vascular plasma protein concentration impacts on the driving forces for fluid exchange within the tissue segment.

The dimensionless effective fluid chemical potential of the luminal fluid associated with a permeable boundary b, $\tilde{\mu}_{\text{eff}}^{\text{b}}$, is given by $\tilde{P}^{\text{b}} - \sigma^{\text{b}} \tilde{\Pi}^{\text{b}}$. Following a drop in protein concentration in the plasma, the effective plasma protein osmotic pressure, $\sigma^{\text{b}} \tilde{\Pi}^{\text{b}}$, decreases by an equal amount in both the arteriolar and the venular capillary. The effective colloid osmotic pressure of the peritoneal fluid, however, remains unchanged. Hence, following the drop in plasma protein concentration in the blood, $\tilde{\mu}_{\text{eff}}^{\text{art}}$ increases from 0.218 to 0.692, $\tilde{\mu}_{\text{eff}}^{\text{ven}}$ increases from -0.215 to 0.259, and $\tilde{\mu}_{\text{eff}}^{\text{mes}}$ remains -0.136 for boundary condition 2 and 0 for boundary condition 3.

The overall driving force for the exchange of fluid from one luminal compartment to another is given by the difference in the effective fluid chemical potential between the two compartments. Table (5.1) lists these for the various pairs of compartments. The following general observations are made.

1. While both $\tilde{\mu}_{\text{eff}}^{\text{art}}$ and $\tilde{\mu}_{\text{eff}}^{\text{ven}}$ increase, the difference between the two, $\tilde{\mu}_{\text{eff}}^{\text{art}} - \tilde{\mu}_{\text{eff}}^{\text{ven}}$, remains unchanged from pre-perturbation to post-perturbation in all cases.

State	Boundary Condition 1	Boundary Condition 2			Boundary Condition 3		
	$\bar{\mu}_{\text{eff}}^{\text{art}} - \bar{\mu}_{\text{eff}}^{\text{ven}}$	$\bar{\mu}_{\text{eff}}^{\text{art}} - \bar{\mu}_{\text{eff}}^{\text{ven}}$	$\bar{\mu}_{\text{eff}}^{\text{art}} - \bar{\mu}_{\text{eff}}^{\text{mes}}$	$\bar{\mu}_{\text{eff}}^{\text{ven}} - \bar{\mu}_{\text{eff}}^{\text{mes}}$	$\bar{\mu}_{\text{eff}}^{\text{art}} - \bar{\mu}_{\text{eff}}^{\text{ven}}$	$\bar{\mu}_{\text{eff}}^{\text{art}} - \bar{\mu}_{\text{eff}}^{\text{mes}}$	$\bar{\mu}_{\text{eff}}^{\text{ven}} - \bar{\mu}_{\text{eff}}^{\text{mes}}$
Pre-Upset	0.433	0.433	0.354	-0.079	0.433	0.218	-0.215
Post-Upset	0.433	0.433	0.828	0.395	0.433	0.692	0.259

Table 5.1: **Fluid chemical potential differences between the various luminal compartments before and after the initiation of hypoproteinemia.**

2. The magnitude of $\bar{\mu}_{\text{eff}}^{\text{art}} - \bar{\mu}_{\text{eff}}^{\text{mes}}$ increases in all cases where the mesothelium is permeable.

3. $\bar{\mu}_{\text{eff}}^{\text{ven}} - \bar{\mu}_{\text{eff}}^{\text{mes}}$ also increases in all cases where the mesothelium is permeable. Furthermore, $\bar{\mu}_{\text{eff}}^{\text{ven}} - \bar{\mu}_{\text{eff}}^{\text{mes}}$ changes from a negative value to a positive value in each of these cases.

We will return to these general observations in later discussions of fluid and plasma protein exchange during hypoproteinemia.

Mass Exchange Assuming an Impermeable Mesothelial Layer

Fluid Exchange The transient fluid exchange rates across the arteriolar boundary, for those cases in which the mesothelium is impermeable, are illustrated in Figure (5.1). Since the tissue segment and fluid are both incompressible, the fluid exchange at the venular boundary is equal in magnitude to that at the arteriolar boundary, and hence is not shown. The net driving force for fluid exchange within the system is $\bar{\mu}_{\text{eff}}^{\text{art}} - \bar{\mu}_{\text{eff}}^{\text{ven}}$. As mentioned earlier, this quantity remains unaffected by the drop in vascular plasma protein content. In addition, because the mesothelium is impermeable, fluid entering the interstitium from one vascular compartment must pass through the entire interstitial space before re-entering the blood at the other end of the tissue segment. Therefore, the overall effective hydraulic resistance of the system remains constant and equal to the sum of the two vascular wall resistances and the total resistance associated with the interstitial space.

Given this, one would expect no change in fluid exchange within the system following the
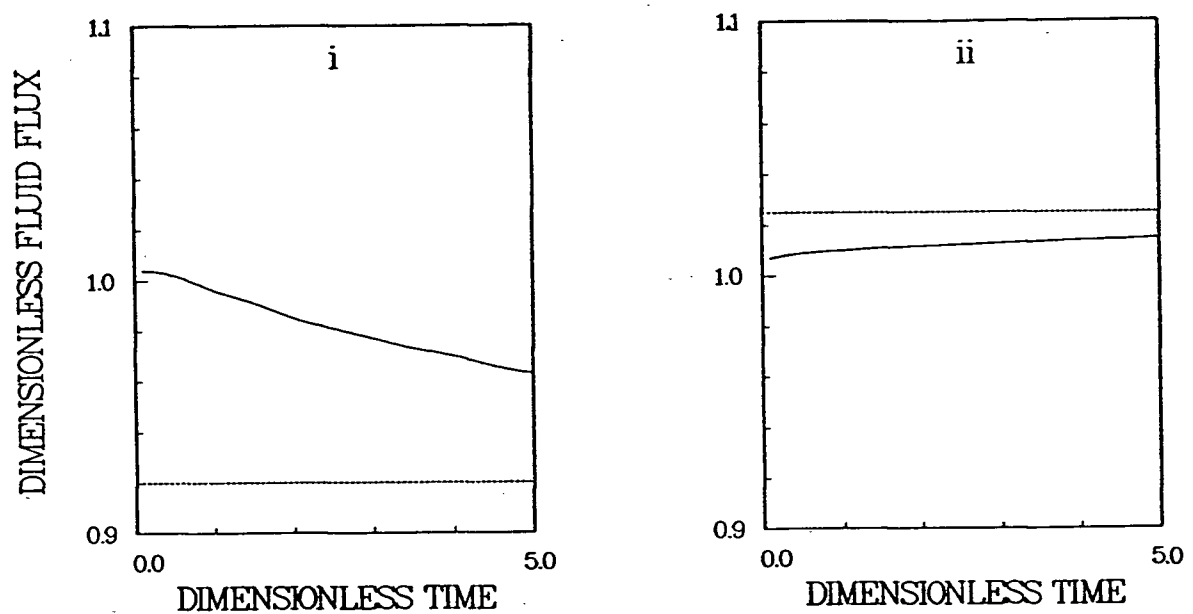
Figure 5.1: The average transient fluid flux across the arteriolar capillary wall following hypoproteinemia is shown assuming an impermeable mesothelium and (i) ξ equal to unity, and (ii) ξ equal to zero. In both cases the fluid flux is normalized with respect to its initial value prior to the upset. The dotted line represents the new steady-state value in each case.

drop in systemic plasma protein concentration, provided that the transcapillary fluid exchange and interstitial fluid flux were both independent of interstitial colloid osmotic pressures. The transient changes in fluid exchange within the tissue segment must therefore reflect the variations in the interstitial osmotic pressure distribution, and hence the interstitial plasma protein distribution, with time.

For the case where ξ is unity, the system experiences a marginal increase in fluid exchange shortly after the drop in vascular plasma protein concentration. (At $\tilde{t}$ equal to 0.1, or 15 minutes after initiation of hypoproteinemia, the dimensionless fluid flux crossing the arteriolar boundary has increased in magnitude by only a factor of 1.004, from -0.3982 to -0.3999.) This is illustrated in panel (i) of Figure (5.1), which shows the transient flux across this boundary, normalized with respect to its value prior to the onset of hypoproteinemia. The marginal rise in fluid exchange rate is attributed to the increase in $\bar{\mu}_{\mathrm{eff}}^{\mathrm{art}}$, which is only partially offset by a concomitant increase in $\bar{P}^1$. The effective interstitial osmotic pressure at the boundary, $\sigma^{\mathrm{art}} \cdot \bar{\Pi}^{\mathrm{art}}$, meanwhile, is still near its pre-upset value since insufficient time has elapsed to significantly reduce the concentration of interstitial plasma proteins there. Hence, the arteriolar fluid exchange rate, given by Starling's Law, is slightly greater following the upset. Subsequently, as the local plasma protein content near the boundary decreases with time, the dimensionless fluid flux across this boundary also declines so that, at $\tilde{t}$ of 5.0 (i.e., 12.5 hours), it is -0.3836. This represents 48.4 % of the total drop that occurs before the system reaches its new steady-state value of 0.3662.

When ξ is zero, the transient fluid exchange within the system follows a different pattern (see panel (ii) of Figure (5.1)). Again, there is a marginal increase in the fluid exchange rate across the arteriolar boundary (i.e., at $\tilde{t}$ equal to 0.1 units, the dimensionless fluid flux has increased in magnitude from 0.3378 to 0.3400). However, in this case the magnitude of the dimensionless fluid flux across this boundary continues to increase with time until it reaches a new steady-state value of 0.3462, which represents a 2.5 % increase over the initial value of 0.3378. At $\tilde{t}$ equal 5.0, the arteriolar fluid flux has undergone 59.5 % of the total increase from initial to final steady-state conditions, indicating that the relaxation time for this case may be

somewhat less than, though of the same order of magnitude as, that when ξ equals one.

The fact that the the fluid exchange rate within the system increases with time when ξ is zero, but decreases with time when ξ is one, indicates that, with an impermeable mesothelium, the interstitial plasma protein transport mechanisms play a significant role in determining the transient fluid exchange within the model system following the onset of hypoproteinemia. As mentioned earlier, this can only be attributed to differences between the transient adjustments in the interstitial colloid osmotic pressure distributions for the two cases.

Plasma Protein Exchange and Interstitial Plasma Protein Distribution   The transient plasma protein exchange between the vascular and interstitial compartments is coupled to the fluid exchange between these via the convective transport of the macromolecules across the vascular boundary. In addition, plasma proteins enter the interstitium from the vascular compartment by diffusion. The relative importance of these two transport mechanisms depends on the magnitude of the fluid flux across a given permeable boundary, the degree of sieving at the boundary, and the differences in plasma protein concentration on either side of the boundary. Assuming that convection dominates, the total plasma protein flux across a permeable boundary b from vascular to interstitial compartments, expressed as a dimensionless quantity, is equal to $(1 - \sigma^b) \cdot \tilde{j}_w^0 \cdot \tilde{C}^b$. Likewise, if the exchange is from the interstitium to the vascular compartment and assuming that convection dominates, the plasma protein flux is given by $(1 - \sigma^b) \cdot \tilde{j}_w^0 \cdot [\tilde{C}^1]_b$.

Figures (5.2) (i) and (ii) illustrate the transient plasma protein exchange across the arteriolar and venular capillaries assuming ξ equal to 1 and ξ equal to 0, respectively. In each case the flux is normalized with respect to its value prior to the upset. Consider first the case where ξ equals 1. During the entire transient phase and subsequent steady-state, the plasma protein transport from the arteriolar capillary to the interstitium is predominantly convective. Hence the transient flux of plasma proteins across this boundary follows the general trend of the transient fluid flux profile there. However, the former profile is further characterized by a dramatic reduction in the plasma protein exchange rate immediately after the perturbation,

due to the reduced vascular concentration of plasma proteins.

At the venular boundary, convective plasma protein exchange likewise dominates during the transient period and the subsequent new steady-state. However, since the interstitial plasma protein concentration near the boundary is greater than the vascular plasma protein concentration during the transient period, the plasma protein flux across the venular boundary exceeds the plasma protein flux across the arteriolar boundary. This results in a net exchange of plasma proteins from the interstitium to the blood and subsequent reduction in interstitial plasma protein content. Furthermore, while the dimensionless arteriolar plasma protein exchange rate is only 4.7 % greater than the steady-state value at $\bar{t}$ of 5.0, the venular exchange rate is still 66.3 % greater than its steady-state value. The length of the transient period is therefore determined by the time required to remove the excess plasma proteins from the interstitial space by way of the venular capillary. This is further illustrated in the transient interstitial plasma protein distributions shown in the left panel of Figure (5.3).

Within the interstitium itself, both convection and diffusion play significant roles during the entire transient period. For example, the ratio of convection to diffusion within the interstitial space adjacent the arteriolar boundary varies from -1.15 to -1.33 from a $\bar{t}$ of 0.1 units to the new steady-state. The negative values for these ratios indicate that diffusion and convection occur in opposite directions.

When ξ is 0, plasma protein exchange across the arteriolar and venular capillaries is, likewise, predominantly convective. The arteriolar plasma protein exchange rate drops slightly below, and then slowly rises to, the ultimate steady-state value so that, at $\bar{t}$ equal 5.0, the dimensionless arteriolar plasma protein exchange rate is approximately 1 % less than at steady-state. Meanwhile, the dimensionless plasma protein flux across the venular boundary first rises above its initial value of 0.0507, then steadily decreases until reaching a new steady-state value of 0.0260. By $\bar{t}$ equal 5.0, the venular plasma protein exchange rate is approximately 69 % greater than the final steady-state value. The length of the transient period when ξ is zero is therefore close to that when ξ is one.
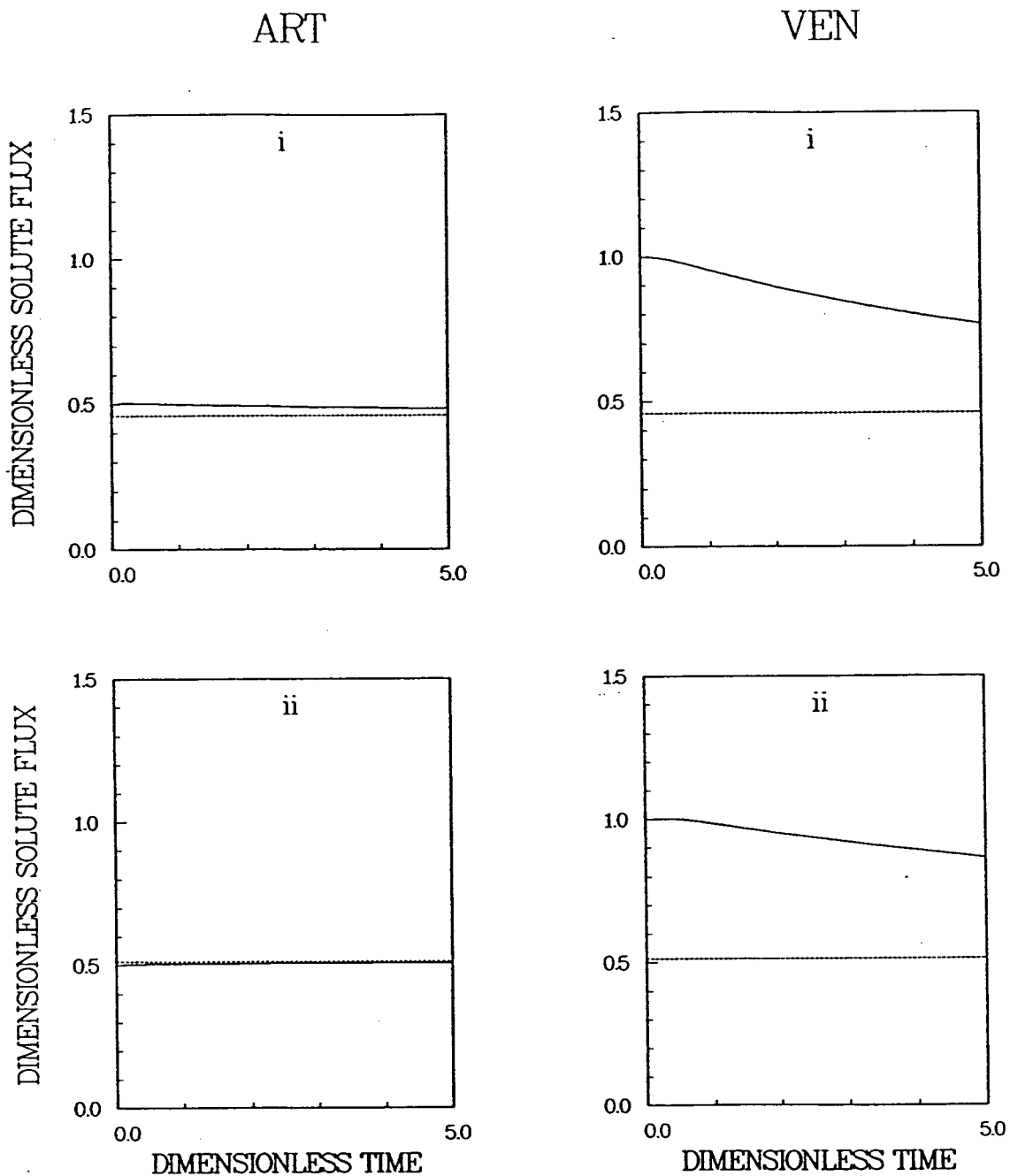
Figure 5.2: The average transient plasma protein flux across the arteriolar and venu-lar capillary walls following hypoproteinemia is shown assuming an impermeable mesothelium and (i) ξ equal to unity, and (ii) ξ equal to zero. In both cases the protein flux is normalized with respect to its initial value prior to the upset. The dotted line in each case represents the new steady-state value.
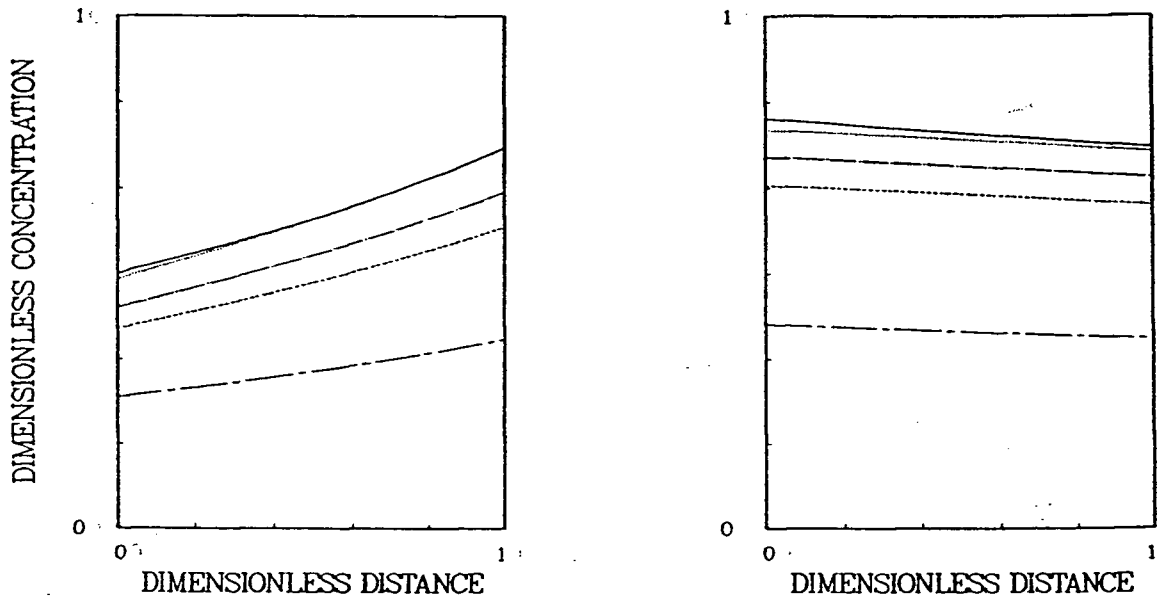
Figure 5.3: The transient total dimensionless plasma protein concentration distributions ($\tilde{C}^t$) following hypoproteinemia and assuming an impermeable mesothelium are shown for (i) the case where ξ is 1 (left panel) and (ii) for the case where ξ is 0 (right panel). In each case the solid line represents the initial condition, the dotted line is at $\tilde{t}$ equal 0.5, the chain-dot line is at $\tilde{t}$ equal 2.5, the dashed line corresponds to $\tilde{t}$ equal 5.0, and the chain-dash line represents the final steady-state condition.

Because the plasma protein content in the blood decreases following the onset of hypoproteinemia, the rate of plasma protein exchange across the arteriolar capillary drops. Meanwhile, the interstitial plasma protein concentration adjacent the venular boundary is near its initial condition. The net exchange rate across the venular boundary therefore exceeds the exchange across the arteriolar boundary during the course of the transient period so that, once again, there is a net loss of plasma proteins from the interstitium to the blood. This is reflected in the concentration profiles in the right panel of Figure (5.3). However, unlike the case where ξ is one, the fluid exchange rate within the system remains elevated above its initial condition despite the washout of plasma proteins from the interstitium.

Mass Exchange Assuming Mesothelial Transport Properties Similar to Those of the Vascular Walls

In these simulations, it is assumed that the mesothelial transport properties are identical to those of the arteriolar capillary wall. Since the mesothelium is permeable, fluid and plasma proteins may be exchanged between the arteriolar capillary and the peritoneum, the venular capillary and the peritoneum, and the arteriolar and venular capillaries. In addition, the over-all effective resistance of the tissue segment to mass exchange depends on the flow patterns within the interstitium itself, since fluid and plasma proteins are able to bypass regions of the interstitium via the peritoneum.

In fact, the steady-state analysis of Chapter 4 suggests that, when the mesothelium is permeable, the majority of fluid and plasma proteins exchanged between the various luminal compartments passes through only a small portion of the interstitial space. Further, interstitial fluid and plasma proteins located in the central portions of the tissue segment need only travel a short distance to reach the mesothelial surface. Hence, when all bounding surfaces are permeable, the system can achieve its new steady-state following the onset of hypoproteinemia much more quickly here than for those cases in which the mesothelial layer is impermeable.

Fluid Exchange In the previous discussion of luminal driving forces it was noted that, following the drop in vascular plasma protein concentration, $\bar{\mu}_{\text{eff}}^{\text{art}} - \bar{\mu}_{\text{eff}}^{\text{mes}}$ and $\bar{\mu}_{\text{eff}}^{\text{ven}} - \bar{\mu}_{\text{eff}}^{\text{mes}}$ both increase in magnitude, suggesting that the fluid exchange between these respective compartments should increase following the systemic upset. In addition, it was noted that $\bar{\mu}_{\text{eff}}^{\text{ven}} - \bar{\mu}_{\text{eff}}^{\text{mes}}$ changes from a negative quantity to a positive one, which would imply a reversal in the direction of fluid exchange between the venular capillary and the peritoneum. In fact these trends are observed both when ξ is zero and when ξ is one, as discussed below.

Consider first the case in which the convective hindrance, ξ, is unity. Initially following the drop in vascular protein, there is a substantial increase in the rate of fluid exchange across each of the three permeable boundaries (see Table (5.2)). Further, the fluid exchange rate across the venular capillary changes direction, so that the vessel moves from a state of fluid re-absorption to one of fluid filtration. Likewise, the direction of the mesothelial fluid flux near the venular boundary changes direction, as shown in Figure (5.4). The system has reached steady-state with respect to fluid exchange by $\bar{t}$ equal 3.0 units (i.e., 7.5 hours), as illustrated in Figure (5.5).

ξ	Period	Boundary Condition 2			Boundary Condition 3		
		Art	Ven	Mes	Art	Ven	Mes
1.0	Pre-Upset	-2.387	0.656	0.087	-3.551	0.762	0.139
1.0	Post-Upset	-5.567	-3.253	0.441	-8.600	-6.243	0.742
1.0	Steady-State	-5.527	-3.247	0.439	-8.305	-5.238	0.677
0.0	Pre-Upset	-2.313	0.632	0.084	-3.570	0.803	0.138
0.0	Post-Upset	-5.439	-3.187	0.431	-8.630	-6.273	0.745
0.0	Steady-State	-5.444	-3.180	0.431	-8.319	-5.263	0.679

Table 5.2: **The average transient fluid fluxes across the permeable boundaries following hypoproteinemia, for the mesothelial boundary conditions 2 and 3. In each case the table reports the flux prior to the upset ('pre-upset'), at $\bar{t}$ equal 0.001 post-upset ('post-upset'), and at the new system steady-state ('steady-state'). A negative flux indicates a flow into the interstitium.**

Upon examining the distribution of $\bar{P}^1 - \bar{\Pi}^1$ at $\bar{t}$ equal 2.5 (see Figure (5.6)), it is clear that

Figure 5.4: **The dimensionless transient fluid flux distribution across the mesothelium following hypoproteinemia, assuming mesothelial transport properties equal to those of the arteriolar capillary and a ξ of 1, are shown at the pre-perturbation state (panel (i)), and at a $\tilde{t}$ of 0.001 (panel (ii)), 0.05 (panel (iii)), 0.5 (panel (iv)), and at the final steady-state (panel (v)).**
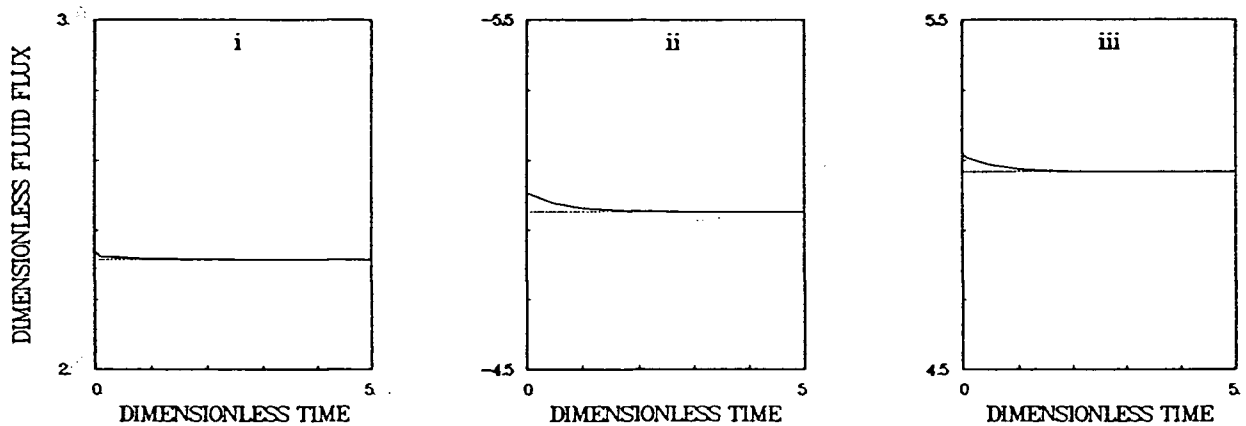
Figure 5.5: The average transient fluid fluxes across the permeable boundaries following hypoproteinemia, assuming mesothelial transport properties equal to those of the arteriolar capillary and a ξ of 1, are shown in the three panels above. Panel (i) shows the fluid flux across the arteriolar capillary, panel (ii) corresponds to the fluid flux across the venular capillary, and panel (iii) represents the net fluid flux across the mesothelium. In each case the fluxes are normalized with respect to their respective pre-perturbation values. The dotted line represents the new steady-state value in each case.
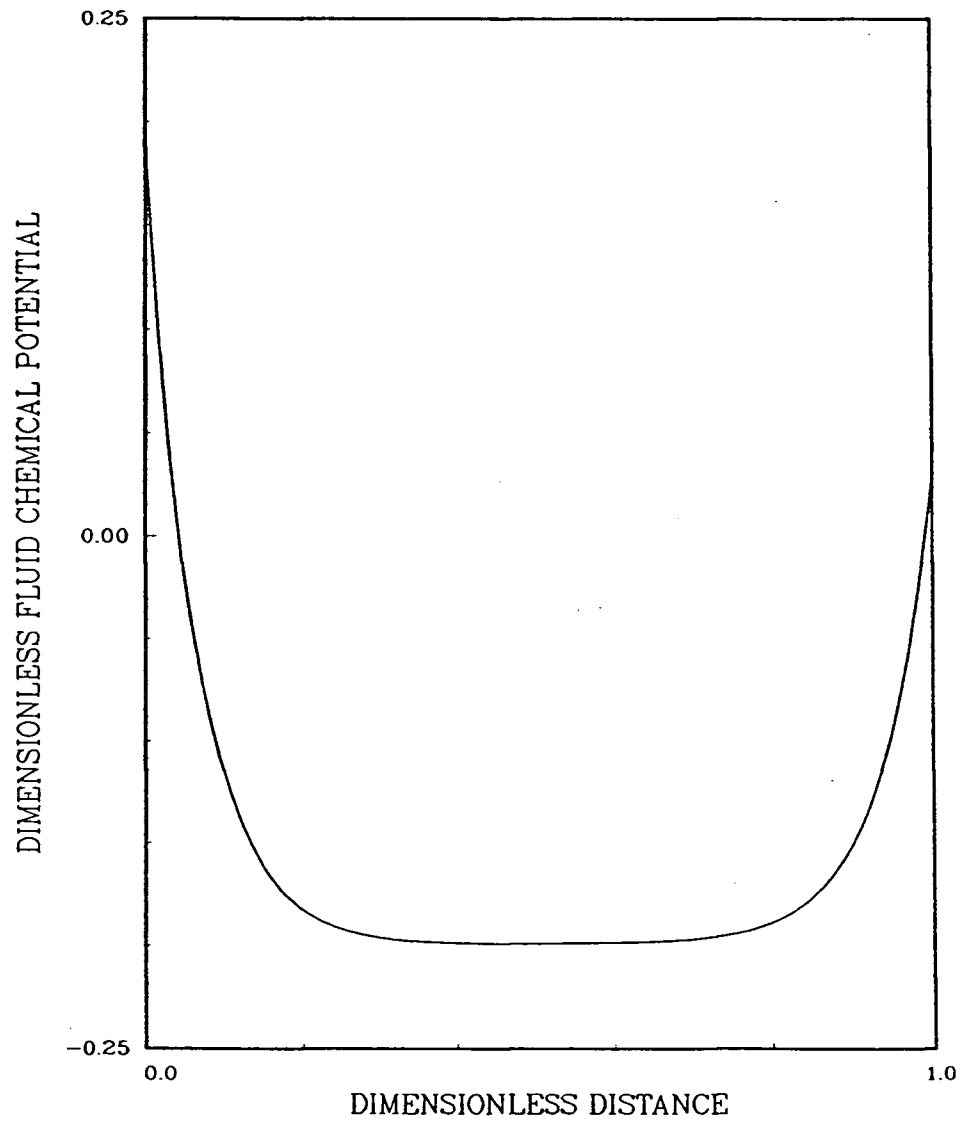
Figure 5.6: The dimensionless interstitial fluid chemical potential distribution ($\tilde{P}^1 - \tilde{\Pi}^1$) is shown at $\bar{t}$ equal 2.5 following hypoproteinemia for the case where the mesothelial transport properties equal those of the arteriolar capillary and ζ is 1.

the majority of interstitial fluid flow occurs in the regions near the blood vessels; the central regions of the tissue space are relatively quiescent. Movement of fluid within the interstitial space near the vessels is towards the central regions of the tissue. Conservation of fluid mass, meanwhile, is satisfied by a local, concomitant exchange of fluid across the mesothelial boundary.

The transient fluid exchange within the system for the case where ξ equals 0 is much the same as when ξ is one. There is a rapid increase in fluid exchange across each of the permeable boundaries immediately following the onset of hypoproteinemia, as shown in Table 5.2. Again, the venular capillary shifts from a state of fluid re-absorption to one of fluid filtration. Further, the transient fluid flux distribution across the mesothelial boundary parallels that for ξ equal to one, and so is not shown. However, the fluid fluxes reach their new steady-state values by $\bar{t}$ equal 1.0 (i.e., 2.5 hours), indicating a shorter transient period than that found when ξ is one.

Plasma Protein Exchange and Interstitial Plasma Protein Distribution When ξ is equal to one, the plasma protein transport across each of the permeable boundaries is predominantly convective. Therefore, since both the arteriolar and venular capillaries are filtering fluid, the plasma protein exchange rates across these boundaries follow the respective transient fluid fluxes. For example, the plasma protein flux across each of these boundaries reaches a new steady-state value at the same time as the fluid fluxes. However, since the vascular plasma protein content is lower subsequent to the perturbation, the increase in the plasma protein fluxes across these boundaries is not as pronounced as increase in the fluid exchange rates (see Table (5.3)).

The exchange rate of plasma proteins across the mesothelium is also enhanced following the onset of hypoproteinemia. Again, since the exchange is largely convective, the plasma protein flux distribution across the mesothelium is qualitatively the same as the fluid flux distribution. The transient plasma protein fluxes across each of these boundaries is illustrated in Figure (5.7). In this case, the system reaches a new steady-state by a dimensionless time of 3.0.

Since, during the transient period, the total efflux of plasma proteins across the mesothelium

ξ	Period	Boundary Condition 2			Boundary Condition 3		
		Art	Ven	Mes	Art	Ven	Mes
1.0	Pre-Upset	-0.358	0.072	0.014	-0.533	0.762	0.025
1.0	Post-Upset	-0.417	-0.244	0.049	-0.645	-0.468	0.148
1.0	Steady-State	-0.415	-0.244	0.033	-0.623	-0.393	0.051
0.0	Pre-Upset	-0.347	0.063	0.014	-0.535	0.036	0.025
0.0	Post-Upset	-0.408	-0.239	0.049	-0.647	-0.471	0.151
0.0	Steady-State	-0.408	-0.239	0.032	-0.624	-0.395	0.051

Table 5.3: **The average transient plasma protein fluxes across the permeable boundaries following hypoproteinemia, for the mesothelial boundary conditions 2 and 3. In each case the table reports the flux prior to the upset ('pre-upset'), at $\tilde{t}$ equal 0.001 post-upset ('post-upset'), and at the new system steady-state ('steady-state'). A negative flux indicates a flow into the interstitium.**

exceeds the influx of protein across the other two boundaries, there is a net loss of plasma proteins from the interstitium to the peritoneum. This is to be expected for the following reasons. Prior to the onset of hypoproteinemia, the net plasma protein transport into the system is zero because steady-state conditions prevail. Immediately following the upset, there is increased fluid exchange from the blood to the interstitium. The concentration of plasma proteins within the fluid is more dilute, however, so that convective transport of plasma proteins across the vascular boundaries does not increase in proportion to the increased fluid fluxes. At the same time, the fluid exchange from the interstitium to the peritoneum increases by an amount equal to the increase in fluid exchange across the blood vessels. This increases the convective transport of plasma proteins from the interstitium to the peritoneum. However, the interstitial fluid crossing the mesothelium has virtually the same plasma protein concentration as that prior to the onset of hypoproteinemia, so that the increase in plasma protein exchange across this boundary is substantial. Since the vascular fluid replacing the interstitial fluid is somewhat diluted, compared to the conditions before the upset, there is a net loss of plasma proteins from the interstitial space. Furthermore, plasma protein exchange across the mesothelium does not

reach its new steady-state value until the wash-out of interstitial plasma proteins is complete.

The transient dimensionless plasma protein distributions assuming ξ is one are shown in the left panel of Figure (5.8). By a dimensionless time of 0.001, the profile has been altered substantially in the region of the venular blood vessel, so that the gradient in interstitial plasma protein concentration changes direction following the shift from plasma protein re-absorption to filtration at that boundary. Furthermore, by this time there is a slight increase in the local interstitial plasma protein concentration near the arteriolar and venular capillaries. This appears to be similar, qualitatively, to the buildup of plasma proteins seen in several of the steady-state cases of Chapter 4 and is presumably due to the same effects, namely the combination of significant convective plasma protein transport within the interstitium and the sieving of proteins at the mesothelium. However, these local maxima in interstitial plasma protein concentration are soon dissipated as interstitial plasma proteins continue to be lost to the peritoneum. (Compare, for example, the profiles at a $\bar{t}$ of 0.001 and 0.05.) It is still conceivable that, in some circumstances, irregularities in the mesothelial fluid and plasma protein flux distributions, similar to those discussed in Chapter 4, might occur as transient phenomena during hypoproteinemia.

As Figure (5.6) showed, convective transport of plasma proteins is directed towards the central regions of the tissue, with the largest convective velocities occurring near the blood vessels. Based on the concentration gradients of Figure (5.8), then, plasma protein convection and diffusion continue to oppose one another in the vicinity of the vascular boundaries during the entire transient phase. Furthermore, there is very little plasma protein transport in the central portions of the tissue throughout that period. The fact that diffusion and convection oppose one another may offer one explanation for the longer transient period of fluid exchange when ξ is one, compared to that when ξ is zero.

The overall transient exchange of plasma proteins within the system when the interstitial convective hindrance of zero is much the same as for the case where ξ is unity (see Table (5.3)). Once again, the plasma protein transport across each of the boundaries is largely convective. The transient distributions of dimensionless plasma protein fluxes across the mesothelium are
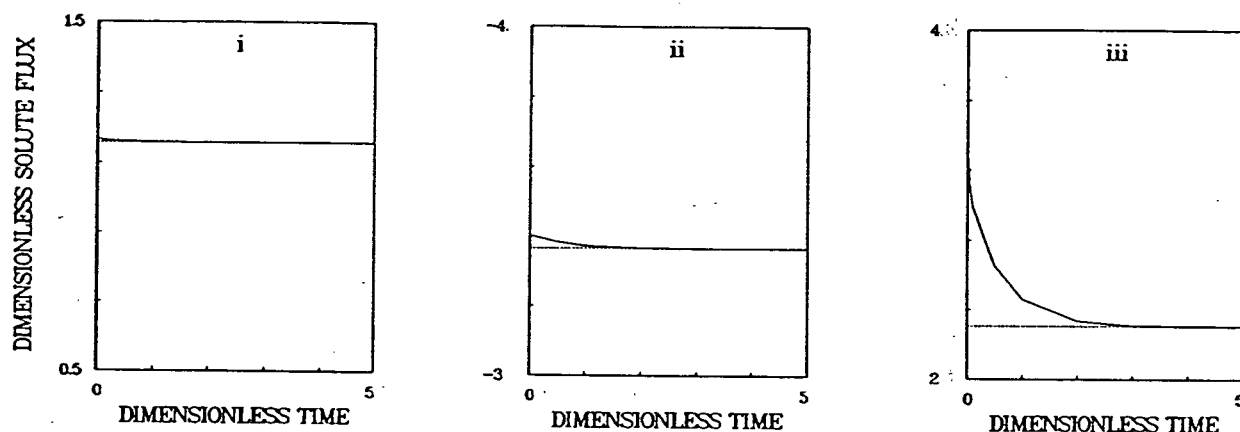
Figure 5.7: The average transient plasma protein fluxes across the permeable boundaries following hypoproteinemia, assuming mesothelial transport properties equal to those of the arteriolar capillary and a ξ of 1, are shown in the three panels above. Panel (i) shows the protein flux across the arteriolar capillary, panel (ii) corresponds to the protein flux across the venular capillary, and panel (iii) represents the net protein flux across the mesothelium. In each case the fluxes are normalized with respect to their respective pre-perturbation values. The dotted line represents the new steady-state value in each case.

Figure 5.8: The transient dimensionless total plasma protein concentration distributions ($\tilde{C}^t$) following hypoproteinemia and assuming that the mesothelial transport properties are equal to those of the arteriolar capillary are shown for (i) the case where ξ is 1 (left panel) and (ii) for the case where ξ is 0 (right panel). In each case the solid line corresponds to the initial condition, the dotted line is at $\bar{t}$ equal 0.001, the chain-dot line is at $\bar{t}$ equal 0.05, the dashed line corresponds to $\bar{t}$ equal 0.5, and the chain-dash line represents the final steady-state condition.

similar here to the case where ξ is one and so are not shown.

The transient distribution of interstitial plasma proteins assuming ξ is zero is illustrated in the right panel of Figure (5.8). Since the venular boundary shifts from a re-absorbing to a filtering one, and since the only means of interstitial plasma protein transport is by diffusion, the gradient is forced to reverse directions immediately following the onset of the perturbation. Further, because the plasma protein exchange across the permeable boundaries is largely convective, there is a net loss of plasma proteins from the interstitium to the peritoneum, for the same reasons given when ξ is one. The mean interstitial plasma protein concentration therefore decreases with time, as illustrated in Figure (5.8).

It is clear from these results that, although the transient variations in the interstitial plasma protein distributions depend strongly on the value of ξ assumed, the overall transient exchange of fluid and plasma proteins within the system does not. This further emphasizes the fact that, when the mesothelium is permeable, the interstitium contributes less to the overall resistance within the system, so that the interstitial plasma protein transport mechanisms have less impact on the behavior of the system as a whole.

Mass Exchange Assuming a Highly Permeable Mesothelium

In the final set of simulations of hypoproteinemia, it is assumed that the mesothelial transport properties are given by boundary condition 3 of Chapter 4; that is, the mesothelium is much more permeable than the capillary walls and offers no sieving of proteins (σ^{mes} is zero).

Fluid Exchange   Once again, the simulations suggest that the transient fluid exchange within the model mesenteric tissue is affected little by the interstitial plasma protein transport mechanisms (see Table (5.2)). Further, the general trends are similar to those found when the mesothelial transport properties mimic the arteriolar capillary, except that the fluxes are typically an order of magnitude larger and the time to reach steady-state is an order of magnitude smaller. The reduced time for the transient is attributed to the lower mass transfer resistance of the mesothelial layer. Hence, following an initial increase immediately after the onset of

hypoproteinemia, fluid exchange across each of the boundaries declines slightly over time to reach a new steady-state value by a $\bar{t}$ of 0.5 (i.e., 1.25 hours).

The dimensionless fluid flux distribution across the mesothelial boundary for the case where ξ is one is shown in Figure (5.9). Figure (5.9) shows that the majority of the fluid exchange across the mesothelium occurs in close proximity to the blood vessels. However, although it is not apparent in the figure, there is some exchange in the central portions of the tissue segment as well. Again, the trend is virtually identical when ξ is zero.

Following the drop in vascular plasma protein content, then, the interstitial fluid flow is directed towards the central regions of the tissue, independent of the value of ξ. Again, the fluid material balance constraints are met by the appropriate fluid exchange across the mesothelium.

Plasma Protein Exchange and Interstitial Plasma Protein Distribution   Since plasma protein transport is largely convective, the transients follow the fluid flux behavior, except that the increase in protein exchange across the arteriolar boundary is limited by the fact that the filtering fluid contains less plasma proteins following the upset. Again, the transient plasma protein exchange across the permeable boundaries is affected only marginally by the transport mechanisms within the interstitial space.

Both when ξ is one and when ξ is zero, plasma proteins leave the interstitium by way of the mesothelial boundary. Since the exchange across this boundary is largely convective, the distribution of the plasma protein flux across the mesothelium follows closely the fluid flux profile, and so is not shown here. The transient distribution of plasma proteins for the two values of ξ investigated are shown in Figure (5.10). In both cases the massive plasma protein fluxes across the mesothelium in the vicinity of the blood vessels reduce the plasma protein content in those regions. This causes the local depletion of interstitial plasma proteins in the vicinity of the arteriolar and venular boundaries over time, so that diffusive transport tends to move interstitial plasma proteins from the central regions of the tissue towards the vascular boundaries. For the case where ξ is one, this is counteracted in part by a convective flux of plasma proteins towards the central portions of the tissue. However, when plasma protein transport is limited to
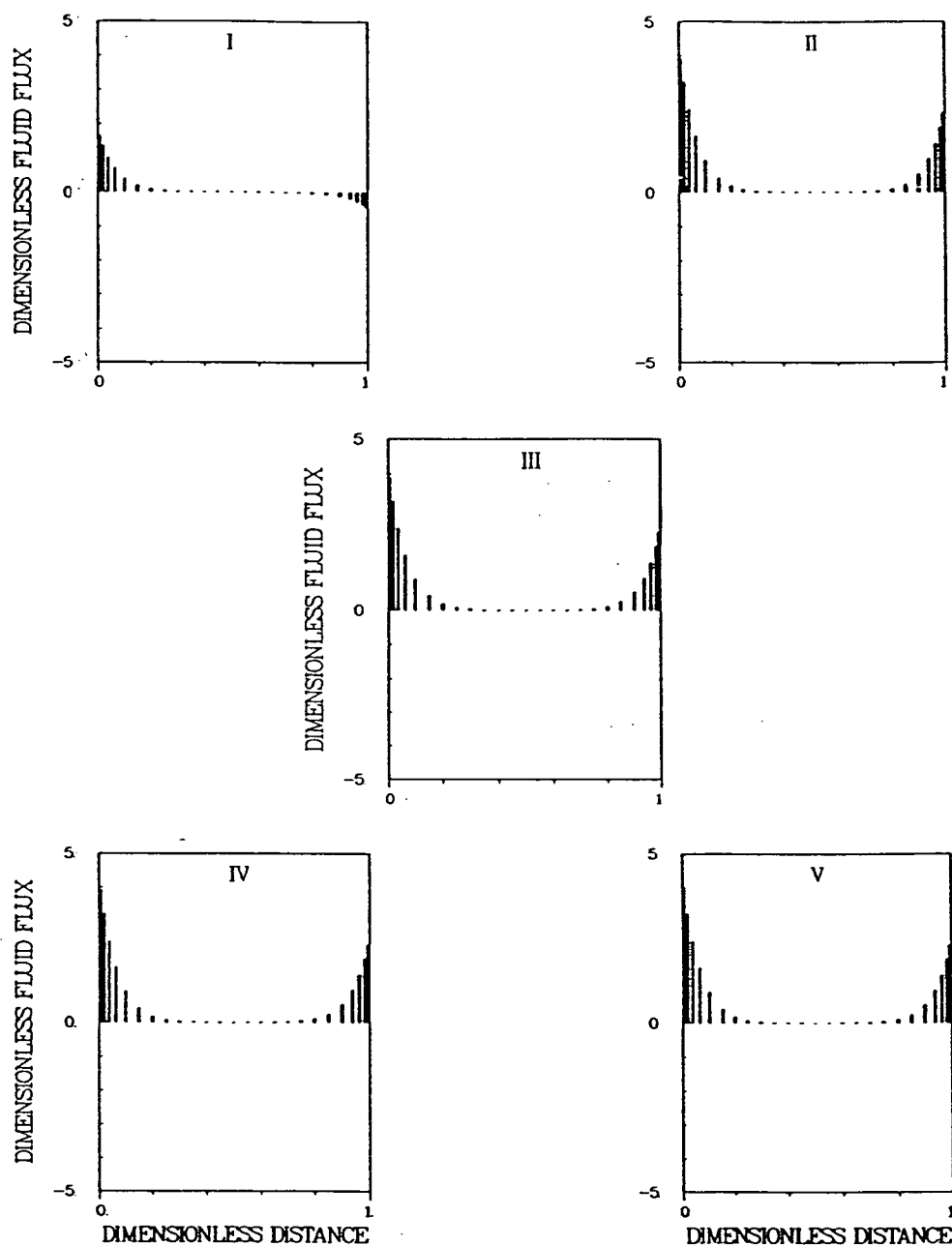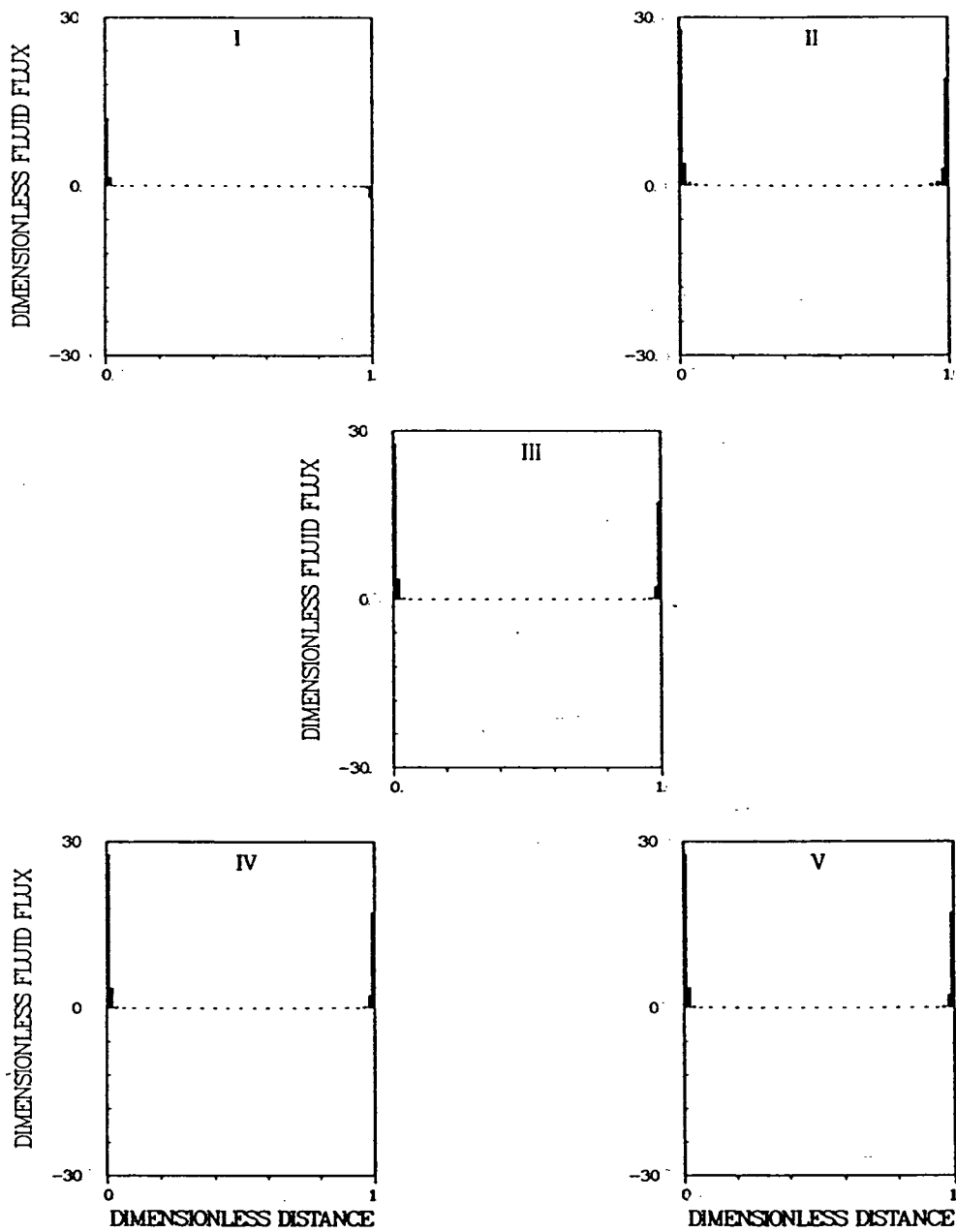
Figure 5.9: The dimensionless transient fluid flux distribution across the mesothelium following hypoproteinemia, assuming the mesothelial transport properties are given by boundary condition 3 and ζ equals 1, are shown at the pre-perturbation state (panel (i)), and at a $\tilde{t}$ of 0.001 (panel (ii)), 0.05 (panel (iii)), 0.5 (panel (iv)), and at the final steady-state (panel (v)).
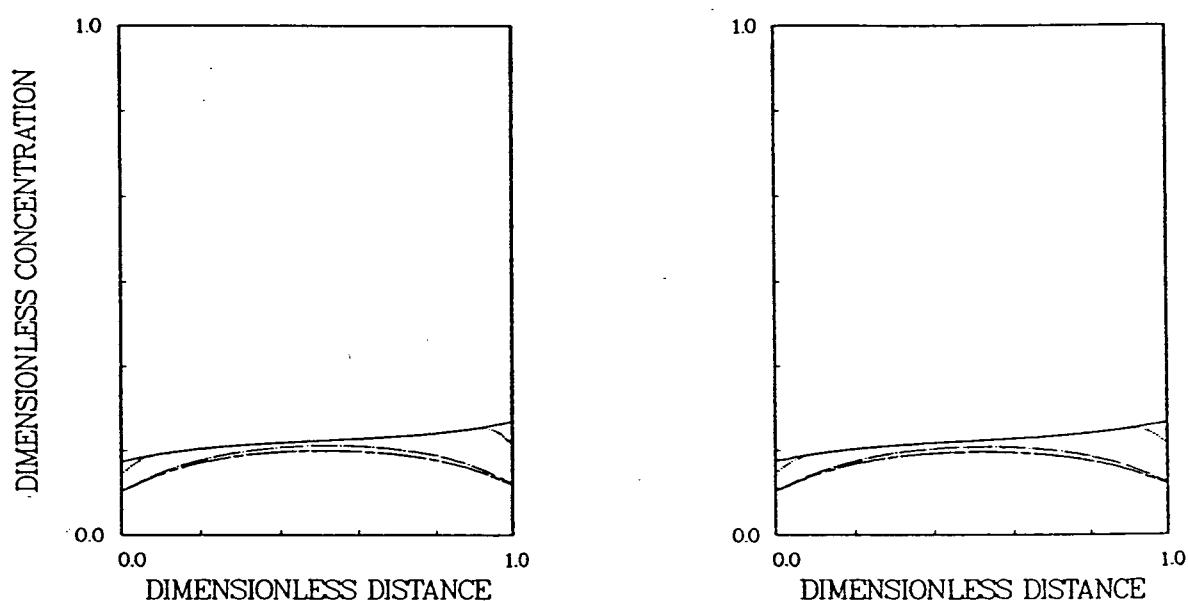
Figure 5.10: The transient dimensionless total plasma protein concentration distributions ($\tilde{C}^t$) following hypoproteinemia and assuming a highly permeable mesothelium (boundary condition 3) are shown for (i) the case where ξ is 1 (left panel) and (ii) for the case where ξ is 0 (right panel). The solid line corresponds to the initial condition, the dotted line is at $\tilde{t}$ equal 0.001, the chain-dot line corresponds to $\tilde{t}$ equal 0.05, the dashed line is at $\tilde{t}$ equal 0.5, and the chain-dash line corresponds to the final steady-state conditions.

diffusion, the interstitial plasma protein concentration distribution undergoes further alterations so that, by the time the system has reached its new steady-state, there is a net diffusion of interstitial plasma proteins from the vascular boundaries towards the center of the interstitial space in the regions adjacent the blood vessels. Because the magnitude of the shift is small and limited to the region adjacent the capillary walls, it is not apparent in Figure (5.10).

Once again the interstitial plasma protein content decreases following hypoproteinemia, both when ξ is one and when ξ is zero. This occurs for the same reasons presented earlier when discussing plasma protein exchange assuming the mesothelial transport properties equal those of the arteriolar capillary wall.

Summary of Hypoproteinemia Simulations

In all cases considered here, the onset of hypoproteinemia led to a washout of interstitial plasma proteins. The transient behavior of the system during the washout, however, depended on the transport properties of the mesothelium and, to a lesser degree, on the interstitial plasma protein transport properties. When the mesothelium is assumed to be impermeable, fluid and plasma proteins must traverse the entire interstitial length in their journey from the arteriolar end of the system to the venular end. However, when it is assumed that the mesothelium is permeable, the distance travelled by material leaving the interstitium is reduced substantially. As a result, the response time of the model system to hypoproteinemia varied inversely with the permeability of the mesothelial layer.

Further, when the mesothelium is impermeable, the interstitium represents a substantial portion of the total resistance to mass exchange within the system. Hence, the behavior of the system as a whole is influenced to a great degree by the conditions prevailing within the interstitial space. For example, in this case the transient changes to the interstitial colloid osmotic pressure distribution had a significant effect on the transient fluid exchange within the tissue segment. The transient fluid exchange across the boundaries of the system therefore varied according to changes in the interstitial plasma protein distribution, which depended

further on the interstitial plasma protein transport properties.

However, when the mesothelium is assumed to be permeable, the behavior of the system with respect to mass exchange is dominated by the transport properties of this boundary. In addition, the interstitial plasma protein transport mechanisms have less impact on the transient distribution of interstitial plasma proteins as the transport properties of the mesothelium are enhanced.

5.4.2 Transient Exchange During Sustained Venous Congestion

In this set of simulations, the system response to sustained venous congestion is studied as a function of the mesothelial transport properties and interstitial transport mechanisms outlined in the investigation of hypoproteinemia. Once again, it is instructive to consider first the effect that venous congestion has on the driving forces for fluid and plasma protein exchange between the luminal compartments.

The Effect of Venous Congestion on the Luminal Driving Forces

During venous congestion, the venous pressure rises, resulting in an increase in hydrostatic pressure throughout the microcirculation. However, according to Eqs. (5.11) and (5.12), the incremental increases in arteriolar and venular capillary pressures are not equal. In fact, the arteriolar pressure increases by 1.538×10^4 dyne/cm^2 (11.5 mmHg), while the venular pressure rises by 1.725×10^4 dyne/cm^2 (12.9 mmHg). The hydrostatic pressure of the peritoneal fluid, meanwhile, is assumed to remain at 0 dyne/cm^2.

Since the vascular plasma protein content is unchanged following the perturbation, the effective fluid chemical potential in each of the two blood vessels of the tissue segment increases according to the change in the hydrostatic pressures. The effective chemical potential of the peritoneal fluid is unaffected by the systemic disturbance. Further, the driving force for diffusive plasma protein exchange between the various luminal compartments is unchanged following venous congestion.

State	Boundary Condition 1	Boundary Condition 2			Boundary Condition 3		
	$\bar{\mu}_{\text{eff}}^{\text{art}} - \bar{\mu}_{\text{eff}}^{\text{ven}}$	$\bar{\mu}_{\text{eff}}^{\text{art}} - \bar{\mu}_{\text{eff}}^{\text{ven}}$	$\bar{\mu}_{\text{eff}}^{\text{art}} - \bar{\mu}_{\text{eff}}^{\text{mes}}$	$\bar{\mu}_{\text{eff}}^{\text{ven}} - \bar{\mu}_{\text{eff}}^{\text{mes}}$	$\bar{\mu}_{\text{eff}}^{\text{art}} - \bar{\mu}_{\text{eff}}^{\text{ven}}$	$\bar{\mu}_{\text{eff}}^{\text{art}} - \bar{\mu}_{\text{eff}}^{\text{mes}}$	$\bar{\mu}_{\text{eff}}^{\text{ven}} - \bar{\mu}_{\text{eff}}^{\text{mes}}$
Pre-Upset	0.433	0.433	0.354	-0.079	0.433	0.218	-0.215
Post-Upset	0.370	0.370	0.602	0.232	0.370	0.738	0.368

Table 5.4: **Fluid chemical potential differences between the various luminal compartments before and after the initiation of venous congestion.**

Table (5.4) lists the differences in effective fluid chemical potential for the various pairs of compartments both before and after the onset of venous congestion. The following general observations are made.

1. While in all cases both $\bar{\mu}_{\text{eff}}^{\text{art}}$ and $\bar{\mu}_{\text{eff}}^{\text{ven}}$ increase, the difference between the two, $\bar{\mu}_{\text{eff}}^{\text{art}} - \bar{\mu}_{\text{eff}}^{\text{ven}}$, decreases.

2. $\bar{\mu}_{\text{eff}}^{\text{art}} - \bar{\mu}_{\text{eff}}^{\text{mes}}$ increases in all cases where the mesothelium is permeable.

3. The magnitude of $\bar{\mu}_{\text{eff}}^{\text{ven}} - \bar{\mu}_{\text{eff}}^{\text{mes}}$ also increases in all cases where the mesothelium is permeable. Furthermore, $\bar{\mu}_{\text{eff}}^{\text{ven}} - \bar{\mu}_{\text{eff}}^{\text{mes}}$ changes from a negative value to a positive value in each of these cases.

We will return to these general observations in later discussions of fluid and plasma protein exchange during venous congestion.

Mass Exchange Assuming an Impermeable Mesothelium

Fluid Exchange   Based on the information of Table (5.4), the fluid exchange rate within the system for this set of mesothelial boundary conditions is expected to decline following the onset of venous congestion, since $\bar{\mu}_{\text{eff}}^{\text{art}} - \bar{\mu}_{\text{eff}}^{\text{ven}}$ decreases with the increase in systemic blood pressure. In fact this trend is observed, both for the case of ξ equal to one and for the case where ξ is zero.
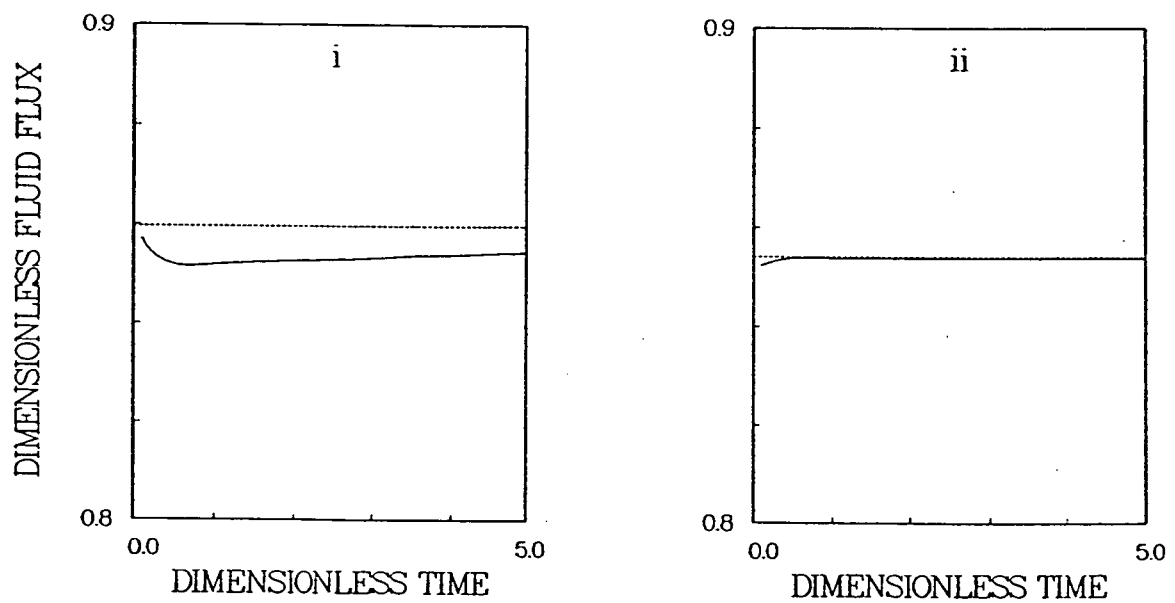
Figure 5.11: The average transient fluid flux across the arteriolar capillary wall following venous congestion is shown assuming an impermeable mesothelium and (i) ξ equal to unity, and (ii) ξ equal to zero. In both cases the fluid flux is normalized with respect to its steady-state value prior to the upset. The dotted line represents the new steady-state value in each case.

With ξ equal to one, the dimensionless fluid flux across the arteriolar capillary wall drops from its pre-upset value of -0.3982 to 86 % of that (i.e., -0.3422) by $\bar{t}$ equal 0.1 (i.e., 15 minutes). This flux declines further with time to -0.3401, then gradually increases to its new steady-state value of -0.3423 (see panel (i) of Figure (5.11)).

The transient fluid exchange within the system when ξ is zero somewhat different. Again, by a $\bar{t}$ of 0.1, the dimensionless arteriolar fluid flux has dropped from its original value of -0.3378 to 85 % of that (i.e., -0.2879). However, by a $\bar{t}$ of 0.5 (i.e., 1.25 hours), this flux has risen slightly to -0.2884 and, by steady-state, has reached -0.2885. Hence, in this case fluid exchange within the system is very close to its steady-state by 1.25 hours (see panel (ii) of Figure (5.11)). Note that, when ξ is zero, the interstitial plasma protein distribution remains virtually unchanged following the onset of venous congestion (see Figure (5.13)). Since the interstitial plasma protein washout is less here than when ξ is one, the system response time is shorter.

Plasma Protein Exchange and Interstitial Plasma Protein Distribution   Consider first the case where ξ is one. Plasma protein transport across the arteriolar and venular boundaries is predominantly convective during the transient period and subsequent steady-state. The rate of plasma protein exchange across the arteriolar boundary therefore closely follows the fluid flux pattern there. Shortly after the perturbation, the dimensionless plasma protein flux across this boundary drops from its original value of -0.05973 to 86 % of that, or -0.0512. It declines further to -0.509, then slowly rises to eventually reach its new steady-state value of -0.0514. At the venular end, the dimensionless plasma protein flux drops from 0.05973 to approximately 83 % of that, or 0.0498 shortly after the onset of venous congestion. By $\bar{t}$ equal to 0.5, the protein flux has dropped to 0.0497. From this point it rises slowly to achieve the steady-state value of 0.0514. This is illustrated in panel (i) of Figure (5.12).

These transients have the following effect on the interstitial plasma protein concentration distribution. Under the initial conditions, interstitial plasma protein diffusion is from the venular boundary towards the arteriolar boundary, as illustrated in the left panel of Figure (5.13).
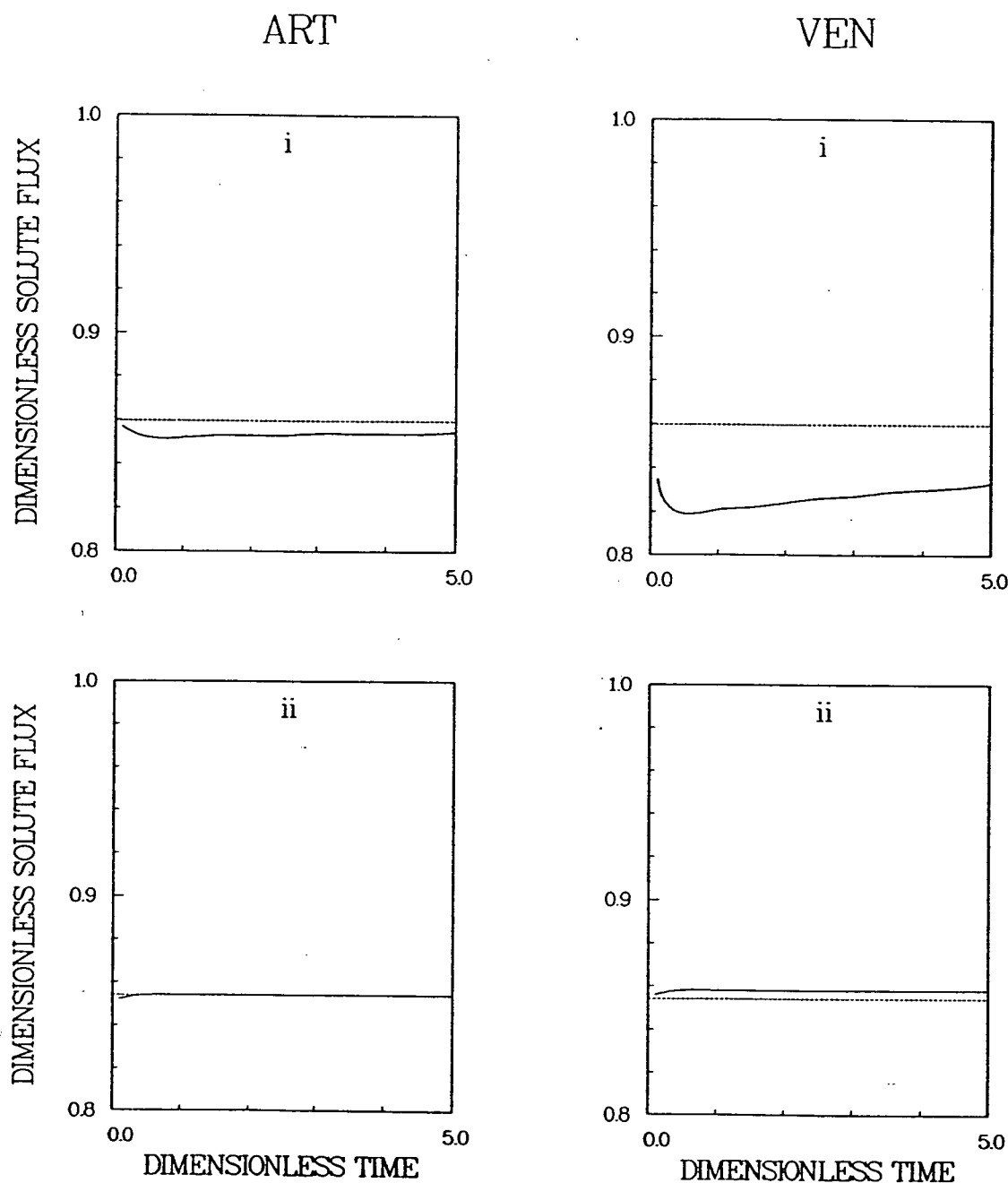
Figure 5.12: **The average transient plasma protein flux across the arteriolar and venular capillary walls following venous congestion is shown assuming an impermeable mesothelium and (i) ξ equal to unity, and (ii) ξ equal to zero. In both cases the protein flux is normalized with respect to its steady-state value prior to the upset. The dotted line in each case represents the new steady-state value.**
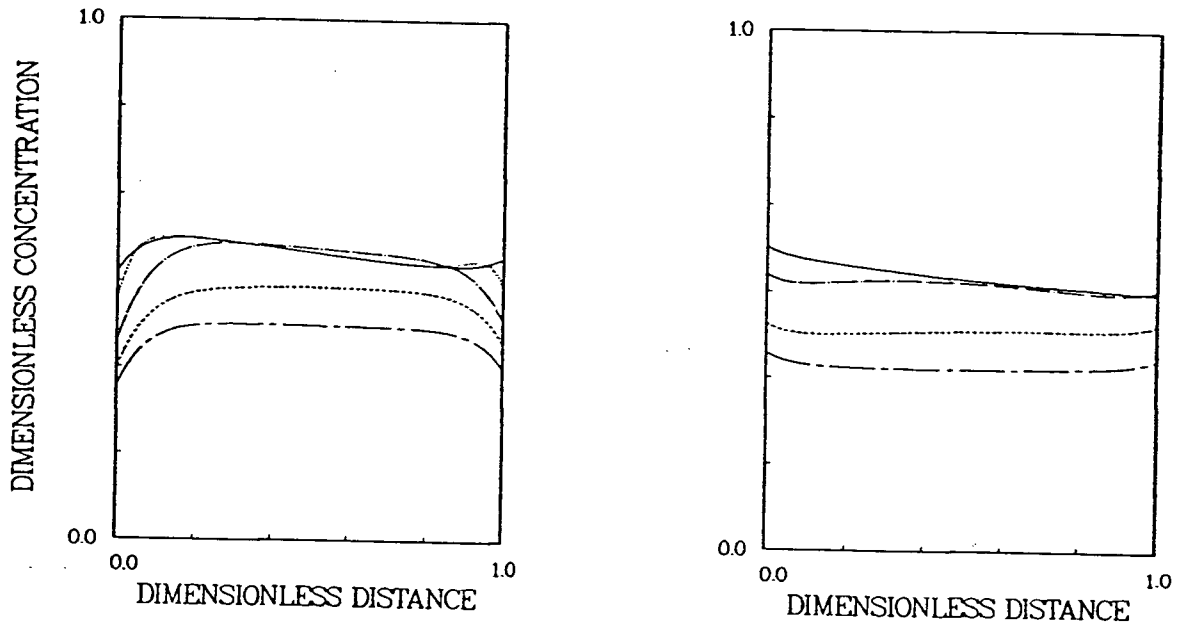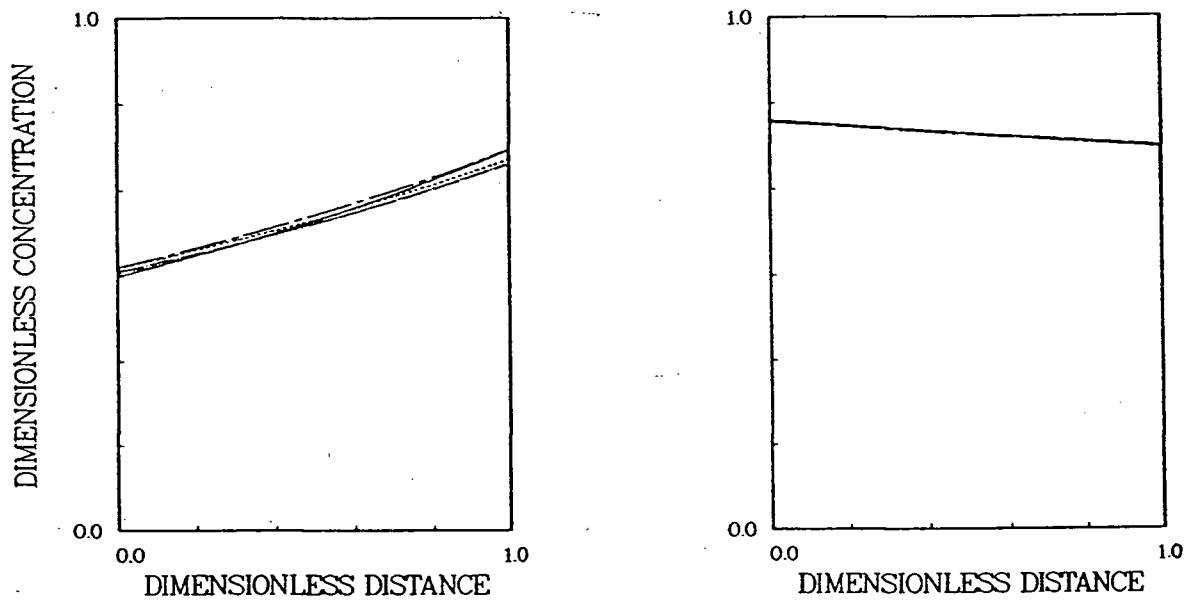
Figure 5.13: The transient dimensionless total plasma protein concentration distributions ($\tilde{C}^t$) following venous congestion and assuming an impermeable mesothelium are shown for (i) the case where ξ is 1 (left panel) and (ii) for the case where ξ is 0 (right panel). In each case the solid line represents the initial condition, the dotted line is at $\tilde{t}$ equal 0.1, the chain-dot line is at $\tilde{t}$ equal 0.5, the dashed line corresponds to $\tilde{t}$ equal 5.0, and the chain-dash line represents the final steady-state condition.

Since fluid flows from the arteriolar capillary to the venular capillary, interstitial plasma protein convection and diffusion are in opposite directions throughout the tissue space. As the fluid flow through the system decreases following the onset of venous congestion, so does the convective transport of plasma proteins through the interstitial space. With the decrease in convective plasma protein transport, diffusion within the interstitium tends to diminish the gradient in interstitial plasma protein concentration. Hence the interstitial plasma protein concentration near the arteriolar wall increases while the plasma protein concentration near the venular boundary decreases.

Now the transport of plasma proteins into the system across the arteriolar boundary is largely convective, so that it is approximately equal to $(1 - \sigma^{\text{art}}) \cdot \bar{j}_w^0 \cdot \bar{C}^{\text{art}}$. By the time the system achieves a new steady-state, this influx of plasma proteins must be balanced by the efflux of proteins at the venular boundary. This latter quantity is approximately equal to $(1 - \sigma^{\text{art}}) \cdot \bar{j}_w^0 \cdot [\bar{C}^1]_{\text{ven}}$, where $[\bar{C}^1]_{\text{ven}}$ is the interstitial plasma protein concentration in the accessible space adjacent the venular boundary. Since σ^{art} equals σ^{ven}, $[\bar{C}^1]_{\text{ven}}$ must eventually equal the plasma protein concentration in the arteriolar vessel to satisfy continuity. Hence the plasma protein concentration in that region eventually increases to its original value, as seen in the left panel of Figure (5.13).

When ξ is zero, convective plasma protein exchange across the permeable boundaries dominates once again. Hence, the trends in the transient dimensionless plasma protein fluxes follow the variations in dimensionless fluid exchange. Specifically, the dimensionless protein flux across the arteriolar boundary drops from -0.0507 to -0.0432 by a $\bar{t}$ of 0.1 units. This flux then increases slowly with time to eventually reach the steady-state value of -0.0433. At the venular boundary, the dimensionless plasma protein flux drops from 0.0507 to 0.0434 by $\bar{t}$ equal to 0.1 units, and continues to drop, albeit slowly, to eventually reach the steady-state value of 0.0433 (see panel (ii) of Figure (5.12)).

The onset of venous congestion has a marginal effect on the interstitial plasma protein distribution when interstitial plasma protein transport is restricted to diffusion only (see the

right panel of Figure (5.13)). The drop in transcapillary transport of plasma proteins into the interstitium at the arteriolar end of the system results in the net loss of plasma proteins from the interstitium via the venular capillary. Since this reduction in plasma protein transport into the system is sustained, the net diffusive flux of plasma proteins through the interstitium must drop as the system approaches its new steady-state. Hence, the interstitial plasma protein concentration gradient must be slightly less under the new steady-state conditions, compared to the initial state. However, by the time the system has reached steady-state, conservation of plasma proteins within the system dictates that $[\tilde{C}^1]_{ven}$ equal $\hat{C}^{art}$. The interstitial plasma protein concentration adjacent the arteriolar boundary therefore increases to satisfy the constraints imposed by continuity and the fact that diffusion of interstitial plasma protein transport is less under the new steady-state conditions.

Mass Exchange Assuming Mesothelial Transport Properties Similar to Those of the Vascular Walls

Fluid Exchange The shifts in the effective chemical potential of the various luminal fluids following venous congestion suggest that subsequent fluid exchange between the blood and the peritoneum should increase and that fluid flow across the venular capillary wall should change direction. In fact, this is observed both when ξ is one and when it is zero (see Table (5.5)).

Figure (5.14) shows the transient fluid exchange across the three permeable boundaries following venous congestion and assuming that ξ is unity. The fluid fluxes increase dramatically following the onset of venous congestion, then continue to rise more slowly, so that the system achieves steady-state ·by a $\tilde{t}$ of 5.0. However, when ξ is zero, the system reaches steady-state with respect to fluid exchange almost immediately after the onset of the perturbation.

The transient distribution of fluid exchange across the mesothelial boundary is qualitatively the same as shown in Figure (5.4), both when ξ is one and when it is zero. Fluid exchange across the mesothelium in the vicinity of the venular capillary shifts direction so that, following the onset of venous congestion, fluid is transported from the interstitium to the peritoneum
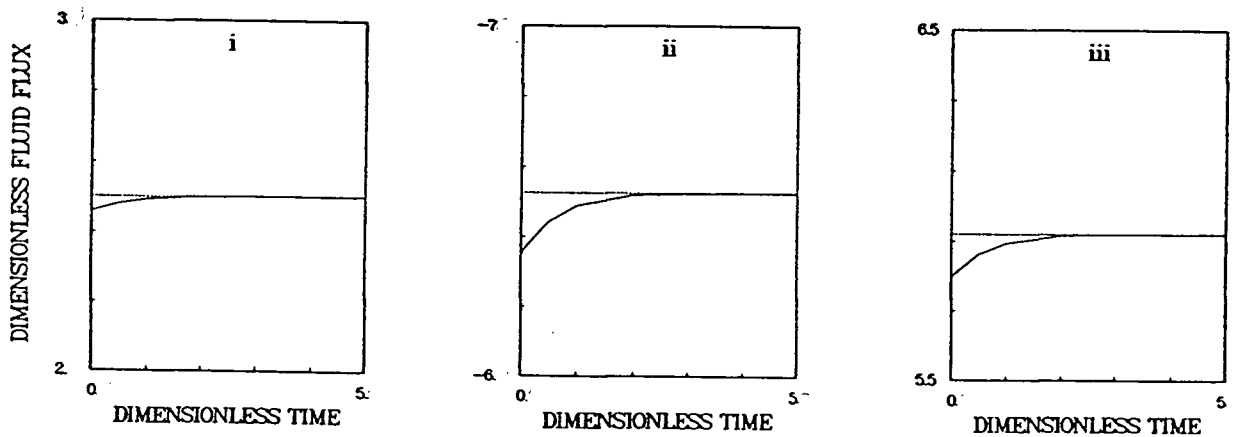
Figure 5.14: The average transient fluid fluxes across the permeable boundaries following venous congestion, assuming mesothelial transport properties equal to those of the arteriolar capillary and a ζ of 1, are shown in the three panels above. Panel (i) shows the fluid flux across the arteriolar capillary, panel (ii) corresponds to the fluid flux across the venular capillary, and panel (iii) represents the net fluid flux across the mesothelium. In each case the fluxes are normalized with respect to their respective pre-perturbation values. The dotted line represents the new steady-state value in each case.

ξ	Period	Boundary Condition 2			Boundary Condition 3		
		Art	Ven	Mes	Art	Ven	Mes
1.0	Pre-Upset	-2.387	-0.656	0.087	-3.551	-0.762	0.139
1.0	Post-Upset	-5.857	-4.134	0.500	-9.232	-8.070	0.865
1.0	Steady-State	-5.971	-4.278	0.513	-9.143	-7.347	0.825
0.0	Pre-Upset	-2.313	0.632	0.084	-3.570	0.803	0.138
0.0	Post-Upset	-5.720	-4.048	0.488	-9.259	-8.100	0.868
0.0	Steady-State	-5.708	-4.024	0.487	-9.153	-7.364	0.826

Table 5.5: **The average transient fluid fluxes across the permeable boundaries follow-ing venous congestion, for the mesothelial boundary conditions 2 and 3. In each case the table reports the flux prior to the upset ('pre-upset'), at $\tilde{t}$ equal 0.001 post-upset ('post-upset'), and at the new system steady-state ('steady-state'). A negative flux indicates a flow into the interstitium.**

along the entire length of the mesothelial boundary.

Plasma Protein Exchange and Interstitial Plasma Protein Distribution Table (5.6) lists the transient plasma protein fluxes across each of the three boundaries following venous congestion. Figure (5.15), meanwhile, shows the dimensionless plasma protein flux across the three boundaries as a function of time and assuming that ξ is one. Because the plasma protein exchange across the boundaries is predominantly convective, the transient plasma protein exchange parallels the transient fluid exchange behavior. However, as this figure illustrates, the relative changes in protein fluxes across the permeable boundaries are more dramatic than the relative changes in fluid exchange rates. Further, the transient behavior assuming ξ is zero is qualitatively the same as when ξ is one, except that the length of the transient period is somewhat shorter.

Both when ξ equals zero and when it equals one, the time needed for the mesothelial boundary to achieve steady-state with respect to plasma protein exchange is longer than the period required for the other two boundaries. Since the arteriolar and venular capillaries filter fluid and plasma proteins following the upset, and since the transport of proteins across these
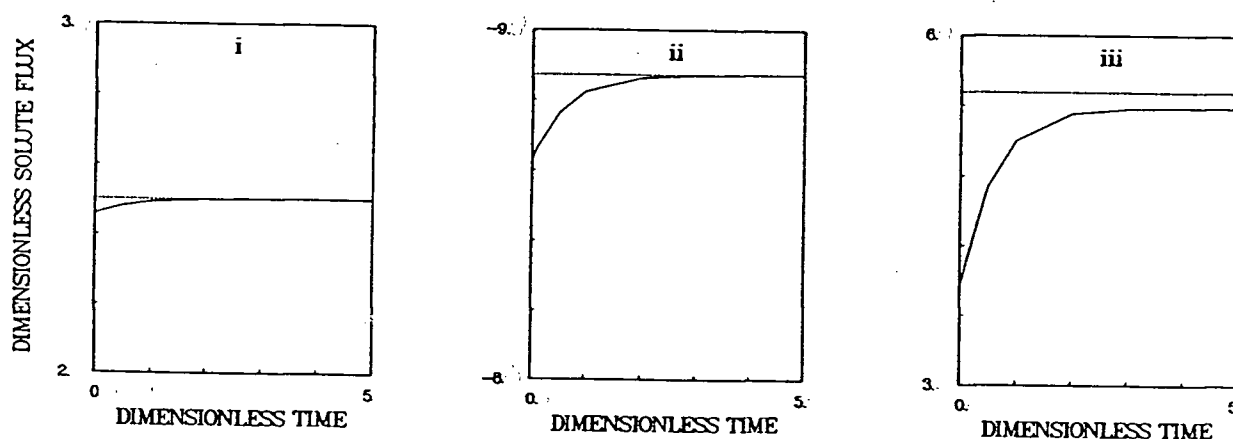
Figure 5.15: The average transient plasma protein fluxes across the permeable boundaries following venous congestion, assuming mesothelial transport properties equal to those of the arteriolar capillary and a ξ of 1, are shown in the three panels above. Panel (i) shows the protein flux across the arteriolar capillary, panel (ii) corresponds to the protein flux across the venular capillary, and panel (iii) represents the net protein flux across the mesothelium. In each case the fluxes are normalized with respect to their respective pre-perturbation values. The dotted line represents the new steady-state value in each case.
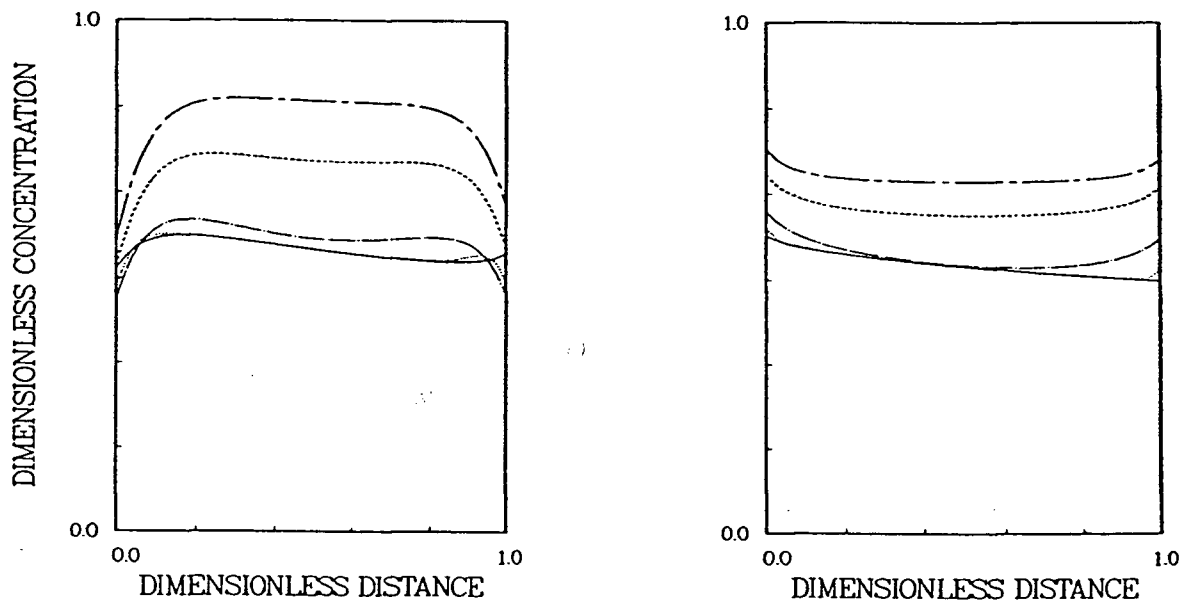
Figure 5.16: The transient dimensionless total plasma protein concentration distributions ($\tilde{C}^t$) following venous congestion and assuming mesothelial transport properties equal to those of the arteriolar capillary are shown for (i) the case where ξ is 1 (left panel) and (ii) for the case where ξ is 0 (right panel). In each case the solid line represents the initial condition, the dotted line is at $\tilde{t}$ equal 0.001, the chain-dot line is at $\tilde{t}$ equal 0.05, the dashed line corresponds to $\tilde{t}$ equal 0.5, and the chain-dash line represents the final steady-state condition.

ξ	Period	Boundary Condition 2			Boundary Condition 3		
		Art	Ven	Mes	Art	Ven	Mes
1.0	Pre-Upset	-0.358	0.072	0.014	-0.533	0.762	0.025
1.0	Post-Upset	-0.878	-0.620	0.059	-1.385	-1.210	0.188
1.0	Steady-State	-0.896	-0.604	0.077	-1.371	-1.102	0.124
0.0	Pre-Upset	-0.347	0.063	0.014	-0.535	0.036	0.025
0.0	Post-Upset	-0.858	-0.607	0.055	-1.389	-1.215	0.192
0.0	Steady-State	-0.856	-0.604	0.073	-1.373	-1.105	0.124

Table 5.6: **The average transient plasma protein fluxes across the permeable boundaries following venous congestion, for the mesothelial boundary conditions 2 and 3. In each case the table reports the flux prior to the upset ('pre-upset'), at $\tilde{t}$ equal 0.001 post-upset ('post-upset'), and at the new system steady-state ('steady-state'). A negative flux indicates a flow into the interstitium.**

boundaries is largely convective, the length of the transient associated with plasma protein exchange is approximately equal to that for fluid exchange. However, as indicated in the plasma protein distributions of Figure (5.16), a considerable increase in the total interstitial plasma protein content occurs following the initiation of venous congestion. This filling period is much longer than the time required for the fluid exchange rates within the system to adjust. Further, plasma protein exchange across the mesothelial boundary cannot reach steady-state until the interstitial plasma protein concentration distribution stabilizes.

The left-hand panel of Figure (5.16) shows the transient distributions of the dimensionless interstitial plasma protein concentration assuming ξ is equal to one. In this case, there is a local buildup of interstitial plasma proteins in the vicinity of the arteriolar and venular vessels shortly after the onset of venous congestion, similar to the buildup observed during the early stages of hypoproteinemia. This is likely due to the same causes cited in that case, namely the combination of plasma protein convection within the interstitium and sieving at the mesothelial boundary. Furthermore, since interstitial fluid flow is directed towards the center of the tissue, interstitial plasma protein convection and diffusion generally act in opposite directions, as evidenced by the interstitial plasma protein concentration gradients of the left

panel of Figure (5.16). When ξ is zero, the gradient near the venular boundary changes direction following the perturbation (see the right panel), reflecting the shift in plasma protein exchange across that boundary.

In contrast to the situation during hypoproteinemia, we have already noted that the interstitial plasma protein content following venous congestion increases with time for both values of ξ (see Figure (5.16)). This occurs for the following reason. The average plasma protein concentration in the interstitium prior to the upset is less than that in the serum. Following the perturbation, the convective flux of plasma proteins from the blood into the interstitium rises. The convective flux of plasma proteins from the interstitium to the peritoneum likewise increases. However, since the sieving properties of the three boundaries are the same (i.e., $\sigma^{art} = \sigma^{ven} = \sigma^{mes}$), and since the interstitial plasma protein concentration is less than that of the serum, the concentration of plasma proteins in the incoming fluid is higher than that of the fluid leaving the interstitium. In addition, since the rate of fluid flow into the interstitium equals the rate of fluid flow out of the interstitium at all times (because the interstitium is rigid), the convective flow of proteins into the tissue space must then exceed the convective flow of proteins out of the interstitium, thereby increasing the interstitial plasma protein content.

Mass Exchange Assuming a Highly Permeable Mesothelium

Fluid Exchange The data of Table (5.4) suggest that the fluid exchange within the system should increase following the onset of venous congestion. In fact, as illustrated in Table (5.5), this is true for both values of ξ investigated. The normalized transient fluid fluxes across the permeable boundaries are illustrated graphically in Figure (5.17) for the case where ξ is one. A similar pattern is seen when ξ is zero, except that, once again, the transient period is somewhat shorter when plasma protein transport occurs by diffusion alone.

The transient distribution of fluid fluxes across the mesothelium is qualitatively the same as that of Figure (5.9), both when ξ is one and when it is zero. Therefore, the fluid flow across the mesothelium in the vicinity of the venular capillary changes direction so that, following
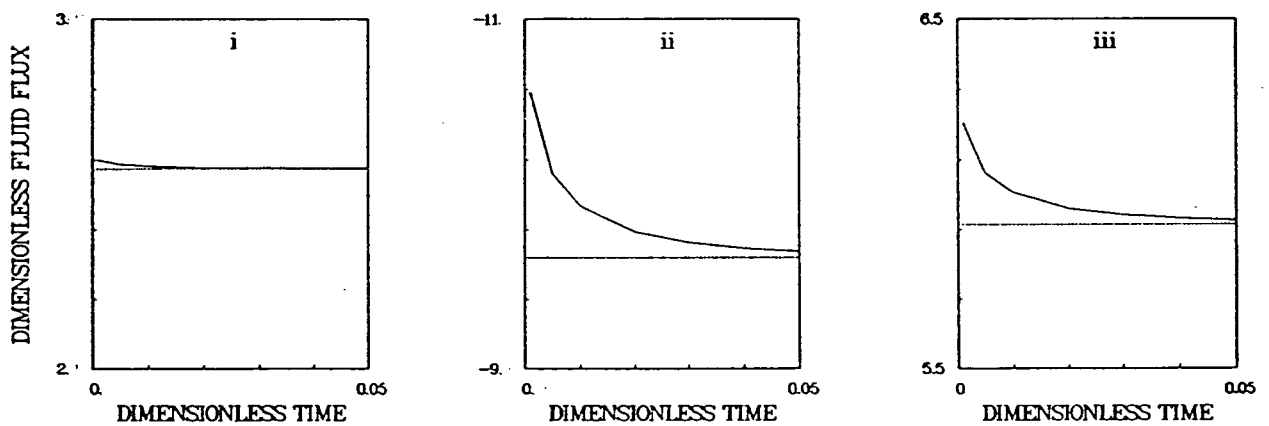
Figure 5.17: The average transient fluid fluxes across the permeable boundaries following venous congestion, assuming a highly permeable mesothelium (boundary condition 3) and a ζ of 1, are shown in the three panels above. Panel (i) shows the fluid flux across the arteriolar capillary, panel (ii) corresponds to the fluid flux across the venular capillary, and panel (iii) represents the net fluid flux across the mesothelium. In each case the fluxes are normalized with respect to their respective pre-perturbation values. The dotted line represents the new steady-state value in each case.

the onset of venous congestion, fluid movement is from the interstitium to the peritoneum. Furthermore, interstitial fluid flow is directed from the vascular boundaries towards the center of the tissue segment in both cases.

Plasma Protein Exchange and Interstitial Plasma Protein Distribution The exchange of plasma proteins across the various boundaries is largely convective for both values of ξ. Hence, the transient behavior of the system with respect to plasma protein exchange follows its pattern of fluid exchange. Further, the transient distribution of plasma protein fluxes across the mesothelium is qualitatively the same as that shown in Figure (5.9). Figure (5.18) shows the normalized transient plasma protein exchange across the three boundaries for a ξ of one. In each case, there is an initial rise in the plasma protein flux, followed by a decay in the exchange rate. A similar behavior is observed when ξ is zero, except that, once more, the length of the transient period is shorter.

The transient plasma protein distribution for the two values of ξ are shown in Figure (5.19). Whereas, when the mesothelium behaves as a sieving boundary the interstitial plasma protein content increases following venous congestion (see Figure (5.16)), in this case the mean interstitial plasma protein content decreases with time. Following the onset of venous congestion, the fluid exchange across the vascular boundaries increases, so that the convective flux of plasma proteins also increases. However, as fluid enters into the interstitium from the vascular compartments, plasma proteins are sieved. In contrast, the fluid crossing the mesothelial boundary is not filtered so that, as the fluid flux across the mesothelium increases, there is a net loss of plasma proteins from the interstitium to the peritoneal fluid. This demonstrates that the sieving properties of the drainage system within a tissue (in this case, the mesothelium) play a major role in determining the ratio of interstitial plasma protein concentration to vascular plasma protein concentration.

Once again the simulations suggest that, when both interstitial plasma protein convection and diffusion occur, they oppose one another. The comparatively high interstitial plasma protein content initially found in the vicinity of the venular boundary is soon depleted, as
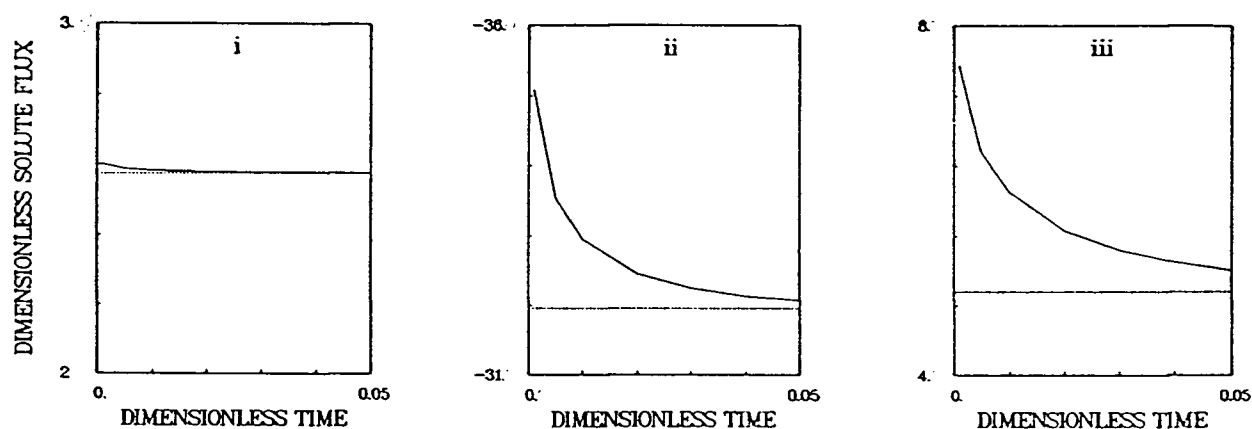
Figure 5.18: The transient plasma protein fluxes across the permeable boundaries following venous congestion, assuming a highly permeable mesothelium (boundary condition 3) and a ξ of 1, are shown in the three panels above. Panel (i) shows the protein flux across the arteriolar capillary, panel (ii) corresponds to the protein flux across the venular capillary, and panel (iii) represents the net protein flux across the mesothelium. In each case the fluxes are normalized with respect to their respective pre-perturbation values. The dotted line represents the new steady-state value in each case.
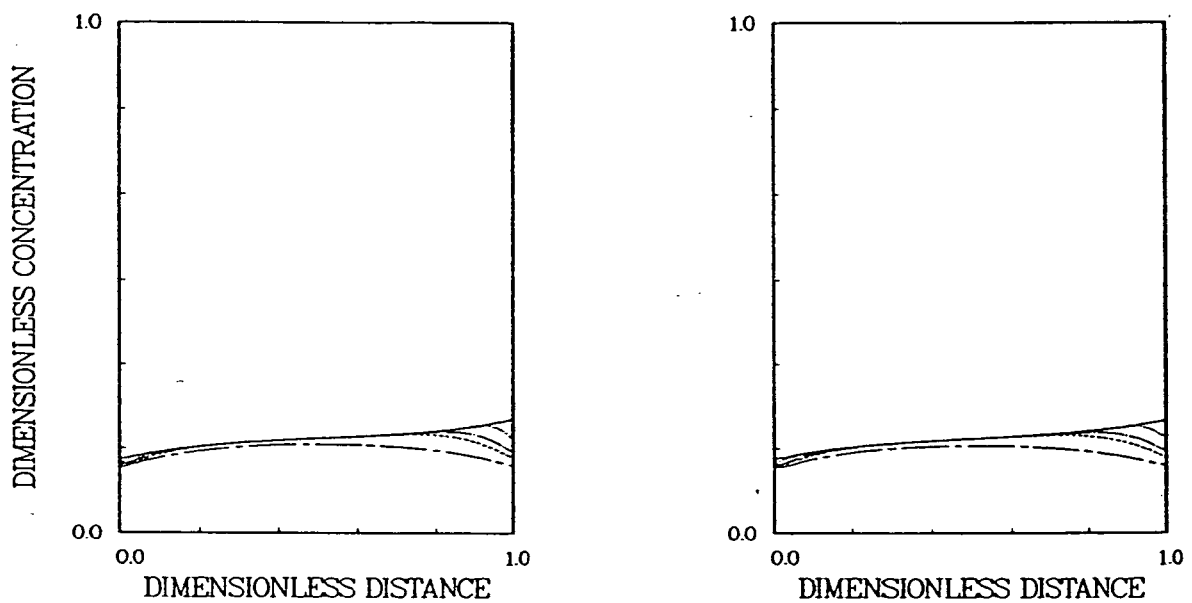
Figure 5.19: The transient dimensionless total plasma protein concentration distributions ($\tilde{C}^t$) following venous congestion and assuming a highly permeable mesothelium (boundary condition 3) are shown for (i) the case where ξ is 1 and (ii) for the case where ξ is 0. In each case the solid line represents the initial condition, the dotted line is at $\tilde{t}$ equal 0.001, the chain-dot line is at $\tilde{t}$ equal 0.005, the dashed line corresponds to $\tilde{t}$ equal 0.01, and the chain-dash line represents the final steady-state condition.

the venular capillary shifts from a re-absorbing to a filtering vessel. When interstitial plasma protein transport is limited to diffusion, there is a change in gradient in interstitial plasma protein concentration some distance from the venular boundary shortly after the perturbation begins. This is due to the increased protein exchange from the interstitium to the peritoneum there. However, adjacent the venular capillary wall, plasma protein diffusion is directed into the interstitium, due to the transfer of proteins the from blood to the interstitium at that boundary. Since this shift in the interstitial plasma protein concentration gradient occurs over a very short distance just outside of the venular boundary, it is not discernable in Figure (5.19).

Summary of Venous Congestion Simulations

As in the case of hypoproteinemia, the length of the transient period varied inversely with the permeability of the mesothelial layer. Further, when it is assumed that the mesothelium is impermeable, the transient behavior of the fluid and plasma protein fluxes entering and leaving the system are strongly influenced by the interstitial plasma protein transport mechanisms and by the transient distribution of plasma proteins within the interstitial space. Once again, this is due to the greater role that the interstitium has here in determining the overall resistance of the system.

In contrast to the simulations of hypoproteinemia, however, some of the simulations of venous congestion predicted an increase in the interstitial plasma protein content with time. A determining factor for this behavior appears to be the plasma protein sieving properties of the filtering boundary relative to the sieving properties of the draining boundary. This provides a possible explanation for the differences in the interstitial plasma protein content within selected tissues observed in clinical settings during venous congestion, and is discussed further below.

5.4.3   Clinical Observations of Hypoproteinemia and Venous Congestion

According to the simulations presented above, the rate of fluid exchange within the model tissue segment typically increases following hypoproteinemia. However, because of the reduced plasma

protein content in the filtering fluid, the net rate at which plasma proteins enter the interstitial space is less than that prior to the upset. This causes a 'washout' of plasma proteins from the interstitium and leads to a somewhat reduced interstitial plasma protein content by the time the system has achieved a new steady-state. These findings are in keeping with the clinical observations reported by Witte and co-workers [114]. The authors state that hypoproteinemia is followed by a lowering of interstitial plasma protein content.

The simulations of venous congestion revealed several interesting phenomena that might shed further light on clinical observations of this state. Clinical data show that, in most peripheral tissues, the plasma protein concentration in lymph decreases with the onset of venous congestion, suggesting that the interstitial plasma protein concentration likewise drops [113]. Witte and co-authors attribute the washout of plasma proteins to the increased filtration rates that accompany an elevation in systemic pressure. However, the simulations presented here demonstrate that an increased filtration rate does not assure washout of plasma proteins from the interstitium of mesentery, for example. On the contrary, the majority of the simulations predicted an increase in interstitial plasma protein content within the model tissue. Only in those cases in which the sieving of proteins at the draining boundary (e.g., the mesothelium) was less than the sieving at the filtering boundaries did the interstitial plasma protein content decrease following venous congestion.

The simulations suggest that it is the relative sieving properties of the draining and filtering boundaries, and not simply the filtration rate, that determines whether plasma protein washout occurs. Since it is generally thought that the terminal lymphatics do not sieve proteins to any great extent [77], it follows that, in most tissues, we would expect a decrease in plasma protein content to accompany enhanced filtration, as seen clinically. The notion that the relative sieving properties are important in determining changes in interstitial plasma protein content is further supported by the fact that the plasma protein content in hepatic lymph (and so, presumably, the plasma protein content in the interstitium of the liver) increases under venous congestion [114]. Since the exchange vessels of the liver are sinusoids, far less sieving occurs across the

vascular walls in this tissue, so that the sieving properties of the filtering and the draining boundaries are similar.

One other characteristic of venous congestion is the accumulation of fluid in the pleural cavity. This pathological state is called *ascites* [51]. The increased fluid exchange across the mesothelium predicted by the model seems to support this clinical observation. Further, the simulations indicate that this increase accompanies a shift from fluid re-absorption to fluid filtration at the venular capillary, due to the increase in hydrostatic pressure in that vessel. This suggests that there may be some limiting value for venular hydrostatic pressure, corresponding to the shift in the direction of transcapillary fluid flux there, that leads to ascites.

5.5 Concluding Remarks

In this chapter we studied the response of the model tissue segment to two systemic perturbations, namely hypoproteinemia and venous congestion. Since the simplified version of the model employed in these simulations does not include all of the features of the microvascular exchange system (for example, interstitial swelling is neglected) the results are, at best, qualitative. However, the simulations reveal several interesting features of the model microvascular exchange system. These are summarized below.

1. When the mesothelium is permeable, the trends in fluid and plasma protein exchange following a systemic perturbation can be anticipated by considering the effect that the given upset has on the effective chemical potential of the luminal fluids. In such instances the interstitium may not be the major resistance within the system. However, when the mesothelium is impermeable, fluid and plasma proteins must cross the entire interstitial space in their journey from the filtering vessel to the re-absorbing vessel, so that the interstitium comprises a large fraction of the system's total resistance to mass exchange. In these cases the distribution of interstitial plasma proteins plays a greater role in determining the overall behavior of the model tissue. Further, the length of the transient period following an upset is typically shorter for those cases in which the mesothelium is

permeable.

2. Following hypoproteinemia, the interstitial plasma protein content of the tissue segment typically decreases with time, due to a decrease in plasma protein exchange across the vascular boundaries and an increase in the total rate of fluid exchange within the system. This is in keeping with qualitative clinical observations.

3. Following venous congestion, the fluid exchange rate and plasma protein exchange rate within the system both typically increase. However, the change in interstitial plasma protein content depends, in part, on the relative sieving properties of the filtering and draining boundaries. When the reflection coefficients of these two sets of boundaries are similar, the interstitial plasma protein content increases due to the increased protein exchange rate across the filtering boundaries and sieving of interstitial plasma proteins at the draining boundaries. As the reflection coefficient of the draining boundaries decreases relative to that of the filtering boundaries, there is a net loss of plasma proteins from the interstitial space, resulting in a decrease in total interstitial plasma protein content over time. These results are supported by the clinical observation that interstitial plasma protein content in the liver increases during venous congestion. Since this tissue is serviced by sinusoids, the sieving properties of the filtering blood vessels and the draining lymphatic vessels are similar. (It should be noted, however, that both the filtering and draining vessels of the liver offer little sieving of plasma proteins.) In addition, the model predicts an increase in fluid transfer from the mesentery to the peritoneal fluid, supporting the clinical observation of ascites formation.

The trends in system behavior predicted by the simplified model are, for the most part, in keeping with the limited number of clinical observations associated with hypoproteinemia and venous congestion discussed here. Furthermore, the simulations provide a clearer picture of the relationship between the vascular wall transport properties, the interstitial transport properties, and the transient behavior of the system as a whole following these upsets.

Chapter 6

A Preliminary Study of Tracer Transport through the Interstitium

6.1 Introduction

Thus far we have considered the transport of a single, aggregate plasma protein species through the interstitium of a model tissue. In fact, numerous types of macromolecules are exchanged between the blood and the interstitium under normal conditions. In addition, certain clinical procedures, such as chemotherapy, involve the exchange of small quantities of foreign substances between the blood stream and a particular organ or tissue. The exchange of multiple solute species within the microcirculation is therefore of interest to physiologists and clinicians alike.

This chapter presents a study of the relative exchange rates of two different macromolecular tracers representing albumin and γ – globulin within a hypothetical, one-dimensional tissue. Specifically, the study investigates the time required for the concentration of the tracer in the outlet stream to reach 50 % of its steady-state value, subsequent to its introduction in the blood at a dimensionless concentration of 0.01, as a function of the following:

1. the transport properties of the capillary wall to the tracer,

2. the transport properties of the tracer through the interstitial space, and

3. the interstitial distribution volume of tracer.

The results of the study suggest that the distribution volume of a particular solute species can play a major role in determining its rate of transport through the interstitium. Further, the exclusion properties of the interstitium can create conditions for a 'gel-chromatographic effect', whereby larger macromolecules pass through the interstitial space more quickly than smaller

149

macromolecules. (This mechanism is to be distinguished from the 'free-fluid phase – gel phase' mechanism proposed by Watson and Grodins [104] that lacks substantial structural evidence.)

The chapter is divided into five remaining sections. Section 6.2 describes the model tissue segment and the equations applying to the transient movement of a solute species through that tissue segment. Section 6.3 outlines the particular numerical experiments constituting the study, while Section 6.4 outlines the numerical procedures employed to solve the relevant mathematical expressions. The results of the study are then discussed in Section 6.5. Finally, Section 6.6 summarizes the ramifications of these findings to the interpretation of transient tracer experiments and the delivery of substances to specific tissue sites.

6.2 Defining the System

Consider a flat, thin, sheet-like tissue analogous to the mesenteric tissue of Chapter 4 and bounded left and right by a blood capillary and a terminal lymphatic vessel, respectively. It is assumed that the upper and lower surfaces of the tissue are impermeable and that the intervening interstitium is both homogeneous and isotropic. Furthermore, the tissue properties and conditions are considered uniform in the direction parallel to the vessels' axes, so that the model tissue can be treated as a one-dimensional system.

Contained within the tissue is an aggregate plasma protein species representative of the various osmotically active plasma protein species found *in vivo*. These display the same characteristics as the aggregate plasma proteins of Chapters 4 and 5. It is further assumed that, at some time t_o, a macromolecular tracer is introduced into the blood vessel. Since this macromolecule is present in minute quantities only (i.e., one percent of the total plasma protein concentration), its contribution to the system osmotic pressure is negligible and therefore it does not alter the exchange of fluid or the exchange of aggregate plasma protein species within the system. Given this, the interstitial fluid flux depends only on the local gradient in fluid hydrostatic pressure, P^1, and aggregate protein osmotic pressure, Π^1, according to Eq. (5.2). The fluid material balance is then given by Eq. (5.4), with the added constraint that L_p^{mes} is

zero. With these assumptions, the transient tracer distribution problem is uncoupled from the steady-state problem of fluid and aggregate plasma protein transport.

The material balance expression for the aggregate plasma protein species is therefore given by the steady-state version of Eq. (5.7), assuming further that j_s^{mes} (given by Eq. (5.6)) is zero. Meanwhile, the transient distribution of interstitial tracer concentration, C^2, is described by an analogous form of Eq. (5.7), assuming once more that no exchange of tracer occurs across the upper and lower surfaces of the tissue segment. Furthermore, since the tracer's osmotic pressure is negligible compared to that of the aggregate plasma protein species, then the fluid chemical potential in the tracer's distribution volume is equal to $P^1 - \Pi^1$.

The exchanges of fluid and solutes across the capillary wall are described by the same set of boundary conditions as presented in Chapter 4 (see Eqs. (4.13), (4.14), and (4.15)). However, the conditions prevailing at the lymphatic vessel warrant some discussion.

It is typically assumed [3, 14, 70, 108] that, under normal conditions, the flow of fluid across the lymphatic wall is proportional to the interstitial hydrostatic fluid pressure, P^1. That is,

$$\left[j_w^0\right]_{lym} = L_p^{lym} \cdot \left(\left[P^1\right]_{lym} - P^{lym}\right), \tag{6.1}$$

where $L_p^{lym} \cdot P^{lym}$ is some reference lymph drainage rate. This type of relationship can be viewed as a specific form of the Starling relationship in which the reflection coefficient of the lymphatic wall, σ^{lym}, is zero. If we further assume, for simplicity, that the hydrostatic pressure within the lymphatic vessel, P^{lym}, is zero, we then have

$$\left[j_w^0\right]_{lym} = L_p^{lym} \cdot \left[P^1\right]_{lym}. \tag{6.2}$$

Solutes, meanwhile, are assumed to cross the lymphatic wall by unhindered convection [3, 14, 75, 108]. The valve-like behavior of the overlapping endothelial cells of the lymphatic wall prevents back-flow of solutes from the lymph to the tissue space. Hence, assuming that a thin fluid film separates the lymphatic wall and the interstitium (analogous to that at the vascular boundary), the rate of exchange of aggregate proteins across the vessel wall ($\left[j_s^1\right]_{lym}$), for example, is

$$\left[j_s^1\right]_{lym} = \left[j_w^0\right]_{lym} \cdot \left[C^1\right]_{lym}. \tag{6.3}$$

A similar expression applies for the exchange of a particular tracer species 2, namely,

$$\left[j_s^2\right]_{lym} = \left[j_w^0\right]_{lym} \cdot \left[C^2\right]_{lym}. \tag{6.4}$$

An alternative boundary condition for the exchange of a given solute species k at the lymphatic vessel wall might be

$$\left[j_s^k\right]_{lym} = \left[j_w^0\right]_{lym} \cdot \frac{n^k}{n^0} \cdot \left[C^k\right]_{lym}, \tag{6.5}$$

where $\frac{n^k}{n^0} \cdot \left[C^k\right]_{lym}$ is equivalent to the average plasma protein concentration based on the total mobile fluid volume fraction. In this fashion, Eq. (6.5) eliminates the 'thin film' assumption. However, since all previous simulations used the thin film approach, it is retained here as well.

The dimensionless form of the mass balance equations can be found in Chapters 4 and 5. Note that the tracer mass balance equation is non-dimensionalized with respect to the parameters for the aggregate plasma protein species. For example, the dimensionless diffusivity of tracer species k is $n^k \cdot D_{eff}^k / D_{eff}^1$. The dimensionless forms of Eqs. (6.2) and (6.3), meanwhile, are, respectively,

$$-\left[\frac{d(\tilde{P}^1 - \tilde{\Pi}^1)}{d\tilde{x}}\right]_{lym} = \tilde{L}_p^{lym} \cdot \left[\tilde{P}^1\right]_{lym}, \tag{6.6}$$

and

$$\left[\tilde{j}_s^1\right]_{lym} = \left[\tilde{j}_w^0\right]_{lym} \cdot \left[\tilde{C}^1\right]_{lym}, \tag{6.7}$$

where $\tilde{L}_p^{lym} = L_p^{lym} L / K^0$. As before, all pressures and concentrations are normalized with respect to P^{art} and $C^{1,art}$ (the arteriolar concentration of the aggregate plasma protein species), respectively. Equations (6.6) and (6.7) are combined with the appropriate dimensionless forms of the aggregate plasma protein mass balance equation, the tracer mass balance equation, the fluid mass balance equation, the capillary wall boundary conditions, and the initial conditions to describe the movement of both the aggregate plasma protein species and the tracer through the interstitium.

6.3 Case Studies

In order to carry out the numerical simulations, the various model parameters must first be assigned values. These parameters can be divided into three groups: those parameters characterizing fluid and aggregate plasma protein exchange across the capillary wall and the transport of these materials through the interstitium; those parameters characterizing the transcapillary exchange and interstitial transport of the tracers; and the parameters characterizing mass exchange across the lymphatic wall.

The first group of parameters were assigned the same set of values as in the steady-state analysis of fluid and aggregate plasma protein exchange in mesentery (see Table (4.1) in Chapter 4), assuming further that the aggregate protein convective hindrance, ξ, equalled 0.5. The properties of the aggregate plasma protein species are therefore close to, but not identical with, the values described below for the albumin tracer.

The following tracer parameters were assumed. The capillary wall permeabilities to the albumin and globulin tracers, $D^{art,alb}$ and $D^{art,glob}$, assumed values of 2.4×10^{-8} cm/s and 1.39×10^{-8} cm/s respectively. These values fall within the range reported in the literature for these two species [83]. The values of the reflection coefficients for the albumin tracer and the globulin tracer, σ^{alb} and σ^{glob}, were 0.89 and 0.91 respectively, based on data reported for dog hindpaw [82]. The distribution volume fractions assumed for the two tracers, meanwhile, were 0.68 and 0.5, respectively, based on rabbit skin data [13]. The effective interstitial diffusivity of the albumin tracer, D_{eff}^{alb}, assumed a value of 1.0×10^{-7} cm^2/s, based on the data of Fox and Wayland [38]. Since no value was available for the interstitial diffusivity of globulin, D_{eff}^{glob}, this parameter was assigned a value such that $D_{eff}^{alb}/D_{eff}^{glob}$ equalled $D^{art,alb}/D^{art,glob}$. This yielded a D_{eff}^{glob} of 0.58×10^{-7} cm^2/s.

The product $\xi^k \cdot \beta^k$ for the albumin and globulin tracers was varied over a range of values by establishing first the lower limits for ξ^k and β^k individually. The lower limit for ξ^k was arbitrarily set equal to 0.25. The lower limit for β^k, meanwhile, was set equal to the ratio n^k/n^0, thereby assuming that the flow conductivity of the interstitial space was uniformly distributed

throughout the various mobile fluid volume fractions. Under this assumption the regions of the interstitial space accessible to the macromolecular tracers were no more conductive to fluid than the excluded regions of the interstitium. On this basis, a lower limit for $\beta^k \cdot \xi^k$ of 0.21 for albumin and 0.16 for globulin was determined. However, in all likelihood, macromolecules excluded from portions of the interstitial matrix will be limited to pathways of higher conductivity, leading to somewhat larger values of $\beta^k \cdot \xi^k$. Hence, additional values of $\beta^k \cdot \xi^k$ equal to 0.5 and 0.9 were assumed for each of the two tracers during the sensitivity analyses discussed below.

According to Eqs. (6.2) and (6.3), mass exchange across the lymphatic vessel wall is characterized by a single parameter – the lymphatic hydraulic conductance, L_p^{lym}. Since no information could be found in the literature to quantify L_p^{lym}, a set of simulations was first performed to investigate the influence of this parameter on the exchange of fluid within the system. Increasing L_p^{lym} from 1.35×10^{-9} cm^3/(dyne-s) to 1.35×10^{-7} cm^3/(dyne-s) caused the fluid exchange rate within the system to increase by less than 7 %, indicating that fluid flow was relatively insensitive to the value of L_p^{lym} in this range. The lymphatic hydraulic conductance was therefore arbitrarily assigned a value of 1.35×10^{-9} cm^3/(dyne-s), equal to the value applied to the arteriolar boundary.

Having established the reference values for the model parameters, a series of numerical simulations was performed to investigate the effect of several system parameters on the transport rates of the albumin and globulin tracers through the model tissue. These system parameters are summarized below:

1. the transport characteristics of the capillary wall to each of the two tracers;

2. the interstitial distribution volume fraction of the globulin tracer; and

3. the diffusivity of the albumin tracer.

In each case, the product $\beta^k \cdot \xi^k$ of the tracer was varied over the range of values described earlier to provide a factorial design. In all, 21 transient simulations were performed, as well as 21 corresponding steady-state runs.

6.4 Numerical Procedures

A numerical procedure similar to that reported in Chapter 5 that combined the finite element and finite difference methods was used here to solve for the transient distribution of tracer throughout the interstitium. Again, the interstitium was divided into 25 elements and 51 nodal points. The initial time step size was determined by specifying an initial Courant number of 0.05. As a further check of the validity of the numerical solution, one of the simulations was repeated assuming an initial Courant number of 0.025, thereby doubling the number of time steps performed during the run. As a result, the dimensionless time taken for the tracer concentration at the lymphatic vessel to reach 50 % of its steady-state value, $\bar{t}_{50\%}$, changed by less than .05 %. In another test, the initial Courant number was reduced from 0.05 to 0.01, resulting in a 5-fold increase in the number of time steps taken during the simulation. The reduced time step produced no significant change in the model predictions.

6.5 Results and Discussion

This section is divided into three parts. The first discusses the effect of the capillary wall transport properties on the transport rates of the globulin and albumin tracers, assuming various values of $\beta^k \cdot \xi^k$ for these macromolecules. The second part considers the effect of the globulin interstitial distribution volume on the transport of that tracer for different values of $\beta^{glob} \cdot \xi^{glob}$. Finally, the third part of this section discusses the effect of interstitial diffusivity on the transport rate of the albumin tracer as a function of $\beta^{alb} \cdot \xi^{alb}$.

6.5.1 The Effect of Capillary Boundary Conditions on Tracer Transit Time

The first set of simulations explored the combined effect of the $\beta^k \cdot \xi^k$ and the capillary wall transport properties on the exchange of each of the two tracers. Two 2×3 factorial studies were performed in which each tracer was subjected to first the globulin boundary conditions and then the albumin boundary conditions for each value of $\beta^k \cdot \xi^k$ considered. (Recall that the

albumin boundary condition corresponds to a reflection coefficient of 0.89 and a permeability, D^{art}, of 2.4×10^{-8} cm/s at the capillary wall, while the globulin boundary condition implies a reflection coefficient of 0.91 and a permeability of 1.39×10^{-8} cm/s.)

Tracer	Boundary Condition	$\xi \cdot \beta$	Steady-State Outlet Concentration
Globulin	Globulin	0.16	0.00091
		0.50	0.00091
		0.90	0.00091
Globulin	Albumin	0.16	0.00113
		0.50	0.00113
		0.90	0.00113
Albumin	Albumin	0.21	0.00113
		0.50	0.00113
		0.90	0.00113
Albumin	Globulin	0.21	0.00091
		0.50	0.00091
		0.90	0.00091

Table 6.1: **The effect of capillary wall boundary conditions on the steady-state concentration of the tracers in the outlet (lymphatic) stream.**

Table (6.1) presents the steady-state dimensionless concentrations for the albumin and the globulin tracers in the lymphatic vessel (i.e., their plasma/lymph ratios) as functions of $\beta \cdot \xi$ and the capillary wall boundary conditions. Recall that the outlet concentration in the lymphatic vessel equals the interstitial concentration within the tracer's distribution volume in the vicinity of the lymphatic vessel. It is clear from Table (6.1) that the steady-state concentration of a tracer is determined by the boundary conditions at the capillary wall, and not the transport

mechanisms within the interstitial space. In fact, the outlet concentration is determined largely by the capillary wall reflection coefficient since, in the simulations presented here, the principle mechanism for the transcapillary exchange of tracer is convective transport. Hence, the influx of some tracer k into the system is proportional to $(1 - \sigma^k)$. Under steady-state conditions and for this model tissue, then, the flux of tracer across the lymphatic vessel wall must also be proportional to $(1 - \sigma^k)$, so that the outlet stream composition is determined by the degree of sieving at the capillary wall.

Table (6.2) presents the dimensionless time required for the tracer's outlet stream concentration to reach 50 % of its steady-state value, $\tilde{t}_{50\%}$, as a function of $\beta \cdot \xi$ and the capillary wall reflection coefficient for both the globulin tracer and the albumin tracer. The breakthrough curves associated with these simulations are shown in Figure (6.1). In each case $\tilde{t}_{50\%}$ decreases with increasing $\beta \cdot \xi$, due to the enhanced convective transport of the tracer accompanying such an increase. In addition, when the capillary wall is assigned the more permeable (albumin) transport properties, the time required for each tracer to reach 50 % of its steady-state value decreases marginally (i.e., by less than 0.5 %) in each case. Hence, the capillary transport properties exert a stronger influence on the ultimate steady-state outlet concentration than on the transit times through the interstitium, for the range of permeabilities and reflection coefficients considered here.

Of greater significance is the difference in transit times between the albumin and globulin tracers. In all cases, the globulin tracer reaches 50 % of its steady-state value in a significantly shorter time than the albumin tracer, even when both tracers are subject to the same boundary conditions (and hence achieve the same ultimate outlet concentrations), and despite the fact that the globulin interstitial diffusivity is less than that of albumin. For example, when $\beta \cdot \xi$ is 0.90 and assuming globulin boundary conditions, the $\tilde{t}_{50\%}$ for the globulin tracer is 1.636, compared to a $\tilde{t}_{50\%}$ of 2.115 for the albumin tracer. Therefore, only two model parameters remain to account for this difference in transit times: the tracer distribution volume and interstitial diffusivity. These are investigated separately below.
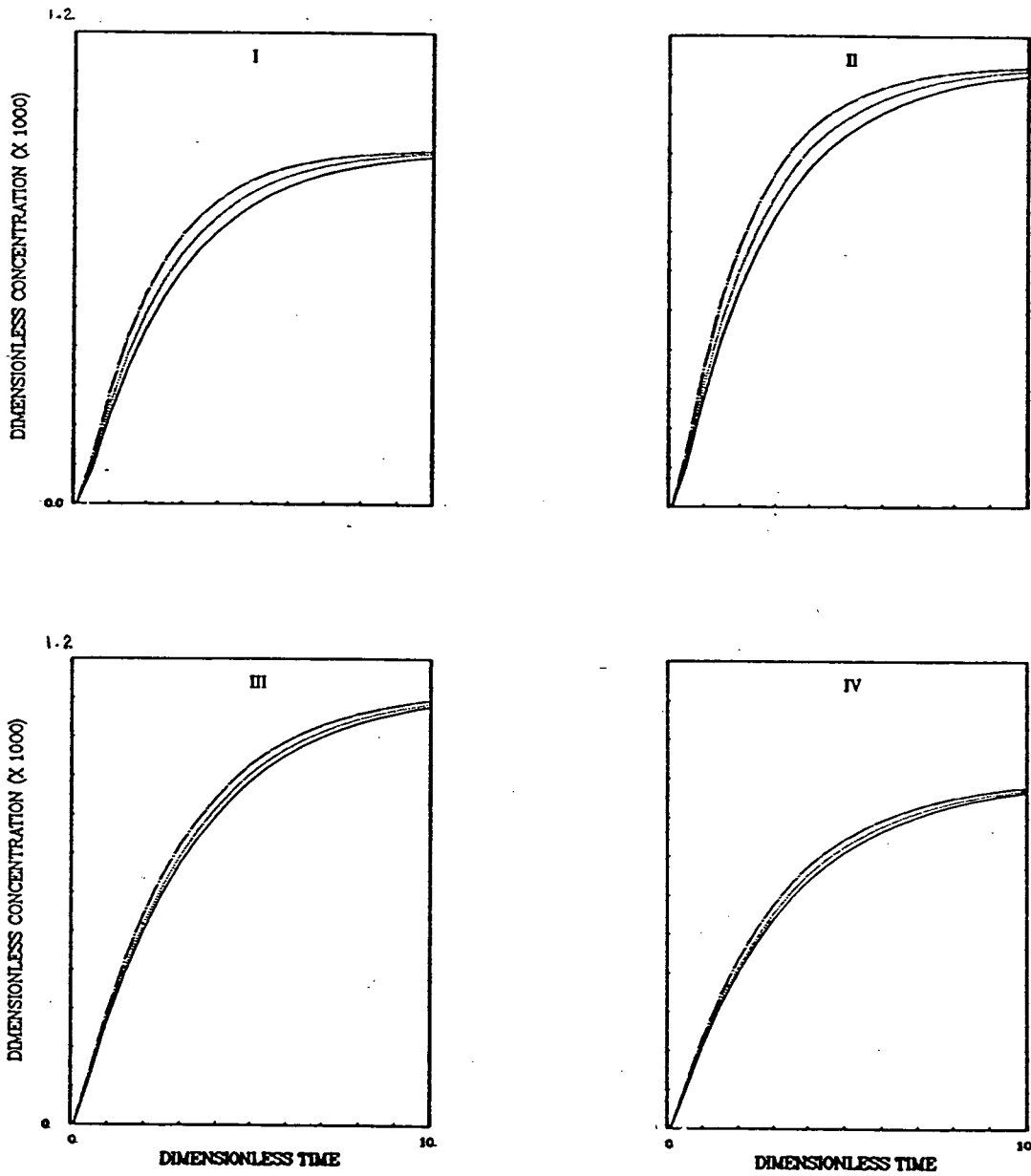
Figure 6.1: The breakthrough curves for various values of $\beta \cdot \xi$ are shown (I) for glob-
ulin, assuming globulin boundary conditions; (II) for globulin, assuming albumin
boundary conditions; (III) for albumin, assuming albumin boundary conditions;
and (IV) for albumin, assuming globulin boundary conditions. In each case the
top (chain-dot) curve corresponds to $\beta \cdot \xi$ equal to 0.90, the middle (dotted) curve
corresponds to $\beta \cdot \xi$ equal to 0.50, and the lower (solid) curve corresponds to $\beta \cdot \xi$
equal to 0.16 for globulin and 0.21 for albumin.

Tracer	$\xi \cdot \beta$	$\bar{t}_{50\%}$ Assuming Albumin B.C.	$\bar{t}_{50\%}$ Assuming Globulin B.C.
Albumin	0.21	2.355	2.349
	0.50	2.254	2.247
	0.90	2.119	2.115
Globulin	0.16	2.064	2.057
	0.50	1.853	1.849
	0.90	1.639	1.636

Table 6.2: **Transit times of Albumin and Globulin tracers as functions of $\beta \cdot \xi$ and the capillary wall transport properties.**

6.5.2 The Effect of Tracer Distribution Volume on Globulin Transit Times

Table (6.3) shows the $\bar{t}_{50\%}$ for the globulin tracer assuming a distribution volume of first 0.50 and then 0.68, and compares these values to the $\bar{t}_{50\%}$ for albumin (which has a distribution volume of 0.68). In each case globulin boundary conditions prevail. The breakthrough curves for these cases are illustrated in Figure (6.2). The increase in globulin distribution volume results in a dramatic increase in the transit time for that tracer. In fact, when both the globulin tracer's distribution volume and $\beta \cdot \xi$ equal those of the albumin tracer, the $\bar{t}_{50\%}$ for the globulin tracer exceeds the $\bar{t}_{50\%}$ for the albumin tracer, due to the globulin tracer's lower interstitial diffusivity. Assuming a $\beta \cdot \xi$ of 0.50, for example, the $\bar{t}_{50\%}$ for globulin increases by 29 %, from 1.853 to 2.394, as the tracer's distribution volume is raised from 0.50 to 0.68. This is to be compared to the $\bar{t}_{50\%}$ of 2.247 for the albumin tracer at the same $\beta \cdot \xi$ and a distribution volume of 0.68.

The rise in transit time accompanying the increase in distribution volume is attributed to the increased capacity of the interstitium to contain the given tracer. Altering the distribution volume from 0.50 to 0.68 represents a 36 % increase in the interstitial volume available to the globulin tracer. It is not surprising, then, that an increase in the distribution volume leads to a

$\xi \cdot \beta$	$\tilde{t}_{50\%}$ $n^{glob} = 0.50$	$\tilde{t}_{50\%}$ $n^{glob} = 0.68$	$\tilde{t}_{50\%}$ Albumin Tracer
0.16	2.064	2.607	2.355*
0.50	1.853	2.394	2.254
0.90	1.639	2.177	2.119

* evaluated at $\beta \cdot \xi = 0.21$

Table 6.3: **The effect of interstitial distribution volume on the transit time of a globulin tracer through the interstitium. The last column of values presents the transit times for the albumin tracer assuming the same capillary boundary conditions as those for the globulin tracer, and assuming that the distribution volume of the albumin tracer equals 0.68.**

concomitant rise in the length of the transient for a given tracer, since the tracer must fill the available interstitial space before steady-state conditions prevail.

This finding offers an alternative mechanism for the 'gel chromatographic effect' discussed in Chapter 3. Recall that some experimental data suggests that, in certain instances, larger probes pass through the interstitial space more rapidly than smaller ones [48]. To date, only one paper has addressed this phenomenon from a theoretical standpoint [104]. In that work, the authors assumed that the interstitium contained a 'free-fluid phase', in which macromolecules moved by convection and diffusion, and a 'gel phase', in which the transport of macromolecules was limited to restricted diffusion alone. Assuming, then, that the larger molecules were limited to the free-fluid phase while smaller molecules penetrated both phases, the transit time through the interstitium for the smaller tracer could conceivably exceed that of the larger probe.

As was mentioned in Chapter 2, the concept of continuous, distinct free-fluid and gel phases lacks solid evidence. Macromolecular exclusion, on the other hand, is well documented (see, for example, [13]). Hence this latter mechanism for the 'gel chromatographic effect' requires no additional assumptions regarding the structure of the interstitium, and so is preferred over the

'gel phase – free-fluid phase' mechanism of Watson and Grodins [104]. It is also conceivable that variations in the convective hindrances for various macromolecular species may, under certain conditions, create conditions for the gel chromatographic effect, as described in Chapter 3. Again, this mechanism does not rest on a 'gel phase – free-fluid phase' model of the interstitium.

6.5.3 The Effect of Interstitial Diffusivity on Albumin Transit Times

Finally, consider the effect of interstitial diffusivity on the transit time of the albumin tracer through the interstitium. Table (6.3) presents $\bar{t}_{50\%}$ for the various values of $\beta \cdot \xi$, assuming three different values of $D_{\text{eff}}^{\text{alb}}$: 0.58×10^{-7} cm^2/s (i.e., equal to $D_{\text{eff}}^{\text{glob}}$), 1.0×10^{-7} cm^2/s, and 1.5×10^{-7} cm^2/s. The breakthrough curves are shown in Figure (6.3).

$\xi \cdot \beta$	$\bar{t}_{50\%}$ $D_{\text{eff}}^{\text{alb}} = 0.58 \times 10^{-7}$ cm^2/s	$\bar{t}_{50\%}$ $D_{\text{eff}}^{\text{alb}} = 1.00 \times 10^{-7}$ cm^2/s	$\bar{t}_{50\%}$ $D_{\text{eff}}^{\text{alb}} = 1.50 \times 10^{-7}$ cm^2/s
0.21	2.564	2.349	2.246
0.50	2.389	2.247	2.174
0.90	2.173	2.115	2.081

Table 6.4: **The effect of interstitial diffusivity on the transit time of an albumin tracer through the interstitium.**

In general, varying the interstitial diffusivity according to these amounts had only a small to moderate effect on the value of $\bar{t}_{50\%}$ for the albumin tracer. For example, increasing the diffusivity from 0.58×10^{-7} cm^2/s to 1.0×10^{-7} cm^2/s, assuming a $\beta \cdot \xi$ of 0.50, reduced $\bar{t}_{50\%}$ by less than 6 %. Further increases in the tracer diffusivity had an even less pronounced effect on the transit time of the macromolecule. For example, increasing the diffusivity of the albumin tracer from 1.0×10^{-7} cm^2/s to 1.5×10^{-7} cm^2/s, at a $\beta \cdot \xi$ of 0.50, only dropped $\bar{t}_{50\%}$ by an additional 3.2 %. This trend was observed for all values of $\beta \cdot \xi$ considered in the study. Furthermore, even at the higher diffusivity, the transit time for the albumin tracer exceeded

the transit time for the globulin tracer for all values of $\beta \cdot \xi$ investigated. Within the limits of this study, then, it appears that interstitial diffusion has less impact on the transit time of an interstitial macromolecule than does the interstitial distribution volume of that species.
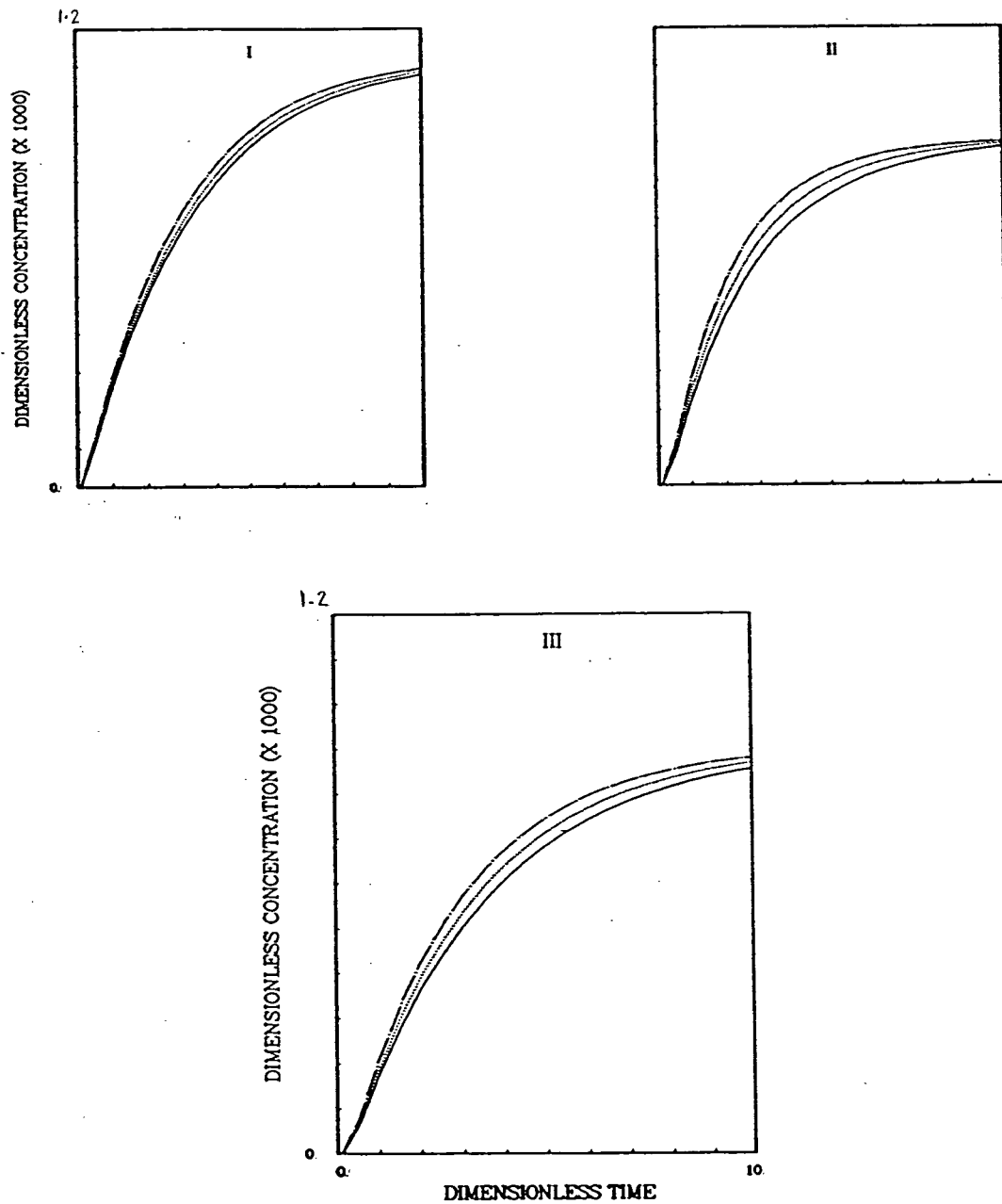
Figure 6.2: The breakthrough curves for various values of $\beta \cdot \xi$ and globulin boundary conditions are shown (i) for albumin; (ii) for globulin, assuming a distribution volume of 0.50; and (iii) for globulin, assuming a distribution volume of 0.68. In each case the top (chain-dot) curve corresponds to $\beta \cdot \xi$ equal to 0.90, the middle (dotted) curve corresponds to $\beta \cdot \xi$ equal to 0.50, and the lower (solid) curve corresponds to $\beta \cdot \xi$ equal to 0.16 for globulin and 0.21 for albumin.
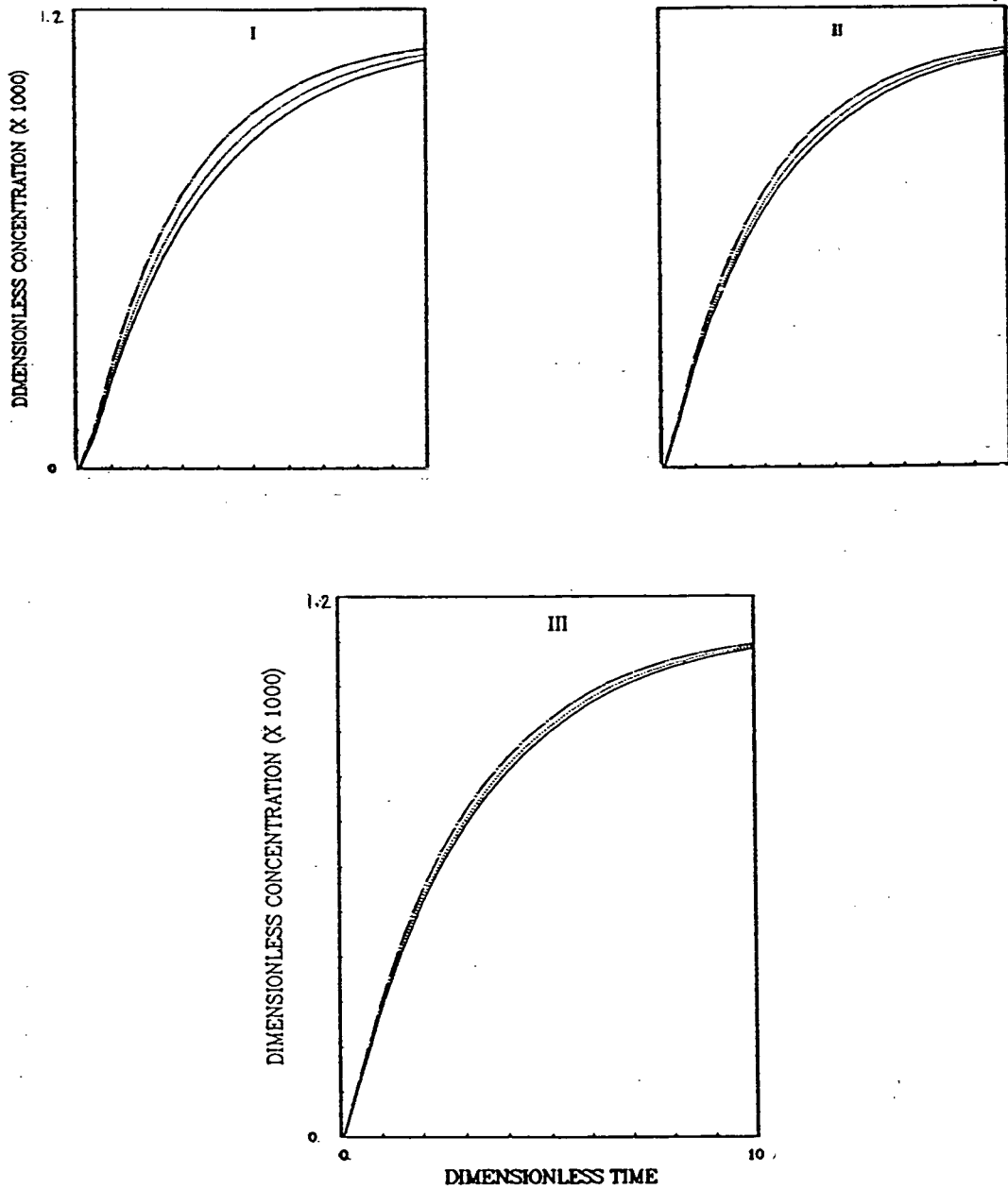
Figure 6.3: The breakthrough curves for albumin, assuming various values of $\beta \cdot \xi$, are shown for (i) $D_{eff}^{alb} = 0.58 \times 10^{-7}$ cm^2/s, (ii) $D_{eff}^{alb} = 1.00 \times 10^{-7}$ cm^2/s, and (iii) $D_{eff}^{alb} = 1.50 \times 10^{-7}$ cm^2/s. In each case the top (chain-dot) curve corresponds to $\beta \cdot \xi$ equal to 0.90, the middle (dotted) curve corresponds to $\beta \cdot \xi$ equal to 0.50, and the lower (solid) curve corresponds to $\beta \cdot \xi$ equal to 0.16 for globulin and 0.21 for albumin.

6.6   Concluding Remarks

This chapter presented the results of a preliminary study that investigated the effects of interstitial convection and diffusion, interstitial distribution volume, and capillary transport properties on the transit times of two macromolecular tracers representative of albumin and γ – globulin for a specific set of interstitial fluid flow conditions. The findings are summarized below.

1. As to be expected, the transit time of the tracers varied inversely with the degree of convective transport within the interstitium.

2. Increasing the interstitial diffusivity of the albumin tracer also led to a moderate decrease in the transit time for that tracer.

3. The capillary transport properties had only a marginal effect on the transit times of the tracers, for the range of capillary permeabilities and reflection coefficients considered. However, these properties (and, in particular, the reflection coefficient) had a more pronounced effect on the ultimate steady-state concentration in the outlet stream.

4. The interstitial distribution volume of a given tracer had the greatest influence on the time required to achieve steady-state. This is attributed to the increased filling times associated with the larger interstitial distribution volumes. These findings suggest that the 'gel chromatographic effect' [48] observed in some tissues could possibly be explained on the basis of varying distribution volumes, rather than the hypothetical 'gel phase – free-fluid phase' model proposed by Watson and Grodins [104].

Clearly, much more experimental and theoretical research is needed before the interstitial transport of multiple tracer species can be well characterized. However, this study suggests that the relative transport rates of different macromolecules is governed by a number of interstitial properties, including the interstitial distribution volume. This may ultimately bear clinical import, particularly in the use of macromolecular carriers for drug delivery.

Chapter 7

Summary of Conclusions

In this dissertation, mathematical relationships are developed to describe the transient flow and distribution of fluid and various macromolecular solute species within the interstitium, yielding a system of coupled, nonlinear partial differential equations. The resultant mathematical model describes the combined effects of a number of interstitial properties (such as exclusion and swelling characteristics) and transport mechanisms (such as solute convection, diffusion, and dispersion) on mass transport within the interstitium.

Despite the complexity of the model, it is limited in several respects. First, the description of interstitial deformation applies to small strains only (on the order of ten percent), and so is not suited to analyzing extreme cases of edema formation. Further, the model uses a compliance relationship to characterize swelling which assumes that any change in volume is a function of the interstitial hydrostatic pressure. It therefore neglects the influence of shear stresses on interstitial deformation. However, since the model concerns itself primarily with the effect that swelling has on the various transport properties and material characteristics of the interstitial space (such as the hydraulic conductivity, effective diffusivities, and various distribution volume fractions), rather than a description of the deformed geometry of the interstitium, this approach provides a reasonable first approximation to the complete theory of deformation for porous systems developed by Biot [19]. The use of Biot's theory to describe interstitial swelling must await further experimentation to quantify the material properties of the various interstitial components.

Interstitial fluid flow is assumed to be proportional to the gradient in fluid chemical potential alone, thus neglecting any coupling between fluid flow and solute chemical potential, for

166

example. However, the theory developed here could be modified to include these additional effects, given better information about the nature of fluid transport within the interstitium. Further research in the area of fluid flow within osmotically active, partially restricting matrices is therefore needed. However, because the interstitial fluid flow expression presented here includes the influence of colloid osmotic as well as hydrostatic pressure gradients, it is considered more general than that offered in previous models [87, 36, 22].

Despite these limitations, the model of Chapter 3 provides a far more comprehensive description of interstitial transport than that offered by any of the previous models to appear in the literature. Its strength lies in the general, self-consistent, and self-contained nature of the mathematical formulation. It therefore provides a framework in which to further understand the interstitium and its role in microvascular exchange.

Subsequent chapters of the dissertation have used simplified versions of the general model to conduct theoretical investigations of microvascular exchange under normal and pathological states. In Chapter 4, for example, the model is used to describe the steady-state exchange of fluid and plasma proteins in mesenteric tissue, which is treated as a two-dimensional, rigid system. This tissue was selected both for its simple geometry and because it is a popular tissue for experimental studies of interstitial transport and microvascular exchange. The array of plasma protein species found *in vivo* was approximated by a single, 'aggregate' species that displayed average properties.

The simulations of Chapter 4 indicate that convective transport of plasma proteins is significant, even at reduced values of convective hindrance, ζ. This supports a recent study of the movement of labelled albumin in rat mesentery suggesting that convection plays a significant role in interstitial plasma protein transport within that tissue [74]. However, the simulations also show that exact nature of interstitial plasma protein transport cannot be determined from protein distributions alone.

The model predictions also reveal that the hydrodynamics within the interstitial space can

be complex, resulting, for example, in the development of fluid recirculation patterns. The hydrodynamics can also lead to irregularities in the distribution of fluid and plasma protein fluxes across a permeable boundary, such as the mesothelium, even when the boundary's transport properties are uniform. This behavior, which is strongly influenced by the transport properties of the mesothelial layer, could lead to the erroneous identification of 'leaky sites' within the system.

Finally, the model predicts significant interstitial osmotic pressure gradients in some instances, suggesting that the Darcy expression evoked in a number of previous models [22, 36, 87], that considers hydrostatic gradients only, is inadequate for describing interstitial fluid transport.

The analysis of Chapter 4 is extended to transient perturbations in Chapter 5. Again, a rigid model of mesenteric tissue is used although, in this case, the two-dimensional tissue is replaced by a one-dimensional analogue. Two systemic perturbations are considered: namely hypoproteinemia and venous congestion.

The simulations of Chapter 5 demonstrate that, assuming a permeable mesothelium, the trends in fluid and plasma protein exchange can be anticipated by considering the effect that a particular upset has on the effective chemical potential of the luminal fluids. In these instances the interstitium is not the major resistance within the system, due to by-passing. However, when the mesothelium is impermeable, fluid and plasma proteins must cross the entire interstitial space in their journey from the filtering vessel to the re-absorbing vessel, so that the interstitium comprises a large fraction of the system's total resistance to mass exchange. In these cases the distribution of interstitial plasma proteins plays a greater role in determining the overall behavior of the system.

The simulations indicate further that, following hypoproteinemia, interstitial plasma protein content decreases, while the rate of fluid exchange within the tissue increases. This is in keeping (qualitatively, at least) with clinical observations of hypoproteinemia. In the case of venous congestion, however, the change in interstitial plasma protein content depends, in part, on the relative sieving properties of the filtering and draining vessels. When the reflection coefficients

of these two sets of boundaries are similar, the interstitial plasma protein content increases due to the increased plasma protein exchange rate across the filtering boundaries and sieving of interstitial plasma proteins at the draining boundaries. This effect is further supported by the clinical observation that interstitial plasma protein content in liver increases during venous congestion. Since this tissue is serviced by sinusoids, the sieving properties of the filtering blood vessels and the draining lymphatic vessels are similar. The simulations also predict that, as the reflection coefficient of the draining boundaries decreases relative to that of the filtering boundaries, there is a net loss of plasma proteins from the interstitium, resulting in a decrease in the total interstitial plasma protein content over time (i.e., the familiar 'plasma protein washout').

In Chapter 6 a one-dimensional model of a hypothetical tissue was used in a preliminary study investigating the effects of interstitial plasma protein convection and diffusion, plasma protein exclusion, and the capillary transport properties on the transit times of two macro-molecular tracers representative of albumin and γ-globulin. As was expected, the transit times of each of the tracers through the model tissue varied inversely with the degree of convective transport. Increasing the interstitial diffusivity of the albumin tracer also led to a moderate decrease in the transit time for that tracer. The capillary wall transport properties, meanwhile, had only a marginal effect on the transit time for the range of capillary permeabilities and reflection coefficients considered. However, these properties (and, in particular, the reflection coefficient) had a more pronounced effect on the ultimate steady-state concentration of the tracer in the outlet stream.

It was the interstitial distribution volume of a given tracer that had the greatest impact on the time required for the outlet tracer concentration to reach 50 % of its steady-state value. This was attributed to the increased filling times associated with larger interstitial distribution volumes. These findings suggest that the 'gel chromatographic effect' [48] observed in some tissues could possibly be explained on the basis of varying distribution volumes, rather than the hypothetical 'gel phase – free fluid phase' model proposed by Watson and Grodins [104].

Finally, in Appendix C, we investigate the possible influence of mechanical dispersion on mass exchange within the model tissue. While it influenced the distribution of interstitial plasma proteins to some extent, mechanical dispersion had less impact on the overall exchange of fluid and plasma proteins within the system.

Clearly, much more experimental and theoretical research is needed before the interstitial transport of fluid and multiple solute species can be well characterized. However, it is hoped that the work presented here offers some further insight into the mechanisms governing interstitial transport and microvascular exchange. Continued research in this area will not only contribute to a fundamental understanding of the operation of the microvascular exchange system, but will assist clinicians in developing more effective techniques for fluid resuscitation and drug delivery.

Chapter 8

Recommendations

In the preceding chapters we investigated the combined effects of a number of system parameters (such as the interstitial hydraulic conductivity, the interstitial plasma protein diffusivity, and the plasma protein convective hindrance) on the steady-state and transient exchange of fluid and various plasma protein species within a model tissue representative of mesentery. However, many questions regarding the nature of the interstitium and its influence on mass exchange within tissues remain unanswered. These include, among others, the effect of interstitial swelling on microvascular exchange and the nature of interstitial fluid flow. To address these and other questions, the analysis presented in this dissertation might be extended to include the following.

1. The equations describing interstitial deformation should be incorporated into the numerical simulations to include the influence of tissue swelling on microvascular exchange. Alternate expressions suitable for large changes in interstitial hydration should be sought out and applied, where possible.

2. The analysis of mass exchange in mesentery should be extended to other tissue models. Such models would include, for example, a more rigorous description of lymphatic drainage.

3. The effect of local gradients in interstitial colloid osmotic pressure on local interstitial fluid flow should be investigated, possibly by introducing an 'effective interstitial reflection coefficient' analogous to the capillary wall reflection coefficient into the extended Darcy flux expression. However, a rigorous theoretical description of interstitial fluid flow is to be desired over the introduction of an arbitrary parameter such as this.

171

4. Finally, the preliminary study of the transient movement of multiple tracer species through the interstitium should be expanded to consider other species having a broader range of solute transport characteristics.

Nomenclature

SYMBOL	DESCRIPTION	UNITS
A_i, i=1,2,3	first, second, and third virial coefficients of colloid osmotic pressure relationship for aggregate plasma protein species	$F \cdot L^i/M^i$
C^b	plasma protein concentration of luminal fluid associated with boundary b	M/L^3
$C^{k,l}$	local concentration of plasma protein species k in incremental volume fraction l (δn^l)	M/L^3
C^k	local concentration of plasma protein species k in species' distribution volume fraction (n^k)	M/L^3
Cr	Courant number	
D	permeability of membrane boundary to aggregate plasma protein species	L/θ
D_d	local dispersion coefficient of interstitial plasma protein species k	L^2/θ
D_{eff}^k	local effective diffusion coefficient of interstitial plasma protein species k	L^2/θ
F^k	function relating excluded volume fraction for plasma protein species k to the solid volume fraction (n^s)	
F^s	function relating the immobile fluid phase volume fraction to the solid volume fraction (n^s)	
G^k	function relating the osmotic pressure of plasma protein species k (Π^k) to its concentration (C^k)	
H	mesentery thickness	L
H^{eff}	effective resistance thickness for one-dimensional mesentery	L

SYMBOL	DESCRIPTION	UNITS
$j_{c_i}^k$	local convective flux of protein species k in x_i direction, relative to moving solids	$M/(L^2 \cdot \theta)$
$j_{d_i}^k$	local diffusive flux of protein species k in x_i direction, relative to convective flux	$M/(L^2 \cdot \theta)$
$j_{md_i}^k$	local mechanical dispersive flux of protein species k in x_i direction, relative to convective flux	$M/(L^2 \cdot \theta)$
j_s	transcapillary plasma protein flux	$M/(L^2 \cdot \theta)$
$j_{s_i}^k$	total local flux of plasma protein species k in x_i direction,	$M/(L^2 \cdot \theta)$
j_v	transcapillary fluid flux	L/θ
$j_{w_i}^k$	local volumetric fluid flux in x_i direction through distribution volume of protein species k, relative to the moving solids	L/θ
$j_{w_i}^0$	local total volumetric fluid flux in x_i direction, relative to moving solids	L/θ
j_{w_i}	local non-specific fluid flux in x_i direction, relative to moving solids	L/θ
K^k	local interstitial hydraulic conductivity associated with distribution volume of protein species k	$L^4/(F \cdot \theta)$
K^0	local total interstitial hydraulic conductivity	$L^4/(F \cdot \theta)$
K'	local interstitial specific hydraulic conductivity	L^2
L	distance separating arteriolar and venular capillaries	L
L_p	hydraulic conductance of membrane boundary	$L^3/F \cdot \theta$
l_{x_i}	x_ith component of outward normal, n, of boundary	
Δl	maximum dimension of finite element	
n	unit outward normal of boundary	
n^k	local distribution volume fraction of protein species k	
n^{ek}	local excluded volume fraction of protein species k	

SYMBOL	DESCRIPTION	UNITS
n^0	local total mobile fluid volume fraction	
n^{im}	local immobile fluid volume fraction	
n^s	local solid phase volume fraction	
P^l	local fluid hydrostatic pressure in incremental volume fraction l (δn^l)	F/L^2
P_{av}	average local hydrostatic fluid pressure	F/L^2
Pe	Peclet number	
$q^0_{w_i}$	local total volumetric fluid flux in x_i direction, relative to stationary coordinates	L/θ
R	universal gas constant	$F/(MOL \cdot T)$
R^k_f	retardation factor of plasma protein species k	
R^{tot}_w	effective hydraulic resistance of in y direction for one-dimensional mesentery	$\theta \cdot F/L^3$
R^{tot}_d	effective diffusive resistance of in y direction for one-dimensional mesentery	θ/L
T	absolute temperature	T
t	time	θ
$t^k_{50\%}$	time for breakthrough curve of species k to reach 50 % of its steady-state value	θ
U_i	local solid phase displacement in x_i direction	L
$\tilde{V}^l_w$	partial molar volume of fluid in incremental volume fraction l (δn^l)	L^3/MOL
$\tilde{V}_w$	molar volume of pure fluid	L^3/MOL
$\bar{v}^k_{c_i}$	local mean convective velocity of protein species k in x_i direction, relative to solid phase velocity (v_{s_i})	L/θ
v_{s_i}	local solid phase velocity	L/θ
v_{sc}	local superficial convective solute velocity	L/θ

SYMBOL	DESCRIPTION	UNITS
v_{sd}	local superficial dispersive solute velocity	L/θ
$\bar{v}_{w_i}^k$	local mean fluid velocity in x_i direction through distribution volume of protein species k, relative to solid phase velocity (v_{s_i})	L/θ
$v^{\sim}$	ratio of particle velocity to local fluid velocity, for arbitrary spherical particle travelling in cylindrical channel	L/θ
X_w^1	local fluid mole fraction in incremental volume fraction 1 (δn^1)	
x_i	local spatial coordinate	L
x_i'	local spatial coordinate of deformed medium	L
α	ratio of interstitial resistance to plasma protein diffusion to interstitial resistance to fluid flow ($K^0 P^{art}/D_{eff}$)	
α_l^k	longitudinal dispersivity of protein species k in interstitium	L
α_t^k	transverse dispersivity of protein species k in interstitium	L
β^k	ratio of hydraulic conductivity in distribution volume k to total interstitial hydraulic conductivity (K^k/K^0)	
$\beta^{\sim}$	ratio of immobile fluid phase volume fraction to solid phase volume fraction (n^{im}/n^s)	
γ_w	fluid phase activity coefficient	
Δ	difference sign	
δ_{ij}	Kronecker delta function	
δn^1	incremental volume fraction 1	
ϵ_i	local solid strain in the x_i direction	
ϵ_v	local volumetric dilation of interstitium	
ϑ_{ij}^k	local coefficient of mechanical dispersion for protein species k	L^2/θ
λ	ratio of particle diameter to channel diameter for arbitrary spherical particle travelling in cylindrical channel	

SYMBOL	DESCRIPTION	UNITS
μ_{eff}^{b}	effective fluid chemical potential of luminal fluid associated with boundary b	F/L^2
μ_w	general solvent chemical potential	$F \cdot L/MOL$
μ_w^l	local chemical potential of fluid in incremental volume fraction l (δn^l)	$F \cdot L/MOL$
μ_w^{ref}	reference fluid chemical potential	$F \cdot L/MOL$
ξ^k	local convective hindrance of protein species k	
$\Pi^{k,l}$	local osmotic pressure of protein species k in incremental volume fraction l (δn^l)	F/L^2
Π^k	local osmotic pressure of protein species k averaged over its distribution volume fraction (n^k)	F/L^2
σ^b	reflection coefficient of membrane boundary b	
σ_{ij}	component of total stress tensor in interstitium	
σ_{ij}^{eff}	component of effective stress tensor in interstitium	
ς_i	finite element weighting function	
Φ	solid displacement potential function	
ϕ_i	finite element basis function	
Ω	interstitial compliance function	
$\hat{\Omega}$	specific interstitial compliance function	
$[\cdot]_b$	interstitial quantity evaluated at boundary b	

Superscripts and Subscripts

alb	albumin	
anal	analytical solution of dependent variable	
art	arteriolar capillary	
b	unspecified permeable boundary	

Superscripts and Subscripts

glob	globulin
grid	finite element grid quantity
int	interstitium
lym	lymphatic
mes	mesothelium
p	plasma
simul	numerical simulation solution of dependent variable
tot	total 'effective' quantity for one-dimensional mesentery
ven	venular capillary
$\tilde{}$	dimensionless quantity (see text for specific definitions)

References

[1] Anderson, M.P. Movement of contaminants in groundwater: groundwater transport— advection and dispersion. In: *Groundwater Contamination*. Washington: National Academy Press, 1984, p. 37-45.

[2] Aroesty, J., and J.F. Gross. Convection and diffusion in the microcirculation. *Microvasc. Res. 2*: 247-267, 1970.

[3] Arturson, G., T. Groth, A. Hedlund, and B. Zaar. Potential use of computer simulation in treatment of burns with special regard to oedema formation. *Scand. J. Plast. Reconstr. Surg. 18*: 39-48, 1984.

[4] Aukland, K., and G. Nicolaysen. Interstitial fluid volume: local regulatory mechanisms. *Physiol. Rev 61: 556-643,* 1981.

[5] Aukland, K., and R. Reed. Interstitial-lymphatic mechanisms in the control of extracellular fluid volume. Submitted to *Physiol. Rev.,* 1989.

[6] Baxter, L.T., and R.K. Jain. Transport of fluid and macromolecules in tumors I. Role of interstitial pressure and convection. *Microvasc. Res. 37*: 77-104, 1989.

[7] Baxter, L.T., R.K. Jain, and E. Svensö. Vascular permeability and interstitial diffusion of macromolecules in the hamster cheek pouch: effects of vasoactive drugs. *Microvasc. Res. 34*: 336-348, 1987.

[8] Bear, J. *Dynamics of Fluids in Porous Media*. New York: Elsevier, 1972, p. 579-663.

[9] Bekey, G.A. Models and reality: some reflections on the art and science of simulation. *Simulation* , 161-164, November, 1977.

179

[10] Benoit, J.N., C.A. Navia, A.E. Taylor, and D.N. Granger. Mathematical model of intestinal transcapillary fluid and protein exchange. In: *Physiology of the Intestinal Circulation*, edited by A.P. Shepherd and D.N. Granger. New York: Raven, 1984, p. 275-287.

[11] Bert, J.L., J.M. Mathieson, and R.H. Pearce. The exclusion of human serum albumin by human dermal collagenous fibers and within dermis. *Biochem. J. 201*: 395-403, 1982.

[12] Bert, J.L., J.M. Mathieson, R.H. Pearce, and S.J. Warner. Characterization of collagenous meshworks by volume exclusion of dextrans. *Biochem. J. 191*: 761-768, 1980.

[13] Bert, J.L., and R.H. Pearce. The interstitium and microvascular exchange. In: *Handbook of Physiology. The Cardiovascular System. Microcirculation*, edited by E. Renkin and C.C. Michel. Bethesda: American Physiological Society, 1984, p. 521-547.

[14] Bert, J.L., B.D. Bowen, and R.K. Reed. Microvascular exchange and interstitial volume regulation in the rat: model validation. *Am. J. Physiol. 254 (Heart and Circ. Physiol. 23)*: H384-H399, 1988.

[15] Bert, J.L., and K.L. Pinder. Computer simulation of fluid and plasma protein transport in the lungs. *Can. J. Chem Eng. 63*: 310-313, 1985.

[16] Bert, J.L., and K.L. Pinder. Pulmonary microvascular exchange : an analog computer simulation. *Microvasc. Res. 27*: 51-70, 1984.

[17] Bert, J.L., and K.L. Pinder. From which compartment in the interstitium does lymph originate? *Microvasc. Res. 26*: 116-121, 1983.

[18] Bert, J.L., and K.L. Pinder. An analog computer simulation showing the effect of volume exclusion on capillary fluid exchange. *Microvasc. Res. 24*: 94-103, 1982.

[19] Biot, M.A. General theory of three-dimensional consolidation. *J. Appl. Phys. 12*: 155-164, 1941.

[20] Biot, M.A. Theory of deformation of porous viscoeleastic anisotropic solid. *J. Appl. Phys.* *27*: 459-467, 1956.

[21] Biot, M.A. Theory of finite deformations of porous solids. *Indiana Univ. Math. J. 21*: 597-620, 1972.

[22] Blake, T.R., and J.F. Gross. Analysis of coupled intra- and extraluminal flows for single and multiple capillaries. *Math. Biosci. 59:* 173-206, 1982.

[23] Brenner, H., and L.J. Gaydos. The constrained Brownian movement of spherical particles in cylindrical pores of comparable radius. *J. Colloid Interface Sci. 58*: 312-356, 1977.

[24] Carnaghan, B., H.A. Luther and J.O. Wilkes. *Applied Numerical Methods.* NewYork: John Wiley, 1969, p. 508.

[25] Carson, E.R., and L. Finkelstein. *The Mathematical Modeling of Metabolic and Endocrine Systems - Model Formulation, Identification, and Validation.* New York: John Wiley and Sons, 1982, p. 9-54.

[26] Comper, W.D. Interstitium. In: *Edema*, edited by N.C. Staub and A.E. Taylor. New York: Raven, 1984, p. 229-262.

[27] Comper, W.D., and T.C. Laurent. Physiological function of connective tissue polysaccharides. *Physiol. Rev. 58: 255-315, 1978*.

[28] Corapcioglu, M.Y., and J. Bear. Land subsidence—b. a regional mathematical model for land subsidence due to pumping. In: *Fundamentals of Transport Phenomena in Porous Media*, edited by J. Bear and M.Y. Corapcioglu. Dordrecht: Martinus Nijhoff, 1984, p.445-493.

[29] Colella, A.M., M.J. O'Sullivan, and D.J. Carlino. *Systems Simulation - Methods and Applications.* Lexington: Lexington Books, 1974, p. 1-55.

[30] Curry, F.E. Determinants of capillary permeability: a review of mechanisms based on single capillary studies in the frog. *Circ. Res. 59*: 367-380, 1986.

[31] Curry, F.E. Mechanics and thermodynamics of transcapillary exchange. In: *Handbook of Physiology. The Cardiovascular System. Microcirculation*, edited by E. Renkin and C.C. Michel. Bethesda: American Physiological Society, 1984, p. 309-374.

[32] Dibona, D.R., and J.A. Schafer. Cellular transport phenomena. In: *Edema*, edited by N.C. Staub and A.E. Taylor. New York: Raven Press, 1984, p. 61-80.

[33] Drake, R., G.A. Laine, S.J. Allen, J. Katz, and J.C. Gabel. A model of the lung interstitial-lymphatic system. *Microvasc. Res. 34*: 96-107, 1987.

[34] Fadnes, H.O. Effect of increased venous pressure on the hydrostatic and colloid osmotic pressure in subcutanteous interstitial fluid in rats: edema-preventing mechanisms. *Scand. J. Clin. Lab. Invest. 36*: 371-377, 1976.

[35] Fatt, I., and T.K. Goldstick. Dynamics of water transport in swelling membranes. *J. Colloid Sci. 20*: 962, 1965.

[36] Fleischman, G.J., and T.W. Secomb. Effect of extravascular pressure gradients on capillary fluid exchange. *Math. Biosci. 81:* 145-164, 1986.

[37] Flessner, M.F., R.L. Dedrick, and J.S. Schultz. A distributed model of peritoneal-plasma transport: analysis of experimental data in the rat. *Am. J. Physiol. 248 (Renal Fluid Electrolyte Physiol. 17)*: F413-F424, 1985.

[38] Fox, J.R., and H. Wayland. Interstitial diffusion of macromolecules in the rat mesentery. *Microvasc. Res. 18*: 255-276, 1979.

[39] Fraser, P.A., L.H. Smaje, and V. Verrinder. Microvascular pressures and filtration coefficients in the cat mesentery. *J. Physiol. 283*: 439-456, 1978.

[40] Friedman, J.J., and S. Witte. The radial protein concentration distribution in the interstitial space of rat ileal mesentery. *Microvasc. Res. 31*: 277-278, 1986.

[41] Friedman, M.H. General theory of tissue swelling with application to the corneal stroma. *J. Theor. Biol. 30*: 93-109, 1971.

[42] Frind, E.O. Simulation of long-term transient density-dependent transport in groundwater. *Adv. Water Resources 5*: 73-98, 1982.

[43] Fry, D.L. Mathematical models of arteriolar transmural transport. *Am. J. Physiol. 248 (Heart Circ. Physiol. 17)*: H240-H263, 1985.

[44] Fung, Y.C. *Biodynamics – Circulation*. New York: Springer-Verlag, 1984, p. 224-238.

[45] Gabel, J.C. and R.E. Drake. Plasma proteins and protein osmotic pressure. In: *Edema*, edited by N.C. Staub and A.E. Taylor. New York: Raven, 1984, p. 371-381.

[46] Gagnon, W.F. *Review of Medical Physiology*. Los Altos: Lange Medical Publications, 1985, p. 421-458.

[47] Gersh, I., and H.R. Catchpole. The nature of the ground substance of connective tissue. *Perspect. Biol. Med. 3*: 282-319, 1960.

[48] Garlick, D.G., and E.M. Renkin. Transport of large molecules from plasma to interstitial fluid and lymph in dogs. *Am. J. Physiol. 219*: 1595-1605, 1970.

[49] Gnepp, D.R. Lymphatics. In: *Edema*, edited by N.C. Staub and A.E. Taylor. New York: Raven Press, 1984, p. 263-298.

[50] *Gray's Anatomy*, edited by P.L. Williams and R. Warwick. Norwich: Longman, 1980, p. 1257-1270.

[51] Granger, D.N., and J.A. Barrowman. Gastrointestinal and liver edema. In: *Edema,* edited by N.C. Staub and A.E. Taylor. New York: Raven, 1984, p. 615-656.

[52] Granger, D.N., M.A.Perry, P.R. Kvietys, and A.E.Taylor. Interstitium-to-blood movement of macromolecules in the absorbing small intestine. *Am J. Physiol. 241 (Gastrointest. Liver Physiol. 4)*: G31-G36, 1981.

[53] Granger, H.J. Physicochemical properties of the extracellular matrix. In: *Tissue Fluid Pressure and Composition*, edited by A.R. Hargins. Baltimore: Williams & Wilkins, 1981, p.43-61.

[54] Granger, H.J., and A.P. Shepherd. Dynamics and control of the microcirculation. *Adv. Biomed. Eng. 7*: 1-63, 1979.

[55] Grodzinsky, A.J. Electromechanical and physicochemical properties of connective tissue. *C.R.C. Crit. Rev. Biomed. Eng. 9*: 133-199, 1983.

[56] Guyton, A.G., T.G. Coleman, and H.J. Granger. Circulation: overall regulation. *Ann. Rev. Physiol. 34*: p. ,1972.

[57] Grodzinsky, A.J. Electromechanical and physicochemical properties of connective tissue. *C.R.C. Crit. Rev. Biomed. Eng. 9*: 133-199, 1983.

[58] Haraldsson, B. Physiological studies of macromolecular transport across capillary walls. *Acta Physiol. Scand. Suppl. 553*: 1-40, 1986.

[59] Huyakorn, P.S., and G.F. Pinder. *Computational Methods in Subsurface Flow*. New York: Academic Press, 1983, p. 229-288.

[60] Jackson, G.W., and D.F. James. The permeability of fibrous porous media. *Can J. Chem. Eng. 64*: 364-374, 1986.

[61] Jain, R.K. Transport of molecules in tumor interstitium: a review. *Cancer Res. 47*: 3039-3051, 1987.

[62] Katz, M.A., and E.H. Bresler. Osmosis. In: *Edema*, edited by N.C. Staub and A.E. Taylor. New York: Raven, 1984, p. 39-60.

[63] Landis, E.M. The capillary blood pressure in mammalian mesentery as determined by the micro–injection method. *Am. J. Physiol. 93:* 353-362, 1930.

[64] Landis, E.M., and J.R. Pappenheimer. Exchange of substances through capillary walls. In: *Handbook of Physiology. Circulation, Volume II*, edited by W.F. Hamilton. Washington: American Physiological Society, 1963, p. 961-1034.

[65] Lenhoff, A.M., and E.N. Lightfoot. The effects of axial diffusion and permeability on the transient response of tissue cylinders. III. Solution in the time domain. *J. Theor. Biol. 106:* 207-238, 1984.

[66] Levick, J.R. Flow through interstitium and other fibrous matrices. *Quart. J. Exp. Physiol. 72:* 409-438, 1987.

[67] Lewis, R.N., and B.A. Schrefler. *The Finite Element Method in the Deformation and Consolidation of Porous Media*. Chichester: John Wiley, 1987, p. 421-458.

[68] Lincoff, M., H.S. Borovetz, and W.H. Inskeep. Characterization of the unsteady transport of labelled species in permeable capillaries: role of convective dispersion. *Phys. Med. Biol. 28:* 1191-1208, 1983.

[69] Maroudas, A. Biophysical chemistry of cartilaginous tissues with special reference to solute and fluid transport. *Biorheology 12:* 233-248, 1975.

[70] Mazzoni, M.C., P. Borgström, K-E. Arfors, and M. Intaglietta. Dynamic fluid redistribution in hyperosmotic resuscitation of hypovolemic hemorrhage. *Am. J. Physiol. 255 (Heart Circ. Physiol. 24):* H629-h637, 1988.

[71] Michel, C.C. Fluid movements through capillary walls. In: *Handbook of Physiology. The Cardiovascular System. Microcirculation*, edited by E. Renkin and C.C. Michel. Bethesda: American Physiological Society, 1984, p.375-409.

[72] Ogston, A.G. The role of the extracellular space. In: *Biology of Fibroblast*, edited by E. Kulonen and J. Pikkarainen. London: Academic Press, 1973, p. 9-12.

[73] Ogston, A.G., and C.C. Michel. General descriptions of passive transport of neutral solute and solvent through membranes. *Prog. Biophys. Molec. Biol. 34*: 197-217, 1978.

[74] Papenfuss, H.D., and S. Witte. Perivascular flow and transport of macromolecules: comparison between intravital microscopic and theoretical studies. In: *Microcirculation–An Update, Volume 1, International Congress Series 775*, edited by M. Tsuchiya, M. Asano, Y. Mishima, and M. Oda. Amsterdam: Excerpta Medica, 1987.

[75] Parker, J.C., M.A. Perry, and A.E. Taylor. Permeability of the microvascular barrier. In: *Edema*, edited by N.C. Staub and A.E. Taylor. New York: Raven, 1984, p. 143-187.

[76] Patlak, C.S., D.A. Goldstein, and J.F. Hoffman. The flow of solute and solvent across a two-membrane system. *J. Theor. Biol. 5*: 426-442, 1963.

[77] Reddy, N. Lymph circulation: physiology, pharmacology, and biomechanics. In: *C.R.C. Crit. Rev. Biomed. Eng. 14*: 45-91, 1986.

[78] Reed, R.K. Interstitial fluid volume,colloid osmotic and hydrostatic pressures in rat skeletal muscle. Effect of hypoproteinemia. *Acta Physiol. Scand. 112*: 141-147, 1981.

[79] Reed, R.K., and H. Wiig. Compliance of the interstitial space in rats. III. Contribution of skin and skeletal muscle interstitial fluid volume to changes in total extracellular fluid volume. *Acta Physiol. Scand. 121*: 57-63, 1984.

[80] Renkin, E.M. Transport pathways and processes. In: *Endothelial Cell Biology*, edited by N. Simionescu and M. Simionescu. Plenum Publishing, 1988, p. 51-68.

[81] Renkin, E.M. Some consequences of capillary permeability to macromolecules: Starling's hypothesis reconsidered. *Am. J. Physiol. 250 (Heart Circ. Physiol. 19)*: H706-H710, 1986.

[82] Renkin, E.M. Capillary transport of macromolecules: pores and other endothelial pathways. *J. Appl. Physiol. 58(2):*, 315-325, 1985.

[83] Renkin, E.M. Multiple pathways of capillary permeability. *Circ. Res. 41:* 735-743, 1977.

[84] Renkin, E.M., and F.E. Curry. Endothelial permeability: pathways and modulations. In: *Annals of the New York Academy of Sciences*, New York Academy of Science, 1982, p. 248-259.

[85] Roselli, R.J., R.E. Parker, and T.R. Harris. Comparison between pore model predictions and sheep lung fluid and protein transport. *Microvasc. Res. 29:* 320-339, 1985.

[86] Rutili, G. Transport of macromolecules in subcutaneous tissue studied by FITC–dextrans. *Ph.D Dissertation*, Upsala, Sweden: Univ. Upsaliensis, 1978.

[87] Salathé, E.P., and R. Venkataraman. Role of extravascular protein in capillary–tissue fluid exchange. *Am.J.Physiol. 234 (Heart Circ. Physiol. 3):* H52–H58, 1978.

[88] Sherwood, T.K., R.L. Pigford, and C.R. Wilke. *Mass Transfer*. New York: McGraw–Hill, 1975, p. 8-53.

[89] Silberberg, A. The significance of hydrostatic pressure in the fluid phase of a structured tissue space. In: *Tissue Fluid Pressure and Composition*, edited by A.R. Hargins. Baltimore: Williams & Wilkins, 1981, p.71-75.

[90] Simionescu, M., and N. Simionescu. Ultrastructure of the microvascular wall: functional correlations. In: *The Handbook of Physiology. The Cardiovascular System. Microcirculation*, edited by E.M. Renkin and C.C. Michel. Bethesda: American Physiological Society, 1984, p. 41-101.

[91] Soodak, H., and A. Iberall. Forum on osmosis. IV. More on osmosis and diffusion. *Am. J. Physiol. 237 (Regulatory Integrative Comp. Physiol. 6):* R114-R122, 1979.

(

[92] Swabb, E.A., J. Wei, and P.M. Gullino. Diffusion and convection in normal and neoplastic tissues. *Cancer Res. 34*: 2814-2822, 1974.

[93] Taylor, A.E., and D.N. Granger. Exchange of macromolecules across the microcirculation. In: *Handbook of Physiology. The Cardiovascular System. Microcirculation*, edited by E.M. Renkin and C.C. Michel. Bethesda: American Physiological Society, 1984, p. 467-520.

[94] Taylor, D.G., J.L. Bert, and B.D. Bowen. A mathematical model of interstitial transport. I Theory. In Press *Microvasc. Res.,* 1990.

[95] Taylor, D.G., J.L. Bert, and B.D. Bowen. A mathematical model of interstitial transport. II Microvascular exchange in mesentery. In Press *Microvasc. Res.,* 1990.

[96] Taylor, G.I. Dispersion of soluble matter in solvent flowing slowly through a tube. *Proc. Roy. Soc. A 219*: 186-203, 1953.

[97] Taylor, G.I. The dispersion of matter in turbulent flow through a pipe. *Proc. Roy. Soc. A 223*: 446-468, 1954.

[98] Terzaghi, K. *Theoretical Soil Mechanics*. New York: John Wiley, 1943.

[99] Tyldseley, J.R. *An Introduction to Tensor Analysis for Engineers and Applied Scientists*. London: Longman, p. 1-13, 1975.

[100] *UBC Matrix–A Guide to Solving Matrix Problems*, edited by T. Nicol, Vancouver: University of British Columbia Computing Center, 1982, p. 65-70.

[101] Verruijt, A. The theory of consolidation. In: *Fundamentals of Transport Phenomena in Porous Media*, edited by J. Bear and M.Y. Corapcioglu. Dordrecht: Martinus Nijhoff, 1984, p. 349-368.

[102] Verruijt, A. Elastic storage of aquifers. In: *Flow Through Porous Media*, edited by R. Deweist. New York: Academic Press, 1969, p.331-375.

[103] Wagner, R.C. and C.S. Robinson. High voltage electron microscopy of capillary endothelial vesicles. *Microvasc. Res. 28*: 197-205, 1984.

[104] Watson, P.D., and F.S. Grodins. An analysis of the effects of the interstitial matrix on plasma-lymph transport. *Microvasc. Res. 16*: 19-41, 1987.

[105] Weaver, L.J. and C.J. Carrico. Congestive heart failure and edema. In: *Edema*, edited by N.C. Staub and A.E. Taylor. New York: Raven, 1984, p. 543-562.

[106] Whitaker, S. Advances in theory of fluid motion in porous media. *Ind. Eng. Chem. 61*: 14-28, 1969.

[107] Wiederhielm, C.A. The tissue pressure controversy, a semantic dilemma. In: *Tissue Fluid Pressure and Composition*, edited by A.R. Hargins. Baltimore: Williams & Wilkins, 1981, p.21-33.

[108] Wiederhielm, C.A. Dynamics of capillary fluid exchange: a nonlinear computer simulation. *Microvasc. Res. 18*: 48-82, 1979.

[109] Wiedeman, M.P. Architecture. In: *Handbook of Physiology. The Cardiovascular System. Microcirculation*, edited by E. Renkin and C.C. Michel. Bethesda: American Physiological Society, 1984, p. 11-40.

[110] Wiig, H., E.Tveit, Hultborn, R.K. Reed, and L. Weiss. Interstitial fluid pressure in Dmba-induced rat mammary tumours. *Scand. J. Clin. Lab. Invest. 42*: 159-164, 1982.

[111] Winters, A.D., and S. Kruger. Drug effect on bulk flow through mesenteric membrane. *Arch. Int. Pharacodyn. Ther. 173*: 213-225, 1968.

[112] Wissig, S.L., and A.S. Charonis. Capillary ultrastructure. In: *Edema*, edited by N.C. Staub and A.E. Taylor. New York: American Physiological Society, 1984, p. 117-142.

[113] Witte, C.L., M.H. Witte, A.E. Dumont, W.R. Cole, and J.R. Smith. Protein content in lymph and edema fluids in congestive heart failure. *Circulation 40*: 623-630, 1969.

[114] Witte, C.L., M.H. Witte, and A.E. Dumont. Pathophysiology of chronic edema, lymphedema, and fibrosis. In: *Edema*, edited by N.C. Staub and A.E. Taylor. New York: Raven, 1984, p. 521-542.

[115] Witte, S., G. Strässle, P. Schwarzmann, and H.D. Papenfuss. Transvascular and perivascular transport of fluorescent-labelled molecules. In: *Microcirculation—An Update. International Congress Series 755*, edited by M. Tsuchiya, M. Asano, Y. Mishima, and M. Oda. Amsterdam: Excerpta Medica, 1987.

[116] Zienkiewicz, O.C., and K. Morgan. *Finite Elements and Approximation.* New York: John Wiley, p. 266-308.

[117] Zweifach, B.W., and A. Silberberg. The interstitial-lymphatic flow system. In: *International Review of Physiology. Cardiovascular physiology III, Volume 18*, edited by A.C. Guyton and B.D. Young. Baltimore: University Park Press, 1979, p. 215-260.

Appendix A

One Dimensional Approximation to the Two Dimensional Model Mesentery

A.1 Introduction

The mathematical model developed earlier to describe interstitial transport and microvascular exchange in mesentery treats the tissue as a two–dimensional structure. However, the fact that the distance separating the arteriolar and venular vessels is an order of magnitude greater than the tissue thickness provokes the question: can the behavior of the tissue segment be adequately described by a one–dimensional model. As initial evidence that this in fact is the case, one need only examine the surface plots of interstitial fluid pressure and interstitial plasma protein concentration from the two–dimensional simulation presented earlier (see Figure (4.5) of Chapter 4). In this case the gradients in the transverse (y) direction are insignificant compared to those in the longitudinal (x) direction. However, this represents the results of only one of 26 simulations. Hence a detailed study was undertaken to determine under what conditions a one–dimensional description of the system would prove adequate.

The presentation will take the following form. In Section A.2 the mathematical expressions describing interstitial fluid and plasma protein transport are developed. These equations, along with the various boundary conditions, are then cast in dimensionless form. Section A.3 describes the simulations performed in this study, while Section A.4 outlines the numerical procedures used. In Section A.5 the results of the study are presented and the ramifications discussed. Section A.6 summarizes the work. We will now develop the one–dimensional model of interstitial transport in mesentery.

A.2 One–Dimensional Approximations to the Two–Dimensional Equations

Consider the steady flow of fluid and plasma proteins through a thin, two–dimensional segment of mesenteric tissue (see Figure (4.1) of Chapter 4). The interstitium is assumed to be homogeneous and isotropic. In addition, it is assumed that variations in the y–direction can be neglected, so that the analysis is reduced to one spatial dimension. We will now develop expressions for the conservation of fluid mass and plasma protein content within the interstitium, given this simplification.

A.2.1 Conservation of Fluid Mass
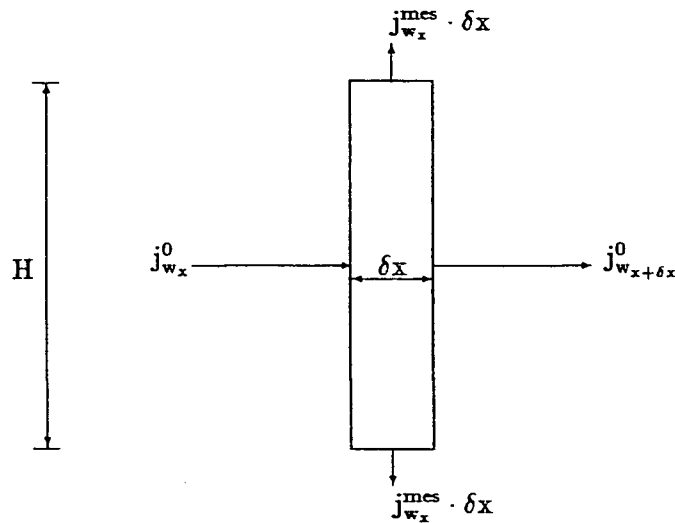
Figure A.1: A schematic diagram of a one-dimensional segment of mesenteric tissue of thickness H and differential length δx showing the various fluid fluxes.

Figure (A.1) is a schematic diagram of a differential element of interstitium of length δx and thickness H. The upper and lower boundaries of the element consist of segments of mesothelium that are permeable to both fluid and plasma proteins. Let $j^0_{w_x}$ be the fluid flux in the x–direction at some position x in the interstitium. Furthermore, let $j^{mes}_{w_x}$ represent the fluid flux crossing either of the two mesothelial segments and entering the peritoneum at that same point. A

material balance on the fluid within the volume element gives

$$H \cdot \left[j_{w_x}^0 - j_{w_{x+\delta x}}^0 \right] - 2 \cdot j_{w_x}^{mes} \cdot \delta x = 0. \tag{A.1}$$

Rearranging Eq. (A.1) and taking the limit as $\delta x \longrightarrow 0$ gives

$$\frac{dj_w^0}{dx} + \frac{2}{H} \cdot j_w^{mes} = 0. \tag{A.2}$$

The local fluid flux is related to the local hydrostatic and colloid osmotic pressures in the available space, P^1 and Π^1 respectively, via an extended Darcy relationship:

$$j_w^0 = -K^0 \frac{d(P^1 - \Pi^1)}{dx}. \tag{A.3}$$

The fluid exchange rate between the interstitium and the peritoneum, meanwhile, is described by Starling's Law:

$$j_w^{mes} = L_p^{mes} \left[P^1 - P^{mes} - \sigma^{mes} \left(\Pi^1 - \Pi^{mes} \right) \right]. \tag{A.4}$$

Substituting Eqs. (A.3) and (A.4) into Eq. (A.2) then gives

$$\frac{d^2(P^1 - \Pi^1)}{dx^2} - \frac{2L_p^{mes}}{HK^0} \left[P^1 - P^{mes} - \sigma^{mes} \left(\Pi^1 - \Pi^{mes} \right) \right] = 0. \tag{A.5}$$

Equation (A.5) provides an expression for the hydrostatic pressure distribution in the accessible space as a function of the interstitial material properties, the mesothelial boundary parameters, and the interstitial colloid osmotic pressure distribution. This latter distribution can be related to the plasma protein distribution in the accessible space through a colloid osmotic relationship. It is assumed here that

$$\Pi^1 = A_1 \left(C^1 \right) + A_2 \left(C^1 \right)^2 + A_3 \left(C^1 \right)^3, \tag{A.6}$$

where A_1, A_2, and A_3 are constants.

A.2.2 Conservation of Interstitial Plasma Proteins

Consider once more a differential element of interstitium (see Figure (A.2)). Let j_{c_x} represent the convective flux of plasma proteins through the accessible space and in the x–direction at
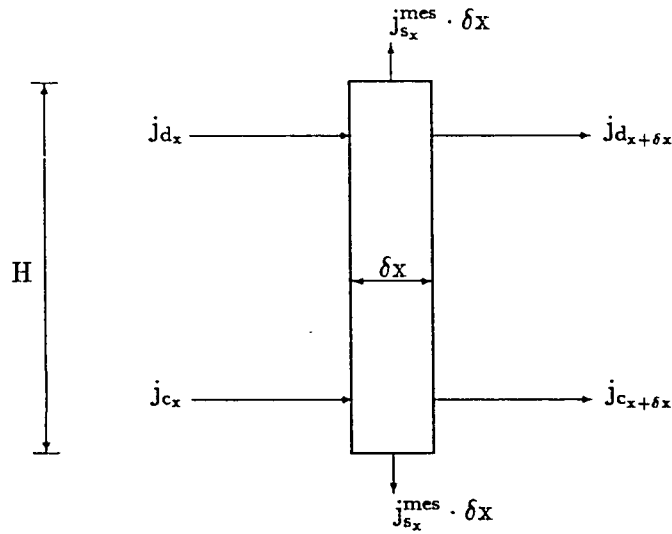
Figure A.2: **A schematic diagram of a one-dimensional segment of mesenteric tissue of thickness H and differential length δx showing the various plasma protein fluxes.**

some point x in the interstitium. Let j_{d_x} be the dispersive flux of plasma proteins through that space and in the x–direction at that same point. Finally, let $j_{s_x}^{mes}$ be the local flux of plasma proteins from the accessible space to the peritoneum crossing one of the mesothelial segments at that point.

A material balance on the plasma proteins within the differential element under steady–state conditions gives

$$H \cdot \left[j_{d_x} - j_{d_{x+\delta x}} + j_{c_x} - j_{c_{x+\delta x}} \right] - 2 \cdot j_{s_x}^{mes} \cdot \delta x = 0. \tag{A.7}$$

In the limit, as $\delta x \longrightarrow 0$, Eq. (A.7) becomes

$$\frac{d(j_c + j_d)}{dx} + \frac{2}{H} \cdot j_s^{mes} = 0. \tag{A.8}$$

The local convective flux, j_c, is related to the local fluid flux, j_w^0, by

$$j_c = \xi \cdot \beta \cdot j_w^0 \cdot C^1. \tag{A.9}$$

The local dispersive flux, j_d, is given by Fick's Law:

$$j_d = -n^1 \cdot D_d \cdot \frac{dC^1}{dx}. \tag{A.10}$$

where the coefficient of mechanical dispersion, D_d, is (see Appendix C)

$$D_d = \frac{|\xi \cdot \beta \cdot j_w^0|}{n^1} \cdot \alpha_1 + D_{eff}. \tag{A.11}$$

Finally, we will assume that the flux of plasma proteins crossing each of the mesothelial boundary segments, j_s^{mes}, is given by the nonlinear flux equation. That is,

$$j_s^{mes} = (1 - \sigma^{mes}) \cdot j_w^{mes} \cdot \frac{[C^1 - C^{mes} \exp(-Pe^{mes})]}{[1 - \exp(-Pe^{mes})]}, \tag{A.12}$$

where

$$Pe^{mes} = \frac{(1 - \sigma^{mes})j_w^{mes}}{D^{mes}}. \tag{A.13}$$

Equation (A.8) then becomes

$$\xi \cdot \beta \cdot \frac{d(j_w^0 \cdot C^1)}{dx} - n^1 \cdot \frac{d}{dx}\left(D_d \cdot \frac{dC^1}{dx}\right) + \frac{2}{H} \cdot (1 - \sigma^{mes}) \cdot j_w^{mes} \cdot \frac{[C^1 - C^{mes}\exp(-Pe^{mes})]}{[1 - \exp(-Pe^{mes})]} = 0. \tag{A.14}$$

That is, the sum of the net convective plasma protein flux per unit volume of interstitium, the net dispersive flux of plasma proteins per unit volume of interstitium, and the net exchange of plasma proteins between the interstitium and the peritoneum, per unit volume of interstitium, equals zero at steady–state.

The differential in the convective term may be expanded as follows:

$$\frac{dj_w^0 \cdot C^1}{dx} = j_w^0 \cdot \frac{dC^1}{dx} + C^1 \cdot \frac{dj_w^0}{dx}. \tag{A.15}$$

Similarly, the diffusive term may be expanded to give

$$\frac{d}{dx}\left(D_d \cdot \frac{dC^1}{dx}\right) = \frac{dD_d}{dx} \cdot \frac{dC^1}{dx} + D_d \cdot \frac{d^2C^1}{dx^2}. \tag{A.16}$$

However, D_d may be related to the fluid flux, j_w^0, via Eq. (A.11), so that

$$\frac{dD_d}{dx} = \frac{\xi \cdot \beta \cdot \alpha_1}{n^1} \cdot \frac{d|j_w^0|}{dx}. \tag{A.17}$$

Equation (A.17) further assumes that ξ, β, n^1, D_{eff}, and α_1 are all spatially invariant. However, according to Eq. (A.2) dj_w^0/dx is equal to $-2j_w^{mes}/H$. Hence Eq. (A.15) becomes

$$\frac{dj_w^0 \cdot C^1}{dx} = j_w^0 \cdot \frac{dC^1}{dx} - C^1 \cdot \frac{2}{H} \cdot j_w^{mes}. \tag{A.18}$$

Substituting Eq. (A.18) into the convective term of Eq. (A.14) and Eq. (A.17) in the diffusive term, the final form of the solute transport equation becomes

$$\xi \cdot \beta \cdot \left[j_w^0 \cdot \frac{dC^1}{dx} - \frac{2}{H} C^1 j_w^{mes} \right] - n^1 \left[D_d \frac{d^2 C^1}{dx^2} + \frac{\xi \, \beta \, \alpha_1}{n^1} \cdot \frac{d \, |j_w^0|}{dx} \cdot \frac{dC^1}{dx} \right] +$$

$$+ \frac{2}{H} \cdot (1 - \sigma^{mes}) j_w^{mes} \frac{[C^1 - C^{mes} \exp(-Pe^{mes})]}{[1 - \exp(-Pe^{mes})]} = 0. \qquad (A.19)$$

A.2.3 Boundary Conditions

A complete description of fluid and plasma protein transport within the interstitium requires expressions for fluid and plasma protein exchange at each of the arteriolar and venular capillaries. These boundary conditions are the same as those for the two–dimensional system analyzed earlier. That is,

$$\left[j_w^0 \right]_b \cdot l_x = L_p^b \left[\left[P^1 \right]_b - P^b - (1 - \sigma^b) \left(\left[\Pi^1 \right]_b - \Pi^b \right) \right], \qquad (A.20)$$

and

$$[j_d + j_c]_b \cdot l_x = (1 - \sigma^b) \cdot \left[j_w^0 \right]_b \cdot l_x \frac{\left(\left[C^1 \right]_b - C^b \exp(-Pe^b) \right)}{\left(1 - \exp(-Pe^b) \right)}, \qquad (A.21)$$

where

$$Pe^b = \frac{(1 - \sigma^b) \cdot \left[j_w^0 \right]_b \cdot l_x}{D^b}, \qquad (A.22)$$

and where $[\cdot]_b$ represents an interstitial parameter evaluated at a point adjacent to the boundary b.

A.2.4 Non–Dimensional Form of the Equations

The set of coupled, ordinary differential equations developed above can be recast in dimensionless form by introducing the following dimensionless parameters: $\tilde{P} = P/P^{art}$, $\tilde{C} = C/C^{art}$, $\tilde{\Pi} = \Pi/P^{art}$, $\tilde{x} = x/L$, $\tilde{H} = H/L$, $\alpha = (K^0 \cdot P^{art})/D_{eff}$, $\beta = K^1/K^0$, $\gamma = (\xi \beta \alpha_1)/(Ln^1)$, $\tilde{j}_w^0 = j_w^0 L/D_{eff}$, $\tilde{j}_d = j_d L/(D_{eff} C^{art})$, $\tilde{j}_c = j_c L/(D_{eff} C^{art})$, $\tilde{j}_w^{mes} = j_w^{mes} L/D_{eff}$, $\tilde{\alpha}_1 = \alpha_1/L$, $\tilde{D}_d = D_d/D_{eff}$, $\tilde{A}_1 = A_1 \cdot C^{art}/P^{art}$, $\tilde{A}_2 = A_2 \cdot (C^{art})^2/P^{art}$, $\tilde{A}_3 = A_3 \cdot (C^{art})^3/P^{art}$, $\tilde{L}_p^b = (L_p^b \cdot L)/K^0$, and $\tilde{D}^b = (D^b \cdot L)/D_{eff}$. The equations then take the following form.

1. Fluid Transport within the Interstitium:

$$\frac{d^2(\tilde{P}^1 - \tilde{\Pi}^1)}{d\tilde{x}^2} - \frac{2}{\tilde{H}} \tilde{L}_p^{mes} \left[\tilde{P}^1 - \tilde{P}^{mes} - \sigma^{mes} \left(\tilde{\Pi}^1 - \tilde{\Pi}^{mes} \right) \right] = 0, \qquad (A.23)$$

$$\tilde{\Pi}^1 = \tilde{A}_1 \left(\tilde{C}^1 \right) + \tilde{A}_2 \left(\tilde{C}^1 \right)^2 + \tilde{A}_3 \left(\tilde{C}^1 \right)^3, \qquad (A.24)$$

$$\tilde{j}_w^0 = -\alpha \frac{d(\tilde{P}^1 - \tilde{\Pi}^1)}{d\tilde{x}}. \qquad (A.25)$$

2. Plasma Protein Transport within the Interstitium:

$$\xi \cdot \beta \cdot \left[\tilde{j}_w^0 \cdot \frac{d\tilde{C}^1}{d\tilde{x}} - \frac{2}{\tilde{H}} \cdot \tilde{j}_w^{mes} \cdot \tilde{C}^1 \right] - n^1 \cdot \left[\tilde{D}_d \cdot \frac{d^2\tilde{C}^1}{d\tilde{x}^2} + \gamma \cdot \frac{d \left| \tilde{j}_w^0 \right|}{d\tilde{x}} \cdot \frac{d\tilde{C}^1}{d\tilde{x}} \right] +$$

$$+ \frac{2}{\tilde{H}} \cdot (1 - \sigma^{mes}) \cdot \tilde{j}_w^{mes} \cdot \frac{\left[\tilde{C}^1 - \tilde{C}^{mes} \exp(-\tilde{P}e^{mes}) \right]}{\left[1 - \exp(-\tilde{P}e^{mes}) \right]} = 0, \qquad (A.26)$$

$$\tilde{j}_c = \xi \cdot \beta \cdot \tilde{j}_w^0 \cdot \tilde{C}^1, \qquad (A.27)$$

$$\tilde{j}_d = -n^1 \cdot \tilde{D}_d \cdot \frac{d\tilde{C}^1}{d\tilde{x}}, \qquad (A.28)$$

$$\tilde{j}_w^{mes} = \alpha \cdot \tilde{L}_p^{mes} \left[\tilde{P}^1 - \tilde{P}^{mes} - \sigma^{mes} \left(\tilde{\Pi}^1 - \tilde{\Pi}^{mes} \right) \right]. \qquad (A.29)$$

3. Boundary Conditions:

$$\left[-\frac{d(\tilde{P}^1 - \tilde{\Pi}^1)}{d\tilde{x}} \right]_b \cdot l_x = \tilde{L}_p^b \left(\left[\tilde{P}^1 \right]_b - \tilde{P}^b - \sigma^b \left(\left[\tilde{\Pi}^1 \right]_b - \tilde{\Pi}^b \right) \right), \qquad (A.30)$$

$$\left[\tilde{j}_c + \tilde{j}_d \right]_b \cdot l_x = \left(1 - \sigma^b \right) \cdot \left[\tilde{j}_w^0 \right]_b \cdot l_x \cdot \frac{\left(\left[\tilde{C}^1 \right]_b - \tilde{C}^b \exp \left(-\tilde{P}e^b \right) \right)}{\left(1 - \exp \left(-\tilde{P}e^b \right) \right)}, \qquad (A.31)$$

$$\tilde{P}e^b = \frac{\left(1 - \sigma^b \right) \cdot \left[\tilde{j}_w^0 \right]_b \cdot l_x}{\tilde{D}^b}. \qquad (A.32)$$

Equations (A.23) through (A.32) fully describe the system.

A.2.5 Influence of the 1–D Approximation on Characterizing the Mesothelial Transport Properties

The equations developed earlier provide a one–dimensional approximation to the two–dimensional equations describing fluid and plasma protein transport within a segment of mesenteric tissue. The validity of this simplification rests on the assumption that variations in the transverse (y) direction are negligible. However, a further consequence of this simplification is that the resistance of the interstitium to fluid and plasma protein transport in the transverse direction is ignored. This presents no real problem, provided that the permeable boundaries, and not the interstitium, are the major sources of resistance to mass exchange. However, should the interstitial resistance to fluid and plasma protein transport be significant, the hydraulic conductance and permeability of the mesothelial layer, L_p^{mes} and D^{mes} respectively, must be reduced in the one–dimensional case to account for the contribution of the interstitium to the overall resistance of the system in this direction.

Let H^{eff} be the effective thickness of the interstitium which contributes to the overall resistance to transport in the transverse direction. Given the symmetry of the system about the longitudinal axis of the interstitium, then $H/2$, the half–thickness of the tissue, serves as an upper bound to H^{eff}. However, H^{eff} will in fact depend on the hydrodynamics within the tissue itself. For example, should the majority of fluid and plasma proteins be transported within a fraction of the total tissue thickness, H^{eff} will be less than $H/2$. The magnitude of H^{eff} can therefore only be determined by first investigating mass transport in the two–dimensional system.

Suppose that the effective tissue thickness is known. The resistance of the interstitium to fluid flow, R_w^{int}, is then given by

$$R_w^{int} = \frac{H^{eff}}{K^0},$$
(A.33)

where K^0 is the hydraulic conductivity of the interstitial space. The resistance of the mesothelial

layer, R_w^{mes}, on the other hand, is

$$R_w^{mes} = \frac{1}{L_p^{mes}}. \tag{A.34}$$

The total resistance to fluid flow in the transverse direction is given by the sum of these two:

$$R_w^{tot} = R_w^{int} + R_w^{mes}. \tag{A.35}$$

The total hydraulic conductivity of the system in the transverse direction, L_p^{tot}, is then given by

$$L_p^{tot} = \frac{1}{R_w^{tot}}. \tag{A.36}$$

The same argument can be applied to the resistance to protein diffusion in the transverse direction. For example, the resistance of the interstitium to plasma protein diffusion, R_d^{int} is

$$R_d^{int} = \frac{H^{eff}}{n^1 D_d}, \tag{A.37}$$

where, as before, D_d is the dispersion coefficient. The resistance associated with the mesothelial boundary, meanwhile, is

$$R_d^{mes} = \frac{1}{D^{mes}}. \tag{A.38}$$

The total resistance to diffusion, R_d^{tot} is then

$$R_d^{tot} = R_d^{int} + R_d^{mes}, \tag{A.39}$$

while the system's total transverse permeability to plasma proteins, D^{tot}, is given by

$$D^{tot} = \frac{1}{R_d^{tot}}. \tag{A.40}$$

Since the dispersion coefficient is linked to the fluid flow, the interstitial resistance to diffusion will vary with the hydrodynamics of the interstitium. If mechanical dispersion is negligible compared to molecular diffusion, D_d can be replaced by D_{eff} in Eq. (A.37). (Note that, in the numerical analysis that follows, mechanical dispersion is neglected so that D_d reduces to D_{eff}, the coefficient of molecular diffusion.)

The above analysis fails to consider the additional effect of convective retardation on the plasma protein transport properties of the mesothelium in the one–dimensional approximation. Presumably, the influence of the retardation factor can be accounted for by adjusting the reflection coefficient of the mesothelium. The exact way in which this can be described is unclear. Initially, one might assume that if $\xi \cdot \beta$ is less than $(1 - \sigma^{mes})$, the former replaces the latter. However, this fails to consider the possibility of a change in plasma protein transport mechanisms at the boundary itself. In the extreme case, σ^{mes} and ξ might both equal 0. Hence, plasma protein transport would be restricted to diffusion alone in the interstitium, while considerable convective transport might take place across the mesothelial layer. The matter of adjusting σ^{mes} in the one–dimensional case will therefore be left unresolved at this time.

A.3 Case Studies

The various parameters associated with the one–dimensional model were assigned the same values as those used in the two–dimensional simulations. A $3 \times 3 \times 3$ factorial study was performed as before, with α varying as 0.09117, 0.9117, and 9.117, ξ assuming values of 1.0, 0.5, and 0.0, and where the mesothelial transport properties varied according to boundary condition 1, boundary condition 2, and boundary condition 3 outlined previously (see Chapter 4).

Four additional simulations were performed to study the influence of the interstitial resistance in the transverse direction, discussed in Section A.2, on microvascular exchange in the tissue segment. In these latter simulations α assumed a value of 9.117 and the mesothelial transport properties were defined by boundary condition 3 — the mesothelium's most permeable state. ξ was assigned values of 0.5 and 0.0. (An ξ value of 1.0 was not considered since no two–dimensional simulation was available for comparison.) Two values of H^{eff} were considered: 1.5×10^{-3} cm (i.e., the tissue half-thickness) and 1.5×10^{-4} cm. These corresponded to a total hydraulic conductivity in the y–direction, L_p^{tot}, of 2.04×10^{-6} cm^3/(dyne-s) and 1.79×10^{-7}

$cm^3/(dyne-s)$, respectively, while the total transverse plasma protein permeability, D^{tot}, assumed values of 2.28×10^{-6} cm/s and 2.39×10^{-6} cm/s, respectively. These 'effective values' of hydraulic conductivity and permeability were then used to characterize the mesothelium.

A.4   Numerical Procedures

The numerical procedure used to solve the two–dimensional problem was applied to the one-dimensional system as well. Again, the finite element method was employed, with second-order Lagrange polynomials serving as basis functions. The tissue domain was divided into 25 elements resulting in a system of 51 nodal points. Nodal values of $\tilde{P}^1$ and $\tilde{C}^1$ were determined iteratively. A tolerance of 10^{-6} served as the criterion for convergence (see Section 4.4 of Chapter 4 on numerical procedures for the two–dimensional simulations for details).

Global material balances on fluid and plasma protein exchange were performed to verify the numerical solution. In all cases the material balances were accurate to within 0.005 percent.

A.5   Results and Discussion

A.5.1   General Comparison of the 1–Dimensional and 2–Dimensional Simulations

Panels i through ix of Figure (A.3) yield the profiles of the total plasma protein concentration, $\tilde{C}^t$, as a function of position $\tilde{x}$ for each of the 27 1–dimensional simulations. Recall that the total concentration is related to the concentration in the accessible space, $\tilde{C}^1$, by

$$\tilde{C}^t = \frac{n^1}{(1 - n^s)} \cdot \tilde{C}^1, \tag{A.41}$$

where n^1 and n^s are accessible phase volume fraction and the solid phase volume fraction, respectively. Each panel of Figure (A.3) contains three curves corresponding to the three values of α considered, as in the concentration plots from the 2–dimensional simulations (see Figure (4.9) of Chapter 4). In each case H^{eff} is assumed to be zero. Comparing the curves from the 1–dimensional simulations to the corresponding curves from the 2–dimensional simulations, it is clear that, for the most part, the curves closely resemble one another.
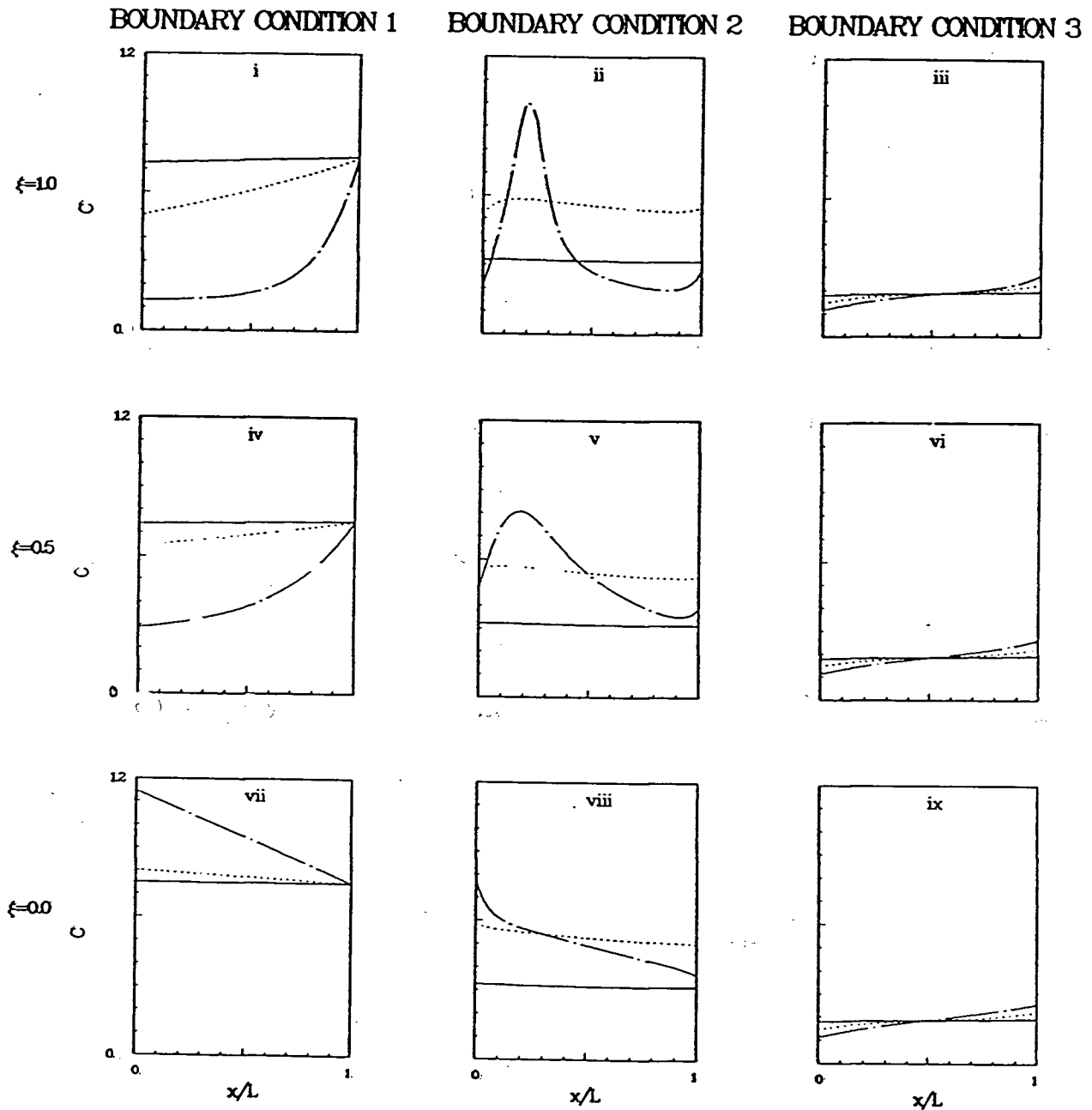
Figure A.3: The dimensionless total concentration, $\bar{C}^t$, as a function of dimensionless position, $\bar{x}$. The nine plots correspond to the nine different combinations of boundary conditions (columns) and values of ζ (rows) studied. Each plot contains three curves corresponding to the three values of α considered (i.e., the solid line corresponds to α equal to 0.09117, the dotted line corresponds to α equal 0.9117, and the chain-dot line corresponds to α equal to 9.117).

One exception to this is the case where ξ equals 1.0, α is 9.117, and the mesothelial transport properties are defined by boundary condition 2. The plot from the 1–dimensional simulation reveals a sharper peak in the total concentration than the corresponding curve from the 2–dimensional simulation. This discrepancy is attributed largely to the finer grid density, and hence the greater definition, in the 1–dimensional simulation. At the very least, the two curves show good qualitative agreement. The similarity is further substantiated when we consider the distribution of fluid and solute fluxes crossing the mesothelium predicted by the two simulations. Panel i of Figure (A.4) corresponds to the 1–dimensional simulation, while panel ii corresponds to the 2–dimensional simulation.

Other significant differences in the concentration profiles predicted by the 1–dimensional and 2–dimensional simulations are restricted to those cases for which the mesothelial transport properties are given by boundary condition 3. The differences are most pronounced in the vicinity of the arteriolar and venular walls when α is 9.117. However, these discrepancies will be fully addressed in Section A.5.2.

The average fluid and solute fluxes across each of the permeable boundaries predicted by the 1–dimensional simulations are compared to those from the 2–dimensional simulations in Table A.1 and Table A.2, respectively. With exception of those simulations associated with boundary condition 3, the 1–dimensional model predictions and 2–dimensional model predictions are in close agreement. Consider, for example, the fluxes across the arteriolar wall for boundary condition 1 and 2. In all cases the fluid and solute fluxes predicted by the two models agreed to within 6.6 percent of each other, and generally agreed to within 4.6 percent. Similarly, the ratio of the average convective protein flux to the average diffusive protein flux in the vicinity of the arteriolar wall differed by no more than 4.6 percent (see Table A.3). A comparison of the one-dimensional and two-dimensional model predictions assuming the mesothelial boundary condition 3 follows.
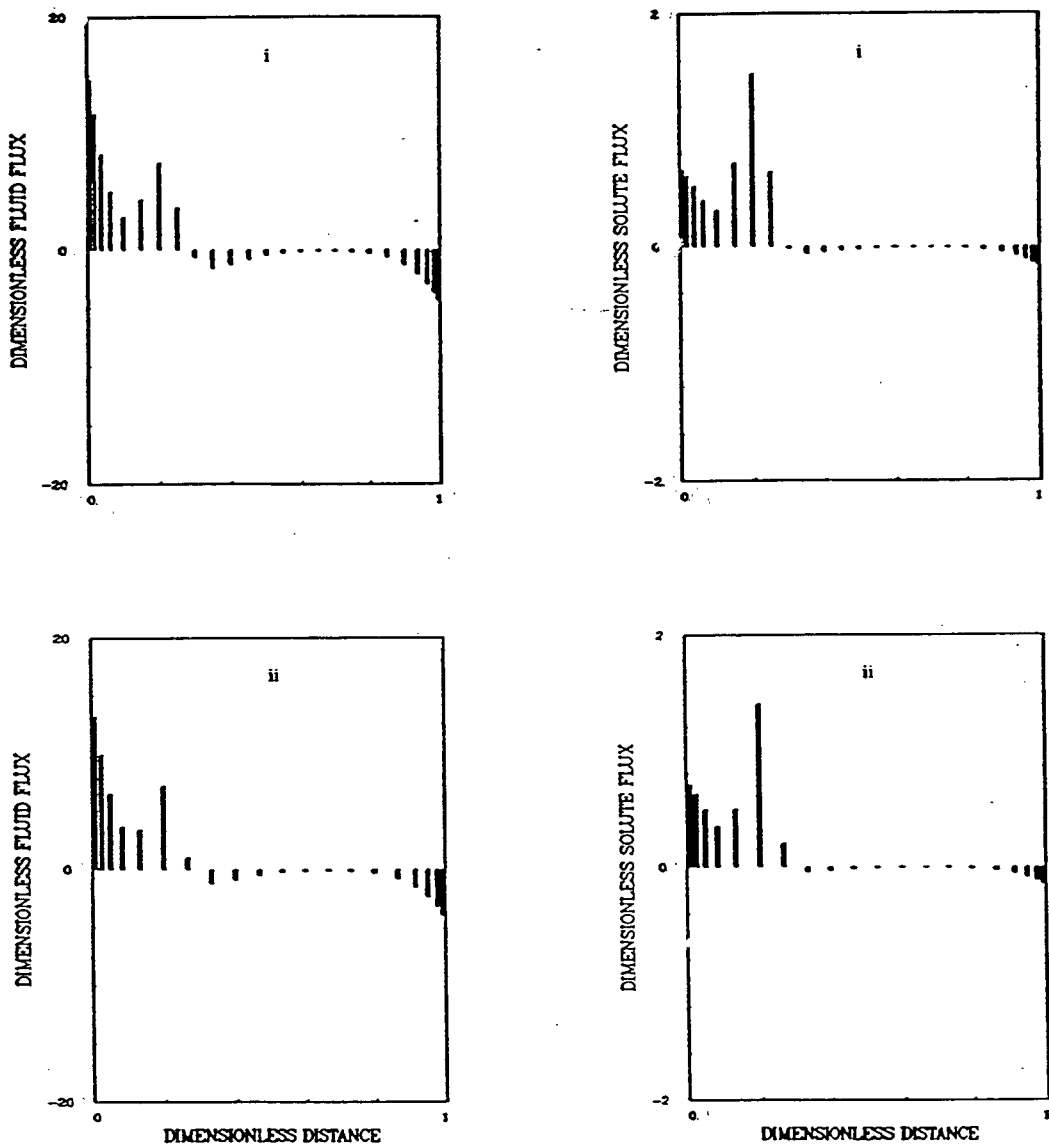
Figure A.4: The mesothelial fluid and plasma protein flux distributions, assuming ζ is 1.0, α is 9.117, and the mesothelial transport properties are given by boundary condition 2, are shown for the one-dimensional model (panels i) and the two-dimensional model (panels ii).

ξ	α	Boundary Condition 1			Boundary Condition 2			Boundary Condition 3		
		Art	Ven	Mes	Art	Ven	Mes	Art	Ven	Mes
1.0	0.09117	-0.04	0.04	—	-0.22	0.06	0.01	-0.31	0.09	0.01
1.0	0.9117	-0.40	0.40	—	-2.30	0.63	0.08	-2.87	0.65	0.11
1.0	9.117	-4.49	4.49	—	-25.16	6.84	0.92	No Convergence		
0.5	0.09117	-0.04	0.04	—	-0.22	0.06	0.01	-0.31	0.09	0.01
0.5	0.9117	-0.37	0.37	—	-2.26	0.61	0.08	-2.87	0.66	0.11
0.5	9.117	-4.30	4.30	—	-24.90	6.46	0.92	-26.14	2.47	1.18
0.0	0.09117	-0.03	0.03	—	-0.22	0.06	0.01	-0.31	0.09	0.01
0.0	0.9117	-0.34	0.34	—	-2.21	0.60	0.08	-2.86	0.66	0.11
0.0	9.117	-2.42	2.42	—	-20.20	5.70	0.72	-25.58	2.92	1.13

ξ	α	Boundary Condition 1			Boundary Condition 2			Boundary Condition 3		
		Art	Ven	Mes	Art	Ven	Mes	Art	Ven	Mes
1.0	0.09117	-0.04	0.04	—	-0.23	0.06	0.01	-0.38	0.12	0.01
1.0	0.9117	-0.40	0.40	—	-2.39	0.66	0.09	-3.55	0.76	0.14
1.0	9.117	-4.49	4.49	—	-25.83	7.03	0.94	-33.06	2.25	1.54
0.5	0.09117	-0.04	0.04	—	-0.23	0.06	0.01	-0.38	0.12	0.01
0.5	0.9117	-0.37	0.37	—	-2.35	0.64	0.09	-3.56	0.78	0.14
0.5	9.117	-4.30	4.30	—	-25.64	6.69	0.95	-33.17	2.47	1.53
0.0	0.09117	-0.03	0.03	—	-0.23	0.06	0.01	-0.38	0.12	0.01
0.0	0.9117	-0.34	0.34	—	-2.31	0.63	0.08	-3.57	0.80	0.14
0.0	9.117	-2.42	2.42	—	-21.53	6.05	0.77	-33.23	3.19	1.50

Table A.1: The upper table presents the average dimensionless fluid fluxes across the various permeable boundaries assuming a two-dimensional model of the mesentery. The same data is shown in the lower table for the case of a one-dimensional model of the tissue segment. A negative value indicates a fluid flux entering the interstitial space, while a positive value denotes a flux leaving the interstitium.

ξ	α	Boundary Condition 1			Boundary Condition 2			Boundary Condition 3		
		Art	Ven	Mes	Art	Ven	Mes	Art	Ven	Mes
1.0	0.09117	-0.005	0.005	—	-0.034	0.000	0.002	-0.046	0.001	0.002
1.0	0.9117	-0.060	0.060	—	-0.345	0.069	0.014	-0.430	0.029	0.020
1.0	9.117	-0.673	0.673	—	-3.774	0.396	0.169	No Convergence		
0.5	0.09117	-0.005	0.005	—	-0.034	-0.000	0.002	-0.046	-0.001	0.002
0.5	0.9117	-0.056	0.056	—	-0.339	0.064	0.014	-0.430	0.029	0.020
0.5	9.117	-0.645	0.645	—	-3.736	0.512	0.161	-3.920	0.130	0.189
0.0	0.09117	-0.005	0.005	—	-0.034	-0.000	0.002	-0.046	0.001	0.002
0.0	0.9117	-0.051	0.051	—	-0.332	0.060	0.014	-0.430	0.028	0.020
0.0	9.117	-0.364	0.364	—	-3.030	0.433	0.130	-3.840	0.144	0.184

ξ	α	Boundary Condition 1			Boundary Condition 2			Boundary Condition 3		
		Art	Ven	Mes	Art	Ven	Mes	Art	Ven	Mes
1.0	0.09117	-0.005	0.005	—	-0.035	0.000	0.002	-0.058	0.001	0.003
1.0	0.9117	-0.060	0.060	—	-0.358	0.072	0.014	-0.533	0.034	0.025
1.0	9.117	-0.673	0.673	—	-3.874	0.395	0.174	-4.959	0.120	0.242
0.5	0.09117	-0.005	0.005	—	-0.035	0.000	0.002	-0.058	-0.001	0.003
0.5	0.9117	-0.056	0.056	—	-0.353	0.067	0.014	-0.534	0.035	0.025
0.5	9.117	-0.645	0.645	—	-3.846	0.521	0.166	-4.976	0.130	0.242
0.0	0.09117	-0.005	0.005	—	-0.035	0.000	0.002	-0.058	0.001	0.003
0.0	0.9117	-0.051	0.051	—	-0.347	0.063	0.014	-0.536	0.036	0.025
0.0	9.117	-0.364	0.364	—	-3.229	0.445	0.139	-4.985	0.164	0.241

Table A.2: **The upper table presents the average dimensionless plasma protein fluxes across the various permeable boundaries assuming a two-dimensional model of the mesentery. The same data is shown in the lower table for the case of a one-dimensional model of the tissue segment. A negative value indicates a protein flux entering the interstitial space, while a positive value denotes a flux leaving the interstitium.**

ξ	α	Boundary Condition 1			Boundary Condition 2			Boundary Condition 3		
		Art	Ven	Mes	Art	Ven	Mes	Art	Ven	Mes
1.0	0.09117	-1.22	-1.21	—	-1.69	-0.99	-2.26	-3.54	-0.97	23.22
1.0	0.9117	-1.35	-1.21	—	-1.34	-1.21	-1.34	-7.89	-1.21	5.73
1.0	9.117	-64.51	-1.21	—	-2.71	-1.21	-1.23	No Convergence		
0.5	0.09117	-1.55	-1.53	—	-5.28	-0.98	9.16	2.34	-0.93	0.92
0.5	0.9117	-1.67	-1.53	—	-1.89	-1.53	-1.98	1.52	-1.53	0.75
0.5	9.117	-9.22	-1.53	—	-2.30	-1.53	-1.62	1.80	-1.53	0.71

ξ	α	Boundary Condition 1			Boundary Condition 2			Boundary Condition 3		
		Art	Ven	Mes	Art	Ven	Mes	Art	Ven	Mes
1.0	0.09117	-1.22	-1.21	—	-1.68	-1.01	—	-3.61	-1.06	—
1.0	0.9117	-1.35	-1.21	—	-1.33	-1.21	—	-8.91	-1.21	—
1.0	9.117	-65.46	-1.21	—	-2.60	-1.21	—	10.69	-1.21	—
0.5	0.09117	-1.55	-1.53	—	-5.05	-1.01	—	2.25	-1.11	—
0.5	0.9117	-1.67	-1.53	—	-1.88	-1.53	—	1.34	-1.53	—
0.5	9.117	-9.21	-1.53	—	-2.21	-1.53	—	0.95	-1.53	—

Table A.3: **The upper table presents the ratios of the average dimensionless convective plasma protein flux to the average dimensionless diffusive protein flux across the various permeable boundaries assuming a two-dimensional model of the mesentery. The same data is shown in the lower table for the case of a one-dimensional model of the tissue segment. A negative value indicates that the two protein fluxes are in opposite directions.**

A.5.2 Effect of H^{eff} on Exchange in the 1–D Simulations

The results from the 27 simulations suggest that the 1–dimensional model is, under most circumstances, a reasonable approximation to the 2–dimensional formulation. Notable exceptions are those cases in which the mesothelial transport properties are given by boundary condition 3. Here the 1–dimensional simulations predict substantially higher fluxes across each of the permeable boundaries when compared to the 2–dimensional simulations. Four additional simulations were therefore performed to evaluate the effect of the interstitial matrix resistance on mass exchange for those cases in which the mesothelium was most permeable. In these simulations α was set equal to 9.117, since the differences between the 2–dimensional and the 1–dimensional simulations were greatest under these conditions. Two values of ζ were considered: namely 0.5 and 0.0. A ζ value of 1.0 was not included in the study since the corresponding 2–dimensional simulation failed to converge to a solution. For each value of ζ two simulations were performed in which H^{eff} assumed values of 1.5×10^{-3} cm and 1.5×10^{-4} cm. Together with the initial 1–dimensional simulations, in which H^{eff} was zero, this gave a total of three cases with H^{eff} ranging from zero to the tissue half–thickness. The results of these predictions were then compared with the corresponding 2–dimensional simulations.

In general, an increase in H^{eff} was accompanied by a substantial decrease in the local dimensionless fluid and plasma protein fluxes across the mesothelium. This is illustrated in Figure (A.5), where ζ equals 0.5, and Figure (A.6), in which ζ equals 0.0. Panels i through iii of these figures plot the local dimensionless fluid and plasma protein fluxes as a function of position, $\bar{x}$, for H^{eff} equal to 0 cm, 1.5×10^{-4} cm, and 1.5×10^{-3} cm, respectively. Consider, for example, those cases where ζ equals 0.5. The maximum dimensionless fluid flux drops from approximately 116 to something less than 25 as H^{eff} increases from 0 to 1.5×10^{-3} cm. In addition, the fraction of the mesothelial surface over which fluid and plasma proteins are exchanged increases with H^{eff}. A similar trend is observed for those simulations in which ζ equals 0. The reduced fluxes and greater portion of mesothelial surface area active in exchange associated with increased H^{eff} both compare more favorably with the 2–dimensional predictions.

This is shown for the case where ξ equals 0.5 in panels i and ii of Figure (A.7).

The average dimensionless fluid and plasma protein fluxes across the permeable boundaries, assuming various values of H^{eff} and ξ equal to 0.5, are compared to the 2–dimensional simulation in the upper data of Table (A.4). Similar data for the case where ξ equals 0 are given in the lower set of panels of Table (A.4). Again, the data suggest that the interstitial matrix contributes significantly to the overall resistance when the mesothelium assumes its most permeable state and α equals 9.117. Consider, for example, the case where ξ equals 0.5. When H^{eff} is zero, the average dimensionless fluid flux across the arteriolar vessel, $\bar{j}_w^{art}$, is approximately 27 percent higher than that predicted by the 2–dimensional simulation. This increased influx of fluid into the interstitium is attributed to the enhanced capacity of the system to exchange material with the peritoneum, due to the elimination of the interstitial resistance in the transverse direction. This effect is also reflected in the average fluid flux across the mesothelium when H^{eff} is zero, which is approximately 53 percent higher than the mesothelial fluid flux associated with the 2–dimensional simulation.

The enhanced fluid exchange is accompanied by a concomitant increase in plasma protein exchange in the system. Again assuming ξ equals 0.5 and H^{eff} is zero, the plasma protein fluxes across the arteriolar wall and the mesothelium are 27 percent and 28 percent higher, respectively, than the fluxes predicted in the 2–dimensional simulation.

The situation is reversed when we assume a value of 1.5×10^{-3} cm for H^{eff}. In this case the 1–dimensional simulations underestimate $\bar{j}_w^{art}$ and $\bar{j}_w^{mes}$ by 16 percent and 19 percent, respectively, suggesting that the effective thickness of the interstitium is something less than the tissue half–thickness. A similar conclusion may be drawn from the solute flux data since, with a H^{eff} of 1.5×10^{-3}, the 1–dimensional simulation underestimates $\bar{j}_s^{art}$ and $\bar{j}_s^{mes}$ by 16 percent and 17 percent, respectively. Furthermore, since a value of 1.5×10^{-4} cm for H^{eff} again leads to an overestimate of the various fluxes across the arteriolar and mesothelial boundaries, it is concluded that the effective thickness lies between this and 1.5×10^{-3} cm.

Finally, it is observed that the 1–dimensional model's prediction of the relative importance
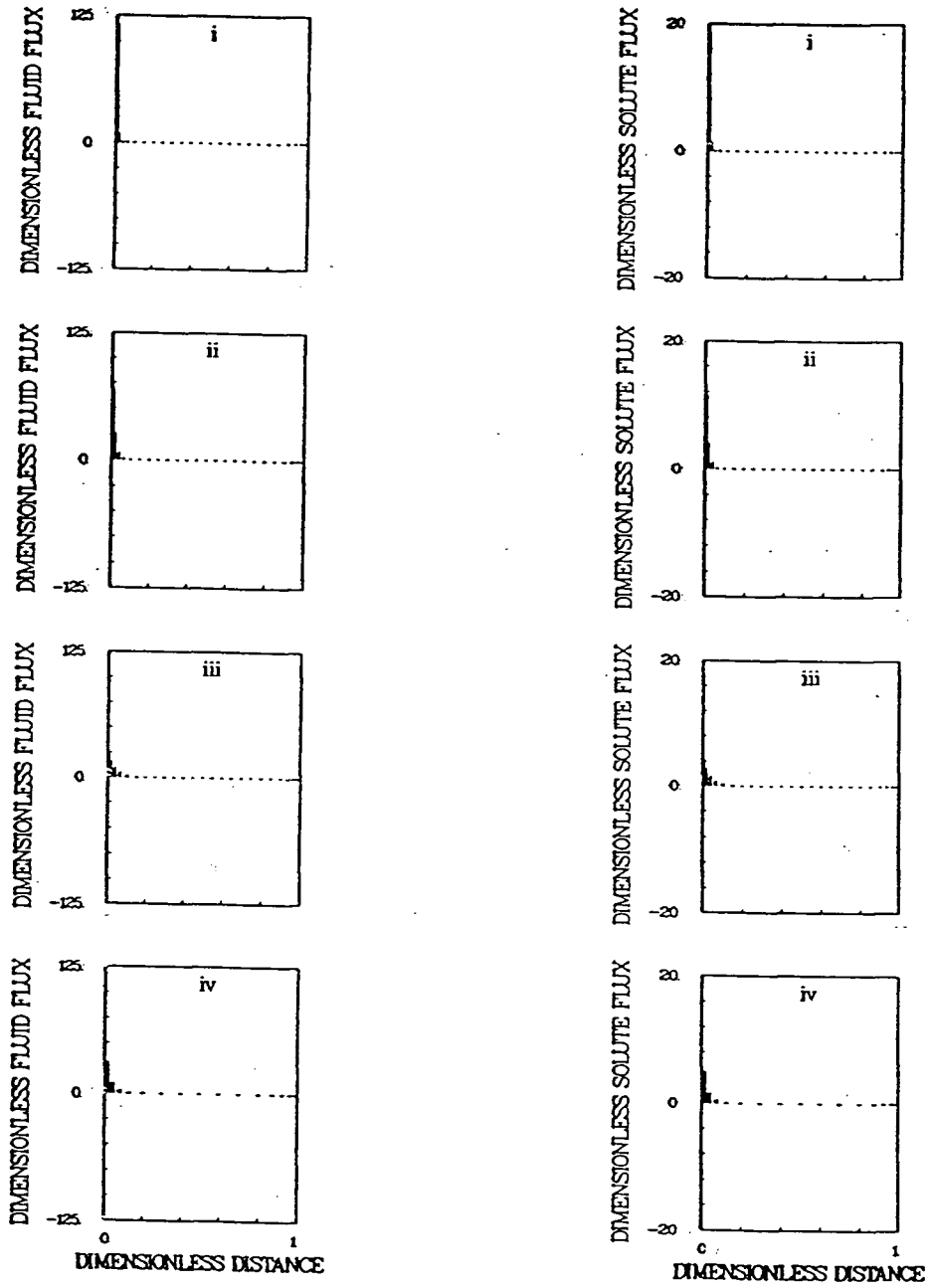
Figure A.5: This figure illustrates the effect of varying H^{eff} on the fluid and plasma protein flux distribution across the mesothelium in the one-dimensional model of mesentery, assuming ζ equal to 0.5. Panel i assumes H^{eff} is 0 cm, Panel ii assumes H^{eff} equals 1.5×10^{-4} cm, and panel iii assumes H^{eff} equals 1.5×10^{-3} cm. Panel iv provides the results from the 2-dimensional model.
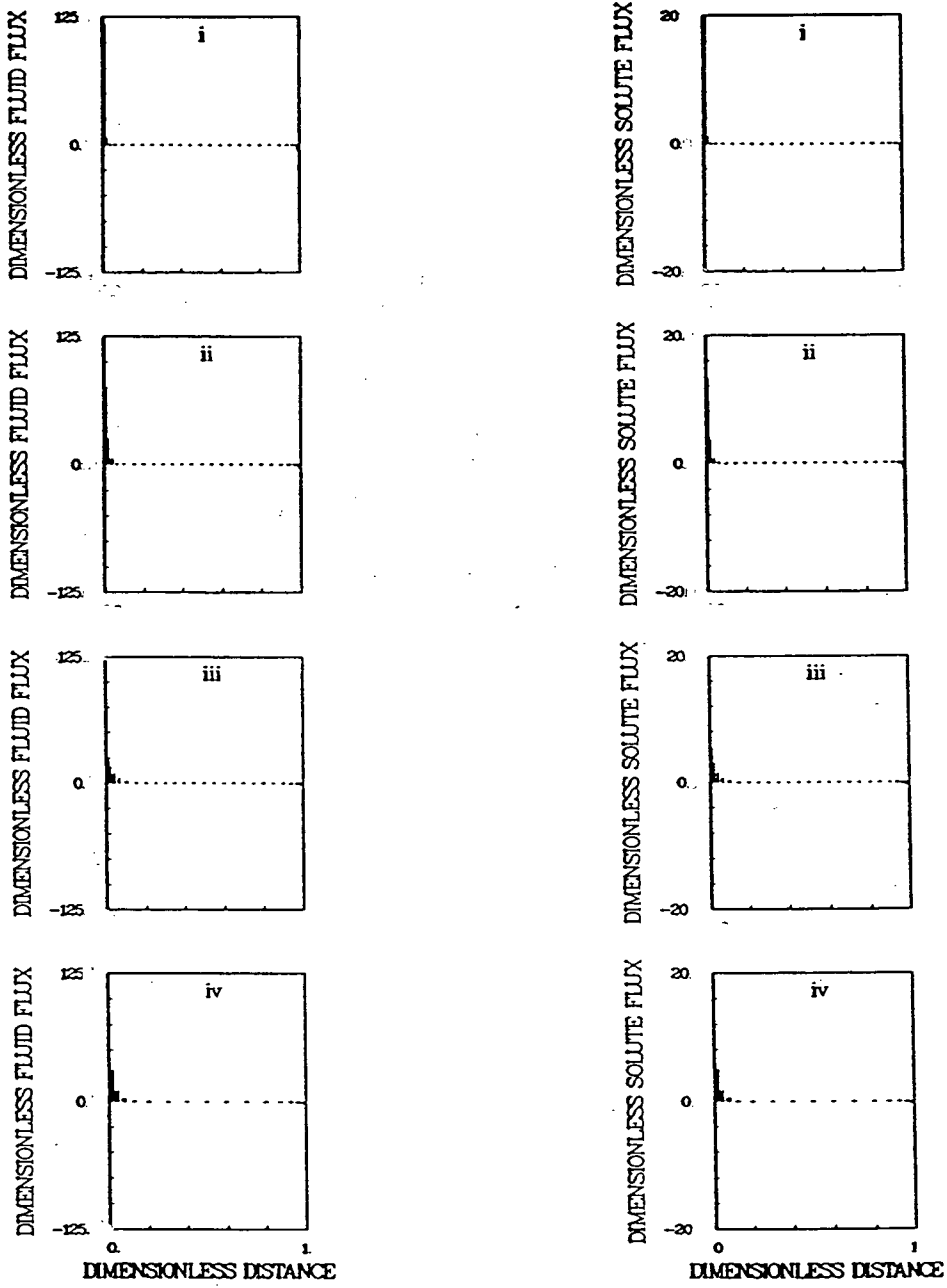
Figure A.6: This figure illustrates the effect of varying H^{eff} on the fluid and plasma protein flux distribution across the mesothelium in the one-dimensional model of mesentery assuming ζ equal to 0. Panel i assumes H^{eff} is 0 cm, Panel ii assumes H^{eff} equals 1.5×10^{-4} cm, and panel iii assumes H^{eff} equals 1.5×10^{-3} cm. Panel iv provides the results from the 2-dimensional model.
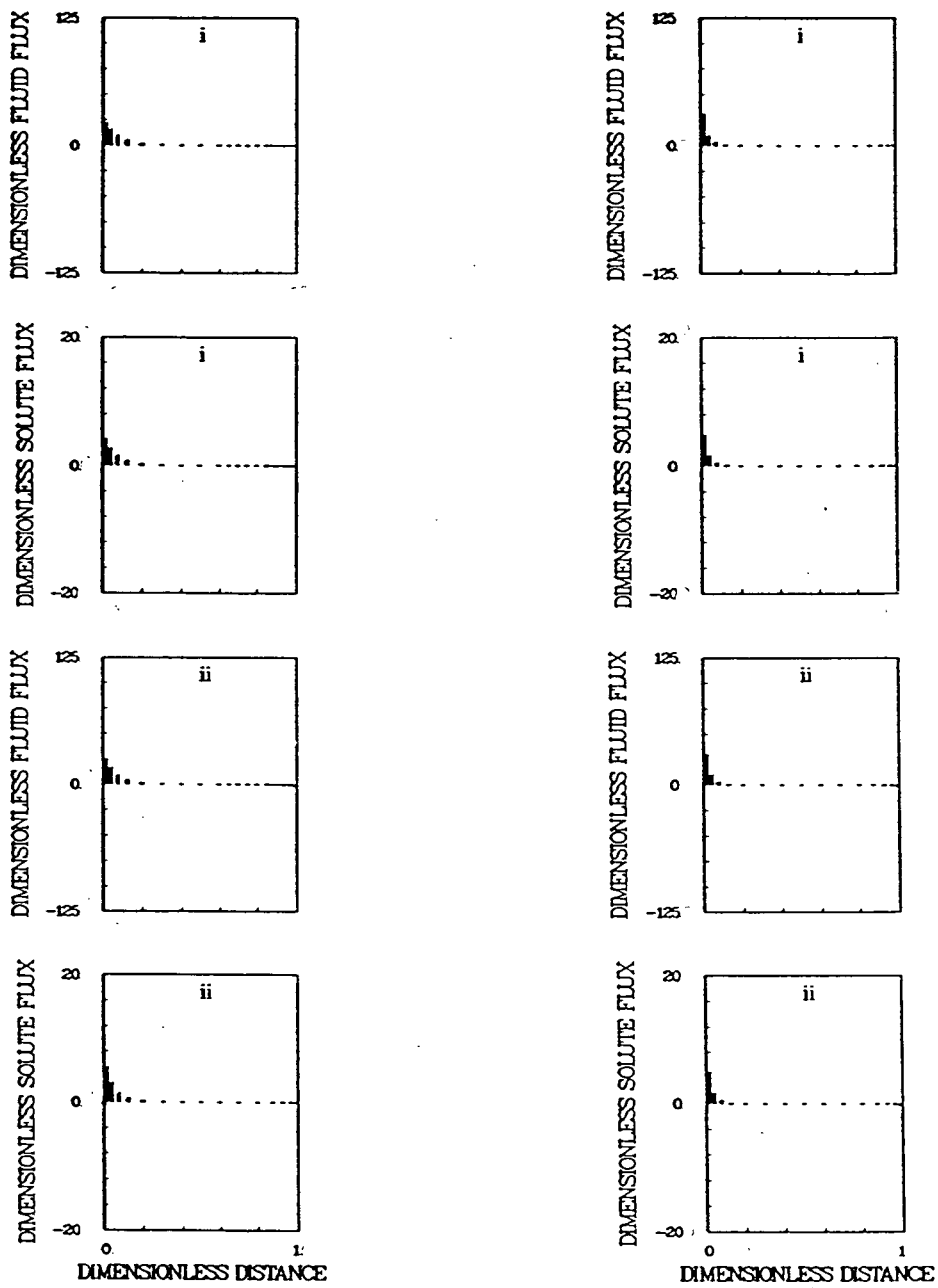
Figure A.7: This figure compares the fluid and plasma protein flux distributions across the mesothelium for the one-dimensional model (left column) and the two-dimensional model (right column) assuming ξ equal to 0.5 (panels i) and ξ equal to 0 (panels ii) and with H^{eff} equal to 1.5×10^{-3} cm.

H^{eff}	$\bar{j}_w^{art}$	$\bar{j}_w^{ven}$	$\bar{j}_w^{mes}$	$\bar{j}_s^{art}$	$\bar{j}_s^{ven}$	$\bar{j}_s^{mes}$	$\bar{j}_c^{art}/\bar{j}_d^{art}$	$\bar{j}_c^{ven}/\bar{j}_d^{ven}$
0.0	-33.17	2.47	1.53	-4.976	0.130	0.242	0.95	-1.53
1.5×10^{-4}	-29.29	2.50	1.34	-4.393	0.132	0.213	1.10	-1.53
1.5×10^{-3}	-21.69	2.53	0.96	-3.254	0.132	0.156	1.41	-1.53
2–D	-26.14	2.47	1.18	-3.920	0.130	0.189	1.52	-1.53

H^{eff}	$\bar{j}_w^{art}$	$\bar{j}_w^{ven}$	$\bar{j}_w^{mes}$	$\bar{j}_s^{art}$	$\bar{j}_s^{ven}$	$\bar{j}_s^{mes}$	$\bar{j}_c^{art}/\bar{j}_d^{art}$	$\bar{j}_c^{ven}/\bar{j}_d^{ven}$
0.0	-33.23	3.19	1.50	-4.985	0.164	0.241	0.0	0.0
1.5×10^{-4}	-29.23	3.15	1.30	-4.385	0.160	0.211	0.0	0.0
1.5×10^{-3}	-21.56	3.08	0.92	-3.233	0.151	0.154	0.0	0.0
2–D	-25.58	2.92	1.13	-3.840	0.144	0.184	0.0	0.0

Table A.4: The upper table presents the effect of H^{eff} on the the average fluid and plasma protein fluxes across the permeable boundaries for the case where ξ is 0.5. The same data are shown for ξ equal to 0 in the lower table.

of convection to diffusion within the interstitial space depends, in part, on the value of H^{eff} assumed. With ξ equal to 0.5 and an H^{eff} of zero, the ratio of the average convective flux of proteins to the average diffusive flux adjacent the arteriolar vessel, $\bar{j}_c^{art}/\bar{j}_d^{art}$, is 0.95. When H^{eff} is increased to 1.5×10^{-3} cm, the ratio of convection to diffusion also increases to 1.41. The 2–dimensional simulation predicts a ratio of 1.52. This effect is further illustrated in panel i of Figure (A.8), which plots the total interstitial plasma protein concentration as a function of $\bar{x}$ for the various values of H^{eff}. From this figure it is clear that the concentration gradient adjacent the arteriolar vessel increases with decreasing H^{eff}, implying more diffusion in that region as H^{eff} approaches zero. This may be explained by the following. As H^{eff} decreases, the rate of plasma protein exchange between the interstitium and the peritoneum is enhanced near the arteriolar wall (see panels i, ii, and iii of Figure (A.5)). This greater rate of protein depletion near the wall increases the concentration gradient there, which in turn enhances diffusion. The same phenomenon is seen in the case where ξ is 0, as shown in panel ii of Figure (A.8). While in each case the profile associated with an H^{eff} of zero follows closely the y–averaged concentration profile from the 2–dimensional simulation in the central portions of the tissue, it deviates from the 2–D profile in the vicinity of the arteriolar and venular boundaries, where the majority of the mass exchange occurs. On the other hand, the concentration profile associated with an H^{eff} of 1.5×10^{-3} cm, while it never coincides with the 2–D profile, follows more closely the trend of latter curve in the vicinity of the arteriolar and venular capillaries, and therefore provides a more accurate description of the plasma protein transport processes there.

A.6 Concluding Remarks

In the preceding sections we developed a one–dimensional model of interstitial transport and microvascular exchange in mesentery and compared the model predictions to·those based on a two–dimensional representation of the tissue. In general it was found that the one–dimensional simulations were in close agreement with the two–dimensional simulations, suggesting that the one–dimensional model was an adequate approximation of the real system.
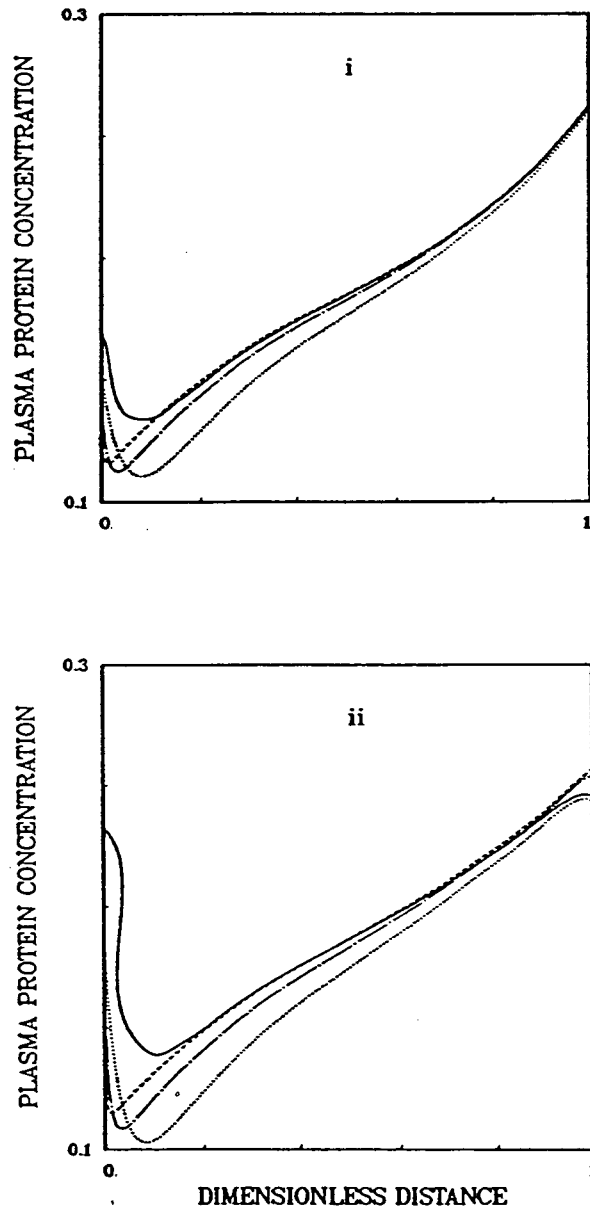
Figure A.8: The upper panel (i) shows the effect of varying H^{eff} on the dimensionless interstitial plasma protein distribution ($\tilde{C}^t$ assuming an ξ of 0.5. The same data is illustrated in panel (ii) for the case where ξ equals 0. In each plot, the solid line represents the results from the two-dimensional simulation, the dotted line assumes H^{eff} is 1.5×10^{-3} cm, the chain-dotted line assumes H^{eff} is 1.5×10^{-4} cm, and the dashed line assumes H^{eff} is 0.

Notable exceptions to this were those cases in which the mesothelium assumed its most permeable state. Under these conditions the interstitium contributed significantly to the overall resistance to mass transport in the transverse direction. Hence the one–dimensional simulations tended to over–estimate the amount of fluid and plasma proteins exchanged within the tissue. However, it was also shown that the interstitial resistance could be accounted for, at least in part, by reducing the hydraulic conductance and permeability of the mesothelium. An 'effective thickness', H^{eff}, was proposed as one method of characterizing the interstitium's contribution to the overall resistance in the transverse direction.

Finally, given the general effectiveness of the one–dimensional model to describe the system's behavior under steady–state conditions, and the substantial savings in computational effort it offers over the two–dimensional model, the one–dimensional model is used in the transient analysis presented in Chapters 5 and 6. Further, since the analysis of these chapters is qualitative, and since the the one-dimensional simulations are, for the most part, in close agreement to the two dimensional predictions, no attempt is made in the simulations of Chapters 5 and 6 to adjust the mesothelial resistances to account for the interstitial resistance.

Appendix B

An Overview of the Combined Finite Element – Finite Difference Technique

B.1 Introduction

The transient one–dimensional solute mass balance equation developed in Appendix A represents the most general partial differential equation we will consider, in that it contains both spatial and temporal terms. This equation has therefore been selected to provide an example of the numerical procedures used in this research to solve the system of equations describing microvascular exchange in the model tissue.

In dimensionless form, the transient form of the solute mass balance equation for a single solute species is

$$\xi \cdot \beta \left[\tilde{j}_w^0 \frac{\partial \tilde{C}^1}{\partial \tilde{x}} - \frac{2}{\tilde{H}} \tilde{j}_w^{mes} \cdot \tilde{C}^1 \right] - n^1 \left[\tilde{D}_d \frac{\partial^2 \tilde{C}^1}{\partial \tilde{x}^2} + \frac{\partial \tilde{D}_d}{\partial \tilde{x}} \frac{\partial \tilde{C}^1}{\partial \tilde{x}} \right] +$$

$$+ \frac{2}{\tilde{H}} (1 - \sigma^{mes}) \tilde{j}_w^{mes} \frac{\left[\tilde{C}^1 - \tilde{C}^{mes} \exp\left(-\tilde{Pe}^{mes} \right) \right]}{\left[1 - \exp\left(-\tilde{Pe}^{mes} \right) \right]} = -n^1 \frac{\partial \tilde{C}^1}{\partial \tilde{t}}. \tag{B.1}$$

The solution to Eq. (B.1) is obtained numerically using a combined finite element – finite difference scheme. This approach has been used to solve, for example, problems of consolidation and solute transport in porous media [67, 42]. The original partial differential equation is reduced to a set of time–dependent ordinary differential equations by applying the finite element method of weighted residuals to the spatial components of the partial differential equation. (The selective application of the finite element procedure to the spatial elements of the equation is referred to in the literature as the *partial discretization method* , or *Kantorovich's method* [116].) This set of coupled ordinary differential equations is then reduced to a set of coupled algebraic expressions by applying a semi–implicit finite difference scheme to the time derivatives.

The system of simultaneous algebraic equations can then be solved using appropriate matrix techniques.

The sequential applications of the finite element procedure and the finite difference technique to the solute mass balance equation are discussed in detail in Sections B.2, B.3, and B.4. For more information on the techniques and their application to transport problems, the reader may refer to any number of sources in the literature (see, for example, [67, 42, 59, 116]).

Finally, in Section B.5 we discuss briefly, by way of two examples, some of the techniques used to validate the simulator.

B.2 Solving for the Spatial Variation in Concentration Using Finite Elements

The finite element method partitions the domain (in this case, the mesenteric tissue segment) into a set of connected subregions, the so-called *finite elements* of the system (see, for example, Figure (4.2) of Chapter 4). Each element contains a number of nodes representing discrete locations within the domain. Associated with each node j is a basis function, ϕ_j, that takes on a value of 1 at node j and is zero at all other nodes within the system. The value of the basis functions elsewhere in the domain depend only on position (in fact, the basis functions are typically polynomial relationships in the spatial coordinates). The basis functions are combined with the nodal values of the dependent variable (e.g., the dimensionless plasma protein concentration, $\tilde{C}^1$) to create a continuous approximation to the dependent variable throughout the region. Specifically, the approximating function $\hat{C}^1$ to the interstitial plasma protein concentration $\tilde{C}^1$ is

$$\hat{C}^1 = \sum_{j=1}^{m} \phi_j \cdot \tilde{C}_j^1, \tag{B.2}$$

where $\tilde{C}_j^1$ is the value of $\tilde{C}^1$ at node j, and where m is the total number of nodes in the system. Since the plasma protein concentration varies with time, the nodal values $\hat{C}_j^1$ will vary with time as well. However, they represent constant coefficients with respect to the spatial variation of $\tilde{C}^1$.

The dependence of the basis functions on position is known *a priori*. However, we must

determine the m nodal values of $\hat{C}^1$ before the interstitial plasma protein distribution is known. These are calculated as follows. First, the piecewise approximating function $\hat{C}^1$ is substituted into Eq. (B.1). Since $\hat{C}^1$ is only an approximation to the true function $\tilde{C}^1$, $\hat{C}^1$ will not, in general, satisfy the differential equation completely. Rather, there will be some residual error, $\epsilon(\tilde{x})$, associated with the approximation. That is, assuming the temporal variation of $\tilde{C}^1$ is known,

$$\epsilon = \xi \cdot \beta \left[\tilde{j}_w^0 \frac{\partial \hat{C}^1}{\partial \tilde{x}} - \frac{2}{\tilde{H}} \tilde{j}_w^{\text{mes}} \cdot \hat{C}^1 \right] - n^1 \left[\tilde{D}_d \frac{\partial^2 \hat{C}^1}{\partial \tilde{x}^2} + \frac{\partial \tilde{D}_d}{\partial \tilde{x}} \frac{\partial \hat{C}^1}{\partial \tilde{x}} \right] +$$
$$+ \frac{2}{\tilde{H}} (1 - \sigma^{\text{mes}}) \tilde{j}_w^{\text{mes}} \frac{\left[\hat{C}^1 - \tilde{C}^{\text{mes}} \exp\left(-\tilde{P}e^{\text{mes}} \right) \right]}{\left[1 - \exp\left(-\tilde{P}e^{\text{mes}} \right) \right]} + n^1 \frac{\partial \hat{C}^1}{\partial \tilde{t}}. \tag{B.3}$$

To minimize the residual error, the nodal values $\hat{C}_j^1$ are chosen such that the weighted integral of ϵ over the entire domain D is zero for m different choices of weighting functions, $\varsigma_i, i = 1, 2, ..., m$. That is,

$$\int_D \varsigma_i \cdot \epsilon \, d\tilde{x} = 0, \ i = 1, 2, ..., m. \tag{B.4}$$

Hence the solution of the system of m equations represented by Eq. (B.4) yields the m nodal values of $\tilde{C}^1$ which minimize the error associated with the piecewise approximating function, $\hat{C}^1$.

The choice of weighting functions, ς_i, is arbitrary; however, each weighting function must be independent of the others. In the Galerkin procedure (used in this research) the weighting function ς_i is set equal to the basis function ϕ_i. The set of weighted residual equations then becomes

$$\int_D \phi_i \left\{ \xi \cdot \beta \left[\tilde{j}_w^0 \frac{\partial \hat{C}^1}{\partial \tilde{x}} - \frac{2}{\tilde{H}} \tilde{j}_w^{\text{mes}} \cdot \hat{C}^1 \right] - n^1 \left[\tilde{D}_d \frac{\partial^2 \hat{C}^1}{\partial \tilde{x}^2} + \frac{\partial \tilde{D}_d}{\partial \tilde{x}} \frac{\partial \hat{C}^1}{\partial \tilde{x}} \right] + \right.$$
$$\left. + \frac{2}{\tilde{H}} (1 - \sigma^{\text{mes}}) \tilde{j}_w^{\text{mes}} \frac{\left[\hat{C}^1 - \tilde{C}^{\text{mes}} \exp\left(-\tilde{P}e^{\text{mes}} \right) \right]}{\left[1 - \exp\left(-\tilde{P}e^{\text{mes}} \right) \right]} + n^1 \frac{\partial \hat{C}^1}{\partial \tilde{t}} \right\} d\tilde{x} = 0, \ i = 1, 2, ..., m. \tag{B.5}$$

Since $\hat{C}^1$ is only C^0 continuous in D (i.e., the derivatives of $\hat{C}^1$ are not necessarily continuous), and to facilitate the introduction of the boundary conditions into the weighted residual

expressions, we reduce the second–order dispersive term in Eq. (B.5) to a first–order term and a boundary integral using Green's Second Theorem:

$$\int_D \phi_i \tilde{D}_d \frac{\partial^2 \hat{C}^1}{\partial \tilde{x}^2}\, dD = \int_B \phi_i \tilde{D}_d \frac{\partial \hat{C}^1}{\partial \tilde{x}} \cdot l_x\, dB - \int_D \frac{d(\phi_i \tilde{D}_d)}{d\tilde{x}} \frac{\partial \hat{C}^1}{\partial \tilde{x}}\, dD. \tag{B.6}$$

where l_x is the direction cosine of a unit outward normal to the boundary, B. Note that, for the one–dimensional system, Green's Second Theorem is equivalent to integration by parts since the boundary integral reduces to an evaluation of the integrand at the domain's two end-points. The second term on the right-hand-side of Eq. (B.6) can be expanded as follows:

$$\int_D \frac{d(\phi_i \tilde{D}_d)}{d\tilde{x}} \frac{\partial \hat{C}^1}{\partial \tilde{x}}\, dD = \int_D \phi_i \frac{d\tilde{D}_d}{d\tilde{x}} \frac{\partial \hat{C}^1}{\partial \tilde{x}}\, dD + \int_D \tilde{D}_d \frac{d\phi_i}{d\tilde{x}} \frac{\partial \hat{C}^1}{\partial \tilde{x}}\, dD. \tag{B.7}$$

Substituting Eqs. (B.6) and (B.7) into Eq. (B.5) yields the 'weak form' [116] of the weighted residual equations:

$$\int_D \left[\phi_i \left\{ \xi \cdot \beta \left[\tilde{j}_w^0 \frac{\partial \hat{C}^1}{\partial \tilde{x}} - \frac{2}{\tilde{H}} \tilde{j}_w^{mes} \cdot \hat{C}^1 \right] + n^1 \tilde{D}_d \frac{d\phi_i}{d\tilde{x}} \frac{\partial \hat{C}^1}{\partial \tilde{x}} + \right.\right.$$

$$\left.\left. + \frac{2}{\tilde{H}}(1 - \sigma^{mes}) \tilde{j}_w^{mes} \frac{\left[\hat{C}^1 - \tilde{C}^{mes} \exp\left(-\tilde{P}e^{mes}\right) \right]}{\left[1 - \exp\left(-\tilde{P}e^{mes}\right) \right]} + n^1 \frac{\partial \hat{C}^1}{\partial \tilde{t}} \right\} + \right] d\tilde{x}$$

$$= \int_B \phi_i \tilde{D}_d \frac{\partial \hat{C}^1}{\partial \tilde{x}} \cdot l_x\, dB, \quad i = 1, 2, ..., m. \tag{B.8}$$

Based on the definition of $\hat{C}^1$ (see Eq. (B.2)), Eq. (B.8) can be written in matrix form as

$$\mathbf{M} \cdot \frac{d\hat{C}^1}{d\tilde{t}} + \mathbf{A} \cdot \hat{C}^1 = \mathbf{b}, \tag{B.9}$$

where

$$M_{i,j} = \int_D \phi_i \cdot \phi_j\, d\tilde{x}, \tag{B.10}$$

$$\hat{C}_i^1 = \tilde{C}_i^1, \tag{B.11}$$

$$A_{i,j} = \int_D \left[\phi_i \left\{ \xi \beta \left[\tilde{j}_w^0 \frac{d\phi_j}{d\tilde{x}} - \frac{2}{\tilde{H}} \tilde{j}_w^{mes} \phi_j \right] + n^1 \tilde{D}_d \frac{d\phi_i}{d\tilde{x}} \frac{d\phi_j}{d\tilde{x}} + \right.\right.$$

$$\left.\left. + \frac{2}{\tilde{H}}(1 - \sigma^{mes}) \tilde{j}_w^{mes} \frac{\phi_j}{\left[1 - \exp\left(-\tilde{P}e^{mes}\right) \right]} \right\} \right] d\tilde{x}, \tag{B.12}$$

and

$$
b_i = \int_B \phi_i \, \tilde{D}_d \, \frac{\partial \hat{C}^1}{\partial \tilde{x}} \cdot l_x \, dB + \int_D \phi_i \left[\frac{2}{\tilde{H}} (1 - \sigma^{mes}) \tilde{j}_w^{mes} \frac{\tilde{C}^{mes} \exp\left(-\tilde{P}e^{mes}\right)}{\left[1 - \exp\left(-\tilde{P}e^{mes}\right)\right]} \right] d\tilde{x}. \qquad (B.13)
$$

The boundary conditions are incorporated into the finite element expressions as follows. We have at each vascular boundary the condition

$$
\left[-\tilde{D}_d \frac{\partial \hat{C}^1}{\partial \tilde{x}} + \xi \beta \tilde{j}_w^0 \, \hat{C}^1 \right]_b \cdot l_x = \left(1 - \sigma^b\right) \cdot \left[\tilde{j}_w^0\right]_b \cdot l_x \frac{\left(\left[\hat{C}^1\right]_b - \tilde{C}^b \exp\left(-\tilde{P}e^b\right)\right)}{\left(1 - \exp\left(\tilde{P}e^b\right)\right)}. \qquad (B.14)
$$

Rearranging Eq. (B.14) and substituting into the boundary integral term gives

$$
\int_B \phi_i \left[D_d \frac{\partial \hat{C}^1}{\partial \tilde{x}} \right] \cdot l_x \, dB =
$$

$$
\int_B \phi_i \left[\tilde{j}_w^0\right]_b \cdot l_x \left[\left[\hat{C}^1\right]_b \left(\xi \cdot \beta - \frac{1}{\left[1 - \exp\left(\tilde{P}e^b\right)\right]} \right) + \frac{\tilde{C}^b \exp\left(-\tilde{P}e^b\right)}{\left[1 - \exp\left(\tilde{P}e^b\right)\right]} \right] dB. \qquad (B.15)
$$

The **A** matrix is then adjusted to include those components of the boundary integral that contain $\hat{C}^1$ (i.e., the first term in the right-hand-side integral), while the remaining terms are retained in the expression for the **b** vector. That is, the boundary contributions $A_{i,j}^b$ and b_i^b are introduced into the **A** matrix and **b** vector where

$$
A_{i,j}^b = -\int_B \phi_i \left[\tilde{j}_w^0\right]_b \cdot l_x \phi_j \left(\xi \cdot \beta - \left(1 - \sigma^b\right) \frac{1}{\left[1 - \exp\left(\tilde{P}e^b\right)\right]} \right) dB, \qquad (B.16)
$$

and

$$
b_i^b = \int_B \phi_i \left[\tilde{j}_w^0\right]_b \cdot l_x \left(1 - \sigma^b\right) \frac{\tilde{C}^b \exp\left(-\tilde{P}e^b\right)}{\left[1 - \exp\left(\tilde{P}e^b\right)\right]} dB. \qquad (B.17)
$$

We are now left with the task of representing the temporal derivative in the matrix Eq. (B.9) using the finite difference method. This will be discussed in the next section.

B.3 Solving for the Temporal Variation in Concentration Using Finite Differences

As we have seen, the finite element method reduces the second order p.d.e. (Eq. (B.1)) to a set of first order o.d.e.'s in the nodal values of $\hat{C}^1$. We are now free to apply a finite difference

scheme to Eq. (B.9) to approximate the time differential. The semi–implicit method will be presented here (for more information on this technique see, for example [59]).

Let θ be a parameter bounded by $[0,1]$. Let k and k+1 be adjacent finite difference time levels. Then the value of $\hat{C}^1$ at time level $k + \theta$ is

$$\left[\mathbf{A} \cdot \hat{\mathbf{C}}^1\right]^{k+\theta} = (1 - \theta) \cdot \left[\mathbf{A} \cdot \hat{\mathbf{C}}^1\right]^{k} + \theta \cdot \left[\mathbf{A} \cdot \hat{\mathbf{C}}^1\right]^{k+1}. \tag{B.18}$$

Similarly, if the **b** vector varies with time

$$\mathbf{b}^{k+\theta} = (1 - \theta) \cdot \mathbf{b}^k + \theta \cdot \mathbf{b}^{k+1}. \tag{B.19}$$

The temporal derivative at time level $k + \theta$ is

$$\left[\frac{d\hat{\mathbf{C}}^1}{d\tilde{t}}\right]^{k+\theta} = \frac{\left[\hat{\mathbf{C}}^1\right]^{k+1} - \left[\hat{\mathbf{C}}^1\right]^{k}}{\Delta \tilde{t}}, \tag{B.20}$$

where $\Delta \tilde{t}$ is the finite difference time step.

Substituting Eqs. (B.18), (B.19), and (B.20) into Eq. (B.9) gives the semi–implicit finite difference form of the matrix equation:

$$\frac{\mathbf{M}}{\Delta \tilde{t}} \cdot \left(\left[\hat{\mathbf{C}}^1\right]^{k+1} - \left[\hat{\mathbf{C}}^1\right]^{k}\right) + \left([1 - \theta] \cdot \mathbf{A}^k \cdot \left[\hat{\mathbf{C}}^1\right]^{k} + \theta \cdot \mathbf{A}^{k+1} \cdot \left[\hat{\mathbf{C}}^1\right]^{k+1}\right) = \theta \cdot \mathbf{b}^{k+1} + (1 - \theta) \cdot \mathbf{b}^k. \tag{B.21}$$

When θ is equal to 0, Eq. (B.21) reduces to the fully explicit form, while a θ value of 1 transforms Eq. (B.21) to the fully implicit scheme. A θ of 0.5 represents the Crank–Nicolson form of the finite difference method. The Crank-Nicolson method was used in the transient simulations of Chapters 5 and 6.

B.4 Guidelines for Selecting Grid and Time Step Sizes

In general, numerical techniques for solving partial differential equations, be they finite element or finite difference schemes, are subject to some numerical error. For example, when the convective component of the local solute flux is significant relative to the dispersive flux, the finite element method suffers from spatial oscillations when estimating the solute concentration in

the vicinity of the advancing front [59]. These oscillations can be reduced by using a finer grid. For this reason, and to assure an accurate solution to the model equations in general, tests were performed in each of the numerical studies to confirm that the grid size was sufficiently small.

Guidelines have been established for selecting grid size as a function of the local convective velocity and dispersion coefficient for a limited number of problems [59]. These guidelines are expressed in terms of a local grid Peclet number, $\mathrm{Pe^{grid}}$, where

$$\mathrm{Pe^{grid}} = \frac{\tilde{v}_{sc} \, \Delta \tilde{l}}{\tilde{D}_d},$$ (B.22)

and where $\tilde{v}_{sc}$ is the local superficial convective velocity of the solute within an element, $\Delta \tilde{l}$ is the maximum dimension of the element, and $\tilde{D}_d$ is the dispersion coefficient. The superficial convective velocity is related to the convective solute flux, $\tilde{j}_c$, by

$$\tilde{v}_{sc} = \frac{\tilde{j}_c}{\tilde{C}^1}.$$ (B.23)

It has been found that, when using linear basis functions at least, the spatial oscillations previously mentioned are virtually non-existent provided $\mathrm{Pe^{grid}}$ is less than 2. The maximum grid Peclet number was therefore monitored in all simulations as a further check of numerical accuracy.

The criterion for selecting the time step size utilizes the local grid Courant number, $\mathrm{Cr^{grid}}$, where

$$\mathrm{Cr^{grid}} = \frac{\tilde{v}_{sc} \, \Delta \tilde{t}}{\Delta \tilde{l}},$$ (B.24)

and where $\Delta \tilde{t}$ is the time step size. Since, for our system, the superficial dispersive velocity is frequently of the same order of magnitude as the superficial convective velocity, $\tilde{v}_{sc}$, in Eq. (B.24) is replaced by the total superficial solute velocity, $\tilde{v}_{sd} + \tilde{v}_{sc}$. The superficial dispersive velocity is related to the dispersive flux, $\tilde{j}_d$ by

$$\tilde{v}_{sd} = \frac{\tilde{j}_d}{\tilde{C}^1}.$$ (B.25)

According to Huyakorn and Pinder [59], the local grid Courant number should not exceed 1. (A value greater than 1 would imply that a solute particle passes through an entire element

in less time than the time step size. The simulation would therefore be unable to describe the transient interactions occurring within that element due to the presence of that solute particle from one time interval to the next.) In fact, in this research, the maximum Cr^{grid} was assigned an initial value much less than one (see appropriate sections on numerical procedures for details), and monitored during the course of the simulations.

B.5 Validation of Simulator

To assure an accurate numerical solution to a given problem, the computer program itself must be validated. One source of validation for steady-state simulations is through a global material balance (see, for example, Chapter 4). For transient problems the simulation can be run until the system achieves steady-state (see Chapter 5 for an example of this approach). This final solution can then be compared to the solution obtained using the steady-state simulator.

As further validation, the governing equations and boundary conditions can be simplified, by a judicious choice of system parameters, to a point where an analytical solution is possible. The computer predictions are then compared to the analytical solution. Clearly, this latter validation procedure must consider all of the features of a given model equation. For example, simplifying the steady-state plasma protein transport equation to a simple diffusion equation does not validate that part of the simulator responsible for the convection term. However, in some cases it is not possible to retain all of the salient features of the differential equation and still obtain an analytical solution. In such instances the validation procedure must be conducted in stages, considering the various terms within the equation one at a time. In fact, this procedure was used to test the ability of the simulator to accurately determine a solution to the fluid and plasma protein mass balance equations under steady-state and transient conditions. In the following pages we will demonstrate the process by way of some examples.

B.5.1   Validation of the Fluid Mass Balance Equation and Starling Boundary Conditions in a One-Dimensional Mesentery

Recall from Appendix A that the dimensionless fluid mass balance equation for the one-dimensional model of the mesentery is

$$\frac{d^2(\tilde{P}^1 - \tilde{\Pi}^1)}{d\tilde{x}^2} - \frac{2}{\tilde{H}}\tilde{L}_p^{mes}\left[\tilde{P}^1 - \tilde{P}^{mes} - \sigma^{mes}\left(\tilde{\Pi}^1 - \tilde{\Pi}^{mes}\right)\right] = 0, \qquad (B.26)$$

where the local interstitial colloid osmotic pressure, $\tilde{\Pi}^1$, is related to the local interstitial plasma protein concentration, $\tilde{C}^1$, by a third-order polynomial:

$$\tilde{\Pi}^1 = \tilde{A}_1\left(\tilde{C}^1\right) + \tilde{A}_2\left(\tilde{C}^1\right)^2 + \tilde{A}_3\left(\tilde{C}^1\right)^3. \qquad (B.27)$$

The boundary condition at a vascular wall b, meanwhile, is given by Starling's Law so that

$$\left[-\frac{d(\tilde{P}^1 - \tilde{\Pi}^1)}{d\tilde{x}}\right]_b \cdot 1_x = \tilde{L}_p^b\left(\left[\tilde{P}^1\right]_b - \tilde{P}^b - \sigma^b\left(\left[\tilde{\Pi}^1\right]_b - \tilde{\Pi}^b\right)\right). \qquad (B.28)$$

Equation (B.26) can be simplified as follows. Assume first that $\tilde{C}^1$ equals $\tilde{x}$ throughout the interstitial space. Assume further that $\tilde{A}_1$ and $\tilde{A}_2$ are identically equal to zero. It then follows that

$$\tilde{\Pi}^1 = \tilde{A}_3 \cdot \tilde{x}^3. \qquad (B.29)$$

If we also assume that $\tilde{P}^{mes}$ and $\tilde{\Pi}^{mes}$ are zero, then Eq. (B.26) reduces to

$$\frac{d^2\tilde{P}^1}{d\tilde{x}^2} - \frac{2\,\tilde{L}_p^{mes}\,\tilde{P}^1}{\tilde{H}} = 6\,\tilde{A}_3\,\tilde{x} - \frac{2\,\tilde{L}_p^{mes}}{\tilde{H}} \cdot \sigma^{mes} \cdot \tilde{A}_3 \cdot \tilde{x}^3. \qquad (B.30)$$

The boundary condition, meanwhile, becomes

$$-\left[\frac{d\tilde{P}^1}{d\tilde{x}}\right]_b \cdot 1_x = \tilde{L}_p^b\left(\left[\tilde{P}^1\right]_b - \tilde{P}^b - \sigma^b\left[\tilde{A}_3 \cdot ([\tilde{x}]_b)^3 - \tilde{\Pi}^b\right]\right). \qquad (B.31)$$

By virtue of the simplifying assumptions $\tilde{x}$, $\tilde{C}^1$, $\tilde{\Pi}^1$ and $d\tilde{\Pi}^1/d\tilde{x}$ are all zero at the arteriolar capillary wall. Hence, at this boundary we have

$$\left[\frac{d\tilde{P}^1}{d\tilde{x}}\right]_{art} = \tilde{L}_p^{art}\left(\left[\tilde{P}^1\right]_{art} - \tilde{P}^{art} - \sigma^b \cdot \tilde{\Pi}^{art}\right). \qquad (B.32)$$

To simplify the problem we further assume that the interstitial pressure, $\tilde{P}^1$, is a specified constant, K, at the venular end of the system (i.e., at $\tilde{x} = 1$). That is,

$$\left[\tilde{P}^1\right]_{\text{ven}} = K. \tag{B.33}$$

The solution to Eq. (B.31), given boundary conditions (B.32) and (B.33), is

$$\tilde{P}^1 = B_0 \exp\left(\sqrt{\frac{2\,\tilde{L}_p^{\text{mes}}}{\tilde{H}}}\,\tilde{x}\right) + B_1 \exp\left(-\sqrt{\frac{2\,\tilde{L}_p^{\text{mes}}}{\tilde{H}}}\,\tilde{x}\right)$$
$$+ \frac{3\,\tilde{A}_3\,\tilde{H}}{\tilde{L}_p^{\text{mes}}}\cdot[\sigma^{\text{mes}}-1]\cdot\tilde{x} + \sigma^{\text{mes}}\,\tilde{A}_3\,\tilde{x}^3, \tag{B.34}$$

where

$$B_1 = \cfrac{\exp\left(-\sqrt{\frac{2\,\tilde{L}_p^{\text{mes}}}{\tilde{H}}}\right)\cdot\left[K+\frac{3\,\tilde{A}_3\,\tilde{H}}{\tilde{L}_p^{\text{mes}}}\cdot(1-\sigma^{\text{mes}})-\sigma^{\text{mes}}\,\tilde{A}_3\right] - \cfrac{\frac{3\,\tilde{H}\,\tilde{A}_3}{\tilde{L}_p}\cdot[1-\sigma^{\text{mes}}]+\tilde{L}_p^{\text{art}}\left[\sigma^{\text{art}}\,\tilde{\Pi}^{\text{art}}-\tilde{P}^{\text{art}}\right]}{\sqrt{\frac{2\,\tilde{L}_p^{\text{mes}}}{\tilde{H}}}-\tilde{L}_p^{\text{art}}}}{\cfrac{\left(\sqrt{\frac{2\,\tilde{L}_p^{\text{mes}}}{\tilde{H}}}+\tilde{L}_p^{\text{art}}\right)}{\left(\sqrt{\frac{2\,\tilde{L}_p^{\text{mes}}}{\tilde{H}}}-\tilde{L}_p^{\text{art}}\right)}+\exp\left(-2\sqrt{\frac{2\,\tilde{L}_p^{\text{mes}}}{\tilde{H}}}\right)} \tag{B.35}$$

and

$$B_0 = \cfrac{\left(\sqrt{\frac{2\,\tilde{L}_p^{\text{mes}}}{\tilde{H}}}+\tilde{L}_p^{\text{art}}\right)}{\left(\sqrt{\frac{2\,\tilde{L}_p^{\text{mes}}}{\tilde{H}}}-\tilde{L}_p^{\text{art}}\right)}\cdot B_1 + \cfrac{\frac{3\,\tilde{H}\,\tilde{A}_3}{\tilde{L}_p}\cdot[1-\sigma^{\text{mes}}]+\tilde{L}_p^{\text{art}}\left[\sigma^{\text{art}}\,\tilde{\Pi}^{\text{art}}-\tilde{P}^{\text{art}}\right]}{\sqrt{\frac{2\,\tilde{L}_p^{\text{mes}}}{\tilde{H}}}-\tilde{L}_p^{\text{art}}}. \tag{B.36}$$

The analytical equation given above was used validate the numerical solution to the fluid mass balance equation assuming a Starling boundary condition at the arteriolar wall. Let the relative error, ϵ^{rel}, between the simulation estimate of $\tilde{P}^1$ at some point $\tilde{x}_i$, $\tilde{P}^1_{\text{simul},i}$, and the analytical solution at that point, $\tilde{P}^1_{\text{anal},i}$, be defined as

$$\epsilon^{\text{rel}} = \frac{\left|\tilde{P}^1_{\text{simul},i} - \tilde{P}^1_{\text{anal},i}\right|}{\tilde{P}^1_{\text{anal,max}}}, \tag{B.37}$$

where $\tilde{P}^1_{\text{anal,max}}$ is the maximum value of $\tilde{P}^1$ within the domain. Then the maximum relative error associated with the numerical solution of the problem described above was less than 0.001%

with 50 finite elements. Similar approaches were used to validate the numerical solutions to the Starling boundary condition at the venular capillary wall, the steady-state solute mass balance equation, and the nonlinear flux boundary conditions for solute exchange at the arteriolar and venular boundaries. In each case the numerical and analytical solutions were in excellent agreement.

B.5.2 Validation of the Transient Solute Mass Balance Equation in a One-Dimensional Mesentery

Having validated the spatial components of the program, we are left with testing the simulator's ability to accurately predict temporal variations in the distribution of interstitial plasma proteins. Again, this is acheived by simplifying the governing equation to a point where an analytical solution to the problem is attainable.

In this case, it is assumed that $\bar{j}_w^0$ is constant and that $\bar{j}_w^{mes}$ and $\bar{j}_s^{mes}$ are both zero. It then follows that $d\bar{j}_w^0/d\tilde{x}$ is zero and that, according to Eq (A.17), $d\tilde{D}_d/d\tilde{x}$ is also zero. Equation (B.1) then becomes

$$- n^1 \frac{\partial \tilde{C}^1}{\partial \tilde{t}} = - n^1 \, \tilde{D}_d \frac{\partial^2 \tilde{C}^1}{\partial \tilde{x}^2} + \xi \, \beta \, \bar{j}_w^0 \frac{\partial \tilde{C}^1}{\partial \tilde{x}}, \qquad (B.38)$$

where $\tilde{D}_d$, a constant, is given by

$$\tilde{D}_d = \frac{\xi \, \beta \, \bar{j}_w^0 \, \tilde{\alpha}_1}{n^1} + 1. \qquad (B.39)$$

We will assume further that the interstitial solute concentration at the arteriolar wall is equal to some constant, K_0, for all time. Likewise, the solute concentration at the venular wall remains constant and, in this case, zero for all time. With the added assumption that the interstitial space initially contains no solute, the solution to Eq. (B.38) is [8]

$$\tilde{C}^1 = \frac{K_0}{2} \cdot \left[\text{erfc} \left(\frac{\tilde{x} - \frac{\xi \beta \bar{j}_w^0}{n^1} \cdot \tilde{t}}{2 \sqrt{\tilde{D}_d \, \tilde{t}}} \right) + \exp \left(\frac{\xi \, \beta \, \bar{j}_w^0 \tilde{x}}{n^1 \, \tilde{D}_d} \right) \cdot \text{erfc} \left(\frac{\tilde{x} + \frac{\xi \beta \bar{j}_w^0}{n^1} \cdot \tilde{t}}{2 \sqrt{\tilde{D}_d \, \tilde{t}}} \right) \right]. \qquad (B.40)$$

Equation (B.38) was also solved numerically by the combined finite element – finite difference technique outlined earlier, using a grid of 25 elements, an initial Courant number of 0.1, and

a Crank-Nicolson time stepping procedure (corresponding to a θ equal to 0.5). After 160 time steps the relative error associated with the numerical solution was less than 0.0025%.

Appendix C

A Preliminary Study of Interstitial Plasma Protein Dispersion

C.1 Introduction

In the analyses presented in Chapters 4, 5, and 6, the interstitial transport of plasma proteins was limited to restricted convection and molecular diffusion. However, as was discussed in Chapter 3, the convective transport of a solute through a porous medium can give rise to mechanical dispersion which, through a convective process at the microscopic level, appears similar to molecular diffusion at the macroscale. The extent to which mechanical dispersion affects the overall transport of a solute within the interstitium will depend on several factors, including the structure of the interstitial matrix and the magnitude of the convective velocity of the solute relative to its diffusive velocity. To date there is nothing reported in the literature that investigates the possible ramifications of mechanical dispersion on the interstitial transport and exchange of macromolecules or other solute species. Hence, in the following sections we will take a cursory look at the possible effects of this phenomenon on the steady-state interstitial transport and microvascular exchange of an aggregate plasma protein species within a one-dimensional model tissue representative of mesentery.

C.2 Defining the System

Recall from Chapter 3 that the coefficient of mechanical dispersion for some interstitial solute species k, ϑ_{ij}^k, is related to the three principle components of the local convective velocity of the solute by

$$\vartheta_{ij}^k = \alpha_t^k \left| \bar{v}_c^k \right| \delta_{ij} + \left(\alpha_l^k - \alpha_t^k \right) \frac{\bar{v}_{c_i}^k \cdot \bar{v}_{c_j}^k}{\left| \bar{v}_c^k \right|}. \tag{C.1}$$

As Eq. (C.1) indicates, ϑ_{ij}^k is a second-order tensor. The longitudinal and transverse dispersivities, α_l and α_t, meanwhile, are functions of the interstitial matrix structure and have units of length.

The dispersivities are typically fitted parameters [1]. In geologic formations, which can extend for many hundreds or thousands of meters, α_l may vary from 3 m to 200 m [1]. α_t, meanwhile, is generally 1/10 to 1/100 the magnitude of α_l. Unfortunately, it is not yet possible to accurately estimate the magnitude of the dispersivities from measured properties of a porous structure. Hence, there are no correlations to predict the value of the dispersivities in tissues. One can only infer from the data for geological formations that the dispersivities will be somewhat less than the overall dimensions of the system.

Confining ourselves to the steady-state version of the one-dimensional model of the mesentery first developed in Appendix A and considering an aggregate plasma protein species only, then the coefficient of mechanical dispersion reduces to a scalar quantity given by

$$\vartheta = \alpha_l \left| \bar{v}_c \right|, \tag{C.2}$$

where

$$\bar{v}_c = \frac{\xi \, \beta \, j_w^0}{n^1}. \tag{C.3}$$

The total dispersive flux of interstitial plasma proteins is given by Fick's Law, with the coefficient of total dispersion given by the sum $\vartheta + D_{eff}$. The relative importance of the mechanical dispersive component compared to molecular diffusion will depend on the magnitude of the local convective velocity, $\bar{v}_c$, and the structure of the interstitial matrix, characterized by α_l in the one-dimensional system considered here. It follows from Eqs. (C.2) and (C.3) that the mechanical dispersive flux is zero when one or more of α_l, ξ, and j_w^0 are zero.

The dimensionless form of the longitudinal dispersivity, $\tilde{\alpha}_l$, is α_l/L for the case of the one-dimensional model. The dimensionless coefficient of mechanical dispersion, $\tilde{\vartheta}$, is then defined as $\tilde{\alpha}_l \, \xi \, \beta \, \tilde{j}_w^0/n^1$. These expressions are combined with the appropriate forms of fluid and plasma protein mass balance equations and auxiliary equations (see Appendix A) to describe

the dispersive and convective fluxes of interstitial plasma proteins within the one-dimensional tissue model under steady-state conditions.

C.3 Case Studies

According to Eqs. (C.2) and (C.3), the coefficient of mechanical dispersion is directly proportional to the interstitial plasma protein convective hindrance, ζ, and the longitudinal dispersivity, $\bar{\alpha}_l$. A series of numerical simulations were performed to investigate the coupled effects of ζ and $\bar{\alpha}_l$ on the exchange and interstitial distribution of the aggregate plasma protein species for each of the three mesothelial boundary conditions outlined in Chapter 4. The interstitial plasma protein convective hindrance assumed values of 1.0 and 0.5, while the dimensionless longitudinal dispersivity was assigned values of 0.0, 0.01, 0.1, and 1.0. The ratio of interstitial hydraulic conductivity to interstitial plasma protein diffusivity, α, meanwhile, was assigned its intermediate value of 0.9117. All other system parameters were kept at their baseline values (see Table (4.2) for details). This resulted in a $2 \times 4 \times 3$ factorial study.

As discussed further in this appendix, convective dispersion had very little effect on the system behavior when α equalled 0.9117. Since increasing α results in a concomitant increase in the fluid exchange within the system, and hence enhanced convective transport of interstitial plasma proteins at any given nonzero value of ζ, the same factorial set of numerical simulations outlined above was repeated at an elevated value of α (i.e., 9.117). In total, then, 48 simulations were carried out in the study.

C.4 Numerical Procedure

Based on the previous simulations of Appendix A, the one-dimensional tissue space was divided into a set of 25 elements and 51 nodal points. The steady-state values of $\tilde{C}^1$ and $\tilde{P}^1$ were then determined using the iterative procedure outlined in Chapter 4 assuming a tolerance of 10^{-6} and limiting the total number of iterations to 999. In all cases it was necessary to use under-relaxation techniques [24] to assure convergence within the specified number of iterations. The

under-relaxation parameter assumed values between 0.1 and 0.2 in all cases.

As a further check of the numerical solution, overall material balances were performed around the boundaries of the system. In all cases, the total inflow of fluid and plasma proteins equalled to total outflow, to within 0.002 %.

C.5 Results and Discussion

Figure C.1 shows the effect of ξ, α_1 and the mesothelial boundary conditions assuming α is equal to 0.9117. It is clear from this figure that, for these conditions, mechanical dispersion has no significant effect on the interstitial plasma protein concentration profiles. The most significant variation is found when ξ equals one and the mesothelium is assumed to be impermeable. In this case, the enhanced dispersion associated with increased values of $\tilde{\alpha}_1$ tended to reduce the gradient in the interstitial plasma protein distribution. However, in all cases varying $\tilde{\alpha}_1$ from 0 to 1 had only a marginal effect on the interstitial transport and microvascular exchange of fluid and plasma proteins within the model tissue.

Given these results, a similar set of numerical simulations was performed assuming that α equalled 9.117. The findings from these simulations are illustrated in Figure (C.2). To be expected, the increase in dispersive transport of interstitial plasma proteins associated with increasing values of $\tilde{\alpha}_1$ yields reduced gradients in the plasma protein concentration distribution within the interstitium. This reduction in the protein concentration gradient is particularly well illustrated in the case where ξ is 1 and the mesothelial transport properties are defined by boundary condition 2. The sharp increase in the interstitial plasma protein concentration found in the vicinity of the arteriolar vessel is nearly obliterated as $\tilde{\alpha}_1$ increases from 0 to 1. As a result, the irregular fluid flux distribution across the mesothelial layer associated with no mechanical dispersion and discussed in detail in Chapter 4 is eliminated as the longitudinal dispersivity achieves a value of 1.

Table (C.1) summarizes the effect of varying $\tilde{\alpha}_1$ on the rate of fluid exchange across each of

BOUNDARY CONDITION 1   BOUNDARY CONDITION 2   BOUNDARY CONDITION 3
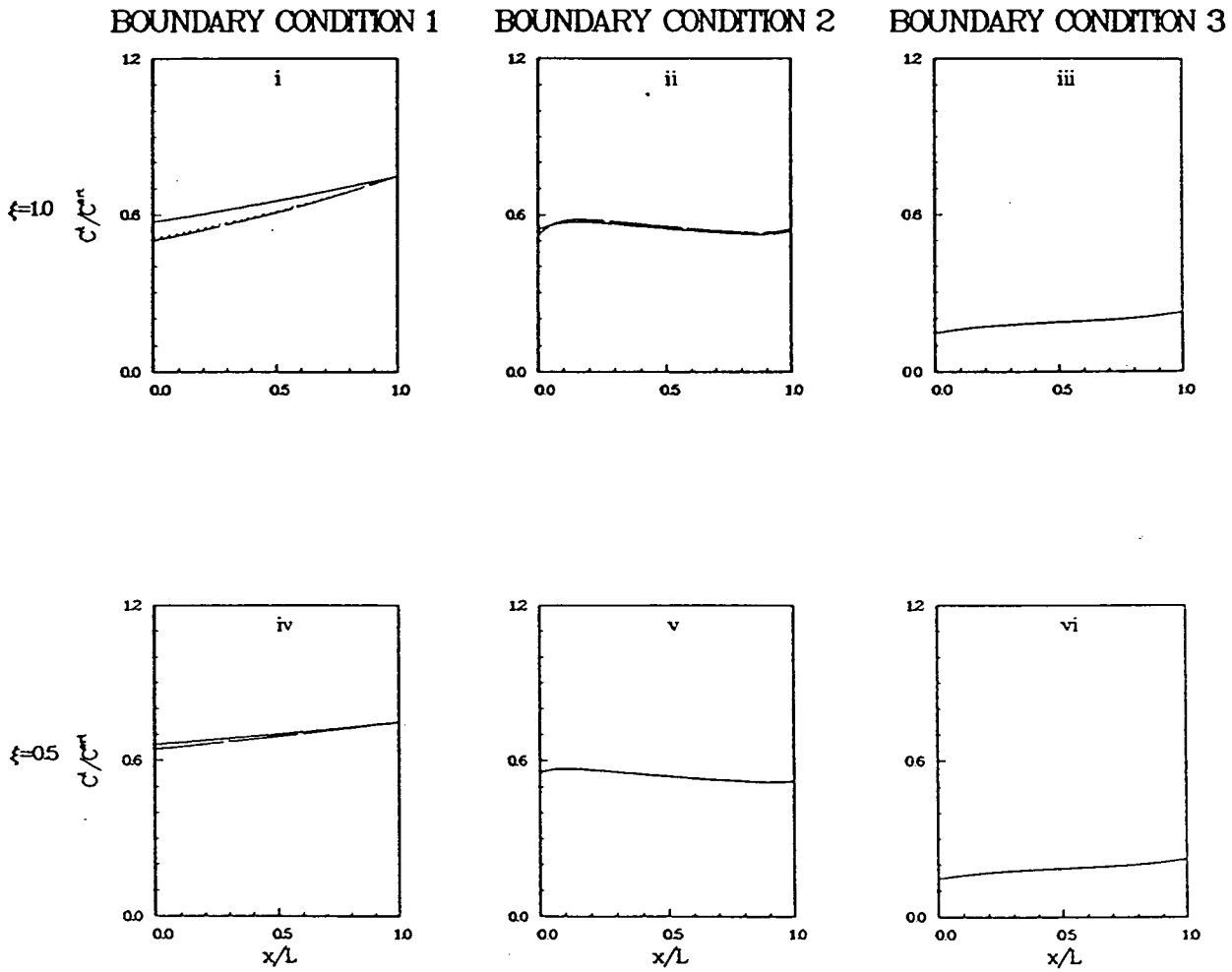
Figure C.1: The dimensionless interstitial plasma protein distribution is shown for the various cases where α equals 0.9117. The solid line represents the distribution assuming $\tilde{\alpha}_l$ equal to 1.0, the dotted line corresponds to $\tilde{\alpha}_l$ equal 0.1, the chain-dotted line represents the distribution assuming $\tilde{\alpha}_l$ equal to 0.01, and the dashed line corresponds to an $\tilde{\alpha}_l$ of 0.0.

BOUNDARY CONDITION 1   BOUNDARY CONDITION 2   BOUNDARY CONDITION 3

$\xi=1.0$ c'/c'' i   ii   iii

$\xi=0.5$ c'/c'' iv   v   vi

x/L   x/L   x/L

Figure C.2: The dimensionless interstitial plasma protein distribution is shown for the various cases where α equals 9.117. The solid line represents the distribution assuming $\tilde{\alpha}_1$ equal to 1.0, the dotted line corresponds to $\tilde{\alpha}_1$ equal 0.1, the chain-dotted line represents the distribution assuming $\tilde{\alpha}_1$ equal to 0.01, and the dashed line corresponds to an $\tilde{\alpha}_1$ of 0.0.

the permeable boundaries. With α equal to 9.117, the rate of fluid exchange across the arteriolar boundary, for example, typically increased slightly with decreased dispersion. However, the increase in the rate of fluid exchange across this boundary as $\bar{\alpha}_1$ varied from 1 to 0 was less than 10 % for all values of ζ and all mesothelial boundary conditions considered in this study. Moreover, for those cases in which the mesothelium was most permeable (i.e., boundary condition 3), the fluid exchange rate across the arteriolar capillary varied by less than 1.2 %. These results emphasize further that, for the conditions assumed in this study, the net rate of fluid exchange within the system is determined primarily by the chemical potential of the luminal fluids and the transport properties of the permeable boundaries, and not by the interstitial plasma protein transport mechanisms.

ζ	α_1	Boundary Condition 1			Boundary Condition 2			Boundary Condition 3		
		Art	Ven	Mes	Art	Ven	Mes	Art	Ven	Mes
1.0	1.00	-4.15	4.15	—	-23.75	6.55	0.86	-33.45	2.78	1.53
1.0	0.10	-4.47	4.47	—	-25.38	6.90	0.92	-33.12	2.13	1.55
1.0	0.01	-4.49	4.49	—	-25.86	7.01	0.94	-33.07	2.22	1.54
1.0	0.00	-4.49	4.49	—	-25.83	7.03	0.94	-33.06	2.25	1.54
0.5	1.00	-3.99	3.99	—	-23.60	6.43	0.86	-33.47	2.95	1.52
0.5	0.10	-4.26	4.26	—	-24.65	6.61	0.90	-33.27	2.51	1.54
0.5	0.01	-4.29	4.29	—	-25.48	6.68	0.94	-33.19	2.47	1.54
0.5	0.00	-4.34	4.34	—	-25.64	6.69	0.95	-33.17	2.47	1.54

Table C.1: **The average dimensionless fluid fluxes across each of the permeable boundaries as a function of ζ, the mesothelial boundary conditions and $\bar{\alpha}_1$, assuming α equals 9.117. A negative value indicates a flux entering the interstitial space, while a positive value denotes a flux leaving the interstitium.**

Since the rate of plasma protein exchange across the permeable boundaries is largely convective, the average plasma protein fluxes across the boundaries for the various cases follow the same behavior as the fluid fluxes. The results are summarized in Table (C.2). Again, the change in plasma protein exchange rate across the arteriolar capillary is never more than 10 % as $\bar{\alpha}_1$ is varied from 0 to 1 and, in most cases, is much less.

ξ	α_1	Boundary Condition 1			Boundary Condition 2			Boundary Condition 3		
		Art	Ven	Mes	Art	Ven	Mes	Art	Ven	Mes
1.0	1.00	-0.62	0.62	—	-3.56	0.58	0.15	-5.01	0.15	0.24
1.0	0.10	-0.67	0.67	—	-3.81	0.46	0.17	-4.97	0.11	0.24
1.0	0.01	-0.67	0.67	—	-3.88	0.40	0.17	-4.96	0.12	0.24
1.0	0.00	-0.67	0.67	—	-3.87	0.39	0.17	-4.96	0.12	0.24
0.5	1.00	-0.60	0.60	—	-3.54	0.55	0.15	-5.02	0.15	0.24
0.5	0.10	-0.64	0.64	—	-3.70	0.52	0.16	-4.99	0.13	0.24
0.5	0.01	-0.64	0.64	—	-3.82	0.52	0.17	-4.98	0.13	0.24
0.5	0.00	-0.64	0.64	—	-3.85	0.52	0.17	-4.98	0.13	0.24

Table C.2: **The average dimensionless plasma protein flux across each of the permeable boundaries as a function of ξ, the mesothelial boundary conditions and $\tilde{\alpha}_1$, assuming α equals 9.117. A negative value indicates a flux entering the interstitial space, while a positive value denotes a flux leaving the interstitium.**

While varying $\tilde{\alpha}_1$ from 0 to 1 had little effect on the net rates of fluid and plasma protein exchange across the permeable boundaries, it did alter substantially the relative roles of plasma protein convection and dispersion within the regions of the interstitium adjacent the boundaries. The results are reported in Table (C.3). The most dramatic effect is seen when it is assumed that the mesothelium is impermeable (i.e., boundary condition 1). In this case, the ratio of interstitial plasma protein convection to dispersion adjacent the arteriolar boundary decreases in magnitude by a factor of 44 (i.e, from -65.44 to -1.48).

C.6 Concluding Remarks

In summary, when the interstitial hydraulic conductivity and interstitial plasma protein diffusivity assume their baseline values (corresponding to an α of 0.9117), mechanical dispersion has only a marginal effect on the exchange of fluid and plasma proteins within the model tissue. As the interstitial hydraulic conductivity is increased relative to the interstitial plasma protein diffusivity, however, mechanical dispersion does have a noticeable, albeit small, effect on the

ξ	α_1	Boundary Condition 1			Boundary Condition 2			Boundary Condition 3		
		Art	Ven	Mes	Art	Ven	Mes	Art	Ven	Mes
1.0	1.00	-1.48	-1.21	—	-1.26	-1.21	-1.25	-16.73	-1.21	5.35
1.0	0.10	-8.92	-1.21	—	-1.42	-1.21	-1.24	-10.67	-1.21	5.91
1.0	0.01	-48.18	-1.21	—	-2.17	-1.21	-1.23	-10.56	-1.21	5.78
1.0	0.00	-65.44	-1.21	—	-2.60	-1.21	-1.23	-10.68	-1.21	5.71
0.5	1.00	-2.08	-1.53	—	-1.67	-1.53	-1.65	0.91	-1.53	0.71
0.5	0.10	-5.48	-1.53	—	-1.84	-1.53	-1.63	0.91	-1.53	0.74
0.5	0.01	-8.62	-1.53	—	-2.12	-1.53	-1.63	0.94	-1.53	0.74
0.5	0.00	-9.21	-1.53	—	-2.21	-1.53	-1.63	0.95	-1.53	0.74

Table C.3: **The ratio of the average dimensionless convective plasma protein flux to the average dimensionless dispersive flux normal to each of the permeable boundaries as a function of ξ, the mesothelial boundary conditions and $\tilde{\alpha}_1$, assuming α equals 9.117. A negative value indicates that convection and dispersion are in opposite directions.**

rates of fluid and plasma protein exchange within the system. Further, the relative rates of interstitial plasma protein convection and dispersion are altered substantially, thereby modifying the distribution of plasma proteins within the interstitium.

The results of the study, though limited in scope, suggest that, for the conditions presented here, mechanical dispersion likely has only a marginal effect on the rates of fluid and plasma protein exchange within the model tissue. However, much more research is needed before any general conclusions can be drawn regarding the nature and importance of mechanical dispersion in tissues.

Appendix D

Program Listings

D.1 Parameter List for Steady-State and Transient Simulators

```
*************************************************************************
*                                                                       *
*      A LIST OF THE PROGRAM VARIABLES FOR THE SIMULATORS MES8NOD.FOR,   *
*      MESDISP.FOR, MES2P.FOR, TRANS.FOR, AND TRANS2P.FOR                *
*                                                                       *
*************************************************************************


                 *******************************
                 *GRID AND TOLERANCE PARAMETERS *
                 *******************************


          COUR: INITIAL COURANT NUMBER
          DELT: INITIAL TIME STEP SIZE
            DX: X-INCREMENTS BETWEEN NODES
            DY: Y-INCREMENTS BETWEEN NODES
        DISPMX: MAXIMUM LOCAL DISPERSION COEFFICIENT
           EPS: TOLERANCE FOR ITERATIVE IMPROVEMENT FOR MATRIX SOLVER DGBAND
                (DGBND1)
         IDISP: ELEMENT LOCATION OF MAXIMUM DISPERSION COEFFICIENT
  IMAX (ITMAX): MAXIMUM NUMBER OF ITERATIONS FOR CONVERGENCE OF POLD, COLD
          IMAX: MAXIMUM NUMBER OF TIME STEPS
          IPEC: ELEMENT LOCATION OF THE MAXIMUM GRID PECLET NUMBER
             M: NUMBER OF NODES IN THE Y DIRECTION (M=1 FOR 1-D MODEL)
             N: NUMBER OF NODES IN THE X DIRECTION
         NP,NT: TOTAL NUMBER OF NODES
         NECHO: IF 0, DO NOT ECHO INPUT DATA
           NEX: NUMBER OF ELEMENTS IN THE X DIRECTION
           NEY: NUMBER OF ELEMENTS IN THE Y DIRECTION
          NEXY: TOTAL NUMBER OF ELEMENTS IN GRID (NEX*NEY)
         NODEL: MATRIX CONTAINING NODE REFERENCES FOR A GIVEN FINITE ELEMENT
        OMEGAF: RELAXATION PARAMETER FOR PRESSURE DISTRIBUTION
        OMEGAC: RELAXATION PARAMETER FOR PROTEIN DISTRIBUTION
        PECMAX: MAXIMUM GRID PECLET NUMBER
         TFACT: TIME STEP ACCELERATION FACTOR
         THETA: SEMI-IMPLICIT FACTOR (THETA=0.5 - CRANK-NICOLSON FINITE DIFF)
          TOLC: CONVERGENCE TOLERANCE FOR THE PROTEIN DISTRIBUTION
          TOLP: CONVERGENCE TOLERANCE FOR THE PRESSURE DISTRIBUTION
          XNOD: VECTOR OF X COORDINATES OF NODAL POINTS
          YNOD: VECTOR OF Y COORDINATES OF NODAL POINTS


                 **************************
                 *    MATRIX VARIABLES    *
                 **************************


        BCTIME: THETA*SOLUTB + (1-THETA)*SBOLDT - (1-THETA)*SCOLDT
         CFLUX: MATRIX OF LOCAL CONVECTIVE INTERSTITIAL PROTEIN FLUXES
          COLD: VECTOR CONTAINING PREVIOUS ESTIMATE OF PROTEIN DISTRIBUTION
         COLDT: PROTEIN DISTRIBUTION FROM PREVIOUS TIME STEP
         DFLUX: MATRIX OF LOCAL DIFFUSIVE INTERSTITIAL PLASMA PROTEIN FLUXES
          ELOC: COORDINATE LOCATION OF INTERSTITIAL FLUXES (FFLUX,CFLUX,DFLUX)
```

```
*                TRANS2P.FOR), PARAMETERS AFFILIATED WITH INDIVIDUAL SOLUTES   *
*                ARE DISTINGIUSHED BY NUMBERS 1 AND 2 (E.G., SIGM1 AND SIGM2). *
******************************************************************************
```

D.2 Two Dimensional Simulator: MES8NOD.FOR

```
C      THIS PROGRAM MODELS THE STEADY TRANSPORT OF FLUID AND PROTEIN
C      THROUGH THE INTERSTITIAL SPACE OF THE MESENTERY.  IT ASSUMES
C      THAT THE TISSUE BEHAVES AS A RIGID POROUS MEDIUM.   IT IS
C      FURTHER ASSUMED THAT THE FLUID PRESSURE IN THE EXCLUDED
C      SPACE IS IN EQUILIBRIUM WITH THAT IN THE AVAILABLE SPACE.
C
C
       IMPLICIT REAL*8(A-H,O-Z)
       DIMENSION HOLD(2000),IPERM(2000),RES(2000),HOLDS(2000),
      #RESS(2000),IPERMS(2000),GAUS(4),W(4)
       COMMON/BLK1/NODEL(600,8),XNOD(2000),YNOD(2000)
       COMMON/BLK2/DX(41),DY(41)
       COMMON/MATBAL/QFC(40),QCC(40),QSC(40),QFV(40),QCV(40),QSV(40),
      #QFM(40),QCM(40),QSM(40)
       COMMON/FLUMAT/FLUID(210000)
       COMMON/OLD/POLD(2000),COLD(2000)
       COMMON/SOLB/SOLUTB(2000)
       COMMON/FLUB/FLUIDB(2000)
       COMMON/SOLMAT/SOLUTE(210000)
       COMMON/OSMOT/AOSM,BOSM,COSM
       COMMON/TISDAT/AK,DEFF,ALPHL,ALPHT,PHIA,PHIT,RET,SIGT
       COMMON/CAPDAT/PC,CC
       COMMON/WALL/DLC,DLV,DLM,DDC,DDV,DDM,PDC,PDV,PDM,PIDC,PIDV,PIDM,
      #SIGC,SIGV,SIGM,CDC,CDV,CDM
       COMMON/FLUXES/FFLUX(600,2),CFLUX(600,2),DFLUX(600,2),
      #ELOC(600,2)
       DATA T1,T2,T3,T4,T5,T6,T7,T8,T9/9*0.D0/
       DATA W/.347854845137454D0,.652145154862546D0,
      #.652145154862546D0,.347854845137454D0/
       DATA GAUS/-.861136311594053D0,-.339981043584856D0,
      #.339981043584856D0,.861136311594053D0/
C
C      SET MARKER AND TOLERANCE VALUES
C
       READ(5,504)OMEGAF,OMEGAC,TOLP,TOLC,PECMAX,EPS
       READ(5,550)IMAX,ITER,NECHO,N,M
  550  FORMAT(5I3)
       NEX=(N-1)/2
       NNUM=NEX+1
       NEY=(M-1)/2
       MNUM=NEY+1
       NEXY=NEX*NEY
       NT=NEX*(3*NEY+2)+2*NEY+1
       LUB=3*NEY+4
       ICOUNT=0
C
C      READ IN THE DATA FROM EXTERNAL FILE
C
       DO 1 I=1,NNUM
       READ(5,501) DX(I)
  501  FORMAT(E12.6)
    1  CONTINUE
C
       YLL=0.D0
       DO 2 J=1,MNUM
       READ(5,501) DY(J)
       YLL=YLL+DY(J)
    2  CONTINUE
C
```

```
      READ(5,502)  AOSM,BOSM,COSM,AK,PC,PHIA,PHIT,RET,PHIS
      READ(5,504)  ALPHL,ALPHT,AL,DEFF,SIGT,CC
      READ(5,504)  CONC,CONV,CONM,PERMC,PERMV,PERMM
      READ(5,504)  DDC,DDV,DDM,SIGC,SIGV,SIGM
      READ(5,504)  CDC,CDV,CDM,DLC,DLV,DLM
      READ(5,506)  PDC,PDV,PDM
      READ(5,506)  AOS1,BOS1,COS1
      YL=YLL*AL
      PIDC=CDC*(AOS1+CDC*(BOS1+CDC*COS1))
      PIDV=CDV*(AOS1+CDV*(BOS1+CDV*COS1))
      PIDM=CDM*(AOS1+CDM*(BOS1+CDM*COS1))
      PV=PDV*PC
      PM=PDM*PC
      CV=CDV*CC
      CM=CDM*CC
C
C
C
  502 FORMAT(9E10.4)
  503 FORMAT(5E10.4)
  504 FORMAT(6E10.4)
  506 FORMAT(3E10.4)
C
      DO 21 I=1,NT
      READ(5,505) POLD(I),COLD(I)
  505 FORMAT(2E10.4)
   21 CONTINUE
C     ECHO DATA IF NECHO N.E. 0
C
      IF(NECHO.EQ.0) GO TO 999
C
C     PRINT OUT INPUT DATA
C
      WRITE(6,611)
  611 FORMAT(1X,'STEADY-STATE  FLUID PRESSURE AND SOLUTE CONCENTRATION'
     #)
      WRITE(6,667)
  667 FORMAT(1X,'PROFILES  FOR TWO DIMENSIONAL  TISSUE SYSTEM',//)
      WRITE(6,612)
      WRITE(6,612)
  612 FORMAT(//,1X,'_____'
     #,//)
      WRITE(6,660)
  660 FORMAT(1X,'INPUT  PARAMETERS')
      WRITE(6,612)
      WRITE(6,613)
  613 FORMAT(1X,'1.  GRID DATA:',//)
      WRITE(6,614)NEX,DX(2)
  614 FORMAT(1X,'NUMBER  OF ELEMENTS  IN  X-DIRECTION:',1X,I2,/,1X,
     #'SMALLEST  X INCREMENTS:',19X,E10.4,/)
      WRITE(6,615)NEY,DY(2)
  615 FORMAT(1X,'NUMBER  OF ELEMENTS  IN  Y-DIRECTION:',1X,I2,/,1X,
     #'SMALLEST  Y INCREMENTS:',19X,E10.4,/)
      WRITE(6,616)NT,NEXY
  616 FORMAT(1X,'TOTAL  NUMBER  OF NODES:',10X,I4,/,1X,
     #'TOTAL  NUMBER OF ELEMENTS:',6X,I4)
      WRITE (6,612)
      WRITE(6,617) TOLP,TOLC,IMAX,OMEGAF,OMEGAC,PECMAX
  617 FORMAT(1X,'2. CONVERGENCE  CRITERIA:',//,1X,'PRESSURE   TOLERANCE:'
     #,17X,E10.4,/,1X,'SOLUTE   TOLERANCE:',20X,E10.4,/,1X,
     #'MAXIMUM NUMBER OF LOOP ITERATIONS:',2X,I3,/,1X,
     #'PRESSURE  RELAXATION PARAMETER:',6X,E10.4,/,1X,
     #'SOLUTE  RELAXATION PARAMETER:',9X,E10.4,/,1X,
     #'MAXIMUM  DESIRED  GRID PECLET  NUMBER:',1X,E10.4)
      WRITE(6,612)
      PIC=PIDC*PC
```

```
      PIV=PIDV*PC
      PIM=PIDM*PC
C
      WRITE(6,618) AL,YL,CC,CV,CM,PC,PV,PM,PIC,PIV,PIM,AK,DEFF,SIGT
  618 FORMAT(1X,'3. DIMENSIONAL INPUT PARAMETERS:',//,1X,
     #'TISSUE X-DIMENSION (CM):',21X,E10.4,/,1X,
     #'TISSUE Y-DIMENSION (CM):',21X,E10.4,/,1X,
     #'CAP. PROTEIN CONC. (GRAMS/DL):',14X,E10.4,/,1X,
     #'VEN. PROTEIN CONC. (GRAMS/DL):',14X,E10.4,/,1X,
     #'MES. PROTEIN CONC. (GRAMS/DL):',14X,E10.4,/,1X,
     #'CAP. DYN. PRESSURE (DYN/CM**2):',14X,E10.4,/,1X,
     #'VEN. DYN. PRESSURE (DYN/CM**2):',14X,E10.4,/,1X,
     #'MES. DYN. PRESSURE (DYN/CM**2):',14X,E10.4,/,1X,
     #'CAP. OSM. PRESSURE (DYN/CM**2):',14X,E10.4,/,1X,
     #'VEN. OSM. PRESSURE (DYN/CM**2):',14X,E10.4,/,1X,
     #'MES. OSM. PRESSURE (DYN/CM**2):',14X,E10.4,/,1X,
     #'TISSUE FLUID CONDUCTIVITY (CM**4/(DYN-SEC):',2X,E10.4,/,1X,
     #'TISSUE SOLUTE DIFFUSIVITY (CM**2/SEC):',7X,E10.4,/,1X,
     #'TISSUE REFLECTION COEFFICIENT:',15X,E10.4)
      WRITE(6,653) RET
  653 FORMAT(1X,'RETARDATION FACTOR:',26X,E10.4)
      WRITE(6,626) CONC,CONV,CONM,PERMC,PERMV,PERMM
  626 FORMAT(1X,'CAP. CONDUCTIVITY (CM**3/(DYN-S));',11X,E10.4,/,1X,
     #'VEN. CONDUCTIVITY (CM**3/(DYN-S)):',11X,E10.4,/,1X,
     #'MES. CONDUCTIVITY (CM**3/(DYN-S)):',11X,E10.4,/,1X,
     #'CAP. PERMEABILITY (CM/S):',21X,E10.4,/,1X,
     #'VEN. PERMEABILITY (CM/S):',21X,E10.4,/,1X,
     #'MES. PERMEABILITY (CM/S):',21X,E10.4)
      WRITE(6,612)
      WRITE(6,619)PDC,PIDC,PDV,PIDV,PDM,PIDM
  619 FORMAT(1X,'4. DIMENSIONLESS INPUT PARAMETERS:',//,1X,
     #'PRESSURE:',6X,'DYNAMIC',5X,'OSMOTIC',//,1X,'CAPILLARY:',5X,
     #E10.4,
     #2X,E10.4,/,1X,'VENULE:',8X,E10.4,2X,E10.4,/,1X,'MESOTHELIUM:',
     #3X,E10.4,2X,E10.4,//)
      WRITE(6,620)CDC,CDV,CDM
  620 FORMAT(1X,'CONCENTRATIONS:',//,1X,'CAPILLARY:',5X,E10.4,/,1X,
     #'VENULE:',9X,E10.4,/,1X,'MESOTHELIUM:',1X,E10.4,//)
      WRITE(6,621)SIGC,SIGV,SIGM
  621 FORMAT(1X,'REFLECTION COEFFICIENTS:',//,1X,'CAPILLARY:',5X,
     #E10.4,/,1X,'VENULE:',9X,E10.4,/,1X,'MESOTHELIUM:',1X,E10.4,//)
      WRITE(6,622)DLC,DLV,DLM
  622 FORMAT(1X,'VESSEL FLUID CONDUCTANCES:',//,1X,'CAPILLARY:',5X,
     #E10.4,/,1X,'VENULE:',9X,E10.4,/,1X,'MESOTHELIUM:',1X,E10.4,//)
      WRITE(6,625)AOSM,BOSM,COSM
  625 FORMAT(1X,'VIRIAL COEFFICIENTS:',//,1X,'AOSM:',1X,E10.4,/,1X,
     #'BOSM:',1X,E10.4,/,1X,'COSM:',1X,E10.4,//)
      WRITE(6,623)DDC,DDV,DDM
  623 FORMAT(1X,'VESSEL SOLUTE PERMEABILITIES:',//,1X,'CAPILLARY:',5X,
     #E10.4,/,1X,'VENULE:',9X,E10.4,/,1X,'MESOTHELIUM:',1X,E10.4,//)
      WRITE(6,624)PHIT,PHIA,PHIS
  624 FORMAT(1X,'TOTAL TISSUE FLUID VOLUME FRACTION:',2X,E10.4,/,1X,
     #'SOLUTE DISTRIBUTION VOLUME FRACTION:',1X,E10.4,/,1X,
     #'TOTAL SOLIDS VOLUME FRACTION:',8X,E10.4,///)
C
C
C
  999 CALL GRID(NEX,NEY)
C
C     INITIALIZE FLUID VECTOR
C
      CALL SETMAT(NEX,NEY,0,PEC,IEL)
C
C     ADJUST FLUID VECTOR TO FIT BOUNDARY CONDITIONS
```

```
C
      CALL ASTAR(NEX,NEY,0)
      CALL VSTAR(NEX,NEY,0)
C     CALL MESTAR(NEX,NEY,0)
C
C     ENTER ITERATION LOOP, CHECK COUNTER VALUE
C
C
  100 ICOUNT=ICOUNT+1
      IF(ICOUNT.GT.IMAX)GO TO 200
C
C
C     INITIALIZE FLUIDB VECTOR AND ADJUST TO FIT BOUNDARY CONDITIONS
C
      CALL SETMAT(NEX,NEY,1,PEC,IEL)
C
      CALL ASTAR(NEX,NEY,1)
      CALL VSTAR(NEX,NEY,1)
C     CALL MESTAR(NEX,NEY,1)
C
C     SOLVE THE FLUID SYSTEM
C
      EP=EPS
      CALL DGBAND(FLUID,FLUIDB,NT,LUB,LUB,ICOUNT,IPERM,DET,JEXP,HOLD,
     #RES,ITER,EP)
C
C     DETERMINE THE MAXIMUM CHANGE IN P FROM ONE ITERATION TO THE NEXT
C     AND UPDATE POLD USING A RELAXATION PROCEDURE. PDIFMX WILL BE
C     COMPARED TO TOLP TO ESTABLISH CONVERGENCE
C
      PMAX=0.DO
      PDIFMX=0.DO
      DO 3 I=1,NT
      IF(DABS(FLUIDB(I)).GT.PMAX)  PMAX=DABS(FLUIDB(I))
      TEST=DABS(FLUIDB(I)-POLD(I))
      IF(TEST.GT.PDIFMX)  PDIFMX=TEST
      POLD(I)=(OMEGAF)*(FLUIDB(I)-POLD(I))+POLD(I)
    3 CONTINUE
      PDIFMX=PDIFMX/PMAX
C
C     NOW INITIALIZE SOLUTE AND SOLUTB. STORE MAX. GRID PECLET
C     NUMBER IN PECLET. ADJUST SOLUTE AND SOLUTB TO SUIT BOUNDARY
C     CONDITIONS
C
      CALL SETMAT(NEX,NEY,2,PEC,IEL)
      PECLET=PEC
      IELE=IEL
      CALL SETMAT(NEX,NEY,3,PEC,IEL)
      CALL PATART(NEX,NEY)
      CALL PATVEN(NEX,NEY)
C     CALL PATMES(NEX,NEY)
C
C
C     SOLVE THE SYSTEM OF EQUATIONS FOR THE SOLUTE FLOW EQUATION
C
      EP1=EPS
      CALL DGBND1(SOLUTE,SOLUTB,NT,LUB,LUB,1,IPERMS,DET,JEXP,HOLDS,
     #RESS,ITER,EP1)
C
C     DETERMINE THE MAXIMUM CHANGE IN CALCULATED CONCENTRATION FROM
C     ONE ITERATION TO THE NEXT, AND UPDATE COLD USING A RELAXATION
C     PROCEDURE. CDIFMX WILL BE COMPARED TO TOLC TO ESTABLISH
C     CONVERGENCE
C
C
      CMAX=0.DO
      CDIFMX=0.DO
      DO 4 I=1,NT
      IF(DABS(SOLUTB(I)).GT.CMAX)  CMAX=DABS(SOLUTB(I))
      TEST=DABS(SOLUTB(I)-COLD(I))
```

```
      IF(TEST.GT.CDIFMX) CDIFMX=TEST
      COLD(I)=(OMEGAC)*(SOLUTB(I)-COLD(I))+COLD(I)
 4    CONTINUE
      CDIFMX=CDIFMX/CMAX
C
C     CHECK TO SEE IF FURTHER ITERATION IS REQUIRED
C
      IF(PDIFMX.GT.TOLP) GO TO 100
      IF(CDIFMX.GT.TOLC) GO TO 100
C
      GO TO 300


C
C     MAXIMUM NUMBER OF ITERATIONS REACHED. PRINT OUT WARNING.
C
 200  ICOUNT=ICOUNT-1
      WRITE(6,600) ICOUNT
 600  FORMAT(//,1X,'WARNING.  CONVERGENCE CRITERIA NOT MET AFTER',
     #1X,I3,1X,'ITERATIONS')
      WRITE(6,601) PDIFMX,CDIFMX
 601  FORMAT(//,1X,'MAXIMUM  FRACTIONAL  CHANGE  IN  P',2X,
     #'MAXIMUM  FRACTIONAL  CHANGE  IN  C',//,11X,E9.4,22X,E9.4,//)
C
 300  IF(PECLET.LT.PECMAX) GO TO 400
      WRITE(6,603) PECLET,IELE
 603  FORMAT(//,'WARNING.  GRID PECLET NUMBER EQUALS',1X,E9.4,3X,
     #'ELEMENT LOCATION:',1X,I4)
C
 400  WRITE(6,604) ICOUNT
 604  FORMAT('1',//,'STEADY-STATE  SOLUTION ACHIEVED AFTER',1X,I3,1X,
     #'ITERATIONS:')
      WRITE(6,670) PECLET,IELE
 670  FORMAT(//,1X,'MAXIMUM  GRID PECLET NUMBER:',1X,E9.4,3X,
     #'ELEMENT LOCATION:',1X,I4)
      WRITE(6,601)PDIFMX,CDIFMX
      WRITE(6,605)
 605  FORMAT(//,1X,'X  POSITION',2X,'DYN.  PRESS',2X,'OSM.  PRESS',2X,
     #'TOT.  PRESS',2X,'AVAIL.  CONC.',2X,'TOTAL  CONC.',//)
C
      WRITE(7,701)NEX,NEY
 701  FORMAT(1X,I2,1X,I2)
C
C     CALCULATE THE Y-AVERAGED PROTEIN CONCENTRATION, CAV, PRESSURE,
C     PAV, AND PROTEIN OSMOTIC PRESSURE,PIAV
C
      X=0.D0
      DO 5 I=1,NEX
C
C     IDENTIFY X-COORDINATE FOR AVERAGED QUANTITIES
C
      X=X+DX(I)
      PAV=0.D0
      PIAV=0.D0
      CAV=0.D0
C
C     ENTER LOOP FOR INTEGRATION, IDENTIFYING APPROPRIATE BASIS FUNCS
C
        DO 6 IT=1,4
        T=GAUS(IT)
        B1=(T-1.D0)*T*.5D0
        B7=(T+1.D0)*T*.5D0
        B8=1.D0-T*T
C
C       NOW INTEGRATE IN THE Y-DIRECTION, ELEMENT BY ELEMENT
C
          DO 7 J=1,NEY
C
C         IDENTIFY THE ELEMENT NUMBER, EL
C
```

```
            NEL=(I-1)*NEY+J
C
C           CALCULATE  C(S,T)
C
            CST=B1*COLD(NODEL(NEL,1))+B7*COLD(NODEL(NEL,7))+
     #          B8*COLD(NODEL(NEL,8))
            PAV=PAV+(B1*POLD(NODEL(NEL,1))+B7*POLD(NODEL(NEL,7))+
     #          B8*POLD(NODEL(NEL,8)))*W(IT)*DY(J+1)*.5D0
            CAV=CAV+CST*W(IT)*DY(J+1)*.5D0
            PIAV=PIAV+CST*(AOSM+CST*(BOSM+CST*COSM))*W(IT)*DY(J+1)*.5D0
    7       CONTINUE
    6     CONTINUE
          CAV=CAV/YLL
          C1=CAV*PHIA/(1.D0-PHIS)
          PAV=PAV/YLL
          PIAV=PIAV/YLL
          PTOT=PAV-PIAV
          WRITE(6,606)  X,PAV,PIAV,PTOT,CAV,C1
  606     FORMAT(1X,E9.3,2X,E10.4,2X,E10.4,2X,E10.4,2X,E10.4,3X,E10.4)
          WRITE(7,606)  X,C1,PAV,PIAV,PTOT,CAV
    5   CONTINUE
C
C       AND FINALLY WE CONSIDER THE VENULAR BOUNDARY
C
        X=X+DX(NEX+1)
        CAV=0.D0
        PAV=0.D0
        PIAV=0.D0
        DO 8 IT=1,4
        T=GAUS(IT)
        B3=(T-1.D0)*T*.5D0
        B4=1.D0-T*T
        B5=(T+1.D0)*T*.5D0
          DO 9 J=1,NEY
          NEL=(NEX-1)*NEY+J
          CST=B3*COLD(NODEL(NEL,3))+B4*COLD(NODEL(NEL,4))+
     #        B5*COLD(NODEL(NEL,5))
          PAV=PAV+(B3*POLD(NODEL(NEL,3))+B4*POLD(NODEL(NEL,4))+
     #        B5*POLD(NODEL(NEL,5)))*W(IT)*DY(J+1)*.5D0
          PIAV=PIAV+(CST*(AOSM+CST*(BOSM+CST*COSM)))*W(IT)*DY(J+1)*.5D0
          CAV=CAV+CST*W(IT)*DY(J+1)*.5D0
    9     CONTINUE
    8   CONTINUE

C
        PAV=PAV/YLL
        PIAV=PIAV/YLL
        CAV=CAV/YLL
        C1=CAV*PHIA/(1.D0-PHIS)
        PTOT=PAV-PIAV
        WRITE(6,606)  X,PAV,PIAV,PTOT,CAV,C1
        WRITE(7,606)  X,C1,PAV,PIAV,PTOT,CAV
C
C
        WRITE(6,607)
  607   FORMAT('1',//,1X,'MASS  BALANCE DATA'////)
        CALL MASFC(NEX,NEY)
        CALL MASFV(NEX,NEY)
C       CALL MASFM(NEX,NEY)
        CALL MASSC(NEX,NEY)
        CALL MASSV(NEX,NEY)
C       CALL MASSM(NEX,NEY)
        DO 10 I=1,NEY
        T1=T1+QFC(I)
        T2=T2+QSC(I)
        T3=T3+QFV(I)
        T4=T4+QSV(I)
        T7=T7+QCC(I)
```

```
        T8=T8+QCV(I)
   10   CONTINUE
C       WRITE(6,612)
C       DO 11 I=1,NEX
C       T5=T5+QFM(I)
C       T6=T6+QSM(I)
C       T9=T9+QCM(I)
C 11    CONTINUE
        WRITE(6,608)
  608   FORMAT(///,1X,'NET DIMENSIONLESS FLUID FLOWS')
        TF=T1+T3+T5
        WRITE(6,609) T5,T1,T3,TF
  609   FORMAT(//,1X,'MES:',1X,E12.4,/,1X,'CAP:',
       #E12.4,/,1X,'VEN:',1X,E12.4,/,1X,'TOT:',1X,E12.4)
        WRITE(6,661)
  661   FORMAT(///,1X,'NET DIMENSIONLESS SOLUTE FLOWS')
        TS=T2+T4+T6
        WRITE(6,609)T6,T2,T4,TS
        WRITE(6,662)
  662   FORMAT(//,1X,'CONVECTIVE  COMPONENTS OF DIMENSIONLESS SOLUTE
       #FLOWS')
        TC=T8+T9+T7
        WRITE(6,610) T9,T7,T8,TC
  610   FORMAT(//,1X,'MES:',1X,E12.4,/,1X,'CAP:',1X,E12.4,/,1X,'VEN:',
       #1X,E12.4,/,1X,'TOT:',1X,E12.4)
C
C       WRITE OUT THE MESOTHELIAL FLUID FLUXES TO DEVICE 7
C
        QFMAX=0.D0
        QSMAX=0.D0
        QSMIN=0.D0
        QFMIN=0.D0
        QCSMIN=0.D0
        QCSMAX=0.D0
        X=DX(1)
C       DO 12 I=1,NEX
C       IP=I+1
C       X=X+DX(IP)*.5D0
C       QF=QFM(I)/DX(IP)
C       IF(QF.GT.QFMAX)  QFMAX=QF
C       IF(QF.LT.QFMIN)  QFMIN=QF
C       QS=QSM(I)/DX(IP)
C       IF(QS.GT.QSMAX)  QSMAX=QS
C       IF(QS.LT.QSMIN)  QSMIN=QS
C       QC=QCM(I)/DX(IP)
C       IF(QC.LT.QCSMIN)  QCSMIN=QC
C       IF(QC.GT.QCSMAX)  QCSMAX=QC
C       WRITE(7,702)  X,QF,QS,QC
C702    FORMAT(1X,E10.4,1X,E10.4,1X,E10.4,1X,E10.4)
C       X=X+DX(IP)*.5D0
C12       CONTINUE
C
C       WRITE FLUX DATA FOR 2-D PLOTS
C
C       CALL FLUX(NEX,NEY)
C       NEL=NEX*NEY
C       DO 15 I=1,NEL
C       WRITE(7,705) ELOC(I,1),ELOC(I,2),FFLUX(I,1),FFLUX(I,2),
C      #CFLUX(I,1),CFLUX(I,2),DFLUX(I,1),DFLUX(I,2)
CC
C 705   FORMAT(8(1X,E10.4))
C 15    CONTINUE
C
C       NOW WRITE THE CONTOUR INFORMATION TO DEVICE 7
C
        CMIN=0.D0
        CMAX=0.D0
        DO 13 I=1,NT
```

```
        PI=COLD(I)*(AOSM+COLD(I)*(BOSM+COLD(I)*COSM))
        C=COLD(I)*PHIA/(1.D0-PHIS)
        WRITE(7,703)XNOD(I),YNOD(I),C,POLD(I),PI
  703   FORMAT(1X,E10.4,1X,E10.4,3(1X,E12.6))
        IF(C.GT.CMAX) CMAX=C
        IF(C.LT.CMIN) CMIN=C
  13    CONTINUE
C
        WRITE(7,704) CMIN,CMAX,QFMIN,QFMAX,QSMIN,QSMAX,QCSMIN,QCSMAX
  704   FORMAT(1X,E7.2,1X,E7.2,1X,E7.2,1X,E7.2,1X,E7.2,1X,E7.2,1X,E7.2,
       #1X,E7.2)
        STOP
        END


        SUBROUTINE GRID(NEX,NEY)
C
C       THIS SUBROUTINE ESTABLISHES A RECTANGULAR GRID CONSISTING OF
C       EIGHT-NODE ISOPARAMETRIC ELEMENTS.
C
        IMPLICIT REAL*8(A-H,O-Z)
        COMMON/BLK1/NODEL(600,8),XNOD(2000),YNOD(2000)
        COMMON/BLK2/DX(41),DY(41)
C
C       THE TOTAL NUMBER OF NODES IS GIVEN BY NEX*(3*NEY+2)+2*NEY+1,
C       WHERE NEX IS THE TOTAL NUMBER OF ELEMENTS IN THE X DIRECTION,
C       AND NEY IS THE TOTAL IN THE Y DIRECTION.
C
        X=0.D0
C
        DO 1 I=1,NEX
        X=X+DX(I)
        IP=I+1
        DXH=DX(IP)*.5D0
        Y=0.D0
C
        DO 2 J=1,NEY
        Y=Y+DY(J)
        JP=J+1
        DYH=DY(JP)*.5D0
        IT=(I-1)*NEY+J
        NODEL(IT,1)=(3*NEY+2)*(I-1)+2*J-1
        NODEL(IT,2)=NODEL(IT,1)+2*NEY+2-J
        NODEL(IT,3)=NODEL(IT,2)+NEY+J
        NODEL(IT,4)=NODEL(IT,3)+1
        NODEL(IT,5)=NODEL(IT,4)+1
        NODEL(IT,6)=NODEL(IT,2)+1
        NODEL(IT,7)=NODEL(IT,1)+2
        NODEL(IT,8)=NODEL(IT,1)+1
C
        XNOD(NODEL(IT,1))=X
        YNOD(NODEL(IT,1))=Y
        XNOD(NODEL(IT,2))=X+DXH
        YNOD(NODEL(IT,2))=Y
        XNOD(NODEL(IT,3))=X+DX(IP)
        YNOD(NODEL(IT,3))=Y
        XNOD(NODEL(IT,4))=X+DX(IP)
        YNOD(NODEL(IT,4))=Y+DYH
        XNOD(NODEL(IT,5))=X+DX(IP)
        YNOD(NODEL(IT,5))=Y+DY(JP)
        XNOD(NODEL(IT,6))=X+DXH
        YNOD(NODEL(IT,6))=Y+DY(JP)
        XNOD(NODEL(IT,7))=X
        YNOD(NODEL(IT,7))=Y+DY(JP)
        XNOD(NODEL(IT,8))=X
        YNOD(NODEL(IT,8))=Y+DYH
C
  2        CONTINUE
```

```
  1       CONTINUE
          RETURN
          END
C
C

          SUBROUTINE SETMAT(NEX,NEY,IND,PE,IPEC)
C
C         THIS SUBROUTINE INITIALIZES THE STIFFNESS MATRICES FOR THE
C         FLUID FLOW AND PROTEIN TRANSPORT EQUATIONS, CONVERTING THE
C         BANDED MATRICES TO VECTOR EQUIVALENTS WHICH STORE ONLY THE
C         BANDS OF THE MATRICES. AN ELEMENT LOCATION (I,J) IS PLACED
C         IN THE VECTOR LOCATION (K) WHERE K=(3*LUB)*J+I-LUB,  AND
C         LUB IS THE HALF BANDWIDTH OF THE MATRIX (EXCLUDING THE
C         DIAGONAL). LUB IS RELATED TO NEY BY LUB=3*NEY+4.
C
          IMPLICIT REAL*8(A-H,O-Z)
          COMMON/BLK1/NODEL(600,8),XNOD(2000),YNOD(2000)
          COMMON/BLK2/DX(41),DY(41)
          COMMON/FLUMAT/AF(210000)
          COMMON/SOLMAT/AS(210000)
          COMMON/TISDAT/AK,DEFF,AL,AT,PHIA,PHIT,RET,SIGT
          COMMON/OSMOT/AO,BO,CO
          COMMON/CAPDAT/PC,CC
          COMMON/OLD/POLD(2000),COLD(2000)
          COMMON/FLUB/BF(2000)
          COMMON/SOLB/BS(2000)
C
          DIMENSION GAUS(4),W(4),B(8),DBS(8),DBT(8),DBX(8),DBY(8),
         #AJAC(2,2),AJACIN(2,2)
C
          DATA NGAUS/4/
          DATA W/.347854845137454D0,.652145154862546D0,
         #.652145154862546D0,.347854845137454D0/
          DATA GAUS/-.861136311594053D0,-.339981043584856D0,
         #.339981043584856D0,.861136311594053D0/
C         DATA NGAUS/3/
C         DATA W/0.5555555555556D0,0.8888888888889D0,0.5555555555556D0/
C         DATA GAUS/-0.774596669241483D0,0.D0,0.774596669241483D0/
C
C         DATA NGAUS/2/
C         DATA W/1.0D0,1.0D0,0.D0/
C         DATA GAUS/-0.577350269189626D0,0.577350269189626D0,0.D0/
C
C         ZERO APPROPRIATE ARRAY
C
C
          IF(IND.EQ.3)GO TO 999
C
          IF(IND.NE.2)GO TO 900
          DO 90 I=1,210000
          AS(I)=0.D0
 90       CONTINUE
C
          PE=0.D0
C
          GO TO 101
C
 900      IF(IND.NE.0) GO TO 901
          DO 91 I=1,210000
          AF(I)=0.D0
 91       CONTINUE
C
          GO TO 101
C
 901      DO 92 I=1,2000
          BF(I)=0.D0
 92       CONTINUE
C
C
```

```
C
C        CARRY OUT THE INTEGRATION ELEMENT BY ELEMENT. INTEGRATION IS
C        ACCORDING TO A THREE POINT GAUSS QUADRATURE.
C
  101    LUB=3*NEY+4
         LP=3*LUB
         NEL=NEX*NEY
C
C        ENTER LOOP WHICH EVALUATES INTEGRAND AT APPROPRIATE (S,T)
C        POINTS FOR GAUSS QUADRATURE.
C
         DO 1 II=1,NGAUS
         S=GAUS(II)
C
         DO 2 JJ=1,NGAUS
         T=GAUS(JJ)
C
C        DEFINE THE BASIS FUNCTIONS AND THEIR S AND T DERIVATIVES,
C        EVALUATED AT THE QUADRATURE POINTS
C
         B(1)=(S-1.D0)*(1.D0-T)*(1.D0+S+T)*.25D0
         B(2)=(1.D0-S*S)*(1.D0-T)*.5D0
         B(3)=(1.D0+S)*(T-1.D0)*(1.D0-S+T)*.25D0
         B(4)=(1.D0-T*T)*(1.D0+S)*.5D0
         B(5)=(1.D0+S)*(1.D0+T)*(T+S-1.D0)*.25D0
         B(6)=(1.D0-S*S)*(1.D0+T)*.5D0
         B(7)=(S-1.D0)*(1.D0+T)*(1.D0+S-T)*.25D0
         B(8)=(1.D0-T*T)*(1.D0-S)*.5D0
         DBS(1)=(1.D0-T)*(T+2.D0*S)*.25D0
         DBT(1)=(1.D0-S)*(S+2.D0*T)*.25D0
         DBS(2)=S*(T-1.D0)
         DBT(2)=(S*S-1.D0)*.5D0
         DBS(3)=(1.D0-T)*(2.D0*S-T)*.25D0
         DBT(3)=(1.D0+S)*(2.D0*T-S)*.25D0
         DBS(4)=(1.D0-T*T)*.5D0
         DBT(4)=-T*(1.D0+S)
         DBS(5)=(1.D0+T)*(2.D0*S+T)*.25
         DBT(5)=(1.D0+S)*(2.D0*T+S)*.25
         DBS(6)=-S*(1.D0+T)
         DBT(6)=(1.D0-S*S)*.5D0
         DBS(7)=(1.D0+T)*(2.D0*S-T)*.25D0
         DBT(7)=(1.D0-S)*(2.D0*T-S)*.25D0
         DBS(8)=(T*T-1.D0)*.5D0
         DBT(8)=T*(S-1.D0)
C
C        NOW CONSIDER EACH ELEMENT ONE BY ONE
C
         DO 110 ITX=1,NEX
         DO 100 ITY=1,NEY
         IT=(ITX-1)*NEY+ITY
C
C        WE NOW CALCULATE THE JACOBIAN MATRIX, AJAC, ITS DETERMINANT,
C        DETJ, AND ITS INVERSE AJACIN.
C
C
         AJAC(1,1)=0.D0
         AJAC(2,1)=0.D0
         AJAC(1,2)=0.D0
         AJAC(2,2)=0.D0
C
         DO 3 JAK=1,8
         AJAC(1,1)=AJAC(1,1)+DBS(JAK)*XNOD(NODEL(IT,JAK))
         AJAC(1,2)=AJAC(1,2)+DBS(JAK)*YNOD(NODEL(IT,JAK))
         AJAC(2,1)=AJAC(2,1)+DBT(JAK)*XNOD(NODEL(IT,JAK))
         AJAC(2,2)=AJAC(2,2)+DBT(JAK)*YNOD(NODEL(IT,JAK))
  3      CONTINUE
C
         DETJ=AJAC(1,1)*AJAC(2,2)-AJAC(1,2)*AJAC(2,1)
C
```

```
C      CHECK TO SEE IF THE DETERMINANT IS ZERO
C
       IF(DETJ.GT.1.D-16) GO TO 777
       WRITE(6,601) IT
  601  FORMAT(1X,'DETERMINANT=0  AT ELEMENT',1X,I4)
       STOP
C
  777  AJACIN(1,1)=AJAC(2,2)/DETJ
       AJACIN(1,2)=-AJAC(1,2)/DETJ
       AJACIN(2,1)=-AJAC(2,1)/DETJ
       AJACIN(2,2)=AJAC(1,1)/DETJ
C
C      WE CAN NOW CALCULATE D(B(I))/DX AND D(B(I))/DY, EVALUATED AT
C      (X(S,T),Y(S,T)), USING JACIN
C
       DO 4 I=1,8
       DBX(I)=DBS(I)*AJACIN(1,1)+DBT(I)*AJACIN(1,2)
       DBY(I)=DBS(I)*AJACIN(2,1)+DBT(I)*AJACIN(2,2)
  4    CONTINUE
C
C      DETERMINE WHICH MATRIX IS TO BE EVALUATED
C
       IF(IND.EQ.0)GO TO 902
C
C      WE NOW HAVE SUFFICIENT INFORMATION TO DETERMINE QX,QY, AND C,
C      ALL EVALUATED AT (S,T). THIS INFORMATION WILL BE USED TO
C      CALCULATE AF.
C
       CST=0.D0
       DPX=0.D0
       DPY=0.D0
       DCX=0.D0
       DCY=0.D0
C
       DO 5 J=1,8
       DPX=POLD(NODEL(IT,J))*DBX(J)+DPX
       DPY=POLD(NODEL(IT,J))*DBY(J)+DPY
       DCX=COLD(NODEL(IT,J))*DBX(J)+DCX
       DCY=COLD(NODEL(IT,J))*DBY(J)+DCY
       CST=COLD(NODEL(IT,J))*B(J)+CST
  5    CONTINUE
C
       DPIX=DCX*(A0+CST*(2.D0*B0+3.D0*C0*CST))*SIGT
       DPIY=DCY*(A0+CST*(2.D0*B0+3.D0*C0*CST))*SIGT
C
C      IF IND EQUALS 1, THEN EVALUATE BF VECTOR
C
       IF(IND.NE.2)GO TO 903
C
       QXST=-AK*PC*PHIA/(DEFF*PHIT)*RET*(DPX-DPIX)
       QYST=-AK*PC*PHIA/(DEFF*PHIT)*RET*(DPY-DPIY)
C
C
C
C      NOW CALCULATE THE DISPERSION COEFFICIENTS DXX,DXY,DYY, WHERE
C      DXX=(AL*QX**2/QMAG+AT*QY**2/QMAG)+PHIA,  ETC
C
       QMAG=DSQRT(QXST*QXST+QYST*QYST)
C
C      CHECK TO SEE IF QMAG IS NONZERO
C
       IF(QMAG.GT.1.D-10)GO TO 500
       DXX=PHIA
       DXY=0.D0
       DYY=PHIA
       GO TO 600
C
  500  DXX=(AL*QXST*QXST+AT*QYST*QYST)/QMAG+PHIA
       DXY=(AL-AT)*QXST*QYST/QMAG
```

```
       DYY=(AL*QYST*QYST+AT*QXST*QXST)/QMAG+PHIA
C
C
 600   DO 6 M=1,8
       MM=NODEL(IT,M)
C
       DO 7 N=1,8
       NN=NODEL(IT,N)
C
C      CONVERT INDEX(M,N) TO K BY FORMULA K=LP*N+M-LUB
C      AND THEN DETERMINE AS(K)
C
       K=LP*NN+MM-LUB
C
       AS(K)=AS(K)+(DBX(M)*(DXX*DBX(N)+DXY*DBY(N))+
      #DBY(M)*(DXY*DBX(N)+DYY*DBY(N))+
      #(QXST*DBX(N)+QYST*DBY(N))*B(M))*W(II)*W(JJ)*DETJ
C
 7     CONTINUE
 6     CONTINUE
C
C      NOW CALCULATE THE LOCAL GRID PECLET NUMBER EVALUATED AT (S,T),
C      AND COMPARE TO PE
C
       QMAX=DMAX1(QXST,QYST)
       DIFMIN=DMIN1(DXX,DYY)
       DLMAX=DMAX1(DX(ITX+1),DY(ITY+1))
       PEST=DLMAX*QMAX/DIFMIN
       IF(PEST.LT.PE)GO TO 100
       PE=PEST
       IPEC=IT
C
       GO TO 100
C
C      CALCULATE AF
C
C
 902   DO 8 M=1,8
       MM=NODEL(IT,M)
C
       DO 9 N=1,8
       NN=NODEL(IT,N)
C
       K=LP*NN+MM-LUB
C
       AF(K)= AF(K)+(DBX(M)*DBX(N)+DBY(M)*DBY(N))*W(II)*W(JJ)*DETJ
C
 9     CONTINUE
 8     CONTINUE
C
       GO TO 100
C
C      CALCULATE BF
C
 903   DO 10 M=1,8
       MM=NODEL(IT,M)
C
       BF(MM)=BF(MM)+(DBX(M)*DPIX+DBY(M)*DPIY)*W(JJ)*W(II)*DETJ
C
 10    CONTINUE
C
 100   CONTINUE
C
 110   CONTINUE
C
 2     CONTINUE
 1     CONTINUE
C
 999   DO 93 I=1,2000
       BS(I)=0.D0
```

```
  93   CONTINUE
C
       RETURN
       END
C


C
       SUBROUTINE ASTAR(NEX,NEY,IND)
C
C      THIS SUBROUTINE ADJUSTS THE AF AND BF VECTORS TO SUIT THE
C      BOUNDARY CONDITION Jv=Lpc*(P-Pc-sigc*(Pi-Pic))  AT THE CAPILLARY
C      WALL. IF IND=0 THEN THE AF VECTOR IS ADJUSTED.
C
       IMPLICIT REAL*8(A-H,O-Z)
       DIMENSION B(3),INDEX(3),GAUS(3),W(3)
       COMMON/BLK1/NODEL(600,8),XNOD(2000),YNOD(2000)
       COMMON/BLK2/DX(41),DY(41)
       COMMON/FLUMAT/AF(210000)
       COMMON/FLUB/BF(2000)
       COMMON/OLD/POLD(2000),COLD(2000)
       COMMON/OSMOT/A0,B0,C0
       COMMON/WALL/DLC,DLV,DLM,DDC,DDV,DDM,PDC,PDV,PDM,PIDC,PIDV,PIDM,
      #SIGC,SIGV,SIGM,CDC,CDV,CDM
C
       DATA W/0.5555555555556D0,0.8888888888889D0,0.5555555555556D0/
       DATA NGAUS,GAUS/3,-.774596669241483D0,0.D0,.774596669241483D0/
C
C      DEFINE PARAMETERS FOR INDEXING AF VECTOR
C
       LUB=3*NEY+4
       LP=3*LUB
C
C      CONSIDER THE CAPILLARY WALL, ELEMENT BY ELEMENT.
C
       DO 1 IT=1,NEY
       IP=IT+1
C
C      ENTER LOOP FOR GAUSS QUADRATURE INTEGRATION. IDENTIFY T VARIABLE
C
       DO 2 M=1,NGAUS
C
       T=GAUS(M)
C
C      DEFINE BASIS FUNCTIONS B(1)=B1,  B(2)=B7,  B(3)=B8, EVALUATED
C      AT (-1,T)
C
       B(1)=(T-1.D0)*T*.5D0
       B(2)=(T+1.D0)*T*.5D0
       B(3)=1.D0-T*T
C
C      SEE IF AF VECTOR IS TO BE ADJUSTED
C
       IF(IND.EQ.0)GO TO 100
C
C      ADJUST THE BF VECTOR
C
       C=COLD(NODEL(IT,1))*B(1)+COLD(NODEL(IT,7))*B(2)+
      #COLD(NODEL(IT,8))*B(3)
C
       PI=C*(A0+C*(B0+C*C0))
C
       BF(NODEL(IT,1))=BF(NODEL(IT,1))+B(1)*DLC*W(M)*DY(IP)*.5D0*(PDC
      #                +SIGC*(PI-PIDC))
C
       BF(NODEL(IT,7))=BF(NODEL(IT,7))+B(2)*DLC*W(M)*DY(IP)*.5D0*(PDC
      #                +SIGC*(PI-PIDC))
C
       BF(NODEL(IT,8))=BF(NODEL(IT,8))+B(3)*DLC*W(M)*DY(IP)*.5D0*(PDC
      #                +SIGC*(PI-PIDC))
C
```

```
        GO TO 2
C
C       ADJUST THE AF VECTOR
C
  100   INDEX(1)=NODEL(IT,1)
        INDEX(2)=NODEL(IT,7)
        INDEX(3)=NODEL(IT,8)
C
        DO 3 I=1,3
        DO 4 J=1,3
        K=LP*INDEX(J)+INDEX(I)-LUB
        AF(K)=AF(K)+B(I)*B(J)*W(M)*DY(IP)*.5D0*DLC
    4   CONTINUE
    3   CONTINUE
C
    2   CONTINUE
    1   CONTINUE
C
        RETURN
        END
C


C
        SUBROUTINE VSTAR(NEX,NEY,IND)
C
C       THIS SUBROUTINE ADJUSTS THE AF AND BF VECTORS TO SUIT THE
C       BOUNDARY CONDITION Jv=Lpc*(P-Pv-sigv*(Pi-Piv))  AT THE VENULAR
C       WALL. IF IND=0 THEN THE AF VECTOR IS ADJUSTED.
C
        IMPLICIT REAL*8(A-H,O-Z)
        DIMENSION B(3),INDEX(3),GAUS(3),W(3)
        COMMON/BLK1/NODEL(600,8),XNOD(2000),YNOD(2000)
        COMMON/BLK2/DX(41),DY(41)
        COMMON/FLUMAT/AF(210000)
        COMMON/FLUB/BF(2000)
        COMMON/OLD/POLD(2000),COLD(2000)
        COMMON/OSMOT/A0,B0,C0
        COMMON/WALL/DLC,DLV,DLM,DDC,DDV,DDM,PDC,PDV,PDM,PIDC,PIDV,PIDM,
       #SIGC,SIGV,SIGM,CDC,CDV,CDM
C
        DATA W/0.5555555555556D0,0.8888888888889D0,0.5555555555556D0/
        DATA NGAUS,GAUS/3,-.774596669241483D0,0.D0,.774596669241483D0/
C
C       DEFINE PARAMETERS FOR INDEXING AF VECTOR
C
        LUB=3*NEY+4
        LP=3*LUB
C
C       CONSIDER THE VENULAR WALL, ELEMENT BY ELEMENT.
C
        DO 1 ITT=1,NEY
        IP=ITT+1
        IT=(NEX-1)*NEY+ITT
C
C       ENTER LOOP FOR GAUSS QUADRATURE INTEGRATION. IDENTIFY T VARIABLE
C
        DO 2 M=1,NGAUS
C
        T=GAUS(M)
C
C       DEFINE BASIS FUNCTIONS B(1)=B3, B(2)=B4, B(3)=B5, EVALUATED
C       AT (1,T)
C
        B(1)=(T-1.D0)*T*.5D0
        B(3)=(T+1.D0)*T*.5D0
        B(2)=1.D0-T*T
C
C       SEE IF AF VECTOR IS TO BE ADJUSTED
C
        IF(IND.EQ.0)GO TO 100
```

```
C
C     ADJUST THE BF VECTOR
C
      C=COLD(NODEL(IT,3))*B(1)+COLD(NODEL(IT,4))*B(2)+
     #COLD(NODEL(IT,5))*B(3)
C
      PI=C*(A0+C*(B0+C*C0))
C
      BF(NODEL(IT,3))=BF(NODEL(IT,3))+B(1)*DLV*W(M)*DY(IP)*.5D0*(PDV
     #                   +SIGV*(PI-PIDV))
C
      BF(NODEL(IT,4))=BF(NODEL(IT,4))+B(2)*DLV*W(M)*DY(IP)*.5D0*(PDV
     #                   +SIGV*(PI-PIDV))
C
      BF(NODEL(IT,5))=BF(NODEL(IT,5))+B(3)*DLV*W(M)*DY(IP)*.5D0*(PDV
     #                   +SIGV*(PI-PIDV))
C
      GO TO 2
C
C     ADJUST THE AF VECTOR
C
  100 INDEX(1)=NODEL(IT,3)
      INDEX(2)=NODEL(IT,4)
      INDEX(3)=NODEL(IT,5)
C
      DO 3 I=1,3
      DO 4 J=1,3
      K=LP*INDEX(J)+INDEX(I)-LUB
      AF(K)=AF(K)+B(I)*B(J)*W(M)*DY(IP)*.5D0*DLV
    4 CONTINUE
    3 CONTINUE
C
    2 CONTINUE
    1 CONTINUE
C
      RETURN
      END
C
C
      SUBROUTINE MESTAR(NEX,NEY,IND)
C
C     THIS SUBROUTINE ADJUSTS THE AF AND BF VECTORS TO SUIT THE
C     BOUNDARY CONDITION Jv=Lpc*(P-Pm-sigm*(Pi-Pim))  AT THE MESOTHEL.
C     WALL. IF IND=0 THEN THE AF VECTOR IS ADJUSTED.
C
      IMPLICIT REAL*8(A-H,O-Z)
      DIMENSION B(3),INDEX(3),GAUS(3),W(3)
      COMMON/BLK1/NODEL(600,8),XNOD(2000),YNOD(2000)
      COMMON/BLK2/DX(41),DY(41)
      COMMON/FLUMAT/AF(210000)
      COMMON/FLUB/BF(2000)
      COMMON/OLD/POLD(2000),COLD(2000)
      COMMON/OSMOT/A0,B0,C0
      COMMON/WALL/DLC,DLV,DLM,DDC,DDV,DDM,PDC,PDV,PDM,PIDC,PIDV,PIDM,
     #SIGC,SIGV,SIGM,CDC,CDV,CDM
C
      DATA W/0.5555555555556D0,0.8888888888889D0,0.5555555555556D0/
      DATA NGAUS,GAUS/3,-.774596669241483D0,0.D0,.774596669241483D0/
C
C     DEFINE PARAMETERS FOR INDEXING AF VECTOR
C
      LUB=3*NEY+4
      LP=3*LUB
C
C     CONSIDER THE MESOTHELIAL WALL, ELEMENT BY ELEMENT.
C
      DO 1 ITT=1,NEX
      IP=ITT+1
      IT=ITT*NEY
C
```

```
C      ENTER LOOP FOR GAUSS QUADRATURE INTEGRATION. IDENTIFY S VARIABLE
C
       DO 2 M=1,NGAUS
C
       S=GAUS(M)
C
C      DEFINE BASIS FUNCTIONS B(1)=B5, B(2)=B6, B(3)=B7, EVALUATED
C      AT (S,1)
C
       B(3)=(S-1.D0)*S*.5D0
       B(1)=(S+1.D0)*S*.5D0
       B(2)=1.D0-S*S
C
C      SEE IF AF VECTOR IS TO BE ADJUSTED
C
       IF(IND.EQ.0)GO TO 100
C
C      ADJUST THE BF VECTOR
C
       CST=COLD(NODEL(IT,5))*B(1)+COLD(NODEL(IT,6))*B(2)+
      #COLD(NODEL(IT,7))*B(3)
C
       PIST=AO*CST+BO*CST*CST+CO*CST*CST*CST
C
       BF(NODEL(IT,5))=BF(NODEL(IT,5))+
      #B(1)*DLM*DX(IP)*W(M)*.5D0*(PDM+SIGM*(PIST-PIDM))
C
       BF(NODEL(IT,6))=BF(NODEL(IT,6))+
      #B(2)*DLM*DX(IP)*W(M)*.5D0*(PDM+SIGM*(PIST-PIDM))
C
       BF(NODEL(IT,7))=BF(NODEL(IT,7))+
      #B(3)*DLM*DX(IP)*W(M)*.5D0*(PDM+SIGM*(PIST-PIDM))
C
       GO TO 2
C
C      ADJUST THE AF VECTOR
C
  100  INDEX(1)=NODEL(IT,5)
       INDEX(2)=NODEL(IT,6)
       INDEX(3)=NODEL(IT,7)
C
       DO 3 I=1,3
       DO 4 J=1,3
       K=LP*INDEX(J)+INDEX(I)-LUB
       AF(K)=AF(K)+B(I)*B(J)*W(M)*DX(IP)*.5D0*DLM
   4   CONTINUE
   3   CONTINUE
C
   2   CONTINUE
   1   CONTINUE
C
       RETURN
       END


C
       SUBROUTINE PATART(NEX,NEY)
C
C      THIS SUBROUTINE ADJUSTS THE AF AND BF VECTORS TO SUIT THE
C      NONLINEAR FLUX BOUNDARY CONDITION AT THE CAPILLARY
C      WALL.
C
       IMPLICIT REAL*8(A-H,O-Z)
       DIMENSION B(3),INDEX(3),GAUS(3),W(3)
       COMMON/BLK1/NODEL(600,8),XNOD(2000),YNOD(2000)
       COMMON/BLK2/DX(41),DY(41)
       COMMON/SOLMAT/AS(210000)
       COMMON/SOLB/BS(2000)
       COMMON/OLD/POLD(2000),COLD(2000)
       COMMON/OSMOT/AO,BO,CO
       COMMON/WALL/DLC,DLV,DLM,DDC,DDV,DDM,PDC,PDV,PDM,PIDC,PIDV,PIDM,
```

```
      #SIGC,SIGV,SIGM,CDC,CDV,CDM
      COMMON/TISDAT/AK,DEFF,AL,AT,PHIA,PHIT,RET,SIGT
      COMMON/CAPDAT/PC,CC
C
      DATA W/0.5555555555556D0,0.8888888888889D0,0.5555555555556D0/
      DATA NGAUS,GAUS/3,-.774596669241483D0,0.D0,.774596669241483D0/
C
C     DEFINE PARAMETERS FOR INDEXING AF VECTOR
C
      LUB=3*NEY+4
      LP=3*LUB
C
C     CONSIDER THE CAPILLARY WALL, ELEMENT BY ELEMENT.
C
      DO 1 IT=1,NEY
      IP=IT+1
C
C     ENTER LOOP FOR GAUSS QUADRATURE INTEGRATION.  IDENTIFY T VARIABLE
C
      DO 2 M=1,NGAUS
C
      T=GAUS(M)
C
C     DEFINE BASIS FUNCTIONS B(1)=B1, B(2)=B7, B(3)=B8, EVALUATED
C     AT (-1,T)
C
      B(1)=(T-1.D0)*T*.5D0
      B(2)=(T+1.D0)*T*.5D0
      B(3)=1.D0-T*T
C
      INDEX(1)=NODEL(IT,1)
      INDEX(2)=NODEL(IT,7)
      INDEX(3)=NODEL(IT,8)
C
C     CALCULATE C(S,T), PI(S,T) AND Q(S,T)
C
      CST=0.D0
      QST=0.D0
      DO 3 I=1,3
      CST=CST+COLD(INDEX(I))*B(I)
      QST=QST+POLD(INDEX(I))*B(I)
   3  CONTINUE
      PIST=CST*(A0+CST*(B0+CST*C0))
      QST=(QST-PDC-SIGC*(PIST-PIDC))*(AK*PC*DLC)/DEFF
      F=PHIA/PHIT
      PEC=QST*(1.D0-SIGC)/DDC
C
C     CHECK TO SEE IF CONVECTIVE COMPONENT DOMINATES
C
      IF(PEC.GT.170.D0)GO TO 101
      IF(PEC.LT.-170.D0)GO TO 102
C
C     CHECK TO SEE IF CONVECTIVE COMPONENT IS SIGNIFICANT
C
      TEST=1.D0-DEXP(-PEC)
      IF(DABS(TEST).LT.1.D-10) GO TO 100
C
C     ADJUST THE AS VECTOR AND BS VECTOR
C
      DO 4 I=1,3
         DO 5 J=1,3
         K=LP*INDEX(J)+INDEX(I)-LUB
         AS(K)=AS(K)-
    #    (RET*F-(1.D0-SIGC)/TEST)*QST*B(I)*B(J)*DY(IP)*.5D0*W(M)
   5  CONTINUE
      BS(INDEX(I))=BS(INDEX(I))+
    #B(I)*QST*(1.D0-SIGC)*CDC*DEXP(-PEC)/TEST*DY(IP)*.5D0*W(M)
   4  CONTINUE
      GO TO 2
C
```

```
C     ADJUST AS AND BS FOR CASE WHERE SOLUTE FLUX IS PREDOMINANTLY
C     DIFFUSIVE
C
 100  DO 6 I=1,3
          DO 7 J=1,3
          K=LP*INDEX(J)+INDEX(I)-LUB
          AS(K)=AS(K)+(DDC-F*RET*QST)*B(I)*B(J)*DY(IP)*.5D0*W(M)
 7        CONTINUE
      BS(INDEX(I))=BS(INDEX(I))+B(I)*DDC*CDC*DY(IP)*.5D0*W(M)
 6    CONTINUE
C
      GO TO 2
C
C     ADJUST AS AND BS FOR CASES WHERE CONVECTIVE TRANSPORT DOMINATES
 101  DO 8 I=1,3
          DO 9 J=1,3
          K=LP*INDEX(J)+INDEX(I)-LUB
          AS(K)=AS(K)-(RET*F-(1.D0-SIGC))*QST*B(I)*B(J)*DY(IP)*.5D0*W(M)
 9        CONTINUE
 8    CONTINUE
C
      GO TO 2
C
 102  DO 10 I=1,3
          DO 11 J=1,3
          K=LP*INDEX(J)+INDEX(I)-LUB
          AS(K)=AS(K)-RET*F*QST*B(I)*B(J)*DY(IP)*.5D0*W(M)
 11       CONTINUE
      BS(INDEX(I))=BS(INDEX(I))-
     #(1.D0-SIGC)*QST*CDC*B(I)*DY(IP)*.5D0*W(M)
 10   CONTINUE
C
 2    CONTINUE
 1    CONTINUE
C
      RETURN
      END
C


      SUBROUTINE PATVEN(NEX,NEY)
C
C     THIS SUBROUTINE ADJUSTS THE AF AND BF VECTORS TO SUIT THE
C     NONLINEAR FLUX BOUNDARY CONDITION AT THE VENULAR
C     WALL.
C
      IMPLICIT REAL*8(A-H,O-Z)
      DIMENSION B(3),INDEX(3),GAUS(3),W(3)
      COMMON/BLK1/NODEL(600,8),XNOD(2000),YNOD(2000)
      COMMON/BLK2/DX(41),DY(41)
      COMMON/SOLMAT/AS(210000)
      COMMON/SOLB/BS(2000)
      COMMON/OLD/POLD(2000),COLD(2000)
      COMMON/OSMOT/A0,B0,C0
      COMMON/WALL/DLC,DLV,DLM,DDC,DDV,DDM,PDC,PDV,PDM,PIDC,PIDV,PIDM,
     #SIGC,SIGV,SIGM,CDC,CDV,CDM
      COMMON/TISDAT/AK,DEFF,AL,AT,PHIA,PHIT,RET,SIGT
      COMMON/CAPDAT/PC,CC
C
      DATA W/0.5555555555556D0,0.888888888889D0,0.5555555555556D0/
      DATA NGAUS,GAUS/3,-.774596669241483D0,0.D0,.774596669241483D0/
C
C     DEFINE PARAMETERS FOR INDEXING AF VECTOR
C
      LUB=3*NEY+4
      LP=3*LUB
C
C     CONSIDER THE CAPILLARY WALL, ELEMENT BY ELEMENT.
C
      DO 1 ITT=1,NEY
      IP=ITT+1
```

```
      IT=(NEX-1)*NEY+ITT
C
C     ENTER LOOP FOR GAUSS QUADRATURE INTEGRATION.  IDENTIFY T VARIABLE
C
      DO 2 M=1,NGAUS
C
      T=GAUS(M)
C
C     DEFINE BASIS FUNCTIONS B(1)=B3, B(2)=B4, B(3)=B5, EVALUATED
C     AT (1,T)
C
      B(1)=(T-1.D0)*T*.5D0
      B(3)=(T+1.D0)*T*.5D0
      B(2)=1.D0-T*T
C
      INDEX(1)=NODEL(IT,3)
      INDEX(2)=NODEL(IT,4)
      INDEX(3)=NODEL(IT,5)
C
C     CALCULATE C(S,T), PI(S,T) AND Q(S,T)
C
      CST=0.D0
      QST=0.D0
      DO 3 I=1,3
      CST=CST+COLD(INDEX(I))*B(I)
      QST=QST+POLD(INDEX(I))*B(I)
   3  CONTINUE
      PIST=CST*(A0+CST*(B0+CST*C0))
      QST=(QST-PDV-SIGV*(PIST-PIDV))*(AK*PC*DLV)/DEFF
      F=PHIA/PHIT
      PEC=QST*(1.D0-SIGV)/DDV
C
C     CHECK TO SEE IF CONVECTIVE COMPONENT DOMINATES
C
      IF(PEC.GT.170.D0)GO TO 101
      IF(PEC.LT.-170.D0)GO TO 102
C
C     CHECK TO SEE IF CONVECTIVE COMPONENT IS SIGNIFICANT
C
      TEST=1.D0-DEXP(-PEC)
      IF(DABS(TEST).LT.1.D-10) GO TO 100
C
C     ADJUST THE AS VECTOR AND BS VECTOR
C
      DO 4 I=1,3
         DO 5 J=1,3
         K=LP*INDEX(J)+INDEX(I)-LUB
         AS(K)=AS(K)-
     #   (RET*F-(1.D0-SIGV)/TEST)*QST*B(I)*B(J)*DY(IP)*.5D0*W(M)
   5  CONTINUE
      BS(INDEX(I))=BS(INDEX(I))+
     #B(I)*QST*(1.D0-SIGV)*CDV*DEXP(-PEC)/TEST*DY(IP)*.5D0*W(M)
   4  CONTINUE
      GO TO 2
C
C     ADJUST AS AND BS FOR CASE WHERE SOLUTE FLUX IS PREDOMINANTLY
C     DIFFUSIVE
C
 100  DO 6 I=1,3
         DO 7 J=1,3
         K=LP*INDEX(J)+INDEX(I)-LUB
         AS(K)=AS(K)+(DDV-F*RET*QST)*B(I)*B(J)*DY(IP)*.5D0*W(M)
   7     CONTINUE
      BS(INDEX(I))=BS(INDEX(I))+B(I)*DDV*CDV*DY(IP)*.5D0*W(M)
   6  CONTINUE
C
      GO TO 2
C
C     ADJUST AS AND BS FOR THE CASE WHERE CONVECTION DOMINATES
C
 101  DO 8 I=1,3
```

```
          DO 9 J=1,3
          K=LP*INDEX(J)+INDEX(I)-LUB
          AS(K)=AS(K)-(RET*F-(1.D0-SIGV))*QST*B(I)*B(J)*DY(IP)*.5D0*W(M)
      9   CONTINUE
      8 CONTINUE
C
          GO TO 2
C
 102  DO 10 I=1,3
          DO 11 J=1,3
          K=LP*INDEX(J)+INDEX(I)-LUB
          AS(K)=AS(K)-RET*F*QST*B(I)*B(J)*DY(IP)*.5D0*W(M)
     11   CONTINUE
          BS(INDEX(I))=BS(INDEX(I))-
     #                (1.D0-SIGV)*QST*CDV*B(I)*DY(IP)*.5D0*W(M)
  10  CONTINUE
C
   2  CONTINUE
   1  CONTINUE
C
      RETURN
      END
C


      SUBROUTINE PATMES(NEX,NEY)
C
C     THIS SUBROUTINE ADJUSTS THE AF AND BF VECTORS TO SUIT THE
C     NONLINEAR FLUX BOUNDARY CONDITION AT THE MESOTHELIAL
C     WALL.
C
      IMPLICIT REAL*8(A-H,O-Z)
      DIMENSION B(3),INDEX(3),GAUS(3),W(3)
      COMMON/BLK1/NODEL(600,8),XNOD(2000),YNOD(2000)
      COMMON/BLK2/DX(41),DY(41)
      COMMON/SOLMAT/AS(210000)
      COMMON/SOLB/BS(2000)
      COMMON/OLD/POLD(2000),COLD(2000)
      COMMON/OSMOT/A0,B0,C0
      COMMON/WALL/DLC,DLV,DLM,DDC,DDV,DDM,PDC,PDV,PDM,PIDC,PIDV,PIDM,
     #SIGC,SIGV,SIGM,CDC,CDV,CDM
      COMMON/TISDAT/AK,DEFF,AL,AT,PHIA,PHIT,RET,SIGT
      COMMON/CAPDAT/PC,CC
C
      DATA W/0.5555555555556D0,0.8888888888889D0,0.5555555555556D0/
      DATA NGAUS,GAUS/3,-.774596669241483D0,0.D0,.774596669241483D0/
C
C     DEFINE PARAMETERS FOR INDEXING AF VECTOR
C
      LUB=3*NEY+4
      LP=3*LUB
C
C     CONSIDER THE MESOTHELIAL WALL, ELEMENT BY ELEMENT.
C
      DO 1 ITT=1,NEX
      IP=ITT+1
      IT=ITT*NEY
C
C     ENTER LOOP FOR GAUSS QUADRATURE INTEGRATION. IDENTIFY S VARIABLE
C
      DO 2 M=1,NGAUS
C
      S=GAUS(M)
C
C     DEFINE BASIS FUNCTIONS B(1)=B5, B(2)=B6, B(3)=B7, EVALUATED
C     AT (S,1)
C
      B(3)=(S-1.D0)*S*.5D0
      B(1)=(S+1.D0)*S*.5D0
      B(2)=1.D0-S*S
C
```

```
        INDEX(1)=NODEL(IT,5)
        INDEX(2)=NODEL(IT,6)
        INDEX(3)=NODEL(IT,7)
C
C       CALCULATE C(S,T), PI(S,T) AND Q(S,T)
C
        CST=0.D0
        QST=0.D0
        DO 3 I=1,3
        CST=CST+COLD(INDEX(I))*B(I)
        QST=QST+POLD(INDEX(I))*B(I)
   3    CONTINUE
        PIST=CST*(A0+CST*(B0+CST*C0))
        QST=(QST-PDM-SIGM*(PIST-PIDM))*(AK*PC*DLM)/DEFF
        F=PHIA/PHIT
        PEC=QST*(1.D0-SIGM)/DDM
C
C       CHECK TO SEE IF CONVECTION DOMINATES
C
        IF(PEC.GT.170.D0)GO TO 101
        IF(PEC.LT.-170.D0)GO TO 102
C
C       CHECK TO SEE IF CONVECTIVE COMPONENT IS SIGNIFICANT
C
        TEST=1.D0-DEXP(-PEC)
        IF(DABS(TEST).LT.1.D-10) GO TO 100
C
C       ADJUST THE AS VECTOR AND BS VECTOR
C
        DO 4 I=1,3
           DO 5 J=1,3
           K=LP*INDEX(J)+INDEX(I)-LUB
           AS(K)=AS(K)-
     #     (RET*F-(1.D0-SIGM)/TEST)*QST*B(I)*B(J)*DX(IP)*.5D0*W(M)
   5    CONTINUE
        BS(INDEX(I))=BS(INDEX(I))+
     #B(I)*QST*(1.D0-SIGM)*CDM*DEXP(-PEC)/TEST*DX(IP)*.5D0*W(M)
   4    CONTINUE
        GO TO 2
C
C       ADJUST AS AND BS FOR CASE WHERE SOLUTE FLUX IS PREDOMINANTLY
C       DIFFUSIVE
C
 100    DO 6 I=1,3
           DO 7 J=1,3
           K=LP*INDEX(J)+INDEX(I)-LUB
           AS(K)=AS(K)+(DDM-F*RET*QST)*B(I)*B(J)*DX(IP)*.5D0*W(M)
   7       CONTINUE
        BS(INDEX(I))=BS(INDEX(I))+B(I)*DDM*CDM*DX(IP)*.5D0*W(M)
   6    CONTINUE
C
        GO TO 2
C
C       ADJUST AS AND BS FOR CASES WHERE CONVECTION DOMINATES
C
 101    DO 8 I=1,3
           DO 9 J=1,3
           K=LP*INDEX(J)+INDEX(I)-LUB
           AS(K)=AS(K)-(RET*F-(1.D0-SIGM))*QST*B(I)*B(J)*DX(IP)*.5D0*W(M)
   9       CONTINUE
   8    CONTINUE
C
        GO TO 2
C
 102    DO 10 I=1,3
           DO 11 J=1,3
           K=LP*INDEX(J)+INDEX(I)-LUB
           AS(K)=AS(K)-RET*F*QST*B(I)*B(J)*DX(IP)*.5D0*W(M)
  11       CONTINUE
        BS(INDEX(I))=BS(INDEX(I))-
     #                (1.D0-SIGM)*QST*CDM*B(I)*DX(IP)*.5D0*W(M)
```

```
   10  CONTINUE
C
    2  CONTINUE
    1  CONTINUE
C
       RETURN
       END
C
C


       SUBROUTINE MASFC(NEX,NEY)
C
C      THIS SUBROUTINE CALCULATES THE FLUID FLUX ACROSS THE CAPILLARY
C      WALL, STORING IT IN QFC(NEY), AS WELL AS THE CONVECTIVE FLUX
C      OF PROTEIN TO THE WALL FROM THE INTERSTITIUM (QSC(NEY)).
C
       IMPLICIT REAL*8(A-H,O-Z)
       DIMENSION B(3),INDEX(3),GAUS(3),W(3)
       COMMON/BLK1/NODEL(600,8),XNOD(2000),YNOD(2000)
       COMMON/BLK2/DX(41),DY(41)
       COMMON/SOLMAT/AS(210000)
       COMMON/SOLB/BS(2000)
       COMMON/OLD/POLD(2000),COLD(2000)
       COMMON/OSMOT/A0,B0,C0
       COMMON/WALL/DLC,DLV,DLM,DDC,DDV,DDM,PDC,PDV,PDM,PIDC,PIDV,PIDM,
      #SIGC,SIGV,SIGM,CDC,CDV,CDM
       COMMON/TISDAT/AK,DEFF,AL,AT,PHIA,PHIT,RET,SIGT
       COMMON/CAPDAT/PC,CC
       COMMON/MATBAL/QFC(40),QCC(40),QSC(40),QFV(40),QCV(40),QSV(40),
      #QFM(40),QCM(40),QSM(40)
C
       DATA W/0.5555555555556D0,0.8888888888889D0,0.5555555555556D0/
       DATA NGAUS,GAUS/3,-.774596669241483D0,0.D0,.774596669241483D0/
C
C      CONSIDER THE CAPILLARY WALL, ELEMENT BY ELEMENT.
C
       F=PHIA/PHIT
       DO 1 IT=1,NEY
       IP=IT+1
C
C.     ENTER LOOP FOR GAUSS QUADRATURE INTEGRATION.  IDENTIFY T VARIABLE
C
       DO 2 M=1,NGAUS
C
       T=GAUS(M)
C
C      DEFINE BASIS FUNCTIONS B(1)=B1,  B(2)=B7,  B(3)=B8, EVALUATED
C      AT (-1,T)
C
       B(1)=(T-1.D0)*T*.5D0
       B(2)=(T+1.D0)*T*.5D0
       B(3)=1.D0-T*T
C
       INDEX(1)=NODEL(IT,1)
       INDEX(2)=NODEL(IT,7)
       INDEX(3)=NODEL(IT,8)
C
C      CALCULATE C(S,T), PI(S,T) AND Q(S,T)
C
       CST=0.D0
       QST=0.D0
       DO 3 I=1,3
       CST=CST+COLD(INDEX(I))*B(I)
       QST=QST+POLD(INDEX(I))*B(I)
    3  CONTINUE
       PIST=CST*(A0+CST*(B0+CST*C0))
       QST=(QST-PDC-SIGC*(PIST-PIDC))*(AK*PC*DLC)/DEFF
C
C      NOW CALCULATE THE CONVECTIVE FLUX OF PROTEIN, QCC, AND THE
```

```
C      FLUID FLUX, QFC, BOTH INTEGRATED OVER THE ELEMENTAL BOUNDARY
C
       QFC(IT)=QFC(IT)+QST*DY(IP)*.5D0*W(M)
       QCC(IT)=QCC(IT)+QST*RET*F*CST*DY(IP)*.5D0*W(M)
C
   2   CONTINUE
   1   CONTINUE
       RETURN
       END
C
       SUBROUTINE MASFM(NEX,NEY)
C
C      THIS SUBROUTINE CALCULATES THE FLUID FLUX ACROSS THE MESOTHEL.
C      WALL, STORING IT IN QFM(NEY), AS WELL AS THE CONVECTIVE FLUX
C      OF PROTEIN TO THE WALL FROM THE INTERSTITIUM (QSM(NEY)).
C
       IMPLICIT REAL*8(A-H,O-Z)
       DIMENSION B(3),INDEX(3),GAUS(3),W(3)
       COMMON/BLK1/NODEL(600,8),XNOD(2000),YNOD(2000)
       COMMON/BLK2/DX(41),DY(41)
       COMMON/SOLMAT/AS(210000)
       COMMON/SOLB/BS(2000)
       COMMON/OLD/POLD(2000),COLD(2000)
       COMMON/OSMOT/A0,B0,C0
       COMMON/WALL/DLC,DLV,DLM,DDC,DDV,DDM,PDC,PDV,PDM,PIDC,PIDV,PIDM,
      #SIGC,SIGV,SIGM,CDC,CDV,CDM
       COMMON/TISDAT/AK,DEFF,AL,AT,PHIA,PHIT,RET,SIGT
       COMMON/CAPDAT/PC,CC
       COMMON/MATBAL/QFC(40),QCC(40),QSC(40),QFV(40),QCV(40),QSV(40),
      #QFM(40),QCM(40),QSM(40)
C
       DATA W/0.5555555555556D0,0.8888888888889D0,0.5555555555556D0/
       DATA NGAUS,GAUS/3,-.774596669241483D0,0.D0,.774596669241483D0/
C
C      CONSIDER THE MESOTHELIAL WALL, ELEMENT BY ELEMENT.
C
       F=PHIA/PHIT
       DO 1 ITT=1,NEX
       IT=NEY*ITT
       IP=ITT+1
C
C      ENTER LOOP FOR GAUSS QUADRATURE INTEGRATION.  IDENTIFY T VARIABLE
C
       DO 2 M=1,NGAUS
C
       S=GAUS(M)
C
C      DEFINE BASIS FUNCTIONS B(1)=B5, B(2)=B6, B(3)=B7, EVALUATED
C      AT (S,1)
C
       B(3)=(S-1.D0)*S*.5D0
       B(1)=(S+1.D0)*S*.5D0
       B(2)=1.D0-S*S
C
       INDEX(1)=NODEL(IT,5)
       INDEX(2)=NODEL(IT,6)
       INDEX(3)=NODEL(IT,7)
C
C      CALCULATE C(S,T), PI(S,T) AND Q(S,T)
C
       CST=0.D0
       QST=0.D0
       DO 3 I=1,3
       CST=CST+COLD(INDEX(I))*B(I)
       QST=QST+POLD(INDEX(I))*B(I)
   3   CONTINUE
       PIST=CST*(A0+CST*(B0+CST*C0))
       QST=(QST-PDM-SIGM*(PIST-PIDM))*(AK*PC*DLM)/DEFF
C
```

```
C       NOW CALCULATE THE CONVECTIVE FLUX OF PROTEIN, QCM, AND THE
C       FLUID FLUX, QFM, BOTH INTEGRATED OVER THE ELEMENTAL BOUNDARY
C
        QFM(ITT)=QFM(ITT)+QST*DX(IP)*.5D0*W(M)
        QCM(ITT)=QCM(ITT)+QST*RET*F*CST*DX(IP)*.5D0*W(M)
C
  2     CONTINUE
  1     CONTINUE
        RETURN
        END
C


        SUBROUTINE MASFV(NEX,NEY)
C
C       THIS SUBROUTINE CALCULATES THE FLUID FLUX ACROSS THE VENULAR
C       WALL, STORING IT IN QFV(NEY), AS WELL AS THE CONVECTIVE FLUX
C       OF PROTEIN TO THE WALL FROM THE INTERSTITIUM (QSV(NEY)).
C
        IMPLICIT REAL*8(A-H,O-Z)
        DIMENSION B(3),INDEX(3),GAUS(3),W(3)
        COMMON/BLK1/NODEL(600,8),XNOD(2000),YNOD(2000)
        COMMON/BLK2/DX(41),DY(41)
        COMMON/SOLMAT/AS(210000)
        COMMON/SOLB/BS(2000)
        COMMON/OLD/POLD(2000),COLD(2000)
        COMMON/OSMOT/AO,BO,CO
        COMMON/WALL/DLC,DLV,DLM,DDC,DDV,DDM,PDC,PDV,PDM,PIDC,PIDV,PIDM,
       #SIGC,SIGV,SIGM,CDC,CDV,CDM
        COMMON/TISDAT/AK,DEFF,AL,AT,PHIA,PHIT,RET,SIGT
        COMMON/CAPDAT/PC,CC
        COMMON/MATBAL/QFC(40),QCC(40),QSC(40),QFV(40),QCV(40),QSV(40),
       #QFM(40),QCM(40),QSM(40)
C
        DATA W/0.5555555555556D0,0.8888888888889D0,0.5555555555556D0/
        DATA NGAUS,GAUS/3,-.774596669241483D0,0.D0,.774596669241483D0/
C
C       CONSIDER THE VENULAR WALL, ELEMENT BY ELEMENT.
C
        F=PHIA/PHIT
        DO 1 ITT=1,NEY
        IT=(NEX-1)*NEY+ITT
        IP=ITT+1
C
C       ENTER LOOP FOR GAUSS QUADRATURE INTEGRATION. IDENTIFY T VARIABLE
C
        DO 2 M=1,NGAUS
C
        T=GAUS(M)
C
C       DEFINE BASIS FUNCTIONS B(1)=B3, B(2)=B4, B(3)=B5, EVALUATED
C       AT (1,T)
C
        B(1)=(T-1.D0)*T*.5D0
        B(3)=(T+1.D0)*T*.5D0
        B(2)=1.D0-T*T
C
        INDEX(1)=NODEL(IT,3)
        INDEX(2)=NODEL(IT,4)
        INDEX(3)=NODEL(IT,5)
C
C       CALCULATE C(S,T), PI(S,T) AND Q(S,T)
C
        CST=0.D0
        QST=0.D0
        DO 3 I=1,3
        CST=CST+COLD(INDEX(I))*B(I)
        QST=QST+POLD(INDEX(I))*B(I)
  3     CONTINUE
        PIST=CST*(AO+CST*(BO+CST*CO))
```

```
          QST=(QST-PDV-SIGV*(PIST-PIDV))*(AK*PC*DLV)/DEFF
C
C         NOW CALCULATE THE CONVECTIVE FLUX OF PROTEIN, QCV, AND THE
C         FLUID FLUX, QFV, BOTH INTEGRATED OVER THE ELEMENTAL BOUNDARY
C
          QFV(ITT)=QFV(ITT)+QST*DY(IP)*.5D0*W(M)
          QCV(ITT)=QCV(ITT)+QST*RET*F*CST*DY(IP)*.5D0*W(M)
C
    2     CONTINUE
    1     CONTINUE
          RETURN
          END
C
          SUBROUTINE MASSC(NEX,NEY)
C
C         THIS SUBROUTINE CALCULATES THE PROTEIN FLUX ACROSS THE
C         CAPILLARY WALL, STORING THE INTEGRATED FLUX IN THE VECTOR
C         QSC(40).
C
          IMPLICIT REAL*8(A-H,O-Z)
          DIMENSION B(3),INDEX(3),GAUS(3),W(3)
          COMMON/BLK1/NODEL(600,8),XNOD(2000),YNOD(2000)
          COMMON/BLK2/DX(41),DY(41)
          COMMON/SOLMAT/AS(210000)
          COMMON/SOLB/BS(2000)
          COMMON/OLD/POLD(2000),COLD(2000)
          COMMON/OSMOT/A0,B0,C0
          COMMON/WALL/DLC,DLV,DLM,DDC,DDV,DDM,PDC,PDV,PDM,PIDC,PIDV,PIDM,
         #SIGC,SIGV,SIGM,CDC,CDV,CDM
          COMMON/TISDAT/AK,DEFF,AL,AT,PHIA,PHIT,RET,SIGT
          COMMON/CAPDAT/PC,CC
          COMMON/MATBAL/QFC(40),QCC(40),QSC(40),QFV(40),QCV(40),QSV(40),
         #QFM(40),QCM(40),QSM(40)
C
          DATA W/0.5555555555556D0,0.8888888888889D0,0.5555555555556D0/
          DATA NGAUS,GAUS/3,-.774596669241483D0,0.D0,.774596669241483D0/
C
C         CONSIDER THE CAPILLARY WALL, ELEMENT BY ELEMENT.
C
          DO 1 IT=1,NEY
          IP=IT+1
C
C         ENTER LOOP FOR GAUSS QUADRATURE INTEGRATION. IDENTIFY T VARIABLE
C
          DO 2 M=1,NGAUS
C
          T=GAUS(M)
C
C         DEFINE BASIS FUNCTIONS B(1)=B1, B(2)=B7, B(3)=B8, EVALUATED
C         AT (-1,T)
C
          B(1)=(T-1.D0)*T*.5D0
          B(2)=(T+1.D0)*T*.5D0
          B(3)=1.D0-T*T
C
          INDEX(1)=NODEL(IT,1)
          INDEX(2)=NODEL(IT,7)
          INDEX(3)=NODEL(IT,8)
C
C         CALCULATE C(S,T), PI(S,T) AND Q(S,T)
C
          CST=0.D0
          QST=0.D0
          DO 3 I=1,3
          CST=CST+COLD(INDEX(I))*B(I)
          QST=QST+POLD(INDEX(I))*B(I)
    3     CONTINUE
          PIST=CST*(A0+CST*(B0+CST*C0))
          QST=(QST-PDC-SIGC*(PIST-PIDC))*(AK*PC*DLC)/DEFF
```

```
      PEC=QST*(1.D0-SIGC)/DDC
C
C     CHECK TO SEE IF CONVECTION DOMINATES
C
      IF(PEC.GT.170.D0)GO TO 101
      IF(PEC.LT.-170.D0)GO TO 102
C
C     CHECK TO SEE IF CONVECTIVE COMPONENT IS SIGNIFICANT
C
      TEST=1.D0-DEXP(-PEC)
      IF(DABS(TEST).LT.1.D-10) GO TO 100
C
C     CALCULATE THE INTEGRATED FLUX ALONG THE ELEMENTAL BOUNDARY
C
      QSC(IT)=QSC(IT)+
     #(1.D0-SIGC)*QST*(CST-CDC*DEXP(-PEC))/TEST*DY(IP)*W(M)*.5D0
      IND=1
      WRITE(6,600) IND,M,QST,PEC,IT,QSC(IT)
  600 FORMAT(1X,'CONDITION',I2,1X,'M=',I2,1X,'QST=',F14.7,1X,'PEC=',
     #F14.7,1X,'QSC(',I2,')=',F14.7)
C
      GO TO 2
C
C     CASE WHERE CONVECTIVE TRANSPORT IS INSIGNIFICANT
C
  100 QSC(IT)=QSC(IT)+DDC*(CST-CDC)*DY(IP)*.5D0*W(M)
      IND=2
      WRITE(6,600) IND,M,QST,PEC,IT,QSC(IT)
C
      GO TO 2
C
  101 QSC(IT)=QSC(IT)+(1.D0-SIGC)*QST*CST*DY(IP)*.5D0*W(M)
      IND=3
      WRITE(6,600) IND,M,QST,PEC,IT,QSC(IT)
C
      GO TO 2
C
  102 QSC(IT)=QSC(IT)+(1.D0-SIGC)*QST*CDC*DY(IP)*.5D0*W(M)
      IND=4
      WRITE(6,600) IND,M,QST,PEC,IT,QSC(IT)
C
  2   CONTINUE
  1   CONTINUE
C
      RETURN
      END
C


      SUBROUTINE MASSV(NEX,NEY)
C
C     THIS SUBROUTINE CALCULATES THE PROTEIN FLUX ACROSS THE
C     VENULAR WALL, STORING THE INTEGRATED FLUX IN THE VECTOR
C     QSV(40).
C
      IMPLICIT REAL*8(A-H,O-Z)
      DIMENSION B(3),INDEX(3),GAUS(3),W(3)
      COMMON/BLK1/NODEL(600,8),XNOD(2000),YNOD(2000)
      COMMON/BLK2/DX(41),DY(41)
      COMMON/SOLMAT/AS(210000)
      COMMON/SOLB/BS(2000)
      COMMON/OLD/POLD(2000),COLD(2000)
      COMMON/OSMOT/A0,B0,C0
      COMMON/WALL/DLC,DLV,DLM,DDC,DDV,DDM,PDC,PDV,PDM,PIDC,PIDV,PIDM,
     #SIGC,SIGV,SIGM,CDC,CDV,CDM
      COMMON/TISDAT/AK,DEFF,AL,AT,PHIA,PHIT,RET,SIGT
      COMMON/CAPDAT/PC,CC
      COMMON/MATBAL/QFC(40),QCC(40),QSC(40),QFV(40),QCV(40),QSV(40),
     #QFM(40),QCM(40),QSM(40)
C
      DATA W/0.5555555555556D0,0.8888888888889D0,0.5555555555556D0/
```

```
        DATA NGAUS,GAUS/3,-.774596669241483D0,0.D0,.774596669241483D0/
C
C       CONSIDER THE VENULAR WALL, ELEMENT BY ELEMENT.
C
        DO 1 ITT=1,NEY
        IT=(NEX-1)*NEY+ITT
        IP=ITT+1
C
C       ENTER LOOP FOR GAUSS QUADRATURE INTEGRATION. IDENTIFY T VARIABLE
C
        DO 2 M=1,NGAUS
C
        T=GAUS(M)
C
C       DEFINE BASIS FUNCTIONS B(1)=B3, B(2)=B4, B(3)=B5, EVALUATED
C       AT (1,T)
C
        B(1)=(T-1.D0)*T*.5D0
        B(3)=(T+1.D0)*T*.5D0
        B(2)=1.D0-T*T
C
        INDEX(1)=NODEL(IT,3)
        INDEX(2)=NODEL(IT,4)
        INDEX(3)=NODEL(IT,5)
C
C       CALCULATE C(S,T), PI(S,T) AND Q(S,T)
C
        CST=0.D0
        QST=0.D0
        DO 3 I=1,3
        CST=CST+COLD(INDEX(I))*B(I)
        QST=QST+POLD(INDEX(I))*B(I)
   3    CONTINUE
        PIST=CST*(A0+CST*(B0+CST*C0))
        QST=(QST-PDV-SIGV*(PIST-PIDV))*(AK*PC*DLV)/DEFF
        PEC=QST*(1.D0-SIGV)/DDV
C
C       CHECK TO SEE IF CONVECTION DOMINATES
C
        IF(PEC.GT.170.D0)GO TO 101
        IF(PEC.LT.-170.D0)GO TO 102
C
C       CHECK TO SEE IF CONVECTIVE COMPONENT IS SIGNIFICANT
C
        TEST=1.D0-DEXP(-PEC)
        IF(DABS(TEST).LT.1.D-10) GO TO 100
C
C       CALCULATE THE INTEGRATED FLUX ALONG THE ELEMENTAL BOUNDARY
C
        QSV(ITT)=QSV(ITT)+
       #(1.D0-SIGV)*QST*(CST-CDV*DEXP(-PEC))/TEST*DY(IP)*.5D0*W(M)
        IND=1
        WRITE(6,600) IND,M,QST,PEC,ITT,QSV(ITT)
  600   FORMAT(1X,'CONDITION ',I2,1X,'M=',I2,1X,'QST=',F14.7,1X,'PEC=',
       #F14.7,1X,'QSV(',I2,')=',F14.7)
C
        GO TO 2
C
C       CASE WHERE CONVECTIVE TRANSPORT IS INSIGNIFICANT
C
  100   QSV(ITT)=QSV(ITT)+DDV*(CST-CDV)*DY(IP)*.5D0*W(M)
        IND=2
        WRITE(6,600) IND,M,QST,PEC,ITT,QSV(ITT)
C
        GO TO 2
C
  101   QSV(ITT)=QSV(ITT)+(1.D0-SIGV)*QST*CST*DY(IP)*.5D0*W(M)
        IND=3
        WRITE(6,600) IND,M,QST,PEC,ITT,QSV(ITT)
C
```

```
        GO TO 2
C
 102    QSV(ITT)=QSV(ITT)+(1.D0-SIGV)*QST*CDV*DY(IP)*.5D0*W(M)
        IND=4
        WRITE(6,600) IND,M,QST,PEC,ITT,QSV(ITT)
C
 2      CONTINUE
 1      CONTINUE
C
        RETURN
        END
C


        SUBROUTINE MASSM(NEX,NEY)
C
C       THIS SUBROUTINE CALCULATES THE PROTEIN FLUX ACROSS THE
C       MESOTHELIAL WALL, STORING THE INTEGRATED FLUX IN THE VECTOR
C       QSM(40).
C
        IMPLICIT REAL*8(A-H,O-Z)
        DIMENSION B(3),INDEX(3),GAUS(3),W(3)
        COMMON/BLK1/NODEL(600,8),XNOD(2000),YNOD(2000)
        COMMON/BLK2/DX(41),DY(41)
        COMMON/SOLMAT/AS(210000)
        COMMON/SOLB/BS(2000)
        COMMON/OLD/POLD(2000),COLD(2000)
        COMMON/OSMOT/A0,B0,C0
        COMMON/WALL/DLC,DLV,DLM,DDC,DDV,DDM,PDC,PDV,PDM,PIDC,PIDV,PIDM,
       #SIGC,SIGV,SIGM,CDC,CDV,CDM
        COMMON/TISDAT/AK,DEFF,AL,AT,PHIA,PHIT,RET,SIGT
        COMMON/CAPDAT/PC,CC
        COMMON/MATBAL/QFC(40),QCC(40),QSC(40),QFV(40),QCV(40),QSV(40),
       #QFM(40),QCM(40),QSM(40)
C
        DATA W/0.5555555555556D0,0.8888888888889D0,0.5555555555556D0/
        DATA NGAUS,GAUS/3,-.774596669241483D0,0.D0,.774596669241483D0/
C
C       CONSIDER THE VENULAR WALL, ELEMENT BY ELEMENT.
C
        DO 1 ITT=1,NEX
        IT=NEY*ITT
        IP=ITT+1
C
C       ENTER LOOP FOR GAUSS QUADRATURE INTEGRATION. IDENTIFY S VARIABLE
C
        DO 2 M=1,NGAUS
C
        S=GAUS(M)
C
C       DEFINE BASIS FUNCTIONS B(1)=B5, B(2)=B6, B(3)=B7, EVALUATED
C       AT (S,1)
C
        B(3)=(S-1.D0)*S*.5D0
        B(1)=(S+1.D0)*S*.5D0
        B(2)=1.D0-S*S
C
        INDEX(1)=NODEL(IT,5)
        INDEX(2)=NODEL(IT,6)
        INDEX(3)=NODEL(IT,7)
C
C       CALCULATE C(S,T), PI(S,T) AND Q(S,T)
C
        CST=0.D0
        QST=0.D0
        DO 3 I=1,3
        CST=CST+COLD(INDEX(I))*B(I)
        QST=QST+POLD(INDEX(I))*B(I)
 3      CONTINUE
        PIST=CST*(A0+CST*(B0+CST*C0))
```

```
          QST=(QST-PDM-SIGM*(PIST-PIDM))*(AK*PC*DLM)/DEFF
          PEC=QST*(1.D0-SIGM)/DDM
C
C         CHECK TO SEE IF CONVECTION DOMINATES
C
          IF(PEC.GT.170.D0)GO TO 101
          IF(PEC.LT.-170.D0)GO TO 102
C
C         CHECK TO SEE IF CONVECTIVE COMPONENT IS SIGNIFICANT
C
          TEST=1.D0-DEXP(-PEC)
          IF(DABS(TEST).LT.1.D-10) GO TO 100
C
C         CALCULATE THE INTEGRATED FLUX ALONG THE ELEMENTAL BOUNDARY
C
          QSM(ITT)=QSM(ITT)+
         #(1.D0-SIGM)*QST*(CST-CDM*DEXP(-PEC))/TEST*DX(IP)*W(M)*.5D0
C
          GO TO 2
C
C         CASE WHERE CONVECTIVE TRANSPORT IS INSIGNIFICANT
C
  100     QSM(ITT)=QSM(ITT)+DDM*(CST-CDV)*DX(IP)*.5D0*W(M)
C
          GO TO 2
C
  101     QSM(ITT)=QSM(ITT)+(1.D0-SIGM)*QST*CST*DX(IP)*W(M)*.5D0
C
          GO TO 2
C
  102     QSM(ITT)=QSM(ITT)+(1.D0-SIGM)*QST*CDM*DX(IP)*.5D0*W(M)
C
    2     CONTINUE
    1     CONTINUE
C
          RETURN
          END


          SUBROUTINE FLUX(NEX,NEY)
C
C         THIS SUBROUTINE CALCULATES THE FLUID FLUXES AND CONVECTIVE
C         AS WELL AS DISPERSIVE PROTEIN FLUXES IN EACH ELEMENT,
C         STORING THEM IN VECTORS FFLUX(NEL,2), CFLUX(NEL,2) AND
C         DFLUX(NEL,2), RESPECTIVELY. THE (X,Y) COORDINATES CORRESPONDING
C         TO THESE FLUXES ARE STORED IN ELOC(NEL,2). NOTE THAT THE FLUXES
C         ARE CALCULATED AT THE MIDPOINT OF EACH ISOPARAMETRIC ELEMENT
C         (THAT IS, AT (S,T)=(0,0)).
C
          IMPLICIT REAL*8(A-H,O-Z)
          COMMON/BLK1/NODEL(600,8),XNOD(2000),YNOD(2000)
          COMMON/TISDAT/AK,DEFF,AL,AT,PHIA,PHIT,RET,SIGT
          COMMON/OSMOT/A0,B0,C0
          COMMON/CAPDAT/PC,CC
          COMMON/OLD/POLD(2000),COLD(2000)
          COMMON/FLUXES/FFLUX(600,2),CFLUX(600,2),DFLUX(600,2),
         #ELOC(600,2)
          DIMENSION GAUS(4),W(4),B(8),DBS(8),DBT(8),DBX(8),DBY(8),
         #AJAC(2,2),AJACIN(2,2)
C
          DATA NGAUS/4/
          DATA W/.347854845137454D0,.652145154862546D0,
         #.652145154862546D0,.347854845137454D0/
          DATA GAUS/-.861136311594053D0,-.339981043584856D0,
         #.339981043584856D0,.861136311594053D0/
C         DATA NGAUS/3/
C         DATA W/0.5555555555556D0,0.8888888888889D0,0.5555555555556D0/
C         DATA GAUS/-0.774596669241483D0,0.D0,0.774596669241483D0/
C
C         DATA NGAUS/2/
```

```
C       DATA W/1.0D0,1.0D0,0.D0/
C       DATA GAUS/-0.577350269189626D0,0.577350269189626D0,0.D0/
C
C       CARRY OUT THE EVALUATION ELEMENT BY ELEMENT. FLUXES ARE
C       EVALUATED AT (S,T)=(0,0).
C
        NEL=NEX*NEY
        F=PHIA/PHIT
C
C       DEFINE THE BASIS FUNCTIONS AND THEIR S AND T DERIVATIVES,
C       EVALUATED AT THE QUADRATURE POINT (0,0)
C
        S=0.D0
        T=0.D0
C
        B(1)=(S-1.D0)*(1.D0-T)*(1.D0+S+T)*.25D0
        B(2)=(1.D0-S*S)*(1.D0-T)*.5D0
        B(3)=(1.D0+S)*(T-1.D0)*(1.D0-S+T)*.25D0
        B(4)=(1.D0-T*T)*(1.D0+S)*.5D0
        B(5)=(1.D0+S)*(1.D0+T)*(T+S-1.D0)*.25D0
        B(6)=(1.D0-S*S)*(1.D0+T)*.5D0
        B(7)=(S-1.D0)*(1.D0+T)*(1.D0+S-T)*.25D0
        B(8)=(1.D0-T*T)*(1.D0-S)*.5D0
        DBS(1)=(1.D0-T)*(T+2.D0*S)*.25D0
        DBT(1)=(1.D0-S)*(S+2.D0*T)*.25D0
        DBS(2)=S*(T-1.D0)
        DBT(2)=(S*S-1.D0)*.5D0
        DBS(3)=(1.D0-T)*(2.D0*S-T)*.25D0
        DBT(3)=(1.D0+S)*(2.D0*T-S)*.25D0
        DBS(4)=(1.D0-T*T)*.5D0
        DBT(4)=-T*(1.D0+S)
        DBS(5)=(1.D0+T)*(2.D0*S+T)*.25
        DBT(5)=(1.D0+S)*(2.D0*T+S)*.25
        DBS(6)=-S*(1.D0+T)
        DBT(6)=(1.D0-S*S)*.5D0
        DBS(7)=(1.D0+T)*(2.D0*S-T)*.25D0
        DBT(7)=(1.D0-S)*(2.D0*T-S)*.25D0
        DBS(8)=(T*T-1.D0)*.5D0
        DBT(8)=T*(S-1.D0)
C
C       NOW CONSIDER EACH ELEMENT ONE BY ONE
C
        DO 100 IT=1,NEL
C
C       WE NOW CALCULATE THE JACOBIAN MATRIX, AJAC, ITS DETERMINANT,
C       DETJ, AND ITS INVERSE AJACIN.
C
C
        AJAC(1,1)=0.D0
        AJAC(2,1)=0.D0
        AJAC(1,2)=0.D0
        AJAC(2,2)=0.D0
C
        DO 3 JAK=1,8
        AJAC(1,1)=AJAC(1,1)+DBS(JAK)*XNOD(NODEL(IT,JAK))
        AJAC(1,2)=AJAC(1,2)+DBS(JAK)*YNOD(NODEL(IT,JAK))
        AJAC(2,1)=AJAC(2,1)+DBT(JAK)*XNOD(NODEL(IT,JAK))
        AJAC(2,2)=AJAC(2,2)+DBT(JAK)*YNOD(NODEL(IT,JAK))
3       CONTINUE
C
        DETJ=AJAC(1,1)*AJAC(2,2)-AJAC(1,2)*AJAC(2,1)
C
        AJACIN(1,1)=AJAC(2,2)/DETJ
        AJACIN(1,2)=-AJAC(1,2)/DETJ
        AJACIN(2,1)=-AJAC(2,1)/DETJ
        AJACIN(2,2)=AJAC(1,1)/DETJ
C
C       WE CAN NOW CALCULATE D(B(I))/DX AND D(B(I))/DY, EVALUATED AT
C       (X(S,T),Y(S,T)), USING JACIN
C
```

```
       DO 4 I=1,8
       DBX(I)=DBS(I)*AJACIN(1,1)+DBT(I)*AJACIN(1,2)
       DBY(I)=DBS(I)*AJACIN(2,1)+DBT(I)*AJACIN(2,2)
  4    CONTINUE
C
C      WE NOW HAVE SUFFICIENT INFORMATION TO DETERMINE QX,QY,C,DC/DX,
C      DC/DY, AND THE LOCATION IN (X,Y) ·COORDINATES, ALL CORRESPONDING
C      TO VALUES AT (S,T)=(0,0)
C
       CST=0.D0
       DPX=0.D0
       DPY=0.D0
       DCX=0.D0
       DCY=0.D0
       XEL=0.D0
       YEL=0.D0
C
       DO 5 J=1,8
       DPX=POLD(NODEL(IT,J))*DBX(J)+DPX
       DPY=POLD(NODEL(IT,J))*DBY(J)+DPY
       DCX=COLD(NODEL(IT,J))*DBX(J)+DCX
       DCY=COLD(NODEL(IT,J))*DBY(J)+DCY
       CST=COLD(NODEL(IT,J))*B(J)+CST
       XEL=XEL+XNOD(NODEL(IT,J))*B(J)
       YEL=YEL+YNOD(NODEL(IT,J))*B(J)
  5    CONTINUE
C
       DPIX=DCX*(A0+CST*(2.D0*B0+3.D0*C0*CST))*SIGT
       DPIY=DCY*(A0+CST*(2.D0*B0+3.D0*C0*CST))*SIGT
C
       FFLUX(IT,1)=-AK*PC/(DEFF)*(DPX-DPIX)
       FFLUX(IT,2)=-AK*PC/(DEFF)*(DPY-DPIY)
       ELOC(IT,1)=XEL
       ELOC(IT,2)=YEL
C
       QXST=FFLUX(IT,1)*F*RET
       QYST=FFLUX(IT,2)*F*RET
C
C      NOW CALCULATE THE DISPERSION COEFFICIENTS DXX,DXY,DYY, WHERE
C      DXX=(AL*QX**2/QMAG+AT*QY**2/QMAG)+PHIA,   ETC
C.
       QMAG=DSQRT(QXST*QXST+QYST*QYST)
C
C      CHECK TO SEE IF QMAG IS NONZERO
C
       IF(QMAG.GT.1.D-10)GO TO 500
       DXX=PHIA
       DXY=0.D0
       DYY=PHIA
       GO TO 600
C
 500   DXX=(AL*QXST*QXST+AT*QYST*QYST)/QMAG+PHIA
       DXY=(AL-AT)*QXST*QYST/QMAG
       DYY=(AL*QYST*QYST+AT*QXST*QXST)/QMAG+PHIA
C
 600   DFLUX(IT,1)=-(DXX*DCX+DXY*DCY)
       DFLUX(IT,2)=-(DXY*DCX+DYY*DCY)
       CFLUX(IT,1)=QXST*CST
       CFLUX(IT,2)=QYST*CST
C
 100   CONTINUE
       RETURN
       END
C

       SUBROUTINE DGBND1 (A, B, N, ML, NU, LT, IP, DET, NCN1,
     1                    BB, RZ, ITR1, EPS1)
C
C ROUTINE SOLVES SYSTEM OF LINEAR EQNS. AX=B WHERE A IS A GENERAL
```

```
C  BAND MATRIX. METHOD USED IS GAUSSIAN ELIMINATION WITH PARTIAL
C  PIVOTING. OPTION OF ITERATIVELY IMPROVING SOLUTION IS AVAILABLE.
C  UPPER BAND WIDTH OF MATRIX INCREASES DUE TO INTERCHANGES BY
C  AMOUNT ML. ROUTINE REQUIRES BAND ELEMENTS OF MATRIX TO BE STORED
C  BY COLUMN IN A ONE DIMENSIONAL ARRAY. EACH COLUMN IS OF LENGTH
C  2*ML+NU AND BAND IS TO BE STORED IN ELEMENTS ML+1 TO 2*ML+NU OF
C  EACH COLUMN. ELEMENTS 1 TO ML OF COLUMN ARE SET TO ZERO BY GBAND.
C  IF MATRIX IS SYMMETRIC USER MAY SPECIFY LOWER BAND ONLY IN
C  ELEMENTS ML+NU+1 TO 2*ML+NU OF EACH COLUMN AND GBAND WILL
C  GENERATE REMAINING ELEMENTS. (IF THIS IS DESIRED, SET LT=-1 ON
C  FIRST CALL TO GBAND.)
C    A = 1 DIMENSIONAL ARRAY CONTAINING MATRIX OF COEFFICIENTS.
C    B = 1 DIMENSIONAL ARRAY CONTAINING RIGHT HAND SIDE VECTORS.
C          ON EXIT, B WILL CONTAIN THE SOLUTION VECTOR X.
C    N = ORDER OF MATRIX
C   ML = LENGTH OF LOWER BAND (EXCLUDING DIAGONAL)
C   NU = LENGTH OF UPPER BAND (EXCLUDING DIAGONAL)
C   LT = ABS(LT)=1 IF ONLY 1 B VECTOR OR IF 1ST OF SEVERAL.
C        ABS(LT),=1 FOR SUBSEQUENT B VECTORS.
C        (NOTE. LT=+1 IF FULL BAND WIDTH GIVEN, LT=-1 IF LOWER BAND
C          ONLY OF SYMMETRIC MATRIX GIVEN.)
C   IP = INTEGER ARRAY CONTAINING INTERCHANGE INFORMATION.
C  DET = DETERMINANT OF A = DET*(10**NCN) WHERE 1.D-15<|DET|<1.D+15.
C          IF DET=0.0 MATRIX IS SINGULAR AND ERROR RETURN TAKEN.
C  BB, RZ = ARRAYS REQUIRED FOR IMPROVEMENT OPTION. CAN BE REAL*8
C          VARIABLES IF OPTION NOT REQUIRED.
C  ITER   = 0 IF IMPROVEMENT NOT REQUIRED, OTHERWISE ITER= NO. OF
C          ITERATIONS OR CYCLES.
C  EPS - CONVERGENCE CRITERION.
C
C MODIFIED TO DO ITERATIVE IMPROVEMENT (FORMERLY AVAILABLE ONLY
C WITH THE SINGLE PRECISION VERSION).  MIKE PATTERSON - NOV, 1980
       IMPLICIT REAL*8 (A-H, O-Z)
       COMMON /GBAND$/ NITER
       DIMENSION A(1), B(N), IP(N), BB(N), RZ(N)
       COMPLEX*16 DSUMM, QADDQ, QMULD
       REAL*8 QRNDQ
C TO ASSIGN LOGICAL UNITS 94 AND 95 ONLY ONCE:
       LOGICAL ASSIGN /F/, YES /T/
C STATEMENT FUNCTION TO CALCULATE POINTERS INTO A:
       IFN(I, J) = 1 + (J - 1)*LC + I - J + NUM
C
C·
       NCN=NCN1
       ITR=ITR1
       EPS=EPS1
       ITER = ITR
C
       LCM = NU + 2*ML
       LC = LCM + 1
       NLC = N*LC
       NUM = NU + ML
C  GENERATE REMAINING ELEMENTS OF SYMMETRIC MATRIX
       IF (LT .NE. -1) GO TO 120
       NN = N - 1
       DO 110 I = 1, NN
         IFI = IFN(I, I)
         IFJ = IFI
         II = I + 1
         IML = MINO(I + ML, N)
         DO 100 J = II, IML
           IFI = IFI + 1
           IFJ = IFJ + LCM
100        A(IFJ) = A(IFI)
110    CONTINUE
120    IF (ITER .EQ. 0) GO TO 140
C ASSIGN UNITS 94 AND 95 IF THEY HAVE NOT ALREADY BEEN ASSIGNED:
       IF (ASSIGN) GO TO 125
       CALL FTNCMD ('ASSIGN 94=-GBAND94;')
       CALL FTNCMD ('ASSIGN 95=-GBAND95;')
       ASSIGN = YES
```

```
125     REWIND 94
        REWIND 95
        DO 130 I = 1, N
130     BB(I) = B(I)
140     IF (IABS(LT) .NE. 1) GO TO 280
        IP(N) = 1
        IF (ML .EQ. 0) GO TO 160
C  SET ELEMENTS 1 - ML OF EACH COLUMN TO ZERO
        DO 150 I = 1, N
          IFK = (I - 1)*LC
          DO 150 J = 1, ML
            IFK = IFK + 1
150     A(IFK) = 0.0D0
160     IF (ITER .NE. 0) CALL DWR1 (A, NLC, 94)
        DET = 0.0D0
        NCN = 0
        IF (ML .EQ. 0) GO TO 230
C  LU DECOMPOSITION
        DO 220 K = 1, N
          IFK = IFN(K, K)
          IF (K .EQ. N) GO TO 210
          KP = K + 1
          KPM = MINO(K + ML, N)
          KPN = MINO(K + NUM, N)
          M = K
          IFM = IFK
          IFI = IFK
          DO 170 I = KP, KPM
            IFI = IFI + 1
            IF (DABS(A(IFI)) .LE. DABS(A(IFM))) GO TO 170
            M = I
            IFM = IFI
170       CONTINUE
          IP(K) = M
          T = A(IFM)
          IF (M .NE. K) IP(N) = -IP(N)
          A(IFM) = A(IFK)
          A(IFK) = T
          IF (T .EQ. 0.0D0) GO TO 260
          OT = 1.0D0/T
          IK = IFK
          DO 180 I = KP, KPM
            IK = IK + 1
180       A(IK) = -A(IK)*OT
          KJ = IFK
          MJ = IFM
          DO 200 J = KP, KPN
            KJ = KJ + LCM
            MJ = MJ + LCM
            T = A(MJ)
            A(MJ) = A(KJ)
            A(KJ) = T
            IF (T .EQ. 0.0D0) GO TO 200
            IK = IFK
            IJ = KJ
            DO 190 I = KP, KPM
              IK = IK + 1
              IJ = IJ + 1
190         A(IJ) = A(IJ) + A(IK)*T
200       CONTINUE
210       IF (A(IFK) .EQ. 0.0D0) GO TO 260
220     CONTINUE
230     IFK = IFN(1, 1)
        DET = A(IFK)
        DO 250 K = 2, N
          IFK = IFK + LC
          DET = DET*A(IFK)
          IF (DET .EQ. 0.0D0) GO TO 260
          IF (DABS(DET) .GT. 1.D-15) GO TO 240
          DET = DET*1.D+15
          NCN = NCN - 15
```

```
              GO TO 250
240           IF (DABS(DET) .LT. 1.D+15) GO TO 250
              DET = DET*1.D-15
              NCN = NCN + 15
250        CONTINUE
           DET = DET*IP(N)
           GO TO 280
260        DET = 0.0D0
           WRITE (6, 270) K
270        FORMAT ('0* DGBND1 - matrix is singular. '/
     1     '      Error occurred in attempt to find', I5, 'th pivot.')
           RETURN
280        CALL DSOLV1 (A, B, IP, N, ML, NU)
           IF (ITER .EQ. 0) RETURN
C
C    ITERATIVE IMPROVEMENT
C    RESIDUALS (R) = AX-B ARE FOUND AND STORED IN ARRAY RZ USING
C    EXTENDED PRECISION ARITHMETIC. SYSTEM AZ=R IS SOLVED AND NEW
C    SOLUTION =X+Z IS STORED IN ARRAY B. ABOVE STEPS REPEATED UNTIL
C      (1) MAX(Z)/MAX(X) < EPS OR
C      (2) NO. OF CYCLES > ITER OR
C      (3) IMPROVEMENT STARTS TO DIVERGE.
C    ROUTINE THEN RETURNS AFTER SETTING EPS=MAX(Z) (FOR (1)) OR
C    SETTING EPS=-MAX(Z) AND PRINTING APPROPRIATE ERROR MESSAGE (FOR
C    (2) AND (3))
C
C
           IF (IABS(LT) .EQ. 1) CALL DWR1 (A, NLC, 95)
           XNORM = 0.0D0
           DO 290 K = 1, N
290        XNORM = DMAX1(XNORM, DABS(B(K)))
           IF (XNORM .LE. 0.0D0) RETURN
           ZX = 1.D+60
           LD = 0
           DO 340 L = 1, ITER
             REWIND 94
             CALL DRE1 (A, NLC, 94)
             DO 310 K = 1, N
               DSUMM = (0.D0, 0.D0)
               KPM = MAX0(K - ML, 1)
               KPN = MIN0(K + NU, N)
               IFK = IFN(K, KPM)
               DO 300 J = KPM, KPN
C                  DSUMM = DSUMM + A(IFK)*B(J)
C USING EXTENDED PRECISION:
                   DSUMM = QADDQ(DSUMM, QMULD(A(IFK), B(J)))
300                IFK = IFK + LCM
               RZ(K) = BB(K) - QRNDQ(DSUMM)
310          CONTINUE
             REWIND 95
             CALL DRE1 (A, NLC, 95)
             CALL DSOLV1 (A, RZ, IP, N, ML, NU)
             ZNORM = 0.0D0
             DO 320 K = 1, N
               ERZ = RZ(K)
               ZNORM = DMAX1(ZNORM, DABS(ERZ))
320            B(K) = B(K) + ERZ
             IF (ZNORM .GT. ZX) GO TO 330
             IF ((ZNORM - EPS*XNORM) .LT. 0.0D0) GO TO 390
             ZX = ZNORM
             GO TO 340
330          IF (ZNORM .GT. 10.0D0*ZX) GO TO 360
             LD = LD + 1
             IF (LD .GE. 3) GO TO 360
340        CONTINUE
           L = ITER
           WRITE (6, 350)
350        FORMAT ('0* DGBND1- Iterative improvement did not converge'/)
           GO TO 380
```

```
360     WRITE (6, 370)
370     FORMAT ('0* DGBND1 - Iterative improvement is diverging.'/)
380     EPS = -ZNORM
        NITER = L
        RETURN
390     EPS = ZNORM
        NITER = L
        RETURN
        END

        SUBROUTINE DSOLV1 (A, B, IP, N, ML, NU)
C
C  THIS ROUTINE COMPUTES THE SOLUTION OF A SYSTEM AFTER GBAND HAS
C  DECOMPOSED MATRIX A INTO A LOWER TRIANGULAR MATRIX L AND AN
C  UPPER TRIANGULAR MATRIX U.
C
        IMPLICIT REAL*8 (A-H, O-Z)
        DIMENSION A(1), B(N), IP(N)
        IFN(I, J) = 1 + (J - 1)*LC + I - J + NUM
        LCM = 2*ML + NU
        LC = LCM + 1
        NUM = NU + ML
        MN = N - 1
C  SOLVE FOR Y
        IF (ML .EQ. 0) GO TO 110
        DO 100 K = 1, MN
           KP = K + 1
           M = IP(K)
           T = B(M)
           B(M) = B(K)
           B(K) = T
           KPM = MINO(K + ML, N)
           IFK = IFN(K, K)
           DO 100 I = KP, KPM
              IFK = IFK + 1
100     B(I) = B(I) + A(IFK)*T
C  SOLVE FOR X
110     IFK = IFN(N, N)
        DO 120 KB = 1, MN
           KM = N - KB
           K = KM + 1
           B(K) = B(K)/A(IFK)
           IFK = IFK - LC
           T = -B(K)
           KMN = MAXO(1, K - ML - NU)
           KML = IFN(KMN, K)
           DO 120 I = KMN, KM
              B(I) = B(I) + A(KML)*T
120     KML = KML + 1
        B(1) = B(1)/A(NUM + 1)
        RETURN
        END
        SUBROUTINE DWR1 (A, N, LU)
        REAL*8 A(N)
        WRITE (LU) A
        RETURN
        END
        SUBROUTINE DRE1 (A, N, LU)
        REAL*8 A(N)
        READ (LU) A
        RETURN
        END
```

D.3 One-Dimensional Simulator: MESDISP.FOR

```
C
C      THIS PROGRAM SIMULATES BOTH CONVECTIVE AND DISPERSIVE PLASMA
C      PROTEIN TRANSPORT THROUGH MESENTERY DURING STEADY-STATE
```

```
C       CONDITIONS. THE MESENTERY IS TREATED AS A 1-DIMENSIONAL
C       RECTANGULAR SLAB.
C
        IMPLICIT REAL*8(A-H,O-Z)
        DIMENSION HOLD(1001),IPERM(1001),RES(1001),HOLDS(1000),
       #RESS(1001),IPERMS(1001)
        COMMON/BLK1/NODEL(500,3),XNOD(1001)
        COMMON/BLK2/DX(1001)
        COMMON/MATBAL/QFC,QCC,QSC,QFV,QCV,QSV,QFM,QCM,QSM,QFM1(500),
       #             QCM1(500),QSM1(500)
        COMMON/FLUMAT/FLUID(20000)
        COMMON/OLD/POLD(1001),COLD(1001)
        COMMON/SOLB/SOLUTB(1001)
        COMMON/FLUB/FLUIDB(1001)
        COMMON/SOLMAT/SOLUTE(20000)
        COMMON/OSMOT/AOSM,BOSM,COSM
        COMMON/TISDAT/AK,DEFF,ALPHL,PHIA,PHIT,RET,SIGT,BETA
        COMMON/CAPDAT/PC,CC
        COMMON/WALL/DLC,DLV,DLM,DDC,DDV,DDM,PDC,PDV,PDM,PIDC,PIDV,PIDM,
       #SIGC,SIGV,SIGM,CDC,CDV,CDM,YYL
        COMMON/MAXDAT/DISPMX,IDISP
C
C       SET MARKER AND TOLERANCE VALUES
C
        READ(5,504)OMEGAF,OMEGAC,TOLP,TOLC,PECMAX,EPS
        READ(5,550)IMAX,ITER,NECHO,N
  550   FORMAT(4I3)
        NEX=(N-1)/2
        LUB=2
        ICOUNT=0
C
C       READ IN THE DATA FROM EXTERNAL FILE
C
        DO 1 I=1,N
        READ(5,501) DX(I)
  501   FORMAT(E12.6)
    1   CONTINUE
C
C
        READ(5,502)  AOSM,BOSM,COSM,AK,PC,PHIA,PHIT,RET,PHIS
        READ(5,507)  ALPHL,AL,DEFF,SIGT,CC,YYL,BETA
        READ(5,504)  CONC,CONV,CONM,PERMC,PERMV,PERMM
        READ(5,504)  DDC,DDV,DDM,SIGC,SIGV,SIGM
        READ(5,504)  CDC,CDV,CDM,DLC,DLV,DLM
        READ(5,506)  PDC,PDV,PDM
        READ(5,506)  AOS1,BOS1,COS1
        YL=YYL*AL
        PIDC=CDC*(AOS1+CDC*(BOS1+CDC*COS1))
        PIDV=CDV*(AOS1+CDV*(BOS1+CDV*COS1))
        PIDM=CDM*(AOS1+CDM*(BOS1+CDM*COS1))
        PV=PDV*PC
        PM=PDM*PC
        CV=CDV*CC
        CM=CDM*CC
C
C
  507   FORMAT(7E10.4)
  502   FORMAT(9E10.4)
  503   FORMAT(5E10.4)
  504   FORMAT(6E10.4)
  506   FORMAT(3E10.4)
C
        DO 21 I=1,N
        READ(5,505) POLD(I),COLD(I)
  505   FORMAT(2E10.4)
   21   CONTINUE
C
```

```
C      ECHO DATA IF NECHO N.E. 0
C
       IF(NECHO.EQ.0) GO TO 999
C
C      PRINT OUT INPUT DATA
C
       WRITE(6,611)
  611 FORMAT(1X,'STEADY-STATE  FLUID PRESSURE AND SOLUTE CONCENTRATION'
     #)
       WRITE(6,667)
  667 FORMAT(1X,'PROFILES  FOR ONE DIMENSIONAL TISSUE SYSTEM',//)
       WRITE(6,612)
       WRITE(6,612)
  612 FORMAT(//,1X,'_____'
     #,//)
       WRITE(6,660)
  660 FORMAT(1X,'INPUT  PARAMETERS')
       WRITE(6,612)
       WRITE(6,613)
  613 FORMAT(1X,'1.  GRID DATA:',//)
       WRITE(6,614)NEX,DX(2)
  614 FORMAT(1X,'NUMBER  OF ELEMENTS:',1X,I2,/,1X,
     #'SMALLEST X INCREMENT:',19X,E10.4,/)
       WRITE(6,616)N
  616 FORMAT(1X,'TOTAL  NUMBER OF NODES:',10X,I4,/)
       WRITE (6,612)
       WRITE(6,617)  TOLP,TOLC,IMAX,OMEGAF,OMEGAC,PECMAX
  617 FORMAT(1X,'2.  CONVERGENCE CRITERIA:',//,1X,'PRESSURE   TOLERANCE:'
     #,17X,E10.4,/,1X,'SOLUTE   TOLERANCE:',20X,E10.4,/,1X,
     #'MAXIMUM NUMBER OF LOOP ITERATIONS:',2X,I3,/,1X,
     #'PRESSURE RELAXATION PARAMETER:',6X,E10.4,/,1X,
     #'SOLUTE RELAXATION PARAMETER:',9X,E10.4,/,1X,
     #'MAXIMUM DESIRED GRID PECLET NUMBER:',1X,E10.4)
       WRITE(6,612)
       PIC=PIDC*PC
       PIV=PIDV*PC
       PIM=PIDM*PC
C
       WRITE(6,618)  AL,YL,CC,CV,CM,PC,PV,PM,PIC,PIV,PIM,AK,DEFF
  618 FORMAT(1X,'3.  DIMENSIONAL INPUT PARAMETERS:',//,1X,
     #'TISSUE X-DIMENSION  (CM):',21X,E10.4,/,1X,
     #'TISSUE Y-DIMENSION  (CM):',21X,E10.4,/,1X,
     #'CAP. PROTEIN CONC.  (GRAMS/DL):',14X,E10.4,/,1X,
     #'VEN. PROTEIN CONC.  (GRAMS/DL):',14X,E10.4,/,1X,
     #'MES. PROTEIN CONC.  (GRAMS/DL):',14X,E10.4,/,1X,
     #'CAP. DYN. PRESSURE (DYN/CM**2):',14X,E10.4,/,1X,
     #'VEN. DYN. PRESSURE (DYN/CM**2):',14X,E10.4,/,1X,
     #'MES. DYN. PRESSURE (DYN/CM**2):',14X,E10.4,/,1X,
     #'CAP. OSM. PRESSURE (DYN/CM**2):',14X,E10.4,/,1X,
     #'VEN. OSM. PRESSURE (DYN/CM**2):',14X,E10.4,/,1X,
     #'MES. OSM. PRESSURE (DYN/CM**2):',14X,E10.4,/,1X,
     #'TISSUE FLUID CONDUCTIVITY (CM**4/(DYN-SEC):',2X,E10.4,/,1X,
     #'TISSUE SOLUTE DIFFUSIVITY (CM**2/SEC):',7X,E10.4)
       WRITE(6,626)  CONC,CONV,CONM,PERMC,PERMV,PERMM
  626 FORMAT(1X,'CAP.  CONDUCTIVITY  (CM**3/(DYN-S)):',11X,E10.4,/,1X,
     #'VEN.  CONDUCTIVITY  (CM**3/(DYN-S)):',11X,E10.4,/,1X,
     #'MES.  CONDUCTIVITY  (CM**3/(DYN-S)):',11X,E10.4,/,1X,
     #'CAP.  PERMEABILITY  (CM/S):',21X,E10.4,/,1X,
     #'VEN.  PERMEABILITY  (CM/S):',21X,E10.4,/,1X,
     #'MES.  PERMEABILITY  (CM/S):',21X,E10.4)
       WRITE(6,612)
       WRITE(6,653)  SIGT,RET,BETA,ALPHL
  653  FORMAT(1X,'DIMENSIONLESS  INPUT PARAMETERS:',//,1X,
     #'TISSUE REFLECTION COEFFICIENT:',15X,E10.4,/,
```

```
      #1X,'RETARDATION  FACTOR:',26X,E10.4,/,1X,
      #'HYDRAULIC  CONDUCTIVITY  RATIO, BETA:',15X,E10.4,/,1X,
      #'DIMENSIONLESS  DISPERSIVITY:',21X,E10.4)
        WRITE(6,619)PDC,PIDC,PDV,PIDV,PDM,PIDM
  619 FORMAT(//,1X,
      #'PRESSURE:',6X,'DYNAMIC',5X,'OSMOTIC',//,1X,'CAPILLARY:',5X,
      #E10.4,
      #2X,E10.4,/,1X,'VENULE:',8X,E10.4,2X,E10.4,/,1X,'MESOTHELIUM:',
      #3X,E10.4,2X,E10.4,//)
        WRITE(6,620)CDC,CDV,CDM
  620 FORMAT(1X,'CONCENTRATIONS:',//,1X,'CAPILLARY:',5X,E10.4,/,1X,
      #'VENULE:',9X,E10.4,/,1X,'MESOTHELIUM:',1X,E10.4,//)
        WRITE(6,621)SIGC,SIGV,SIGM
  621 FORMAT(1X,'REFLECTION  COEFFICIENTS:',//,1X,'CAPILLARY:',5X,
      #E10.4,/,1X,'VENULE:',9X,E10.4,/,1X,'MESOTHELIUM:',1X,E10.4,//)
        WRITE(6,622)DLC,DLV,DLM
  622 FORMAT(1X,'VESSEL  FLUID  CONDUCTANCES:',//,1X,'CAPILLARY:',5X,
      #E10.4,/,1X,'VENULE:',9X,E10.4,/,1X,'MESOTHELIUM:',1X,E10.4,//)
        WRITE(6,625)AOSM,BOSM,COSM
  625 FORMAT(1X,'VIRIAL  COEFFICIENTS:',//,1X,'AOSM:',1X,E10.4,/,1X,

      #'BOSM:',1X,E10.4,/,1X,'COSM:',1X,E10.4,//)
        WRITE(6,623)DDC,DDV,DDM
  623 FORMAT(1X,'VESSEL  SOLUTE  PERMEABILITIES:',//,1X,'CAPILLARY:',5X,
      #E10.4,/,1X,'VENULE:',9X,E10.4,/,1X,'MESOTHELIUM:',1X,E10.4,//)
        WRITE(6,624)PHIT,PHIA,PHIS
  624 FORMAT(1X,'TOTAL  TISSUE  FLUID  VOLUME  FRACTION:',2X,E10.4,/,1X,
      #'SOLUTE  DISTRIBUTION  VOLUME  FRACTION:',1X,E10.4,/,1X,
      #'TOTAL  SOLIDS  VOLUME  FRACTION:',8X,E10.4,///)
C
C
C
  999 CALL GRID(NEX)
C
C     INITIALIZE FLUID VECTOR
C
      CALL SETMAT(NEX,0,PEC,IEL,VELMX)
C
C     ADJUST FLUID VECTOR TO FIT BOUNDARY CONDITIONS
C
      CALL ASTAR(NEX,0)
      CALL VSTAR(NEX,0)
C
C     ENTER ITERATION LOOP, CHECK COUNTER VALUE
C
C
  100 ICOUNT=ICOUNT+1
      IF(ICOUNT.GT.IMAX)GO  TO 200
C
C
C     INITIALIZE FLUIDB VECTOR AND ADJUST TO FIT BOUNDARY CONDITIONS
C
      CALL SETMAT(NEX,1,PEC,IEL,VELMX)
C
      CALL ASTAR(NEX,1)
      CALL VSTAR(NEX,1)
C
C     SOLVE THE FLUID SYSTEM
C
      EP=EPS
      CALL DGBAND(FLUID,FLUIDB,N,LUB,LUB,ICOUNT,IPERM,DET,JEXP,HOLD,
      #RES,ITER,EP)
C
C     DETERMINE THE MAXIMUM CHANGE IN P FROM ONE ITERATION TO THE NEXT
C     AND UPDATE POLD USING A RELAXATION PROCEDURE. PDIFMX WILL BE
C     COMPARED TO TOLP TO ESTABLISH CONVERGENCE
C
      PMAX=0.D0
```

```
          PDIFMX=0.D0
          DO 3 I=1,N
          IF(DABS(FLUIDB(I)).GT.PMAX)  PMAX=DABS(FLUIDB(I))
          TEST=DABS(FLUIDB(I)-POLD(I))
          IF(TEST.GT.PDIFMX)  PDIFMX=TEST
   ·      POLD(I)=(OMEGAF)*(FLUIDB(I)-POLD(I))+POLD(I)
    3     CONTINUE
          PDIFMX=PDIFMX/PMAX
C
C         NOW INITIALIZE SOLUTE AND SOLUTB. STORE MAX. GRID PECLET
C         NUMBER IN PECLET. ADJUST SOLUTE AND SOLUTB TO SUIT BOUNDARY
C         CONDITIONS
C
          CALL SETMAT(NEX,2,PEC,IEL,VELMX)
          PECLET=PEC
          IELE=IEL
          CALL PATART(NEX,0)
          CALL PATVEN(NEX,0)
C
C
C         SOLVE THE SYSTEM OF EQUATIONS FOR THE SOLUTE FLOW EQUATION
C
          EP1=EPS
          CALL DGBND1(SOLUTE,SOLUTB,N,LUB,LUB,1,IPERMS,DET,JEXP,HOLDS,
         #RESS,ITER,EP1)
C
C         DETERMINE THE MAXIMUM CHANGE IN CALCULATED CONCENTRATION FROM
C         ONE ITERATION TO THE NEXT, AND UPDATE COLD USING A RELAXATION
C         PROCEDURE. CDIFMX WILL BE COMPARED TO TOLC TO ESTABLISH
C         CONVERGENCE
C
C
          CMAX=0.D0
          CDIFMX=0.D0
          DO 4 I=1,N
          IF(DABS(SOLUTB(I)).GT.CMAX)  CMAX=DABS(SOLUTB(I))
          TEST=DABS(SOLUTB(I)-COLD(I))
          IF(TEST.GT.CDIFMX)  CDIFMX=TEST
          COLD(I)=(OMEGAC)*(SOLUTB(I)-COLD(I))+COLD(I)
    4     CONTINUE
          CDIFMX=CDIFMX/CMAX
C
C·        CHECK TO SEE IF FURTHER ITERATION IS REQUIRED
C
          IF(PDIFMX.GT.TOLP)  GO TO 100
          IF(CDIFMX.GT.TOLC)  GO TO 100
C
          GO TO 300
C
C         MAXIMUM NUMBER OF ITERATIONS REACHED. PRINT OUT WARNING.
C
  200     ICOUNT=ICOUNT-1
          WRITE(6,600) ICOUNT
  600     FORMAT(//,1X,'WARNING.  CONVERGENCE CRITERIA NOT MET AFTER',
         #1X,I3,1X,'ITERATIONS')
          WRITE(6,601) PDIFMX,CDIFMX
  601     FORMAT(//,1X,'MAXIMUM  FRACTIONAL CHANGE IN P',2X,
         #'MAXIMUM FRACTIONAL CHANGE IN C',//,11X,E9.4,22X,E9.4,//)
C
  300     IF(PECLET.LT.PECMAX)  GO TO 400
          WRITE(6,603) PECLET,IELE
  603     FORMAT(//,'WARNING.  GRID PECLET NUMBER EQUALS',1X,E9.4,3X,
         #'ELEMENT LOCATION:',1X,I4)
C
  400     WRITE(6,604) ICOUNT
  604     FORMAT('1',//,'STEADY-STATE  SOLUTION ACHIEVED AFTER',1X,I3,1X,
         #'ITERATIONS:')
          WRITE(6,670) PECLET,IELE,DISPMX,IDISP
  670     FORMAT(//,1X,'MAXIMUM  GRID PECLET NUMBER:',1X,E9.4,3X,
         #'ELEMENT LOCATION:',1X,I4,/,1X,'MAXIMUM  DISPERSION COEFF:',
```

```
       #1X,E9.4,'   ELEMENT LOCATION:',1X,I4)
        WRITE(6,601)PDIFMX,CDIFMX
        WRITE(6,605)
   605 FORMAT(//,1X,'X POSITION',2X,'DYN. PRESS',2X,'OSM. PRESS',2X,
       #'TOT. PRESS',2X,'AVAIL. CONC.',2X,'TOTAL CONC.',//)
C
        X=0.D0
        DO 5 I=1,N
        X=X+DX(I)
        PI=COLD(I)*(AOSM+COLD(I)*(BOSM+COLD(I)*COSM))
        C1=COLD(I)*PHIA/(1.D0-PHIS)
        PTOT=POLD(I)-PI
C
C       WRITE OUT PROFILE DATA TO DEVICES 6 AND 7
C

        WRITE(6,606)  X,POLD(I),PI,PTOT,COLD(I),C1
        WRITE(7,606)  X,POLD(I),PI,PTOT,COLD(I),C1
   606 FORMAT(1X,E9.3,4(2X,E10.4),3X,E10.4)
     5  CONTINUE
C
C       WRITE OUT MESOTHELIAL FLUX DATA TO DEVICE 7
C
        CALL MASBAL(NEX)
        DO 6 I=1,NEX
        I2=2*I
        X=XNOD(I2)
        WRITE(7,702) X,QFM1(I),QSM1(I),QCM1(I)
   702 FORMAT(4(2X,E10.4))
     6  CONTINUE
C
C
        WRITE(6,607)
   607 FORMAT('1',//,1X,'MASS  BALANCE DATA'///)
C
        WRITE(6,608)
   608 FORMAT(///,1X,'NET  DIMENSIONLESS FLUID FLOWS')
        TF=QFC+QFV+QFM*2.D0
        WRITE(6,609)  QFM,QFC,QFV,TF
   609 FORMAT(//,1X,'MES:',1X,E12.4,/,1X,'CAP:',
       #E12.4,/,1X,'VEN:',1X,E12.4,/,1X,'TOT:',1X,E12.4)
        WRITE(6,661)
   661 FORMAT(///,1X,'NET  DIMENSIONLESS SOLUTE FLOWS')
        TS=QSC+QSV+QSM*2.D0
        WRITE(6,609)QSM,QSC,QSV,TS
        WRITE(6,662)
   662 FORMAT(//,1X,'CONVECTIVE  COMPONENTS OF DIMENSIONLESS SOLUTE
       #FLOWS')
        TC=QCM*2.D0+QCC+QCV
        WRITE(6,610)  QCM,QCC,QCV,TC
   610 FORMAT(//,1X,'MES:',1X,E12.4,/,1X,'CAP:',1X,E12.4,/,1X,'VEN:',
       #1X,E12.4,/,1X,'TOT:',1X,E12.4)
C
        WRITE(6,663)
   663 FORMAT(//,1X,'ERROR  IN GLOBAL MATERIAL BALANCES')
        EFLU=TF/QFC
        ESOL=TS/QSC
        WRITE(6,664) EFLU, ESOL
   664 FORMAT(//,1X,'FLUID  BALANCE:',1X,E12.4,/,1X,'SOLUTE  BALANCE:',
       #1X,E12.4)
C
        WRITE(6,665)
   665 FORMAT(//,1X,'RATIO  OF CONVEC. TO DIFF. FLUXES AT BOUNDARIES')
        PECC=QCC/(QSC-QCC)
        PECV=QCV/(QSV-QCV)
        PECM=QCM/(QSM-QCM)
        WRITE(6,668) PECM,PECC,PECV
```

```
  668  FORMAT(//,1X,'MES:',1X,E12.4,/,1X,'CAP:',1X,E12.4,/,1X,'VEN:',
      #1X,E12.4)
       STOP
       END
       SUBROUTINE MASBAL(NEX)
C
C      THIS SUBROUTINE PERFORMS A MATERIAL BALANCE ON THE SYSTEM FOR
C      BOTH FLUID AND PLASMA PROTEINS.
C
       IMPLICIT REAL*8(A-H,O-Z)
       COMMON/MATBAL/QFC,QCC,QSC,QFV,QCV,QSV,QFM,QCM,QSM,QFM1(500),
      #              QCM1(500),QSM1(500)
       COMMON/OLD/POLD(1001),COLD(1001)
       COMMON/BLK1/NODEL(500,3),XNOD(1001)
       COMMON/OSMOT/A0,B0,C0

       COMMON/TISDAT/AK,DEFF,AL,PHIA,PHIT,RET,SIGT,BETA
       COMMON/CAPDAT/PC,CC
       COMMON/WALL/DLC,DLV,DLM,DDC,DDV,DDM,PDC,PDV,PDM,PIDC,PIDV,PIDM,
      #            SIGC,SIGV,SIGM,CDC,CDV,CDM,DH
       DIMENSION GAUS(4),W(4),B(3)
       DATA NGAUS/4/
       DATA W/.347854845137454D0,.652145154862546D0,
      #.652145154862546D0,.347854845137454D0/
       DATA GAUS/-.861136311594053D0,-.339981043584856D0,
      #.339981043584856D0,.861136311594053D0/
C
C      FIRST, CALCULATE THE NET FLOWS ACROSS THE ARTERIOLAR WALL
C
       PIC=COLD(1)*(A0+COLD(1)*(B0+COLD(1)*C0))
       QFC=DH*AK*PC/DEFF*DLC*(POLD(1)-PDC-SIGC*(PIC-PIDC))
       QCC=BETA*QFC*COLD(1)*RET
       PECC=(1.D0-SIGC)*QFC/(DDC*DH)
       IF(PECC.GT.100.D0)GO TO 110
       IF(PECC.LT.-100.D0)GO TO 120
       TEST=1.D0-DEXP(-PECC)
       IF(DABS(TEST).LT.1.D-10)GO TO 130
       QSC=(1.D0-SIGC)*QFC*(COLD(1)-CDC*DEXP(-PECC))/TEST
       GO TO 200
  110  QSC=QFC*(1.D0-SIGC)*COLD(1)
       GO TO 200
  120  QSC=(1.D0-SIGC)*CDC*QFC
       GO TO 200
  130  QSC=DH*DDC*(COLD(1)-CDC)
C
C      NOW FOR THE VENULAR WALL
C
  200  N=NEX*2+1
       PIV=COLD(N)*(A0+COLD(N)*(B0+COLD(N)*C0))
       QFV=DH*AK*PC/DEFF*DLV*(POLD(N)-PDV-SIGV*(PIV-PIDV))
       QCV=BETA*QFV*COLD(N)*RET
       PECV=(1.D0-SIGV)*QFV/(DDV*DH)
       IF(PECV.GT.100.D0)GO TO 210
       IF(PECV.LT.-100.D0)GO TO 220
       TEST=1.D0-DEXP(-PECV)
       IF(DABS(TEST).LT.1.D-10)GO TO 230
       QSV=(1.D0-SIGV)*QFV*(COLD(N)-CDV*DEXP(-PECV))/TEST
       GO TO 300
  210  QSV=QFV*(1.D0-SIGV)*COLD(N)
       GO TO 300
  220  QSV=(1.D0-SIGV)*CDV*QFV
       GO TO 300
  230  QSV=DH*DDV*(COLD(N)-CDV)
C
C      AND FINALLY, THE MESOTHELIAL LAYER
C
C      CONSIDER THE MESOTHELIAL WALL, ELEMENT BY ELEMENT.
C
  300  QSM=0.D0
```

```
      QCM=0.D0
      QFM=0.D0

C
      DO 400 I=1,NEX
      QSM1(I)=0.D0
      QFM1(I)=0.D0
      QCM1(I)=0.D0
 400  CONTINUE
C
      DO 1 II=1,NGAUS
      S=GAUS(II)
          DO 2 I=1,NEX
          X1=XNOD(NODEL(I,1))
          X2=XNOD(NODEL(I,2))
          X3=XNOD(NODEL(I,3))
          S2=(2.D0*X2-(X1+X3))/(X3-X1)
C
          B(1)=(S-S2)*(S-1.D0)/(2.D0*(S2+1.D0))
          B(2)=(S+1.D0)*(S-1.D0)/(S2*S2-1.D0)
          B(3)=(S+1.D0)*(S-S2)/(2.D0*(1.D0-S2))
          DX=(X3-X1)*.5D0
C
C     CALCULATE C(S), PI(S), AND P(S)
C
          CS=0.D0
          PS=0.D0
          DO 3 IT=1,3
          CS=CS+COLD(NODEL(I,IT))*B(IT)
          PS=PS+POLD(NODEL(I,IT))*B(IT)
 3        CONTINUE
          PIS=CS*(A0+CS*(B0+CS*C0))
C
C     CALCULATE THE FLUXES
C
          FLOW=AK*PC/DEFF*DLM*(PS-PDM-SIGM*(PIS-PIDM))*W(II)*DX
          QFM=QFM+FLOW
          QFM1(I)=QFM1(I)+FLOW/(X3-X1)
          QCM=QCM+FLOW*CS*BETA*RET
          QCM1(I)=QCM1(I)+FLOW*CS*BETA/(X3-X1)*RET
C
C     DETERMINE WHICH FORM OF THE NONLINEAR FLUX EQN. IS TO BE USED.
C
          QS=FLOW/(W(II)*DX)
          PECM=QS*(1.D0-SIGM)/DDM
          IF(PECM.GT.100.D0)GO TO 410

          IF(PECM.LT.-100.D0)GO TO 420
          TESTM=1.D0-DEXP(-PECM)
          IF(DABS(TESTM).LT.1.D-10)GO TO 430
C
C     USE THE FULL EXPRESSION
C
          SFLOW=FLOW*(1.D0-SIGM)*(CS-CDM*DEXP(-PECM))/TESTM
          QSM=QSM+SFLOW
          QSM1(I)=QSM1(I)+SFLOW/(X3-X1)
          GO TO 2
C
  410     SFLOW=FLOW*(1.D0-SIGM)*CS
          QSM=QSM+SFLOW
          QSM1(I)=QSM1(I)+SFLOW/(X3-X1)
          GO TO 2
C
  420     SFLOW=FLOW*(1.D0-SIGM)*CDM
          QSM=QSM+SFLOW
          QSM1(I)=QSM1(I)+SFLOW/(X3-X1)
          GO TO 2
C
  430     SFLOW=DDM*(CS-CDM)*DX*W(II)
```

```
            QSM=QSM+SFLOW
            QSM1(I)=QSM1(I)+SFLOW/(X3-X1)
   2        CONTINUE
   1     CONTINUE
         RETURN
         END

         SUBROUTINE GRID(NEX)
C
C        THIS SUBROUTINE CALCULATES THE SPATIAL LOCATION OF THE NODES
C        FOR EACH ELEMENT, ALONG WITH THE NODES ASSOCIATED WITH A
C        GIVEN ELEMENT.
C
         IMPLICIT REAL*8(A-H,O-Z)
         COMMON/BLK1/NODEL(500,3),  XNOD(1001)
         COMMON/BLK2/DX(1001)
C
         K=1
         DO 1 I=1,NEX
         NODEL(I,1)=K
         NODEL(I,2)=K+1
         NODEL(I,3)=K+2
         K=K+2
   1     CONTINUE
C
         X=0.D0
         NP=2*NEX+1
         DO 2 I=1,NP
         X=X+DX(I)
         XNOD(I)=X
   2     CONTINUE
         RETURN
         END
C
         SUBROUTINE VSTAR(NEX,IND)
C
C        THIS SUBROUTINE ADJUSTS THE AF AND BF VECTORS TO ACCOUNT FOR THE
C        STARLING BOUNDARY CONDITION AT THE VENULAR WALL.
C
         IMPLICIT REAL*8(A-H,O-Z)
         COMMON/BLK1/NODEL(500,3),  XNOD(1001)
         COMMON/FLUMAT/AF(20000)
         COMMON/FLUB/BF(1001)
         COMMON/OLD/POLD(1001),COLD(1001)
         COMMON/WALL/DLC,DLV,DLM,DDC,DDV,DDM,PDC,PDV,PDM,PIDC,PIDV,PIDM,
        #          SIGC,SIGV,SIGM,CDC,CDV,CDM,DE
         COMMON/OSMOT/A0,B0,C0
C
         M=NEX*2+1
         LUB=2
         LP=3*LUB
         IF(IND.EQ.1)GO TO 100
         K=LP*M+M-LUB
         AF(K)=AF(K)+ DLV
         GO TO 900
C
  100    PI=COLD(M)*(A0+COLD(M)*(B0+COLD(M)*C0))
         BF(M)=BF(M)+DLV*(PDV+SIGV*(PI-PIDV))
C
  900    RETURN
         END
         SUBROUTINE ASTAR(NEX,IND)
C
C        THIS SUBROUTINE ADJUSTS THE AF AND BF VECTORS TO ACCOUNT FOR THE
C        STARLING BOUNDARY CONDITION AT THE ARTERIOLAR WALL.
C
         IMPLICIT REAL*8(A-H,O-Z)
         COMMON/BLK1/NODEL(500,3),  XNOD(1001)
         COMMON/FLUMAT/AF(20000)
         COMMON/FLUB/BF(1001)
```

```
      COMMON/OLD/POLD(1001),COLD(1001)
      COMMON/WALL/DLC,DLV,DLM,DDC,DDV,DDM,PDC,PDV,PDM,PIDC,PIDV,PIDM,
     #          SIGC,SIGV,SIGM,CDC,CDV,CDM,DH
      COMMON/OSMOT/A0,B0,C0
C
      LUB=2
      LP=3*LUB
C
      IF(IND.EQ.1)GO TO 100
      K=LP+1-LUB
      AF(K)=AF(K)+ DLC
      GO TO 900
C
 100  PI=COLD(1)*(A0+COLD(1)*(B0+COLD(1)*C0))
      BF(1)=BF(1)+DLC*(PDC+SIGC*(PI-PIDC))
C
 900  RETURN
      END


      SUBROUTINE PATART(NEX,IND)
C
C     THIS SUBROUTINE ADJUSTS THE AS AND BS VECTORS TO ACCOUNT FOR THE
C     PATLAK BOUNDARY CONDITION AT THE ARTERIOLAR WALL.
C
      IMPLICIT REAL*8(A-H,O-Z)
      COMMON/BLK1/NODEL(500,3),  XNOD(1001)
      COMMON/SOLMAT/AS(20000)
      COMMON/SOLB/BS(1001)
      COMMON/OLD/POLD(1001),COLD(1001)
      COMMON/TISDAT/AK,DEFF,AL,PHIA,PHIT,RET,SIGT,BETA
      COMMON/CAPDAT/PC,CC
      COMMON/WALL/DLC,DLV,DLM,DDC,DDV,DDM,PDC,PDV,PDM,PIDC,PIDV,PIDM,
     #          SIGC,SIGV,SIGM,CDC,CDV,CDM,DH
      COMMON/OSMOT/A0,B0,C0
C
      LUB=2
      LP=3*LUB
      K=LP+1-LUB
C
      PI=COLD(1)*(A0+COLD(1)*(B0+COLD(1)*C0))
      QART=AK*PC/DEFF*DLC*(POLD(1)-PDC-SIGC*(PI-PIDC))
      PEC=(1.D0-SIGC)/DDC*QART
C
C     DETERMINE WHICH FORM OF THE FLUX EXPRESSION APPLIES
C
      IF(PEC.GT.100.0D0)GO TO 100
      IF(PEC.LT.-100.D0)GO TO 200
      TEST=1.D0-DEXP(-PEC)
      IF(DABS(TEST).LT.1.D-10)GO TO 300
C
      AS(K)=AS(K)-QART*(RET*BETA-(1.D0-SIGC)/TEST)
      BS(1)=BS(1)+(1.D0-SIGC)*QART*CDC*DEXP(-PEC)/TEST
      GO TO 900
C
 100  AS(K)=AS(K)-QART*(BETA*RET-(1.D0-SIGC))
      GO TO 900
C
 200  AS(K)=AS(K)-QART*BETA*RET
      BS(1)=BS(1)-(1.D0-SIGC)*QART*CDC
      GO TO 900
C
 300  AS(K)=AS(K)-QART*BETA*RET+DDC
      BS(1)=BS(1)+DDC*CDC
 900  RETURN
      END
      SUBROUTINE PATVEN(NEX,IND)
C
C     THIS SUBROUTINE ADJUSTS THE AS AND BS VECTORS TO ACCOUNT FOR THE
C     PATLAK BOUNDARY CONDITION AT THE VENULAR WALL.
C
```

```
      IMPLICIT REAL*8(A-H,O-Z)
      COMMON/BLK1/NODEL(500,3),  XNOD(1001)
      COMMON/SOLMAT/AS(20000)
      COMMON/SOLB/BS(1001)
      COMMON/OLD/POLD(1001),COLD(1001)
      COMMON/TISDAT/AK,DEFF,AL,PHIA,PHIT,RET,SIGT,BETA
      COMMON/CAPDAT/PC,CC
      COMMON/WALL/DLC,DLV,DLM,DDC,DDV,DDM,PDC,PDV,PDM,PIDC,PIDV,PIDM,
     #            SIGC,SIGV,SIGM,CDC,CDV,CDM,DH
      COMMON/OSMOT/A0,B0,C0
C
      LUB=2
      LP=3*LUB
      NP=2*NEX+1
      K=LP*NP+NP-LUB
C
      PI=COLD(NP)*(A0+COLD(NP)*(B0+COLD(NP)*C0))
      QART=AK*PC/DEFF*DLV*(POLD(NP)-PDV-SIGV*(PI-PIDV))
      PEC=(1.D0-SIGV)/DDV*QART
C
C     DETERMINE WHICH FORM OF THE FLUX EXPRESSION APPLIES
C
      IF(PEC.GT.100.0D0)GO  TO 100
      IF(PEC.LT.-100.D0)GO  TO 200
      TEST=1.D0-DEXP(-PEC)
      IF(DABS(TEST).LT.1.D-10)GO  TO 300
C
      AS(K)=AS(K)-QART*(RET*BETA-(1.D0-SIGV)/TEST)
      BS(NP)=BS(NP)+(1.D0-SIGV)*QART*CDV*DEXP(-PEC)/TEST
      GO TO 900
C
  100 AS(K)=AS(K)-QART*(BETA*RET-(1.D0-SIGV))
      GO TO 900
C
  200 AS(K)=AS(K)-QART*BETA*RET
      BS(NP)=BS(NP)-(1.D0-SIGV)*QART*CDV
      GO TO 900

C
  300 AS(K)=AS(K)-QART*BETA*RET+DDV
      BS(NP)=BS(NP)+DDV*CDV
  900 RETURN
      END


      SUBROUTINE MATPLY(A,A1,B,C,NP)
C
C     THIS SUBROUTINE MULTIPLIES A MATRIX A BY A VECTOR B AND SCALAR A1
C     TO GIVE  VECTOR C. MATRIX A IS STORED AS A VECTOR, WHERE MATRIX
C     ELEMENT A(I,J) IS STORED AS A(IJ), IJ=3*LUB*J+I-LUB,  AND WHERE
C     LUB IS THE NUMBER OF OFF DIAGONAL BANDS. FOR THIS SUBROUTINE,
C     IT IS ASSUMED THAT THE BANDWIDTH IS 5, SO THAT LUB=2.
C
      IMPLICIT REAL*8(A-H,O-Z)
      DIMENSION A(20000), B(NP), C(NP)
      LUB=2
      LP=3*LUB
C
      DO 1 I=1,NP
      C(I)=0.D0
    1 CONTINUE
C
      K=2
      DO 2 I=1,2
      K=K+1
          DO 3 J=1,K
          IJ=LP*J+I-LUB
          C(I)=C(I)+A(IJ)*A1*B(J)
    3     CONTINUE
    2 CONTINUE
```

```
C       ZERO THE AF VECTOR
C
        DO 700 I=1,20000
        AF(I)=0.D0
 700    CONTINUE
        .GO TO 100
C
C       ZERO THE BF VECTOR
C
 800    DO 801 I=1,1001
        BF(I)=0.D0
 801    CONTINUE
        GO TO 100
C
C       ZERO THE T MATRIX
C
 950    DO 951 I=1,20000
        T(I)=0.D0
 951    CONTINUE
        GO TO 100
C
C       ZERO THE AS AND BS VECTORS
C
 900    DO 901 I=1,20000
        AS(I)=0.D0
 901    CONTINUE
C
        DO 902 I=1,1001
        BS(I)=0.D0
 902    CONTINUE
C
C       BEGIN THE GAUSS INTEGRATION, ELEMENT BY ELEMENT
C
 100    LUB=2
        LP=3*LUB
C
C       EVALUATE THE INTEGRAND AT THE APPROPRIATE QUADRATURE POINT, S.
C
        DO 200 II=1,NGAUS
        S=GAUS(II)
C
C       INITIALIZE THE APPROPRIATE ARRAY, ELEMENT BY ELEMENT.
C
        DO 300 I=1,NEX
C
C       CALCULATE VALUE OF BASIS FUNCTIONS AND DERIVATIVES AT THE
C       QUADRATURE POINT
C
        X1=XNOD(NODEL(I,1))
        X2=XNOD(NODEL(I,2))
        X3=XNOD(NODEL(I,3))
C
        S2=(2.D0*X2-(X1+X3))/(X3-X1)
C
        B(1)=(S-S2)*(S-1.D0)/(2.D0*(S2+1.D0))
        B(2)=(S+1.D0)*(S-1.D0)/(S2*S2-1.D0)
        B(3)=(S+1.D0)*(S-S2)/(2.D0*(1.D0-S2))
        DB(1)=(2.D0*S-S2-1.D0)/(2.D0*(S2+1.D0))
        DB(2)=2.D0*S/(S2*S2-1.D0)
        DB(3)=(2.D0*S-S2+1.D0)/(2.D0*(1.D0-S2))
C
        DX=(X3-X1)*.5D0
C
C       CALCULATE THE T VECTOR
C
        IF(IND.NE.3) GO TO 101
        DO 952 M=1,3
        MM=NODEL(I,M)
           DO 953 N=1,3
           NN=NODEL(I,N)
```

```
            K=LP*NN+MM-LUB
            T(K)=T(K)+PHIA*B(M)*B(N)*DX*W(II)
  953       CONTINUE
  952 CONTINUE
      GO TO 300
C
C     NOW CALCULATE C(S), DC/DS, PI(S), DPI/DS
C
  101 CS=0.D0
      DCS=0.D0
      DO 301 IT=1,3
      CS=CS+COLD(NODEL(I,IT))*B(IT)
      DCS=DCS+COLD(NODEL(I,IT))*DB(IT)
  301 CONTINUE
C
      PIS=CS*(A0+CS*(B0+CS*C0))
      DPIS=(A0+2.D0*B0*CS+3.D0*CS*CS*C0)*DCS
C
C     DETERMINE WHICH VECTOR IS TO BE INITIALIZED
C
      IF(IND.EQ.1)GO TO 500
      IF(IND.EQ.2)GO TO 600
C
C     INITIALIZE THE FLUID VECTOR
C
      DO 401 M=1,3
      MM=NODEL(I,M)
          DO 402 N=1,3
          NN=NODEL(I,N)

          K=LP*NN+MM-LUB
          AF(K)=AF(K)+(B(M)*B(N)*2.D0*DLM/DH*DX+DB(M)*DB(N)/DX)*W(II)
  402     CONTINUE
  401 CONTINUE
      GO TO 300


C
C     INITIALIZE THE FLUID B VECTOR
C
  500 DO 501 M=1,3
      MM=NODEL(I,M)
    . BF(MM)=BF(MM)+(DB(M)*DPIS/DX+B(M)*2.D0*DLM/DH*DX*(PDM+SIGM*
     #    (PIS - PIDM)))*W(II)
  501 CONTINUE
      GO TO 300
C
C     INITIALIZE THE SOLUTE VECTORS, BS AND AS. fIRST CALCULATE VS,
C     QMES, AND THE DISPERSION COEFFICIENT, DISP.
C
  600 DPS=0.D0
      PS=0.D0
      DO 601 IT=1,3
      DPS=DPS+POLD(NODEL(I,IT))*DB(IT)
      PS=PS+POLD(NODEL(I,IT))*B(IT)
  601 CONTINUE
C
      VS=-ALPHA*(DPS-SIGT*DPIS)/DX*RET*BETA/PHIA
      QFMES=ALPHA*DLM*(PS-PDM-SIGM*(PIS-PIDM))
      DISP=DABS(VS)*AL+1.D0
      IF(DISP.LT.DISPMX)  GO TO 650
      DISPMX=DISP
      IDISP=I
C
C     CALCULATE THE MAXIMUM LOCAL SOLUTE VELOCITY, VELMAX
C
  650   IF(DABS(CS).LT.1.D-5)  VELS=DABS(VS)*PHIA
        IF(DABS(CS).GT.1.D-5)  VELS=DABS(VS-(DISP*DCS/DX)/CS)*PHIA
        IF(.5D0*VELS/DX.GT.VELMAX)  VELMAX=.5D0*VELS/DX
C
C     CALCULATE THE GRID PECLET NUMBER, AND SEE IF IT EXCEEDS
```

```
C       THE LIMIT
C
        PEST=DABS(PHIA*VS)*(X3-X1)/DISP
        IF(PEST.LT.PE)GO TO 609
        PE=PEST
        IPEC=I
C
C       NOW DETERMINE WHICH FORM OF THE NONLINEAR FLUX EXPRESSION
C       IS TO BE USED TO CALCULATE SOLUTE FLUX ACROSS MESOTHELIUM.
C
 609    PEC=QFMES*(1.D0-SIGM)/DDM
        IF(PEC.GT.100.D0)GO TO 610
        IF(PEC.LT.-100.D0)GO TO 620
        TEST=1.D0-DEXP(-PEC)
        IF(DABS(TEST).LT.1.D-10)GO TO 630
C
C       CASE 1: USE THE FULL NONLINEAR FLUX EXPRESSION
C
        DO 602 M=1,3
        MM=NODEL(I,M)
                DO 603 N=1,3
                NN=NODEL(I,N)
                K=LP*NN+MM-LUB
                AS(K)=AS(K)+(B(M)*DB(N)*VS*PHIA+DB(M)*DB(N)*DISP*PHIA/DX
     #                +B(M)*B(N)*2.D0*QFMES/TEST/DH*(1.D0-SIGM)*DX
     #                -2.D0/DH*QFMES*RET*BETA*B(M)*B(N)*DX)*W(II)
 603            CONTINUE
        BS(MM)=BS(MM)+B(M)*2.D0/DH*(1.D0-SIGM)*QFMES*CDM*DEXP(-PEC)/TEST
     #          *DX*W(II)
 602    CONTINUE
        GO TO 300
C
C       CASE 2: PEC APPROACHES INFINITY
C
 610    DO 611 M=1,3
        MM=NODEL(I,M)
                DO 612 N=1,3
                NN=NODEL(I,N)
                K=LP*NN+MM-LUB
                AS(K)=AS(K)+(B(M)*DB(N)*VS*PHIA+DB(M)*DB(N)*PHIA*DISP/DX
     #                +B(M)*B(N)*2.D0/DH*(1.D0-SIGM)*QFMES*DX
     #                -QFMES*RET*BETA*B(M)*B(N)*DX*2.D0/DE)*W(II)
 612            CONTINUE
 611    CONTINUE
        GO TO 300
C
C       CASE 3: -PEC APPROACHES INFINITY
C
 620    DO 621 M=1,3
        MM=NODEL(I,M)
                DO 622 N=1,3
                NN=NODEL(I,N)
                K=LP*NN+MM-LUB
                AS(K)=AS(K)+(B(M)*DB(N)*VS*PHIA+DB(M)*DB(H)*PHIA*DISP/DX
     #                -2.D0/DH*BETA*RET*QFMES*B(N)*B(M)*DX)*W(II)
 622            CONTINUE
        BS(MM)=BS(MM)-2.D0/DH*(1.D0-SIGM)*QFMES*CDM*DX*W(II)*B(M)
 621    CONTINUE
        GO TO 300


C
C       CASE 4: PEC APPROACHES 0
C
 630    DO 631 M=1,3
        MM=NODEL(I,M)
                DO 632 N=1,3
                NN=NODEL(I,N)
                K=LP*NN+MM-LUB
                AS(K)=AS(K)+(B(M)*DB(N)*VS*PHIA+DB(M)*DB(H)*PHIA*DISP/DX
     #                +2.D0/DH*DDM*B(M)*B(N)*DX
```

```
     #                  -2.D0/DH*RET*BETA*DX*B(M)*B(N)*QFMES)*W(II)
 632 CONTINUE
     BS(MM)=BS(MM)+2.D0/DH*DDM*B(M)*CDM*DX*W(II)
 631 CONTINUE
C
 300 CONTINUE
 200 CONTINUE
     RETURN
     END


C
     SUBROUTINE DGBND1 (A, B, N, ML, NU, LT, IP, DET, NCN1,
    1                   BB, RZ, ITR1, EPS1)
C
C ROUTINE SOLVES SYSTEM OF LINEAR EQNS. AX=B WHERE A IS A GENERAL
C BAND MATRIX. METHOD USED IS GAUSSIAN ELIMINATION WITH PARTIAL
C PIVOTING. OPTION OF ITERATIVELY IMPROVING SOLUTION IS AVAILABLE.
C UPPER BAND WIDTH OF MATRIX INCREASES DUE TO INTERCHANGES BY
C AMOUNT ML. ROUTINE REQUIRES BAND ELEMENTS OF MATRIX TO BE STORED
C BY COLUMN IN A ONE DIMENSIONAL ARRAY. EACH COLUMN IS OF LENGTH
C 2*ML+NU AND BAND IS TO BE STORED IN ELEMENTS ML+1 TO 2*ML+NU OF
C EACH COLUMN. ELEMENTS 1 TO ML OF COLUMN ARE SET TO ZERO BY GBAND.
C IF MATRIX IS SYMMETRIC USER MAY SPECIFY LOWER BAND ONLY IN
C ELEMENTS ML+NU+1 TO 2*ML+NU OF EACH COLUMN AND GBAND WILL
C GENERATE REMAINING ELEMENTS. (IF THIS IS DESIRED, SET LT=-1 ON
C FIRST CALL TO GBAND.)
C  A = 1 DIMENSIONAL ARRAY CONTAINING MATRIX OF COEFFICIENTS.
C  B = 1 DIMENSIONAL ARRAY CONTAINING RIGHT HAND SIDE VECTORS.
C        ON EXIT, B WILL CONTAIN THE SOLUTION VECTOR X.
C  N = ORDER OF MATRIX
C ML = LENGTH OF LOWER BAND (EXCLUDING DIAGONAL)
C NU = LENGTH OF UPPER BAND (EXCLUDING DIAGONAL)
C LT = ABS(LT)=1 IF ONLY 1 B VECTOR OR IF 1ST OF SEVERAL.
C        ABS(LT),=1 FOR SUBSEQUENT B VECTORS.
C        (NOTE. LT=+1 IF FULL BAND WIDTH GIVEN, LT=-1 IF LOWER BAND
C        ONLY OF SYMMETRIC MATRIX GIVEN.)
C IP = INTEGER ARRAY CONTAINING INTERCHANGE INFORMATION.
C DET = DETERMINANT OF A = DET*(10**NCN) WHERE 1.D-15<|DET|<1.D+15.
C        IF DET=0.0 MATRIX IS SINGULAR AND ERROR RETURN TAKEN.
C BB, RZ = ARRAYS REQUIRED FOR IMPROVEMENT OPTION. CAN BE REAL*8
C        VARIABLES IF OPTION NOT REQUIRED.
C  ITER  = 0 IF IMPROVEMENT NOT REQUIRED, OTHERWISE ITER= NO. OF
C        ITERATIONS OR CYCLES.
C EPS - CONVERGENCE CRITERION.
C
C MODIFIED TO DO ITERATIVE IMPROVEMENT (FORMERLY AVAILABLE ONLY
C WITH THE SINGLE PRECISION VERSION).  MIKE PATTERSON - NOV, 1980
     IMPLICIT REAL*8 (A-H, O-Z)
     COMMON /GBAND$/ NITER
     DIMENSION A(1), B(N), IP(N), BB(N), RZ(N)
     COMPLEX*16 DSUMM, QADDQ, QMULD
     REAL*8 QRNDQ
C TO ASSIGN LOGICAL UNITS 94 AND 95 ONLY ONCE:
     LOGICAL ASSIGN /F/, YES /T/
C STATEMENT FUNCTION TO CALCULATE POINTERS INTO A:
     IFN(I, J) = 1 + (J - 1)*LC + I - J + NUM
C
C
     NCN=NCN1
     ITR=ITR1
     EPS=EPS1
     ITER = ITR
C
     LCM = NU + 2*ML
     LC = LCM + 1
     NLC = N*LC
     NUM = NU + ML
C  GENERATE REMAINING ELEMENTS OF SYMMETRIC MATRIX
     IF (LT .NE. -1) GO TO 120
     NN = N - 1
     DO 110 I = 1, NN
```

```
              IFI = IFN(I, I)
              IFJ = IFI
              II = I + 1
              IML = MINO(I + ML, N)
              DO 100 J = II, IML
                 IFI = IFI + 1
                 IFJ = IFJ + LCM
100           A(IFJ) = A(IFI)
110        CONTINUE
120        IF (ITER .EQ. 0) GO TO 140
C ASSIGN UNITS 94 AND 95 IF THEY HAVE NOT ALREADY BEEN ASSIGNED:
           IF (ASSIGN) GO TO 125
           CALL FTNCMD ('ASSIGN 94=-GBAND94;')
           CALL FTNCMD ('ASSIGN 95=-GBAND95;')
           ASSIGN = YES
125        REWIND 94
           REWIND 95
           DO 130 I = 1, N

130        BB(I) = B(I)
140        IF (IABS(LT) .NE. 1) GO TO 280
           IP(N) = 1
           IF (ML .EQ. 0) GO TO 160
C   SET ELEMENTS 1 - ML OF EACH COLUMN TO ZERO
           DO 150 I = 1, N
              IFK = (I - 1)*LC
              DO 150 J = 1, ML
                 IFK = IFK + 1
150        A(IFK) = 0.0D0
160        IF (ITER .NE. 0) CALL DWR1 (A, NLC, 94)
           DET = 0.0D0
           NCN = 0
           IF (ML .EQ. 0) GO TO 230
C   LU DECOMPOSITION
           DO 220 K = 1, N
              IFK = IFN(K, K)
              IF (K .EQ. N) GO TO 210
              KP = K + 1
              KPM = MINO(K + ML, N)
              KPN = MINO(K + NUM, N)
              M = K
              IFM = IFK
              IFI = IFK
              DO 170 I = KP, KPM
                 IFI = IFI + 1
                 IF (DABS(A(IFI)) .LE. DABS(A(IFM))) GO TO 170
                 M = I
                 IFM = IFI
170           CONTINUE
              IP(K) = M
              T = A(IFM)
              IF (M .NE. K) IP(N) = -IP(N)
              A(IFM) = A(IFK)
              A(IFK) = T
              IF (T .EQ. 0.0D0) GO TO 260
              OT = 1.0D0/T
              IK = IFK
              DO 180 I = KP, KPM
                 IK = IK + 1
180           A(IK) = -A(IK)*OT
              KJ = IFK
              MJ = IFM
              DO 200 J = KP, KPN
                 KJ = KJ + LCM
                 MJ = MJ + LCM
                 T = A(MJ)
                 A(MJ) = A(KJ)
                 A(KJ) = T
                 IF (T .EQ. 0.0D0) GO TO 200
                 IK = IFK
                 IJ = KJ
```

```
            DO 190 I = KP, KPM
               IK = IK + 1
               IJ = IJ + 1
190            A(IJ) = A(IJ) + A(IK)*T
200         CONTINUE
210         IF (A(IFK) .EQ. 0.0D0) GO TO 260
220      CONTINUE
230  .   IFK = IFN(1, 1)
         DET = A(IFK)
         DO 250 K = 2, N
            IFK = IFK + LC
            DET = DET*A(IFK)
            IF (DET .EQ. 0.0D0) GO TO 260
            IF (DABS(DET) .GT. 1.D-15) GO TO 240
            DET = DET*1.D+15
            NCN = NCN - 15
            GO TO 250
240         IF (DABS(DET) .LT. 1.D+15) GO TO 250
            DET = DET*1.D-15
            NCN = NCN + 15
250      CONTINUE
         DET = DET*IP(N)
         GO TO 280
260      DET = 0.0D0
         WRITE (6, 270) K
270      FORMAT ('0* DGBND1 - matrix is singular. '/
        1      '    Error occurred in attempt to find', I5, 'th pivot.')
         RETURN

280      CALL DSOLV1 (A, B, IP, N, ML, NU)
         IF (ITER .EQ. 0) RETURN
C
C     ITERATIVE IMPROVEMENT
C     RESIDUALS (R) = AX-B ARE FOUND AND STORED IN ARRAY RZ USING
C     EXTENDED PRECISION ARITHMETIC. SYSTEM AZ=R IS SOLVED AND NEW
C     SOLUTION =X+Z IS STORED IN ARRAY B. ABOVE STEPS REPEATED UNTIL
C        (1) MAX(Z)/MAX(X) < EPS OR
C        (2) NO. OF CYCLES > ITER OR
C        (3) IMPROVEMENT STARTS TO DIVERGE.
C     ROUTINE THEN RETURNS AFTER SETTING EPS=MAX(Z) (FOR (1)) OR
C     SETTING EPS=-MAX(Z) AND PRINTING APPROPRIATE ERROR MESSAGE (FOR
C.    (2) AND (3))
C
C
         IF (IABS(LT) .EQ. 1) CALL DWR1 (A, NLC, 95)
         XNORM = 0.0D0
         DO 290 K = 1, N

290      XNORM = DMAX1(XNORM, DABS(B(K)))
         IF (XNORM .LE. 0.0D0) RETURN
         ZX = 1.D+60
         LD = 0
         DO 340 L = 1, ITER
            REWIND 94
            CALL DRE1 (A, NLC, 94)
            DO 310 K = 1, N
               DSUMM = (0.D0, 0.D0)
               KPM = MAXO(K - ML, 1)
               KPN = MINO(K + NU, N)
               IFK = IFN(K, KPM)
               DO 300 J = KPM, KPN
C              DSUMM = DSUMM + A(IFK)*B(J)
C USING EXTENDED PRECISION:
               DSUMM = QADDQ(DSUMM, QMULD(A(IFK), B(J)))
300            IFK = IFK + LCM
               RZ(K) = BB(K) - QRNDQ(DSUMM)
310         CONTINUE
            REWIND 95
            CALL DRE1 (A, NLC, 95)
```

```
            CALL DSOLV1 (A, RZ, IP, N, ML, NU)
            ZNORM = 0.0D0
            DO 320 K = 1, N
               ERZ = RZ(K)
               ZNORM = DMAX1(ZNORM, DABS(ERZ))
320         B(K) = B(K) + ERZ
            IF (ZNORM .GT. ZX) GO TO 330
            IF ((ZNORM - EPS*XNORM) .LT. 0.0D0) GO TO 390
            ZX = ZNORM
            GO TO 340
330         IF (ZNORM .GT. 10.0D0*ZX) GO TO 360
            LD = LD + 1
            IF (LD .GE. 3) GO TO 360
340      CONTINUE
         L = ITER
         WRITE (6, 350)
350      FORMAT ('0* DGBND1- Iterative improvement did not converge'/)
         GO TO 380
360      WRITE (6, 370)
370      FORMAT ('0* DGBND1 - Iterative improvement is diverging.'/)
380      EPS = -ZNORM
         NITER = L
         RETURN
390      EPS = ZNORM
         NITER = L
         RETURN
         END
         SUBROUTINE DSOLV1 (A, B, IP, N, ML, NU)
C
C   THIS ROUTINE COMPUTES THE SOLUTION OF A SYSTEM AFTER GBAND HAS
C   DECOMPOSED MATRIX A INTO A LOWER TRIANGULAR MATRIX L AND AN
C   UPPER TRIANGULAR MATRIX U.
C
         IMPLICIT REAL*8 (A-H, O-Z)
         DIMENSION A(1), B(N), IP(N)
         IFN(I, J) = 1 + (J - 1)*LC + I - J + NUM
         LCM = 2*ML + NU
         LC = LCM + 1
         NUM = NU + ML
         MN = N - 1
C   SOLVE FOR Y
         IF (ML .EQ. 0) GO TO 110
         DO 100 K = 1, MN
            KP = K + 1
            M = IP(K)
            T = B(M)
            B(M) = B(K)
            B(K) = T
            KPM = MINO(K + ML, N)
            IFK = IFN(K, K)
            DO 100 I = KP, KPM
               IFK = IFK + 1
100         B(I) = B(I) + A(IFK)*T
C   SOLVE FOR X
110      IFK = IFN(N, N)
         DO 120 KB = 1, MN
            KM = N - KB
            K = KM + 1
            B(K) = B(K)/A(IFK)
            IFK = IFK - LC
            T = -B(K)
            KMN = MAXO(1, K - ML - NU)
            KML = IFN(KMN, K)
            DO 120 I = KMN, KM
               B(I) = B(I) + A(KML)*T
120         KML = KML + 1
         B(1) = B(1)/A(NUM + 1)
         RETURN
         END
         SUBROUTINE DWR1 (A, N, LU)
```

```
      REAL*8 A(N)
      WRITE (LU) A
      RETURN
      END
      SUBROUTINE DRE1 (A, N, LU)
      REAL*8 A(N)
      READ (LU) A
      RETURN
      END
```

D.4   One-Dimensional Transient Simulator: TRANS.FOR

```
C
C     THIS ROTUINE CALCULATES THE TRANSIENT PRESSURE AND CONCENTRATION
C     PROFILE WITHIN MESENTERIC TISSUE. THE TISSUE IS APPROXIMATED
C     BY A ONE-DIMENSIONAL SLAB.
C
      IMPLICIT REAL*8(A-H,O-Z)
      INTEGER ELPEC
      DIMENSION HOLD(1001),IPERM(1001),RES(1001),HOLD1(1000),
     #RES1(1001),IPERM1(1001),TDT(20000),COLDT(1001),DTIME1(100),
     #SBOLDT(1001),SOLDT(20000),BCTIME(1001),STNEW(20000),
     #TCOLDT(1001),SCOLDT(1001)
      COMMON/BLK1/NODEL(500,3),XNOD(1001)
      COMMON/BLK2/DX(1001)
      COMMON/MATBAL/QFC,QCC,QSC,QFV,QCV,QSV,QFM,QCM,QSM,QFM1(500),
     #              QCM1(500),QSM1(500)
      COMMON/FLUMAT/FLUID(20000)
      COMMON/OLD/POLD(1001),COLD(1001)
      COMMON/SOLB/SOLUTB(1001)
      COMMON/FLUB/FLUIDB(1001)
      COMMON/TIME/ T(20000)
      COMMON/FMAX/FLUXMX
      COMMON/SOLMAT/SOLUTE(20000)
      COMMON/OSMOT/AOSM,BOSM,COSM
      COMMON/TISDAT/AK,DEFF,ALPHL,PHIA,PHIT,RET,SIGT,BETA
      COMMON/CAPDAT/PREF,CREF
      COMMON/WALL/DLC,DLV,DLM,DDC,DDV,DDM,PDC,PDV,PDM,PIDC,PIDV,PIDM,
     #SIGC,SIGV,SIGM,CDC,CDV,CDM,YYL
      COMMON/MAXDAT/DISPMX,IDISP
C
C     SET MARKER AND TOLERANCE VALUES
C
      READ(5,504)OMEGAF,OMEGAC,TOLP,TOLC,PECMAX,EPS
      READ(5,507)IMAX,ITER,NECHO,NP,ITMAX
      READ(5,504) THETA,TTOL,COUR,BETA,TFACT,TIMMAX
      READ(5,508) K
      DO 60 I=1,K
      READ(5,501) DTIME1(I)
60    CONTINUE
C
      KK=2
      NEX=(NP-1)/2
      LUB=2
      NDIM=NP*(3*LUB+1)
C
C     READ IN THE DATA FROM EXTERNAL FILE
C
      DO 1 I=1,NP
      READ(5,501) DX(I)
1     CONTINUE
C
C
      READ(5,502) AOSM,BOSM,COSM,AK,PREF,PHIA,PHIT,RET,PHIS
      READ(5,504) ALPHL,AL,DEFF,SIGT,CREF,YYL
      READ(5,504) CONC,CONV,CONM,PERMC,PERMV,PERMM
```

```
      READ(5,504)  DDC,DDV,DDM,SIGC,SIGV,SIGM
      READ(5,504)  CDC,CDV,CDM,DLC,DLV,DLM
      READ(5,506)  PDC,PDV,PDM
      READ(5,506)  AOS1,BOS1,COS1
      YL=YYL*AL
      PIDC=CDC*(AOS1+CDC*(BOS1+CDC*COS1))
      PIDV=CDV*(AOS1+CDV*(BOS1+CDV*COS1))
      PIDM=CDM*(AOS1+CDM*(BOS1+CDM*COS1))
      PC=PDC*PREF
      PV=PDV*PREF
      PM=PDM*PREF
      CC=CDC*CREF
      CV=CDV*CREF
      CM=CDM*CREF
C
C
C
C
      DO 21 I=1,NP
      READ(4,405)  POLD(I),COLD(I)
      COLDT(I)=COLD(I)
   21 CONTINUE
C
  501 FORMAT(E12.6)
  502 FORMAT(9E10.4)
  503 FORMAT(5E10.4)
  504 FORMAT(6E10.4)
  405 FORMAT(2(1X,E17.10))
  506 FORMAT(3E10.4)
  507 FORMAT(5I4)
  508 FORMAT(I3)
C
C     ECHO DATA IF NECHO N.E. 0
C
      IF(NECHO.EQ.0) GO TO 999
C
C     PRINT OUT INPUT DATA
C
      WRITE(6,600)
  600 FORMAT(1X,'TRANSIENT  FLUID PRESSURE AND SOLUTE CONCENTRATION'
     #)
      WRITE(6,601)
  601 FORMAT(1X,'PROFILES  FOR ONE DIMENSIONAL TISSUE SYSTEM',//)


      WRITE(6,602)
      WRITE(6,602)
  602 FORMAT(//,1X,'_____',
     #,//)
      WRITE(6,603)
  603 FORMAT(1X,'INPUT  PARAMETERS')
      WRITE(6,602)
      WRITE(6,604)
  604 FORMAT(1X,'1.  GRID DATA:',//)
      WRITE(6,605)NEX,DX(2)
  605 FORMAT(1X,'NUMBER  OF ELEMENTS:',1X,I2,/,1X,
     #'SMALLEST X INCREMENT:',19X,E10.4,/)
      WRITE(6,606)NP
  606 FORMAT(1X,'TOTAL  NUMBER OF NODES:',10X,I4,/)
      WRITE (6,602)
      WRITE(6,607)  TOLP,TOLC,ITMAX,OMEGAF,OMEGAC,PECMAX
  607 FORMAT(1X,'2.  CONVERGENCE  CRITERIA:',//,1X,'PRESSURE  TOLERANCE:'
     #,17X,E10.4,/,1X,'SOLUTE  TOLERANCE:',20X,E10.4,/,1X,
     #'MAXIMUM NUMBER OF LOOP ITERATIONS:',2X,I3,/,1X,
     #'PRESSURE RELAXATION PARAMETER:',6X,E10.4,/,1X,
     #'SOLUTE RELAXATION PARAMETER:',9X,E10.4,/,1X,
     #'MAXIMUM  DESIRED  GRID PECLET NUMBER:',1X,E10.4)
      WRITE(6,608)  IMAX,TFACT,COUR,THETA
```

```
  608 FORMAT(/,1X,'MAXIMUM NUMBER OF TIME STEPS:',2X,I5,/,1X,
      #'TIME STEP ACCELERATION FACTOR:',6X,E10.4,/,1X,
      #'INITIAL COURANT NUMBER:',14X,E10.4,/,1X,
      #'SEMI-IMPLICIT PARAMETER THETA:',7X,E10.4)
        WRITE(6,602)
        PIC=PIDC*PREF
        PIV=PIDV*PREF
        PIM=PIDM*PREF
C
        WRITE(6,609) AL,YL,CC,CV,CM,PC,PV,PM,PIC,PIV,PIM,AK,DEFF
  609 FORMAT(1X,'3. DIMENSIONAL INPUT PARAMETERS:',//,1X,
      #'TISSUE X-DIMENSION  (CM):',21X,E10.4,/,1X,
      #'TISSUE Y-DIMENSION  (CM):',21X,E10.4,/,1X,
      #'CAP. PROTEIN CONC.  (GRAMS/DL):',14X,E10.4,/,1X,
      #'VEN. PROTEIN CONC.  (GRAMS/DL):',14X,E10.4,/,1X,
      #'MES. PROTEIN CONC.  (GRAMS/DL):',14X,E10.4,/,1X,
      #'CAP. DYN. PRESSURE (DYN/CM**2):',14X,E10.4,/,1X,
      #'VEN. DYN. PRESSURE (DYN/CM**2):',14X,E10.4,/,1X,
      #'MES. DYN. PRESSURE (DYN/CM**2):',14X,E10.4,/,1X,
      #'CAP. OSM. PRESSURE (DYN/CM**2):',14X,E10.4,/,1X,
      #'VEN. OSM. PRESSURE (DYN/CM**2):',14X,E10.4,/,1X,
      #'MES. OSM. PRESSURE (DYN/CM**2):',14X,E10.4,/,1X,
      #'TISSUE FLUID CONDUCTIVITY (CM**4/(DYN-SEC):',2X,E10.4,/,1X,
      #'TISSUE SOLUTE DIFFUSIVITY (CM**2/SEC):',7X,E10.4)
        WRITE(6,611) CONC,CONV,CONM,PERMC,PERMV,PERMM
  611 FORMAT(1X,'CAP. CONDUCTIVITY  (CM**3/(DYN-S));',11X,E10.4,/,1X,
      #'VEN. CONDUCTIVITY  (CM**3/(DYN-S)):',11X,E10.4,/,1X,
      #'MES. CONDUCTIVITY  (CM**3/(DYN-S)):',11X,E10.4,/,1X,
      #'CAP. PERMEABILITY  (CM/S):',21X,E10.4,/,1X,
      #'VEN. PERMEABILITY  (CM/S):',21X,E10.4,/,1X,
      #'MES. PERMEABILITY  (CM/S):',21X,E10.4)
        WRITE(6,602)
        WRITE(6,653) SIGT,RET,BETA,ALPHL
  653 FORMAT(1X,'4. DIMENSIONLESS INPUT PARAMETERS:',//,1X,
      #'TISSUE REFLECTION COEFFICIENT:',15X,E10.4,/,1X,
      #'RETARDATION FACTOR:',26X,E10.4,/,1X,
      #'HYDRAULIC CONDUCTIVITY RATIO, BETA:',15X,E10.4,/,1X,
      #'DIMENSIONLESS DISPERSIVITY:',21X,E10.4)
        WRITE(6,612)PDC,PIDC,PDV,PIDV,PDM,PIDM
  612 FORMAT(//,1X,
      #'PRESSURE:',6X,'DYNAMIC',5X,'OSMOTIC',//,1X,'CAPILLARY:',5X,
      #E10.4,
      #2X,E10.4,/,1X,'VENULE:',8X,E10.4,2X,E10.4,/,1X,'MESOTHELIUM:',
      #3X,E10.4,2X,E10.4,//)
        WRITE(6,613)CDC,CDV,CDM
  613 FORMAT(1X,'CONCENTRATIONS:',//,1X,'CAPILLARY:',5X,E10.4,/,1X,
      #'VENULE:',9X,E10.4,/,1X,'MESOTHELIUM:',1X,E10.4,//)
        WRITE(6,614)SIGC,SIGV,SIGM
  614 FORMAT(1X,'REFLECTION COEFFICIENTS:',//,1X,'CAPILLARY:',5X,
      #E10.4,/,1X,'VENULE:',9X,E10.4,/,1X,'MESOTHELIUM:',1X,E10.4,//)
        WRITE(6,615)DLC,DLV,DLM
  615 FORMAT(1X,'VESSEL FLUID CONDUCTANCES:',//,1X,'CAPILLARY:',5X,
      #E10.4,/,1X,'VENULE:',9X,E10.4,/,1X,'MESOTHELIUM:',1X,E10.4,//)
        WRITE(6,616)AOSM,BOSM,COSM
  616 FORMAT(1X,'VIRIAL COEFFICIENTS:',//,1X,'AOSM:',1X,E10.4,/,1X,
      #'BOSM:',1X,E10.4,/,1X,'COSM:',1X,E10.4,//)
        WRITE(6,617)DDC,DDV,DDM
  617 FORMAT(1X,'VESSEL SOLUTE PERMEABILITIES:',//,1X,'CAPILLARY:',5X,
      #E10.4,/,1X,'VENULE:',9X,E10.4,/,1X,'MESOTHELIUM:',1X,E10.4,//)
        WRITE(6,618)PHIT,PHIA,PHIS
  618 FORMAT(1X,'TOTAL TISSUE FLUID VOLUME FRACTION:',2X,E10.4,/,1X,
      #'SOLUTE DISTRIBUTION VOLUME FRACTION:',1X,E10.4,/,1X,
      #'TOTAL SOLIDS VOLUME FRACTION:',8X,E10.4,///)
C
```

```
C
C .
C
  999   THETAM=1.D0-THETA
        TIME1=DTIME1(1)
        IFLAG=0
C
C       ESTABLISH THE GRID
C

        CALL GRID(NEX)
C

C       CALCULATE THE T VECTOR AND THE FLUID VECTOR, ADJUSTING THE LATTER
C       TO FIT THE BOUNDARY CONDITIONS
C
        CALL SETMAT(NEX,3,PEC,IEL,VELMAX)
        CALL SETMAT(NEX,0,PEC,IEL,VELMAX)
        CALL ASTAR(NEX,0)
        CALL VSTAR(NEX,0)
C
C       CALCULATE THE SOLUTE VECTORS FROM THE STEADY-STATE DATA. THESE
C       WILL SERVE TO GIVE A FIRST ESTIMATE OF THE CONCENTRATION AT THE
C       NEXT TIME STEP BY USING A FULLY EXPLICIT FORM TO START WITH.
C
        CALL SETMAT(NEX,2,PEC,IEL,VELMAX)
        CALL PATART(NEX)
        CALL PATVEN(NEX)
        PECLET=PEC
        ELPEC=IEL
        DMX=DISPMX
        ID=IDISP
        DELT=COUR/VELMAX
C
C       SET THE SOLDT AND SBOLDT VECTORS EQUAL TO THE STEADY-STATE
C       VECTORS ABOVE
C
        DO 2 I=1,NDIM
        SOLDT(I)=SOLUTE(I)
    2   CONTINUE
C
        DO 3 I=1,NP
        SBOLDT(I)=SOLUTB(I)
    3   CONTINUE
C
C       CHECK THAT THE MAXIMUM NUMBER OF TIME STEP ITERATIONS HAVE NOT
C       BEEN EXCEEDED.
C
        ICOUNT=0
        TIME=0
C
        ITSOL=1
  100   ICOUNT=ICOUNT+1
C
C       DETERMINE TOTAL ELAPSED TIME
C
        NITER=0
        DTINV=1.D0/DELT
        TIME=TIME+1.D0/DTINV
        IF(ICOUNT.GT.IMAX)  GO TO 900
        IF(TIME.GT.TIMMAX)  GO TO 910
C
        DO 4 I=1,NDIM
        TDT(I)=T(I)*DTINV
    4   CONTINUE
C
C       DETERMINE THE AS VECTOR AND BS VECTOR FOR THE EXPLICIT SCHEME
C
        CALL MATPLY(T,DTINV,COLDT,TCOLDT,NP)
        CALL MATPLY(SOLDT,1.D0,COLDT,SCOLDT,NP)
```

```
C
      DO 5 I=1,NP
      BCTIME(I)=TCOLDT(I)+SBOLDT(I)-SCOLDT(I)
   5  CONTINUE
C
C     DETERMINE THE INITIAL GUESS FOR CNEW, UPDATING NITER
C
 200  NITER=NITER+1
      EP=EPS
      IF(NITER.GT.ITMAX)GO TO 901
C
C     DETERMINE WHETHER THIS IS THE FIRST PASS, AND HENCE USE THE
C     FULLY EXPLICIT FORM OF THE SOLUTE TRANSPORT EQ., OR IF IT IS
C     A SUBSEQUENT PASS, IN WHICH CASE A SEMI-IMPLICIT SCHEME IS
C     USED. .
C
      IF(NITER.EQ.1) CALL DGBAND(TDT,BCTIME,NP,LUB,LUB,1,IPERM,DET,
     #             JEXP,HOLD,RES,ITER,EP)
C
      IF(NITER.GT.1) CALL DGBAND(STNEW,BCTIME,NP,LUB,LUB,1,IPERM,DET,
     #             JEXP,HOLD,RES,ITER,EP)
C
C     DETERMINE THE MAXIMUM CHANGE IN C FROM ONE ITERATION TO THE
C     NEXT, USING A RELATATION PROCEDURE. CDIFMX WILL BE COMPARED
C     TO CTOL TO ESTABLISH CONVERGENCE FOR TIME STEP ICOUNT.
C
      CMAX=0.DO
      CDIFMX=0.DO
      DO 6 I=1,NP
      IF(DABS(BCTIME(I)).GT.CMAX)  CMAX=DABS(BCTIME(I))
      TEST=DABS(BCTIME(I)-COLD(I))
      IF(TEST.GT.CDIFMX)  CDIFMX=TEST
      COLD(I)=OMEGAC*(BCTIME(I)-COLD(I))+COLD(I)
   6  CONTINUE
      CDIFMX=CDIFMX/CMAX
C
C     NOW INITIALIZE THE FLUID B VECTOR AND SOLVE FOR THE PRESSURE
C     DISTRIBUTION AT THIS NEW TIME STEP
C
C
      CALL SETMAT(NEX,1,PEC,IEL,VELMAX)
      CALL ASTAR(NEX,1)
      CALL VSTAR(NEX,1)


C
C     SOLVE FOR THE NEW PRESSURE
C
      EP=EPS
      CALL DGBND1(FLUID,FLUIDB,NP,LUB,LUB,ITSOL,IPERM1,DET,JEXP,
     #HOLD1,RES1,ITER,EP)
       ITSOL=ITSOL+1
C
C     CHECK TO SEE IF THE SOLUTION HAS CONVERGED
C
      PMAX=0.DO
      PDIFMX=0.DO
      DO 7 I=1,NP
      IF(DABS(FLUIDB(I)).GT.PMAX)  PMAX=FLUIDB(I)
      TEST=DABS(FLUIDB(I)-POLD(I))
      IF(TEST.GT.PDIFMX)  PDIFMX=TEST
      POLD(I)=OMEGAF*(FLUIDB(I)-POLD(I))+POLD(I)
   7  CONTINUE

      PDIFMX=PDIFMX/PMAX
C
C     CHECK FOR CONVERGENCE
C
      IF(PDIFMX.GT.TOLP)  GO TO 300
      IF(CDIFMX.LT.TOLC)  GO TO 301
C
```

```
C     RESET THE SOLUTE MATRIX, SET THE NECESSARY VECTORS FOR A SEMI-
C     IMPLICIT SCHEME
C
  300 CALL SETMAT(NEX,2,PEC,IEL,VELMAX)
      CALL PATART(NEX)
      CALL PATVEN(NEX)
      PECLET=PEC
      ELPEC=IEL
      COUR=VELMAX*DELT
      DMX=DISPMX
      ID=IDISP
      DO 8 I=1,NP
      BCTIME(I)=THETA*SOLUTB(I)+TCOLDT(I)+THETAM*SBOLDT(I)-
     #          THETAM*SCOLDT(I)
    8 CONTINUE
C
      DO 9 I=1,NDIM
      STNEW(I)=T(I)*DTINV+THETA*SOLUTE(I)
    9 CONTINUE
      GO TO 200
C
C     RESET MATRICES FOR NEXT TIME STEP
C
  301 DO 10 I=1,NP
      SBOLDT(I)=SOLUTB(I)
      COLDT(I)=COLD(I)
   10 CONTINUE
C
      DO 11 I=1,NDIM
      SOLDT(I)=SOLUTE(I)
   11 CONTINUE
C
C     DETERMINE IF THE SOLUTION SHOULD BE PRINTED OUT.
C     IF DELT HAS BEEN SET TO (TIME1-TIME), RESET DELT
C     TO DTHOLD, I.E., TO THE LAST VALUE OF DELT BEFORE
C     SETTING IT TO TIME1-TIME
C
      IF(IFLAG.EQ.0)GO TO 400
      DELT=DTHOLD
      IFLAG=0
  400 DELT=DELT*TFACT
      IF(DABS(TIME-TIME1).LT.TTOL)  GO TO 800
      IF(DABS(TIME-TIME1).GT.DELT)  GO TO 100
      DTHOLD=DELT
      IFLAG=1
      DELT=DABS(TIME-TIME1)
  619 FORMAT(//,1X,'NUMBER  OF TIME STEPS:', I4,1X,
     #'REPRESENTING A CUMMULATIVE TIME OF ',F10.7,/,1X,
     #'NUMBER OF ITERATIONS REQUIRED FOR CONVERGENCE:',1X,I3,/,1X,
     #'MAXIMUM COURANT NUMBER:',F10.7,/,1X,
     #'MAXIMUM GRID PECLET NUMBER:',F10.7,1X,'AT  ELEMENT',1X,I4,/,1X,
     #'MAXIMUM DISPERSION COEFFICIENT:',1X,E9.4,1X,'AT  ELEMENT',1X,I4)
      WRITE(6,602)
      GO TO 100
C
C     PRINT OUT THE SOLUTION AT TIME1 TO DEVICE 6 AND 7
C
  800 WRITE(6,619) ICOUNT,TIME,NITER,COUR,PECLET,ELPEC,DMX,ID
      WRITE(6,620)
  620 FORMAT(//,1X,'POSITION',1X,'AVAIL.  CONC.',1X,'TOTAL  CONC.',
     #1X,'HYDRO. PRESS.',1X, 'OSMOTIC PRESS.',1X,'TOTAL PRESS.')
      X=0.D0
      DO 12 I=1,NP
      POSM=COLD(I)*(AOSM+COLD(I)*(BOSM+COSM*COLD(I)))
      PTOT=POLD(I)-POSM
      CTOT=COLD(I)*PHIA/(1.D0-PHIS)
      X=X+DX(I)
      WRITE(6,621) X,COLD(I),CTOT,POLD(I),POSM,PTOT
      WRITE(7,621) X,POLD(I),POSM,PTOT,COLD(I),CTOT
```

```
  621 FORMAT(2X,F6.4,3X,F9.6,4X,F9.6,3X,F9.6,5X,F9.6,6X,F9.6)
   12 CONTINUE
C
      CALL MASBAL(NEX)
C
      DO 20 I=1,NEX
      I2=2*I
      X=XNOD(I2)
      WRITE(7,702) X,QFM1(I),QSM1(I),QCM1(I)
  702 FORMAT(4(2X,E10.4))
   20 CONTINUE
C
      WRITE(6,622)
  622 FORMAT('1',//,1X,'MASS  BALANCE  DATA',///)
      WRITE(6,623)
  623 FORMAT(///,1X,'NET  DIMENSIONLESS  FLUID  FLOWS')
      WRITE(6,624) QFC,QFV,QFM
  624 FORMAT(//,1X,'ART:',1X,E12.4,/,1X,'VEN:',1X,E12.4,/,1X,
     #'MES:',1X,E12.4)
      WRITE(6,625)
  625 FORMAT(///,'NET  DIMENSIONLESS  SOLUTE  FLOWS')
      WRITE(6,624) QSC,QSV,QSM
      WRITE(6,626)
  626 FORMAT(//,1X,'CONVECT.  COMPONENTS OF DIMENSIONLESS SOLUTE FLOW')
      WRITE(6,624) QCC,QCV,QCM
      PECC=QCC/(QSC-QCC)
      PECV=QCV/(QSV-QCV)
      PECM=QCM/(QSM-QCM)
      WRITE(6,627)
  627 FORMAT(//,1X,'RATIO  OF CONVECTION  TO DIFFUSION  AT BOUNDARIES')
      WRITE(6,624) PECC,PECV,PECM
      TIME1=TIME1+DTIME1(KK)
      KK=KK+1
      WRITE(6,602)
      GO TO 100
C
C     PRINT OUT ERROR THAT CONVERGENCE WAS NOT ACHIEVED
C
  901 ICOUNT=ICOUNT-1
      NITER=NITER-1
      WRITE(6,628) NITER,TIME,ICOUNT,PECLET,IEL,COUR
  628 FORMAT(//,1X,'CONVERGENCE  NOT  ACHEIVED  AFTER',I4,'  ITERATIONS.',
     #/,'TIME  OF FAILURE:',F10.6,3X,
     #'NUMBER OF SUCCESSFUL TIME STEPS BEFORE FAILURE:',I5,/,
     #1X,'MAXIMUM GRID PECLET NUMBER IS',1X,F7.4,1X,'AT ELEMENT',I4,/,
     #1X,'MAXIMUM  COURANT  NUMBER IS ',F10.7)
      GO TO 920
  900 WRITE(6,629) TIME
  629 FORMAT(//,1X,'MAXIMUM  NUMBER OF TIME STEPS ACHIEVED AT TIME',
     #E10.4)
      GO TO 920
  910 WRITE(6,630) TIMMAX, ICOUNT
  630 FORMAT(//,1X,'MAXIMUM  TIME OF',1X,E10.4,' EXCEEDED AFTER ',I4,
     # ' TIME  STEPS')
  920 STOP
      END
C
      SUBROUTINE MATPLY(A,A1,B,C,NP)
C
C     THIS SUBROUTINE MULTIPLIES A MATRIX A BY A VECTOR B AND SCALAR A1
C     TO GIVE  VECTOR C. MATRIX A IS STORED AS A VECTOR, WHERE MATRIX
C     ELEMENT A(I,J) IS STORED AS A(IJ), IJ=3*LUB*J+I-LUB,  AND WHERE
C     LUB IS THE NUMBER OF OFF DIAGONAL BANDS. FOR THIS SUBROUTINE,
C     IT IS ASSUMED THAT THE BANDWIDTH IS 5, SO THAT LUB=2.
C
      IMPLICIT REAL*8(A-H,O-Z)
```

```
      DIMENSION A(20000), B(NP), C(NP)
      LUB=2
      LP=3*LUB
C
      DO 1 I=1,NP
      C(I)=0.D0
  1   CONTINUE
C
      K=2
      DO 2 I=1,2
      K=K+1
         DO 3 J=1,K
         IJ=LP*J+I-LUB
         C(I)=C(I)+A(IJ)*A1*B(J)
  3      CONTINUE
  2   CONTINUE
C
      NPM=NP-2
      K=0
      DO 4 I=3,NPM
      K=K+1
      KP=K+4
         DO 5 J=K,KP
         IJ=J*LP+I-LUB
         C(I)=C(I)+A(IJ)*B(J)*A1
  5      CONTINUE
  4   CONTINUE
C
      NPM=NP-1
      K=NP-4
      DO 6 I=NPM,NP
      K=K+1
         DO 7 J=K,NP
         IJ=LP*J+I-LUB
         C(I)=C(I)+A(IJ)*A1*B(J)
  7      CONTINUE
C
  6   CONTINUE
C
      RETURN
      END
C
      SUBROUTINE MASBAL(NEX)
C
C     THIS SUBROUTINE PERFORMS A MATERIAL BALANCE ON THE SYSTEM FOR
C     BOTH FLUID AND PLASMA PROTEINS.
C
      IMPLICIT REAL*8(A-H,O-Z)
      COMMON/MATBAL/QFC,QCC,QSC,QFV,QCV,QSV,QFM,QCM,QSM,QFM1(500),
     #              QCM1(500),QSM1(500)
      COMMON/OLD/POLD(1001),COLD(1001)
      COMMON/BLK1/NODEL(500,3),XNOD(1001)
      COMMON/OSMOT/A0,B0,C0
      COMMON/TISDAT/AK,DEFF,AL,PHIA,PHIT,RET,SIGT,BETA
      COMMON/CAPDAT/PC,CC
      COMMON/WALL/DLC,DLV,DLM,DDC,DDV,DDM,PDC,PDV,PDM,PIDC,PIDV,PIDM,
     #            SIGC,SIGV,SIGM,CDC,CDV,CDM,DH
      DIMENSION GAUS(4),W(4),B(3)
      DATA NGAUS/4/
      DATA W/.347854845137454D0,.652145154862546D0,
     #.652145154862546D0,.347854845137454D0/
      DATA GAUS/-.861136311594053D0,-.339981043584856D0,
     #.339981043584856D0,.861136311594053D0/
C
C     FIRST, CALCULATE THE NET FLOWS ACROSS THE ARTERIOLAR WALL
C
      PIC=COLD(1)*(A0+COLD(1)*(B0+COLD(1)*C0))
      QFC=DH*AK*PC/DEFF*DLC*(POLD(1)-PDC-SIGC*(PIC-PIDC))
      QCC=BETA*QFC*COLD(1)*RET
      PECC=(1.D0-SIGC)*QFC/(DDC*DH)
```

```
      IF(PECC.GT.100.D0)GO TO 110
      IF(PECC.LT.-100.D0)GO TO 120
      TEST=1.D0-DEXP(-PECC)
      IF(DABS(TEST).LT.1.D-10)GO TO 130
      QSC=(1.D0-SIGC)*QFC*(COLD(1)-CDC*DEXP(-PECC))/TEST
      GO TO 200
  110 QSC=QFC*(1.D0-SIGC)*COLD(1)
      GO TO 200
  120 QSC=(1.D0-SIGC)*CDC*QFC
      GO TO 200
  130 QSC=DH*DDC*(COLD(1)-CDC)
C
C     NOW FOR THE VENULAR WALL
C
  200 N=NEX*2+1
      PIV=COLD(N)*(A0+COLD(N)*(B0+COLD(N)*C0))
      QFV=DH*AK*PC/DEFF*DLV*(POLD(N)-PDV-SIGV*(PIV-PIDV))
      QCV=BETA*QFV*COLD(N)*RET
      PECV=(1.D0-SIGV)*QFV/(DDV*DH)
      IF(PECV.GT.100.D0)GO TO 210
      IF(PECV.LT.-100.D0)GO TO 220
      TEST=1.D0-DEXP(-PECV)
      IF(DABS(TEST).LT.1.D-10)GO TO 230
      QSV=(1.D0-SIGV)*QFV*(COLD(N)-CDV*DEXP(-PECV))/TEST
      GO TO 300
  210 QSV=QFV*(1.D0-SIGV)*COLD(N)
      GO TO 300
  220 QSV=(1.D0-SIGV)*CDV*QFV
      GO TO 300
  230 QSV=DH*DDV*(COLD(N)-CDV)
C
C     AND FINALLY, THE MESOTHELIAL LAYER
C
C     CONSIDER THE MESOTHELIAL WALL, ELEMENT BY ELEMENT.
C
  300 QSM=0.D0
      QCM=0.D0
      QFM=0.D0
C
      DO 400 I=1,NEX
      QSM1(I)=0.D0
      QFM1(I)=0.D0
      QCM1(I)=0.D0
  400 CONTINUE

C
      DO 1 II=1,NGAUS
      S=GAUS(II)
          DO 2 I=1,NEX
          X1=XNOD(NODEL(I,1))
          X2=XNOD(NODEL(I,2))
          X3=XNOD(NODEL(I,3))
          S2=(2.D0*X2-(X1+X3))/(X3-X1)
C
          B(1)=(S-S2)*(S-1.D0)/(2.D0*(S2+1.D0))
          B(2)=(S+1.D0)*(S-1.D0)/(S2*S2-1.D0)
          B(3)=(S+1.D0)*(S-S2)/(2.D0*(1.D0-S2))
          DX=(X3-X1)*.5D0
C
C     CALCULATE C(S), PI(S), AND P(S)
C
          CS=0.D0
          PS=0.D0
          DO 3 IT=1,3
          CS=CS+COLD(NODEL(I,IT))*B(IT)
          PS=PS+POLD(NODEL(I,IT))*B(IT)

    3     CONTINUE
          PIS=CS*(A0+CS*(B0+CS*C0))
```

```
C
C       CALCULATE THE FLUXES
C
        FLOW=AK*PC/DEFF*DLM*(PS-PDM-SIGM*(PIS-PIDM))*W(II)*DX
        QFM=QFM+FLOW
        QFM1(I)=QFM1(I)+FLOW/(X3-X1)
        QCM=QCM+FLOW*CS*BETA*RET
        QCM1(I)=QCM1(I)+FLOW*CS*BETA/(X3-X1)*RET
C
C       DETERMINE WHICH FORM OF THE NONLINEAR FLUX EQN. IS TO BE USED.
C
        QS=FLOW/(W(II)*DX)
        PECM=QS*(1.D0-SIGM)/DDM
        IF(PECM.GT.100.D0)GO  TO 410
        IF(PECM.LT.-100.D0)GO  TO 420
        TESTM=1.D0-DEXP(-PECM)
        IF(DABS(TESTM).LT.1.D-10)GO  TO 430
C
C       USE THE FULL EXPRESSION
C
        SFLOW=FLOW*(1.D0-SIGM)*(CS-CDM*DEXP(-PECM))/TESTM
        QSM=QSM+SFLOW
        QSM1(I)=QSM1(I)+SFLOW/(X3-X1)
        GO TO 2
C
  410   SFLOW=FLOW*(1.D0-SIGM)*CS
        QSM=QSM+SFLOW
        QSM1(I)=QSM1(I)+SFLOW/(X3-X1)
        GO TO 2
C
  420   SFLOW=FLOW*(1.D0-SIGM)*CDM
        QSM=QSM+SFLOW
        QSM1(I)=QSM1(I)+SFLOW/(X3-X1)
        GO TO 2
C
  430   SFLOW=DDM*(CS-CDM)*DX*W(II)
        QSM=QSM+SFLOW
        QSM1(I)=QSM1(I)+SFLOW/(X3-X1)
  2     CONTINUE
  1   CONTINUE
      RETURN
      END
      SUBROUTINE GRID(NEX)
C
C       THIS SUBROUTINE CALCULATES THE SPATIAL LOCATION OF THE NODES
C       FOR EACH ELEMENT, ALONG WITH THE NODES ASSOCIATED WITH A
C       GIVEN ELEMENT.
C
      IMPLICIT REAL*8(A-H,O-Z)
      COMMON/BLK1/NODEL(500,3),  XNOD(1001)
      COMMON/BLK2/DX(1001)
C
      K=1
      DO 1 I=1,NEX
      NODEL(I,1)=K
      NODEL(I,2)=K+1
      NODEL(I,3)=K+2
      K=K+2
  1   CONTINUE
C
      X=0.D0
      NP=2*NEX+1
      DO 2 I=1,NP
      X=X+DX(I)
      XNOD(I)=X
  2   CONTINUE
      RETURN
      END
C
```

```
      SUBROUTINE VSTAR(NEX,IND)
C
C     THIS SUBROUTINE ADJUSTS THE AF AND BF VECTORS TO ACCOUNT FOR THE
C     STARLING BOUNDARY CONDITION AT THE VENULAR WALL.
C
      IMPLICIT REAL*8(A-H,O-Z)
      COMMON/BLK1/NODEL(500,3), XNOD(1001)
      COMMON/FLUMAT/AF(20000)
      COMMON/FLUB/BF(1001)
      COMMON/OLD/POLD(1001),COLD(1001)
      COMMON/WALL/DLC,DLV,DLM,DDC,DDV,DDM,PDC,PDV,PDM,PIDC,PIDV,PIDM,
     #          SIGC,SIGV,SIGM,CDC,CDV,CDM,DE
      COMMON/OSMOT/A0,B0,C0
C
      M=NEX*2+1
      LUB=2
      LP=3*LUB
      IF(IND.EQ.1)GO TO 100
      K=LP*M+M-LUB
      AF(K)=AF(K)+ DLV
      GO TO 900
C
  100 PI=COLD(M)*(A0+COLD(M)*(B0+COLD(M)*C0))
      BF(M)=BF(M)+DLV*(PDV+SIGV*(PI-PIDV))
C
  900 RETURN
      END

      SUBROUTINE ASTAR(NEX,IND)
C
C     THIS SUBROUTINE ADJUSTS THE AF AND BF VECTORS TO ACCOUNT FOR THE
C     STARLING BOUNDARY CONDITION AT THE ARTERIOLAR WALL.
C
      IMPLICIT REAL*8(A-H,O-Z)
      COMMON/BLK1/NODEL(500,3), XNOD(1001)
      COMMON/FLUMAT/AF(20000)
      COMMON/FLUB/BF(1001)
      COMMON/OLD/POLD(1001),COLD(1001)
      COMMON/WALL/DLC,DLV,DLM,DDC,DDV,DDM,PDC,PDV,PDM,PIDC,PIDV,PIDM,
     #          SIGC,SIGV,SIGM,CDC,CDV,CDM,DE
      COMMON/OSMOT/A0,B0,C0
C.
      LUB=2
      LP=3*LUB
      IF(IND.EQ.1)GO TO 100
      K=LP+1-LUB
      AF(K)=AF(K)+ DLC
      GO TO 900
C
  100 PI=COLD(1)*(A0+COLD(1)*(B0+COLD(1)*C0))
      BF(1)=BF(1)+DLC*(PDC+SIGC*(PI-PIDC))
C
  900 RETURN
      END
      SUBROUTINE PATART(NEX)
C
C     THIS SUBROUTINE ADJUSTS THE AS AND BS VECTORS TO ACCOUNT FOR THE
C     PATLAK BOUNDARY CONDITION AT THE ARTERIOLAR WALL.
C
      IMPLICIT REAL*8(A-H,O-Z)
      COMMON/BLK1/NODEL(500,3), XNOD(1001)
      COMMON/SOLMAT/AS(20000)
      COMMON/SOLB/BS(1001)
      COMMON/OLD/POLD(1001),COLD(1001)
      COMMON/TISDAT/AK,DEFF,AL,PHIA,PHIT,RET,SIGT,BETA
      COMMON/CAPDAT/PC,CC
      COMMON/WALL/DLC,DLV,DLM,DDC,DDV,DDM,PDC,PDV,PDM,PIDC,PIDV,PIDM,
     #          SIGC,SIGV,SIGM,CDC,CDV,CDM,DE
      COMMON/OSMOT/A0,B0,C0
C
```

```
        LUB=2
        LP=3*LUB
        K=LP+1-LUB
C
        PI=COLD(1)*(A0+COLD(1)*(B0+COLD(1)*C0))
        QART=AK*PC/DEFF*DLC*(POLD(1)-PDC-SIGC*(PI-PIDC))
        PEC=(1.D0-SIGC)/DDC*QART
C
C       DETERMINE WHICH FORM OF THE FLUX EXPRESSION APPLIES
C
        IF(PEC.GT.100.0D0)GO TO 100
        IF(PEC.LT.-100.D0)GO TO 200
        TEST=1.D0-DEXP(-PEC)
        IF(DABS(TEST).LT.1.D-10)GO TO 300
C
        AS(K)=AS(K)-QART*(RET*BETA-(1.D0-SIGC)/TEST)
        BS(1)=BS(1)+(1.D0-SIGC)*QART*CDC*DEXP(-PEC)/TEST
        GO TO 900
C
  100   AS(K)=AS(K)-QART*(BETA*RET-(1.D0-SIGC))
        GO TO 900
C
  200   AS(K)=AS(K)-QART*BETA*RET
        BS(1)=BS(1)-(1.D0-SIGC)*QART*CDC
        GO TO 900
C
  300   AS(K)=AS(K)-QART*BETA*RET+DDC
        BS(1)=BS(1)+DDC*CDC
  900   RETURN
        END
        SUBROUTINE PATVEN(NEX)

C
C       THIS SUBROUTINE ADJUSTS THE AS AND BS VECTORS TO ACCOUNT FOR THE
C       PATLAK BOUNDARY CONDITION AT THE VENULAR WALL.
C
        IMPLICIT REAL*8(A-H,O-Z)
        COMMON/BLK1/NODEL(500,3), XNOD(1001)
        COMMON/SOLMAT/AS(20000)
        COMMON/SOLB/BS(1001)
        COMMON/OLD/POLD(1001),COLD(1001)
        COMMON/TISDAT/AK,DEFF,AL,PHIA,PHIT,RET,SIGT,BETA
        COMMON/CAPDAT/PC,CC
        COMMON/WALL/DLC,DLV,DLM,DDC,DDV,DDM,PDC,PDV,PDM,PIDC,PIDV,PIDM,
       #            SIGC,SIGV,SIGM,CDC,CDV,CDM,DH
        COMMON/OSMOT/A0,B0,C0
C
        LUB=2
        LP=3*LUB
        NP=2*NEX+1
        K=LP*NP+NP-LUB
C
        PI=COLD(NP)*(A0+COLD(NP)*(B0+COLD(NP)*C0))
        QART=AK*PC/DEFF*DLV*(POLD(NP)-PDV-SIGV*(PI-PIDV))
        PEC=(1.D0-SIGV)/DDV*QART
C
C       DETERMINE WHICH FORM OF THE FLUX EXPRESSION APPLIES
C
        IF(PEC.GT.100.0D0)GO TO 100
        IF(PEC.LT.-100.D0)GO TO 200
        TEST=1.D0-DEXP(-PEC)
        IF(DABS(TEST).LT.1.D-10)GO TO 300
C
        AS(K)=AS(K)-QART*(RET*BETA-(1.D0-SIGV)/TEST)
        BS(NP)=BS(NP)+(1.D0-SIGV)*QART*CDV*DEXP(-PEC)/TEST
        GO TO 900
C
  100   AS(K)=AS(K)-QART*(BETA*RET-(1.D0-SIGV))
        GO TO 900
```

```
C
  200   AS(K)=AS(K)-QART*BETA*RET
        BS(NP)=BS(NP)-(1.D0-SIGV)*QART*CDV
        GO TO 900
C
  300   AS(K)=AS(K)-QART*BETA*RET+DDV
        BS(NP)=BS(NP)+DDV*CDV
  900   RETURN
        END
        SUBROUTINE SETMAT(NEX,IND,PE,IPEC,VELMAX)
C
C       THIS SUBROUTINE INITIALIZES THE VARIOUS VECTORS ASSOCIATED
C       WITH SOLUTE AND FLUID TRANSPORT EQUATIONS, AF(K), BF(I), AS(K),
C       AND BS(I). NOTE THAT PARAMETER XL IS THE REFERENCE LENGTH
C       USED TO NONDIMENSIONALIZE  THE EQUATIONS. IN THIS CASE
C       XL IS THE LENGTH OF THE MESENTERIC SLAB.
C
        IMPLICIT REAL*8(A-H,O-Z)
        COMMON/BLK1/NODEL(500,3),XNOD(1001)
        COMMON/FLUMAT/AF(20000)
        COMMON/SOLMAT/AS(20000)
        COMMON/TIME/T(20000)
        COMMON/FLUB/BF(1001)
        COMMON/SOLB/BS(1001)
        COMMON/TISDAT/AK,DEFF,AL,PHIA,PHIT,RET,SIGT,BETA
        COMMON/OSMOT/A0,B0,C0
        COMMON/CAPDAT/PC,CC
        COMMON/OLD/POLD(1001),COLD(1001)
        COMMON/WALL/DLC,DLV,DLM,DDC,DDV,DDM,PDC,PDV,PDM,PIDC,PIDV,PIDM,
       #SIGC,SIGV,SIGM,CDC,CDV,CDM,DH
        COMMON/MAXDAT/DISPMX,IDISP
C
        DIMENSION GAUS(4),W(4),B(3),DB(3)
        DATA NGAUS/4/
        DATA W/.347854845137454D0,.652145154862546D0,
       #.652145154862546D0,.347854845137454D0/
        DATA GAUS/-.861136311594053D0,-.339981043584856D0,
       #.339981043584856D0,.861136311594053D0/
C       DATA GAUS/
C       DATA W/
C       DATA NGAUS/3/
C       DATA GAUS/
C       DATA W/
        DISPMX=0.D0
        ALPHA=AK*PC/DEFF
        PE=0.D0
        VELMAX=0.D0
C
C       ZERO THE APPROPRIATE ARRAY AND INITIALIZE
C
        IF(IND.EQ.1)GO TO 800
        IF(IND.EQ.2)GO TO 900
        IF(IND.EQ.3)GO TO 950
C
C       ZERO THE AF VECTOR
C
        DO 700 I=1,20000
        AF(I)=0.D0
  700   CONTINUE
        GO TO 100
C
C       ZERO THE BF VECTOR
C
C
  800   DO 801 I=1,1001
        BF(I)=0.D0
  801   CONTINUE
        GO TO 100
C
```

```
C     ZERO THE T MATRIX
C
 950  DO 951 I=1,20000
      T(I)=0.D0
 951  CONTINUE
      GO TO 100
C
C     ZERO THE AS AND BS VECTORS
C
 900  DO 901 I=1,20000
      AS(I)=0.D0
 901  CONTINUE
C
      DO 902 I=1,1001
      BS(I)=0.D0
 902  CONTINUE
C
C     BEGIN THE GAUSS INTEGRATION, ELEMENT BY ELEMENT
C
 100  LUB=2
      LP=3*LUB
C
C     EVALUATE THE INTEGRAND AT THE APPROPRIATE QUADRATURE POINT, S.
C
      DO 200 II=1,NGAUS
      S=GAUS(II)
C
C     INITIALIZE THE APPROPRIATE ARRAY, ELEMENT BY ELEMENT.
C
      DO 300 I=1,NEX
C
C     CALCULATE VALUE OF BASIS FUNCTIONS AND DERIVATIVES AT THE
C     QUADRATURE POINT
C
      X1=XNOD(NODEL(I,1))
      X2=XNOD(NODEL(I,2))
      X3=XNOD(NODEL(I,3))
C
      S2=(2.D0*X2-(X1+X3))/(X3-X1)
C
      B(1)=(S-S2)*(S-1.D0)/(2.D0*(S2+1.D0))
      B(2)=(S+1.D0)*(S-1.D0)/(S2*S2-1.D0)
      B(3)=(S+1.D0)*(S-S2)/(2.D0*(1.D0-S2))
      DB(1)=(2.D0*S-S2-1.D0)/(2.D0*(S2+1.D0))
      DB(2)=2.D0*S/(S2*S2-1.D0)
      DB(3)=(2.D0*S-S2+1.D0)/(2.D0*(1.D0-S2))
C
      DX=(X3-X1)*.5D0
C
C     CALCULATE THE T VECTOR
C
      IF(IND.NE.3) GO TO 101
      DO 952 M=1,3
      MM=NODEL(I,M)
        DO 953 N=1,3
        NN=NODEL(I,N)
        K=LP*NN+MM-LUB
        T(K)=T(K)+PHIA*B(M)*B(N)*DX*W(II)
 953    CONTINUE
 952  CONTINUE
      GO TO 300
C
C     NOW CALCULATE C(S), DC/DS, PI(S), DPI/DS
C
 101  CS=0.D0
      DCS=0.D0
      DO 301 IT=1,3
      CS=CS+COLD(NODEL(I,IT))*B(IT)
      DCS=DCS+COLD(NODEL(I,IT))*DB(IT)
```

```
  301  CONTINUE
C
       PIS=CS*(A0+CS*(B0+CS*C0))
       DPIS=(A0+2.D0*B0*CS+3.D0*CS*CS*C0)*DCS
C
C      DETERMINE WHICH VECTOR IS TO BE INITIALIZED
C
       IF(IND.EQ.1)GO TO 500
       IF(IND.EQ.2)GO TO 600
C
C      INITIALIZE THE FLUID VECTOR
C
       DO 401 M=1,3
       MM=NODEL(I,M)
          DO 402 N=1,3
          NN=NODEL(I,N)
          K=LP*NN+MM-LUB
          AF(K)=AF(K)+(B(M)*B(N)*2.D0*DLM/DH*DX+DB(M)*DB(N)/DX)*W(II)
  402     CONTINUE
  401  CONTINUE
       GO TO 300
C
C      INITIALIZE THE FLUID B VECTOR
C
  500 DO 501 M=1,3
       MM=NODEL(I,M)
       BF(MM)=BF(MM)+(DB(M)*DPIS/DX+B(M)*2.D0*DLM/DH*DX*(PDM+SIGM*
     #    (PIS - PIDM)))*W(II)
  501  CONTINUE
       GO TO 300
C
C      INITIALIZE THE SOLUTE VECTORS, BS AND AS. fIRST CALCULATE VS,
C      QMES, AND THE DISPERSION COEFFICIENT, DISP.
C
  600  DPS=0.D0
       PS=0.D0
       DO 601 IT=1,3
       DPS=DPS+POLD(NODEL(I,IT))*DB(IT)
       PS=PS+POLD(NODEL(I,IT))*B(IT)
  601  CONTINUE
C.
       VS=-ALPHA*(DPS-SIGT*DPIS)/DX*RET*BETA/PHIA
       QFMES=ALPHA*DLM*(PS-PDM-SIGM*(PIS-PIDM))
       DISP=DABS(VS)*AL+1.D0
       IF(DISP.LT.DISPMX) GO TO 650
       DISPMX=DISP
       IDISP=I


C
C      CALCULATE THE MAXIMUM LOCAL SOLUTE VELOCITY, VELMAX
C
  650  IF(DABS(CS).LT.1.D-5)  VELS=DABS(VS)*PHIA
       IF(DABS(CS).GT.1.D-5)  VELS=DABS(VS-(DISP*DCS/DX)/CS)*PHIA
       IF(.5D0*VELS/DX.GT.VELMAX)  VELMAX=.5D0*VELS/DX
C
C      CALCULATE THE GRID PECLET NUMBER, AND SEE IF IT EXCEEDS
C      THE LIMIT
C
       PEST=DABS(VS)*(X3-X1)/DISP
       IF(PEST.LT.PE)GO TO 609
       PE=PEST
       IPEC=I
C
C      NOW DETERMINE WHICH FORM OF THE NONLINEAR FLUX EXPRESSION
C      IS TO BE USED TO CALCULATE SOLUTE FLUX ACROSS MESOTHELIUM.
C
  609  PEC=QFMES*(1.D0-SIGM)/DDM
       IF(PEC.GT.100.D0)GO TO 610
       IF(PEC.LT.-100.D0)GO TO 620
```

```
        TEST=1.D0-DEXP(-PEC)
        IF(DABS(TEST).LT.1.D-10)GO  TO 630
C
C       CASE 1: USE THE FULL NONLINEAR FLUX EXPRESSION
C
        DO 602 M=1,3
        MM=NODEL(I,M)
              DO 603 N=1,3
              NN=NODEL(I,N)
              K=LP*NN+MM-LUB
              AS(K)=AS(K)+(B(M)*DB(N)*VS*PHIA+DB(M)*DB(N)*DISP*PHIA/DX
     #             +B(M)*B(N)*2.D0*QFMES/TEST/DH*(1.D0-SIGM)*DX
     #             -2.D0/DH*QFMES*RET*BETA*B(M)*B(N)*DX)*W(II)
 603          CONTINUE
        BS(MM)=BS(MM)+B(M)*2.D0/DH*(1.D0-SIGM)*QFMES*CDM*DEXP(-PEC)/TEST
     #        *DX*W(II)
 602    CONTINUE
        GO TO 300
C
C       CASE 2: PEC APPROACHES INFINITY
C
 610    DO 611 M=1,3
        MM=NODEL(I,M)
              DO 612 N=1,3
              NN=NODEL(I,N)
              K=LP*NN+MM-LUB
              AS(K)=AS(K)+(B(M)*DB(N)*VS*PHIA+DB(M)*DB(N)*PHIA*DISP/DX
     #             +B(M)*B(N)*2.D0/DH*(1.D0-SIGM)*QFMES*DX
     #             -QFMES*RET*BETA*B(M)*B(N)*DX*2.D0/DH)*W(II)
 612          CONTINUE
 611    CONTINUE
        GO TO 300
C
C       CASE 3: -PEC APPROACHES INFINITY
C
 620    DO 621 M=1,3
        MM=NODEL(I,M)
              DO 622 N=1,3
              NN=NODEL(I,N)
              K=LP*NN+MM-LUB
              AS(K)=AS(K)+(B(M)*DB(N)*VS*PHIA+DB(M)*DB(N)*PHIA*DISP/DX
     #             -2.D0/DH*BETA*RET*QFMES*B(N)*B(M)*DX)*W(II)
 622          CONTINUE
        BS(MM)=BS(MM)-2.D0/DH*(1.D0-SIGM)*QFMES*CDM*DX*W(II)*B(M)
 621    CONTINUE
        GO TO 300
C
C       CASE 4: PEC APPROACHES 0
C
 630    DO 631 M=1,3
        MM=NODEL(I,M)
              DO 632 N=1,3
              NN=NODEL(I,N)
              K=LP*NN+MM-LUB
              AS(K)=AS(K)+(B(M)*DB(N)*VS*PHIA+DB(M)*DB(N)*PHIA*DISP/DX
     #             +2.D0/DH*DDM*B(M)*B(N)*DX
     #             -2.D0/DH*RET*BETA*DX*B(M)*B(N)*QFMES)*W(II)
 632    CONTINUE
        BS(MM)=BS(MM)+2.D0/DH*DDM*B(M)*CDM*DX*W(II)
 631    CONTINUE
C
 300    CONTINUE
 200    CONTINUE
        RETURN
        END
C

        SUBROUTINE DGBND1 (A, B, N, ML, NU, LT, IP, DET, NCN1,
     1                      BB, RZ, ITR1, EPS1)
C
```

```
C  ROUTINE SOLVES SYSTEM OF LINEAR EQNS. AX=B WHERE A IS A GENERAL
C  BAND MATRIX. METHOD USED IS GAUSSIAN ELIMINATION WITH PARTIAL
C  PIVOTING. OPTION OF ITERATIVELY IMPROVING SOLUTION IS AVAILABLE.
C  UPPER BAND WIDTH OF MATRIX INCREASES DUE TO INTERCHANGES BY
C  AMOUNT ML. ROUTINE REQUIRES BAND ELEMENTS OF MATRIX TO BE STORED
C  BY COLUMN IN A ONE DIMENSIONAL ARRAY. EACH COLUMN IS OF LENGTH
C  2*ML+NU AND BAND IS TO BE STORED IN ELEMENTS ML+1 TO 2*ML+NU OF
C  EACH COLUMN. ELEMENTS 1 TO ML OF COLUMN ARE SET TO ZERO BY GBAND.

C  IF MATRIX IS SYMMETRIC USER MAY SPECIFY LOWER BAND ONLY IN
C  ELEMENTS ML+NU+1 TO 2*ML+NU OF EACH COLUMN AND GBAND WILL
C  GENERATE REMAINING ELEMENTS. (IF THIS IS DESIRED, SET LT=-1 ON
C  FIRST CALL TO GBAND.)
C   A = 1 DIMENSIONAL ARRAY CONTAINING MATRIX OF COEFFICIENTS.
C   B = 1 DIMENSIONAL ARRAY CONTAINING RIGHT HAND SIDE VECTORS.
C       ON EXIT, B WILL CONTAIN THE SOLUTION VECTOR X.
C   N = ORDER OF MATRIX
C  ML = LENGTH OF LOWER BAND (EXCLUDING DIAGONAL)
C  NU = LENGTH OF UPPER BAND (EXCLUDING DIAGONAL)
C  LT = ABS(LT)=1 IF ONLY 1 B VECTOR OR IF 1ST OF SEVERAL.
C       ABS(LT),=1 FOR SUBSEQUENT B VECTORS.
C       (NOTE. LT=+1 IF FULL BAND WIDTH GIVEN, LT=-1 IF LOWER BAND
C       ONLY OF SYMMETRIC MATRIX GIVEN.)
C  IP = INTEGER ARRAY CONTAINING INTERCHANGE INFORMATION.
C  DET = DETERMINANT OF A = DET*(10**NCN) WHERE 1.D-15<|DET|<1.D+15.
C        IF DET=0.0 MATRIX IS SINGULAR AND ERROR RETURN TAKEN.
C  BB, RZ = ARRAYS REQUIRED FOR IMPROVEMENT OPTION. CAN BE REAL*8
C        VARIABLES IF OPTION NOT REQUIRED.
C  ITER  = 0 IF IMPROVEMENT NOT REQUIRED, OTHERWISE ITER= NO. OF
C        ITERATIONS OR CYCLES.
C  EPS - CONVERGENCE CRITERION.
C
C MODIFIED TO DO ITERATIVE IMPROVEMENT (FORMERLY AVAILABLE ONLY
C WITH THE SINGLE PRECISION VERSION). MIKE PATTERSON - NOV, 1980
      IMPLICIT REAL*8 (A-H, O-Z)
      COMMON /GBAND$/ NITER
      DIMENSION A(1), B(N), IP(N), BB(N), RZ(N)
      COMPLEX*16 DSUMM, QADDQ, QMULD
      REAL*8 QRNDQ
C TO ASSIGN LOGICAL UNITS 94 AND 95 ONLY ONCE:
      LOGICAL ASSIGN /F/, YES /T/
C STATEMENT FUNCTION TO CALCULATE POINTERS INTO A:
      IFN(I, J) = 1 + (J - 1)*LC + I - J + NUM
C
C
      NCN=NCN1
      ITR=ITR1
      EPS=EPS1
      ITER = ITR
C
      LCM = NU + 2*ML
      LC = LCM + 1
      NLC = N*LC
      NUM = NU + ML
C  GENERATE REMAINING ELEMENTS OF SYMMETRIC MATRIX
      IF (LT .NE. -1) GO TO 120
      NN = N - 1
      DO 110 I = 1, NN
         IFI = IFN(I, I)
         IFJ = IFI
         II = I + 1
         IML = MINO(I + ML, N)
         DO 100 J = II, IML
            IFI = IFI + 1
            IFJ = IFJ + LCM
100         A(IFJ) = A(IFI)
110   CONTINUE
120   IF (ITER .EQ. 0) GO TO 140
C ASSIGN UNITS 94 AND 95 IF THEY HAVE NOT ALREADY BEEN ASSIGNED:
      IF (ASSIGN) GO TO 125
      CALL FTNCMD ('ASSIGN 94=-GBAND94;')
```

```
          CALL FTNCMD ('ASSIGN 95=-GBAND95;')
          ASSIGN = YES
125       REWIND 94
          REWIND 95
          DO 130 I = 1, N
130       BB(I) = B(I)
140       IF (IABS(LT) .NE. 1) GO TO 280
          IP(N) = 1
          IF (ML .EQ. 0) GO TO 160
C   SET ELEMENTS 1 - ML OF EACH COLUMN TO ZERO
          DO 150 I = 1, N
             IFK = (I - 1)*LC
             DO 150 J = 1, ML
                IFK = IFK + 1
150       A(IFK) = 0.0D0
160       IF (ITER .NE. 0) CALL DWR1 (A, NLC, 94)
          DET = 0.0D0
          NCN = 0
          IF (ML .EQ. 0) GO TO 230
C   LU DECOMPOSITION
          DO 220 K = 1, N
             IFK = IFN(K, K)
             IF (K .EQ. N) GO TO 210
             KP = K + 1
             KPM = MINO(K + ML, N)
             KPN = MINO(K + NUM, N)

             M = K
             IFM = IFK
             IFI = IFK
             DO 170 I = KP, KPM
                IFI = IFI + 1
                IF (DABS(A(IFI)) .LE. DABS(A(IFM))) GO TO 170
                M = I
                IFM = IFI
170          CONTINUE
             IP(K) = M

             T = A(IFM)
             IF (M .NE. K) IP(N) = -IP(N)
             A(IFM) = A(IFK)
             A(IFK) = T
             IF (T .EQ. 0.0D0) GO TO 260
             OT = 1.0D0/T
             IK = IFK
             DO 180 I = KP, KPM
                IK = IK + 1
180          A(IK) = -A(IK)*OT
             KJ = IFK
             MJ = IFM
             DO 200 J = KP, KPN
                KJ = KJ + LCM
                MJ = MJ + LCM
                T = A(MJ)
                A(MJ) = A(KJ)
                A(KJ) = T
                IF (T .EQ. 0.0D0) GO TO 200
                IK = IFK
                IJ = KJ
                DO 190 I = KP, KPM
                   IK = IK + 1
                   IJ = IJ + 1
190             A(IJ) = A(IJ) + A(IK)*T
200          CONTINUE
210          IF (A(IFK) .EQ. 0.0D0) GO TO 260
220       CONTINUE
230       IFK = IFN(1, 1)
          DET = A(IFK)
          DO 250 K = 2, N
             IFK = IFK + LC
```

```
           DET = DET*A(IFK)
           IF (DET .EQ. 0.0D0) GO TO 260
           IF (DABS(DET) .GT. 1.D-15) GO TO 240
           DET = DET*1.D+15
           NCN = NCN - 15
           GO TO 250
240        IF (DABS(DET) .LT. 1.D+15) GO TO 250
           DET = DET*1.D-15
           NCN = NCN + 15
250        CONTINUE
           DET = DET*IP(N)
           GO TO 280
260        DET = 0.0D0
           WRITE (6, 270) K
270        FORMAT ('0* DGBND1 - matrix is singular. '/
          1        '    Error occurred in attempt to find', I5, 'th pivot.')
           RETURN
280        CALL DSOLV1 (A, B, IP, N, ML, NU)
           IF (ITER .EQ. 0) RETURN
C
C   ITERATIVE IMPROVEMENT
C   RESIDUALS (R) = AX-B ARE FOUND AND STORED IN ARRAY RZ USING
C   EXTENDED PRECISION ARITHMETIC. SYSTEM AZ=R IS SOLVED AND NEW
C   SOLUTION =X+Z IS STORED IN ARRAY B. ABOVE STEPS REPEATED UNTIL
C      (1) MAX(Z)/MAX(X)  < EPS OR
C      (2) NO. OF CYCLES > ITER OR
C      (3) IMPROVEMENT STARTS TO DIVERGE.
C   ROUTINE THEN RETURNS AFTER SETTING EPS=MAX(Z) (FOR (1)) OR
C   SETTING EPS=-MAX(Z) AND PRINTING APPROPRIATE ERROR MESSAGE (FOR
C   (2) AND (3))
C
C
           IF (IABS(LT) .EQ. 1) CALL DWR1 (A, NLC, 95)
           XNORM = 0.0D0
           DO 290 K = 1, N
290        XNORM = DMAX1(XNORM, DABS(B(K)))
           IF (XNORM .LE. 0.0D0) RETURN
           ZX = 1.D+60
           LD = 0
           DO 340 L = 1, ITER
             REWIND 94
             CALL DRE1 (A, NLC, 94)
             DO 310 K = 1, N
               DSUMM = (0.D0, 0.D0)
               KPM = MAXO(K - ML, 1)
               KPN = MINO(K + NU, N)
               IFK = IFN(K, KPM)
               DO 300 J = KPM, KPN
C                DSUMM = DSUMM + A(IFK)*B(J)
C USING EXTENDED PRECISION:
                 DSUMM = QADDQ(DSUMM, QMULD(A(IFK), B(J)))
300              IFK = IFK + LCM
               RZ(K) = BB(K) - QRNDQ(DSUMM)
310          CONTINUE
             REWIND 95
             CALL DRE1 (A, NLC, 95)
             CALL DSOLV1 (A, RZ, IP, N, ML, NU)

             ZNORM = 0.0D0
             DO 320 K = 1, N
               ERZ = RZ(K)
               ZNORM = DMAX1(ZNORM, DABS(ERZ))
320          B(K) = B(K) + ERZ
             IF (ZNORM .GT. ZX) GO TO 330
             IF ((ZNORM - EPS*XNORM) .LT. 0.0D0) GO TO 390
             ZX = ZNORM
             GO TO 340

330          IF (ZNORM .GT. 10.0D0*ZX) GO TO 360
```

```
          LD = LD + 1
          IF (LD .GE. 3) GO TO 360
340    CONTINUE
       L = ITER
       WRITE (6, 350)
350    FORMAT ('0* DGBND1- Iterative improvement did not converge'/)
       GO TO 380
360    WRITE (6, 370)
370    FORMAT ('0* DGBND1 - Iterative improvement is diverging.'/)
380    EPS = -ZNORM
       NITER = L
       RETURN
390    EPS = ZNORM
       NITER = L
       RETURN
       END
       SUBROUTINE DSOLV1 (A, B, IP, N, ML, NU)
C
C  THIS ROUTINE COMPUTES THE SOLUTION OF A SYSTEM AFTER GBAND HAS
C  DECOMPOSED MATRIX A INTO A LOWER TRIANGULAR MATRIX L AND AN
C  UPPER TRIANGULAR MATRIX U.
C.
       IMPLICIT REAL*8 (A-H, O-Z)
       DIMENSION A(1), B(N), IP(N)
       IFN(I, J) = 1 + (J - 1)*LC + I - J + NUM
       LCM = 2*ML + NU
       LC = LCM + 1
       NUM = NU + ML
       MN = N - 1
C  SOLVE FOR Y
       IF (ML .EQ. 0) GO TO 110
       DO 100 K = 1, MN
          KP = K + 1
          M = IP(K)
          T = B(M)
          B(M) = B(K)
          B(K) = T
          KPM = MINO(K + ML, N)
          IFK = IFN(K, K)
          DO 100 I = KP, KPM
             IFK = IFK + 1
100    B(I) = B(I) + A(IFK)*T
C  SOLVE FOR X
110    IFK = IFN(N, N)
       DO 120 KB = 1, MN
          KM = N - KB
          K = KM + 1
          B(K) = B(K)/A(IFK)
          IFK = IFK - LC
          T = -B(K)
          KMN = MAX0(1, K - ML - NU)
          KML = IFN(KMN, K)
          DO 120 I = KMN, KM
             B(I) = B(I) + A(KML)*T
120    KML = KML + 1
       B(1) = B(1)/A(NUM + 1)
       RETURN
       END
       SUBROUTINE DWR1 (A, N, LU)
       REAL*8 A(N)
       WRITE (LU) A
       RETURN
       END
       SUBROUTINE DRE1 (A, N, LU)
       REAL*8 A(N)
       READ (LU) A
       RETURN
       END
```

D.5 Two Protein Steady-State Simulator: MESDISP2.FOR

```
C
C      THIS PROGRAM SIMULATES BOTH CONVECTIVE AND DISPERSIVE PLASMA
C      PROTEIN TRANSPORT THROUGH MESENTERY DURING STEADY-STATE
C      CONDITIONS. THE MESENTERY IS TREATED AS A 1-DIMENSIONAL
C      RECTANGULAR SLAB.
C
       IMPLICIT REAL*8(A-H,O-Z)
       DIMENSION HOLD(1001),IPERM(1001),RES(1001),HOLD1(1000),
      #RES1(1001),IPERM1(1001),HOLD2(1001),RES2(1001),IPERM2(1001)
       COMMON/BLK1/NODEL(500,3),XNOD(1001)
       COMMON/BLK2/DX(1001)
       COMMON/MATBAL/QFC,QCC1,QSC1,QCC2,QSC2,QFV,QCV1,QSV1,QCV2,QSV2,
      #QFM,QCM1,QSM1,QCM2,QSM2,QFM1(500),QCM11(500),QSM11(500),
      #QCM12(500),QSM12(500)
       COMMON/FLUMAT/FLUID(20000)
       COMMON/OLD/POLD(1001),COLD1(1001),COLD2(1001)
       COMMON/SOLB/SOLB1(1001),SOLB2(1001)
       COMMON/FLUB/FLUIDB(1001)
       COMMON/SOLMAT/SOL1(20000),SOL2(20000)
       COMMON/OSMOT/A1,B1,C1,A2,B2,C2
       COMMON/TISDAT/AK,DEFF1,ALPHL1,PHI1,PHIT,RET1,SIGT1,BETA1,
      #DEFF2,ALPHL2,PHI2,RET2,SIGT2,BETA2
       COMMON/CAPDAT/PREF,CREF
       COMMON/WALL/DLC,DLV,DLM,DDC1,DDV1,DDM1,PDC,PDV,PDM,PIDC1,
      #PIDV1,PIDM1,PIDC2,PIDV2,PIDM2,SIGC1,SIGV1,SIGM1,CDC1,CDV1,CDM1,
      #YYL,DDC2,DDV2,DDM2,SIGC2,SIGV2,SIGM2,CDC2,CDV2,CDM2
       COMMON/MAXDAT/DIS1MX,DIS2MX,IDISP1,IDISP2
C

C      SET MARKER AND TOLERANCE VALUES
C
       READ(5,504)OMEGAF,OMEGAC,TOLP,TOLC,PECMAX,EPS
       READ(5,550)IMAX,ITER,NECHO,N
  550  FORMAT(4I3)
       NEX=(N-1)/2
       LUB=2
       ICOUNT=0
C .
C      READ IN THE DATA FROM EXTERNAL FILE
C
       DO 1 I=1,N
       READ(5,501) DX(I)
  501  FORMAT(E12.6)
   1   CONTINUE
C
C
       READ(5,502)  A1,B1,C1,AK,PREF,PHI1,PHIT,RET1,PHIS
       READ(5,504)  A2,B2,C2,PHI2,RET2,BETA2
       READ(5,507)  ALPHL1,AL,DEFF1,SIGT1,CREF,YYL,BETA1
       READ(5,507)  ALPHL2,DEFF2,SIGT2,PERMC2,PERMV2,PERMM2
       READ(5,504)  CONC,CONV,CONM,PERMC1,PERMV1,PERMM1
       READ(5,504)  DDC1,DDV1,DDM1,SIGC1,SIGV1,SIGM1
       READ(5,504)  DDC2,DDV2,DDM2,SIGC2,SIGV2,SIGM2
       READ(5,504)  CDC1,CDV1,CDM1,DLC,DLV,DLM
       READ(5,506)  CDC2,CDV2,CDM2
       READ(5,506)  PDC,PDV,PDM
       READ(5,506)  AOS1,BOS1,COS1
       READ(5,506)  AOS2,BOS2,COS2
       YL=YYL*AL
       PIDC1=CDC1*(AOS1+CDC1*(BOS1+CDC1*COS1))
       PIDC2=CDC2*(AOS2+CDC2*(BOS2+CDC2*COS2))
       PIDV1=CDV1*(AOS1+CDV1*(BOS1+CDV1*COS1))
       PIDV2=CDV2*(AOS2+CDV2*(BOS2+CDV2*COS2))
       PIDM1=CDM1*(AOS1+CDM1*(BOS1+CDM1*COS1))
       PIDM2=CDM2*(AOS2+CDM2*(BOS2+CDM2*COS2))
```

```
      PC=PDC*PREF
      PV=PDV*PREF
      PM=PDM*PREF
      CC1=CDC1*CREF
      CV1=CDV1*CREF
      CM1=CDM1*CREF
      CC2=CDC2*CREF
      CV2=CDV2*CREF
      CM2=CDM2*CREF
C
C
C
  507 FORMAT(7E10.4)
  502 FORMAT(9E10.4)
  503 FORMAT(5E10.4)
  504 FORMAT(6E10.4)
  506 FORMAT(3E10.4)
C
      DO 21 I=1,N
      READ(5,505) POLD(I),COLD1(I),COLD2(I)
  505 FORMAT(3E10.4)
   21 CONTINUE
C
C     ECHO DATA IF NECHO N.E. 0
C
      IF(NECHO.EQ.0)  GO TO 999
C
C     PRINT OUT INPUT DATA
C
      WRITE(6,611)
  611 FORMAT(1X,'STEADY-STATE  FLUID PRESSURE AND SOLUTE CONCENTRATION'
     #)
      WRITE(6,679)
  679 FORMAT(1X,'PROFILES  FOR ONE DIMENSIONAL TISSUE SYSTEM',//)
      WRITE(6,612)
      WRITE(6,612)
  612 FORMAT(//,1X,'_____'
     #,//)
      WRITE(6,660)
  660 FORMAT(1X,'INPUT  PARAMETERS')
      WRITE(6,612)
      WRITE(6,613)
  613 FORMAT(1X,'1.  GRID DATA:',//)
      WRITE(6,614)NEX,DX(2)
  614 FORMAT(1X,'NUMBER  OF ELEMENTS:',1X,I2,/,1X,
     #'SMALLEST  X INCREMENT:',19X,E10.4,/)
      WRITE(6,616)N
  616 FORMAT(1X,'TOTAL  NUMBER OF NODES:',10X,I4,/)
      WRITE (6,612)
      WRITE(6,617) TOLP,TOLC,IMAX,OMEGAF,OMEGAC,PECMAX
  617 FORMAT(1X,'2.  CONVERGENCE  CRITERIA:',//,1X,'PRESSURE  TOLERANCE:'
     #,17X,E10.4,/,1X,'SOLUTE  TOLERANCE:',20X,E10.4,/,1X,
     #'MAXIMUM NUMBER OF LOOP ITERATIONS:',2X,I3,/,1X,
     #'PRESSURE RELAXATION PARAMETER:',6X,E10.4,/,1X,
     #'SOLUTE RELAXATION PARAMETER:',9X,E10.4,/,1X,
     #'MAXIMUM DESIRED GRID PECLET NUMBER:',1X,E10.4)
      WRITE(6,612)

      PIC1=PIDC1*PREF
      PIV1=PIDV1*PREF
      PIM1=PIDM1*PREF
      PIC2=PIDC2*PREF
      PIV2=PIDV2*PREF

      PIM2=PIDM2*PREF
C
      WRITE(6,618)  AL,YL,CC1,CV1,CM1,CC2,CV2,CM2,
```

```
      #PC,PV,PM,PIC1,PIV1,PIM1,PIC2,PIV2,PIM2,AK
  618 FORMAT(1X,'3. DIMENSIONAL INPUT PARAMETERS:',//,1X,
      #'TISSUE X-DIMENSION (CM):',21X,E10.4,/,1X,
      #'TISSUE Y-DIMENSION (CM):',21X,E10.4,/,1X,
      #'CAP. PROTEIN1 CONC.  (GRAMS/DL):',14X,E10.4,/,1X,
      #'VEN. PROTEIN1 CONC.  (GRAMS/DL):',14X,E10.4,/,1X,
      #'MES. PROTEIN1 CONC.  (GRAMS/DL):',14X,E10.4,/,1X,
      #'CAP. PROTEIN2 CONC.  (GRAMS/DL):',14X,E10.4,/,1X,
      #'VEN. PROTEIN2 CONC.  (GRAMS/DL):',14X,E10.4,/,1X,
      #'MES. PROTEIN2 CONC.  (GRAMS/DL):',14X,E10.4,/,1X,
      #'CAP. DYN. PRESSURE (DYN/CM**2):',14X,E10.4,/,1X,
      #'VEN. DYN. PRESSURE (DYN/CM**2):',14X,E10.4,/,1X,
      #'MES. DYN. PRESSURE (DYN/CM**2):',14X,E10.4,/,1X,
      #'CAP. OSM1. PRESSURE (DYN/CM**2):',14X,E10.4,/,1X,
      #'VEN. OSM1. PRESSURE (DYN/CM**2):',14X,E10.4,/,1X,
      #'MES. OSM1. PRESSURE (DYN/CM**2):',14X,E10.4,/,1X,
      #'CAP. OSM2. PRESSURE (DYN/CM**2):',14X,E10.4,/,1X,
      #'VEN. OSM2. PRESSURE (DYN/CM**2):',14X,E10.4,/,1X,
      #'MES. OSM2. PRESSURE (DYN/CM**2):',14X,E10.4,/,1X,
      #'TISSUE FLUID CONDUCTIVITY (CM**4/(DYN-SEC):',2X,E10.4)
      WRITE(6,698) DEFF1,DEFF2
  698 FORMAT(1X,
      #'TISSUE SOLUTE1 DIFFUSIVITY (CM**2/SEC):',7X,E10.4,/,1X,
      #'TISSUE SOLUTE2 DIFFUSIVITY (CM**2/SEC):',7X,E10.4)
      WRITE(6,626) CONC,CONV,CONM,PERMC1,PERMV1,PERMM1,PERMC2,PERMV2,
      #PERMM2
  626 FORMAT(1X,'CAP. CONDUCTIVITY (CM**3/(DYN-S));',11X,E10.4,/,1X,
      #'VEN. CONDUCTIVITY (CM**3/(DYN-S)):',11X,E10.4,/,1X,
      #'MES. CONDUCTIVITY (CM**3/(DYN-S)):',11X,E10.4,/,1X,
      #'CAP. PERMEABILITY 1 (CM/S):',21X,E10.4,/,1X,
      #'VEN. PERMEABILITY 1 (CM/S):',21X,E10.4,/,1X,
    - #'MES. PERMEABILITY 1 (CM/S):',21X,E10.4,/,1X,
      #'CAP. PERMEABILITY 2 (CM/S):',21X,E10.4,/,1X,
      #'VEN. PERMEABILITY 2 (CM/S):',21X,E10.4,/,1X,
      #'MES. PERMEABILITY 2 (CM/S):',21X,E10.4)
      WRITE(6,612)
      WRITE(6,653) SIGT1,RET1,BETA1,ALPHL1,SIGT2,RET2,BETA2,ALPHL2
  653 FORMAT(1X,'DIMENSIONLESS INPUT PARAMETERS:',//,1X,
      #'TISSUE REFLECTION COEFFICIENT 1:',15X,E10.4,/,
      #1X,'RETARDATION FACTOR 1:',26X,E10.4,/,1X,
      #'HYDRAULIC CONDUCTIVITY RATIO, BETA1:',15X,E10.4,/,1X,
      #'DIMENSIONLESS DISPERSIVITY 1:',21X,E10.4,/,1X,
      #'TISSUE REFLECTION COEFFICIENT 2:',15X,E10.4,/,
      #1X,'RETARDATION FACTOR 2:',26X,E10.4,/,1X,
      #'HYDRAULIC CONDUCTIVITY RATIO, BETA2:',15X,E10.4,/,1X,
      #'DIMENSIONLESS DISPERSIVITY 2:',21X,E10.4)
      WRITE(6,619)PDC,PIDC1,PIDC2,PDV,PIDV1,PIDV2,PDM,PIDM1,PIDM2
  619 FORMAT(//,1X,
      #'PRESSURE:',6X,'DYNAMIC',5X,'OSMOTIC1',5X,'OSMOTIC2',
      #//,1X,'CAPILLARY:',5X,  E10.4,2X,E10.4,2X,E10.4,
      #/,1X,'VENULE:',8X,E10.4,2X,E10.4,2X,E10.4,/,1X,'MESOTHELIUM:',
      #3X,E10.4,2X,E10.4,2X,E10.4,//)
      WRITE(6,620)CDC1,CDC2,CDV1,CDV2,CDM1,CDM2
  620 FORMAT(1X,'CONCENTRATIONS:  PROTEIN1   PROTEIN2',
      #//,1X,'CAPILLARY:',6X,E10.4,1X,E10.4,/,1X,
      #'VENULE:',10X,E10.4,1X,E10.4,/,1X,'MESOTHELIUM:',2(1X,E10.4),//)
      WRITE(6,621)SIGC1,SIGC2,SIGV1,SIGV2,SIGM1,SIGM2
  621 FORMAT(1X,'REFLECTION  COEFFICIENTS:  PROTEIN1    PROTEIN2',
      #//,1X,'CAPILLARY:',15X,E10.4,1X,E10.4,/,1X,'VENULE:',19X,
      #E10.4,1X,E10.4,/,1X,'MESOTHELIUM:',13X,E10.4,1X,E10.4,//)
      WRITE(6,622)DLC,DLV,DLM
  622 FORMAT(1X,'VESSEL FLUID CONDUCTANCES:',//,1X,'CAPILLARY:',5X,
      #E10.4,/,1X,'VENULE:',9X,E10.4,/,1X,'MESOTHELIUM:',1X,E10.4,//)
```

```
        WRITE(6,625)A1,B1,C1,A2,B2,C2
625 FORMAT(1X,'VIRIAL  COEFFICIENTS:',//,1X,'A1:',1X,E10.4,/,1X,
   #'B1:',1X,E10.4,/,1X,'C1:',1X,E10.4,/,1X,'A2:',1X,E10.4,/,1X,
   #'B2:',1X,E10.4,/,1X,'C2:',1X,E10.4,//)
        WRITE(6,623)DDC1,DDC2,DDV1,DDV2,DDM1,DDM2
623 FORMAT(1X,'VESSEL SOLUTE PERMEABILITIES: PROTEIN1   PROTEIN2'
   #,//,1X,'CAPILLARY:',19X,E10.4,1X,E10.4,/,1X,'VENULE',22X,E10.4,
   #1X,E10.4,/,1X,'MESOTHELIUM:',17X,E10.4,1X,E10.4,//)
        WRITE(6,624)PHIT,PHI1,PHI2,PHIS
624 FORMAT(1X,'TOTAL  TISSUE FLUID VOLUME FRACTION:',2X,E10.4,/,1X,
   #'SOLUTE 1 DISTRIBUTION VOLUME FRACTION:',1X,E10.4,/,1X,
   #'SOLUTE 2 DISTRIBUTION VOLUME FRACTION:',1X,E10.4,/,1X,
   #'TOTAL SOLIDS VOLUME FRACTION:',8X,E10.4,///)
C
C
C
999 CALL GRID(NEX)
C
C       INITIALIZE FLUID VECTOR
C
        CALL SETMAT(NEX,0,PE1,IE1,VELMX1,PE2,IE2,VELMX2)
C
C       ADJUST FLUID VECTOR TO FIT BOUNDARY CONDITIONS
C
        CALL ASTAR(NEX,0)
        CALL VSTAR(NEX,0)
C
C       ENTER ITERATION LOOP, CHECK COUNTER VALUE
C
C
C
100 ICOUNT=ICOUNT+1
        IF(ICOUNT.GT.IMAX)GO TO 200
C
C
C       INITIALIZE FLUIDB VECTOR AND ADJUST TO FIT BOUNDARY CONDITIONS
C
        CALL SETMAT(NEX,1,PE1,IE1,VELMX1,PE2,IE2,VELMX2)
C
        .CALL ASTAR(NEX,1)
        CALL VSTAR(NEX,1)
C
C       SOLVE THE FLUID SYSTEM
C
        EP=EPS
        CALL DGBAND(FLUID,FLUIDB,N,LUB,LUB,ICOUNT,IPERM,DET,JEXP,HOLD,
   #RES,ITER,EP)
C
C       DETERMINE THE MAXIMUM CHANGE IN P FROM ONE ITERATION TO THE NEXT
C       AND UPDATE POLD USING A RELAXATION PROCEDURE. PDIFMX WILL BE
C       COMPARED TO TOLP TO ESTABLISH CONVERGENCE
C
        PMAX=0.D0
        PDIFMX=0.D0
        DO 3 I=1,N
        IF(DABS(FLUIDB(I)).GT.PMAX)  PMAX=DABS(FLUIDB(I))
        TEST=DABS(FLUIDB(I)-POLD(I))
        IF(TEST.GT.PDIFMX)  PDIFMX=TEST
        POLD(I)=(OMEGAF)*(FLUIDB(I)-POLD(I))+POLD(I)
3       CONTINUE
        PDIFMX=PDIFMX/PMAX
C
C       NOW INITIALIZE SOLUTE AND SOLUTB. STORE MAX. GRID PECLET
C       NUMBER IN PECLET. ADJUST SOLUTE AND SOLUTB TO SUIT BOUNDARY
C       CONDITIONS
C
        CALL SETMAT(NEX,2,PE1,IE1,VELMX1,PE2,IE2,VELMX2)
        PEC1=PE1
```

```
      IEL1=IE1
      PEC2=PE2
      IEL2=IE2
      CALL PATART(NEX)
      CALL PATVEN(NEX)
C
C
C     SOLVE THE SYSTEM OF EQUATIONS FOR THE SOLUTE FLOW EQUATION
C
      EP1=EPS
      CALL DGBND1(SOL1,SOLB1,N,LUB,LUB,1,IPERM1,DET,JEXP,HOLD1,
     #RES1,ITER,EP1)
      EP2=EPS
      CALL DGBND1(SOL2,SOLB2,N,LUB,LUB,1,IPERM2,DET,JEXP,HOLD2,
     #RES2,ITER,EP2)
C
C     DETERMINE THE MAXIMUM CHANGE IN CALCULATED CONCENTRATION FROM
C     ONE ITERATION TO THE NEXT, AND UPDATE COLD USING A RELAXATION
C     PROCEDURE. CDIFMX WILL BE COMPARED TO TOLC TO ESTABLISH
C     CONVERGENCE
C
C
      CMAX1=0.D0
      CDMX1=0.D0
      CMAX2=0.D0
      CDMX2=0.D0
      DO 4 I=1,N
      IF(DABS(SOLB1(I)).GT.CMAX1)  CMAX1=DABS(SOLB1(I))
      TEST1=DABS(SOLB1(I)-COLD1(I))
      IF(TEST1.GT.CDMX1)  CDMX1=TEST1
      COLD1(I)=(OMEGAC)*(SOLB1(I)-COLD1(I))+COLD1(I)
      IF(DABS(SOLB2(I)).GT.CMAX2)  CMAX2=DABS(SOLB2(I))
      TEST2=DABS(SOLB2(I)-COLD2(I))
      IF(TEST2.GT.CDMX2)  CDMX2=TEST2
      COLD2(I)=(OMEGAC)*(SOLB2(I)-COLD2(I))+COLD2(I)
    4 CONTINUE
      CDMX1=CDMX1/CMAX1
      CDMX2=CDMX2/CMAX2
C
C     CHECK TO SEE IF FURTHER ITERATION IS REQUIRED
C
      IF(PDIFMX.GT.TOLP) GO TO 100
      IF(CDMX1.GT.TOLC) GO TO 100
      IF(CDMX2.GT.TOLC) GO TO 100
C
      GO TO 300
C
C     MAXIMUM NUMBER OF ITERATIONS REACHED. PRINT OUT WARNING.
C
  200 ICOUNT=ICOUNT-1
      WRITE(6,600) ICOUNT
  600 FORMAT(//,1X,'WARNING.  CONVERGENCE CRITERIA NOT MET AFTER',
     #1X,I3,1X,'ITERATIONS')
      WRITE(6,601) PDIFMX,CDMX1,CDMX2
  601 FORMAT(//,1X,'MAX.  FRAC.  CHANGE IN P',2X,
     #'MAX.  FRAC.  CHANGE IN C1',2X,
     #'MAX.  FRAC.  CHANGE IN C2',
     #//,6X,E9.4,14X,E9.4,14X,E9.4,//)
C
  300 IF(PEC1.LT.PECMAX)  GO TO 400
      IF(PEC2.LT.PECMAX)GO TO 400
      WRITE(6,603) PEC1,IEL1,PEC2,IEL2
  603 FORMAT(//,1X,'WARNING.  PROTEIN 1 GRID PECLET NUMBER EQUALS',
     #1X,E9.4,3X,'ELEMENT  LOCATION:',1X,I4,//,1X,
     #'PROTEIN  2 GRID PECLET NUMBER EQUALS',1X,E9.4,3X,

     #'ELEMENT LOCATION:',1X,I4,//)
C
  400 WRITE(6,604) ICOUNT
  604 FORMAT('1',//,'STEADY-STATE  SOLUTION ACHIEVED AFTER',1X,I3,1X,
```

```
      #'ITERATIONS:')
         WRITE(6,670) PEC1,IEL1,DIS1MX,IDISP1,PEC2,IEL2,DIS2MX,IDISP2
  670 FORMAT(//,1X,'MAXIMUM  GRID PECLET1 NUMBER:',1X,E9.4,3X,
      #'ELEMENT LOCATION:',1X,I4,/,1X,'MAXIMUM  DISPERSION COEFF1:',
      #1X,E9.4,'   ELEMENT LOCATION:',1X,I4,
      #/,1X,'MAXIMUM GRID PECLET2 NUMBER:',1X,E9.4,3X,
      #'ELEMENT LOCATION:',1X,I4,/,1X,'MAXIMUM  DISPERSION COEFF2:',
      #1X,E9.4,'   ELEMENT LOCATION:',1X,I4)
         WRITE(6,601)PDIFMX,CDMX1,CDMX2
C

         WRITE(6,605)
  605 FORMAT(//,1X,'X POSITION',2X,'DYN. PRESS',2X,'OSM. PRESS',2X,
      #'AVAIL. CONC1',2X,'TOTAL CONC1',2X,'AVAIL. CONC2',2X,
      #'TOTAL CONC2',//)
C
         X=0.D0
         DO 5 I=1,N
         X=X+DX(I)
         PI=COLD1(I)*(A1+COLD1(I)*(B1+COLD1(I)*C1))
      #   +COLD2(I)*(A2+COLD2(I)*(B2+COLD2(I)*C2))
         CON1=COLD1(I)*PHI1/(1.D0-PHIS)
         CON2=COLD2(I)*PEI2/(1.D0-PHIS)
C
C        WRITE OUT PROFILE DATA TO DEVICES 6 AND 7
C
         WRITE(6,606)  X,POLD(I),PI,COLD1(I),CON1,COLD2(I),CON2
         WRITE(7,606)  X,POLD(I),PI,COLD1(I),CON1,COLD2(I),CON2
         WRITE(4,401)  POLD(I),COLD1(I),COLD2(I)
  606 FORMAT(1X,E9.3,6(2X,E10.4))
  401 FORMAT(3(1X,E14.7))
    5 CONTINUE
C
C        WRITE OUT MESOTHELIAL FLUX DATA TO DEVICE 7
C
         CALL MASBAL(NEX)
         DO 6 I=1,NEX
         I2=2*I
         X=XNOD(I2)
         WRITE(7,702)  X,QFM1(I),QSM11(I),QCM11(I),QSM12(I),QCM12(I)
  702 FORMAT(6(2X,E10.4))
    6 CONTINUE
C
C
         WRITE(6,607)
  607 FORMAT('1',//,1X,'MASS  BALANCE DATA'////)
C
         WRITE(6,608)
  608 FORMAT(///,1X,'NET DIMENSIONLESS FLUID FLOWS')
         TF=QFC+QFV+QFM*2.D0
         WRITE(6,609)  QFC,QFV,QFM,TF
  609 FORMAT(//,1X,'CAP:',1X,E12.4,/,1X,'VEN:',
      #E12.4,/,1X,'MES:',1X,E12.4,/,1X,'TOT:',1X,E12.4)
         WRITE(6,661)
  661 FORMAT(///,1X,'NET DIMENSIONLESS SOLUTE FLOWS: SOLUTE1')
         TS1=QSC1+QSV1+QSM1*2.D0
         WRITE(6,609)QSC1,QSV1,QSM1,TS1
         WRITE(6,662)
  662 FORMAT(//,1X,'CONVECTIVE  COMPONENTS OF DIMENSIONLESS SOLUTE
      #FLOWS: SOLUTE1')
         TC1=QCM1*2.D0+QCC1+QCV1
         WRITE(6,610)  QCC1,QCV1,QCM1,TC1
  610 FORMAT(//,1X,'CAP:',1X,E12.4,/,1X,'VEN:',1X,E12.4,/,1X,'MES:',
      #1X,E12.4,/,1X,'TOT:',1X,E12.4)
C
         WRITE(6,663)
  663 FORMAT(///,1X,'NET DIMENSIONLESS SOLUTE FLOWS: SOLUTE2')
         TS2=QSC2+QSV2+QSM2*2.D0
```

```
      WRITE(6,609)QSC2,QSV2,QSM2,TS2
      WRITE(6,664)
  664 FORMAT(//,1X,'CONVECTIVE  COMPONENTS OF DIMENSIONLESS SOLUTE
     #FLOWS: SOLUTE2')
      TC2=QCM2*2.D0+QCC2+QCV2
      WRITE(6,629) QCC2,QCV2,QCM2,TC2
  629 FORMAT(//,1X,'CAP:',1X,E12.4,/,1X,'VEN:',1X,E12.4,/,1X,'MES:',
     #1X,E12.4,/,1X,'TOT:',1X,E12.4)
C
      WRITE(6,669)
  669 FORMAT(//,1X,'ERROR  IN GLOBAL MATERIAL BALANCES')
      EFLU=TF/QFC
      ESOL1=TS1/QSC1
      ESOL2=TS2/QSC2
      WRITE(6,665) EFLU, ESOL1,ESOL2
  665 FORMAT(//,1X,'FLUID  BALANCE:',1X,E12.4,/,1X,'SOLUTE  1 BALANCE:',
     #1X,E12.4,/,1X,'SOLUTE  2 BALANCE:',1X,E12.4)
C
      WRITE(6,666)
  666 FORMAT(//,1X,
     #'RATIO OF CONV. TO DIFFUS. FLUXES AT BOUNDARIES: SOLUTE 1')
      IF(DABS(QSC1-QSV1).LT.1.D-9)  THEN
      PECC1=999.999D0
      ELSE
      PECC1=QCC1/(QSC1-QCC1)
      ENDIF
      IF(DABS(QSV1-QCV1).LT.1.D-9)  THEN

      PECV1=999.999D0
      ELSE
      PECV1=QCV1/(QSV1-QCV1)
      ENDIF
      IF(DABS(QSM1-QCM1).LT.1.D-9)  THEN
      PECM1=999.999D0
      ELSE
      PECM1=QCM1/(QSM1-QCM1)
      ENDIF
      WRITE(6,667) PECC1,PECV1,PECM1
  667 FORMAT(//,1X,'CAP:',1X,E12.4,/,1X,'VEN:',1X,E12.4,/,1X,'MES:',
     #1X,E12.4)
C
      WRITE(6,668)
  668 FORMAT(//,1X,
     #'RATIO OF CONV. TO DIFFUS. FLUXES AT BOUNDARIES: SOLUTE 2')
      IF(DABS(QSC2-QCC2).LT.1.D-9)  THEN
      PECC2=999.999D0
      ELSE
      PECC2=QCC2/(QSC2-QCC2)
      ENDIF
      IF(DABS(QSV2-QCV2).LT.1.D-9)  THEN
      PECV2=999.999D0
      ELSE
      PECV2=QCV2/(QSV2-QCV2)
      ENDIF
      IF(DABS(QSM2-QCM2).LT.1.D-9)  THEN
      PECM2=999.999D0
      ELSE
      PECM2=QCM2/(QSM2-QCM2)
      ENDIF
      WRITE(6,667) PECC2,PECV2,PECM2
      STOP
      END
      SUBROUTINE MASBAL(NEX)

C
C     THIS SUBROUTINE PERFORMS A MATERIAL BALANCE ON THE SYSTEM FOR
C     BOTH FLUID AND PLASMA PROTEINS.
C
      IMPLICIT REAL*8(A-H,O-Z)
```

```
      COMMON/MATBAL/QFC,QCC1,QSC1,QCC2,QSC2,QFV,QCV1,QSV1,QCV2,QSV2,
     #QFM,QCM1,QSM1,QCM2,QSM2,QFM1(500),QCM11(500),QSM11(500),
     #QCM12(500),QSM12(500)
      COMMON/OLD/POLD(1001),COLD1(1001),COLD2(1001)
      COMMON/BLK1/NODEL(500,3),XNOD(1001)
      COMMON/OSMOT/A1,B1,C1,A2,B2,C2
      COMMON/TISDAT/AK,DEFF1,AL1,PHI1,PHIT,RET1,SIGT1,BETA1,
     #              DEFF2,AL2,PHI2,RET2,SIGT2,BETA2
      COMMON/CAPDAT/PC,CREF
      COMMON/WALL/DLC,DLV,DLM,DDC1,DDV1,DDM1,PDC,PDV,PDM,PIDC1,PIDV1,
     #PIDM1,PIDC2,PIDV2,PIDM2,SIGC1,SIGV1,SIGM1,CDC1,CDV1,CDM1,DH,
     #              DDC2,DDV2,DDM2,SIGC2,SIGV2,SIGM2,CDC2,CDV2,CDM2
      DIMENSION GAUS(4),W(4),B(3)
      DATA NGAUS/4/
      DATA W/.347854845137454D0,.652145154862546D0,
     #.652145154862546D0,.347854845137454D0/
      DATA GAUS/-.861136311594053D0,-.339981043584856D0,
     #.339981043584856D0,.861136311594053D0/
C
C     FIRST, CALCULATE THE NET FLOWS ACROSS THE ARTERIOLAR WALL
C
      PIC1=COLD1(1)*(A1+COLD1(1)*(B1+COLD1(1)*C1))
      PIC2=COLD2(1)*(A2+COLD2(1)*(B2+COLD2(1)*C2))
      QFC=DH*AK*PC/DEFF1*DLC*(POLD(1)-PDC-SIGC1*(PIC1-PIDC1)-
     #    SIGC2*(PIC2-PIDC2))
      QCC1=BETA1*QFC*COLD1(1)*RET1
      QCC2=BETA2*QFC*COLD2(1)*RET2
      PECC1=(1.D0-SIGC1)*QFC/(DDC1*DH)
      IF(PECC1.GT.100.D0)GO TO 110
      IF(PECC1.LT.-100.D0)GO TO 120
      TEST=1.D0-DEXP(-PECC1)
      IF(DABS(TEST).LT.1.D-10)GO TO 130
      QSC1=(1.D0-SIGC1)*QFC*(COLD1(1)-CDC1*DEXP(-PECC1))/TEST
      GO TO 101
110   QSC1=QFC*(1.D0-SIGC1)*COLD1(1)
      GO TO 101
120   QSC1=(1.D0-SIGC1)*CDC1*QFC
      GO TO 101
130   QSC1=DH*DDC1*(COLD1(1)-CDC1)
C
101   PECC2=(1.D0-SIGC2)*QFC/(DDC2*DH)
      IF(PECC2.GT.100.D0)GO TO 111
      IF(PECC2.LT.-100.D0)GO TO 121
      TEST=1.D0-DEXP(-PECC2)
      IF(DABS(TEST).LT.1.D-10)GO TO 131
      QSC2=(1.D0-SIGC2)*QFC*(COLD2(1)-CDC2*DEXP(-PECC2))/TEST
      GO TO 200
111   QSC2=QFC*(1.D0-SIGC2)*COLD2(1)
      GO TO 200
121   QSC2=(1.D0-SIGC2)*CDC2*QFC
      GO TO 200
131   QSC2=DH*DDC2*(COLD2(1)-CDC2)
C
C     NOW FOR THE VENULAR WALL
C
200   N=NEX*2+1
      PIV1=COLD1(N)*(A1+COLD1(N)*(B1+COLD1(N)*C1))
      PIV2=COLD2(N)*(A2+COLD2(N)*(B2+COLD2(N)*C2))

      QFV=DH*AK*PC/DEFF1*DLV*(POLD(N)-PDV-SIGV1*(PIV1-PIDV1)   -
     #    SIGV2*(PIV2-PIDV2))
      QCV1=BETA1*QFV*COLD1(N)*RET1
      QCV2=BETA2*QFV*COLD2(N)*RET2
      PECV1=(1.D0-SIGV1)*QFV/(DDV1*DH)
      IF(PECV1.GT.100.D0)GO TO 210
      IF(PECV1.LT.-100.D0)GO TO 220
      TEST=1.D0-DEXP(-PECV1)
      IF(DABS(TEST).LT.1.D-10)GO TO 230
      QSV1=(1.D0-SIGV1)*QFV*(COLD1(N)-CDV1*DEXP(-PECV1))/TEST
```

```
        GO TO 201
  210   QSV1=QFV*(1.DO-SIGV1)*COLD1(N)
        GO TO 201
  220   QSV1=(1.DO-SIGV1)*CDV1*QFV
        GO TO 201
  230   QSV1=DH*DDV1*(COLD1(N)-CDV1)
C
  201   PECV2=(1.DO-SIGV2)*QFV/(DDV2*DH)
        IF(PECV2.GT.100.DO)GO  TO 211
        IF(PECV2.LT.-100.DO)GO  TO 221
        TEST=1.DO-DEXP(-PECV2)
        IF(DABS(TEST).LT.1.D-10)GO  TO 231
        QSV2=(1.DO-SIGV2)*QFV*(COLD2(N)-CDV2*DEXP(-PECV2))/TEST
        GO TO 300
  211   QSV2=QFV*(1.DO-SIGV2)*COLD2(N)
        GO TO 300
  221   QSV2=(1.DO-SIGV2)*CDV2*QFV
        GO TO 300
  231   QSV2=DH*DDV2*(COLD2(N)-CDV2)
C
C       AND FINALLY, THE MESOTHELIAL LAYER
C
C       CONSIDER THE MESOTHELIAL WALL, ELEMENT BY ELEMENT.
C
  300   QSM1=0.DO
        QCM1=0.DO
        QSM2=0.DO
        QCM2=0.DO
        QFM=0.DO
C
        DO 401 I=1,NEX
        QSM11(I)=0.DO
        QFM1(I)=0.DO
        QCM11(I)=0.DO
        QSM12(I)=0.DO
        QCM12(I)=0.DO
  401   CONTINUE
C
        DO 1 II=1,NGAUS
        S=GAUS(II)
            DO 2 I=1,NEX
            X1=XNOD(NODEL(I,1))
            X2=XNOD(NODEL(I,2))
            X3=XNOD(NODEL(I,3))
            S2=(2.DO*X2-(X1+X3))/(X3-X1)
C
            B(1)=(S-S2)*(S-1.DO)/(2.DO*(S2+1.DO))
            B(2)=(S+1.DO)*(S-1.DO)/(S2*S2-1.DO)
            B(3)=(S+1.DO)*(S-S2)/(2.DO*(1.DO-S2))
            DX=(X3-X1)*.5DO
C
C       CALCULATE C(S), PI(S), AND P(S)
C
            CS1=0.DO
            CS2=0.DO
            PS=0.DO
            DO 3 IT=1,3
            CS1=CS1+COLD1(NODEL(I,IT))*B(IT)
            CS2=CS2+COLD2(NODEL(I,IT))*B(IT)
            PS=PS+POLD(NODEL(I,IT))*B(IT)
  3         CONTINUE
            PIS1=CS1*(A1+CS1*(B1+CS1*C1))
            PIS2=CS2*(A2+CS2*(B2+CS2*C2))
C
C       CALCULATE THE FLUXES
C
            FLOW=AK*PC/DEFF1*DLM*(PS-PDM-SIGM1*(PIS1-PIDM1)
      #          - SIGM2*(PIS2-PIDM2))*W(II)*DX
            QFM=QFM+FLOW
```

```
            QFM1(I)=QFM1(I)+FLOW/(X3-X1)
            QCM1=QCM1+FLOW*CS1*BETA1*RET1
            QCM2=QCM2+FLOW*CS2*BETA2*RET2
            QCM11(I)=QCM11(I)+FLOW*CS1*BETA1/(X3-X1)*RET1
            QCM12(I)=QCM12(I)+FLOW*CS2*BETA2/(X3-X1)*RET2
C
C       DETERMINE WHICH FORM OF THE NONLINEAR FLUX EQN. IS TO BE USED.
C
            QS=FLOW/(W(II)*DX)
            PECM1=QS*(1.D0-SIGM1)/DDM1
            IF(PECM1.GT.100.D0)GO  TO 410
            IF(PECM1.LT.-100.D0)GO  TO 420
            TESTM=1.D0-DEXP(-PECM1)
            IF(DABS(TESTM).LT.1.D-10)GO  TO 430
C
C       USE THE FULL EXPRESSION
C
            SFLOW1=FLOW*(1.D0-SIGM1)*(CS1-CDM1*DEXP(-PECM1))/TESTM
            QSM1=QSM1+SFLOW1

            QSM11(I)=QSM11(I)+SFLOW1/(X3-X1)
            GO TO 500
C
  410       SFLOW1=FLOW*(1.D0-SIGM1)*CS1
            QSM1=QSM1+SFLOW1
            QSM11(I)=QSM11(I)+SFLOW1/(X3-X1)
            GO TO 500
C
  420       SFLOW1=FLOW*(1.D0-SIGM1)*CDM1
            QSM1=QSM1+SFLOW1
            QSM11(I)=QSM11(I)+SFLOW1/(X3-X1)
            GO TO 500
C
  430       SFLOW1=DDM1*(CS1-CDM1)*DX*W(II)
            QSM1=QSM1+SFLOW1
            QSM11(I)=QSM11(I)+SFLOW1/(X3-X1)
C
  500       PECM2=QS*(1.D0-SIGM2)/DDM2
            IF(PECM2.GT.100.D0)GO  TO 510
            IF(PECM2.LT.-100.D0)GO  TO 520
            TESTM=1.D0-DEXP(-PECM2)
            IF(DABS(TESTM).LT.1.D-10)GO  TO 530
C
C       USE THE FULL EXPRESSION
C
            SFLOW2=FLOW*(1.D0-SIGM2)*(CS2-CDM2*DEXP(-PECM2))/TESTM
            QSM2=QSM2+SFLOW2
            QSM12(I)=QSM12(I)+SFLOW2/(X3-X1)
            GO TO 2
C
  510       SFLOW2=FLOW*(1.D0-SIGM2)*CS2
            QSM2=QSM2+SFLOW2
            QSM12(I)=QSM12(I)+SFLOW2/(X3-X1)
            GO TO 2
C
  520       SFLOW2=FLOW*(1.D0-SIGM2)*CDM2
            QSM2=QSM2+SFLOW2
            QSM12(I)=QSM12(I)+SFLOW2/(X3-X1)
            GO TO 2
C
  530       SFLOW2=DDM2*(CS2-CDM2)*DX*W(II)
            QSM2=QSM2+SFLOW2
            QSM12(I)=QSM12(I)+SFLOW2/(X3-X1)
C
  2         CONTINUE
  1     CONTINUE
        RETURN
        END
        SUBROUTINE GRID(NEX)
C
```

```
C      THIS SUBROUTINE CALCULATES THE SPATIAL LOCATION OF THE NODES
C      FOR EACH ELEMENT, ALONG WITH THE NODES ASSOCIATED WITH A
C      GIVEN ELEMENT.
C
       IMPLICIT REAL*8(A-H,O-Z)
       COMMON/BLK1/NODEL(500,3),  XNOD(1001)
       COMMON/BLK2/DX(1001)
C
       K=1
       DO 1 I=1,NEX
       NODEL(I,1)=K
       NODEL(I,2)=K+1
       NODEL(I,3)=K+2
       K=K+2
  1    CONTINUE
C
       X=0.DO
       NP=2*NEX+1
       DO 2 I=1,NP
       X=X+DX(I)
       XNOD(I)=X
  2    CONTINUE
       RETURN
       END
C
       SUBROUTINE VSTAR(NEX,IND)
C

C      THIS SUBROUTINE ADJUSTS THE AF AND BF VECTORS TO ACCOUNT FOR THE
C      STARLING BOUNDARY CONDITION AT THE VENULAR WALL.
C
       IMPLICIT REAL*8(A-H,O-Z)
       COMMON/BLK1/NODEL(500,3),  XNOD(1001)
       COMMON/FLUMAT/AF(20000)
       COMMON/FLUB/BF(1001)
       COMMON/OLD/POLD(1001),COLD1(1001),COLD2(1001)
       COMMON/WALL/DLC,DLV,DLM,DDC1,DDV1,DDM1,PDC,PDV,PDM,PIDC1,PIDV1,
      #PIDM1,PIDC2,PIDV2,PIDM2,SIGC1,SIGV1,SIGM1,CDC1,CDV1,CDM1,DH,
      #          DDC2,DDV2,DDM2,SIGC2,SIGV2,SIGM2,CDC2,CDV2,CDM2
       COMMON/OSMOT/A1,B1,C1,A2,B2,C2
C
       M=NEX*2+1
       LUB=2
       LP=3*LUB
       IF(IND.EQ.1)GO TO 100
       K=LP*M+M-LUB
       AF(K)=AF(K)+ DLV
       GO TO 900
C
 100   PI1=COLD1(M)*(A1+COLD1(M)*(B1+COLD1(M)*C1))
       PI2=COLD2(M)*(A2+COLD2(M)*(B2+COLD2(M)*C2))
       BF(M)=BF(M)+DLV*(PDV+SIGV1*(PI1-PIDV1)+SIGV2*(PI2-PIDV2))
C
 900   RETURN
       END
       SUBROUTINE ASTAR(NEX,IND)
C
C      THIS SUBROUTINE ADJUSTS THE AF AND BF VECTORS TO ACCOUNT FOR THE
C      STARLING BOUNDARY CONDITION AT THE ARTERIOLAR WALL.
C
       IMPLICIT REAL*8(A-H,O-Z)
       COMMON/BLK1/NODEL(500,3),  XNOD(1001)
       COMMON/FLUMAT/AF(20000)
       COMMON/FLUB/BF(1001)
       COMMON/OLD/POLD(1001),COLD1(1001),COLD2(1001)
       COMMON/WALL/DLC,DLV,DLM,DDC1,DDV1,DDM1,PDC,PDV,PDM,PIDC1,PIDV1,
      #PIDM1,PIDC2,PIDV2,PIDM2,SIGC1,SIGV1,SIGM1,CDC1,CDV1,CDM1,DH,
      #          DDC2,DDV2,DDM2,SIGC2,SIGV2,SIGM2,CDC2,CDV2,CDM2
```

```
      COMMON/OSMOT/A1,B1,C1,A2,B2,C2
C
      LUB=2
      LP=3*LUB
      IF(IND.EQ.1)GO TO 100
      K=LP+1-LUB
      AF(K)=AF(K)+ DLC
      GO TO 900
C
  100 PI1=COLD1(1)*(A1+COLD1(1)*(B1+COLD1(1)*C1))
      PI2=COLD2(1)*(A2+COLD2(1)*(B2+COLD2(1)*C2))
      BF(1)=BF(1)+DLC*(PDC+SIGC1*(PI1-PIDC1)+SIGC2*(PI2-PIDC2))
C
  900 RETURN
      END
      SUBROUTINE PATART(NEX)
C
C     THIS SUBROUTINE ADJUSTS THE AS AND BS VECTORS TO ACCOUNT FOR THE
C     PATLAK BOUNDARY CONDITION AT THE ARTERIOLAR WALL.
C
      IMPLICIT REAL*8(A-H,O-Z)
      COMMON/BLK1/NODEL(500,3), XNOD(1001)
      COMMON/SOLMAT/AS1(20000),AS2(20000)
      COMMON/SOLB/BS1(1001),BS2(1001)
      COMMON/OLD/POLD(1001),COLD1(1001),COLD2(1001)
      COMMON/TISDAT/AK,DEFF1,ALPHL1,PHI1,PHIT,RET1,SIGT1,BETA1,
     #DEFF2,ALPHL2,PHI2,RET2,SIGT2,BETA2
      COMMON/CAPDAT/PC,CREF
      COMMON/WALL/DLC,DLV,DLM,DDC1,DDV1,DDM1,PDC,PDV,PDM,PIDC1,
     #PIDV1,PIDM1,PIDC2,PIDV2,PIDM2,SIGC1,SIGV1,SIGM1,CDC1,CDV1,CDM1,
     #DH,DDC2,DDV2,DDM2,SIGC2,SIGV2,SIGM2,CDC2,CDV2,CDM2
      COMMON/OSMOT/A1,B1,C1,A2,B2,C2
C
      LUB=2
      LP=3*LUB
      K=LP+1-LUB
C
      PI1=COLD1(1)*(A1+COLD1(1)*(B1+COLD1(1)*C1))
      PI2=COLD2(1)*(A2+COLD2(1)*(B2+COLD2(1)*C2))
      QART=AK*PC/DEFF1*DLC*(POLD(1)-PDC-SIGC1*(PI1-PIDC1)-
     #SIGC2*(PI2-PIDC2))
      PEC1=(1.D0-SIGC1)/DDC1*QART
C
C     DETERMINE WHICH FORM OF THE FLUX EXPRESSION APPLIES
C
      IF(PEC1.GT.100.0D0)GO TO 100
      IF(PEC1.LT.-100.D0)GO TO 200
      TEST=1.D0-DEXP(-PEC1)
      IF(DABS(TEST).LT.1.D-10)GO TO 300
C
      AS1(K)=AS1(K)-QART*(RET1*BETA1-(1.D0-SIGC1)/TEST)
      BS1(1)=BS1(1)+(1.D0-SIGC1)*QART*CDC1*DEXP(-PEC1)/TEST
      GO TO 900
C
  100 AS1(K)=AS1(K)-QART*(BETA1*RET1-(1.D0-SIGC1))
      GO TO 900
C
  200 AS1(K)=AS1(K)-QART*BETA1*RET1
      BS1(1)=BS1(1)-(1.D0-SIGC1)*QART*CDC1
      GO TO 900
C
  300 AS1(K)=AS1(K)-QART*BETA1*RET1+DDC1
      BS1(1)=BS1(1)+DDC1*CDC1
C
  900 PEC2=(1.D0-SIGC2)/DDC2*QART
C
C     DETERMINE WHICH FORM OF THE FLUX EXPRESSION APPLIES
C
      IF(PEC2.GT.100.0D0)GO TO 101
      IF(PEC2.LT.-100.D0)GO TO 201
```

```
        TEST=1.D0-DEXP(-PEC2)
        IF(DABS(TEST).LT.1.D-10)GO  TO 301
C
        AS2(K)=AS2(K)-QART*(RET2*BETA2-(1.D0-SIGC2)/TEST)
        BS2(1)=BS2(1)+(1.D0-SIGC2)*QART*CDC2*DEXP(-PEC2)/TEST
        GO TO 901
C
  101   AS2(K)=AS2(K)-QART*(BETA2*RET2-(1.D0-SIGC2))
        GO TO 901
C
  201   AS2(K)=AS2(K)-QART*BETA2*RET2
        BS2(1)=BS2(1)-(1.D0-SIGC2)*QART*CDC2
        GO TO 901
C
  301   AS2(K)=AS2(K)-QART*BETA2*RET2+DDC2
        BS2(1)=BS2(1)+DDC2*CDC2
C
C
  901   RETURN
        END
        SUBROUTINE PATVEN(NEX)
C
C       THIS SUBROUTINE ADJUSTS THE AS AND BS VECTORS TO ACCOUNT FOR THE
C       PATLAK BOUNDARY CONDITION AT THE VENULAR WALL.
C
        IMPLICIT REAL*8(A-H,O-Z)
        COMMON/BLK1/NODEL(500,3),  XNOD(1001)
        COMMON/SOLMAT/AS1(20000),AS2(20000)
        COMMON/SOLB/BS1(1001),BS2(1001)
        COMMON/OLD/POLD(1001),COLD1(1001),COLD2(1001)
        COMMON/TISDAT/AK,DEFF1,ALPHL1,PHI1,PHIT,RET1,SIGT1,BETA1,
       #DEFF2,ALPHL2,PHI2,RET2,SIGT2,BETA2
        COMMON/CAPDAT/PC,CREF
        COMMON/WALL/DLC,DLV,DLM,DDC1,DDV1,DDM1,PDC,PDV,PDM,PIDC1,
       #PIDV1,PIDM1,PIDC2,PIDV2,PIDM2,SIGC1,SIGV1,SIGM1,CDC1,CDV1,CDM1,
       #DH,DDC2,DDV2,DDM2,SIGC2,SIGV2,SIGM2,CDC2,CDV2,CDM2
        COMMON/OSMOT/A1,B1,C1,A2,B2,C2
C
        LUB=2
        LP=3*LUB
        NP=2*NEX+1
        K=LP*NP+NP-LUB
C
        PI1=COLD1(NP)*(A1+COLD1(NP)*(B1+COLD1(NP)*C1))
        PI2=COLD2(NP)*(A2+COLD2(NP)*(B2+COLD2(NP)*C2))
        QART=AK*PC/DEFF1*DLV*(POLD(NP)-PDV-SIGV1*(PI1-PIDV1)-
       #SIGV2*(PI2-PIDV2))
        PEC1=(1.D0-SIGV1)/DDV1*QART
C
C       DETERMINE WHICH FORM OF THE FLUX EXPRESSION APPLIES
C
        IF(PEC1.GT.100.0D0)GO  TO 100
        IF(PEC1.LT.-100.D0)GO  TO 200
        TEST=1.D0-DEXP(-PEC1)
        IF(DABS(TEST).LT.1.D-10)GO  TO 300
C
        AS1(K)=AS1(K)-QART*(RET1*BETA1-(1.D0-SIGV1)/TEST)
        BS1(NP)=BS1(NP)+(1.D0-SIGV1)*QART*CDV1*DEXP(-PEC1)/TEST
        GO TO 900
C
  100   AS1(K)=AS1(K)-QART*(BETA1*RET1-(1.D0-SIGV1))
        GO TO 900
C
  200   AS1(K)=AS1(K)-QART*BETA1*RET1
        BS1(NP)=BS1(NP)-(1.D0-SIGV1)*QART*CDV1
        GO TO 900
C
  300   AS1(K)=AS1(K)-QART*BETA1*RET1+DDV1
        BS1(NP)=BS1(NP)+DDV1*CDV1
```

```
C
 900   PEC2=(1.D0-SIGV2)/DDV2*QART
C
C      DETERMINE WHICH FORM OF THE FLUX EXPRESSION APPLIES
C
       IF(PEC2.GT.100.0D0)GO  TO 101
       IF(PEC2.LT.-100.D0)GO  TO 201
       TEST=1.D0-DEXP(-PEC2)
       IF(DABS(TEST).LT.1.D-10)GO  TO 301
C
       AS2(K)=AS2(K)-QART*(RET2*BETA2-(1.D0-SIGV2)/TEST)
       BS2(NP)=BS2(NP)+(1.D0-SIGV2)*QART*CDV2*DEXP(-PEC2)/TEST
       GO TO 901
C
 101   AS2(K)=AS2(K)-QART*(BETA2*RET2-(1.D0-SIGV2))
       GO TO 901
C
 201   AS2(K)=AS2(K)-QART*BETA2*RET2
       BS2(NP)=BS2(NP)-(1.D0-SIGV2)*QART*CDV2
       GO TO 901
C
 301   AS2(K)=AS2(K)-QART*BETA2*RET2+DDV2
       BS2(NP)=BS2(NP)+DDV2*CDV2
C
 901   RETURN
       END
        SUBROUTINE MATPLY(A,A1,B,C,NP)
C
C      THIS SUBROUTINE MULTIPLIES A MATRIX A BY A VECTOR B AND SCALAR A1
C      TO GIVE  VECTOR C. MATRIX A IS STORED AS A VECTOR, WHERE MATRIX
C      ELEMENT A(I,J) IS STORED AS A(IJ), IJ=3*LUB*J+I-LUB,  AND WHERE
C      LUB IS THE NUMBER OF OFF DIAGONAL BANDS. FOR THIS SUBROUTINE,
C      IT IS ASSUMED THAT THE BANDWIDTH IS 5, SO THAT LUB=2.
C
       IMPLICIT REAL*8(A-H,O-Z)
       DIMENSION A(20000), B(NP), C(NP)
       LUB=2
       LP=3*LUB
C
       DO 1 I=1,NP

       C(I)=0.D0
 1     CONTINUE
C
       K=2
       DO 2 I=1,2
       K=K+1
          DO 3 J=1,K
          IJ=LP*J+I-LUB
          C(I)=C(I)+A(IJ)*A1*B(J)
 3        CONTINUE
 2     CONTINUE
C
       NPM=NP-2
       K=0
       DO 4 I=3,NPM
       K=K+1
       KP=K+4
          DO 5 J=K,KP
          IJ=J*LP+I-LUB

          C(I)=C(I)+A(IJ)*B(J)*A1
 5        CONTINUE
 4     CONTINUE
C
       NPM=NP-1
       K=NP-4
       DO 6 I=NPM,NP
       K=K+1
          DO 7 J=K,NP
```

```
          IJ=LP*J+I-LUB
          C(I)=C(I)+A(IJ)*A1*B(J)
    7     CONTINUE
    6    CONTINUE
C
     RETURN
     END
     SUBROUTINE SETMAT(NEX,IND,PE1,IPEC1,VMAX1,PE2,IPEC2,VMAX2)
C
C    THIS SUBROUTINE INITIALIZES THE VARIOUS VECTORS ASSOCIATED
C    WITH SOLUTE AND FLUID TRANSPORT EQUATIONS, AF(K), BF(I), AS1(K),
C    AS2(I),BS1(I), BS2(I).
C
     IMPLICIT REAL*8(A-H,O-Z)
     COMMON/BLK1/NODEL(500,3),XNOD(1001)
     COMMON/FLUMAT/AF(20000)
     COMMON/OLD/POLD(1001),COLD1(1001),COLD2(1001)
     COMMON/SOLB/BS1(1001),BS2(1001)
     COMMON/FLUB/BF(1001)
     COMMON/SOLMAT/AS1(20000),AS2(20000)
     COMMON/OSMOT/A1,B1,C1,A2,B2,C2
     COMMON/TISDAT/AK,DEFF1,AL1,PHI1,PHIT,RET1,SIGT1,BETA1,
    #DEFF2,AL2,PHI2,RET2,SIGT2,BETA2
     COMMON/CAPDAT/PC,CREF
     COMMON/WALL/DLC,DLV,DLM,DDC1,DDV1,DDM1,PDC,PDV,PDM,PIDC1,
    #PIDV1,PIDM1,PIDC2,PIDV2,PIDM2,SIGC1,SIGV1,SIGM1,CDC1,CDV1,CDM1,
    #DH,DDC2,DDV2,DDM2,SIGC2,SIGV2,SIGM2,CDC2,CDV2,CDM2
     COMMON/TIME/T(20000)
     COMMON/MAXDAT/DMX1,DMX2,IDISP1,IDISP2
C
     DIMENSION GAUS(4),W(4),B(3),DB(3)
     DATA NGAUS/4/
     DATA W/.347854845137454D0,.652145154862546D0,
    #.652145154862546D0,.347854845137454D0/
     DATA GAUS/-.861136311594053D0,-.339981043584856D0,
    #.339981043584856D0,.861136311594053D0/
C    DATA GAUS/
C    DATA W/
C    DATA NGAUS/3/
C    DATA GAUS/
C    DATA W/
     DMX1=0.D0
     DMX2=0.D0
     ALPHA=AK*PC/DEFF1
     PE1=0.D0
     VMAX1=0.D0
     PE2=0.D0
     VMAX2=0.D0
C
C
C    ZERO THE APPROPRIATE ARRAY AND INITIALIZE
C
     IF(IND.EQ.1)GO TO 800
     IF(IND.EQ.2)GO TO 900
     IF(IND.EQ.3)GO TO 950
C
C    ZERO THE AF VECTOR
C
     DO 700 I=1,20000
     AF(I)=0.D0
  700 CONTINUE
     GO TO 100
C
C    ZERO THE BF VECTOR
C
  800 DO 801 I=1,1001
     BF(I)=0.D0
  801 CONTINUE
     GO TO 100
```

```
C

C     ZERO THE T MATRIX
C
 950  DO 951 I=1,20000
      T(I)=0.D0
 951  CONTINUE
      GO TO 100
C
C     ZERO THE AS AND BS VECTORS
C
 900  DO 901 I=1,20000
      AS1(I)=0.D0
      AS2(I)=0.D0
 901  CONTINUE
C
      DO 902 I=1,1001
      BS1(I)=0.D0
      BS2(I)=0.D0
 902  CONTINUE
C
C     BEGIN THE GAUSS INTEGRATION, ELEMENT BY ELEMENT
C
 100  LUB=2
      LP=3*LUB
C
C     EVALUATE THE INTEGRAND AT THE APPROPRIATE QUADRATURE POINT, S.
C
      DO 200 II=1,NGAUS
      S=GAUS(II)
C
C     INITIALIZE THE APPROPRIATE ARRAY, ELEMENT BY ELEMENT.
C
      DO 300 I=1,NEX
C
C     CALCULATE VALUE OF BASIS FUNCTIONS AND DERIVATIVES AT THE
C     QUADRATURE POINT
C
      X1=XNOD(NODEL(I,1))
      X2=XNOD(NODEL(I,2))
      X3=XNOD(NODEL(I,3))
C

      S2=(2.D0*X2-(X1+X3))/(X3-X1)
C
      B(1)=(S-S2)*(S-1.D0)/(2.D0*(S2+1.D0))
      B(2)=(S+1.D0)*(S-1.D0)/(S2*S2-1.D0)
      B(3)=(S+1.D0)*(S-S2)/(2.D0*(1.D0-S2))
      DB(1)=(2.D0*S-S2-1.D0)/(2.D0*(S2+1.D0))
      DB(2)=2.D0*S/(S2*S2-1.D0)
      DB(3)=(2.D0*S-S2+1.D0)/(2.D0*(1.D0-S2))
C
      DX=(X3-X1)*.5D0
C
C     CALCULATE THE T VECTOR
C
      IF(IND.NE.3) GO TO 101
      DO 952 M=1,3
      MM=NODEL(I,M)
         DO 953 N=1,3
         NN=NODEL(I,N)
         K=LP*NN+MM-LUB
         T(K)=T(K)+B(M)*B(N)*DX*W(II)
 953     CONTINUE
 952  CONTINUE
      GO TO 300
C
C     NOW CALCULATE C1(S), DC1/DS, PI1(S), DPI1/DS,C2(S),...
C
 101  CS1=0.D0
```

```
      CS2=0.D0
      DCS1=0.D0
      DCS2=0.D0
      DO 301 IT=1,3
      CS1=CS1+COLD1(NODEL(I,IT))*B(IT)
      CS2=CS2+COLD2(NODEL(I,IT))*B(IT)
      DCS1=DCS1+COLD1(NODEL(I,IT))*DB(IT)
      DCS2=DCS2+COLD2(NODEL(I,IT))*DB(IT)
  301 CONTINUE
C
      PIS1=CS1*(A1+CS1*(B1+CS1*C1))
      PIS2=CS2*(A2+CS2*(B2+CS2*C2))
      DPIS2=(A2+2.D0*B2*CS2+3.D0*CS2*CS2*C2)*DCS2
      DPIS1=(A1+2.D0*B1*CS1+3.D0*CS1*CS1*C1)*DCS1
C
C     DETERMINE WHICH VECTOR IS TO BE INITIALIZED
C
      IF(IND.EQ.1)GO TO 500
      IF(IND.EQ.2)GO TO 600
C
C     INITIALIZE THE FLUID VECTOR
C
      DO 401 M=1,3
      MM=NODEL(I,M)
          DO 402 N=1,3
          NN=NODEL(I,N)
          K=LP*NN+MM-LUB
          AF(K)=AF(K)+(B(M)*B(N)*2.D0*DLM/DH*DX+DB(M)*DB(N)/DX)*W(II)
  402     CONTINUE
  401 CONTINUE
      GO TO 300


C
C     INITIALIZE THE FLUID B VECTOR
C
  500 DO 501 M=1,3
      MM=NODEL(I,M)
      BF(MM)=BF(MM)+(DB(M)*(DPIS1*SIGT1+DPIS2*SIGT2)/DX+B(M)*
     #2.D0*DLM/DH*DX*(PDM+SIGM1*(PIS1   - PIDM1)+SIGM2*(PIS2-PIDM2)
     #))*W(II)
  501 CONTINUE
    . GO TO 300
C
C     INITIALIZE THE SOLUTE VECTORS, BS AND AS. fIRST CALCULATE VS1,VS2
C     QMES, AND THE DISPERSION COEFFICIENTS, DISP1 AND DISP2.
C
  600 DPS=0.D0
      PS=0.D0
      DO 601 IT=1,3
      DPS=DPS+POLD(NODEL(I,IT))*DB(IT)
      PS=PS+POLD(NODEL(I,IT))*B(IT)
  601 CONTINUE
C
      VS1=-ALPHA*(DPS-SIGT1*DPIS1-SIGT2*DPIS2)/DX*RET1*BETA1/PHI1
      VS2=-ALPHA*(DPS-SIGT1*DPIS1-SIGT2*DPIS2)/DX*RET2*BETA2/PHI2
      QFMES=ALPHA*DLM*(PS-PDM-SIGM1*(PIS1-PIDM1)-SIGM2*(PIS2-PIDM2))
      DISP1=DABS(VS1)*AL1+1.D0
      IF(DISP1.LT.DMX1) GO TO 655
      DMX1=DISP1
      IDISP1=I
  655 DISP2=DABS(VS2)*AL2+DEFF2/DEFF1
      IF(DISP2.LT.DMX2) GO TO 656
      DMX2=DISP2
      IDISP2=I
C
C     CALCULATE THE MAXIMUM LOCAL SOLUTE VELOCITY, VELMAX
C
  656 IF(DABS(CS1).LT.1.D-5)  VELS1=DABS(VS1)*PHI1
      IF(DABS(CS1).GT.1.D-5)  VELS1=DABS(VS1-(DISP1*DCS1/DX)/CS1)*PHI1
      IF(DABS(CS2).LT.1.D-5)  VELS2=DABS(VS2)*PHI2
```

```
         IF(DABS(CS2).GT.1.D-5)  VELS2=DABS(VS2-(DISP2*DCS2/DX)/CS2)*PHI2
         IF(.5D0*VELS1/DX.GT.VMAX1)  VMAX1=.5D0*VELS1/DX
         IF(.5D0*VELS2/DX.GT.VMAX2)  VMAX2=.5D0*VELS2/DX
C
C        CALCULATE THE GRID PECLET NUMBER, AND SEE IF IT EXCEEDS
C        THE LIMIT
C
         PEST1=DABS(VS1)*(X3-X1)/DISP1
         IF(PEST1.LT.PE1)GO  TO  609
         PE1=PEST1
         IPEC1=I
  609    PEST2=DABS(VS2)*(X3-X1)/DISP2
         IF(PEST2.LT.PE2)GO  TO  610
         PE2=PEST2
         IPEC2=I
C
C        NOW DETERMINE WHICH FORM OF THE NONLINEAR FLUX EXPRESSION
C        IS TO BE USED TO CALCULATE SOLUTE FLUX ACROSS MESOTHELIUM.
C
C
  610    PEC1=QFMES*(1.D0-SIGM1)/DDM1
         IF(PEC1.GT.100.D0)GO  TO  611
         IF(PEC1.LT.-100.D0)GO  TO  620
         TEST=1.D0-DEXP(-PEC1)
         IF(DABS(TEST).LT.1.D-10)GO   TO  630
C


C        CASE  1: USE THE FULL NONLINEAR FLUX EXPRESSION
C
         DO 602 M=1,3
         MM=NODEL(I,M)
               DO 603 N=1,3
               NN=NODEL(I,N)
               K=LP*NN+MM-LUB
               AS1(K)=AS1(K)+(B(M)*DB(N)*VS1*PHI1+
     #                DB(M)*DB(N)*DISP1*PHI1/DX
     #                +B(M)*B(N)*2.D0*QFMES/TEST/DH*(1.D0-SIGM1)*DX
     #                -2.D0/DH*QFMES*RET1*BETA1*B(M)*B(N)*DX)*W(II)
  603          CONTINUE
         BS1(MM)=BS1(MM)+
     #           B(M)*2.D0/DH*(1.D0-SIGM1)*QFMES*CDM1*DEXP(-PEC1)/TEST
     #           *DX*W(II)
  602    CONTINUE
         GO TO 640
C
C        CASE  2: PEC APPROACHES INFINITY
C
  611    DO 612 M=1,3
         MM=NODEL(I,M)
               DO 613 N=1,3
               NN=NODEL(I,N)
               K=LP*NN+MM-LUB
               AS1(K)=AS1(K)+
     #             (B(M)*DB(N)*VS1*PHI1+DB(M)*DB(N)*PHI1*DISP1/DX
     #             +B(M)*B(N)*2.D0/DH*(1.D0-SIGM1)*QFMES*DX
     #             -QFMES*RET1*BETA1*B(M)*B(N)*DX*2.D0/DH)*W(II)
  613          CONTINUE
  612    CONTINUE
         GO TO 640
C
C        CASE  3: -PEC APPROACHES INFINITY
C
C
  620    DO 621 M=1,3
         MM=NODEL(I,M)
               DO 622 N=1,3
               NN=NODEL(I,N)
               K=LP*NN+MM-LUB
               AS1(K)=AS1(K)+
     #             (B(M)*DB(N)*VS1*PHI1+DB(M)*DB(N)*PHI1*DISP1/DX
```

```
      #                     -2.D0/DH*BETA1*RET1*QFMES*B(N)*B(M)*DX)*W(II)
  622          CONTINUE
      BS1(MM)=BS1(MM)-2.D0/DH*(1.D0-SIGM1)*QFMES*CDM1*DX*W(II)*B(M)
  621 CONTINUE
      GO TO 640
C
C     CASE 4: PEC APPROACHES 0
C
  630 DO 631 M=1,3
      MM=NODEL(I,M)
            DO 632 N=1,3
            NN=NODEL(I,N)
            K=LP*NN+MM-LUB
            AS1(K)=AS1(K)+
      #                (B(M)*DB(N)*VS1*PHI1+DB(M)*DB(N)*PHI1*DISP1/DX
      #               +2.D0/DH*DDM1*B(M)*B(N)*DX
      #               -2.D0/DH*RET1*BETA1*DX*B(M)*B(N)*QFMES)*W(II)
  632 CONTINUE
      BS1(MM)=BS1(MM)+2.D0/DH*DDM1*B(M)*CDM1*DX*W(II)
  631 CONTINUE
C
  640 PEC2=QFMES*(1.D0-SIGM2)/DDM2
      IF(PEC2.GT.100.D0)GO TO 650
      IF(PEC2.LT.-100.D0)GO TO 660
      TEST=1.D0-DEXP(-PEC2)
      IF(DABS(TEST).LT.1.D-10)GO TO 670
C
C     CASE 1: USE THE FULL NONLINEAR FLUX EXPRESSION
C
      DO 641 M=1,3
      MM=NODEL(I,M)
            DO 642 N=1,3
            NN=NODEL(I,N)
            K=LP*NN+MM-LUB
            AS2(K)=AS2(K)+(B(M)*DB(N)*VS2*PHI2+
      #            DB(M)*DB(N)*DISP2*PHI2/DX
      #           +B(M)*B(N)*2.D0*QFMES/TEST/DH*(1.D0-SIGM2)*DX
      #           -2.D0/DH*QFMES*RET2*BETA2*B(M)*B(N)*DX)*W(II)
  642          CONTINUE
      BS2(MM)=BS2(MM)+
      #      B(M)*2.D0/DH*(1.D0-SIGM2)*QFMES*CDM2*DEXP(-PEC2)/TEST
      #      *DX*W(II)
  641 CONTINUE
      GO TO 300
C
C     CASE 2: PEC APPROACHES INFINITY
C
  650 DO 651 M=1,3
      MM=NODEL(I,M)
            DO 652 N=1,3
            NN=NODEL(I,N)
            K=LP*NN+MM-LUB
            AS2(K)=AS2(K)+
      #           (B(M)*DB(N)*VS2*PHI2+DB(M)*DB(N)*PHI2*DISP2/DX
      #           +B(M)*B(N)*2.D0/DH*(1.D0-SIGM2)*QFMES*DX
      #           -QFMES*RET2*BETA2*B(M)*B(N)*DX*2.D0/DH)*W(II)
  652          CONTINUE
  651 CONTINUE
      GO TO 300
C
C     CASE 3: -PEC APPROACHES INFINITY
C
  660 DO 661 M=1,3
      MM=NODEL(I,M)
            DO 662 N=1,3
            NN=NODEL(I,N)
            K=LP*NN+MM-LUB
            AS2(K)=AS2(K)+
      #           (B(M)*DB(N)*VS2*PHI2+DB(M)*DB(N)*PHI2*DISP2/DX
      #           -2.D0/DH*BETA2*RET2*QFMES*B(N)*B(M)*DX)*W(II)
```

```
 662          CONTINUE
       BS2(MM)=BS2(MM)-2.D0/DH*(1.D0-SIGM2)*QFMES*CDM2*DX*W(II)*B(M)
 661   CONTINUE
       GO TO 300
C
C      CASE 4: PEC APPROACHES 0
C
 670   DO 671 M=1,3
       MM=NODEL(I,M)
             DO 672 N=1,3
             NN=NODEL(I,N)
             K=LP*NN+MM-LUB
             AS2(K)=AS2(K)+
     #             (B(M)*DB(N)*VS2*PHI2+DB(M)*DB(N)*PHI2*DISP2/DX
     #             +2.D0/DH*DDM2*B(M)*B(N)*DX
     #             -2.D0/DH*RET2*BETA2*DX*B(M)*B(N)*QFMES)*W(II)
 672   CONTINUE
       BS2(MM)=BS2(MM)+2.D0/DH*DDM2*B(M)*CDM2*DX*W(II)
 671   CONTINUE
C
 300   CONTINUE
 200   CONTINUE

       RETURN
       END
C


       SUBROUTINE DGBND1 (A, B, N, ML, NU, LT, IP, DET, NCN1,
      1                   BB, RZ, ITR1, EPS1)
C
C  ROUTINE SOLVES SYSTEM OF LINEAR EQNS. AX=B WHERE A IS A GENERAL
C  BAND MATRIX. METHOD USED IS GAUSSIAN ELIMINATION WITH PARTIAL
C  PIVOTING. OPTION OF ITERATIVELY IMPROVING SOLUTION IS AVAILABLE.
C  UPPER BAND WIDTH OF MATRIX INCREASES DUE TO INTERCHANGES BY
C  AMOUNT ML. ROUTINE REQUIRES BAND ELEMENTS OF MATRIX TO BE STORED
C  BY COLUMN IN A ONE DIMENSIONAL ARRAY. EACH COLUMN IS OF LENGTH
C  2*ML+NU AND BAND IS TO BE STORED IN ELEMENTS ML+1 TO 2*ML+NU OF
C  EACH COLUMN. ELEMENTS 1 TO ML OF COLUMN ARE SET TO ZERO BY GBAND.
C  IF MATRIX IS SYMMETRIC USER MAY SPECIFY LOWER BAND ONLY IN
C  ELEMENTS ML+NU+1 TO 2*ML+NU OF EACH COLUMN AND GBAND WILL
C  GENERATE REMAINING ELEMENTS. (IF THIS IS DESIRED, SET LT=-1 ON
C  FIRST CALL TO GBAND.)
C  A = 1 DIMENSIONAL ARRAY CONTAINING MATRIX OF COEFFICIENTS.
C  B = 1 DIMENSIONAL ARRAY CONTAINING RIGHT HAND SIDE VECTORS.
C      ON EXIT, B WILL CONTAIN THE SOLUTION VECTOR X.
C  N = ORDER OF MATRIX
C  ML = LENGTH OF LOWER BAND (EXCLUDING DIAGONAL)
C  NU = LENGTH OF UPPER BAND (EXCLUDING DIAGONAL)
C  LT = ABS(LT)=1 IF ONLY 1 B VECTOR OR IF 1ST OF SEVERAL.
C       ABS(LT),=1 FOR SUBSEQUENT B VECTORS.
C       (NOTE. LT=+1 IF FULL BAND WIDTH GIVEN, LT=-1 IF LOWER BAND
C       ONLY OF SYMMETRIC MATRIX GIVEN.)
C  IP = INTEGER ARRAY CONTAINING INTERCHANGE INFORMATION.
C  DET = DETERMINANT OF A = DET*(10**NCN) WHERE 1.D-15<|DET|<1.D+15.
C        IF DET=0.0 MATRIX IS SINGULAR AND ERROR RETURN TAKEN.
C  BB, RZ = ARRAYS REQUIRED FOR IMPROVEMENT OPTION. CAN BE REAL*8
C           VARIABLES IF OPTION NOT REQUIRED.
C  ITER  = 0 IF IMPROVEMENT NOT REQUIRED, OTHERWISE ITER= NO. OF
C           ITERATIONS OR CYCLES.
C  EPS - CONVERGENCE CRITERION.
C
C MODIFIED TO DO ITERATIVE IMPROVEMENT (FORMERLY AVAILABLE ONLY
C WITH THE SINGLE PRECISION VERSION). MIKE PATTERSON - NOV, 1980
       IMPLICIT REAL*8 (A-H, O-Z)
       COMMON /GBAND$/ NITER
       DIMENSION A(1), B(N), IP(N), BB(N), RZ(N)
       COMPLEX*16 DSUMM, QADDQ, QMULD
       REAL*8 QRNDQ
C TO ASSIGN LOGICAL UNITS 94 AND 95 ONLY ONCE:
       LOGICAL ASSIGN /F/, YES /T/
```

```
C STATEMENT FUNCTION TO CALCULATE POINTERS INTO A:
      IFN(I, J) = 1 + (J - 1)*LC + I - J + NUM
C
C
      NCN=NCN1
      ITR=ITR1
      EPS=EPS1
      ITER = ITR
C
      LCM = NU + 2*ML
      LC = LCM + 1
      NLC = N*LC
      NUM = NU + ML
C  GENERATE REMAINING ELEMENTS OF SYMMETRIC MATRIX
      IF (LT .NE. -1) GO TO 120
      NN = N - 1
      DO 110 I = 1, NN
        IFI = IFN(I, I)
        IFJ = IFI
        II = I + 1
        IML = MINO(I + ML, N)
        DO 100 J = II, IML
           IFI = IFI + 1
           IFJ = IFJ + LCM
100     A(IFJ) = A(IFI)
110     CONTINUE
120     IF (ITER .EQ. 0) GO TO 140
C ASSIGN UNITS 94 AND 95 IF THEY HAVE NOT ALREADY BEEN ASSIGNED:
      IF (ASSIGN) GO TO 125
      CALL FTNCMD ('ASSIGN 94=-GBAND94;')
      CALL FTNCMD ('ASSIGN 95=-GBAND95;')
      ASSIGN = YES
125   REWIND 94
      REWIND 95
      DO 130 I = 1, N
130   BB(I) = B(I)
140   IF (IABS(LT) .NE. 1) GO TO 280
      IP(N) = 1
      IF (ML .EQ. 0) GO TO 160
C  SET ELEMENTS 1 - ML OF EACH COLUMN TO ZERO
      DO 150 I = 1, N
        IFK = (I - 1)*LC
        DO 150 J = 1, ML
           IFK = IFK + 1
150   A(IFK) = 0.0D0
160   IF (ITER .NE. 0) CALL DWR1 (A, NLC, 94)
      DET = 0.0D0
      NCN = 0
      IF (ML .EQ. 0) GO TO 230
C  LU DECOMPOSITION
      DO 220 K = 1, N
        IFK = IFN(K, K)

        IF (K .EQ. N) GO TO 210
        KP = K + 1
        KPM = MINO(K + ML, N)
        KPN = MINO(K + NUM, N)
        M = K
        IFM = IFK
        IFI = IFK
        DO 170 I = KP, KPM
           IFI = IFI + 1
           IF (DABS(A(IFI)) .LE. DABS(A(IFM))) GO TO 170
           M = I
           IFM = IFI
170     CONTINUE

        IP(K) = M
        T = A(IFM)
        IF (M .NE. K) IP(N) = -IP(N)
```

```
          A(IFM) = A(IFK)
          A(IFK) = T
          IF (T .EQ. 0.0D0) GO TO 260
          OT = 1.0D0/T
          IK = IFK
          DO 180 I = KP, KPM
             IK = IK + 1
180       A(IK) = -A(IK)*OT
          KJ = IFK
          MJ = IFM
          DO 200 J = KP, KPN
             KJ = KJ + LCM
             MJ = MJ + LCM
             T = A(MJ)
             A(MJ) = A(KJ)
             A(KJ) = T
             IF (T .EQ. 0.0D0) GO TO 200
             IK = IFK
             IJ = KJ
             DO 190 I = KP, KPM
                IK = IK + 1
                IJ = IJ + 1
190          A(IJ) = A(IJ) + A(IK)*T
200       CONTINUE
210       IF (A(IFK) .EQ. 0.0D0) GO TO 260
220    CONTINUE
230    IFK = IFN(1, 1)
       DET = A(IFK)
       DO 250 K = 2, N
          IFK = IFK + LC
          DET = DET*A(IFK)
          IF (DET .EQ. 0.0D0) GO TO 260
          IF (DABS(DET) .GT. 1.D-15) GO TO 240
          DET = DET*1.D+15
          NCN = NCN - 15
          GO TO 250
240       IF (DABS(DET) .LT. 1.D+15) GO TO 250
          DET = DET*1.D-15
          NCN = NCN + 15
250    CONTINUE
       DET = DET*IP(N)
       GO TO 280
260    DET = 0.0D0
       WRITE (6, 270) K
270    FORMAT ('0* DGBND1 - matrix is singular. '/
      1     '    Error occurred in attempt to find', I5, 'th pivot.')
       RETURN
280    CALL DSOLV1 (A, B, IP, N, ML, NU)
       IF (ITER .EQ. 0) RETURN
C
C   ITERATIVE IMPROVEMENT
C   RESIDUALS (R) = AX-B ARE FOUND AND STORED IN ARRAY RZ USING
C   EXTENDED PRECISION ARITHMETIC. SYSTEM AZ=R IS SOLVED AND NEW
C   SOLUTION =X+Z IS STORED IN ARRAY B. ABOVE STEPS REPEATED UNTIL
C     (1) MAX(Z)/MAX(X) < EPS OR
C     (2) NO. OF CYCLES > ITER OR
C     (3) IMPROVEMENT STARTS TO DIVERGE.
C   ROUTINE THEN RETURNS AFTER SETTING EPS=MAX(Z) (FOR (1)) OR
C   SETTING EPS=-MAX(Z) AND PRINTING APPROPRIATE ERROR MESSAGE (FOR
C   (2) AND (3))
C
C
       IF (IABS(LT) .EQ. 1) CALL DWR1 (A, NLC, 95)
       XNORM = 0.0D0
       DO 290 K = 1, N
290    XNORM = DMAX1(XNORM, DABS(B(K)))
       IF (XNORM .LE. 0.0D0) RETURN
       ZX = 1.D+60
       LD = 0
       DO 340 L = 1, ITER
```

```
            REWIND 94
            CALL DRE1 (A, NLC, 94)
            DO 310 K = 1, N
               DSUMM = (0.D0, 0.D0)
               KPM = MAXO(K - ML, 1)
               KPN = MINO(K + NU, N)
               IFK = IFN(K, KPM)
               DO 300 J = KPM, KPN
C              DSUMM = DSUMM + A(IFK)*B(J)
C USING EXTENDED PRECISION:
               DSUMM = QADDQ(DSUMM, QMULD(A(IFK), B(J)))
300            IFK = IFK + LCM

               RZ(K) = BB(K) - QRNDQ(DSUMM)
310         CONTINUE
            REWIND 95
            CALL DRE1 (A, NLC, 95)
            CALL DSOLV1 (A, RZ, IP, N, ML, NU)
            ZNORM = 0.0D0
            DO 320 K = 1, N
               ERZ = RZ(K)
               ZNORM = DMAX1(ZNORM, DABS(ERZ))
320         B(K) = B(K) + ERZ
            IF (ZNORM .GT. ZX) GO TO 330
            IF ((ZNORM - EPS*XNORM) .LT. 0.0D0) GO TO 390
            ZX = ZNORM
            GO TO 340
330         IF (ZNORM .GT. 10.0D0*ZX) GO TO 360
            LD = LD + 1
            IF (LD .GE. 3) GO TO 360
340      CONTINUE
            L = ITER
            WRITE (6, 350)
350      FORMAT ('0* DGBND1- Iterative improvement did not converge'/)
            GO TO 380
360      WRITE (6, 370)
370      FORMAT ('0* DGBND1 - Iterative improvement is diverging.'/)
380      EPS = -ZNORM
            NITER = L
            RETURN
390      EPS = ZNORM
            NITER = L
            RETURN
            END


         SUBROUTINE DSOLV1 (A, B, IP, N, ML, NU)
C
C   THIS ROUTINE COMPUTES THE SOLUTION OF A SYSTEM AFTER GBAND HAS
C   DECOMPOSED MATRIX A INTO A LOWER TRIANGULAR MATRIX L AND AN
C   UPPER TRIANGULAR MATRIX U.
C
         IMPLICIT REAL*8 (A-H, O-Z)
         DIMENSION A(1), B(N), IP(N)
         IFN(I, J) = 1 + (J - 1)*LC + I - J + NUM
         LCM = 2*ML + NU
         LC = LCM + 1
         NUM = NU + ML
         MN = N - 1
C   SOLVE FOR Y
         IF (ML .EQ. 0) GO TO 110
         DO 100 K = 1, MN
            KP = K + 1
            M = IP(K)
            T = B(M)
            B(M) = B(K)
            B(K) = T
            KPM = MINO(K + ML, N)
            IFK = IFN(K, K)
            DO 100 I = KP, KPM
```

```
           IFK = IFK + 1
100    B(I) = B(I) + A(IFK)*T
C   SOLVE FOR X
110    IFK = IFN(N, N)
       DO 120 KB = 1, MN
         KM = N - KB
         K = KM + 1
         B(K) = B(K)/A(IFK)
         IFK = IFK - LC
         T = -B(K)
         KMN = MAXO(1, K - ML - NU)
         KML = IFN(KMN, K)
         DO 120 I = KMN, KM
         B(I) = B(I) + A(KML)*T
120    KML = KML + 1
       B(1) = B(1)/A(NUM + 1)
       RETURN
       END
       SUBROUTINE DWR1 (A, N, LU)
       REAL*8 A(N)
       WRITE (LU) A
       RETURN
       END
       SUBROUTINE DRE1 (A, N, LU)
       REAL*8 A(N)
       READ (LU) A
       RETURN
       END
```

D.6   Two Protein Transient Simulator: TRANS2P.FOR

```
C
C      THIS PROGRAM SIMULATES BOTH CONVECTIVE AND DISPERSIVE PLASMA
C      PROTEIN TRANSPORT THROUGH MESENTERY DURING TRANSIENT
C      CONDITIONS FOR TWO PLASMA PROTEIN SPECIES.
C      THE MESENTERY IS TREATED AS A 1-DIMENSIONAL
C      RECTANGULAR SLAB.
C
       IMPLICIT REAL*8(A-H,O-Z)
       DIMENSION HOLD(1001),IPERM(1001),RES(1001),HOLD1(1000),
      #RES1(1001),IPERM1(1001),HOLD2(1001),RES2(1001),IPERM2(1001),
      #RES3(1001),IPERM3(1001),HOLD3(1001),DTIME1(100),TDT1(20000),
      #TDT2(20000),COLDT1(1001),COLDT2(1001),SBOLD1(1001),

      #SBOLD2(1001),SOLDT1(20000),SOLDT2(20000),BCTIM1(1001),
      #BCTIM2(1001),STNEW1(20000),STNEW2(20000),TCOLD1(1001),
      #TCOLD2(1001),SCOLD1(1001),SCOLD2(1001)
       COMMON/FLUX/FLUXMX
       COMMON/BLK1/NODEL(500,3),XNOD(1001)
       COMMON/BLK2/DX(1001)
       COMMON/MATBAL/QFC,QCC1,QSC1,QCC2,QSC2,QFV,QCV1,QSV1,QCV2,QSV2,
      #QFM,QCM1,QSM1,QCM2,QSM2,QFM1(500),QCM11(500),QSM11(500),
      #QCM12(500),QSM12(500)
       COMMON/FLUMAT/FLUID(20000)
       COMMON/OLD/POLD(1001),COLD1(1001),COLD2(1001)
       COMMON/TIME/T(20000)
       COMMON/SOLB/SOLB1(1001),SOLB2(1001)
       COMMON/FLUB/FLUIDB(1001)
       COMMON/SOLMAT/SOL1(20000),SOL2(20000)
       COMMON/OSMOT/A1,B1,C1,A2,B2,C2
       COMMON/TISDAT/AK,DEFF1,ALPHL1,PHI1,PHIT,RET1,SIGT1,BETA1,
      #DEFF2,ALPHL2,PHI2,RET2,SIGT2,BETA2
       COMMON/CAPDAT/PREF,CREF
       COMMON/WALL/DLC,DLV,DLM,DDC1,DDV1,DDM1,PDC,PDV,PDM,PIDC1,
      #PIDV1,PIDM1,PIDC2,PIDV2,PIDM2,SIGC1,SIGV1,SIGM1,CDC1,CDV1,CDM1,
      #YYL,DDC2,DDV2,DDM2,SIGC2,SIGV2,SIGM2,CDC2,CDV2,CDM2
```

```
      COMMON/MAXDAT/DISMX1,DISMX2,IDISP1,IDISP2
C
C     SET MARKER AND TOLERANCE VALUES
C
      READ(5,504)OMEGAF,OMEGAC,TOLP,TOLC,PECMAX,EPS
      READ(5,509)IMAX,ITER,NECHO,N,ITMAX
      READ(5,503)  THETA,TTOL,COUR,TFACT,TIMMAX
      READ(5,508)  K
      DO 1 I=1,K
      READ(5,501) DTIME1(I)
  1   CONTINUE
C
      KK=2
      NEX=(N-1)/2
      LUB=2
      NDIM=N*(3*LUB+1)
C
C     READ IN THE DATA FROM EXTERNAL FILE
C
      DO 2 I=1,N
      READ(5,501) DX(I)
  2   CONTINUE
C
C
      READ(5,502) A1,B1,C1,AK,PREF,PHI1,PHIT,RET1,PHIS
      READ(5,504) A2,B2,C2,PHI2,RET2,BETA2
      READ(5,507) ALPHL1,AL,DEFF1,SIGT1,CREF,YYL,BETA1
      READ(5,507) ALPHL2,DEFF2,SIGT2,PERMC2,PERMV2,PERMM2
      READ(5,504) CONC,CONV,CONM,PERMC1,PERMV1,PERMM1
      READ(5,504) DDC1,DDV1,DDM1,SIGC1,SIGV1,SIGM1
      READ(5,504) DDC2,DDV2,DDM2,SIGC2,SIGV2,SIGM2
      READ(5,504) CDC1,CDV1,CDM1,DLC,DLV,DLM
      READ(5,506) CDC2,CDV2,CDM2
      READ(5,506) PDC,PDV,PDM
      READ(5,506) AOS1,BOS1,COS1
      READ(5,506) AOS2,BOS2,COS2
      YL=YYL*AL
      PIDC1=CDC1*(AOS1+CDC1*(BOS1+CDC1*COS1))
      PIDC2=CDC2*(AOS2+CDC2*(BOS2+CDC2*COS2))
      PIDV1=CDV1*(AOS1+CDV1*(BOS1+CDV1*COS1))
      PIDV2=CDV2*(AOS2+CDV2*(BOS2+CDV2*COS2))
      PIDM1=CDM1*(AOS1+CDM1*(BOS1+CDM1*COS1))
      PIDM2=CDM2*(AOS2+CDM2*(BOS2+CDM2*COS2))
      PC=PDC*PREF
      PV=PDV*PREF
      PM=PDM*PREF
      CC1=CDC1*CREF
      CV1=CDV1*CREF
      CM1=CDM1*CREF
      CC2=CDC2*CREF
      CV2=CDV2*CREF
      CM2=CDM2*CREF
C
C
C
  501 FORMAT(E12.6)
  502 FORMAT(9E10.4)
  503 FORMAT(5E10.4)
  504 FORMAT(6E10.4)
  505 FORMAT(3E10.4)
  506 FORMAT(3E10.4)
  507 FORMAT(7E10.4)
  508 FORMAT(I2)
  509 FORMAT(5I5)
C
      DO 3  I=1,N
      READ(4,*) POLD(I),COLD1(I),COLD2(I)
      COLDT1(I)=COLD1(I)
      COLDT2(I)=COLD2(I)
```

```
   3   CONTINUE

C
C      ECHO DATA IF NECHO N.E. 0
C
       IF(NECHO.EQ.0) GO TO 999
C
C      PRINT OUT INPUT DATA

C
       WRITE(6,600)
 600 FORMAT(1X,'TRANSIENT  FLUID PRESSURE AND SOLUTE CONCENTRATION'
    #)
       WRITE(6,601)
 601 FORMAT(1X,'PROFILES  FOR ONE DIMENSIONAL TISSUE SYSTEM',//)
       WRITE(6,602)
       WRITE(6,602)
 602 FORMAT(//,1X,'_____',
    #,//)
       WRITE(6,603)
 603 FORMAT(1X,'INPUT  PARAMETERS')
       WRITE(6,602)
       WRITE(6,604)
 604 FORMAT(1X,'1.  GRID DATA:',//)
       WRITE(6,605)NEX,DX(2)
 605 FORMAT(1X,'NUMBER OF ELEMENTS:',1X,I2,/,1X,
    #'SMALLEST X INCREMENT:',19X,E10.4,/)
       WRITE(6,606)N
 606 FORMAT(1X,'TOTAL  NUMBER OF NODES:',10X,I4,/)
       WRITE (6,602)
       WRITE(6,607) TOLP,TOLC,ITMAX,OMEGAF,OMEGAC,PECMAX
 607 FORMAT(1X,'2.  CONVERGENCE CRITERIA:',//,1X,'PRESSURE   TOLERANCE:'
    #,17X,E10.4,/,1X,'SOLUTE   TOLERANCE:',20X,E10.4,/,1X,
    #'MAXIMUM  NUMBER OF LOOP ITERATIONS:',2X,I3,/,1X,
    #'PRESSURE RELAXATION PARAMETER:',6X,E10.4,/,1X,
    #'SOLUTE RELAXATION PARAMETER:',9X,E10.4,/,1X,
    #'MAXIMUM DESIRED GRID PECLET NUMBER:',1X,E10.4)
       WRITE(6,608)  IMAX,TFACT,COUR,THETA
 608 FORMAT(/,1X,'MAXIMUM  NUMBER  OF TIME STEPS:',2X,I6,/,1X,
    #'TIME STEP ACCELERATION FACTOR:',6X,E10.4,/,1X,
    #'INITIAL COURANT NUMBER:',14X,E10.4,/,1X,
    #'SEMI-IMPLICIT PARAMETER THETA:',7X,E10.4)
       WRITE(6,602)
       PIC1=PIDC1*PREF
       PIV1=PIDV1*PREF
       PIM1=PIDM1*PREF
       PIC2=PIDC2*PREF
       PIV2=PIDV2*PREF
       PIM2=PIDM2*PREF
C
       WRITE(6,609)   AL,YL,CC1,CV1,CM1,CC2,CV2,CH2,
    #PC,PV,PM,PIC1,PIV1,PIM1,PIC2,PIV2,PIM2,AK
 609 FORMAT(1X,'3.  DIMENSIONAL INPUT PARAMETERS:',//,1X,
    #'TISSUE X-DIMENSION  (CM):',21X,E10.4,/,1X,
    #'TISSUE Y-DIMENSION  (CM):',21X,E10.4,/,1X,
    #'CAP. PROTEIN1 CONC.  (GRAMS/DL):',14X,E10.4,/,1X,
    #'VEN. PROTEIN1 CONC.  (GRAMS/DL):',14X,E10.4,/,1X,
    #'MES. PROTEIN1 CONC.  (GRAMS/DL):',14X,E10.4,/,1X,
    #'CAP. PROTEIN2 CONC.  (GRAMS/DL):',14X,E10.4,/,1X,
    #'VEN. PROTEIN2 CONC.  (GRAMS/DL):',14X,E10.4,/,1X,
    #'MES. PROTEIN2 CONC.  (GRAMS/DL):',14X,E10.4,/,1X,
    #'CAP. DYN. PRESSURE (DYN/CM**2):',14X,E10.4,/,1X,
    #'VEN. DYN. PRESSURE (DYN/CM**2):',14X,E10.4,/,1X,
    #'MES. DYN. PRESSURE (DYN/CM**2):',14X,E10.4,/,1X,
    #'CAP. OSM1. PRESSURE (DYN/CM**2):',14X,E10.4,/,1X,
```

```
     #'VEN. OSM1. PRESSURE (DYN/CM**2):',14X,E10.4,/,1X,
     #'MES. OSM1. PRESSURE (DYN/CM**2):',14X,E10.4,/,1X,
     #'CAP. OSM2. PRESSURE (DYN/CM**2):',14X,E10.4,/,1X,
     #'VEN. OSM2. PRESSURE (DYN/CM**2):',14X,E10.4,/,1X,
     #'MES. OSM2. PRESSURE (DYN/CM**2):',14X,E10.4,/,1X,
     #'TISSUE FLUID CONDUCTIVITY (CM**4/(DYN-SEC):',2X,E10.4)
     WRITE(6,610) DEFF1,DEFF2
 610 FORMAT(1X,
     #'TISSUE SOLUTE1 DIFFUSIVITY (CM**2/SEC):',7X,E10.4,/,1X,
     #'TISSUE SOLUTE2 DIFFUSIVITY (CM**2/SEC):',7X,E10.4)
     WRITE(6,611) CONC,CONV,CONM,PERMC1,PERMV1,PERMM1,PERMC2,PERMV2,
     #PERMM2
 611 FORMAT(1X,'CAP. CONDUCTIVITY (CM**3/(DYN-S));',11X,E10.4,/,1X,
     #'VEN. CONDUCTIVITY (CM**3/(DYN-S)):',11X,E10.4,/,1X,
     #'MES. CONDUCTIVITY (CM**3/(DYN-S)):',11X,E10.4,/,1X,
     #'CAP. PERMEABILITY 1 (CM/S):',21X,E10.4,/,1X,
     #'VEN. PERMEABILITY 1 (CM/S):',21X,E10.4,/,1X,
     #'MES. PERMEABILITY 1 (CM/S):',21X,E10.4,/,1X,
     #'CAP. PERMEABILITY 2 (CM/S):',21X,E10.4,/,1X,
     #'VEN. PERMEABILITY 2 (CM/S):',21X,E10.4,/,1X,
     #'MES. PERMEABILITY 2 (CM/S):',21X,E10.4)
     WRITE(6,602)
     WRITE(6,612) SIGT1,RET1,BETA1,ALPHL1,SIGT2,RET2,BETA2,ALPHL2
 612 FORMAT(1X,'DIMENSIONLESS INPUT PARAMETERS:',//,1X,
     #'TISSUE REFLECTION COEFFICIENT 1:',15X,E10.4,/,
     #1X,'RETARDATION FACTOR 1:',26X,E10.4,/,1X,
     #'HYDRAULIC CONDUCTIVITY RATIO, BETA1:',15X,E10.4,/,1X,
     #'DIMENSIONLESS DISPERSIVITY 1:',21X,E10.4,/,1X,
     #'TISSUE REFLECTION COEFFICIENT 2:',15X,E10.4,/,
     #1X,'RETARDATION FACTOR 2:',26X,E10.4,/,1X,
     #'HYDRAULIC CONDUCTIVITY RATIO, BETA2:',15X,E10.4,/,1X,
     #'DIMENSIONLESS DISPERSIVITY 2:',21X,E10.4)
     WRITE(6,613)PDC,PIDC1,PIDC2,PDV,PIDV1,PIDV2,PDM,PIDM1,PIDM2
 613 FORMAT(//,1X,
     #'PRESSURE:',6X,'DYNAMIC',5X,'OSMOTIC1',5X,'OSMOTIC2',
     #//,1X,'CAPILLARY:',5X, E10.4,2X,E10.4,2X,E10.4,
     #/,1X,'VENULE:',8X,E10.4,2X,E10.4,2X,E10.4,/,1X,'MESOTHELIUM:',
     #3X,E10.4,2X,E10.4,2X,E10.4,//)
     WRITE(6,614)CDC1,CDC2,CDV1,CDV2,CDM1,CDM2
 614 FORMAT(1X,'CONCENTRATIONS:   PROTEIN1   PROTEIN2',
     #//,1X,'CAPILLARY:',6X,E10.4,1X,E10.4,/,1X,
     #'VENULE:',10X,E10.4,1X,E10.4,/,1X,'MESOTHELIUM:',2(1X,E10.4),//)
     WRITE(6,615)SIGC1,SIGC2,SIGV1,SIGV2,SIGM1,SIGM2
 615 FORMAT(1X,'REFLECTION COEFFICIENTS: PROTEIN1   PROTEIN2',

     #//,1X,'CAPILLARY:',15X,E10.4,1X,E10.4,/,1X,'VENULE:',19X,
     #E10.4,1X,E10.4,/,1X,'MESOTHELIUM:',13X,E10.4,1X,E10.4,//)
     WRITE(6,616)DLC,DLV,DLM
 616 FORMAT(1X,'VESSEL FLUID CONDUCTANCES:',//,1X,'CAPILLARY:',5X,
     #E10.4,/,1X,'VENULE:',9X,E10.4,/,1X,'MESOTHELIUM:',1X,E10.4,//)
     WRITE(6,617)A1,B1,C1,A2,B2,C2
 617 FORMAT(1X,'VIRIAL COEFFICIENTS:',//,1X,'A1:',1X,E10.4,/,1X,
     #'B1:',1X,E10.4,/,1X,'C1:',1X,E10.4,/,1X,'A2:',1X,E10.4,/,1X,
     #'B2:',1X,E10.4,/,1X,'C2:',1X,E10.4,//)
     WRITE(6,618)DDC1,DDC2,DDV1,DDV2,DDM1,DDM2
 618 FORMAT(1X,'VESSEL SOLUTE PERMEABILITIES: PROTEIN1   PROTEIN2'
     #,//,1X,'CAPILLARY:',19X,E10.4,1X,E10.4,/,1X,'VENULE',22X,E10.4,
     #1X,E10.4,/,1X,'MESOTHELIUM:',17X,E10.4,1X,E10.4,//)
     WRITE(6,619)PHIT,PHI1,PHI2,PHIS
 619 FORMAT(1X,'TOTAL TISSUE FLUID VOLUME FRACTION:',2X,E10.4,/,1X,
     #'SOLUTE 1 DISTRIBUTION VOLUME FRACTION:',1X,E10.4,/,1X,
     #'SOLUTE 2 DISTRIBUTION VOLUME FRACTION:',1X,E10.4,/,1X,
     #'TOTAL SOLIDS VOLUME FRACTION:',8X,E10.4,///)
```

```
      C
      C
  999 THETAM=1.D0-THETA
      TIME1=DTIME1(1)
      IFLAG=0
      C
      C     ESTABLISH THE GRID
      C
      CALL GRID(NEX)
      C
      C     INITIALIZE FLUID VECTOR AND T VECTOR
      C
      CALL SETMAT(NEX,0,PE1,IE1,VELMX1,PE2,IE2,VELMX2)
      CALL SETMAT(NEX,3,PE1,IE1,VELMX1,PE2,IE2,VELMX2)
      C
      C     ADJUST FLUID VECTOR TO FIT BOUNDARY CONDITIONS
      C
      CALL ASTAR(NEX,0)
      CALL VSTAR(NEX,0)
      C
      C     CALCULATE THE SOLUTE VECTORS FROM THE STEADY-STATE DATA. THESE
      C     WILL SERVE TO GIVE A FIRST ESTIMATE OF THE CONCENTRATION AT
      C     THE NEXT TIME-STEP BY USING A FULLY EXPLICIT FORM TO BEGIN
      C     THE SIMULATION.
      C
      CALL SETMAT(NEX,2,PE1,IE1,VELMX1,PE2,IE2,VELMX2)
      CALL PATART(NEX)
      CALL PATVEN(NEX)
      PEC1=PE1
      PEC2=PE2
      IPEC1=IE1
      IPEC2=IE2
      DMX1=DISMX1
      DMX2=DISMX2
      ID1=IDISP1
      ID2=IDISP2
      VMAX=VELMX2
      IF(VELMX1.GT.VELMX2)  VMAX=VELMX1
      DELT=COUR/VMAX
      C
      C     SET THE SOLDT1, SOLDT2, SBOLD1, AND SBOLD2 VECTORS EQUAL
      C     TO THE STEADY-STATE VECTORS ABOVE
      C
      DO 4 I=1,NDIM
      SOLDT1(I)=SOL1(I)
      SOLDT2(I)=SOL2(I)
    4 CONTINUE
      C
      DO 5 I=1,NP
      SBOLD1(I)=SOLB1(I)
      SBOLD2(I)=SOLB2(I)
    5 CONTINUE
      C
      C     CHECK THAT THE MAXIMUM NUMBER OF TIME STEPS HAS NOT BEEN
      C     EXCEEDED
      C
      ICOUNT=0
      TIME=0
      ITSOL=1
      C
      C     ENTER ITERATION LOOP, CHECK COUNTER VALUE
      C
      C
  100 ICOUNT=ICOUNT+1
      C
      C     DETERMINE THE TOTAL ELAPSED TIME
      C
      NITER=0
      DTINV=1.D0/DELT
      TIME=TIME+1.D0/DTINV
      IF(ICOUNT.GT.IMAX)  GO TO 900
```

```
      IF(TIME.GT.TIMMAX)GO TO 910
C
      DO 6  I=1,NDIM
      TDT1(I)=T(I)*PHI1*DTINV
      TDT2(I)=T(I)*PHI2*DTINV
  6   CONTINUE
C
C     DETERMINE THE AS AND BS VECTORS FOR THE EXPLICIT SCHEME
C

      CALL MATPLY(TDT1,1.DO,COLDT1,TCOLD1,N)
      CALL MATPLY(TDT2,1.DO,COLDT2,TCOLD2,N)
      CALL MATPLY(SOLDT1,1.DO,COLDT1,SCOLD1,N)
      CALL MATPLY(SOLDT2,1.DO,COLDT2,SCOLD2,N)
C
      DO  7 I=1,N
      BCTIM1(I)=TCOLD1(I)+SBOLD1(I)-SCOLD1(I)
      BCTIM2(I)=TCOLD2(I)+SBOLD2(I)-SCOLD2(I)
  7   CONTINUE
C
C     DETERMINE THE INITIAL GUESS FOR CNEW, UPDATING NITER
C
  200 NITER=NITER+1
      EP=EPS
      IF(NITER.GT.ITMAX)GO TO 901
C
C     DETERMINE WHETHER THIS IS THE FIRST PASS, AND HENCE
C     USE THE FULLY EXPLICIT SCHEME FOR THE SOLUTE TRANSPORT
C     EQUATIONS. IN THE CASE OF SUBSEQUENT PASSES, USE THE
C     SEMI-IMPLICIT SCHEME
C
      IF(NITER.EQ.1) CALL DGBAND(TDT1,BCTIM1,N,LUB,LUB,1,IPERM1,DET,
     #JEXP,HOLD1,RES1,ITER,EP)
      EP=EPS
      IF(NITER.EQ.1) CALL DGBAND(TDT2,BCTIM2,N,LUB,LUB,1,IPERM2,DET,
     #JEXP,HOLD2,RES2,ITER,EP)
      IF(NITER.GT.1) CALL DGBAND(STNEW1,BCTIM1,N,LUB,LUB,1,IPERM1,DET,
     #JEXP,HOLD1,RES1,ITER,EP)
      EP=EPS
      IF(NITER.GT.1) CALL DGBAND(STNEW2,BCTIM2,N,LUB,LUB,1,IPERM2,DET,
     #JEXP,HOLD2,RES2,ITER,EP)
C
C     DETERMINE THE MAXIMUM CHANGE IN C1 AND C2 FROM ONE ITERATION
C     TO THE NEXT USING A RELAXATION PROCEDURE. CDIFMX WILL BE
C     COMPARED TO TOLC TO ESTABLISH CONVERGENCE FOR TIME STEP ICOUNT
C
      CMAX1=0.DO
      CMAX2=0.DO
      CDMX1=0.DO
      CDMX2=0.DO
      DO 8 I=1,N
      IF(DABS(BCTIM1(I)).GT.CMAX1) CMAX1=DABS(BCTIM1(I))
      TEST1=DABS(BCTIM1(I)-COLD1(I))
      IF(TEST1.GT.CDMX1) CDMX1=TEST1
      COLD1(I)=OMEGAC*(BCTIM1(I)-COLD1(I))+COLD1(I)
      IF(DABS(BCTIM2(I)).GT.CMAX2) CMAX2=DABS(BCTIM2(I))
      TEST2=DABS(BCTIM2(I)-COLD2(I))
      IF(TEST2.GT.CDMX2) CDMX2=TEST2
      COLD2(I)=OMEGAC*(BCTIM2(I)-COLD2(I))+COLD2(I)
  8   CONTINUE
      CDMX1=CDMX1/CMAX1
      CDMX2=CDMX2/CMAX2
C
C     NOW INITIALIZE THE FLUID B VECTOR AND SOLVE FOR THE PRESSURE
C     DISTRIBUTION AT THIS NEW TIME STEP
C
      CALL SETMAT(NEX,1,PE1,IE1,VELMX1,PE2,IE2,VELMX2)
      CALL ASTAR(NEX,1)
      CALL VSTAR(NEX,1)
```

```
C
      EP=EPS
      CALL DGBND1(FLUID,FLUIDB,N,LUB,LUB,ITSOL,IPERM3,DET,JEXP,
     #HOLD3,RES3,ITER,EP)
      ITSOL=ITSOL+1
C
C     CHECK TO SEE IF THE SOLUTION HAS CONVERGED
C
      PMAX=0.D0
      PDIFMX=0.D0
      DO 9 I=1,N
      IF(DABS(FLUIDB(I)).GT.PMAX)  PMAX=DABS(FLUIDB(I))
      TEST=DABS(FLUIDB(I)-POLD(I))
      IF(TEST.GT.PDIFMX)  PDIFMX=TEST
      POLD(I)=OMEGAF*(FLUIDB(I)-POLD(I))+POLD(I)
  9   CONTINUE
      PDIFMX=PDIFMX/PMAX
C
C     CHECK FOR CONVERGENCE
C
      IF(PDIFMX.GT.TOLP)GO TO 300
      IF(CDMX1.GT.TOLC)GO TO 300
      IF(CDMX2.LT.TOLC)GO TO 301
C
C     RESET THE SOLUTE MATRICES, SET THE NECESSARY VECTORS FOR THE
C     SEMI-IMPLICIT SCHEME
C
 300  CALL SETMAT(NEX,2,PE1,IE1,VELMX1,PE2,IE2,VELMX2)
      CALL PATART(NEX)
      CALL PATVEN(NEX)
      PEC1=PE1
      PEC2=PE2
      IEL1=IE1
      IEL2=IE2
      COUR1=VELMX1*DELT
      COUR2=VELMX2*DELT
      DMX1=DISMX1
      DMX2=DISMX2
      ID1=IDISP1

      ID2=IDISP2
C
      DO 10 I=1,N
      BCTIM1(I)=THETA*SOLB1(I)+TCOLD1(I)+THETAM*SBOLD1(I)-
     #          THETAM*SCOLD1(I)
      BCTIM2(I)=THETA*SOLB2(I)+TCOLD2(I)+THETAM*SBOLD2(I)-
     #          THETAM*SCOLD2(I)
 10   CONTINUE
C
      DO 11 I=1,NDIM
      STNEW1(I)=T(I)*PHI1*DTINV+THETA*SOL1(I)
      STNEW2(I)=T(I)*PHI2*DTINV+THETA*SOL2(I)
 11   CONTINUE
      GO TO 200
C
C     RESET MATRICES FOR NEXT TIME STEP
C
 301  DO 12 I=1,N
      SBOLD1(I)=SOLB1(I)
      SBOLD2(I)=SOLB2(I)
      COLDT1(I)=COLD1(I)
      COLDT2(I)=COLD2(I)
 12   CONTINUE
C
      DO 13 I=1,NDIM
      SOLDT1(I)=SOL1(I)
      SOLDT2(I)=SOL2(I)
 13   CONTINUE
C
C     DETERMINE IF THE SOLUTION SHOULD BE PRINTED OUT. IF DELT
C     HAS BEEN SET TO (TIME1-TIME), RESET DELT TO DTHOLD, I.E.,
```

```
C      TO THE LAST VALUE OF DELT BEFORE SETTING IT TO TIME1-TIME.
C
       IF(IFLAG.EQ.0)GO TO 400
       DELT=DTHOLD
       IFLAG=0
  400  DELT=DELT*TFACT
       IF(DABS(TIME-TIME1).LT.TTOL)GO TO 800
       IF(DABS(TIME-TIME1).GT.DELT)GO TO 100
       DTHOLD=DELT
       IFLAG=1
       DELT=DABS(TIME-TIME1)
       GO TO 100
C
C      PRINT OUT THE SOLUTION AT TIME1 TO DEVICE 6 AND 7
C
  800  WRITE(6,602)
       WRITE(6,620) ICOUNT,TIME,NITER,COUR1,PEC1,IEL1,DMX1,ID1,COUR2,
      #             PEC2,IEL2,DMX2,ID2
  620  FORMAT(//,1X,'NUMBER OF TIME STEPS:',I7,1X,/,1X,
      #'REPRESENTING A CUMMULATIVE TIME OF ',F10.7,/,1X,
      #'NUMBER OF ITERATIONS REQUIRED FOR CONVERGENCE:',1X,I4,/,1X,
      #'MAXIMUM COURANT NUMBER FOR SOLUTE 1:',1X,F10.7,/,1X,
      #'MAXIMUM GRID PECLET NUMBER FOR SOLUTE 1:',1X,F10.7,1X,
      #'AT ELEMENT',1X,I4,/,1X,
      #'MAXIMUM DISPERSION COEFFICIENT FOR SOLUTE 1:',1X,F10.7,1X,
      #'AT ELEMENT', 1X,I4,/,1X,
      #'MAXIMUM COURANT NUMBER FOR SOLUTE 2:',1X,F10.7,/,1X,
      #'MAXIMUM GRID PECLET NUMBER FOR SOLUTE 2:',1X,F10.7,1X,
      #'AT ELEMENT',1X,I4,/,1X,
      #'MAXIMUM DISPERSION COEFFICIENT FOR SOLUTE 2:',1X,F10.7,1X,
      #'AT ELEMENT', 1X,I4)
C
       WRITE(6,621)
  621  FORMAT(//,1X,'X POSITION',2X,'DYN. PRESS',2X,'OSM. PRESS',2X,
      #'AVAIL. CONC1',2X,'TOTAL CONC1',2X,'AVAIL. CONC2',2X,
      #'TOTAL CONC2',//)
C
       X=0.D0
       DO 14 I=1,N
       X=X+DX(I)
       PI=COLD1(I)*(A1+COLD1(I)*(B1+COLD1(I)*C1))
      #  +COLD2(I)*(A2+COLD2(I)*(B2+COLD2(I)*C2))
       CON1=COLD1(I)*PHI1/(1.D0-PHIS)
       CON2=COLD2(I)*PHI2/(1.D0-PHIS)
C
C      WRITE OUT PROFILE DATA TO DEVICES 6 AND 7
C
       WRITE(6,622) X,POLD(I),PI,COLD1(I),CON1,COLD2(I),CON2
       WRITE(7,622) X,POLD(I),PI,COLD1(I),CON1,COLD2(I),CON2
  622  FORMAT(1X,E9.3,6(2X,E10.4))
  14   CONTINUE
C
C      WRITE OUT MESOTHELIAL FLUX DATA TO DEVICE 7
C
       CALL MASBAL(NEX)
       DO 15 I=1,NEX
       I2=2*I
       X=XNOD(I2)
       WRITE(7,702) X,QFM1(I),QSM11(I),QCM11(I),QSM12(I),QCM12(I)
  702  FORMAT(6(2X,E10.4))
  15   CONTINUE
C
C
       WRITE(6,623)
  623  FORMAT('1',//,1X,'MASS BALANCE DATA'///)
C
       WRITE(6,624)

  624  FORMAT(///,1X,'NET DIMENSIONLESS FLUID FLOWS')
```

```
      WRITE(6,625) QFC,QFV,QFM
  625 FORMAT(//,1X,'ART:',1X,E12.4,/,1X,'VEN:',
     #E12.4,/,1X,'MES:',1X,E12.4)
      WRITE(6,626)
  626 FORMAT(///,1X,'NET DIMENSIONLESS SOLUTE FLOWS: SOLUTE1')
      WRITE(6,625)QSC1,QSV1,QSM1
      WRITE(6,627)
  627 FORMAT(//,1X,'CONVECTIVE COMPONENTS OF DIMENSIONLESS SOLUTE
     #FLOWS: SOLUTE1')
      WRITE(6,625) QCC1,QCV1,QCM1
C
      WRITE(6,628)
  628 FORMAT(///,1X,'NET DIMENSIONLESS SOLUTE FLOWS: SOLUTE2')
      WRITE(6,625)QSC2,QSV2,QSM2
      WRITE(6,629)
  629 FORMAT(//,1X,'CONVECTIVE COMPONENTS OF DIMENSIONLESS SOLUTE
     #FLOWS: SOLUTE2')
      WRITE(6,625) QCC2,QCV2,QCM2
C
      WRITE(6,630)
  630 FORMAT(//,1X,
     #'RATIO OF CONV. TO DIFFUS. FLUXES AT BOUNDARIES: SOLUTE 1')
      IF(DABS(QSC1-QCC1).LT.1.D-9)  THEN
      PECC1=999.999D0
      ELSE
      PECC1=QCC1/(QSC1-QCC1)
      ENDIF
      IF(DABS(QSV1-QCV1).LT.1.D-9)  THEN
      PECV1=999.999D0
      ELSE
      PECV1=QCV1/(QSV1-QCV1)
      ENDIF
      IF(DABS(QSM1-QCM1).LT.1.D-9)  THEN
      PECM1=999.999D0
      ELSE
      PECM1=QCM1/(QSM1-QCM1)
      ENDIF
      WRITE(6,625) PECC1,PECV1,PECM1
C
      WRITE(6,631)
  631 FORMAT(//,1X,
     #'RATIO OF CONV. TO DIFFUS. FLUXES AT BOUNDARIES: SOLUTE 2')
      IF(DABS(QSC2-QCC2).LT.1.D-9)  THEN
      PECC2=999.999D0
      ELSE
      PECC2=QCC2/(QSC2-QCC2)
      ENDIF
      IF(DABS(QSV2-QCV2).LT.1.D-9)  THEN
      PECV2=999.999D0
      ELSE
      PECV2=QCV2/(QSV2-QCV2)
      ENDIF
      IF(DABS(QSM2-QCM2).LT.1.D-9)  THEN
      PECM2=999.999D0
      ELSE
      PECM2=QCM2/(QSM2-QCM2)
      ENDIF
      WRITE(6,625) PECC2,PECV2,PECM2
C
      TIME1=TIME1+DTIME1(KK)
      KK=KK+1
      WRITE(6,602)
      GO TO 100


C
C     MAXIMUM NUMBER OF ITERATIONS REACHED. PRINT OUT WARNING.
C
  901 ICOUNT=ICOUNT-1
      NITER=NITER-1
```

```
      WRITE(6,632) NITER,TIME,ICOUNT
  632 FORMAT(//,1X,'WARNING.  CONVERGENCE CRITERIA NOT MET AFTER',
     #1X,I6,1X,'ITERATIONS',/,1X,
     #'TIME OF FAILURE:',1X,F10.6,3X,
     #'NUMBER OF SUCCESSFUL TIME STEPS BEFORE FAILURE:',1X,I7)
C
      WRITE(6,633) PDIFMX,CDMX1,CDMX2
  633 FORMAT(//,1X,'MAX. FRAC. CHANGE IN P',2X,
     #'MAX. FRAC. CHANGE IN C1',2X,
     #'MAX. FRAC. CHANGE IN C2',
     #//,6X,E9.4,14X,E9.4,14X,E9.4,//)
      WRITE(6,634) PEC1,IEL1,COUR1,PEC2,IEL2,COUR2
  634 FORMAT(1X,'MAXIMUM GRID PECLET NUMBER FOR SOLUTE 1:',1X,F7.4,
     #' AT ELEMENT ',I5,/,1X,'COURANT NUMBER FOR SOLUTE 1:',1X,F10.7,
     #/,1X,'MAXIMUM GRID PECLET NUMBER FOR SOLUTE 2:',1X,F7.4,
     #' AT ELEMENT ',I5,/,1X,'COURANT NUMBER FOR SOLUTE 2:',1X,F10.7)
      GO TO 920
  900 WRITE(6,635) TIME
  635 FORMAT(//,1X,'MAXIMUM  NUMBER OF TIME STEPS ACHEIVED AT TIME',
     #E10.4)
      GO TO 920
  910 WRITE(6,636) TIMMAX,ICOUNT
  636 FORMAT(//,1X,'MAXIMUM TIME OF ',E10.4,1X,'EXCEEDED  AFTER ',
     #I7,' TIME STEPS')
  920 STOP
      END
      SUBROUTINE MASBAL(NEX)
C
C     THIS SUBROUTINE PERFORMS A MATERIAL BALANCE ON THE SYSTEM FOR
C
C     BOTH FLUID AND PLASMA PROTEINS.
C
      IMPLICIT REAL*8(A-H,O-Z)
      COMMON/MATBAL/QFC,QCC1,QSC1,QCC2,QSC2,QFV,QCV1,QSV1,QCV2,QSV2,
     #QFM,QCM1,QSM1,QCM2,QSM2,QFM1(500),QCM11(500),QSM11(500),
     #QCM12(500),QSM12(500)
      COMMON/OLD/POLD(1001),COLD1(1001),COLD2(1001)
      COMMON/BLK1/NODEL(500,3),XNOD(1001)
      COMMON/OSMOT/A1,B1,C1,A2,B2,C2
      COMMON/TISDAT/AK,DEFF1,AL1,PHI1,PHIT,RET1,SIGT1,BETA1,
     #              DEFF2,AL2,PHI2,RET2,SIGT2,BETA2
      COMMON/CAPDAT/PC,CREF
      COMMON/WALL/DLC,DLV,DLM,DDC1,DDV1,DDM1,PDC,PDV,PDM,PIDC1,PIDV1,
     #PIDM1,PIDC2,PIDV2,PIDM2,SIGC1,SIGV1,SIGM1,CDC1,CDV1,CDM1,DH,
     #              DDC2,DDV2,DDM2,SIGC2,SIGV2,SIGM2,CDC2,CDV2,CDM2
      DIMENSION GAUS(4),W(4),B(3)
      DATA NGAUS/4/
      DATA W/.347854845137454D0,.652145154862546D0,
     #.652145154862546D0,.347854845137454D0/
      DATA GAUS/-.861136311594053D0,-.339981043584856D0,
     #.339981043584856D0,.861136311594053D0/
C
C     FIRST, CALCULATE THE NET FLOWS ACROSS THE ARTERIOLAR WALL
C
      PIC1=COLD1(1)*(A1+COLD1(1)*(B1+COLD1(1)*C1))
      PIC2=COLD2(1)*(A2+COLD2(1)*(B2+COLD2(1)*C2))
      QFC=DH*AK*PC/DEFF1/DLC*(POLD(1)-PDC-SIGC1*(PIC1-PIDC1)-
     #    SIGC2*(PIC2-PIDC2))
      QCC1=BETA1*QFC*COLD1(1)*RET1
      QCC2=BETA2*QFC*COLD2(1)*RET2
      PECC1=(1.D0-SIGC1)*QFC/(DDC1*DH)
      IF(PECC1.GT.100.D0)GO  TO 110
      IF(PECC1.LT.-100.D0)GO TO 120
      TEST=1.D0-DEXP(-PECC1)
      IF(DABS(TEST).LT.1.D-10)GO  TO 130
      QSC1=(1.D0-SIGC1)*QFC*(COLD1(1)-CDC1*DEXP(-PECC1))/TEST
      GO TO 101
```

```fortran
  110   QSC1=QFC*(1.D0-SIGC1)*COLD1(1)
        GO TO 101
  120   QSC1=(1.D0-SIGC1)*CDC1*QFC
        GO TO 101
  130   QSC1=DH*DDC1*(COLD1(1)-CDC1)
C
  101   PECC2=(1.D0-SIGC2)*QFC/(DDC2*DH)
        IF(PECC2.GT.100.D0)GO TO 111
        IF(PECC2.LT.-100.D0)GO TO 121
        TEST=1.D0-DEXP(-PECC2)
        IF(DABS(TEST).LT.1.D-10)GO TO 131
        QSC2=(1.D0-SIGC2)*QFC*(COLD2(1)-CDC2*DEXP(-PECC2))/TEST
        GO TO 200
  111   QSC2=QFC*(1.D0-SIGC2)*COLD2(1)
        GO TO 200
  121   QSC2=(1.D0-SIGC2)*CDC2*QFC
        GO TO 200
  131   QSC2=DH*DDC2*(COLD2(1)-CDC2)
C
C       NOW FOR THE VENULAR WALL
C
  200   N=NEX*2+1
        PIV1=COLD1(N)*(A1+COLD1(N)*(B1+COLD1(N)*C1))
        PIV2=COLD2(N)*(A2+COLD2(N)*(B2+COLD2(N)*C2))
        QFV=DH*AK*PC/DEFF1*DLV*(POLD(N)-PDV-SIGV1*(PIV1-PIDV1)    -
     #    SIGV2*(PIV2-PIDV2))
        QCV1=BETA1*QFV*COLD1(N)*RET1
        QCV2=BETA2*QFV*COLD2(N)*RET2
        PECV1=(1.D0-SIGV1)*QFV/(DDV1*DH)
        IF(PECV1.GT.100.D0)GO TO 210
        IF(PECV1.LT.-100.D0)GO TO 220
        TEST=1.D0-DEXP(-PECV1)
        IF(DABS(TEST).LT.1.D-10)GO TO 230
        QSV1=(1.D0-SIGV1)*QFV*(COLD1(N)-CDV1*DEXP(-PECV1))/TEST
        GO TO 201
  210   QSV1=QFV*(1.D0-SIGV1)*COLD1(N)
        GO TO 201
  220   QSV1=(1.D0-SIGV1)*CDV1*QFV
        GO TO 201
  230   QSV1=DH*DDV1*(COLD1(N)-CDV1)
C
  201   PECV2=(1.D0-SIGV2)*QFV/(DDV2*DH)
        IF(PECV2.GT.100.D0)GO TO 211
        IF(PECV2.LT.-100.D0)GO TO 221
        TEST=1.D0-DEXP(-PECV2)
        IF(DABS(TEST).LT.1.D-10)GO TO 231
        QSV2=(1.D0-SIGV2)*QFV*(COLD2(N)-CDV2*DEXP(-PECV2))/TEST
        GO TO 300

  211   QSV2=QFV*(1.D0-SIGV2)*COLD2(N)
        GO TO 300
  221   QSV2=(1.D0-SIGV2)*CDV2*QFV
        GO TO 300
  231   QSV2=DH*DDV2*(COLD2(N)-CDV2)
C
C       AND FINALLY, THE MESOTHELIAL LAYER
C
C       CONSIDER THE MESOTHELIAL WALL, ELEMENT BY ELEMENT.
C
  300   QSM1=0.D0
        QCM1=0.D0
        QSM2=0.D0

        QCM2=0.D0
        QFM=0.D0
C
        DO 400 I=1,NEX
        QSM11(I)=0.D0
        QFM1(I)=0.D0
        QCM11(I)=0.D0
```

```
        QSM12(I)=0.D0
        QCM12(I)=0.D0
 400    CONTINUE
C
        DO 1 II=1,NGAUS
        S=GAUS(II)
            DO 2 I=1,NEX
            X1=XNOD(NODEL(I,1))
            X2=XNOD(NODEL(I,2))
            X3=XNOD(NODEL(I,3))
            S2=(2.D0*X2-(X1+X3))/(X3-X1)
C
            B(1)=(S-S2)*(S-1.D0)/(2.D0*(S2+1.D0))
            B(2)=(S+1.D0)*(S-1.D0)/(S2*S2-1.D0)
            B(3)=(S+1.D0)*(S-S2)/(2.D0*(1.D0-S2))
            DX=(X3-X1)*.5D0
C
C       CALCULATE C(S), PI(S), AND P(S)
C
            CS1=0.D0
            CS2=0.D0
            PS=0.D0
            DO 3 IT=1,3
            CS1=CS1+COLD1(NODEL(I,IT))*B(IT)
            CS2=CS2+COLD2(NODEL(I,IT))*B(IT)
            PS=PS+POLD(NODEL(I,IT))*B(IT)
 3          CONTINUE
            PIS1=CS1*(A1+CS1*(B1+CS1*C1))
            PIS2=CS2*(A2+CS2*(B2+CS2*C2))
C
C       CALCULATE THE FLUXES
C
            FLOW=AK*PC/DEFF1*DLM*(PS-PDM-SIGM1*(PIS1-PIDM1)
     #            - SIGM2*(PIS2-PIDM2))*W(II)*DX
            QFM=QFM+FLOW
            QFM1(I)=QFM1(I)+FLOW/(X3-X1)
            QCM1=QCM1+FLOW*CS1*BETA1*RET1
            QCM2=QCM2+FLOW*CS2*BETA2*RET2
            QCM11(I)=QCM11(I)+FLOW*CS1*BETA1/(X3-X1)*RET1
            QCM12(I)=QCM12(I)+FLOW*CS2*BETA2/(X3-X1)*RET2
C
C       DETERMINE WHICH FORM OF THE NONLINEAR FLUX EQN. IS TO BE USED.
C
            QS=FLOW/(W(II)*DX)
            PECM1=QS*(1.D0-SIGM1)/DDM1
            IF(PECM1.GT.100.D0)GO  TO 410
            IF(PECM1.LT.-100.D0)GO  TO 420
            TESTM=1.D0-DEXP(-PECM1)
            IF(DABS(TESTM).LT.1.D-10)GO  TO 430
C
C       USE THE FULL EXPRESSION
C
            SFLOW1=FLOW*(1.D0-SIGM1)*(CS1-CDM1*DEXP(-PECM1))/TESTM
            QSM1=QSM1+SFLOW1
            QSM11(I)=QSM11(I)+SFLOW1/(X3-X1)
            GO TO 500
C
 410        SFLOW1=FLOW*(1.D0-SIGM1)*CS1
            QSM1=QSM1+SFLOW1
            QSM11(I)=QSM11(I)+SFLOW1/(X3-X1)
            GO TO 500
C
 420        SFLOW1=FLOW*(1.D0-SIGM1)*CDM1
            QSM1=QSM1+SFLOW1
            QSM11(I)=QSM11(I)+SFLOW1/(X3-X1)
            GO TO 500
C
 430        SFLOW1=DDM1*(CS1-CDM1)*DX*W(II)
            QSM1=QSM1+SFLOW1
```

```fortran
                QSM11(I)=QSM11(I)+SFLOW1/(X3-X1)
C
   500          PECM2=QS*(1.D0-SIGM2)/DDM2
                IF(PECM2.GT.100.D0)GO  TO 510
                IF(PECM2.LT.-100.D0)GO  TO 520
                TESTM=1.D0-DEXP(-PECM2)
                IF(DABS(TESTM).LT.1.D-10)GO  TO 530
C
C      USE THE FULL EXPRESSION
C
                SFLOW2=FLOW*(1.D0-SIGM2)*(CS2-CDM2*DEXP(-PECM2))/TESTM
                QSM2=QSM2+SFLOW2
                QSM12(I)=QSM12(I)+SFLOW2/(X3-X1)
                GO TO 2
C
   510          SFLOW2=FLOW*(1.D0-SIGM2)*CS2
                QSM2=QSM2+SFLOW2
                QSM12(I)=QSM12(I)+SFLOW2/(X3-X1)
                GO TO 2
C
   520          SFLOW2=FLOW*(1.D0-SIGM2)*CDM2
                QSM2=QSM2+SFLOW2
                QSM12(I)=QSM12(I)+SFLOW2/(X3-X1)
                GO TO 2


C
   530          SFLOW2=DDM2*(CS2-CDM2)*DX*W(II)
                QSM2=QSM2+SFLOW2
                QSM12(I)=QSM12(I)+SFLOW2/(X3-X1)
C
   2            CONTINUE
   1        CONTINUE
            RETURN

            END
            SUBROUTINE GRID(NEX)
C
C      THIS SUBROUTINE CALCULATES THE SPATIAL LOCATION OF THE NODES
C      FOR EACH ELEMENT, ALONG WITH THE NODES ASSOCIATED WITH A
C      GIVEN ELEMENT.
C
            IMPLICIT REAL*8(A-H,O-Z)
            COMMON/BLK1/NODEL(500,3),   XNOD(1001)
            COMMON/BLK2/DX(1001)
C
            K=1
            DO 1 I=1,NEX
            NODEL(I,1)=K
            NODEL(I,2)=K+1
            NODEL(I,3)=K+2
            K=K+2
   1        CONTINUE
C
            X=0.D0
            NP=2*NEX+1
            DO 2 I=1,NP
            X=X+DX(I)
            XNOD(I)=X
   2        CONTINUE
            RETURN
            END
C
            SUBROUTINE VSTAR(NEX,IND)
C
C      THIS SUBROUTINE ADJUSTS THE AF AND BF VECTORS TO ACCOUNT FOR THE
C      STARLING BOUNDARY CONDITION AT THE VENULAR WALL.
C
            IMPLICIT REAL*8(A-H,O-Z)
            COMMON/BLK1/NODEL(500,3),   XNOD(1001)
            COMMON/FLUMAT/AF(20000)
```

```
      COMMON/FLUB/BF(1001)
      COMMON/OLD/POLD(1001),COLD1(1001),COLD2(1001)
      COMMON/WALL/DLC,DLV,DLM,DDC1,DDV1,DDM1,PDC,PDV,PDM,PIDC1,PIDV1,
     #PIDM1,PIDC2,PIDV2,PIDM2,SIGC1,SIGV1,SIGM1,CDC1,CDV1,CDM1,DH,
     #          DDC2,DDV2,DDM2,SIGC2,SIGV2,SIGM2,CDC2,CDV2,CDM2
      COMMON/OSMOT/A1,B1,C1,A2,B2,C2
C
      M=NEX*2+1
      LUB=2
      LP=3*LUB
      IF(IND.EQ.1)GO TO 100
      K=LP*M+M-LUB
      AF(K)=AF(K)+ DLV
    , GO TO 900
C
 100  PI1=COLD1(M)*(A1+COLD1(M)*(B1+COLD1(M)*C1))
      PI2=COLD2(M)*(A2+COLD2(M)*(B2+COLD2(M)*C2))
      BF(M)=BF(M)+DLV*(PDV+SIGV1*(PI1-PIDV1)+SIGV2*(PI2-PIDV2))
C
 900  RETURN
      END
      SUBROUTINE ASTAR(NEX,IND)
C
C     THIS SUBROUTINE ADJUSTS THE AF AND BF VECTORS TO ACCOUNT FOR THE
C     STARLING BOUNDARY CONDITION AT THE ARTERIOLAR WALL.
C
      IMPLICIT REAL*8(A-H,O-Z)
      COMMON/BLK1/NODEL(500,3),  XNOD(1001)
      COMMON/FLUMAT/AF(20000)
      COMMON/FLUB/BF(1001)
      COMMON/OLD/POLD(1001),COLD1(1001),COLD2(1001)
      COMMON/WALL/DLC,DLV,DLM,DDC1,DDV1,DDM1,PDC,PDV,PDM,PIDC1,PIDV1,
     #PIDM1,PIDC2,PIDV2,PIDM2,SIGC1,SIGV1,SIGM1,CDC1,CDV1,CDM1,DH,
     #          DDC2,DDV2,DDM2,SIGC2,SIGV2,SIGM2,CDC2,CDV2,CDM2
      COMMON/OSMOT/A1,B1,C1,A2,B2,C2
C
      LUB=2
      LP=3*LUB
      IF(IND.EQ.1)GO TO 100
      K=LP+1-LUB
      AF(K)=AF(K)+ DLC
      GO TO 900
C
 100  PI1=COLD1(1)*(A1+COLD1(1)*(B1+COLD1(1)*C1))
      PI2=COLD2(1)*(A2+COLD2(1)*(B2+COLD2(1)*C2))
      BF(1)=BF(1)+DLC*(PDC+SIGC1*(PI1-PIDC1)+SIGC2*(PI2-PIDC2))
C
 900  RETURN
      END


      SUBROUTINE PATART(NEX)
C
C     THIS SUBROUTINE ADJUSTS THE AS AND BS VECTORS TO ACCOUNT FOR THE

C     PATLAK BOUNDARY CONDITION AT THE ARTERIOLAR WALL.
C
      IMPLICIT REAL*8(A-H,O-Z)
      COMMON/BLK1/NODEL(500,3),  XNOD(1001)
      COMMON/SOLMAT/AS1(20000),AS2(20000)
      COMMON/SOLB/BS1(1001),BS2(1001)
      COMMON/OLD/POLD(1001),COLD1(1001),COLD2(1001)
      COMMON/TISDAT/AK,DEFF1,ALPHL1,PHI1,PHIT,RET1,SIGT1,BETA1,
     #DEFF2,ALPHL2,PHI2,RET2,SIGT2,BETA2
      COMMON/CAPDAT/PC,CREF
      COMMON/WALL/DLC,DLV,DLM,DDC1,DDV1,DDM1,PDC,PDV,PDM,PIDC1,
     #PIDV1,PIDM1,PIDC2,PIDV2,PIDM2,SIGC1,SIGV1,SIGM1,CDC1,CDV1,CDM1,
     #DH,DDC2,DDV2,DDM2,SIGC2,SIGV2,SIGM2,CDC2,CDV2,CDM2
      COMMON/OSMOT/A1,B1,C1,A2,B2,C2
C
```

```
        LUB=2
        LP=3*LUB
        K=LP+1-LUB
C
        PI1=COLD1(1)*(A1+COLD1(1)*(B1+COLD1(1)*C1))
        PI2=COLD2(1)*(A2+COLD2(1)*(B2+COLD2(1)*C2))
        QART=AK*PC/DEFF1*DLC*(POLD(1)-PDC-SIGC1*(PI1-PIDC1)-
       #SIGC2*(PI2-PIDC2))
        PEC1=(1.D0-SIGC1)/DDC1*QART
C
C       DETERMINE WHICH FORM OF THE FLUX EXPRESSION APPLIES
C
        IF(PEC1.GT.100.0D0)GO  TO 100
        IF(PEC1.LT.-100.D0)GO  TO 200
        TEST=1.D0-DEXP(-PEC1)
        IF(DABS(TEST).LT.1.D-10)GO  TO 300
C
        AS1(K)=AS1(K)-QART*(RET1*BETA1-(1.D0-SIGC1)/TEST)
        BS1(1)=BS1(1)+(1.D0-SIGC1)*QART*CDC1*DEXP(-PEC1)/TEST
        GO TO 900
C
  100   AS1(K)=AS1(K)-QART*(BETA1*RET1-(1.D0-SIGC1))
        GO TO 900
C
  200   AS1(K)=AS1(K)-QART*BETA1*RET1
        BS1(1)=BS1(1)-(1.D0-SIGC1)*QART*CDC1
        GO TO 900
C
  300   AS1(K)=AS1(K)-QART*BETA1*RET1+DDC1
        BS1(1)=BS1(1)+DDC1*CDC1
C
  900   PEC2=(1.D0-SIGC2)/DDC2*QART
C
C       DETERMINE WHICH FORM OF THE FLUX EXPRESSION APPLIES
C
        IF(PEC2.GT.100.0D0)GO  TO 101
        IF(PEC2.LT.-100.D0)GO  TO 201
        TEST=1.D0-DEXP(-PEC2)
        IF(DABS(TEST).LT.1.D-10)GO  TO 301
C
        AS2(K)=AS2(K)-QART*(RET2*BETA2-(1.D0-SIGC2)/TEST)
        BS2(1)=BS2(1)+(1.D0-SIGC2)*QART*CDC2*DEXP(-PEC2)/TEST
        GO TO 901
C
  101   AS2(K)=AS2(K)-QART*(BETA2*RET2-(1.D0-SIGC2))
        GO TO 901
C
  201   AS2(K)=AS2(K)-QART*BETA2*RET2
        BS2(1)=BS2(1)-(1.D0-SIGC2)*QART*CDC2
        GO TO 901
C
  301   AS2(K)=AS2(K)-QART*BETA2*RET2+DDC2
        BS2(1)=BS2(1)+DDC2*CDC2
C
C
  901   RETURN
        END
        SUBROUTINE PATVEN(NEX)
C
C       THIS SUBROUTINE ADJUSTS THE AS AND BS VECTORS TO ACCOUNT FOR THE
C       PATLAK BOUNDARY CONDITION AT THE VENULAR WALL.
C
        IMPLICIT REAL*8(A-H,O-Z)
        COMMON/BLK1/NODEL(500,3),  XNOD(1001)
        COMMON/SOLMAT/AS1(20000),AS2(20000)
        COMMON/SOLB/BS1(1001),BS2(1001)
        COMMON/OLD/POLD(1001),COLD1(1001),COLD2(1001)
        COMMON/TISDAT/AK,DEFF1,ALPHL1,PHI1,PHIT,RET1,SIGT1,BETA1,
       #DEFF2,ALPHL2,PHI2,RET2,SIGT2,BETA2
        COMMON/CAPDAT/PC,CREF
```

```
      COMMON/WALL/DLC,DLV,DLM,DDC1,DDV1,DDM1,PDC,PDV,PDM,PIDC1,
     #PIDV1,PIDM1,PIDC2,PIDV2,PIDM2,SIGC1,SIGV1,SIGM1,CDC1,CDV1,CDM1,
     #DH,DDC2,DDV2,DDM2,SIGC2,SIGV2,SIGM2,CDC2,CDV2,CDM2
      COMMON/OSMOT/A1,B1,C1,A2,B2,C2
C
      LUB=2
      LP=3*LUB
      NP=2*NEX+1
      K=LP*NP+NP-LUB
C
      PI1=COLD1(NP)*(A1+COLD1(NP)*(B1+COLD1(NP)*C1))
      PI2=COLD2(NP)*(A2+COLD2(NP)*(B2+COLD2(NP)*C2))
      QART=AK*PC/DEFF1*DLV*(POLD(NP)-PDV-SIGV1*(PI1-PIDV1)-
     #SIGV2*(PI2-PIDV2))
      PEC1=(1.D0-SIGV1)/DDV1*QART


C
C     DETERMINE WHICH FORM OF THE FLUX EXPRESSION APPLIES
C
      IF(PEC1.GT.100.0D0)GO  TO 100
      IF(PEC1.LT.-100.D0)GO  TO 200
      TEST=1.D0-DEXP(-PEC1)
      IF(DABS(TEST).LT.1.D-10)GO  TO 300
C
      AS1(K)=AS1(K)-QART*(RET1*BETA1-(1.D0-SIGV1)/TEST)
      BS1(NP)=BS1(NP)+(1.D0-SIGV1)*QART*CDV1*DEXP(-PEC1)/TEST
      GO TO 900
C
  100 AS1(K)=AS1(K)-QART*(BETA1*RET1-(1.D0-SIGV1))
      GO TO 900
C
  200 AS1(K)=AS1(K)-QART*BETA1*RET1
      BS1(NP)=BS1(NP)-(1.D0-SIGV1)*QART*CDV1
      GO TO 900
C
  300 AS1(K)=AS1(K)-QART*BETA1*RET1+DDV1
      BS1(NP)=BS1(NP)+DDV1*CDV1
C
  900 PEC2=(1.D0-SIGV2)/DDV2*QART
C
C     DETERMINE WHICH FORM OF THE FLUX EXPRESSION APPLIES
C
      IF(PEC2.GT.100.0D0)GO  TO 101
      IF(PEC2.LT.-100.D0)GO  TO 201
      TEST=1.D0-DEXP(-PEC2)
      IF(DABS(TEST).LT.1.D-10)GO  TO 301
C
      AS2(K)=AS2(K)-QART*(RET2*BETA2-(1.D0-SIGV2)/TEST)
      BS2(NP)=BS2(NP)+(1.D0-SIGV2)*QART*CDV2*DEXP(-PEC2)/TEST
      GO TO 901
C
  101 AS2(K)=AS2(K)-QART*(BETA2*RET2-(1.D0-SIGV2))
      GO TO 901
C
  201 AS2(K)=AS2(K)-QART*BETA2*RET2
      BS2(NP)=BS2(NP)-(1.D0-SIGV2)*QART*CDV2
      GO TO 901
C
  301 AS2(K)=AS2(K)-QART*BETA2*RET2+DDV2
      BS2(NP)=BS2(NP)+DDV2*CDV2
C
  901 RETURN
      END
      SUBROUTINE MATPLY(A,A1,B,C,NP)
C
C     THIS SUBROUTINE MULTIPLIES A MATRIX A BY A VECTOR B AND SCALAR A1
C     TO GIVE  VECTOR C. MATRIX A IS STORED AS A VECTOR, WHERE MATRIX
C     ELEMENT A(I,J) IS STORED AS A(IJ), IJ=3*LUB*J+I-LUB,  AND WHERE
C     LUB IS THE NUMBER OF OFF DIAGONAL BANDS. FOR THIS SUBROUTINE,
C     IT IS ASSUMED THAT THE BANDWIDTH IS 5, SO THAT LUB=2.
```

```fortran
C
      IMPLICIT REAL*8(A-H,O-Z)
      DIMENSION A(20000), B(NP), C(NP)
      LUB=2
      LP=3*LUB
C
      DO 1 I=1,NP
      C(I)=0.D0
  1   CONTINUE
C
      K=2
      DO 2 I=1,2
      K=K+1
         DO 3 J=1,K
         IJ=LP*J+I-LUB
         C(I)=C(I)+A(IJ)*A1*B(J)
  3      CONTINUE
  2   CONTINUE
C
      NPM=NP-2
      K=0
      DO 4 I=3,NPM
      K=K+1
      KP=K+4
         DO 5 J=K,KP
         IJ=J*LP+I-LUB
         C(I)=C(I)+A(IJ)*B(J)*A1
  5      CONTINUE
  4   CONTINUE
C
      NPM=NP-1
      K=NP-4
      DO 6 I=NPM,NP
      K=K+1
         DO 7 J=K,NP
         IJ=LP*J+I-LUB
         C(I)=C(I)+A(IJ)*A1*B(J)
  7      CONTINUE
  6   CONTINUE
C
      RETURN
      END

      SUBROUTINE SETMAT(NEX,IND,PE1,IPEC1,VMAX1,PE2,IPEC2,VMAX2)
C
C     THIS SUBROUTINE INITIALIZES THE VARIOUS VECTORS ASSOCIATED
C     WITH SOLUTE AND FLUID TRANSPORT EQUATIONS, AF(K), BF(I), AS1(K),
C     AS2(I),BS1(I),  BS2(I).
C
      IMPLICIT REAL*8(A-H,O-Z)
      COMMON/BLK1/NODEL(500,3),XNOD(1001)
      COMMON/FLUMAT/AF(20000)
      COMMON/OLD/POLD(1001),COLD1(1001),COLD2(1001)
      COMMON/SOLB/BS1(1001),BS2(1001)
      COMMON/FLUB/BF(1001)
      COMMON/SOLMAT/AS1(20000),AS2(20000)
      COMMON/OSMOT/A1,B1,C1,A2,B2,C2
      COMMON/TISDAT/AK,DEFF1,AL1,PHI1,PHIT,RET1,SIGT1,BETA1,
     #DEFF2,AL2,PHI2,RET2,SIGT2,BETA2
      COMMON/CAPDAT/PC,CREF
      COMMON/WALL/DLC,DLV,DLM,DDC1,DDV1,DDM1,PDC,PDV,PDM,PIDC1,
     #PIDV1,PIDM1,PIDC2,PIDV2,PIDM2,SIGC1,SIGV1,SIGM1,CDC1,CDV1,CDM1,
     #DH,DDC2,DDV2,DDM2,SIGC2,SIGV2,SIGM2,CDC2,CDV2,CDM2
      COMMON/TIME/T(20000)
      COMMON/MAXDAT/DMX1,DMX2,IDISP1,IDISP2
C
      DIMENSION GAUS(4),W(4),B(3),DB(3)
      DATA NGAUS/4/
      DATA W/.347854845137454D0,.652145154862546D0,
     #.652145154862546D0,.347854845137454D0/
```

```
      DATA GAUS/-.861136311594053D0,-.339981043584856D0,
     #.339981043584856D0,.861136311594053D0/
C     DATA GAUS/
C     DATA W/
C     DATA NGAUS/3/
C     DATA GAUS/
C     DATA W/
      DMX1=0.D0
      DMX2=0.D0
      ALPHA=AK*PC/DEFF1
      PE1=0.D0
      VMAX1=0.D0
      PE2=0.D0
      VMAX2=0.D0
C
C
C     ZERO THE APPROPRIATE ARRAY AND INITIALIZE
C
      IF(IND.EQ.1)GO TO 800
      IF(IND.EQ.2)GO TO 900
      IF(IND.EQ.3)GO TO 950
C
C     ZERO THE AF VECTOR
C
      DO 700 I=1,20000
      AF(I)=0.D0
  700 CONTINUE
      GO TO 100
C
C     ZERO THE BF VECTOR
C
  800 DO 801 I=1,1001
      BF(I)=0.D0
  801 CONTINUE
      GO TO 100
C
C     ZERO THE T MATRIX
C
  950 DO 951 I=1,20000
      T(I)=0.D0
  951 CONTINUE
      GO TO 100
C
C     ZERO THE AS AND BS VECTORS
C
  900 DO 901 I=1,20000
      AS1(I)=0.D0
      AS2(I)=0.D0
  901 CONTINUE
C
      DO 902 I=1,1001
      BS1(I)=0.D0
      BS2(I)=0.D0
  902 CONTINUE
C
C     BEGIN THE GAUSS INTEGRATION, ELEMENT BY ELEMENT
C
  100 LUB=2
      LP=3*LUB
C
C     EVALUATE THE INTEGRAND AT THE APPROPRIATE QUADRATURE POINT, S.
C
      DO 200 II=1,NGAUS
      S=GAUS(II)
C
C     INITIALIZE THE APPROPRIATE ARRAY, ELEMENT BY ELEMENT.
C
      DO 300 I=1,NEX
C
C     CALCULATE VALUE OF BASIS FUNCTIONS AND DERIVATIVES AT THE
```

```
C       QUADRATURE POINT
C

        X1=XNOD(NODEL(I,1))
        X2=XNOD(NODEL(I,2))
        X3=XNOD(NODEL(I,3))
C
        S2=(2.D0*X2-(X1+X3))/(X3-X1)
C
        B(1)=(S-S2)*(S-1.D0)/(2.D0*(S2+1.D0))
        B(2)=(S+1.D0)*(S-1.D0)/(S2*S2-1.D0)
        B(3)=(S+1.D0)*(S-S2)/(2.D0*(1.D0-S2))
        DB(1)=(2.D0*S-S2-1.D0)/(2.D0*(S2+1.D0))
        DB(2)=2.D0*S/(S2*S2-1.D0)
        DB(3)=(2.D0*S-S2+1.D0)/(2.D0*(1.D0-S2))
C
        DX=(X3-X1)*.5D0
C ...
C       CALCULATE THE T VECTOR
C
        IF(IND.NE.3) GO TO 101
        DO 952 M=1,3
        MM=NODEL(I,M)
            DO 953 N=1,3
            NN=NODEL(I,N)
            K=LP*NN+MM-LUB
            T(K)=T(K)+B(M)*B(N)*DX*W(II)
  953       CONTINUE
  952 CONTINUE
        GO TO 300
C
C       NOW CALCULATE C1(S), DC1/DS, PI1(S), DPI1/DS,C2(S),...
C
  101 CS1=0.D0
        CS2=0.D0
        DCS1=0.D0
        DCS2=0.D0
        DO 301 IT=1,3
        CS1=CS1+COLD1(NODEL(I,IT))*B(IT)
        CS2=CS2+COLD2(NODEL(I,IT))*B(IT)
        DCS1=DCS1+COLD1(NODEL(I,IT))*DB(IT)
        DCS2=DCS2+COLD2(NODEL(I,IT))*DB(IT)
  301 CONTINUE
C
        PIS1=CS1*(A1+CS1*(B1+CS1*C1))
        PIS2=CS2*(A2+CS2*(B2+CS2*C2))
        DPIS2=(A2+2.D0*B2*CS2+3.D0*CS2*CS2*C2)*DCS2
        DPIS1=(A1+2.D0*B1*CS1+3.D0*CS1*CS1*C1)*DCS1
C
C       DETERMINE WHICH VECTOR IS TO BE INITIALIZED
C
        IF(IND.EQ.1)GO TO 500
        IF(IND.EQ.2)GO TO 600
C
C       INITIALIZE THE FLUID VECTOR
C
        DO 401 M=1,3
        MM=NODEL(I,M)
            DO 402 N=1,3
            NN=NODEL(I,N)
            K=LP*NN+MM-LUB
            AF(K)=AF(K)+(B(M)*B(N)*2.D0*DLM/DH*DX+DB(M)*DB(N)/DX)*W(II)
  402       CONTINUE
  401 CONTINUE
        GO TO 300
C
C       INITIALIZE THE FLUID B VECTOR
C
  500 DO 501 M=1,3
        MM=NODEL(I,M)
```

```
       BF(MM)=BF(MM)+(DB(M)*(DPIS1*SIGT1+DPIS2*SIGT2)/DX+B(M)*
      #2.DO*DLM/DH*DX*(PDM+SIGM1*(PIS1   - PIDM1)+SIGM2*(PIS2-PIDM2)
      #))*W(II)
  501  CONTINUE
       GO TO 300
C
C      INITIALIZE THE SOLUTE VECTORS, BS AND AS. fIRST CALCULATE VS1,VS2
C      QMES, AND THE DISPERSION COEFFICIENTS, DISP1 AND DISP2.
C
  600  DPS=0.DO
       PS=0.DO
       DO 601 IT=1,3
       DPS=DPS+POLD(NODEL(I,IT))*DB(IT)
       PS=PS+POLD(NODEL(I,IT))*B(IT)
  601  CONTINUE
C
       VS1=-ALPHA*(DPS-SIGT1*DPIS1-SIGT2*DPIS2)/DX*RET1*BETA1/PHI1
       VS2=-ALPHA*(DPS-SIGT1*DPIS1-SIGT2*DPIS2)/DX*RET2*BETA2/PHI2
       QFMES=ALPHA*DLM*(PS-PDM-SIGM1*(PIS1-PIDM1)-SIGM2*(PIS2-PIDM2))
       DISP1=DABS(VS1)*AL1+1.DO
       IF(DISP1.LT.DMX1)  GO TO 655
       DMX1=DISP1
       IDISP1=I
  655  DISP2=DABS(VS2)*AL2+DEFF2/DEFF1
       IF(DISP2.LT.DMX2)  GO TO 656
       DMX2=DISP2
       IDISP2=I
C
C      CALCULATE THE MAXIMUM LOCAL SOLUTE VELOCITY, VELMAX
C
  656  IF(DABS(CS1).LT.1.D-5)  VELS1=DABS(VS1)*PHI1
       IF(DABS(CS1).GT.1.D-5)  VELS1=DABS(VS1-(DISP1*DCS1/DX)/CS1)*PHI1
       IF(DABS(CS2).LT.1.D-5)  VELS2=DABS(VS2)*PHI2
       IF(DABS(CS2).GT.1.D-5)  VELS2=DABS(VS2-(DISP2*DCS2/DX)/CS2)*PHI2
       IF(.5DO*VELS1/DX.GT.VMAX1)  VMAX1=.5DO*VELS1/DX
       IF(.5DO*VELS2/DX.GT.VMAX2)  VMAX2=.5DO*VELS2/DX
C
C      CALCULATE THE GRID PECLET NUMBER, AND SEE IF IT EXCEEDS
C      THE LIMIT
C
       PEST1=DABS(VS1)*(X3-X1)/DISP1
       IF(PEST1.LT.PE1)GO TO 609
       PE1=PEST1
       IPEC1=I
  609  PEST2=DABS(VS2)*(X3-X1)/DISP2
       IF(PEST2.LT.PE2)GO TO 610
       PE2=PEST2
       IPEC2=I
C
C      NOW DETERMINE WHICH FORM OF THE NONLINEAR FLUX EXPRESSION
C      IS TO BE USED TO CALCULATE SOLUTE FLUX ACROSS MESOTHELIUM.
C
C
  610  PEC1=QFMES*(1.DO-SIGM1)/DDM1
       IF(PEC1.GT.100.DO)GO TO 611
       IF(PEC1.LT.-100.DO)GO TO 620
       TEST=1.DO-DEXP(-PEC1)
       IF(DABS(TEST).LT.1.D-10)GO TO 630
C
C      CASE 1: USE THE FULL NONLINEAR FLUX EXPRESSION
C
       DO 602 M=1,3
       MM=NODEL(I,M)
           DO 603 N=1,3
           NN=NODEL(I,N)
           K=LP*NN+MM-LUB
           AS1(K)=AS1(K)+(B(M)*DB(N)*VS1*PHI1+
      #             DB(M)*DB(N)*DISP1*PHI1/DX
      #             +B(M)*B(N)*2.DO*QFMES/TEST/DH*(1.DO-SIGM1)*DX
      #             -2.DO/DH*QFMES*RET1*BETA1*B(M)*B(N)*DX)*W(II)
```

```
  603          CONTINUE
        BS1(MM)=BS1(MM)+
     #          B(M)*2.D0/DH*(1.D0-SIGM1)*QFMES*CDM1*DEXP(-PEC1)/TEST
     #          *DX*W(II)
  602  CONTINUE
        GO TO 640
C
C      CASE 2: PEC APPROACHES INFINITY
C
  611  DO 612 M=1,3
        MM=NODEL(I,M)
              DO 613 N=1,3
              NN=NODEL(I,N)
              K=LP*NN+MM-LUB
              AS1(K)=AS1(K)+
     #            (B(M)*DB(N)*VS1*PHI1+DB(M)*DB(N)*PHI1*DISP1/DX
     #            +B(M)*B(N)*2.D0/DH*(1.D0-SIGM1)*QFMES*DX
     #            -QFMES*RET1*BETA1*B(M)*B(N)*DX*2.D0/DH)*W(II)
  613          CONTINUE
  612  CONTINUE
        GO TO 640
C
C      CASE 3: -PEC APPROACHES INFINITY
C
  620  DO 621 M=1,3
        MM=NODEL(I,M)
              DO 622 N=1,3
              NN=NODEL(I,N)
              K=LP*NN+MM-LUB
              AS1(K)=AS1(K)+
     #            (B(M)*DB(N)*VS1*PHI1+DB(M)*DB(N)*PHI1*DISP1/DX
     #            -2.D0/DH*BETA1*RET1*QFMES*B(N)*B(M)*DX)*W(II)
  622          CONTINUE
         BS1(MM)=BS1(MM)-2.D0/DH*(1.D0-SIGM1)*QFMES*CDM1*DX*W(II)*B(M)
  621  CONTINUE
        GO TO 640
C
C      CASE 4: PEC APPROACHES 0
C
  630  DO 631 M=1,3
        MM=NODEL(I,M)
              DO 632 N=1,3
              NN=NODEL(I,N)
              K=LP*NN+MM-LUB
              AS1(K)=AS1(K)+
     #            (B(M)*DB(N)*VS1*PHI1+DB(M)*DB(N)*PHI1*DISP1/DX
     #            +2.D0/DH*DDM1*B(M)*B(N)*DX
     #            -2.D0/DH*RET1*BETA1*DX*B(M)*B(N)*QFMES)*W(II)
  632  CONTINUE
        BS1(MM)=BS1(MM)+2.D0/DH*DDM1*B(M)*CDM1*DX*W(II)
  631  CONTINUE
C
  640  PEC2=QFMES*(1.D0-SIGM2)/DDM2
        IF(PEC2.GT.100.D0)GO  TO 650
        IF(PEC2.LT.-100.D0)GO  TO 660
        TEST=1.D0-DEXP(-PEC2)
        IF(DABS(TEST).LT.1.D-10)GO  TO 670
C
C      CASE 1: USE THE FULL NONLINEAR FLUX EXPRESSION
C
        DO 641 M=1,3
        MM=NODEL(I,M)
              DO 642 N=1,3
              NN=NODEL(I,N)
              K=LP*NN+MM-LUB
              AS2(K)=AS2(K)+(B(M)*DB(N)*VS2*PHI2+
     #            DB(M)*DB(N)*DISP2*PHI2/DX
     #            +B(M)*B(N)*2.D0*QFMES/TEST/DH*(1.D0-SIGM2)*DX
     #            -2.D0/DH*QFMES*RET2*BETA2*B(M)*B(N)*DX)*W(II)
  642          CONTINUE
```

```
            BS2(MM)=BS2(MM)+
      #          B(M)*2.D0/DH*(1.D0-SIGM2)*QFMES*CDM2*DEXP(-PEC2)/TEST
      #          *DX*W(II)
  641   CONTINUE
        GO TO 300
C
C       CASE 2: PEC APPROACHES INFINITY
C
  650   DO 651 M=1,3
        MM=NODEL(I,M)
              DO 652 N=1,3
              NN=NODEL(I,N)
              K=LP*NN+MM-LUB
              AS2(K)=AS2(K)+
      #              (B(M)*DB(N)*VS2*PHI2+DB(M)*DB(N)*PHI2*DISP2/DX
      #              +B(M)*B(N)*2.D0/DH*(1.D0-SIGM2)*QFMES*DX
      #              -QFMES*RET2*BETA2*B(M)*B(N)*DX*2.D0/DH)*W(II)
  652         CONTINUE
  651   CONTINUE
        GO TO 300
C
C       CASE 3: -PEC APPROACHES INFINITY
C
  660   DO 661 M=1,3
        MM=NODEL(I,M)
              DO 662 N=1,3
              NN=NODEL(I,N)
              K=LP*NN+MM-LUB
              AS2(K)=AS2(K)+
      #              (B(M)*DB(N)*VS2*PHI2+DB(M)*DB(N)*PHI2*DISP2/DX
      #              -2.D0/DH*BETA2*RET2*QFMES*B(N)*B(M)*DX)*W(II)
  662         CONTINUE
        BS2(MM)=BS2(MM)-2.D0/DH*(1.D0-SIGM2)*QFMES*CDM2*DX*W(II)*B(M)
  661   CONTINUE
        GO TO 300


C
C       CASE 4: PEC APPROACHES 0
C
  670   DO 671 M=1,3
        MM=NODEL(I,M)
              DO 672 N=1,3
              NN=NODEL(I,N)
              K=LP*NN+MM-LUB
              AS2(K)=AS2(K)+
      #              (B(M)*DB(N)*VS2*PHI2+DB(M)*DB(N)*PHI2*DISP2/DX
      #              +2.D0/DH*DDM2*B(M)*B(N)*DX
      #              -2.D0/DH*RET2*BETA2*DX*B(M)*B(N)*QFMES)*W(II)
  672   CONTINUE
        BS2(MM)=BS2(MM)+2.D0/DH*DDM2*B(M)*CDM2*DX*W(II)
  671   CONTINUE
C
  300   CONTINUE
  200   CONTINUE
        RETURN
        END
C
        SUBROUTINE DGBED1 (A, B, N, ML, NU, LT, IP, DET, NCN1,
      1                    BB, RZ, ITR1, EPS1)
C
C ROUTINE SOLVES SYSTEM OF LINEAR EQNS. AX=B WHERE A IS A GENERAL
C BAND MATRIX. METHOD USED IS GAUSSIAN ELIMINATION WITH PARTIAL
C PIVOTING. OPTION OF ITERATIVELY IMPROVING SOLUTION IS AVAILABLE.
C UPPER BAND WIDTH OF MATRIX INCREASES DUE TO INTERCHANGES BY
C AMOUNT ML. ROUTINE REQUIRES BAND ELEMENTS OF MATRIX TO BE STORED
C BY COLUMN IN A ONE DIMENSIONAL ARRAY. EACH COLUMN IS OF LENGTH
C 2*ML+NU AND BAND IS TO BE STORED IN ELEMENTS ML+1 TO 2*ML+NU OF
C EACH COLUMN. ELEMENTS 1 TO ML OF COLUMN ARE SET TO ZERO BY GBAND.
C IF MATRIX IS SYMMETRIC USER MAY SPECIFY LOWER BAND ONLY IN
C ELEMENTS ML+NU+1 TO 2*ML+NU OF EACH COLUMN AND GBAND WILL
```

```
C   GENERATE REMAINING ELEMENTS. (IF THIS IS DESIRED, SET LT=-1 ON
C   FIRST CALL TO GBAND.)
C     A = 1 DIMENSIONAL ARRAY CONTAINING MATRIX OF COEFFICIENTS.
C     B = 1 DIMENSIONAL ARRAY CONTAINING RIGHT HAND SIDE VECTORS.
C           ON EXIT, B WILL CONTAIN THE SOLUTION VECTOR X.
C     N = ORDER OF MATRIX
C     ML = LENGTH OF LOWER BAND (EXCLUDING DIAGONAL)
C     NU = LENGTH OF UPPER BAND (EXCLUDING DIAGONAL)
C     LT = ABS(LT)=1 IF ONLY 1 B VECTOR OR IF 1ST OF SEVERAL.
C          ABS(LT),=1 FOR SUBSEQUENT B VECTORS.
C           (NOTE. LT=+1 IF FULL BAND WIDTH GIVEN, LT=-1 IF LOWER BAND
C           ONLY OF SYMMETRIC MATRIX GIVEN.)
C     IP = INTEGER ARRAY CONTAINING INTERCHANGE INFORMATION.
C     DET = DETERMINANT OF A = DET*(10**NCN) WHERE 1.D-15<|DET|<1.D+15.
C           IF DET=0.0 MATRIX IS SINGULAR AND ERROR RETURN TAKEN.
C     BB, RZ = ARRAYS REQUIRED FOR IMPROVEMENT OPTION. CAN BE REAL*8
C           VARIABLES IF OPTION NOT REQUIRED.
C     ITER   = 0 IF IMPROVEMENT NOT REQUIRED, OTHERWISE ITER= NO. OF
C           ITERATIONS OR CYCLES.
C     EPS - CONVERGENCE CRITERION.
C
C   MODIFIED TO DO ITERATIVE IMPROVEMENT (FORMERLY AVAILABLE ONLY
C   WITH THE SINGLE PRECISION VERSION). MIKE PATTERSON - NOV, 1980
        IMPLICIT REAL*8 (A-H, O-Z)
        COMMON /GBAND$/ NITER
        DIMENSION A(1), B(N), IP(N), BB(N), RZ(N)
        COMPLEX*16 DSUMM, QADDQ, QMULD
        REAL*8 QRNDQ
C   TO ASSIGN LOGICAL UNITS 94 AND 95 ONLY ONCE:
        LOGICAL ASSIGN /F/, YES /T/
C   STATEMENT FUNCTION TO CALCULATE POINTERS INTO A:
        IFN(I, J) = 1 + (J - 1)*LC + I - J + NUM
C
C
        NCN=NCN1
        ITR=ITR1
        EPS=EPS1
        ITER = ITR
C
        LCM = NU + 2*ML
        LC = LCM + 1
        NLC = N*LC
        NUM = NU + ML
C   GENERATE REMAINING ELEMENTS OF SYMMETRIC MATRIX
        IF (LT .NE. -1) GO TO 120
        NN = N - 1
        DO 110 I = 1, NN
          IFI = IFN(I, I)
          IFJ = IFI
          II = I + 1
          IML = MINO(I + ML, N)
          DO 100 J = II, IML
            IFI = IFI + 1
            IFJ = IFJ + LCM
100         A(IFJ) = A(IFI)
110       CONTINUE
120     IF (ITER .EQ. 0) GO TO 140
C   ASSIGN UNITS 94 AND 95 IF THEY HAVE NOT ALREADY BEEN ASSIGNED:
        IF (ASSIGN) GO TO 125
        CALL FTNCMD ('ASSIGN 94=-GBAND94;')
        CALL FTNCMD ('ASSIGN 95=-GBAND95;')
        ASSIGN = YES
125     REWIND 94
        REWIND 95
        DO 130 I = 1, N
130     BB(I) = B(I)
140     IF (IABS(LT) .NE. 1) GO TO 280
        IP(N) = 1
        IF (ML .EQ. 0) GO TO 160
C   SET ELEMENTS 1 - ML OF EACH COLUMN TO ZERO
        DO 150 I = 1, N
```

```
              IFK = (I - 1)*LC
              DO 150 J = 1, ML
                 IFK = IFK + 1
150        A(IFK) = 0.0D0
160        IF (ITER .NE. 0) CALL DWR1 (A, NLC, 94)
           DET = 0.0D0
           NCN = 0
           IF (ML .EQ. 0) GO TO 230
C   LU DECOMPOSITION

           DO 220 K = 1, N
              IFK = IFN(K, K)
              IF (K .EQ. N) GO TO 210
              KP = K + 1
              KPM = MINO(K + ML, N)
              KPN = MINO(K + NUM, N)
              M = K
              IFM = IFK
              IFI = IFK
              DO 170 I = KP, KPM
                 IFI = IFI + 1
                 IF (DABS(A(IFI)) .LE. DABS(A(IFM))) GO TO 170
                 M = I
                 IFM = IFI
170           CONTINUE
              IP(K) = M
              T = A(IFM)
              IF (M .NE. K) IP(N) = -IP(N)
              A(IFM) = A(IFK)
              A(IFK) = T
              IF (T .EQ. 0.0D0) GO TO 260
              OT = 1.0D0/T
              IK = IFK
              DO 180 I = KP, KPM
                 IK = IK + 1
180           A(IK) = -A(IK)*OT
              KJ = IFK
              MJ = IFM
              DO 200 J = KP, KPN
                 KJ = KJ + LCM
                 MJ = MJ + LCM
                 T = A(MJ)
                 A(MJ) = A(KJ)
                 A(KJ) = T
                 IF (T .EQ. 0.0D0) GO TO 200
                 IK = IFK
                 IJ = KJ
                 DO 190 I = KP, KPM
                    IK = IK + 1
                    IJ = IJ + 1
190              A(IJ) = A(IJ) + A(IK)*T
200           CONTINUE
210        IF (A(IFK) .EQ. 0.0D0) GO TO 260
220        CONTINUE
230        IFK = IFN(1, 1)
           DET = A(IFK)
           DO 250 K = 2, N
              IFK = IFK + LC
              DET = DET*A(IFK)
              IF (DET .EQ. 0.0D0) GO TO 260
              IF (DABS(DET) .GT. 1.D-15) GO TO 240
              DET = DET*1.D+15
              NCN = NCN - 15
              GO TO 250
240           IF (DABS(DET) .LT. 1.D+15) GO TO 250
              DET = DET*1.D-15
              NCN = NCN + 15
250        CONTINUE
           DET = DET*IP(N)
           GO TO 280
260        DET = 0.0D0
```

```
        WRITE (6, 270) K
270     FORMAT ('0* DGBND1 - matrix is singular. '/
     1        '    Error occurred in attempt to find', I5, 'th pivot.')
        RETURN
280     CALL DSOLV1 (A, B, IP, N, ML, NU)
        IF (ITER .EQ. 0) RETURN
C
C   ITERATIVE IMPROVEMENT
C   RESIDUALS (R) = AX-B ARE FOUND AND STORED IN ARRAY RZ USING
C   EXTENDED PRECISION ARITHMETIC. SYSTEM AZ=R IS SOLVED AND NEW
C   SOLUTION =X+Z IS STORED IN ARRAY B. ABOVE STEPS REPEATED UNTIL
C       (1) MAX(Z)/MAX(X) < EPS OR
C       (2) NO. OF CYCLES > ITER OR
C       (3) IMPROVEMENT STARTS TO DIVERGE.
C   ROUTINE THEN RETURNS AFTER SETTING EPS=MAX(Z) (FOR (1)) OR
C   SETTING EPS=-MAX(Z) AND PRINTING APPROPRIATE ERROR MESSAGE (FOR
C   (2) AND (3))
C
C
        IF (IABS(LT) .EQ. 1) CALL DWR1 (A, NLC, 95)
        XNORM = 0.0D0
        DO 290 K = 1, N
290     XNORM = DMAX1(XNORM, DABS(B(K)))
        IF (XNORM .LE. 0.0D0) RETURN
        ZX = 1.D+60
        LD = 0
        DO 340 L = 1, ITER
          REWIND 94
          CALL DRE1 (A, NLC, 94)
          DO 310 K = 1, N
            DSUMM = (0.D0, 0.D0)
            KPM = MAX0(K - ML, 1)
            KPN = MIN0(K + NU, N)
            IFK = IFN(K, KPM)
            DO 300 J = KPM, KPN
C              DSUMM = DSUMM + A(IFK)*B(J)
C USING EXTENDED PRECISION:

              DSUMM = QADDQ(DSUMM, QMULD(A(IFK), B(J)))
300           IFK = IFK + LCM
          RZ(K) = BB(K) - QRNDQ(DSUMM)
310     CONTINUE
        REWIND 95
        CALL DRE1 (A, NLC, 95)
        CALL DSOLV1 (A, RZ, IP, N, ML, NU)
        ZNORM = 0.0D0
        DO 320 K = 1, N
          ERZ = RZ(K)
          ZNORM = DMAX1(ZNORM, DABS(ERZ))
320       B(K) = B(K) + ERZ
        IF (ZNORM .GT. ZX) GO TO 330
        IF ((ZNORM - EPS*XNORM) .LT. 0.0D0) GO TO 390
        ZX = ZNORM
        GO TO 340
330     IF (ZNORM .GT. 10.0D0*ZX) GO TO 360
        LD = LD + 1
        IF (LD .GE. 3) GO TO 360
340     CONTINUE
        L = ITER
        WRITE (6, 350)
350     FORMAT ('0* DGBND1- Iterative improvement did not converge'/)
        GO TO 380
360     WRITE (6, 370)
370     FORMAT ('0* DGBND1 - Iterative improvement is diverging.'/)
380     EPS = -ZNORM
        NITER = L
        RETURN
390     EPS = ZNORM
        NITER = L
```

```
      RETURN
      END
      SUBROUTINE DSOLV1 (A, B, IP, N, ML, NU)
C
C  THIS ROUTINE COMPUTES THE SOLUTION OF A SYSTEM AFTER GBAND HAS
C  DECOMPOSED MATRIX A INTO A LOWER TRIANGULAR MATRIX L AND AN
C  UPPER TRIANGULAR MATRIX U.
C
      IMPLICIT REAL*8 (A-H, O-Z)
      DIMENSION A(1), B(N), IP(N)
      IFN(I, J) = 1 + (J - 1)*LC + I - J + NUM
      LCM = 2*ML + NU
      LC = LCM + 1
      NUM = NU + ML
      MN = N - 1
C  SOLVE FOR Y
      IF (ML .EQ. 0) GO TO 110
      DO 100 K = 1, MN
      KP = K + 1
      M = IP(K)
      T = B(M)
      B(M) = B(K)
      B(K) = T
      KPM = MINO(K + ML, N)
      IFK = IFN(K, K)
      DO 100 I = KP, KPM
      IFK = IFK + 1
100   B(I) = B(I) + A(IFK)*T
C  SOLVE FOR X
110   IFK = IFN(N, N)
      DO 120 KB = 1, MN
      KM = N - KB
      K = KM + 1
      B(K) = B(K)/A(IFK)
      IFK = IFK - LC
      T = -B(K)
      KMN = MAXO(1, K - ML - NU)
      KML = IFN(KMN, K)
      DO 120 I = KMN, KM
      B(I) = B(I) + A(KML)*T
120   KML = KML + 1
      B(1) = B(1)/A(NUM + 1)
      RETURN
      END
      SUBROUTINE DWR1 (A, N, LU)
      REAL*8 A(N)
      WRITE (LU) A
      RETURN
      END
      SUBROUTINE DRE1 (A, N, LU)
      REAL*8 A(N)
      READ (LU) A
      RETURN
      END
```